Vol. 66 August, 1962 No. 8

# THE JOURNAL OF PHYSICAL CHEMISTRY

(Registered in U. S. Patent Office)

CONTENTS



NOTES



*Contents continued on inside front cover*

# THE JOURNAL OF PHYSICAL CHEMISTRY

(Registered in U. S. Patent Office)



Published monthly by the American Chemical Society at 20th and Northampton Sts., Easton, Pa. Second-class postage paid at Easton, Pa.

The *Journal of Physical Chemistry* is devoted to the publication of selected symposia in the broad field of physical chemistry and to other contributed papers.

Manuscripts originating in the British Isles, Europe, and Africa should be sent to F. C. Tompkins, The Faraday Society, 6 Gray's Inn Square, London W. C. 1, England.

Manuscripts originating elsewhere should be sent to W. Albert Noyes, Jr., Department of Chemistry, University of Rochester, Rochester 20, N. Y.

Correspondence regarding accepted copy, proofs, and reprints should be directed to Assistant Editor, Allen D. Bliss, ACS Office, Mack Printing Company, 20th and Northampton Sts., Easton, Pa.

Advertising Office: Reinhold Publishing Corporation, 430 Park Avenue, New York 22, N. Y.

Articles must be submitted in duplicate, typed, and double spaced. They should have at the beginning a brief Abstract, in no case exceeding 300 words. Original drawings should accompany the manuscript. Lettering at the sides of graphs (black on white or blue) may be pencilled in and will be typeset. Figures and tables should be held to a minimum consistent with adequate presentation of information. Photographs will not be printed on glossy paper except by special arrangement. All footnotes and references to the literature should be numbered consecutively and placed in the manuscript at the proper places. Initials of authors referred to in citations should be given. Nomenclature should conform to that used in *Chemical Abstracts*, mathematical characters be marked for italic, Greek letters carefully made or annotated, and subscripts and superscripts clearly shown. Articles should be written as briefly as possible consistent with clarity and should avoid historical background unnecessary for specialists.

Symposium papers should be sent in all cases to Secretaries of Divisions sponsoring the symposium, who will be responsible for their transmittal to the Editor. The Secretary of the Division by agreement with the Editor will specify a time after which symposium papers cannot be accepted. The Editor reserves the right to refuse to publish symposium articles, for valid scientific reasons. Each symposium paper may not exceed four printed pages (about sixteen double spaced typewritten pages) in length except by prior arrangement with the Editor.

Claims for missing numbers will not be allowed (1) if received more than sixty days from date of issue (because of delivery hazards, no claims can be honored from subscribers in Central Europe, Asia, or Pacific Islands other than Hawaii), (2) if loss was due to failure of notice of change of address to be received before the date specified in the preceding paragraph, or (3) if the reason for the claim is "missing from files."

Subscription rates (1962): members of American Chemical Society, $12.00 for 1 year; to non-members, $24.00 for 1 year. Postage to countries in the Pan-American Union $0.80; Canada, $0.40; all other countries, $1.20. Single copies, current volume, $2.50; foreign postage, $0.15; Canadian postage $0.10; Pan-American Union, $0.10. Back volumes (Vol. 56–65) $30.00 per volume; foreign postage, per volume $1.20, Canadian, $0.40; Pan-American Union, $0.80. Single copies: back issues, $3.00; for current year, $2.50; postage, single copies: foreign, $0.15; Canadian, $0.10; Pan-American Union, $0.10.

The American Chemical Society and the Editors of the *Journal of Physical Chemistry* assume no responsibility for the statements and opinions advanced by contributors to This Journal.

The American Chemical Society also publishes *Journal of the American Chemical Society*, *Chemical Abstracts*, *Industrial and Engineering Chemistry*, International Edition of *Industrial and Engineering Chemistry*, *Chemical and Engineering News*, *Analytical Chemistry*, *Journal of Agricultural and Food Chemistry*, *Journal of Organic Chemistry*, *Journal of Chemical and Engineering Data*, *Chemical Reviews*, *Chemical Titles*, *Journal of Chemical Documentation*, *Journal of Medicinal and Pharmaceutical Chemistry*, *Inorganic Chemistry*, *Biochemistry*, and *CA — Biochemical Sections*. Rates on request.

THE JOURNAL OF PHYSICAL CHEMISTRY

(Registered in U. S. Patent Office) (© Copyright, 1962, by the American Chemical Society)

VOLUME 66 AUGUST 14, 1962 NUMBER 8

# INFLUENCE OF SODIUM CHLORIDE ON LIGHT SCATTERING BY COLLOIDAL SILICA[1]

BY GJ. DEŽELIC AND J. P. KRATOHVIL[2]

*Laboratory of Physical Chemistry, Faculty of Science, University of Zagreb, Zagreb, Croatia, Yugoslavia, and Clarkson College of Technology, Potsdam, New York*

*Received October 24, 1961*

The particle diameters and second virial coefficients of a sample of "Ludox" colloidal silica have been determined from turbidity measurements at several concentrations of sodium chloride (in the range 0.025–0.300 *M*). No significant change of average particle diameter could be noted as the sodium chloride concentration increased. For solutions with no sodium chloride added light scattering data gave apparently lower values for particle diameter. The second virial coefficient decreased with increasing concentration of sodium chloride. The results are discussed in terms of Stigter's theory of light scattering by colloidal electrolytes. The experimentally determined second virial coefficient of "Ludox" compared remarkably well to those estimated on the basis of Stigter's treatment.

## Introduction

In the course of a study of the properties of "Ludox"[3] colloidal silica[4,5] differences have been noted in apparent particle size determined by light scattering measurements on sols diluted with water as compared to those diluted with sodium chloride solutions. The particle size from light scattering experiments on sols containing sodium chloride agreed with electron microscopic data, while the results obtained with sols in the absence of electrolyte were apparently lower. Goring, *et al.*,[6] were the first who noted this difference, but they did not discuss it.

We have recently had the opportunity of carrying out some additional experiments on "Ludox" which seem to be related to this problem. These experiments are described in this paper and discussed in terms of Stigter's treatment of light scattering by colloidal electrolytes.[7] The experimentally determined second virial coefficients of "Ludox" at several concentrations of sodium chloride are compared to those computed on the basis of Stigter's treatment.

## Experimental

A sample of "Ludox" HS sol containing about 30% of $SiO_2$ and less than 0.4% of electrolytes, kindly supplied by E. I. du Pont de Nemours & Co., Wilmington, Del., and investigated previously,[4,5] has been used. The stock sol was freed from aggregates by centrifugation and dilutions were made by adding appropriate amounts of sodium chloride stock solution and water to obtain a series of dilutions of the same electrolyte concentration. The content of sodium chloride varied from 0–0.3 *M*. The amount of electrolytes present in the original sol could be neglected after dilution. Prior to turbidity measurements the diluted solutions were filtered through Selas 03 filter candles. Concentrations were determined by evaporating an aliquot sample and drying to constant weight at 110°, taking into account the amount of sodium chloride added.

Transmission measurements for obtaining turbidity data were carried out by using 10-cm. path length cells in a Beckman Model DU spectrophotometer with a specially built attachment similar to the construction of Bateman, *et al.*[8] It has been shown[8,9] that in the case of polystyrene latexes of much larger particle sizes than "Ludox" the use of this attachment with blackened cells effectively eliminated, in the same way as the apparatus used by Heller, *et al.*,[10,11], the effects of scattered straight light, secondary scattering, and too large solid angles. Besides, it has been established[5] that the turbidities measured in 10-cm. cells

(1) Presented before the Division of Colloid and Surface Chemistry at the 140th National Meeting of the American Chemical Society, Chicago, Illinois, September, 1961.

(2) Clarkson College of Technology, Potsdam, New York. Supported in part by the U.S. Atomic Energy Commission Contract No. AT(30–1)-1801.

(3) Registered trademark of E. I. du Pont de Nemours & Co., Inc., Wilmington, Delaware. See Product Information Bulletin "Ludox Colloidal Silica."

(4) Gj. Deželić, M. Wrischer, Z. Devidé, and J. P. Kratohvil, *Kolloid-Z.*, **171**, 42 (1960).

(5) Gj. Deželić and J. P. Kratohvil, *ibid.*, **173**, 38 (1960).

(6) D. A. Goring, M. Senez, B. Melanson, and M. M. Huque, *J. Colloid Sci.*, **12**, 412 (1957).

(7) D. Stigter, *J. Phys. Chem.*, **64**, 842 (1960).

(8) J. B. Bateman, E. J. Weneck, and D. C. Eshler, *J. Colloid Sci.*, **14**, 308 (1959); see also Gj. Deželić *Croat. Chem. Acta*, **33**, 51 (1961).

(9) Gj. Deželić and J. P. Kratohvil, *J. Colloid Sci.*, **16**, 561 (1961).

(10) R. M. Tabibian, W. Heller, and J. N. Epel, *ibid.*, **11**, 195 (1956).

(11) W. Heller and R. M. Tabibian, *ibid.*, **12**, 25 (1956).

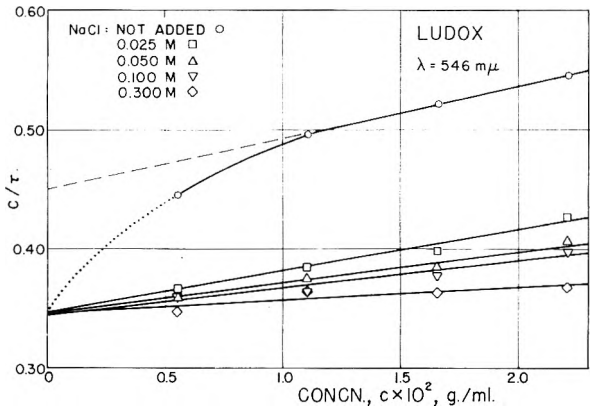


Fig. 1.—Plot of $c_2/\tau$ *vs.* $c_2$ for "Ludox" sol at different concentrations of NaCl.

were practically identical with the values obtained by extrapolation to zero cell length. No time effects were noted and even for diluted sols containing 0.3 *M* NaCl the turbidities were constant for at least several days. All measurements were carried out at the wave length *in vacuo* $\lambda_0$ 546 mμ and at room temperature (23 ± 2°). Details of the experimental procedure can be found in a previous paper.[5]

## Results

Linear plots of reduced turbidity, $c_2/\tau$ *vs.* concentration, $c_2$, of "Ludox" were obtained for solutions containing NaCl as represented by Fig. 1. The turbidity measurements were evaluated as described in detail earlier[5,12] and the results are collected in Table I. The experimental error in $D_w$, the weight-average diameter of "Ludox" particles, was estimated to be ±0.4 mμ. The particle diameters given in Table I correspond to a molecular (particle) weight of $M_2 = 7.1 \times 10^6$.

TABLE I

LIMITING REDUCED TURBIDITIES, $(c_2/\tau)_0$, PARTICLE DIAMETERS, $D_w$, AND SECOND VIRIAL COEFFICIENTS, $b_2$, FOR "LUDOX" MEASURED AT VARIOUS CONCENTRATIONS OF SODIUM CHLORIDE; $\lambda_0$ = 546 mμ

| $c_{NaCl}$ (moles l.$^{-1}$) | $(c_2/\tau)_0$ (g. cm.$^{-2}$) | $D_w$ (mμ) | $b_2 \times 10^7$ (cm.$^3$ g.$^{-2}$ mole) |
|---|---|---|---|
| 0.025 | 0.347 | 22.0 | 6.43 |
| .050 | .344 | 22.1 | 5.04 |
| .100 | .344 | 22.1 | 4.29 |
| .300 | .346 | 22.0 | 2.01 |

It should be pointed out that the treatment of experimental results as employed here and described earlier[5,12] is not exactly correct for a system of charged particles (see Discussion, particularly eq. 1 and Table III). However, as will become apparent later, the error introduced is comparable to the experimental error and cannot in any way invalidate the analysis presented.

Whereas the lines for all concentrations of NaCl give the same intercept, $(c_2/\tau)_0$, indicating the absence of coagulation, the points for water-diluted sol seem to be on a curve. Only above $c_2 = 0.01$ g./ml. could the data be described by a linear relationship. Below $c_2 \simeq 0.005$ g./ml., the turbidity measurements by transmission method for such small particles as in "Ludox" sols are rather precarious and we could not establish the trend of the curve in this low concentration region. The dotted curve is approximately the one to be expected if "Ludox" behaves in the same way as other similar systems in the absence of added electrolyte and calls for no special comment. If only the data above $c_2 = 0.01$ g./ml. are taken into account, the extrapolated $(c_2/\tau)_0$ value leads to too low apparent particle size (20.2 mμ). It has been shown previously[4,5] that the weight-average particle diameters derived from turbidity measurements on diluted "Ludox" sols, brought to 0.05 *M* NaCl, were in agreement with the electron-microscopic determinations rather than those obtained in the absence of added electrolyte.

## Discussion

The dependence of second virial coefficients of "Ludox" sol on the concentration of NaCl offers a possibility of correlating these results with the derivations of Stigter's[7] theory of light scattering by colloidal electrolytes. The starting point for our consideration is eq. 16 in Stigter's paper.[7] For "Ludox", plots of $c_2/\tau$ *vs.* $c_2$ show good linearity (Fig. 1) suggesting negligibly small values of higher coefficients in Stigter's equation. Thus, his equation reduces in our case to

$$\frac{Hc_2}{\tau} = \frac{1 + 2B_2^0N_2}{M_2\,(1 + fN_3^0A_1^0)^2} \qquad (1)$$

Here $\tau$ is the excess turbidity, $H$ the usual optical constant, and $N_i$ the number of particles (or ions) i per unit volume of solution ($N_i = N_A c_i \rho/M_i$, where $N_A$ is Avogadro's number, $c_i$ concentration in grams per unit volume of solution, $\rho$ density of solution, and $M_i$ molecular weight). $A_1$ and $B_2$ are the virial coefficients in the expansion series in powers of colloid concentration for salt distribution and osmotic pressure, respectively, as defined by Stigter and Hill[13,14] and

$$f = \frac{(\partial n/\partial N_3)}{(\partial n/\partial N_2)} = \frac{(\partial n/\partial c_3)M_3}{(\partial n/\partial c_2)M_2} \qquad (2)$$

where $n$ is the refractive index of solution. The subscripts of the concentration terms ($c$ and $N$) and particle (molecular) weight, $M$, refer to water (1), colloid electrolyte (2), and 1–1 salt (3). The subscripts of the virial coefficients $A$ and $B$ refer to the order in the corresponding expansion series.[13,14] The superscript zero refers to solution properties at $c_2 = N_2 = 0$. $B_2^0$ is related to the limiting slope $b_2$ of the Debye plot of $Hc_2/\tau$ *vs.* $c_2$ [neglecting the term $(1 + fN_3^0A_1^0)^2$] through the equation

$$b_2 = N_A\rho B_2^0/M_2^2 \qquad (3)$$

It has been shown[14] that for spherical particles, for which the Gouy–Chapman model of the ionic double layer can be applied, the virial coefficients $B_2^0$ and $A_1^0$ are related to the "cluster integrals"

$$\kappa^3 B_2^0 = 2\pi \int_0^\infty (1 - e^{-W(x)/kT})\, x^2 dx \qquad (4)$$

$$\kappa^3 A_1^0 = -4\pi \int_0^\infty (1 - e^{-W'(x)/kT})\, x^2 dx \qquad (5)$$

(12) J. P. Kratohvil and Gj. Deželić, *Kolloid-Z.*, **180**, 67 (1962).

(13) D. Stigter, *J. Phys. Chem.*, **64**, 838 (1960).

(14) D. Stigter and T. L. Hill, *ibid.*, **63**, 551 (1959).

TABLE II

CHARGE DENSITIES, $\sigma$, SURFACE POTENTIALS, $\psi_0$, AND FUNCTIONS $F$ AND $G$ FOR "LUDOX" SOL

| $c_{NaCl}$ (mole/l.) | $\kappa \times 10^{-6}$ | $\sigma$ ($\mu$coulomb/cm.$^2$) | $\Phi_0$ | $\psi_0 \times 10^4$ (c.g.s. units) | $\gamma$ | $F$ | $G$ |
|---|---|---|---|---|---|---|---|
| 0.025 | 5.20 | 6.4 | 3.61 | 3.04 | 1.218 | $5.40 \times 10^7$ | $4.49 \times 10^3$ |
| .050 | 7.38 | 7.3 | 3.28 | 2.76 | 1.197 | $7.35 \times 10^9$ | $6.21 \times 10^4$ |
| .100 | 10.4 | 8.5 | 2.90 | 2.44 | 1.166 | $5.19 \times 10^{12}$ | $1.96 \times 10^6$ |
| .300 | 18.0 | 10.6 | 2.41 | 2.03 | 1.119 | $8.61 \times 10^{19}$ | $1.05 \times 10^{10}$ |

Here $1/\kappa$ is the Debye–Hückel thickness of ionic atmosphere, $k$ the Boltzmann constant, $T$ the absolute temperature, and $x = \kappa R$, where $R$ is the distance between the centers of two particles. $W(x)$ is the potential of average force between two spherically symmetrical colloid particles and $W'(x)$ is the potential of average force between a colloid particle and a small ion in the limiting case of $N_2 \rightarrow 0$.

The functions $W(x)$ and $W'(x)$ are related to the Debye–Hückel surface potential $\psi_0$ of the colloid particles by the relations

$$W(x)/kT = F\frac{e^{-x}}{x} \qquad (6)$$

$$W'(x)/kT = G\frac{e^{-x}}{x} \qquad (7)$$

where

$$F = \frac{\epsilon\kappa a^2}{kT}\left(\frac{\psi_0}{\gamma}\right)^2 e^{2\kappa a} \qquad (8)$$

$$G = \frac{z_i e\kappa a}{kT}\frac{\psi_0}{\gamma}e^{\kappa a} \qquad (9)$$

$\epsilon$ is the dielectric constant, $a$ the particle radius, $e$ the electron charge, $z_i$ the valency, and $\gamma$ a correction factor for the case of high surface potentials.

The problem of calculating $B_2$ and $A_1$ for the special case of "Ludox" sols reduces, thus, to the determination of surface potentials $\psi_0$ of "Ludox" particles. In the absence of the electrokinetic data for "Ludox" sols (as well as for any other silica sol) as a function of pH and electrolyte concentration, only an approximate estimate of $\psi_0$ was feasible using Bolt's data[15] for the charge density of a commercial sample of "Ludox" as a function of pH and concentration of NaCl as derived from titration experiments.

According to Heston, *et al.*,[16] the number of $OH^-$ ions per unit area adsorbed on a silica surface is relatively independent of the concentration of silica sol and particle size, if pH and $c_{NaCl}$ are constant, in the pH range 7–10.5. Whereas in the experiments described here $c_{NaCl}$ was constant within one series of measurements, pH varied both with dilution and with $c_{NaCl}$. The variations were within 0.6 pH unit (from pH 8.3 to 8.9). Since no attempt has been made to control the change of pH upon dilution of the sol and since the estimate of surface potential from titration data is necessarily only approximate, an average value of pH (8.5) was used in the determination, by graphical interpolation, of charge densities at different values of $c_{NaCl}$ from Bolt's data. Later considerations proved, fortunately, that neglecting pH changes did not influence appreciably the values of the computed functions. From the charge densities, $\sigma$, presented in Table II, and utilizing the computations of Loeb, *et al.*,[17] which give directly $\sigma$ as a function of $\kappa$ and the quantity $\Phi_0 = e\psi_0/kT$, the values of surface potential $\psi_0$ were calculated. The correction factor $\gamma$ necessary for calculating functions $F$ and $G$ (eq. 8 and 9) could be obtained graphically from $D\phi$ functions given by Stigter and Mysels[18] (Table II).[19]

From the values of $F$ and $G$ listed in Table II the virial coefficients $B_2^0$ and $A_1^0$ are calculated from eq. 4 and 5 using the method of numerical integration. Inserting into eq. 2 for $(\partial n/\partial c_3)$ a value of 0.161 cm.$^3$ g.$^{-1}$ (Kruis[20]) and $(\partial n/\partial c_2) = 0.0587$ cm.$^3$ g.$^{-1}$ (our data[5]) one obtains $f = 2.25 \times 10^{-5}$. From experimentally determined values of $b_2$ (Table I), the virial coefficients $B_2^0$ were derived by means of eq. 3, assuming $\rho \simeq 1$. The calculations are summarized in Table III.

TABLE III

VIRIAL COEFFICIENTS $B_2^0$ AND $A_1^0$, AND THE FACTOR $(1 + fN_3^0A_1^0)^2$.

| $c_{NaCl}$ (mole/l.) | $B_2^0 \times 10^{17}$ Calcd. | Exptl. | $-A_1^0 \times 10^{16}$ | $(1 + fN_3^0A_1^0)^2$ |
|---|---|---|---|---|
| 0.025 | 5.82 | 5.36 | 11.22 | 0.992 |
| .050 | 4.40 | 4.20 | 9.03 | .988 |
| .100 | 3.53 | 3.58 | 7.57 | .980 |
| .300 | 2.81 | 1.68 | 6.36 | .949 |

Since the virial expansion approach fails at very low ionic strength, the virial coefficients becoming infinitely large,[14] it is not possible to interpret the results for $c_{NaCl} \rightarrow 0$ in the same way.

The agreement between experimental and theoretical results, at least up to 0.1 $M$ NaCl, is remarkably good although it also may be fortuitous. There are several possible sources of uncertainty: the necessarily approximate character of the theoretical derivations, the possible deviations from the model of the potential field applied and from the spherical shape assumed, the polydispersity of the

(15) G. H. Bolt, *J. Phys. Chem.*, **61**, 1166 (1957).

(16) W. M. Heston, Jr., R. K. Iler, and G. W. Sears, Jr., *ibid.*, **64**, 147 (1960).

(17) A. L. Loeb, J. Th. G. Overbeek, and P. H. Wiersema, "The Electrical Double Layer Around a Spherical Colloid Particle," The M.I.T. Press, Cambridge, Mass., 1961; see also J. Th. G. Overbeek and J. Lijklema, in M. Bier (ed.), "Electrophoresis," Academic Press, New York, N. Y., 1959, p. 23.

(18) D. Stigter and K. J. Mysels, *J. Phys. Chem.*, **59**, 45 (1955).

(19) Essentially the same values for $\psi_0$ as in Table II were obtained by utilizing the procedure of Stigter and Mysels[18] for estimating $\psi_0$ from the particle charge. Since computations of Loeb, *et al.*,[17] were performed for large steps of $\kappa a$, a rather large uncertainty may be introduced by interpolation for intermediate values. Thus, it appears that Stigter and Mysels' treatment still may be useful in certain cases.

(20) A. Kruis, *Z. physik. Chem.*, **B34**, 13 (1936).

"Ludox" sol (although much less than in many other hydrosols), the rather crude estimate of the surface potential. However, what seems to be significant and encouraging is the fact that the theoretically determined $B_2^0$ values are anywhere close to those experimentally determined and that they follow the expected trend.

The influence of the coefficient $A_1^0$ on the particle size of "Ludox" is not large, since the third root of the factor $(1 + fN_3^0A_1^0)^2$ has to be applied in correcting $D_w$. The largest difference, amounting to 2%, is obtained for $c_{NaCl} = 0.3\ M$. This falls into the limits of experimental error of particle size determination, and to verify the influence of virial coefficient $A_1^0$ more precise experimental data would be needed.

The experimental part of this work has been done in the Department of Applied Biochemistry, "Andrija Štampar" School of Public Health, Faculty of Medicine, University of Zagreb, Zagreb, Croatia, Yugoslavia.

# THE INFRARED SPECTRUM OF METHYL CHLORIDE IN STANNIC CHLORIDE AND ANTIMONY PENTACHLORIDE SOLUTION

BY H. M. NELSON[1]

*Mellon Institute, Pittsburgh 13, Pennsylvania*

*Received November 8, 1961*

The infrared spectrum of $CH_3Cl$ in $SnCl_4$ solution (at 30 and $-40°$) and in $SbCl_5$ solution (at 28 and $-12°$) has been obtained in an effort to elucidate the structure of the $CH_3Cl:SnCl_4$ and $CH_3Cl:SbCl_5$ addition compounds. No evidence of compound formation was found in the $CH_3Cl$–$SnCl_4$ solutions. A temperature-dependent band at 688 cm.$^{-1}$ in the $CH_3Cl$–$SbCl_5$ solutions is assigned to the C–Cl stretching motion in the $CH_3Cl:SbCl_5$ addition compound. The spectra of the $CH_3Cl$–$SbCl_5$ solutions are consistent with a linear C–Cl–Sb bond in $CH_3Cl:SbCl_5$ but the evidence is insufficient to rule out an angular bond which seems more probable from other considerations. The results suggest that the $CH_3Cl:SnCl_4$ and $CH_3Cl:SbCl_5$ addition compounds are more accurately described as slightly polarized complexes than as ion pairs.

## Introduction

Brown, Eddy, and Wong have suggested[2] that the initial step in the Friedel–Crafts reaction involves the formation of an addition compound (which may or may not undergo ionization) between the alkyl halide and the metal halide catalyst.

$$RX + MX_3 \rightleftarrows RX:MX_3$$

In an effort to clarify the role of the Lewis acid catalyst, Brown and his co-workers have obtained vapor pressure–phase composition data for a number of alkyl halide–metal halide systems.[3,4] Of particular interest to the present work is Byrne's finding[4] that methyl chloride forms 1:1 compounds with stannic chloride ($CH_3Cl:SnCl_4$, dissoc. press. 40.30 mm. at $-64°$, calcd. m.p. $-50°$, heat of formation $-4.69$ kcal./mole) and antimony pentachloride ($CH_3Cl:SbCl_5$, dissoc. press. 6.50 mm. at $-50°$, calcd. m.p. 90°, heat of formation $-8.92$ kcal./mole).

Jungk, Smoot, and Brown[5] present two alternatives for the mechanism of the aluminum bromide-catalyzed alkylation of benzene and toluene: an attack by the aromatic on a polarized addition compound $R^+Br^-:AlBr_3$ or reaction of the aromatic with an ion pair intermediate, $R^+AlBr_4^-$. They point out that there appeared to be no experimental basis for a choice between the two formulations and that the distinction between the two may be somewhat arbitrary. They also suggest, since the alkyl group's ability to accommodate a positive charge increases as it becomes more branched, that at some point in the series—methyl, ethyl, isopropyl, *t*-butyl—the ion pair description becomes more accurate. This discussion raises a question as to the degree to which the alkyl halide halogen is transferred to the metal halide in the addition compounds, *i.e.*, are they better described as polarized complexes or as ion pairs? The vibrational spectra should provide information relevant to this point. Taylor and Moyer[6] have examined the Raman spectra of a number of Lewis acid–base systems, including methyl bromide–aluminum bromide. They assign a band at 554 cm.$^{-1}$ to the C–Br stretching motion in the $CH_3Br:AlBr_3$ addition compound, while a band at 594 cm.$^{-1}$ is assigned to the corresponding motion in the $CH_3Br$ present as solvent. The objectives of the present work were to obtain infrared spectra of some alkyl halide–metal halide addition compounds with particular attention to the effects of compound formation on the alkyl halide spectrum and to interpret these effects in terms of the structure of the compound formed.

## Experimental

**Materials.**—The materials used and the methods for their purification and subsequent handling followed those of the work already mentioned.[2,4]

**Infrared Cells.**—The moisture-sensitivity and generally reactive nature of the materials involved required modification of conventional infrared sampling techniques. The cells

(1) Chemical Products Division, Aerojet-General Corporation, Azusa, Calif.

(2) H. C. Brown, L. P. Eddy, and R. Wong, *J. Am. Chem. Soc.*, **75**, 6275 (1953).

(3) (a) H. C. Brown and W. J. Wallace, *ibid.*, **75**, 6279 (1953); (b) R. Wong and H. C. Brown, *J. Inorg. Nucl. Chem.*, **1**, 402 (1955).

(4) J. J. Byrne, Ph.D. Thesis, Purdue University, 1958; *Dissertation Abstr.*, **18**, 1976 (1958).

(5) H. Jungk, C. R. Smoot, and H. C. Brown, *J. Am. Chem. Soc.*, **78**, 2185 (1956).

(6) R. C. Taylor and J. R. Moyer, Abstracts, 135th Meeting of American Chemical Society, Boston, April 1959; J. R. Moyer, Ph.D. Thesis, University of Michigan, 1958, *Dissertation Abstr.*, **19**, 3149 (1959).

used consisted of a pair of potassium bromide windows separated by a U-shaped Teflon (Du Pont) spacer. The windows were held together by a strip of epoxy cement (Hysol Epoxi-Patch Kit 1C) applied over the line joining them. (Over-all dimensions of the cell were 16 × 48 × 10 mm. with a working cell area of 6 × 43 mm. Cell thicknesses ranged from 0.055 to 0.250 mm.) The open end of the cell proper then was butt-jointed with a fillet of the same cement to a Pyrex U-tube (volume approx. 35 ml.) fitted with sidearms. These cells were easy to construct and proved to be vacuum tight.

**Sample Introduction.**—In order to introduce the sample, the U-tube was attached to a separate branch of the vacuum manifold through a sidearm. It was separated from stopcock grease and mercury by a liquid nitrogen-cooled trap. A section of tubing to which samples of the metal halide and methyl chloride were attached (on either side of a second U-tube trap) was sealed to the other end of the cell U-tube. After evacuation, the fragile tip on the metal halide sample was broken and the metal halide was distilled into the liquid nitrogen-cooled cell U-tube. Then the trap between the methyl chloride sample and the cell U-tube was cooled to −80° and the methyl chloride sample was introduced. This trap served to eliminate traces of mercury contained in the methyl chloride sample. The section of tubing containing the empty sample ampoules then was sealed off and the cell U-tube itself was sealed off from the manifold. After the sample had warmed to room temperature, the apparatus was inverted to allow the sample to run from the cell U-tube into the infrared cell proper. A reference cell of the same thickness was filled with the metal halide solvent in a similar manner. The concentrations of the methyl chloride solutions were unknown because of the unknown distribution of the two components between the liquid and vapor phases. The quantities of materials used were on the order of 1 mmole of the methyl chloride and 1–15 mmoles of the metal halide. The most useful spectra were obtained with mole ratios of about 1:1 and 0.120-mm. cells. The cells resisted attack by the sample to different degrees. With the $SbCl_5$ solutions, discoloration was evident after a few days and unidentified weak new bands appeared in the spectrum. The $SnCl_4$ solutions seemed to be stable for much longer periods. With both kinds of solutions, bands, presumably due to water, began to appear at about 1580 and 3450 cm.$^{-1}$ after several weeks. This type of cell would seem to be generally useful in obtaining spectra of volatile, moisture-, or oxygen-sensitive materials.

**Spectra.**—Spectra were obtained with a Beckman IR-4 instrument using sodium chloride and cesium bromide optics. The absorption frequencies were checked on a Perkin–Elmer 112 instrument equipped with sodium chloride and calcium fluoride prisms. The accuracy of the frequencies is estimated to be ±1 cm.$^{-1}$ for those below 2000 cm.$^{-1}$ and ±5 cm.$^{-1}$ for those above. Spectra were obtained from 400–3500 cm.$^{-1}$. No absorptions were observed in either $SnCl_4$ or $SbCl_5$ solution in the region 400–600 cm.$^{-1}$. The low temperature spectra were obtained by placing the cell in an enclosure constructed of blocks of Styrofoam (Dow) cemented together. This enclosure was slotted to allow passage of the infrared beam. Two "manifolds" were cut into the base of the enclosure with a cork borer in such a way as to allow one stream of nitrogen (Linde H.P. Dry, cooled by passage through a trap immersed in Dry Ice or liquid nitrogen) to flow over the faces of the cell, while a second stream (at room temperature) more removed from the cell faces prevented condensation or entrainment of atmospheric moisture. The cell temperature was measured with a thermocouple inserted in a hole drilled near the edge of one of the cell windows. This device permitted cooling the cell to temperatures as low as −40° for periods of 0.5 hr. or more with no trouble from fogging of the cell faces. The temperature of the cell could be kept constant to within a few degrees by controlling the depth of immersion of the trap through which the nitrogen passed for cooling.

## Results and Discussion

The spectrum of methyl chloride dissolved in stannic chloride at 30° is shown in Fig. 1. The bands are shifted downward 10–30 cm.$^{-1}$ from the values in the vapor state with the exception of $\nu_6$ (the $CH_3$ rocking), as shown in Table I.

TABLE I

$CH_3Cl$ ABSORPTION FREQUENCIES (cm.$^{-1}$)

| | Vapor[a] | $SnCl_4$ soln. | $SbCl_5$ soln. |
|---|---|---|---|
| $\nu_3$(C–Cl str., $A_1$, ∥) | 732.1 | 716 | 714<br>688[b] |
| $\nu_6$($CH_3$ rock, E, ⊥) | 1015.0 | 1014 | 1018 |
| $\nu_2$($CH_3$ def., $A_1$, ∥) | 1354.9 | 1346 | 1343 |
| $\nu_5$($CH_3$ def., E, ⊥) | 1454.6 | 1441 | 1434 |
| $2\nu_5$(∥) | 2878 | 2850 | 2848 |
| $\nu_1$(CH str., $A_1$, ∥) | 2966 | 2955 | 2953 |
| $\nu_4$(CH str., E, ⊥) | 3041.8 | 3026 | 3027 |

[a] Reference 7, p. 313. [b] In $CH_3Cl:SbCl_5$.

Lowering the temperature to −40° (Fig. 1) produces a general increase in intensity, presumably as a result of the increased solubility of the methyl chloride. There is also a slight change in the relative intensities of $\nu_2$ and $\nu_5$ (the $CH_3$ deformation). No new features are evident. In other samples in which $\nu_3$ (the C–Cl stretch) was not totally absorbing at the lower temperature, no splitting was observed.

The spectrum of methyl chloride dissolved in antimony pentachloride at 28° is shown in Fig. 2. The general appearance of the spectrum is the same as that in stannic chloride, all of the bands being shifted downward from their vapor state values with the exception of the methyl rocking band. In addition a new band appears at 688 cm.$^{-1}$ while $\nu_3$ at 714 cm.$^{-1}$ is relatively weaker than in $SnCl_4$ solution. On going to lower temperatures (Fig. 2), the band at 688 cm.$^{-1}$ appears to grow in intensity at the expense of the 714-cm.$^{-1}$ band. There is a relative change in the intensities of $\nu_2$ and $\nu_5$ which is more pronounced than that in $SnCl_4$ solution. There is no evidence of splitting of $\nu_6$, the methyl rocking band, nor of any of the other doubly degenerate vibrations. The temperature dependence of the 688-cm.$^{-1}$ band suggests that it is associated with the $CH_3Cl:SbCl_5$ addition compound. Lowering the temperature would be expected to shift the equilibrium

$$CH_3Cl + SbCl_5 \rightleftharpoons CH_3Cl:SbCl_5$$

in the direction of the addition compound. Because of this and in view of its position, the 688-cm.$^{-1}$ band is assigned to the C–Cl stretching in $CH_3Cl:SbCl_5$.

Jones and Sheppard[8] studied the spectra of methyl bromide and methyl iodide in carbon tetrachloride solution. They found that the parallel bands $\nu_1$ and $\nu_2$ ($\nu_3$ was not observed) showed comparatively small half-widths while the doubly degenerate perpendicular bands $\nu_4$, $\nu_5$ and $\nu_6$ were considerably broader with extensive wings. They attribute this difference in behavior to a restriction of the rotation about axes perpendicular to the symmetry axis (the carbon–halogen bond) while rotation about this axis remains free or quasi-free. The same general behavior is apparent in the spectra discussed here. Of particular

(7) G. Herzberg, "Infrared and Raman Spectra," D. Van Nostrand Co., Inc., New York, N. Y., 1945.

(8) W. J. Jones and N. Sheppard, *Trans. Faraday Soc.*, **56**, 625 (1960).

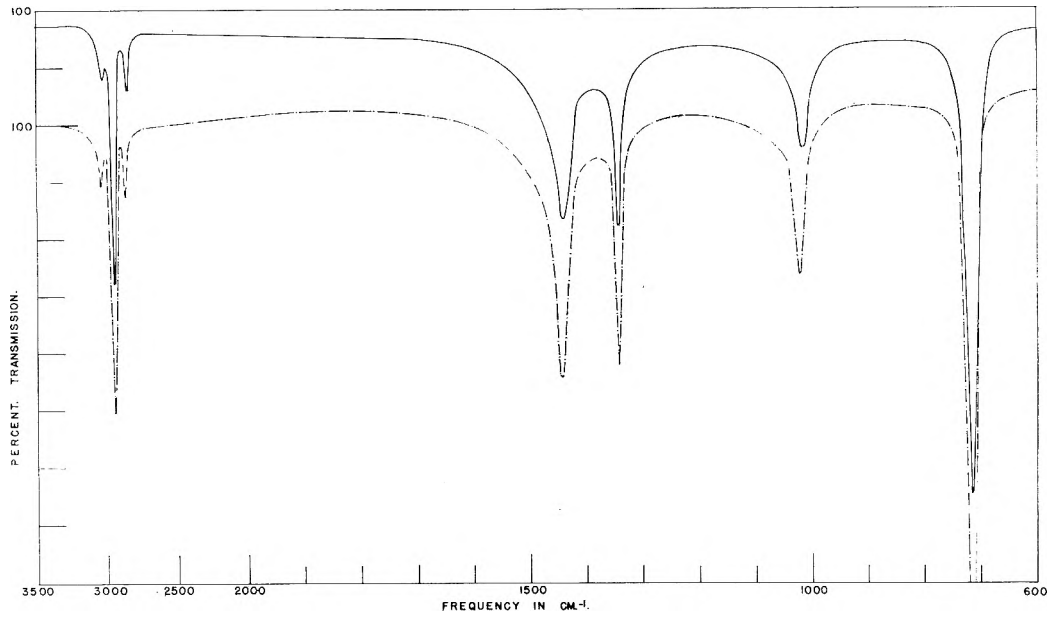


Fig. 1.—Infrared spectrum of methyl chloride in stannic chloride solution: 30 ° ———, −40° — · —·

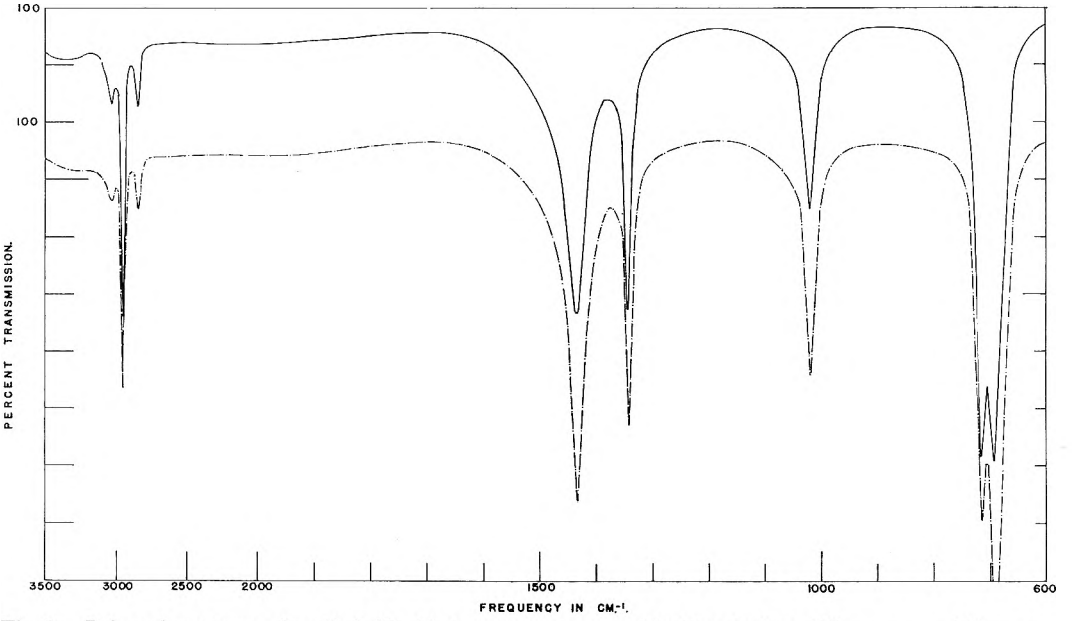


Fig. 2.—Infrared spectrum of methyl chloride in antimony pentachloride solution: 28° ———, −12° — · —·

interest in this connection are the 688 and 714 cm.$^{-1}$ bands in $SbCl_5$ solution. While they are not well resolved, the former, which must be essentially a vibrational motion, appears to have about the same half-width as the latter, thus supporting Jones and Sheppard's views.

The intensity of the 688-cm.$^{-1}$ band in the $CH_3Cl$–$SbCl_5$ solutions indicates that a significant portion of the methyl chloride present is in the form of the addition compound $CH_3Cl:SbCl_5$. In spite of this, no splitting of the doubly degenerate modes is observed. It might be argued on this basis that the methyl chloride effectively retains the $C_{3v}$ symmetry of the free molecule in the addition compound, that is, that the C–Cl–Sb bond is linear. If this bond were bent, the symmetry would be expected to be reduced to $C_s$ with a consequent splitting of the doubly degenerate E species bands. On the other hand, the splitting may be so small as to escape detection, especially in the presence of dissolved but "free" methyl chloride. Thus while the observed spectrum is consistent with a linear structure, the evidence is insufficient to eliminate an angular one. No plausible disposition of the chlorine's bonding electrons gives rise to a linear C–Cl–Sb bond. If the chlorine uses four $\sigma$-electron pairs in $sp^3$ hybrid orbitals, with two lone electron pairs (as in $ClO_2^-$), the resultant complex would be V-shaped with a bent C–Cl–Sb bond.[9] This alternative seems more attractive, even in the absence of evidence from the spectra.

If the spectra are considered in terms of a "tri-

(9) R. J. Gillespie and R. S. Nyholm, *Quart. Rev.*, **11**, 373 (1957).

atomic" RXM model for the addition compounds (where R is the methyl group, X the chlorine, and M the $SbCl_5$ or $SnCl_4$ molecule) and a simple valence force field,[10] it is found that the effect of addition compound formation (regarded as the establishment of an XM bond) on the RX stretching frequency is strongly dependent on the change in the RX stretching force constant on compound formation. The calculation of the RX force constant in terms of this model would require knowledge of the XM stretching and RXM bending frequencies. No attempt was made to observe these bands in view of their probable low frequencies. For the same reason, the effects of compound formation on the metal halide spectra were not examined.

The possibility of an ion pair structure, $CH_3^+$-$SbCl_6^-$, for the $SbCl_5$ addition compound seems unlikely in the absence of any pronounced changes in the methyl group frequencies, in spite of the fact that a large proportion of the $CH_3Cl$ present is in the form of the addition compound. In addition, the decrease in intensity of the 714-cm.$^{-1}$ band which occurs on lowering the temperature appears to be balanced by the increase in the 688-cm.$^{-1}$ band, which would be improbable if an ion pair structure also were participating in the equilibrium.

The failure to observe any clear evidence of compound formation in the $SnCl_4$ solutions may be due to the instability of the $CH_3Cl$:$SnCl_4$ addition compound itself, or to a coincidence of the C–Cl stretching frequency in the addition compound with that in the free, dissolved molecule. The possibility of the formation of an ionic compound seems unlikely in view of the results in $SbCl_5$ solution and the relative instability of the $SnCl_4$ addition compound.

The experimental results suggest that the $CH_3Cl$:$SbCl_5$ and $CH_3Cl$:$SnCl_4$ addition compounds are more accurately described as slightly polarized complexes than as ion pairs.

**Acknowledgments.**—This work was made possible by a grant from the U. S. Army Research Office, Durham. This support is gratefully acknowledged. The author also is indebted to his colleagues, Drs. D. E. Milligan and W. G. Fateley, for helpful discussions.

(10) Reference 7, p. 173.

# LIQUID AMINE AND ION-EXCHANGE RESIN ABSORPTION OF BROMIDE ION FROM AQUEOUS SALT SOLUTIONS; VARIATION WITH AQUEOUS ELECTROLYTE ACTIVITIES[1]

BY S. LINDENBAUM AND G. E. BOYD

*Chemistry Division, Oak Ridge National Laboratory, Oak Ridge, Tennessee*

*Received November 8, 1961*

The absorption of microquantities of bromide ion from aqueous solutions of hydrochloric acid, lithium, sodium, potassium, and cesium chlorides by tri-*n*-octylamine solutions in toluene, and from hydrochloric acid by a strong-base anion exchanger was measured. The departure of the equilibrium distribution coefficients for the liquid ion exchanger from a "mass law" dependence on electrolyte concentration could be explained quantitatively by the non-ideality of the aqueous phase except for the concentrated hydrochloric acid solutions. With the anion-exchange resin, however, corrections for aqueous phase non-ideality and for de-swelling were not sufficient to cause the distribution data to conform to the mass law; in addition, an important correction for the organic phase non-ideality was required. The magnitude of the organic phase non-ideality could be correlated with the invasion of this phase by electrolyte. When the invasion was small, or absent, as with the liquid exchanger, the non-ideality was small and could be neglected.

The role of the secondary cation on the absorption of anionic species from concentrated aqueous electrolyte solutions by strong-base anion-exchange resins has been the subject of several studies.[2-6] It was observed by Kraus and co-workers[5,6] that many metal chloro-complex anions were more strongly absorbed from LiCl than from HCl solutions by Dowex-1. This phenomenon was shown by Horne[2] to be of more general occurrence. This worker and others found, however, that the concentration variation of the distribution coefficients for the $ZnCl_4^{-2}$ anion in acid and alkali metal chloride solutions did not give slopes of $-2$ in log–log plots as expected from the application of the simple law of mass action. It has been suggested[3-6] that the non-ideal variation of the distribution coefficients for this and other anions with the nature and concentration of the aqueous electrolyte was caused by special effects in the organic phase. Schindewolf[7] compared the extraction of Zn(II) from aqueous HCl, LiCl, and CsCl solutions by a quaternary ammonium type anion-exchange resin with that by methyldioctylamine dissolved in trichloroethylene, and noted that the variations of the distribution coefficients with the aqueous electrolyte activity were strikingly similar. The fact that the departures from ideality appeared to be the same for the liquid and resin ion-exchange systems led Schindewolf to suggest that the variation

(1) This paper is based upon work performed at Oak Ridge National Laboratory, which is operated by Union Carbide Corporation for the Atomic Energy Commission.

(2) R. A. Horne, *J. Phys. Chem.*, **61**, 1651 (1957).

(3) B. Chu and R. M. Diamond, *ibid.*, **63**, 2021 (1959).

(4) Y. Marcus and C. D. Coryell, *Bull. Res. Council Israel*, **A8**, 1 (1959).

(5) K. A. Kraus and F. Nelson, *Proc. Intern. Conf. Peaceful Uses At. Energy*, **7**, 113 (1956).

(6) K. A. Kraus, F. Nelson, F. B. Clough, and R. C. Carlston, *J. Am. Chem. Soc.*, **77**, 1391 (1955).

(7) U. Schindewolf, *Z. Elektrochem.*, **62**, 335 (1958).

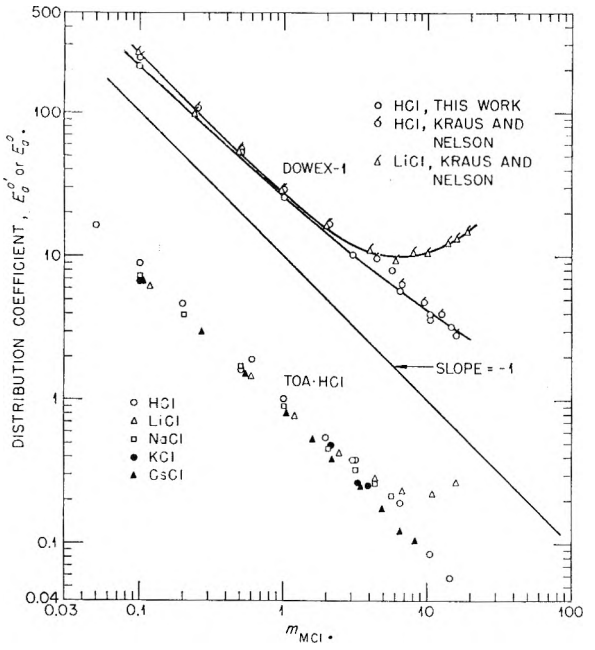


Fig. 1.—Dependence of the extraction of bromide ion from HCl by Dowex-1 and from HCl, LiCl, NaCl, KCl, and CsCl by tri-*n*-octylamine hydrochloride in toluene as a function of the aqueous electrolyte molality. $E_a^{o\prime}$ is defined by eq. 1 for the TOA·HCl in toluene systems and $E_a^{o}$ by eq. 2 for the Dowex-1 system. The data of Kraus and Nelson were kindly provided by the authors.

of the activity coefficient ratio for the aqueous phase might be responsible, at least in part.

The objective in this study was to examine *quantitatively* the contribution of aqueous phase activity coefficients to partition ratios in the extraction by liquid anion exchangers. The extraction of micro-amounts of bromide ion from aqueous chloride solutions by a liquid amine exchanger was chosen because reasonable estimates of the activity coefficients for the constituents in the mixed electrolyte solutions could be made. Surprisingly, it was found that the non-ideality in the concentration variation of the distribution coefficients with neutral aqueous electrolyte solutions could be attributed entirely to the variation in the *aqueous phase* activity coefficient ratios. This was not the case, however, for the extraction of bromide ion from hydrochloric acid solutions where a considerable penetration of the organic phase by acid also occurred. Similarly, for the anion exchange resin, the non-ideality of the concentration dependence of the distribution coefficients with HCl and LiCl solutions could not be attributed solely to activity coefficient ratios for the respective aqueous phases.

## Experimental

**Materials.**—Tri-*n*-octylamine (TOA) (Union Carbide Chemicals Co.) was a pale yellow liquid with a tertiary amine content exceeding 97% as shown by non-aqueous titration.[8] A 1 *M* solution in toluene was equilibrated with 3 *M* HCl to convert the tertiary amine to the hydrochloride (TOA·HCl). This solution was washed with 0.1 *M* HCl and aliquots were analyzed for chloride by argentometric titration in ethanol. Solutions of TOA·HCl in toluene were prepared by accurate dilution.

The strong-base anion-exchange resin, Dowex-1, X-10, was purified and converted to the chloride salt-form following well known procedures. The exchange capacity of the 60/80 mesh particle size fraction of the exchanger was 3.08 ± 0.005 meq. g.$^{-1}$, and its weight swelling when in equilibrium with pure water was 178.6 g. $H_2O$ equiv.$^{-1}$.

Reagent grade chemicals were used throughout. Radioactive bromide tracer (35.9-hr. $Br^{82}$) was prepared by irradiating ammonium bromide in the ORNL Graphite Reactor. In the measurements with highly concentrated HCl solutions it was important to prevent the oxidation of $Br^-$ ion by dissolved air. The addition of a twofold excess of sodium sulfite served very well; this amount of $SO_3^{-2}$ ion was shown not to interfere with the extraction of bromide ion.

**Distribution Coefficients.**—Equal volumes of a 0.122 *m* solution of TOA·HCl in toluene and aqueous chloride solutions to which radiobromide tracer ($c_{Br^-}$ never exceeded $10^{-4}M$) had been added were shaken together for 15–30 min. at room temperature (25 ± 1°) in separatory funnels. Good phase separation was obtained by centrifugation. Each phase was sampled and assayed for its γ-radioactivity by counting in a well-type, NaI scintillation counter. An aliquot from the original aqueous solution also was counted, and radioactivity material balances were established within ±2%. Distribution coefficients, $E_a^{o\prime}$, were calculated according to

$$E_a^{o\prime} = \frac{(\text{counts/min./ml. organic})}{(\text{counts/min./g. water})} = \bar{M}_{Br^-}/m_{Br^-} \quad (1)$$

The experiments were performed on a volume basis; hence, to compute $E_a^{o\prime}$ it was necessary to employ densities for the various electrolyte solutions interpolated from the International Critical Tables.[9] Values of $E_a^{o\prime}$ were plotted (Fig. 1) as a function of molality, *m*, of electrolyte in the aqueous phase.

Ion-exchange resin distribution coefficients were measured for hydrochloric acid solutions according to standardized procedures. Molal distribution coefficients, $E_a^{o}$, were calculated according to

$$E_a^{o} = \frac{\text{resin radioactivity}}{\text{wt. water in resin}} \Big/ \frac{\text{soln. radioactivity}}{\text{wt. water in soln.}} = \bar{m}_{Br^-}/m_{Br^-} \quad (2)$$

To evaluate $E_a^{o}$ it was necessary to measure the weight of water per equivalent in the exchanger as a function of the aqueous hydrochloric acid solution concentration. This was done employing a modification of the centrifuge procedure.[10] Samples of exchanger placed in tared glass tubes fitted with 400-mesh platinum screen bottoms were immersed repeatedly in hydrochloric acid of the desired concentration. After equilibration the tubes were centrifuged at 1000 r.p.m. for 1 hr. The tubes containing the exchanger with imbibed water and HCl were weighed in tared weighing bottles. The resin samples were rinsed with pure water, and the HCl in the rinse water was determined. The weight of dry exchanger was estimated by analyzing for its chloride ion content and dividing this by the exchange capacity. The weight of imbibed water was determined by difference. The resinate molality, $\bar{m}_{HCl}$, (Fig. 2A) and the molal Donnan distribution coefficient for HCl, $\lambda_{D(HCl)}$, (Fig. 2B) were computed from these data

$$\lambda_{D(HCl)} = (\text{moles HCl/kg. } H_2O \text{ in resin})/(\text{moles HCl/kg. } H_2O) = \bar{m}_{HCl}/m_{HCl} \quad (3a)$$

Measurements of $E_a^{o}$ in this Laboratory for the uptake of bromide ion from HCl solutions by a slightly differing Dowex-1 preparation have been reported.[6] Two sets of values ($\lambda_D$) have been published[11,12] for the absorption of HCl

(8) K. B. Brown, private communication; J. G. Moore, K. B. Brown, and C. F. Coleman, ORNL-1922, Aug. 9, 1955.

(9) "International Critical Tables," Vol. 3, McGraw-Hill Book Co., Inc., New York, N. Y., 1930.

(10) K. W. Pepper, D. Reichenberg, and D. K. Hale, *J. Chem. Soc.*, 3129 (1952).

(11) K. A. Kraus and G. E. Moore, *J. Am. Chem. Soc.*, **75**, 1457 (1953).

(12) F. Nelson and K. A. Kraus, *ibid.*, **80**, 4154 (1958).

by the same exchanger; unfortunately these are in serious disagreement. Our $\lambda_D$ determinations (Fig. 2B) appear to support those given in ref. 12, and our $E_a^\circ$ values are in accord with those in ref. 5 (Fig. 1).

Values of $\lambda_{D(HCl)}$ (Fig. 2C) for the TOA·HCl–toluene solutions were measured in experiments where 10-ml. portions of the amine solution were equilibrated with 10 ml. of the aqueous solutions of known concentration

$$\lambda_{D(HCl)} = (\text{excess moles HCl/kg. toluene})/(\text{moles HCl/kg. } H_2O) \quad (3b)^{13}$$

Aliquots were stirred with water and titrated with standard 0.1 *N* sodium hydroxide. A hydrolysis correction was made by subtracting from the measured value the amount of HCl necessary to keep the amine in the hydrochloride form. The invasion of the liquid exchanger by LiCl was determined similarly except chloride ion was measured by argentometric titration. The excess chloride concentration never exceeded $10^{-3}$ *M*. The dissolution of TOA·HCl in the equilibrium aqueous phase was determined by the method of Ashbrook.[14] In all cases the concentration of TOA·HCl in the electrolyte was less than $10^{-5}$ *M*, so that corrections for loss from the organic phase were negligible.

## Treatment of Experimental Data

The ion-exchange extraction of bromide ion from aqueous chloride solutions may be written

$$RCl + Br^- \rightleftarrows RBr + Cl^- \quad (4)$$

where RCl = TOA·HCl for the liquid–liquid extraction system, or, R = quaternary ammonium group for the ion-exchange resin. If the standard states for both phases are taken to be identical, the mass law expression in terms of ionic activities is

$$\bar{a}_{Br^-} \times a_{Cl^-}/a_{Br^-} \times \bar{a}_{Cl^-} = 1 \quad (5)$$

Substituting molalities and molal ionic activity coefficients (mean molal coefficients for the aqueous phase) eq. 5 becomes for micro-concentrations of bromide ion

$$\frac{\bar{m}_{Br^-}}{\bar{m}_{Cl^-}} \times \frac{\bar{\gamma}_{Br^-}}{\bar{\gamma}_{Cl^-}} \times \frac{m^2_{MCl}\,\gamma^2_{\pm MCl}}{m_{MCl}\,m_{MBr}\,\gamma^2_{\pm MBr}} = 1 \quad (6)$$

In eq. 6 the total chloride ion concentration in the liquid ion exchanger, $\bar{M}_{Cl^-}$, is defined by $\bar{M}_{Cl^-} = \bar{M}_{RCl} + \bar{M}_{MCl}$ where $\bar{M}_{RCl}$ is the amine concentration and $\bar{M}_{MCl}$ is the concentration of invaded electrolyte in the organic liquid. The quantity $\bar{m}_{Cl^-}$ for the resinous exchanger is defined analogously. Equations 7a and 7b may be written on introducing the definitions above for $E_a^{\circ\prime}$ and $E_a^\circ$

$$\log E_a^{\circ\prime}\,\gamma^2_{\pm MCl}/\gamma^2_{\pm MBr} = \log \bar{M}_{Cl^-} + \log \bar{\gamma}_{Cl^-}/\bar{\gamma}_{Br^-} - \log m_{MCl} \quad (7a)$$

$$\log E_a^{\circ}\,\gamma^2_{\pm MCl}/\gamma^2_{\pm MBr} = \log \bar{m}_{Cl^-} + \log \bar{\gamma}_{Cl^-}/\bar{\gamma}_{Br^-} - \log m_{MCl} \quad (7b)$$

If it is assumed that the activity coefficient ratio, $\bar{\gamma}_{Cl^-}/\bar{\gamma}_{Br^-}$, for the liquid ion-exchange phase is constant, a plot of log $(E_a^{\circ\prime}\gamma^2_{\pm MCl}\gamma^{-2}_{\pm MBr}\bar{M}^{-1}_{Cl^-})$ *vs.* log $m_{MCl}$ should give a straight line of slope −1. Similarly, for the ion-exchange resin, a plot of log $(E_a^{\circ}\gamma^2_{\pm MCl}\gamma^{-2}_{\pm MBr}\bar{m}^{-1}_{Cl^-})$ *vs.* log $m_{MCl}$ would give a straight line of slope −1 if there were no interaction in the organic phase which changed with the external aqueous electrolyte concentration.

(13) The definitions of $\lambda_D$ in eq. 3a and 3b differ. With the ion-exchange resin, the organic phase was treated as a solution of the functional exchange sites in the imbibed water; with the TOA·HCl solution, the organic phase was a dilute solution of TOA·HCl in toluene.

(14) A. W. Ashbrook, *Analyst*, **84**, 176 (1959).

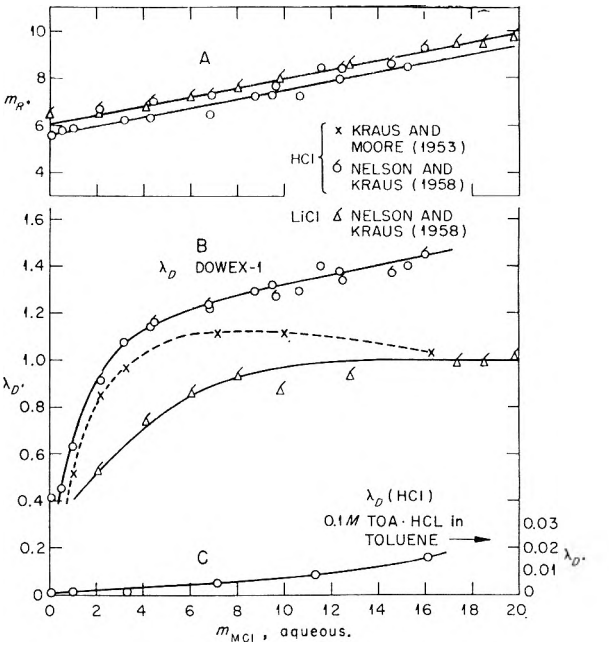


Fig. 2.—A: Dowex-1, X-10 molality as a function of the aqueous phase molality. B: distribution of HCl and LiCl between Dowex-1, X-10, and aqueous solutions as a function of aqueous molality. C: distribution of HCl between 0.1 *M* TOA·HCl in toluene and aqueous HCl as a function of HCl molality.

Values for the activity coefficient of MBr present in vanishingly small concentration in aqueous mixtures with MCl ($\gamma_{(0)MBr}$ in the notation of Harned and Owen)[15] were available only for HCl and KCl solutions. For the other solutions estimates of $\gamma_{(0)MBr}$ were made using Harned's rule[15]

$$\log \gamma_{(0)MBr} = \log \gamma_{MBr(0)} - \alpha_{MBr} m_{MCl} \quad (8)$$

where $\gamma_{MBr(0)}$ is the activity coefficient of the pure bromide salt at the same total molality and $\alpha_{MBr}$ is a constant. Values of $\alpha_{MBr}$ where derived by applying the Åkerlof–Thomas rule[16]

$$\log \gamma_{MBr(0)}/\gamma_{MCl(0)} = B_{MBr} m \quad (9)$$

where $B_{MBr}$ is a constant, and assuming that $\alpha_{MCl} = -\alpha_{MBr}$; then, $B_{MBr} = 2|\alpha|$.[17] It was possible, therefore, to evaluate $\gamma_{(0)MBr}$ from a knowledge of the activity coefficients for the pure chloride and bromide salts.[15,18] Measurements of activity coefficients of aqueous KCl–KBr mixtures have been reported by McCoy and Wallace.[19] They found good agreement between their observed values for $\alpha_{KBr}$ and those calculated using the Harned and Åkerlof–Thomas approximations except at the

(15) H. S. Harned and B. B. Owen, "The Physical Chemistry of Electrolytic Solutions," 3rd Ed., Reinhold Publ. Corp., New York, N. Y., 1959.

(16) G. Åkerlof and H. C. Thomas, *J. Am. Chem. Soc.*, **56**, 593 (1934).

(17) Reference 15, p. 604.

(18) R. A. Robinson and R. H. Stokes, "Electrolyte Solutions," 2nd Ed., Academic Press, New York, N. Y., 1959.

(19) W. H. McCoy and W. E. Wallace, *J. Am. Chem. Soc.*, **78**, 1830 (1956).

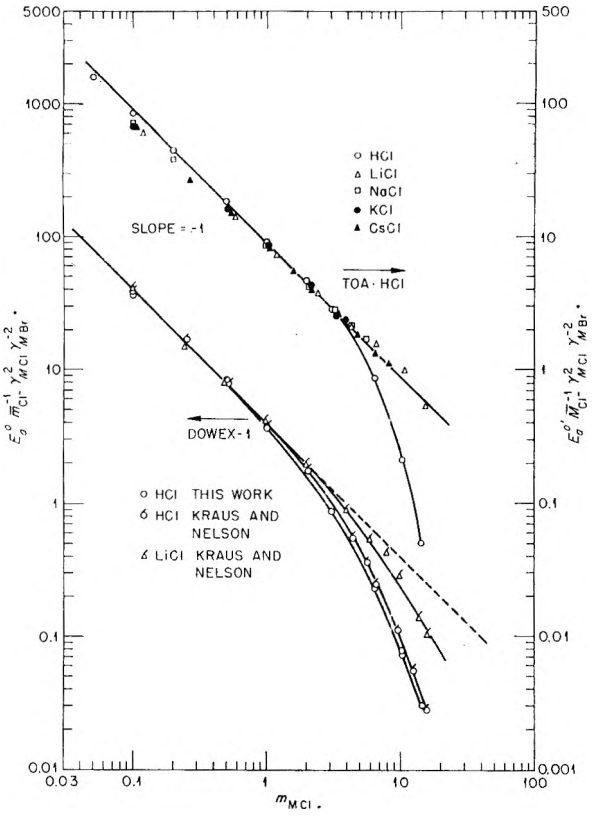


Fig. 3.—Corrected bromide ion distribution coefficients for Dowex-1 and TOA·HCl in toluene as a function of aqueous electrolyte molality. Least squares fit to the equation $\log E_a^{o\prime}\gamma^2_{MCl}\gamma^{-2}_{MBr}\bar{M}_{Cl}^{-1} = a + b \log m_{MCl}$: LiCl: $a = 0.930 \pm 0.016, b = -0.943 \pm 0.021$; NaCl: $a = 0.936 \pm 0.003, b = -0.933 \pm 0.006$; KCl: $a = 0.922 \pm 0.011, b = -0.922 \pm 0.019$; CsCl: $a = 0.920 \pm 0.005, b = -0.958 \pm 0.008$.

highest concentrations. Measured values for $\gamma_{(0)KBr}$ were used in our treatment of the KCl–KBr system. Experimental data for $\alpha_{HBr}$, in agreement with calculated values, were available for the HCl–HBr mixtures for concentrations up to 1 *m*.[20] Between 1 and 3 *m*, data for $\gamma_{HBr(0)}$[21] and $\gamma_{HCl(0)}$[15,18] were used to estimate $B_{HBr}$ values. Beyond 3 *m* it was assumed that $B_{HBr} = 0.036$. For the NaCl–NaBr system, $\gamma_{NaBr(0)}$ data extended only to 4 *m*; it was assumed that $B_{NaBr} = 0.0185$ for higher concentrations. For the CsCl–CsBr system, $\gamma_{CsBr(0)}$ data extended to 5 *m*, and beyond this a value for $B_{CsBr} = -0.004$ was assumed. Data for the activity coefficients of pure LiCl and LiBr, $\gamma_{LiCl(0)}$ and $\gamma_{LiBr(0)}$, were available for the entire concentration range. Values for $B_{LiBr}$ were calculated at each molality with eq. 9. At the highest concentrations (>15 *m*) $B_{MBr}$ was constant at 0.045.

The activity coefficients obtained from eq. 8 and 9 were used to correct the distribution coefficients, $E_a^o$ and $E_a^{o\prime}$, for the aqueous activity coefficient ratio (*cf.* eq. 7). These corrected distribution coefficients were plotted (Fig. 3) as a function of the aqueous electrolyte molality. All the TOA·HCl distribution data except those for the HCl solutions were observed to fall on the same straight line of negative unit slope. The data for the neutral electrolyte solutions were fitted to a straight line by least squares methods. Intercepts, *a*, and slopes, *b*, are given in Fig. 3.

## Discussion

The fact that with the liquid anion exchanger the non-ideal behavior of $E_a^{o\prime}$ could be explained by interactions in the aqueous phase indicated that the assumption that the activity coefficient ratios for the organic phase were invariant as the activity of the aqueous phase changed was valid. The behavior with concentrated hydrochloric acid solutions was an exception, however, and here the failure of the corrected distribution coefficients to conform to the mass law could be related to the invasion of the organic phase by acid.

The extent of the penetration of the anion-exchange resin by acid (Fig. 2B) is especially noteworthy; for aqueous solution concentrations exceeding 3 *m* the concentration of acid in the exchanger was always greater thanth at in the aqueous phase. In the penetration of Dowex-50 exchangers by HCl, in contrast, $\lambda_D$ remains well below unity up to the highest acid concentration. The extraction of bromide from HCl solutions by anion exchangers must be regarded as abnormal, therefore, and a special interaction between HCl and the organic phase must occur. If it is assumed that bichloride ion, $HCl_2^-$, is formed in concentrated acid chloride solutions and is taken up preferentially by anion exchangers, an explanation of the abnormal Donnan coefficient and the negative departure of the bromide ion absorption from mass law behavior becomes possible. Evidence for the existence of bichloride ion has been reported recently,[22,23] and the properties of its compounds with quaternary ammonium groups have been determined. Salts of the type $R_3NH^+HCl_2^-$ are known also, so that the existence of this kind of species in the liquid exchanger cannot be ruled out. The uptake of $Br^-$ ion by exchangers containing bichloride in addition to chloride ion, of course, will not conform to eq. 5.

The invasion of the anion-exchange resin by lithium chloride solutions appears to be typical and no "chemical" interaction seems to be required. The relatively small departure from the mass law shown in Fig. 3 must be caused, therefore, by the non-ideal character of the organic phase. It is of interest to observe that the magnitude of this departure was much smaller than that caused by the interaction in the aqueous electrolyte solution. The liquid anion exchanger was not invaded by LiCl, and conformity with the mass law was found.

The similarity of the variations of anion distribution coefficients with aqueous electrolyte activity for the liquid and resin exchangers can only be superficial, especially at the highest concentrations, because of the differences in extent to which they are invaded by electrolytes. Because they are not penetrated by aqueous neutral electrolyte solutions, liquid anion exchangers are notably superior to resins for use in measurements of activity coefficients and for determinations of complex-ion stability constants in concentrated aqueous

(20) B. B. Owen and T. F. Cook, *J. Am. Chem. Soc.*, **59**, 2277 (1937).
(21) W. J. Biermann and R. S. Yamasaki, *ibid.*, **77**, 241 (1955).
(22) T. C. Waddington, *J. Chem. Soc.*, 1708 (1958).
(23) Y. Pocker, *ibid.*, 1292 (1960).

electrolyte mixtures. Concentrated hydrochloric acid solutions would appear to be poor media for such investigations because of the possible complication arising from bichloride ion formation.

# SOLID-LIQUID PHASE EQUILIBRIA AND SOLID COMPOUND FORMATION IN MIXTURES OF AROMATIC COMPOUNDS WITH CARBON TETRACHLORIDE

BY J. BEVAN OTT, J. REX GOATES, AND ALLEN H. BUDGE

*Department of Chemistry, Brigham Young University, Provo, Utah*

*Received December 11, 1961*

Solid–liquid phase diagrams have been obtained from time–temperature cooling curves for the four binary systems containing carbon tetrachloride with benzene, toluene, pseudocumene, and anisole. Solid compounds with the following empirical formulas were found: $CCl_4 \cdot C_6H_6$, $(CCl_4)_2 \cdot C_6H_6$, $CCl_4 \cdot C_6H_5CH_3$, $CCl_4 \cdot 1,2,4\text{-}C_6H_3(CH_3)_3$, and $(CCl_4)_2 \cdot C_6H_5OCH_3$. A number of other systems composed of carbon tetrachloride and aromatic compounds were screened for possible compound formation. No compounds were observed in the mole fraction range of approximately 0.25 to 0.75 for systems composed of carbon tetrachloride with *o*-xylene, *m*-xylene, chlorobenzene, bromobenzene, or $\alpha,\alpha,\alpha$-trifluorotoluene.

In a previous paper, we reported evidence from heats of mixing and freezing point measurements for the existence of a 1:1 solid compound in the system $CCl_4$–$C_6H_6$.[1] More recently, Rastogi and Nigam[2] found not only a 1:1, but also a 2:1 compound. In an earlier study, Kapustinskii[3] had reported a 3:1 as well as a 1:1 and 2:1 compound in this system. In addition to the problem of the number of compounds, there appears to be some question as to the exact composition of the compound described as 1:1. For these reasons it appeared desirable to obtain in detail the solid–liquid phase diagram of the $CCl_4$–$C_6H_6$ system in the composition range where compound formation is likely. This paper reports the results of such a study, together with the solid–liquid equilibrium properties of solutions of $CCl_4$ with several other aromatic hydrocarbons.

## Experimental

**Chemicals.**—Reagent grade benzene, toluene, anisole, pseudocumene, and carbon tetrachloride were further purified by distillation. The purified reagents contained the following amounts of liquid soluble–solid insoluble impurities: $C_6H_6$, 0.04 mole %; $C_6H_5CH_3$, 0.24 mole %; $C_6H_5OCH_3$, 0.01 mole %; and $CCl_4$, 0.02 mole %.

Because of difficulties in obtaining equilibrium during the freezing of pseudocumene, we were unable to obtain a satisfactory freezing curve from which the per cent impurities in this substance could be calculated. The starting material for the preparation of the sample was Phillips' "pure" grade pseudocumene, which is listed as better than 99% pure. This material was vacuum distilled in a vacuum jacketed, 170-cm. column packed with glass helices and operated at a reflux ratio of 100:1. The center third cut was used. Its index of refraction agreed to the fourth decimal place with the A.P.I.[4] value. Gas chromatograms of the purified chemical showed no impurities detectable by this method. Further evidence of high purity is that the eutectic temperature of the mixtures containing pseudocumene did not vary appreciably with amount of material frozen.

A number of other chemicals were used in only a few exploratory measurements to check on the presence or absence of compound formation. These were either reagent or research grade chemicals that were used without further purification.

**Measurements and Accuracy.**—Both time–temperature cooling and warming curves were obtained with a platinum resistance thermometer in an apparatus that has been described previously.[5] The solutions generally supercooled, and their freezing points were obtained by extrapolation of the time–temperature curve back across the supercooled region. Supercooling was especially pronounced in the anisole and the toluene systems, sometimes being as much as 30°. Most of this supercooling could be eliminated, however, by melting the solid and then freezing a second time. If the sample was not allowed to warm more than about 2° above the freezing point during the melting process, the supercooling during the second freezing generally was reduced to a few tenths of a degree.

The accuracy of the freezing points of the pure substances is estimated to be ±0.05°, and that of the solutions, ±0.1°. The meritectic and eutectic values where stirring was possible also are considered accurate to ±0.1°. Calibration of the resistance thermometer has been described previously.[5] The calibration was rechecked periodically during these measurements at the mercury freezing point (234.29° K.), ice point (273.150° K.), and the sodium sulfate transition point (305.534°K.). No measurable changes in the resistance of the thermometer were found.

## Results

Solid–liquid phase equilibria data were obtained for the four binary systems of carbon tetrachloride with benzene, toluene, pseudocumene, and anisole. The freezing point data for the $CCl_4$–$C_6H_6$ system are summarized in Table I.

Figure 1 is the phase diagram of the $CCl_4$–$C_6H_6$ system over the composition range 0.0 to approximately 0.8 mole fraction $CCl_4$. In all of the phase diagrams of this paper, circles are used for freezing points, triangles for either eutectic or meritectic values, and squares for solid phase transition data. The significant features of Fig. 1 are the meritectic lines at 239.12 and 232.13°K., indicating the presence of two compounds with incongruent melting points. Graphs of the length of meritectic halt *vs.* mole fraction of carbon tetrachloride show maximum values at mole fractions of 0.500 and 0.667, which correspond to compounds with the

(1) J. R. Goates, R. J. Sullivan, and J. B. Ott, *J. Phys. Chem.*, **63**, 589 (1959).

(2) R. P. Rastogi and R. K. Nigam, *Trans. Faraday Soc.*, **55**, 2005 (1959).

(3) A. F. Kapustinskii, *Bull. Acad. Sci. USSR*, 435 (1947).

(4) F. D. Rossini, K. S. Pitzer, W. J. Taylor, J. P. Ebert, J. E. Kilpatrick, C. W. Beckett, M. G. Williams, and H. G. Werner, "Selected Values of Properties of Hydrocarbons," American Petroleum Institute Research Project 44, Natl. Bur. Std. Circ. 461, U. S. Govt. Printing Office, Washington, D. C., 1947.

(5) J. R. Goates, J. B. Ott, and A. N. Budge, *J. Phys. Chem.*, **65**, 2162 (1961).

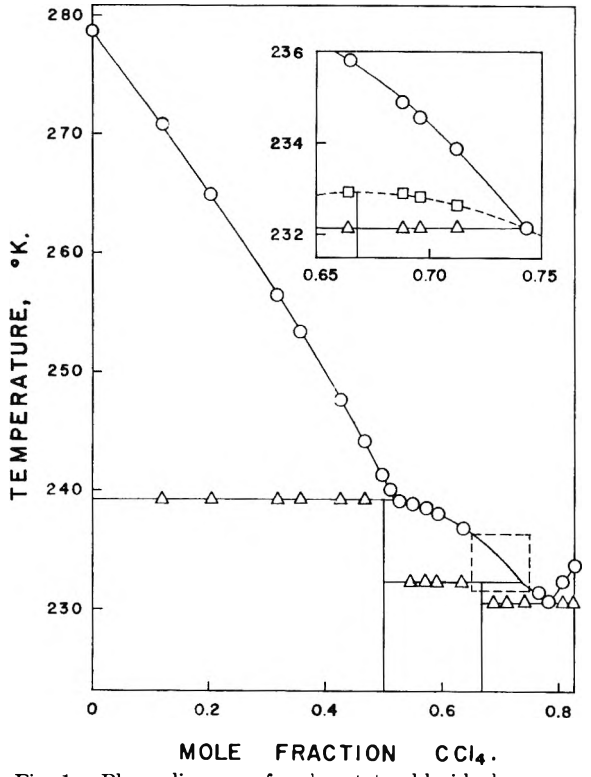


Fig. 1.—Phase diagram of carbon tetrachloride–benzene.

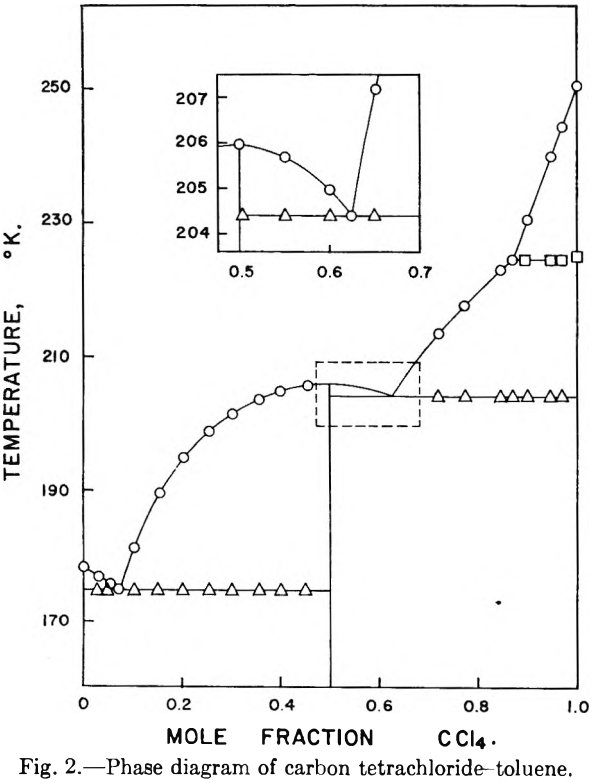


Fig. 2.—Phase diagram of carbon tetrachloride–toluene.

empirical formulas $C_6H_6 \cdot CCl_4$ and $C_6H_6 \cdot (CCl_4)_2$, respectively. No evidence for the 3:1 compound reported by Kapustinskii[3] was found. The eutectic point for this system occurs at a temperature of 230.61°K. and a composition of 0.7840 mole fraction $CCl_4$.

Since the 1:1 compound had been reported earlier to have a congruent melting point and a composition slightly richer in $CCl_4$ than 0.500,[1,2] a very detailed study was made of the region in the 0.4–0.6 mole fraction range. No maximum temperature, which would indicate a congruent melting point, was found. As the composition of the compound was approached, however, the time necessary to establish equilibrium conditions became increasingly longer. Failure to have fully established equilibrium conditions may be the explanation for the eutectic (rather than meritectic) that was observed in the earlier studies.

Solid solutions were found in the region to the right of approximately 0.8 mole fraction $CCl_4$. Freezing points were measured throughout this region, but the solidus point information that could be obtained with our apparatus was too limited to allow us to construct the entire diagram.

The phase diagrams for carbon tetrachloride with toluene, pseudocumene, and anisole are shown in Fig. 2, 3, and 4. The presence of compounds with the empirical formulas of $CCl_4 \cdot C_6H_5CH_3$, $CCl_4 \cdot 1,2,4\text{-}C_6H_3(CH_3)_3$, and $(CCl_4)_2 \cdot C_6H_5OCH_3$, each with a congruent melting point, is evident. The melting points of the compounds in the order just given are 205.97, 229.85, and 215.84°K., respectively. The eutectics are at mole fractions ($CCl_4$) 0.0729 and 0.6231 and temperatures 174.78 and 204.39°K., respectively, in the carbon tetrachloride–toluene system; mole fractions 0.2043 and 0.8043 and temperatures of 221.41 and 220.13° K., respectively, in the carbon tetrachloride–pseudocumene system; and mole fractions 0.5052 and 0.7030 and temperatures of 214.00 and 215.73° K., respectively, in the carbon tetrachloride–anisole system.

The carbon tetrachloride solid phase transition that occurs at approximately 225°K. was observed in solutions of all three systems and also was obtained in pure carbon tetrachloride. The values obtained for carbon tetrachloride in pseudocumene, in anisole, and for pure carbon tetrachloride are

TABLE I

FREEZING POINTS
CARBON TETRACHLORIDE–BENZENE

| Mole fraction $CCl_4$ | Freezing point, °K. | Mole fraction $CCl_4$ | Freezing point, °K. | Mole fraction $CCl_4$ | Freezing point, °K. |
|---|---|---|---|---|---|
| 0.0000 | 278.66[b] | 0.6643[a] | 235.82 | 0.9017 | 238.86 |
| .1179 | 270.81 | .6877[a] | 234.86 | .9031 | 239.01 |
| .2030 | 264.90 | .6948[a] | 234.52 | .9131 | 240.20 |
| .3175 | 256.44 | .7116[a] | 233.80 | .9274 | 241.96 |
| .3557 | 253.42 | .7417 | 232.14 | .9382 | 243.26 |
| .4255 | 247.70 | .7552 | 231.75 | .9484 | 244.38 |
| .4665 | 244.19 | .7658 | 231.40 | .9571 | 245.51 |
| .4983 | 241.26 | .7841 | 230.63 | .9604 | 245.77 |
| .5112 | 240.03 | .8061 | 232.33 | .9617 | 245.82 |
| .5261 | 239.08 | .8265 | 233.72 | .9689 | 246.81 |
| .5491 | 238.83 | .8525 | 235.52 | .9807 | 248.21 |
| .5723 | 238.49 | .8686 | 236.61 | .9892 | 249.12 |
| .5922 | 238.06 | .8831 | 237.59 | 1.0000 | 250.41[b] |
| .6373 | 236.80 | .8982 | 238.65 | | |

[a] Solutions with mole fractions 0.6643, 0.6877, 0.6948, and 0.7116 had metastable freezing points of 232.83, 232.86, 232.84, and 232.71°K., respectively. [b] Corrected to zero per cent impurity, and based on an ice point of 273.15°K.

within 0.3° of the calorimetric value of Hicks, Hooley, and Stephenson.[6] Because the solid phase conversion is slow, it is difficult to establish temperature equilibrium for this transition with time–temperature methods. Consequently, this agreement is about as good as can be expected.

In the carbon tetrachloride–toluene system, the transition occurs approximately 0.8° lower than that of reference 6, which suggests that there is some solubility of toluene in the solid carbon tetrachloride, and that there may be further detail than that shown in Fig. 2 in the region to the right of mole fraction 0.97. Because of the limitations of time–temperature measurements in obtaining solid transition data and because our interest is principally in compound formation, further investigation of this region was not made.

In addition to the five compounds found in this study, compounds of carbon tetrachloride with *p*-xylene[1,6] and 1,2,4,5,-tetramethylbenzene[7] (durene) are known. Exploratory measurements were made on binary mixtures of carbon tetrachloride with several other aromatic compounds to check on the possibility of compound formation. The procedure consisted of obtaining time–temperature cooling curves at several compositions. If all curves showed the same eutectic temperature with no other temperature halts or irregularities, it was concluded that no compound was present between the extreme compositions studied. Solutions of *o*-xylene, *m*-xylene, chlorobenzene, bromobenzene and $\alpha,\alpha,\alpha$-trifluorotoluene with carbon tetrachloride were investigated over the composition range approximately 0.25 to 0.75 mole fraction carbon tetrachloride. This range was chosen to include compositions corresponding to 1:2, 1:1, and 2:1 compounds. The aromatic compounds were chosen so as to have a variety of geometrical structures of varying electron density in the ring. In a previous study,[1] solutions of carbon tetrachloride with nitrobenzene were similarly investigated. None of the above systems formed compounds.

Using the results of the carbon tetrachloride systems on which we have information, one can make several observations: (a) Compounds were formed in systems in which the aromatic compound had high electron density in the ring (benzene, toluene, *p*-xylene, pseudocumene, durene, and anisole). (b) No compounds formed in those systems in which the electron density of the benzene ring had been decreased by the presence of electronegative substituents in the ring (chlorobenzene, bromobenzene, nitrobenzene, and $\alpha,\alpha,\alpha$-trifluorotoluene). (c) Two systems failed to form compounds even though the electron density of the ring was high (*o*- and *m*-xylene).

Such observations suggest that a necessary although not sufficient condition for compound formation in carbon tetrachloride–aromatic compound systems is a high $\pi$-electron density. The failure of the two unsymmetrical xylenes to form compounds with carbon tetrachloride may be due to unfavorable geometry in these systems. One might expect the size and shape of the molecules involved to be very important in determining whether or not a solid compound of low energy of formation will occur. It is interesting to note in this regard that all three xylenes form compounds with $CBr_4$.[7]

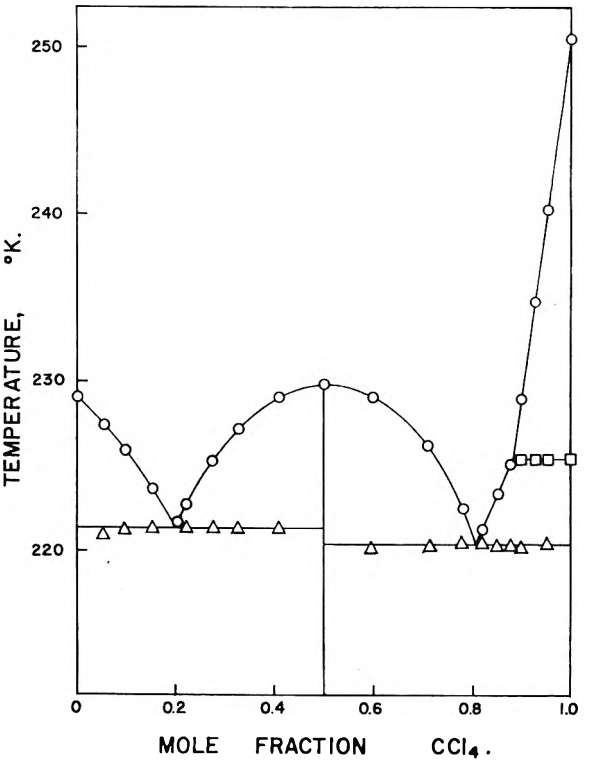


Fig. 3.—Phase diagram of carbon tetrachloride–pseudocumene.

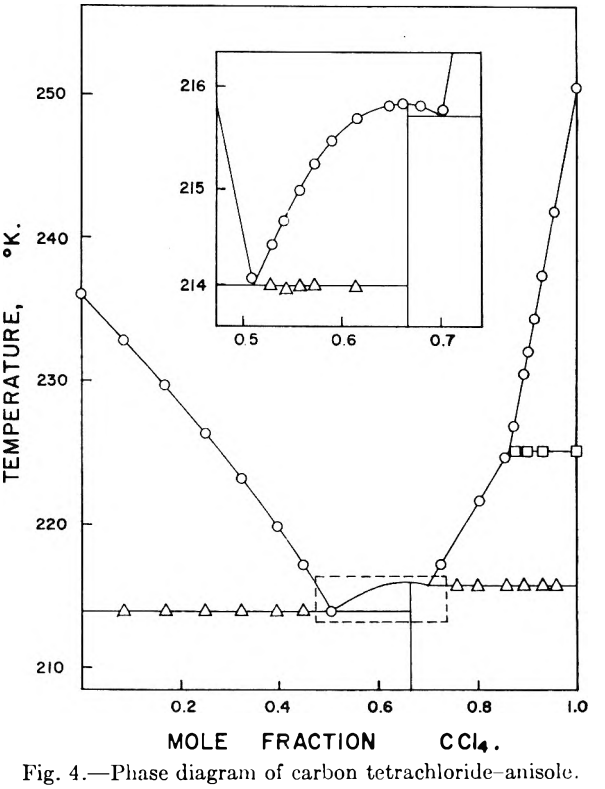


Fig. 4.—Phase diagram of carbon tetrachloride–anisole.

(6) J. F. G. Hicks, J. G. Hooley, and C. C. Stephenson, *J. Am. Chem. Soc.*, **66**, 1064 (1944).

(7) J. E. Clark and R. V. Luthy, *Ind. Eng. Chem.*, **47**, 250 (1955).

Since the size and shape of toluene and $\alpha,\alpha,\alpha$-trifluorotoluene are very nearly the same, a direct comparison of these two systems seems valid. The former with a high electron density forms a compound, the latter of low density does not.

**Acknowledgment.**—The authors gratefully acknowledge the support given this project by the National Science Foundation. We also wish to thank Mr. Frank W. Tsien, who assisted with the freezing point measurements.

# STEREOSPECIFICITY AND DIELECTRIC PROPERTIES OF POLAR POLYMERS

BY HERBERT A. POHL AND HOWARD H. ZABUSKY

*Princeton University Plastics Laboratory, Princeton University, Princeton, N. J.*

*Received January 5, 1962*

A method of determining stereoregularity in polar high polymers by dilute solution dielectric measurements is investigated on polyvinyl isobutyl ethers, polyethyl acrylates, and poly-*p*-chlorostyrenes of differing steric forms. In all cases no significant differences were found in the dielectric constants or dipole moments of the different steric forms of the same polymer. This was generally true of the relaxation times and distribution of relaxation times of the polymers also. The results are compared to those on polymethyl methacrylates where differences were found, and it is concluded that the degree of hindrance to rotation about the carbon–carbon bonds of the main chain and the degree of steric repulsion to positioning of side groups are the determining factors as to whether differences in dielectric properties will be observed. A simple and approximate method of predicting relative polarizations and dipole moments of stereospecific vinyl polymers based on dipole–dipole and repulsion energies is presented. It is concluded that the method of determining stereoregularity in polar polymers by dilute solution dielectric measurements is not generally applicable, but the method is a valuable tool for gaining insight into the flexibility of polar polymer chains.

## Introduction

The object of the present study was to determine if the dielectric behavior of stereoregular polar polymers in dilute solutions is a function of the steric order of the polymer molecule. If it were so, then the dielectric constant or average dipole moment of the polymer in solution could be used as a measure of stereoregularity.

This method has been used in the past on small organic molecules differing in steric configuration, especially on diastereomers,[1-3] molecules containing pairs of asymmetric carbon atoms. Differences in the apparent dipole moment were found between the optically compensated *meso* form and the uncompensated *d-d* or *l-l* forms. Extrapolating this to polymers, the *meso* form would correspond to a syndiotactic polymer and the uncompensated optically active *d-d* or *l-l* form would correspond to an isotactic polymer. The atactic polymer may be thought of as containing random blocks of these two.

Bacskai and Pohl[4] applied this method to isotactic, atactic, and syndiotactic polymethyl methacrylate, and found differences in the dipole moments of the three forms in the order isotactic > atactic > syndiotactic, indicating greater freedom of rotation in the isotactic form. The results were further substantiated by relaxation studies which showed an increase in mean relaxation time and in the distribution of relaxation times in going from the isotactic to the syndiotactic form.

In the present study three polymers were studied with regard to dipole moment and dielectric relaxation—polyvinyl isobutyl ether, polyethyl acrylate, and poly-*p*-chlorostyrene. The polymers each were synthesized in at least two different steric forms. The dielectric properties were measured at a single temperature and at several frequencies. In addition, brief studies were made of polymethyl methacrylates at differing temperatures.

A simple and approximate method was used to try to predict the relative polarizations and dipole moments of the stereospecific polymers. The method consists of considering the monomer units pair by pair as they may lie in space. Each pair can be shown to exist in 18 most probable conformations. Among these 18 conformations the probability and moment of each is calculated. The relative average polarization then is calculated from the weighted average of the pair moments.

## Experimental

**Polymer Preparations.—Polyvinyl Isobutyl Ethers.**—The methods of Schildknecht, *et al.*,[5] were used.

**Rubber-like Atactic Polyvinyl Isobutyl Ether.**—To 100 ml. of pentane was added 15.4 g. (0.154 mole) of vinyl isobutyl ether (Carbon and Carbide Chemicals Co.) freshly distilled from $CaH_2$. The mixture was cooled to $-65°$ in a Dry Ice–acetone bath. $BF_3$ (Matheson Coleman & Bell) was bubbled into 20 ml. of pentane so that the concentration of $BF_3$ was greater than 0.01% that of the monomer. The cooled catalyst mixture was added rapidly to the monomer–pentane mixture, causing a rapid increase in the solution viscosity. Eighty ml. more of pentane was added, the solution was filtered, then precipitated in 10 volumes of methanol. The white, rubbery product was dried under vacuum, giving 10.4 g. (67% yield).

**Crystalline, Isotactic Polyvinyl Isobutyl Ether.** Vinyl isobutyl ether (15.4 g.), distilled from $CaH_2$, was added to 80 ml. of pentane, and a small amount of crushed Dry Ice, and cooled to about $-70°$ in a Dry Ice–methanol bath. Exercising care to exclude moisture, 0.22 g. of $(C_2H_5)_2O$–$BF_3$ complex with 47% $BF_3$ (Matheson Coleman & Bell) was added at the rate of one drop every 10 sec., giving a catalyst concentration of 0.65%. Some instantaneous polymerization resulted and the mixture was allowed to sit 6 hr. The gel formed was dissolved by adding 500 ml. of toluene

(1) A. Weissberger, *J. Org. Chem.*, **2**, 245 (1937–1938); *J. Am. Chem. Soc.*, **67**, 778 (1945).

(2) S. Winstein and R. E. Wood, *ibid.*, **62**, 548 (1940).

(3) V. Ramakrishnan, *Kolloid-Z.*, **132**, 30 (1953).

(4) R. Bacskai and H. A. Pohl, "Stereospecificity and Electric Polarization in High Polymers," Princeton University Plastics Laboratory Report No. 55A, Oct. 1, 1959; *J. Polymer Sci.*, **42**, 151 (1960).

(5) C. E. Schildknecht, S. T. Gross, H. R. Davidson, J. M. Lambert, and A. E. Zoss, *Ind. Eng. Chem.*, **40**, 2104 (1948).

and this mixture precipitated in 10 volumes of methanol. The polymer was washed with additional methanol and dried *in vacuo* 24 hr., giving 12.0 g. (78% yield) of white fibrous non-tacky product.

Polyethyl acrylates were prepared by methods of Garrett, *et al.*[6]

**Syndiotactic Polyethyl Acrylate** (or what is now believed to be this modification).—Benzoin (0.13 g.) was added to 24 g. of ethyl acrylate (Eastman Chemicals) which had been distilled from $CaH_2$. The mixture was degassed by vacuum refreezing and sealed in a tube, then placed in a bed of Dry Ice and subjected to ultraviolet radiation for 2 hr. The product was a clear solid gel. This was dissolved in 750 ml. of warm toluene and precipitated in 4000 ml. of petroleum ether. The product was a high molecular weight, white, elastomeric polymer, 22.2 g. (92% yield).

**Atactic Polyethyl Acrylate.**—Ethylacrylate (30.3 g.) freshly distilled from $CaH_2$, 67.5 ml. of benzene, and 0.1 g. of benzoyl peroxide (Matheson Coleman & Bell) were refluxed under nitrogen for 30 min. and precipitated in 1000 ml. of petroleum ether. The vacuum-dried product (65% yield) was clear, tacky, and elastomeric.

**Isotactic Poly-*p*-chlorostyrene.**—Monomer (Borden Monomer–Polymer Laboratories), vacuum distilled from $CaCl_2$, was dissolved in benzene which had been freshly distilled over sodium metal. Under a dry nitrogen atmosphere, 5.59 g. of *p*-chlorostyrene, 0.19 g. of $TiCl_4$, 0.34 g. of $Al(C_2H_5)_3$, and 12 ml. of benzene were mixed. The mixture was degassed by vacuum refreezing and sealed in a glass tube, then shaken at 70° for 94 hr.[7] The product was precipitated in 350 ml. of methanol, filtered, washed with methanol, and vacuum dried. The polymer was reprecipitated from benzene using methanol, and again vacuum dried. The polymer was obtained in 40% yield as a white powder melting at 125–130°.

**Atactic Poly-*p*-chlorostyrene.**—To 14.3 g. of the purified monomer as above was added 0.10 g. of azobisisobutyronitrile (Brothers Chemical). The mixture, after degassing with the aid of vacuum refreezing, was sealed in glass and agitated 37 hr. at 70°. The reaction mixture then was diluted with 10 ml. of benzene and the polymer precipitated with 200 ml. of methanol, filtered, washed with methanol, and dried. The polymer was redissolved in benzene, reprecipitated with methanol, and vacuum dried; 5.3 g. (37% yield) was obtained.

**Polymethyl Methacrylates.**—Samples of atactic, isotactic, and syndiotactic material were those described earlier in the work of Pohl, *et al.*[4,8]

**Dielectric Polarization Measurements.**—The polymers were examined in dilute benzene solution in apparatus and using techniques described earlier.[9] Dielectric constant, dielectric loss, density, infrared spectra, and X-ray measurements were made as described earlier.[9]

## Results

The values of the polarization measurements made at low frequency are given for polyvinyl isobutyl ether (PVIBE), polyethyl acrylate (PEA), and poly-*p*-chlorostyrene (PCS) in Table I.

These results show no significant variation with steric form in any of these polymers.

The data obtained from the high frequency measurements are shown in Table II. Here $a' = \partial\epsilon'/\partial c$ and $a'' = \partial\epsilon''/\partial c$.[9] In these measurements the two forms of the vinyl ethers and of the chlorostyrenes give identical results, but there is considerable variation in the polyethyl acrylates. At the very high frequency (10 cm.) the atactic form has a higher dielectric constant than the syndiotactic, while the reverse is true at lower frequencies.

TABLE I

AVERAGE MOLAR POLARIZATIONS AND DIPOLE MOMENTS PER MONOMER UNIT FOR DILUTE SOLUTIONS OF POLYMERS AT 30° IN BENZENE

| Polymer | Steric form | $f_2$ × $10^3$ | $\Delta\epsilon/f_2$ | $P_2$ | $P_0$ | $\mu_{app}$ × $10^{18}$ |
|---|---|---|---|---|---|---|
| PVIBE | Atactic | 2.67 | 1.07 | 48.56 | 19.2 | 0.976 |
| PVIBE | Atactic | 4.37 | 1.09 | 48.86 | 19.5 | .983 |
| PVIBE | Isotactic | 2.34 | 1.09 | 48.86 | 19.5 | .983 |
| PVIBE | Isotactic | 4.49 | 1.10 | 49.00 | 19.6 | .987 |
| PEA | Atactic | 3.17 | 3.12 | 45.88 | 21.2 | 1.025 |
| PEA | Atactic | 1.74 | 3.09 | 45.44 | 20.7 | 1.015 |
| PEA | Syndiotactic | 1.28 | 3.13 | 46.03 | 21.3 | 1.029 |
| PEA | Syndiotactic | 5.35 | 3.09 | 45.44 | 20.7 | 1.015 |
| PCS | Atactic | 1.06 | 3.16 | 78.47 | 30.3 | 1.227 |
| PCS | Atactic | 1.81 | 3.14 | 78.18 | 30.0 | 1.221 |
| PCS | Isotactic | 0.93 | 3.14 | 78.18 | 30.0 | 1.221 |
| PCS | Isotactic | 1.72 | 3.16 | 78.47 | 30.3 | 1.227 |
| PCS | Isotactic | 0.88 | 3.11 | 77.74 | 29.5 | 1.211 |

TABLE II

RESULTS OF MICROWAVE MEASUREMENTS

| Polymer | Steric form | 10 cm. $a'$ | 10 cm. $a''$ | 25 cm. $a'$ | 25 cm. $a''$ | 50 cm. $a'$ | 50 cm. $a''$ | Static $a_0$ |
|---|---|---|---|---|---|---|---|---|
| PVIBE | Atactic | 0.31 | 0.15 | 0.38 | 0.19 | 0.45 | 0.24 | 1.08 |
| PVIBE | Isotactic | 0.31 | .12 | 0.39 | .19 | 0.49 | .22 | 1.09 |
| PEA | Atactic | 1.18 | .59 | 2.39 | .68 | 2.47 | .62 | 3.10 |
| PEA | Syndiotactic | 0.51 | .49 | 2.65 | .54 | 2.79 | .51 | 3.11 |
| PCS | Atactic | 1.13 | .09 | 1.47 | .21 | 1.85 | .27 | 3.15 |
| PCS | Isotactic | 1.08 | .12 | 1.48 | .25 | 1.85 | .29 | 3.14 |

The data shown in Table II are shown in Fig. 1 in the form of Cole–Cole plots. From these plots are obtained the most probable relaxation time $\tau_0$, the critical wave length $\lambda_m$, the distribution parameter $\alpha$, and the upper and lower limits of the relaxation distribution $\tau_1$ and $\tau_2$. These results are given in Table III.

TABLE III

RELAXATION DATA OBTAINED FROM COLE–COLE PLOTS

| Polymer | Steric form | $\lambda_m$, cm. | $\tau_0$ × $10^{10}$, sec. | $\alpha$ | $\tau_1$ × $10^{10}$ | $\tau_2$ × $10^{10}$ |
|---|---|---|---|---|---|---|
| PVIBE | Atactic | 113.1 | 6.0 | 0.33 | 0.55 | 65.5 |
| PVIBE | Isotactic | 120.6 | 6.4 | .33 | .59 | 69.8 |
| PEA | Atactic | 20.7 | 1.1 | .29 | .07 | 16.7 |
| PEA | Syndiotactic | 30.2 | 1.6 | .29 | .11 | 24.3 |
| PCS | Atactic | 63.1 | 3.3 | .69 | .006 | 1797.1 |
| PCS | Isotactic | 60.3 | 3.2 | .67 | .009 | 1168.1 |

These results show no significant dependence of relaxation on the steric form for polyvinyl isobutyl ether and poly-*p*-chlorostyrene, but do show a considerable difference in relaxation time between the two polyethyl acrylates.

Low frequency measurements were made on three samples of polymethyl methacrylates at 30 and 60° to observe the effect of temperature on the apparent dipole moment. The results of these measurements are given in Table IV.

The X-ray spectra for films of the polyvinyl ethers were examined. The spectrum of the iso-

(6) B. S. Garrett, W. E. Goode, S. Gratch, J. F. Kincaid, C. L. Levesque, A. Spell, J. D. Stroupe, and W. H. Watanabe, *J. Am. Chem. Soc.*, **81**, 1007 (1959).

(7) G. Natta, F. Danusso, and D. Sianesi, *Makromol. Chem.*, **28**, 253 (1958).

(8) H. A. Pohl, R. Bacskai, and W. P. Purcell, "Steric Order and Dielectric Behavior in Methyl Methacrylates," Princeton Univ. Plastics Laboratory Report No. 57A, April 1, 1960; *J. Phys. Chem.*, **64**, 1701 (1960).

(9) D. A. Pitt and C. P. Smyth, *ibid.*, **63**, 582 (1959).

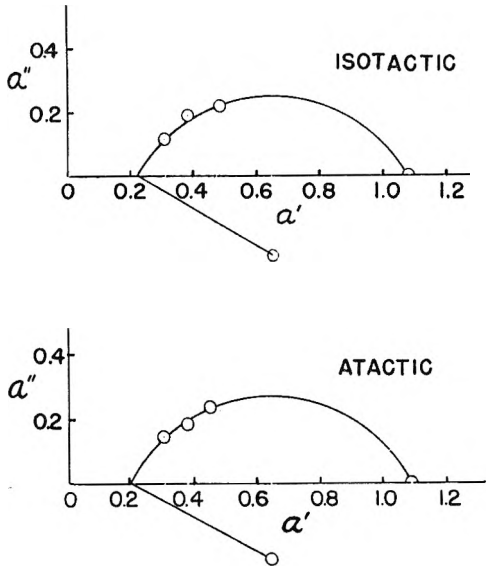


Fig. 1a.—Cole–Cole plots for polyvinyl isobutyl ethers.

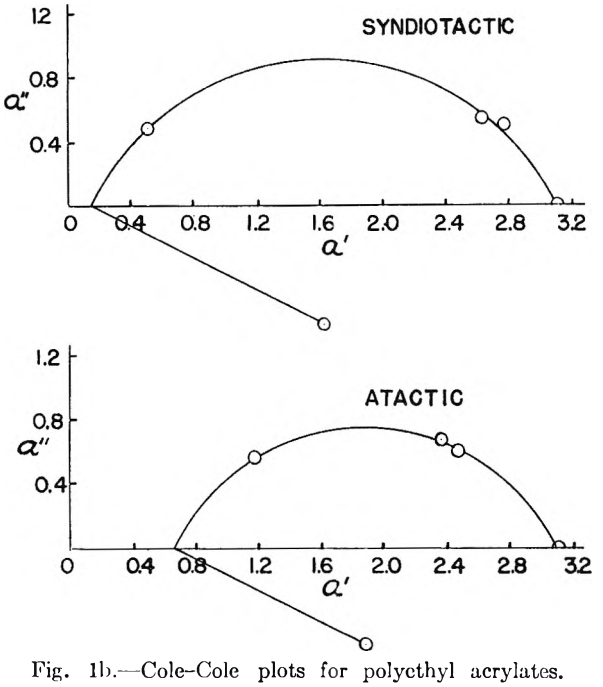


Fig. 1b.—Cole–Cole plots for polyethyl acrylates.

TABLE IV

MOLAR POLARIZATION AND DIPOLE MOMENT OF POLYMETHYL METHACRYLATES AT 30 AND 60°

| Steric form | Temp., °C. | $\Delta\epsilon/f_2$ | $P_2$ | $P_0$ | $\mu^2 \times 10^{35}$ | $\mu \times 10^{18}$ |
|---|---|---|---|---|---|---|
| Atactic | 30 | 2.58 | 61.07 | 36.6 | 1.820 | 1.349 |
| Atactic | 60 | 2.46 | 59.31 | 34.8 | 1.902 | 1.379 |
| Syndiotactic | 30 | 2.48 | 59.60 | 35.1 | 1.745 | 1.321 |
| Syndiotactic | 60 | 2.35 | 57.69 | 33.2 | 1.814 | 1.347 |
| Isotactic | 30 | 2.89 | 65.63 | 41.1 | 2.044 | 1.429 |
| Isotactic | 60 | 2.83 | 64.75 | 40.2 | 2.197 | 1.482 |

tactic polymer shows many peaks indicating crystallinity, while the atactic polymer is void of any evidence of crystallinity.

The infrared spectra of the polymers also were used to distinguish differences between the forms. There are no significant differences between the

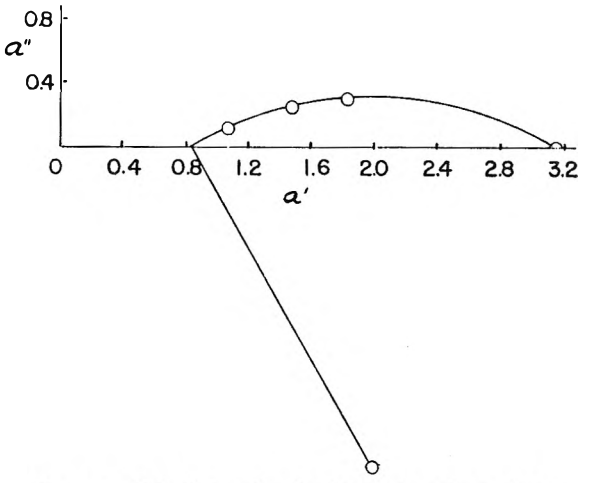


Fig. 1c.—Cole–Cole plot for isotactic poly-*p*-chlorostyrene.

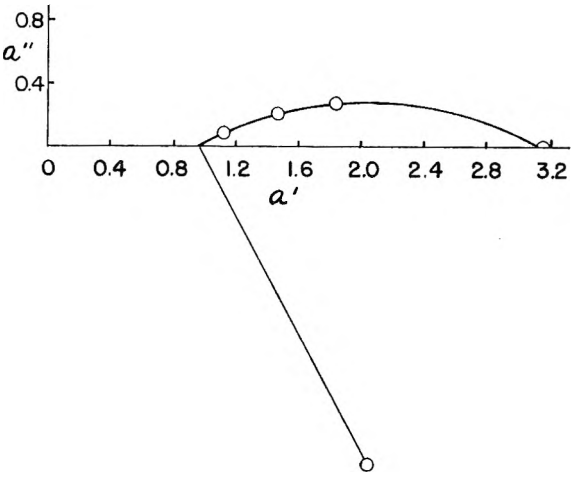


Fig. 1d.—Cole–Cole plot for atactic poly-*p*-chlorostyrene.

isotactic and atactic spectra of polyvinyl isobuty ether or between the atactic and syndiotactic spectra of polyethyl acrylate. In the poly-*p*-chlorostyrene spectra the following differences are observed: at 3.3 $\mu$ the isotactic absorption is twice that of the atactic, there is a small peak at 9.7 $\mu$ in the isotactic which is not evident in the atactic, and there is a large broad absorption at about 14.8 $\mu$ in the isotactic which is about three times as large as that observed for the atactic.

The X-ray spectra of the polyvinyl isobutyl ethers indicate differences between the forms, the infrared spectra indicate differences between the poly-*p*-chlorostyrenes, but there is no such evidence for differences between the polyethyl acrylates.

## Discussion

Briefly summarizing the experimental results, there are no significant differences in the molar polarization or average dipole moments per monomer unit, in the mean relaxation times, or in the distribution of relaxation times between the different steric forms of polyvinyl isobutyl ether and poly-*p*-chlorostyrene. Polyethyl acrylate shows differences in dielectric constant between the two forms at high frequencies but not at low frequency.

There are also significant differences between the relaxation times of the two forms of polyethyl acrylate. The polyethyl acrylates and the poly-*p*-chlorostyrenes have been shown previously to be non-crystallizable in any form,[6,7] and the polyvinyl isobutyl ether is shown to be crystalline in the isotactic form but not in the atactic form.

It is possible to interpret these results by comparing them to the results obtained on polymethyl methacrylate by Bacskai and Pohl[4] and Pohl, Bacskai, and Purcell,[8] where differences among the various steric forms were observed.

The differences observed in the polymethyl methacrylates were explained in terms of hindrance: hindrance to rotation about main chain bonds and hindrance to positioning of chain-attached side groups. Greater hindrance to rotation about the main chain bonds in the syndiotactic polymethyl methacrylate than in the isotactic explains the longer relaxation time and the broader range of relaxation times observed. Differences in steric repulsions to positioning of side groups account for the observed differences in average moments.

Under the influence of an alternating electric field the polar molecules of a system tend to align themselves in the direction of the field. In the case of a polymer the whole molecule does not follow the electric field, but rather we find segmental rotation and alignment with the alternating field. Since the rotating segments may be of different sizes and may be in different environments, the reactions to the field of different segments will vary. This gives rise to a distribution of relaxation times.

It is not surprising, therefore, that hindered rotation about the carbon–carbon bonds will effect the relaxation process. It is apparent from looking at molecular models and from other work[10,11] that rotation about the C–C bond in the polymers studied is hindered. The fact that the most probable relaxation time and the distribution of relaxation times do not vary between steric forms of polyvinyl isobutyl ether and poly-*p*-chlorostyrene leads to the conclusion that the relative location of the bulky side group, *i.e.*, *cis* or *trans*, on adjacent mer units does not affect the degree of freedom of rotation about the carbon–carbon bond. That the situation is different for polymethyl methacrylate possibly could be due to the fact that there are two side groups per mer unit on the main chain of the methacrylate and only one on the other polymers. The addition of the methyl group causes enough additional hindrance so that interactions between adjacent mers take place and the relative positions of the two groups become important.

As for the molar polarizations, the same conclusions can be drawn with regard to specific steric repulsion to positioning of side groups. In the case of polyvinyl isobutyl ether, polyethyl acrylate, and poly-*p*-chlorostyrene, whether the large side groups are *cis* or *trans* to each other on adjacent mer units does not significantly affect the conformations in which the syndiotactic and isotactic forms may lie. In the case of polymethyl methacrylate the additional methyl group is large enough to affect the degree of steric repulsion and change the probability of a given conformation from the isotactic to the syndiotactic form.

The fact that differences in molar polarization are indicated at high frequencies but not at low frequencies, and that there are differences in the relaxation times but not in the distribution parameter for the different polyethyl acrylates cannot be explained adequately at this time. From the results on the polymethyl methacrylates where the differences between the syndiotactic and atactic forms were very slight, there is reason to expect less difference between the syndiotactic and atactic polyethyl acrylates than between the other polymers where an isotactic and atactic form were compared. Atactic polymethyl methacrylate has been shown[6,12] to be largely syndiotactic, but this may not be true in the case of polyethyl acrylate.

With regard to the molar polarization and steric repulsion to positioning, Pohl, Bacskai, and Purcell[8] presented a simple and approximate method of predicting the average moments of polymers by using molecular models and considering successive monomer units pair by pair as they lie in space. Each pair can exist in 18 most probable conformations. Probabilities between 0 and 1 were assigned to each conformation and the moment of the paired monomers calculated. The average polarization of the chain then was calculated from a weighted average of the pair moments. This method, while approximate, gave good results in predicting the observed results on polymethyl methacrylates.

This method was applied independently and without knowing the experimental results to polyvinyl isobutyl ether and polyethyl acrylate in the isotactic and syndiotactic forms. While in both cases the absolute value of the moment may have been uncertain, the method predicted that there would be no significant relative differences in the dipole moments of the two forms of the polymer. This was confirmed by experiment.

The fact that certain conformations are more probable than others and that rotation is restricted indicates an energy barrier to rotation. As the temperature is raised, that is, more energy is put into the system, more and more molecules transcend the barrier and the system tends to overcome the steric hindrance. Table IV shows the effect of changing the temperature from 30 to 60° on the polymethyl methacrylates. In all cases the molar polarization decreased with an increase in temperature. The greater freedom of rotation at the higher temperature would lead to a higher molar polarization, but this is offset by an increase in randomness which results from an increase in temperature. To observe the effect of hindrance only, it is necessary to look at the dipole moment or the square of the dipole moment which is otherwise independent of temperature. In all cases the square of the moment increased slightly with temperature.

As the temperature is increased, one would expect that the dipole moments of the two forms would approach each other. At a temperature where

(10) R. M. Fuoss and J. G. Kirkwood, *J. Am. Chem. Soc.*, **63**, 391 (1941).

(11) J. Marchal and C. Lapp, *J. Polymer Sci.*, **27**, 571 (1958).

(12) F. A. Bovey and G. V. D. Tiers, *ibid.*, **44**, 173 (1960).

enough energy was being added to the system to overcome all steric hindrance, the moments of the two forms would be expected to be equal. The temperature range investigated was not great enough to show any significant change in the ratio of the moments of the two forms. A theoretical investigation considering the repulsion and dipole–dipole energies which leads to the same conclusions is given in the Appendix.

Some support of the discussion of relaxation phenomena is given by Saito and Nakajama,[13] who found an increase in the relaxation time and a corresponding decrease in the glass transition temperature in vinyl chloride–vinylidene chloride copolymers with an increase in vinylidene chloride content, and by Borisova and Mikhailov[14] who found a decrease in the relaxation time of methacrylate–styrene copolymers with an increase in styrene content. In both cases the molecule with the bulkier side group causes an increase in the relaxation time due to the additional hindrance which it provides.

Finally, it is necessary to conclude that the proposed method of determining stereoregularity of polar polymers from dilute solution dielectric measurements is not generally applicable because sufficient steric hindrance to dipole rotation is not always present. There is sufficient hindrance in the case of polymethyl methacrylate but not in the case of polyvinyl isobutyl ether, polyethyl acrylate, or poly-*p*-chlorostyrene to produce ascertainable differences in the average dipole moments, the relaxation times, or the distribution of relaxation times. The method does, however, offer considerable insight into the flexibility of polar polymer chains.

The above computations show that the major source of differing chain flexibility lies in the presence of crowded groups attached to the main chain. This is confirmed by observations on the glass transition temperature, $T_g$, of the isotactic, syndiotactic, and atactic forms of various polymers. Those polymers with little crowding of groups along the main chain show near identity of $T_g$ among their differing stereospecific forms. Polypropylene, poly-1-butene, polystyrene, poly-1-pentene, and polyvinyl isobutyl ether are examples of this. On the other hand, a polymer such as polymethyl methacrylate having crowded side groups on the main chain shows $T_g$ to vary strongly among its stereospecific forms, the isotactic form exhibiting $T_g$ = 45°, the syndiotactic, 115°, and the atactic about 90°.[15]

## Appendix

**The Estimation of Average Moment in Stereospecific Vinyl Polymers.**—In the following, a simple and approximate method is used to try to predict the relative polarizations and dipole moments of stereospecific vinyl polymers. The method consists essentially of considering the monomer units pair by pair as they may lie in space. Each pair can be shown to exist in 18 most probable conformations. Among these 18 conformations the probability and moment of each is calculated. The relative average polarization of the chain then is calculated from the weighted average of the pair moments.

In the specific case of polymethyl methacrylate, the configurations of the isotactic and syndiotactic forms may be written

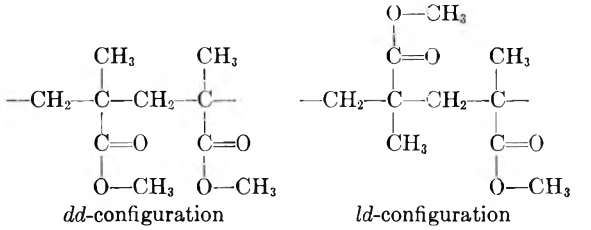

*dd*-configuration *ld*-configuration

As a more complete spatial representation one may refer to Fig. 2, ref. 8. The shorthand method shown in Fig. 3, ref. 8, is adopted for representing the 18 different interlapping conformations of the two asymmetric carbon tetrahedron assemblies. Conformations other than the *gauche*, in which the direct overlapping of groups attached to the tetrahedral corners is present, are regarded *a priori* as too improbable to include in the calculation.

As was shown earlier[8] the moment of the monomer pair, $\mu_p$, is

$$\mu_p = 2\mu_0 \cos(\delta/2) \qquad \text{(A-1)}$$

where $\mu_0$ is the moment of the monomer molecule and $\delta$ is the angle between the average moments of the monomer units as directed along the asymmetric carbon–carboxyl carbon bond. To evaluate the average polarization of the whole polymer, we assume as a good approximation that the average moment, $\mu_{av}$, per monomer unit of the ensemble of monomer pairs in the polymer chain is the root mean square of the weighted moments of the pairs

$$(\mu_{av})^2 = \frac{\sum_i^n f_i\mu_i^2}{4\sum_i^n f_i} = \frac{\mu_0^2\sum_i^n f_i\cos^2(\delta_i/2)}{\sum_i^n f_i} \qquad \text{(A-2)}$$

where $n$ is the number of differing conformations possible in the given polymer species (*e.g.*, 9 for either the isotactic or the syndiotactic species), $\mu_i$ is the moment of the $i$th pair, and $f_i$ is the probability of the individual pair conformations of $\mu_i$ as shown in shorthand form in Fig. 3. Necessarily, $\sum_i^n f_i = 1$.

The evaluation of the $f_i$'s was made using statistical mechanical methods based on reasonable values for dipole–dipole energies and H–H repulsion energies for the separate conformations.

The energy above an arbitrary zero of each dimer conformation, $E_i$, was considered to consist principally of the dipole–dipole interaction energy of the ester group dipoles, $E_D$, and of the repulsion energy $E_R$, arising from the tight placement of the various molecular groups.

$$E_i = E_D + E_R \qquad \text{(A-3)}$$

The dipole–dipole energy for non-polarizable dipoles is

$$E_D = \frac{-3(\boldsymbol{\mu}_1\cdot\mathbf{s})(\boldsymbol{\mu}_2\cdot\mathbf{s})}{s^5} + \frac{\boldsymbol{\mu}_1\cdot\boldsymbol{\mu}_2}{s^3} \qquad \text{(A-4)}$$

$$= \frac{\mu_0^2}{s^3}(\cos\delta - 3\cos\beta\cos\gamma)$$

where $\boldsymbol{\mu}_1$ and $\boldsymbol{\mu}_2$ are the moment vectors of dipoles 1 and 2, $\mu_0$ is the absolute value of the moment of the vectors $\boldsymbol{\mu}_1$ and $\boldsymbol{\mu}_2$, $\mathbf{s}$ is the distance vector expressing the distance between dipole centers, and $\beta$, $\gamma$, and $\delta$ are the angles of the bipole conformation (see F 2).

(13) S. Saito and T. Nakajama, *J. Polymer Sci.*, **37**, 229 (1959).

(14) T. I. Borisova and G. P. Mikhailov, *Vysokomolekul. Soedin.*, **1**, 563 (1959); *J. Polymer Sci.*, **40**, 285 (1959).

(15) N. G. Gaylord and H. F. Mark, "Linear and Stereoregular Addition Polymers," Interscience Publishers, New York, N. Y., 1959, pp. 71, 322.

For $\mu_0 = 1.69$ D., chosen as for a similar simple ester, methyl propionate,[16] and for $s = 1$ Å., $\delta = 0°$, $\beta = 90°$, we obtain

$$E_D^0 = \frac{(1.69)^2(3.33)^2(10^{-30})^2}{(4\pi)(10^{-9}/36\pi)(10^{-10})^3} \frac{\text{coul.}^2\ \text{m.}^2}{\frac{\text{coul.}}{\text{volt-m.}}\ \text{m.}^3}$$

$$= 29.4 \times 10^{-20} \text{ joules}$$

$$= 42.6 \text{ kcal./mole}$$

and eq. A-4 becomes

$$E_D = E_D^0 \left(\frac{\cos\delta - 3\cos\beta\cos\gamma}{s^3}\right) \text{kcal./mole} \qquad \text{(A-5)}$$

where $s$ is in Å.

To obtain the potential energy values for repulsion at various distances between non-bonding hydrogen atoms, the following equations from the valence-bond method can be applied

$$E_R = E_{H,H} = Q_{H,H} - {}^1/_2 J_{h,h} \qquad \text{(A-6)}$$

where $Q_{H,H}$ and $J_{h,h}$ are the coulomb interaction energy and the exchange energy, respectively, for the pair of orbitals of the two H atoms.

Hirschfelder and Linnett[17] showed that $Q_{H,H}$ and $J_{h,h}$ may be obtained from $E(^1\Sigma)$ and $E(^3\Sigma)$ for the singlet and triplet $\sigma$ orbitals

$$E(^1\Sigma) = Q_{H,H} + J_{h,h}$$

$$E(^3\Sigma) = Q_{H,H} - J_{h,h}$$

Figure 3, taken from a private memorandum of Dr. Keniti Higasi, is the result of this estimation. The values of the repulsive energy $E_R = E_{H,H}$ are given as a function of the interatomic distance, $d_{H,H}$, in three different scales. Adrian[18] made a similar calculation for the distance range 1.3 to 3.5 Å.

The values for $E_D$ and $E_R$ used in the present study were calculated after determining the appropriate constants for the 18 conformations. The repulsion energy $E_R$ was calculated using the above relation, $E_R = E_{H,H}$, and values of $d_{H,H}$ were obtained from the conformations using

$$(d_{H,H})_i = d^0 - \Delta_i \qquad \text{(A-7)}$$

where $d^0 = 2.1$ Å., a nominal internuclear distance for close approach of non-bonding hydrogen atoms, $\Delta_i$ = overlap distance of hydrogen atoms in the conformation.

The values of the angles $\beta$, $\gamma$, and $\delta$, and the distances $s$ and $\Delta$ were determined for each conformation by calculations checked by measurement on molecular models (Fisher–Taylor–Hirschfelder). From these parameters, values of $E_D$ and $E_R$ were calculated and used to evaluate $E_i$.

The probability of each state, $f_i$, is given by

$$f_i = p_0 e^{-E_i/RT}$$

$$\sum_i^n f_i = 1 = \sum_i^n p_0\, e^{-E_i/RT} \qquad \text{(A-8)}$$

$$p_0 = \frac{1}{\sum_i^n e^{-E_i/RT}}$$

The measured values of $\beta$, $\gamma$, $\delta$, $s$, $\Delta$, and $d_{H,H}$ are given for all conformations in Table V. The calculated values of $E_R$, $E_D$, $E_i$, $f_i$, and $f_i \cos^2(\delta_i/2)$ are given in Table VI.

(16) C. P. Smyth, "Dielectric Behavior and Structure," McGraw-Hill Book Co., New York, N. Y., 1955, pp. 303-304.

(17) J. O. Hirschfelder and J. W. Linnett, *J. Chem. Phys.*, **18**, 130 (1950).

(18) F. J. Adrian, *ibid.*, **28**, 608 (1958).

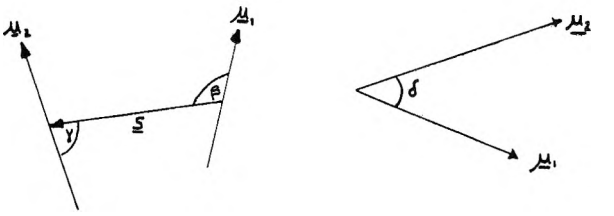


Fig. 2.—Geometry of dipoles.

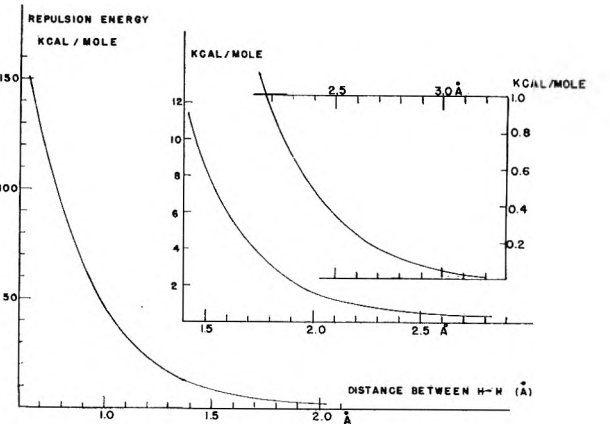


Fig. 3.—Repulsion energy as a function of interatomic distance.

TABLE V

MEASURED VALUES FOR MOLECULAR CONFORMATIONS

| Conformation | $\beta$ | $\gamma$ | $\delta$ | $s$ (Å.) | $\Delta$ (Å.) | $d_{H,H}$ (Å.) |
|---|---|---|---|---|---|---|
| Isotactic | | | | | | |
| I | 120° | 60° | 70° | 3.8 | 0.3 | 1.8 |
| II | 105 | 105 | 40 | 3.5 | .0 | 2.1 |
| III | 135 | 10 | 150 | 6.3 | .8 | 1.3 |
| IV | 120 | 50 | 110 | 6.8 | .6 | 1.5 |
| V | 180 | 75 | 110 | 5.5 | .2 | 1.9 |
| VI | 150 | 55 | 100 | 7.0 | .6 | 1.5 |
| VII | 130 | 30 | 160 | 6.7 | .6 | 1.5 |
| VIII | 90 | 90 | 60 | 3.4 | .3 | 1.8 |
| IX | 100 | 70 | 45 | 4.7 | .8 | 1.3 |
| Syndiotactic | | | | | | |
| I | 130 | 20 | 135 | 6.6 | 0.3 | 1.8 |
| II | 90 | 100 | 20 | 3.7 | .1 | 2.0 |
| III | 90 | 60 | 55 | 4.5 | .8 | 1.3 |
| IV | 160 | 55 | 115 | 6.7 | .6 | 1.5 |
| V | 180 | 60 | 120 | 5.7 | .1 | 2.0 |
| VI | 150 | 60 | 100 | 6.2 | 1.0 | 1.1 |
| VII | 110 | 60 | 55 | 4.7 | 0.7 | 1.4 |
| VIII | 110 | 90 | 55 | 3.8 | 0.0 | 2.1 |
| IX | 120 | 0 | 140 | 6.8 | 1.0 | 1.1 |

For isotactic polymethyl methacrylate, $p_0 = 11.17$ at 30° and 8.415 at 60°. For syndiotactic polymethyl methacrylate, $p_0 = 6.73$ at 30° and 5.12 at 60°.

The values of $\sum_i f_i \cos^2(\delta_i/2)$ obtained were

isotactic —30°—0.7417
isotactic —60°—0.7321
syndiotactic —30°—0.6219
syndiotactic —60°—0.6123

From these values one calculates the average moments of

TABLE VI
CALCULATED VALUES FOR MOLAR CONFORMATIONS

| Conformation | $E_R$, kcal. | $E_D$, kcal. | $E_i$, kcal. | $f_i(30°)$ | $f_i(60°)$ | $f_i \cos^2(\delta_i/2)$ 30° | 60° |
|---|---|---|---|---|---|---|---|
| Isotactic | | | | | | | |
| I | 3.0 | 0.85 | 3.85 | 0.0186 | 0.0248 | 0.0125 | 0.0166 |
| II | 1.1 | .56 | 1.66 | .710 | .681 | .627 | .6020 |
| III | 15 | .21 | 15.21 | 0 | 0 | 0 | 0 |
| IV | 8.4 | .08 | 8.48 | 0 | 0 | 0 | 0 |
| V | 2.2 | .11 | 2.31 | .239 | .255 | .0787 | .0838 |
| VI | 8.4 | .16 | 8.56 | 0 | 0 | 0 | 0 |
| VII | 8.4 | .10 | 8.50 | 0 | 0 | 0 | 0 |
| VIII | 3.0 | .54 | 3.54 | .0313 | .0396 | .0235 | .0297 |
| IX | 15 | .36 | 15.36 | 0 | 0 | 0 | 0 |
| Total | | | | 0.999 | 1.000 | 0.7417 | 0.7321 |
| Syndiotactic | | | | | | | |
| I | 3.0 | 0.17 | 3.17 | 0.0345 | 0.0421 | 0.0051 | 0.0062 |
| II | 1.6 | .79 | 2.39 | .1270 | .1376 | .1228 | .1330 |
| III | 15 | .27 | 15.27 | 0 | 0 | 0 | 0 |
| IV | 8.4 | .17 | 8.57 | 0 | 0 | 0 | 0 |
| V | 1.6 | .23 | 1.83 | .3200 | .3220 | .0800 | .0805 |
| VI | 30 | .21 | 30.21 | 0 | 0 | 0 | 0 |
| VII | 11 | .45 | 11.45 | 0 | 0 | 0 | 0 |
| VIII | 1.1 | .44 | 1.54 | .5225 | .4984 | .4140 | .3926 |
| IX | 30 | − .10 | 29.90 | 0 | 0 | 0 | 0 |
| Total | | | | 1.004 | 1.000 | 0.6219 | 0.6123 |

the polymer species as, for example

$$\mu_{iso,30°} = 1.69\sqrt{.7417} = 1.457$$

Calculated and observed values are compared in Table VII.

TABLE VII
COMPARISON OF CALCULATED AND OBSERVED MOMENTS FOR PMMA

| Steric form | Temp., °C. | $\mu_{av}$ (theor.) | $\mu_{av}$ (obsd.) |
|---|---|---|---|
| Isotactic | 30 | 1.457 | 1.429 |
| Isotactic | 60 | 1.446 | 1.482 |
| Syndiotactic | 30 | 1.333 | 1.321 |
| Syndiotactic | 60 | 1.323 | 1.347 |
| Atactic | 30 | ... | 1.349 |
| Atactic | 60 | ... | 1.379 |

The theory is examined by comparing ratios predicted and observed in Table VIII.

TABLE VIII
COMPARISONS OF THEORETICAL AND OBSERVED RATIOS OF MOMENTS FOR PMMA

| | $\left(\frac{\mu_{iso}}{\mu_{syn}}\right)_{30°}$ | $\left(\frac{\mu_{iso}}{\mu_{syn}}\right)_{60°}$ | $\left(\frac{\mu_{60°}}{\mu_{30°}}\right)_{iso}$ | $\left(\frac{\mu_{60°}}{\mu_{30°}}\right)_{syn}$ |
|---|---|---|---|---|
| Theor. | 1.093 | 1.093 | 0.994 | 0.994 |
| Obsd. | 1.082 ± 0.015 | 1.110 ± 0.025 | 1.037 ± 0.05 | 1.020 ± 0.05 |

($\mu_{60}/\mu_{30}$ for the atactic was observed to be 1.023 ± 0.05)

The agreement is considered quite satisfactory. The larger errors for measurements at higher temperatures are due in part to the volatility of the solvent. A concentration error of perhaps −2 to −4% was observable.

The average moment calculated for the two forms when at "infinite temperature," that is, a temperature high enough to overcome all restrictions to rotation and to positioning, is found by setting $f_i = 1$ for all conformations. On doing this one obtains

$$\mu_{iso} = 1.69\sqrt{.4807} = 1.173$$

$$\mu_{syn} = 1.69\sqrt{.5051} = 1.202$$

An alternative, very qualitative, calculation of the average moment of the polymer can be made by assuming that each momomer loses one degree of rotational freedom on being in the chain. Ignoring special orientation of the moments within the chain, we have

$$\mu_{av}^2 \cong 2/3\ \mu_0^2$$

$$\mu_{av} \cong 1.69\sqrt{2/3} = 1.38$$

It may be noted that the theory predicts and the experiment confirms that little change in the average moment occurs in the experimental 30° temperature interval. This is a consequence of having relatively small "activation energies" for the rotation hindering process. A large energy of activation could produce large changes with small temperature increments.

In the limit of free rotation, the calculation indicates that the syndiotactic form would have a slightly larger moment than the isotactic form (1.202 *vs.* 1.173). One would expect exact equivalence instead of the small difference indicated in the calculation. This may reflect small cumulative errors in the assignment of the $\delta_i$ values.

In summary, it may be said that: 1. The average moments calculated for the isotactic and syndiotactic polymer species are in reasonable agreement with those observed (Table VII). 2. The temperature coefficients of the moments calculated agree closely with those observed (Table VIII). 3. The calculated ratios of the average moments of the isotactic and syndiotactic polymer species agree closely with those observed. 4. The method of considering the average moment of a polar polymer to arise from paired monomer units having enumerable conformations and preassigned degrees of freedom (based on dipole–dipole and repulsion energies) gives a reasonably satisfactory representation of the complex problem of polar polymer moments in polymethyl methacrylates.

**Acknowledgment.**—A portion of this work was supported by Signal Corps Contract No. D-36-039-sc-78105; DA Project 3-99-15–108; ONR 356-375; WADD Project 7371, for which the authors wish to express their appreciation.

# MOLECULAR COMPLEXES OF SOME INTERHALOGEN COMPOUNDS[1]

BY MAX T. ROGERS AND W. K. MEYER[2]

*Kedzie Chemical Laboratory, Michigan State University, East Lansing, Michigan*

*Received January 19, 1962*

Molecular complexes of iodine trichloride, iodine pentafluoride, iodine monochloride, and iodine monobromide with various electron donors, such as dioxane and derivatives of pyridine, have been prepared and some physical properties of the more stable ones have been studied. Dissociation constants of some of these complexes have been determined spectrophotometrically and dipole moments have been estimated from the dielectric polarizations of their solutions in non-polar solvents.

## Introduction

Stable molecular complexes between iodine, iodine monochloride, and iodine monobromide and various electron donors such as pyridine and dioxane long have been known and the stability and various other properties of a number of these have been intensively investigated recently.[3] Apparently the only stable complex of iodine pentafluoride reported is a 1:1 complex with dioxane.[4] Some complexes of iodine trichloride have been reported,[5,6] but no physical measurements appear to have been carried out on them. We therefore have attempted to prepare a variety of complexes of the interhalogen compounds using as electron donors pyridine and pyrazine and some of their derivatives, dioxane, trifluoroacetic anhydride, amines, ethers, etc., and to study some of their physical properties.

It is particularly useful to know the extent to which these complexes dissociate in solution to give the original materials and we therefore have measured spectrophotometrically the dissociation constants of some of them. Since the dielectric constants of the solutions lead to estimated dipole moments for the molecular complexes when the dissociation constants are known, we have measured dielectric constants of a number of the crystalline complexes dissolved in non-polar solvents. From the electric moments of the complexes the extent of electron transfer from donor to acceptor was estimated. The electric moments of the dioxane–iodine and pyridine–iodine complexes in cyclohexane solution have been measured previously and the values 3.0 and 4.5 D., respectively,[7] reported; also, the moment of the pyridine–iodine complex in benzene solution[8] has been reported as 4.17 D.

We also have obtained parts of the phase diagrams for the two-phase solid–liquid systems dioxane–iodine pentafluoride and pyridine–iodine pentafluoride.

(1) This work was supported by a grant from the Atomic Energy Commission.

(2) Abstracted from a thesis submitted by W. K. Meyer in partial fulfillment of the requirements for the Ph.D. degree, Michigan State University, 1958.

(3) A. I. Popov, C. Castellani-Bisi, and Willis B. Person, *J. Phys. Chem.*, **64**, 691 (1960), and preceding papers of that series.

(4) A. F. Scott and J. F. Bunnett, *J. Am. Chem. Soc.*, **64**, 2727 (1942).

(5) E. V. Zappi and M. Fernandez, *Anales Asoc. Quim. Arg.*, **27**, 102 (1939).

(6) R. Cernatescu and M. Poni, *Analele Acad. Rep. Populare Romane, Ser. Mat. Fiz. Chim.*, **3**, 140 (1950).

(7) G. Kortüm and H. Walz, *Z. Elektrochem.*, **57**, 73 (1953).

(8) Y. K. Syrkin and K. M. Anisimova, *Dokl. Akad. Nauk SSSR*, **59**, 14 (1948).

## Experimental

**Materials.**—Benzene ($d^{25}_4$ 0.87336), carbon tetrachloride ($d^{25}_4$ 1.5844), and dioxane (m.p. 11.66°) were purified by partial freezing and distillation over a drying agent. The pyridine and pyrazine derivatives were commercial materials redistilled. A sample of pyrazine was the gift of the Wyandotte Chemical Corp., Wyandotte, Michigan. 2-Fluoropyridine and 3-fluoropyridine were prepared from 2-aminopyridine and 3-aminopyridine by diazotization in 40% fluoroboric acid.[9]

Iodine monochloride (m.p. 27°), iodine trichloride, and iodine monobromide (m.p. 41.5°) were prepared from the elements and (except for iodine trichloride) were purified by recrystallization from the melt. Iodine pentafluoride from the General Chemical Division, Allied Chemical and Dye Co., was fractionally distilled in a Monel–fluorothene still[10] before use (m.p. 9.6°).

**Preparation of Complexes.**—Normally a solution of the interhalogen compound in carbon tetrachloride was added to a solution of the electron donor, also in carbon tetrachloride, and the crystalline complex was removed by filtration, washed with carbon tetrachloride, and dried.

Dioxane–iodine monobromide and dioxane–iodine pentafluoride were prepared by mixing the pure liquids in stoichiometric amounts, filtering, washing with carbon tetrachloride, and drying. Some of the complexes were liquids at room temperature.

Known weights of pure iodine pentafluoride were dispensed from a calibrated 2-ml. Pyrex buret fitted with a stopcock having a Teflon plug. All transfers were carried out in an atmosphere of dry nitrogen.

**Analyses.**—Microanalyses of some complexes were carried out (for C, H, N) by Spang Microanalytical Laboratories, Ann Arbor, Michigan, and are reported in Table I.

Halogen analyses were made for several complexes by determining an iodometric equivalent by the following technique developed for these compounds.

A weighed sample (2–3 meq.) of complex was dissolved in 10 ml. of pyridine, 6 g. of potassium iodide was added, the mixture was cooled to 0°, and 12 ml. of 12 *N* hydrochloric acid was added. Acetone (10 ml.) was added to dissolve the liberated iodine and standard thiosulfate was added until the mixture was yellow. Then 20 ml. of water and 2 ml. of starch solution were added and the titration was continued to the end-point. A blank also was run.

The calculated iodometric equivalent is taken to be the molecular weight of the complex divided by the number of halogen atoms considered to be present. The observed values for the iodine trichloride complexes are somewhat high, corresponding to 5–10% loss of chlorine from the complex.

**Dielectric Constants.**—Dielectric constants of a series of six or seven solutions of the molecular complex in benzene or dioxane, usually varying from 0.0005–0.02 mole fraction of complex, were measured using a heterodyne-beat apparatus; densities were measured with a pycnometer. The methods of measurement of dielectric constant and density as well as the methods of calculation of results have been described.[11] The plots of the dielectric constants and densities of the solutions *vs.* mole fraction of solute were linear within experimental error in every case. Molar refractions were calculated from tables of atomic refractions.

**Phase Diagrams.**—Freezing points of liquid mixtures were measured in a small Pyrex dewar vessel in which the

(9) A. Roe and G. F. Hawkins, *J. Am. Chem. Soc.*, **69**, 2443 (1947).

(10) M. T. Rogers, J. L. Speirs, H. B. Thompson, and M. L. Panish, *ibid.*, **76**, 4843 (1954).

(11) M. T. Rogers, *ibid.*, **77**, 3681 (1955).

TABLE I

SOME PROPERTIES OF CRYSTALLINE MOLECULAR COMPLEXES OF INTERHALOGEN COMPOUNDS[a]

| Complex | M.p., °C. | Color | Stability (25°) | Analyses, % Calcd. C | Calcd. H | Calcd. N | Obsd. C | Obsd. H | Obsd. N | Iodometric equivalent % C Obsd. | Iodometric equivalent % C Calcd. |
|---|---|---|---|---|---|---|---|---|---|---|---|
| Pyridine·$ICl_3$ | 142.6 | Yellow | Loses $Cl_2$ | | | | | | | | |
| Quinoline·$ICl_3$ | 132 | Yellow | ..... | | | | | | | 94.1 | 90.6 |
| 2,6-Dimethylpyridine·$ICl_3$ | 90–95 | Yellow | Loses $Cl_2$ | | | | | | | 90.5 | 85.1 |
| 2-Fluoropyridine·$ICl_3$ | 56–65 | Yellow | Loses $Cl_2$ | | | | | | | 101.6 | 82.5 |
| Quinoline·ICl | 154–155 | Cream | ..... | 37.07 | 2.42 | 4.30 | 36.65 | 2.40 | 4.92 | | |
| Pyrazine·ICl | Dec. 193 | Yellow | Unstable | | | | | | | | |
| 2-Methylpyrazine·ICl | Dec. 115 | Yellow | Unstable | | | | | | | | |
| 2-Fluoropyridine·ICl | 56 | Yellow | ..... | 23.14 | 1.55 | 5.39 | 23.18 | 1.55 | 4.90 | 130.9 | 129.7 |
| 2-Chloropyridine·ICl | 80–82 | Yellow | ..... | 21.76 | 1.46 | 5.07 | 21.54 | 1.47 | 5.33 | 139.3 | 138.0 |
| 3-Fluoropyridine·ICl | 95–97 | Yellow | ..... | 23.14 | 1.55 | 5.39 | 23.02 | 1.56 | 5.35 | 129.7 | 130.9 |
| 3-Bromopyridine·ICl | 90–92 | Orange | ..... | | | | | | | | |
| 3-Chloropyridine·ICl | 56 | Yellow | ..... | 21.76 | 1.46 | 5.07 | 21.94 | 1.44 | 5.06 | | |
| 4-Chloropyridine·ICl | 224–226 | Yellow | ..... | | | | | | | | |
| Quinoline·IBr | 128–129 | Yellow | ..... | 32.16 | 2.09 | 4.16 | 32.13 | 2.06 | 4.23 | 168.6 | 168.0 |
| Pyrazine·IBr | Dec. 156 | Orange | ..... | | | | | | | | |
| 2-Methylpyrazine·IBr | Dec. 115 | Orange | ..... | | | | | | | | |
| 2-Fluoropyridine·IBr | 44–45 | Orange | Dec. slowly | | | | | | | | |
| 2-Chloropyridine·IBr | 44–45 | Orange | ..... | 18.74 | 1.25 | 4.37 | 18.65 | 1.13 | 4.36 | 163.2 | 160.4 |
| 3-Fluoropyridine·IBr | 70–72 | Tan | ..... | | | | | | | 154.7 | 152.0 |
| 3-Bromopyridine·IBr | 77–78 | Orange | ..... | | | | | | | | |
| 3-Chloropyridine·IBr | 47 | Orange | ..... | | | | | | | | |
| 4-Chloropyridine·IBr | 193–195 | Tan | Dec. slowly | | | | | | | | |

[a] (1) M.p. measurements were made on a calibrated melting-point block; (2) most of the compounds show decomposition over a period of months, but those showing decomposition over a short period (a few days) at room temperature are classed as unstable.

TABLE II

APPARENT DIPOLE MOMENTS, MOLAR POLARIZATIONS, MOLAR REFRACTIONS, AND EMPIRICAL CONSTANTS FOR MOLECULAR COMPLEXES

| Compound | Solvent | $T$, °C. | $a$ | $b$ | $P_2$ | $MR_D$ | $\mu$ |
|---|---|---|---|---|---|---|---|
| 2,6-Dimethylpyridine | $CCl_4$ | 25 | 4.16 | 0.324 | 101.9 | 33.31 | 1.83 |
| 2,6-Dimethylpyridine | $C_6H_6$ | 25 | 4.69 | −0.095 | 100.3 | 33.31 | 1.81 |
| 2-Fluoropyridine | $C_6H_6$ | 25 | 15.61 | −0.144 | 259.2 | 23.85 | 3.39 |
| 3-Fluoropyridine | $C_6H_6$ | 25 | 5.67 | −0.315 | 109.1 | 23.85 | 2.04 |
| 3-Chloropyridine | $C_6H_6$ | 25 | 5.86 | −0.948 | 102.8 | 28.88 | 1.90 |
| Pyridine·$IF_5$ | $C_6H_6$ | 15 | 24.55 | −1.713 | 415.0 | 43.24 | 4.19 |
| Pyridine·$IF_5$ | $C_6H_6$ | 25 | 30.99 | −2.246 | 505.7 | 43.24 | 4.56 |
| 2-Fluoropyridine·$IF_5$ | $C_6H_6$ | 15 | 38.24 | −2.432 | 601.0 | 42.95 | 5.13 |
| 2-Fluoropyridine·$IF_5$ | $C_6H_6$ | 25 | 35.93 | −2.486 | 578.8 | 42.95 | 5.12 |
| Dioxane·$IF_5$ | $C_6H_6$ | 15 | 20.75 | −2.870 | 336.7 | 40.85 | 3.73 |
| Dioxane·$IF_5$ | $C_6H_6$ | 25 | 20.06 | −2.650 | 338.5 | 40.85 | 3.81 |
| Dioxane·$IF_5$ | $C_6H_6$ | 35 | 18.51 | −1.980 | 338.1 | 40.85 | 3.87 |
| Trifluoroacetic anhydride·$IF_5$ | $C_6H_6$ | 15 | 22.54 | −3.310 | 393.2 | 40.89 | 4.08 |
| Trifluoroacetic anhydride·$IF_5$ | $C_6H_6$ | 25 | 21.15 | −3.320 | 380.0 | 40.89 | 4.07 |
| 2-Methylpyrazine·$IF_5$ | $C_6H_6$ | 15 | 26.81 | −2.560 | 433.2 | 49.16 | 4.26 |
| 2-Methylpyrazine·$IF_5$ | $C_6H_6$ | 25 | 25.95 | −2.530 | 433.8 | 49.16 | 4.33 |
| 2-Fluoropyridine·ICl | $CCl_4$ | 25 | 30.35 | −0.127 | 535.9 | 43.65 | 4.90 |
| 2-Chloropyridine·ICl | $CCl_4$ | 25 | 54.35 | −0.236 | 926.0 | 48.68 | 6.55 |
| 3-Fluoropyridine·ICl | $CCl_4$ | 25 | 51.14 | −0.258 | 869.6 | 43.65 | 6.35 |
| 3-Chloropyridine·ICl | $CCl_4$ | 25 | 50.40 | −0.194 | 863.4 | 48.68 | 6.31 |
| Dioxane·ICl | Dioxane | 25 | 22.83 | −1.420 | 365.9 | 41.92 | 3.98 |
| 2-Fluoropyridine·IBr | $CCl_4$ | 25 | 33.26 | −0.278 | 585.1 | 46.55 | 5.13 |
| 2-Chloropyridine·IBr | $CCl_4$ | 25 | 44.85 | −0.374 | 773.0 | 51.58 | 5.94 |
| 3-Fluoropyridine·IBr | $CCl_4$ | 25 | 38.79 | −0.335 | 673.0 | 46.55 | 5.53 |
| 3-Chloropyridine·IBr | $CCl_4$ | 25 | 40.39 | −0.330 | 702.3 | 51.58 | 5.64 |
| 3-Bromopyridine·IBr | $CCl_4$ | 25 | 42.66 | −0.500 | 739.9 | 54.48 | 5.79 |
| Dioxane·IBr | Dioxane | 25 | 10.95 | −1.567 | 201.9 | 44.82 | 2.77 |
| $(Pyridine)_2$·$HgI_2$[a] | $C_6H_6$ | 25 | | | | 66.20 | 4.88 |
| 4-Chloropyridine·IBr | $CCl_4$ | 25 | 36.93 | −0.331 | 645.9 | 51.58 | 5.39 |

[a] Calculated as a three-component system assuming dissociation into pyridine plus pyridine·$HgI_2$ in solution; V. V. Zapolskii, *State Inst. Tobacco Invest. (USSR), Bull.*, **81**, 113 (1931).

rate of cooling was controlled by varying the pressure in the partially evacuated air-space and also the temperature of the cooling bath in which the cell was immersed. Temperatures were measured to ±0.01° with a copper–constantan thermocouple calibrated at a series of check points. The method of temperature measurement has been described.[10]

**Absorption Spectra.**—These were measured with a Beckman DK-2 spectrophotometer using capped quartz cells. The technique for determination of dissociation constants of complexes is a standard procedure.[3]

## Results

Some of the crystalline molecular complexes prepared in this work apparently have not been described previously. These compounds, and certain of their properties, are listed in Table I.

White crystalline complexes of iodine pentafluoride with diethyl ether and with quinoline were prepared. Less stable complexes of iodine pentafluoride with isopropyl ether (dec. −30°), pyrazine, 2-methylpyrazine, and ethylene oxide also were prepared at low temperatures. The quinoline–iodine pentafluoride complex first prepared was a tan solid, m.p. ≃ 100°. Remelting or addition of carbon tetrachloride gave a hard white crystalline solid, m.p. 170°. Iodine pentafluoride reacted rapidly with triethylamine, N,N-dimethylaniline, N-methylaniline, piperidine, tetrahydrofuran, and trioxane; no complexes with these electron donors were prepared. Bromine trifluoride reacted rapidly even with solid pyridine at −42° and no stable crystalline complexes of this halogen fluoride were found.

The slopes $a$ and intercepts $\epsilon_1$, and the slopes $b$ and intercepts $v_1$, of the plots of the dielectric constants and specific volumes of the solutions of each compound are shown in Table II. The molar polarizations $P_2$ and dipole moments $\mu$ (assuming no dissociation of the complex) also are shown.

The solid–liquid diagrams for the systems pyridine–iodine pentafluoride and dioxane–iodine pentafluoride are shown in Fig. 1 and 2, respectively. The experimental points are joined by solid lines. The dashed lines represent the probable form of the missing parts of the diagram which we were not able to fill in experimentally. No analyses of the solid phases were made but it is assumed that solid solutions are not formed.

The equilibrium constants for the dissociation of the molecular complexes into components were computed in each case from the absorption spectra of a series of mixtures of varying composition in carbon tetrachloride solution at 25°. The spectra

TABLE III

ABSORPTION SPECTRA AND DISSOCIATION CONSTANTS FOR SOME MOLECULAR COMPLEXES AT 26°

| Compound | $\lambda_{max}$, mμ | $a$[a] | Isosbestic point, mμ | $K_D$ |
|---|---|---|---|---|
| 2-Chloropyridine·ICl | 336 | 217 | 396 | $2.0 \times 10^{-4}$ |
| 3-Chloropyridine·ICl | 302 | 727 | 392 | $1.2 \times 10^{-5}$ |
| 4-Chloropyridine·ICl | 300 | 604 | 389 | $4.8 \times 10^{-7}$ |
| 2-Fluoropyridine·ICl | 335 | 246 | 397 | $1.7 \times 10^{-4}$ |
| 2-Fluoropyridine·$I_2$ | 440 | 700 | 484 | 1 |

[a] $a$ is the molar absorbancy index; the path length of the cells was 1 cm. and the concentrations were expressed in moles/l.

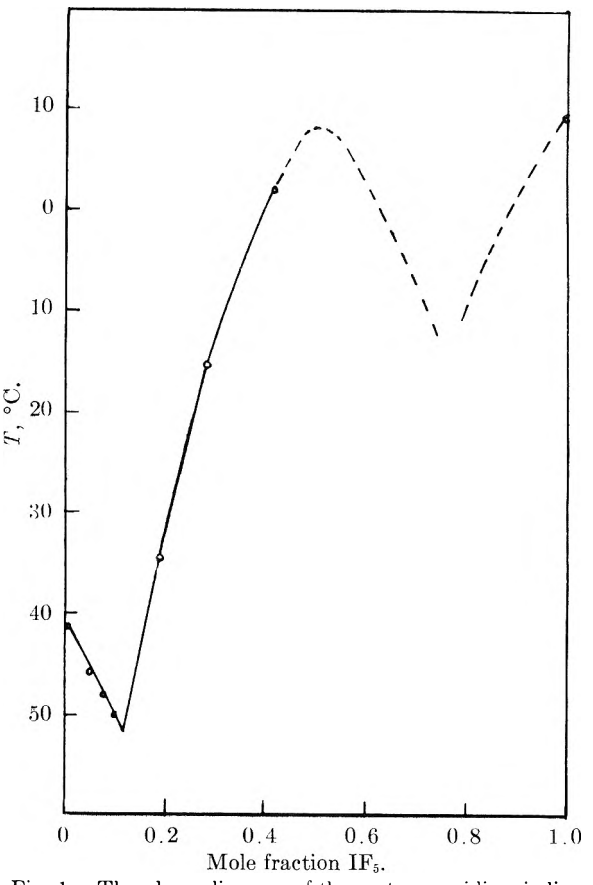


Fig. 1.—The phase diagram of the system pyridine–iodine pentafluoride. The circles are experimental points and are joined by solid lines. The dashed lines indicate the authors' conception of the remaining portion of the diagram.

covered a wave length range 250–700 mμ and for each a well defined isosbestic point[3] was observed. The results are summarized in Table III, which gives the wave length of the absorption maximum of the complex, its molar absorbancy index, the wave length of the isosbestic point, and the measured equilibrium constant (neglecting activity coefficients) for several complexes.

The complexes of iodine pentafluoride are of particular interest. The phase diagrams show that the 1:1 complexes are not particularly stable and in the case of the dioxane·$2IF_5$ complex it is not certain whether the curve shows a true maximum at the 1:2 ratio or merely a peritectic point; the 1:2 compound dissociates into the 1:1 compound and iodine pentafluoride when dried under reduced pressure. Although the solid phases were not analyzed, the eutectic points appear normal. Solutions of the complexes in benzene are relatively stable, whereas pure iodine pentafluoride attacks benzene readily; hence, molecular complexes offer a possible means of moderating the reactivity of halogen fluorides.

The equilibrium constants determined here, and those previously reported in the literature,[8] show that the stability of the pyridine·ICl complex is reduced by substitution of electron-withdrawing groups on the pyridine ring. The stability of the chloropyridine complexes decreases in the order 4-chloro > 3-chloro > 2-chloro as would be expected

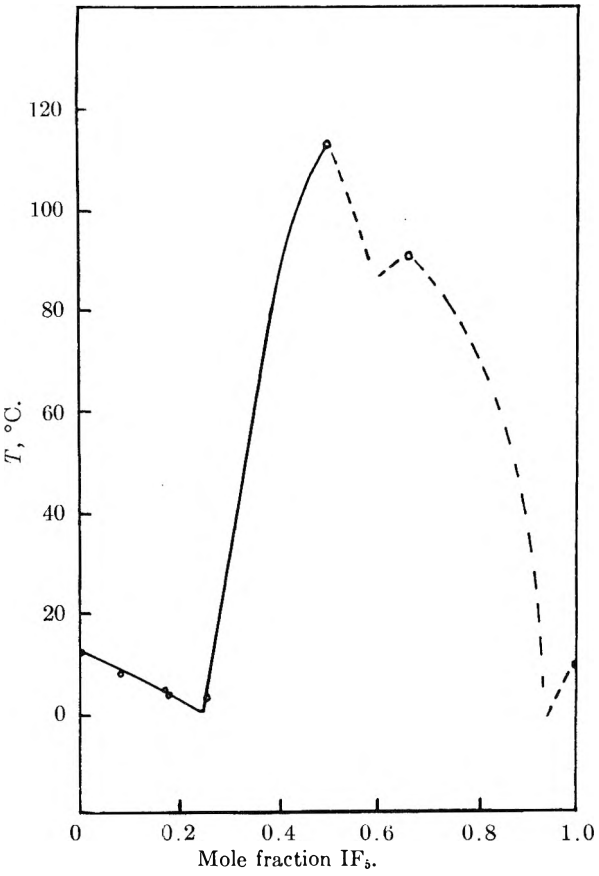


Fig. 2.—The phase diagram for the system dioxane–iodine pentafluoride. The experimental points (circles) are joined by solid lines whereas dashed lines are used to sketch in the authors' conception of the remainder of the diagram.

from the increasing magnitude of the inductive effect as chlorine approaches nitrogen. The difference between the stabilities of the 2-fluoropyridine and 2-chloropyridine complexes is small. The dissociation constants are sufficiently low so that the dissociation can be neglected in computing the electric moments of the complexes from solution measurements.

The electric moments of the complexes should give some indication of their electronic structures. The atomic arrangement in the solid dioxane–iodine and pyridine–iodine monochloride complexes has been studied[12] and the O–I–I and N–I–Cl groups found to be linear with the halogen atoms in the same plane as the ring, the interhalogen distance nearly the normal covalent value, and the O–I or N–I distance considerably longer than the sum of the covalent radii. We assume this arrangement in the compounds studied here and assume that the principal resonance structures for the complexes (in solution in non-polar solvents) are similar to I, II, and III. Structure II requires one extra stable orbital on the iodine atom, which presumably is available. We will, however, neglect II in estimating the extent of charge transfer. The electric moment of I should be 1.50, the vector sum of the moments of dioxane, zero, and iodine monochloride, 1.5. The observed electric moment

(12) O. Hassel and J. Hvoslef, *Acta Chem. Scand.*, **8**, 873 (1954); **10**, 138 (1956); O. Hassel, *Mol. Phys.*, **1**, 241 (1958).

TABLE IV

VALUES OF FRACTIONAL ELECTRON TRANSFER IN MOLECULAR COMPLEXES ESTIMATED FROM DIELECTRIC POLARIZATIONS

| Compound | μ obsd. (25°) | μ calcd. (no electron transfer) | Fractional electron transfer[a] |
|---|---|---|---|
| Dioxane·ICl | 3.98 | 1.49 | 0.11 |
| Dioxane·IBr | 2.77 | 1.21 | .06 |
| Dioxane·$IF_5$ | 3.81 | 2.18 | .07 |
| Pyridine·$IF_5$ | 4.56 | 4.23 | .02 |
| 2-Fluoropyridine·$IF_5$ | 5.12 | 5.15 | 0 |
| 2-Methylpyrazine·$IF_5$ | 4.33 | 2.11 | .11 |
| 2-Fluoropyridine·ICl | 4.90 | 4.64 | .01 |
| 3-Fluoropyridine·ICl | 6.35 | 3.42 | .13 |
| 2-Chloropyridine·ICl | 6.55 | 4.68 | .08 |
| 3-Chloropyridine·ICl | 6.31 | 3.43 | .13 |
| 2-Fluoropyridine·IBr | 5.13 | 4.36 | .03 |
| 3-Fluoropyridine·IBr | 5.53 | 3.14 | .10 |
| 2-Chloropyridine·IBr | 5.94 | 4.40 | .07 |
| 3-Chloropyridine·IBr | 5.64 | 3.15 | .11 |
| 4-Chloropyridine·IBr | 5.39 | 2.05 | .14 |
| 3-Bromopyridine·IBr | 5.79 | 3.13 | .11 |

[a] Calculated moment for complete transfer of one electron is taken as 4.8 times the distance (in Å.) from the nitrogen or oxygen atom of the complex to the halogen atom of III (see text) with the negative charge. The contribution of the rest of the donor or acceptor molecule is neglected since it would normally be less than 20% of the total and would be altered in an unknown way by the charge redistribution in going from separated molecules to the complex.

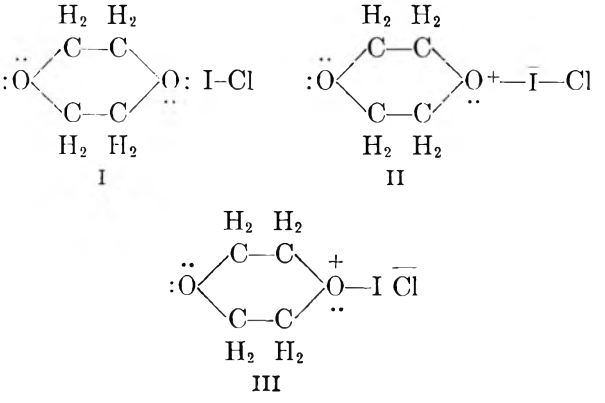


of the complex, 3.98, will be considered to result from some contribution of III to the ground state of the molecule. The fraction of an electronic charge transferred from nitrogen to iodine by resonance between I and III is $(3.98-1.5)/4.8 \times 4.90 = 0.11$, where the O–I and I–Cl distances of 2.60 and 2.30 Å. are those reported in an X-ray study of the solid complex, and the moment of III is taken as the product of the oxygen–chlorine distance and the electronic charge. One may then, at least for comparison purposes, assign the O–I bond an order of 0.11. The bond number $n$ for the O–I bond computed from Pauling's[13] equation for fractional bonds and the observed internuclear distance is 0.1. Similar calculations have been made for the remaining compounds and are given in Table IV. Although, because of the approximations made, they are only estimates, they do

(13) L. Pauling, "The Nature of the Chemical Bond," 3rd edition. Cornell University Press, Ithaca, N. Y., 1960.

give some indication of the electronic structure of the complexes. In general, the complexes with the lowest dissociation constants are those with the highest bond order for the dative bond from iodine to oxygen or nitrogen, but the number of available dissociation constants is too small for any detailed analysis of these relationships.

The fractional electron transfer is larger for the ICl complex than for the corresponding IBr complex, as would be expected from the greater electronegativity of chlorine. Although the $IF_5$ complex shows a smaller fractional electron transfer than the corresponding ICl complex, the geometry is considerably different. Presumably the nitrogen occupies roughly the sixth corner of an irregular octahedron about iodine and both steric and electronic factors may lengthen the I–N bond and weaken the complex relative to the ICl complex.

# THE VANADIUM–VANADIUM CARBIDE SYSTEM[1]

BY E. K. STORMS AND R. J. MCNEAL[2]

*Los Alamos Scientific Laboratory, Los Alamos, New Mexico*

*Received January 25, 1962*

The solid portion of the V–VC phase diagram has been determined above 1000°. The following characteristic temperatures were measured: the melting point of vanadium metal at 1888 ± 10°, a eutectic melting between $VC_{0.09}$ and $VC_{0.33}$ at 1630°, peritectic melting of the $V_2C$-phase between $VC_{0.56}$ and $VC_{0.60}$ at 2165°, and peritectic melting of the VC-phase beginning at $VC_{0.85}$ and extending beyond $VC_{1.0}$ at 2650°. The VC-phase does not extend to $VC_{1.00}$, as has been assumed in the past, but terminates at $VC_{0.88}$ at 1000° and moves to lower carbon contents as the temperature is increased. The variation of lattice parameter of the VC-phase over its homogeneity range was determined. Evidence for an additional phase in the region between $V_2C$ and VC is shown. Vanadium evaporates preferentially from all compositions investigated.

## Introduction

Vanadium shares with niobium and tantalum the formation of two carbides, a hexagonal configuration having the nominal formula $V_2C$ and a face-centered-cubic (NaCl-type) structure which will be referred to as VC. Both of these compounds exist over a range of composition. Gurevich and Ormont[3] have compiled a rather complete bibliography on the subject and may be consulted for information regarding earlier work. As yet, however, a complete phase diagram for this system has not been reported. It is the purpose of this paper to show the relationship between the solid phases which exist in the region between vanadium metal and $VC_{1.00}$, and in the temperature interval between 1000° and the melting point of the material.

## Experimental

Vanadium metal[4] and AUC graphite (99.4% carbon) were used as starting materials. The original 20 mesh metal was made brittle by several methods in order that a 325 mesh product could be obtained. When pure metal was desired, the stock vanadium was hydrided by slow cooling from 800° in hydrogen and the hydride was reduced to 325 mesh in a steel mortar. Iron was removed by magnetic separation or by dilute HCl, after which the powder was dehydrided *in vacuo* at 600°. The impurities remaining in the metal after this treatment are listed in Table I. To prepare starting material for the carbide samples, the stock metal was mixed with outgassed graphite, reacted in a graphite crucible *in vacuo*, ground to 325 mesh, and again heated in a graphite crucible until essentially no additional gas was evolved (to $5 \times 10^{-6}$ torr.). As with the hydride, iron was removed by reflux extraction with constant boiling HCl. Further heating produced a dried and uniform product. This powder then was mixed with either powdered vanadium or graphite, in appropriate amounts, to give the desired composition. Each mixture was cold-pressed into a plug $^3/_8$ in. in diameter and $^3/_4$ in. long. A hole was drilled into each end, one for black-body temperature measurement ($0.040 \times ^3/_8$ in.) and the other to take a 0.060 in. diameter Ta or W support rod. The absence of a crucible eliminated possible contamination and allowed rapid removal of CO from the sample environment.

TABLE I

IMPURITIES CONTAINED IN THE VANADIUM METAL

| Element | Sample 1 | Sample 2 |
|---|---|---|
| Oxygen | 0.33 wt. % | 0.51 wt. % |
| Nitrogen | 0.078 | 0.12 |
| Hydrogen | 25 p.p.m. | 75 p.p.m. |
| Carbon | 90 p.p.m. | .... |
| Boron | <20 p.p.m. | 35 p.p.m. |
| Silicon | 900 p.p.m. | 900 p.p.m. |
| Chromium | 70 p.p.m. | 70 p.p.m. |
| Molybdenum | <180 | 360 p.p.m. |
| Iron | 180 p.p.m. | 1800 p.p.m. |

Li, Be, B, Na, Mg, Al, Ca, Ti, Mn, Co, Ni, Cu, Zn, Sr, Zr, Ag, Sn, Ba, Pb, and Bi below the limit of detection or 20 p.p.m.

Sample 1 was purified by exposure to HCl for 2 hr. Sample 2 was subjected only to magnetic separation.

A typical carbide sample contained less than 500 p.p.m. each of oxygen and nitrogen, in addition to the non-volatile elements contained in the vandium metal.

Heating was done in an induction field using an eddy-current concentrator.[5] High-speed vacuum systems, capable of holding the pressure below $1 \times 10^{-5}$ torr., were used.

Melting points were obtained as follows: the plug was outgassed *in vacuo* until the pressure had dropped below about $5 \times 10^{-5}$ torr., and ~1 atm. of He was added if the composition was above $VC_{0.35}$; otherwise heating was continued *in vacuo*. The temperature was raised quickly to within about 100° of the melting point, then in roughly 20° steps until a liquid phase was observed. This was seen both as a change in brightness of the surface and as a change in the hole as it filled with liquid. The method gives an upper limit to the solidus temperature, but, because very little liquid is needed to detect melting, the error is small. Furthermore, sufficient melt is formed to overshadow premelting of possible

(1) This work done under the auspices of the Atomic Energy Commission.

(2) Guest scientist during the L.A.S.L. Summer Program.

(3) M. A. Gurevich and B. F. Ormont, *Russ. J. Inorg. Chem.*, **2**, 1566 (1957).

(4) High purity metal was furnished by Union Carbide Metals Company, Niagara Falls, New York.

(5) Drawings of an early design may be obtained from Cooper-Trent Blueprint and Microfilm Corporation, 2701 Wilson Blvd., Arlington, Va., Drawings 26Y-70250-1 to 32.

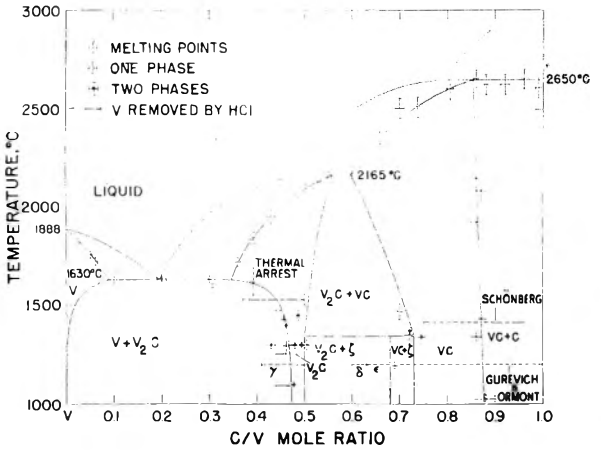


Fig. 1.—Phase diagram for the vanadium–vanadium carbide system: *, average of 2 samples beyond $VC_{1.2}$.

impurity phases within the grain boundaries, and thus eliminates the large error associated with the incipient melting technique. Reproducibility was within 10°, in most cases, and within 25° at the highest temperatures.

Temperature was measured with a Pyro optical pyrometer which was calibrated by observing the melting of the following elements: Ta, 2996°; Rh, 1964°; Pt, 1773°; Co, 1495°, and Au, 1063°. Each of these metals was better than 99% pure. In each case the melting points were observed though the same optical system that was used during the melting of the vanadium carbide samples.

After the heating or melting operation, the samples were reduced to 325 mesh, cleaned of iron in some cases, and analyzed for vanadium and total carbon. Free carbon, oxygen, nitrogen, and iron also were determined when appropriate. Initially, vanadium was determined by ignition at 800° in oxygen. This method, however, gave values that were too low, so a dissolution and titration method was adopted.[6] Total carbon content was obtained by ignition at 1000° in oxygen, and free carbon content was obtained by $HNO_3$ + HF dissolution of the vanadium carbide.[7]

X-Ray patterns were made in a 114.6 mm. Debye–Scherrer camera using Cu radiation ($\lambda_{\alpha 1}$ 1.54051, $\lambda_{\alpha 2}$ 1.54433). Because fluorescence was troublesome, a 0.001-in. thick nickel sheet was placed directly over the film in the camera rather than in the beam. Although the exposure time was increased, very clean, high contrast films resulted. Lattice parameters were calculated from the back reflection lines by applying the least-squares extrapolation of Cohen[8] as modified by Hess.[9] An IBM 704 made this calculation and obtained a standard deviation for each parameter. This error value is associated mainly with the diffuseness of the lines from which the calculations were made.

## Results and Discussion

The phase diagram for the vanadium–vanadium carbide system is shown in Fig. 1. Beginning on the left, there is a solid solution of carbon in vanadium, near the center there is a region in which $V_2C$ is stable, and on the right VC exists as a single phase. Each of these regions will be discussed separately.

**V-Phase.**—Vanadium metal dissolves as much as 2.21 wt. % carbon at the eutectic temperature. However, the solubility drops rapidly as the temperature is lowered. An effort was made to detect the phase boundary at $VC_{0.05}$ by thermal arrest but this was unsuccessful. Schönberg[10] and Gurevich and Ormont[3] found that the solubility of carbon in vanadium is less than $VC_{0.01}$ at about 1000°. A dashed line has been drawn on Fig. 1 to be consistent with these results.

During the course of this work, the melting point of pure vanadium was determined. The details of this measurement will appear later in the paper.

**$V_2C$-Phase.**—Between $VC_{0.09}$ and $VC_{0.35}$, eutectic melting is observed at 1630 ± 20°. No information about the eutectic composition was obtained in this work. Rostoker and Yamamoto[11] reported a eutectic composition somewhere between $VC_{0.17}$ and $VC_{0.22}$, and a eutectic melting temperature of 1650°.

The phase boundary between $V_2C$ and $V_2C$ + V has been determined in three separate ways. In the first, thermal arrest techniques were used, and in the second, the vanadium metal was chemically removed from the two-phase samples and the remainder analyzed to obtain the composition of the remaining $V_2C$, thus the phase boundary. The usual technique of bracketing the boundary was employed as the third method. The appearance of the (110) line of vanadium, the (101) line of $V_2C$, and the (111) and (200) lines of VC indicated the presence of the respective phases.

A bare plug of $VC_{0.39}$ was allowed to cool from 1650° *in vacuo* and the rate of cooling was observed by photometric monitoring of the emitted light.[12] The precipitation of vanadium was observed as a break in the smoothly changing slope of the trace on an oscilloscope screen. Figure 2a shows a reproduction of this trace. At this composition, the precipitation of vanadium occurs above 1614°. (This sample eventually was melted at 1845° by the method described previously.) Because this temperature is near the eutectic melting point, it might be argued that the break in the cooling curve actually was due to the disappearance of a liquid phase. Several studies were made to dispel this notion. A plug of $VC_{\sim 0.40}$ was first heated to 1750° several times while the transition was observed, then annealed at 1440° for 1 hr. No sign of melting could be found by metallographic examination, although precipitation of a phase *within* the grains was clearly evident. Another plug of the same composition was melted in He at 1868° by the method described previously. Examination showed that a small amount of liquid had formed. It also was observed that if the temperature was raised even 25° above the melting point, the plug would quickly topple from the support rod. In order to observe both the melting and precipitation of vanadium by thermal arrest techniques, the starting powder was placed in a graphite crucible and melted. The cooling curve (Fig. 2b) indicates that the last liquid apparently froze at about 1930°. This is higher than the melting point of the bare plug because carbon was absorbed from the crucible into the melt. Upon cooling, another break (Fig. 2c) was observed at about 1515°. Both of these temperatures are somewhat lower than the actual transi-

(6) Vanadium was determined by an adaptation of the method of G. H. Walden, Jr., L. P. Hammett, and S. M. Edmonds, *J. Am. Chem. Soc.*, **56**, 57 (1934).

(7) O. H. Kriege, "The Analysis of Refractory Borides, Carbides, Nitrides and Silicides," Los Alamos Scientific Laboratory Report, LA-2306, 1959.

(8) M. I. Cohen, *Rev. Sci. Instr.*, **6**, 68 (1935); *Z. Krystallogr.*, **94A**, 288 (1936); **94A**, 306 (1936).

(9) J. B. Hess, *Acta Cryst.*, **4**, 209 (1951).

(10) N. Schönberg, *Acta Chem. Scand.*, **8**, 624 (1954).

(11) W. Rostoker and A. Yamamoto, *Trans. ASM*, **46**, 1136 (1954).

(12) G. N. Rupert, "An Apparatus for Observing Phase Transitions of Incandescent Materials," to be published.

tions because of the rapid cooling rates employed. For comparison, the thermal arrest produced by the eutectic is shown in Fig. 2d. In view of these observations, it is clear that the heat effect near 1600° does not involve a liquid phase. Two other samples, having compositions of $VC_{0.43}$ and $VC_{0.48}$, were examined by thermal analysis and showed no heat effect below 1700°.

The second method, the extraction of vanadium metal from a two-phase sample, was carried out as follows: Five samples, listed in Table II, were heated for times sufficient to produce equilibrium. The absence of a third phase and the presence of sharp lines on the diffraction pattern were used as criteria. After reduction to 325 mesh, the samples were exposed to constant boiling HCl in a Soxhlet extractor in order to remove the vanadium metal. The composition of the $V_2C$-phase then was determined by analysis. Three samples of $VC_{0.44}$, heated between 1093 and 1475°, were treated in this manner. The results are shown by arrows on Fig. 1 with the head of the arrow at the final, corrected composition.[13] Powder patterns taken afterward showed no vanadium lines. However, to the extent that all of the metal was not removed, this method gives a lower limit to the phase boundary.

TABLE II

RESULTS OF HCl EXTRACTION PERFORMED ON TWO-PHASE SAMPLES

| Compn. before extraction C/V | Heating temp., °C. | Heating time, hr. | Extraction time, hr. | Cor. compn. after extraction C/V |
|---|---|---|---|---|
| 0.31 | Melted *in* He | | 6 | 0.42 |
| .30 | Melted in *vacuo* | | 4.5 | .44 |
| .44 | 1475° | 2.7 | 6 | .45 |
| .44 | 1254° | 22.0 | 4.5 | .46 |
| .44 | 1093° | 97.0 | 4.5 | .47 |

| Compn. before extraction C/V | Extraction time, hr. | Compn. after extraction C/V |
|---|---|---|
| 0.480 | 4.5 | 0.497 |
| 0.480 | 22 | 0.525 (total)[a] |

[a] Contains 0.17 wt. % free carbon.

In addition to the above methods, the boundary was bracketed between single- and two-phase samples. The one-phase points are designated by an open circle and are listed in Table III.

In order that the presence of vanadium metal could not be attributed to unreacted starting material, a sample of $VC_{0.43}$ was partially melted. This treatment should lead to a rapid dissolution of the metal. Upon cooling, the sample contained vanadium metal which could have resulted only from its precipitation during cooling. Thus, the V–$V_2C$ boundary lies to the right of $VC_{0.43}$ below the breakaway temperature.

(13) A correction had to be applied to allow for the small amount of vanadium removed from the $V_2C$-phase. In order to establish the amount of this correction, two samples, each having a composition within the single-phase region, were treated as shown in Table II. It is interesting to note that $V_2C$ dissolves in HCl leaving a carbon residue.

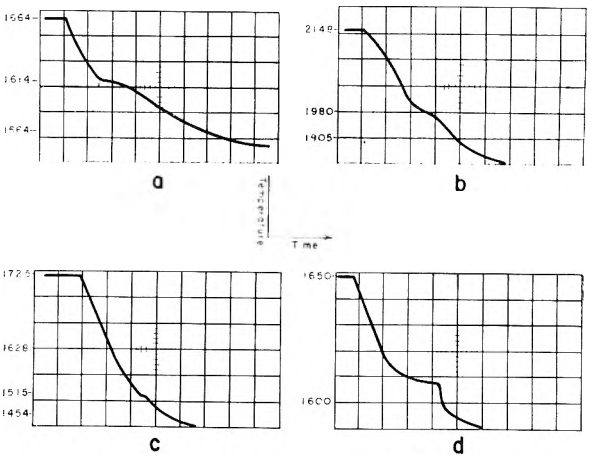


Fig. 2.—Cooling rate studies. Time base: 2 sec./division. (a) $VC_{0.39}$, bare plug, cooled *in vacuo*; (b) $VC_{0.40+}$, melted in a graphite crucible under Ar; (c) $VC_{0.40+}$, after melting, cooled through the low temperature transition; (d) V–$V_2C$ eutectic melted in a graphite crucible under vacuum.

Because it is possible that the composition of the $V_2C$-phase could have changed during cooling, an effort was made to learn at what temperature the phases would cease to be in equilibrium during normal cooling. This temperature will be referred to as the breakaway temperature. Two samples each having a composition of about $VC_{0.30}$ were melted, one in He and the other *in vacuo*. After the metal was removed by HCl, the composition of the $V_2C$-phase was found to be $VC_{0.42}$ when the sample cooled rapidly in He, and $VC_{0.44}$ when the material was cooled more slowly *in vacuo*. Thus, these are the lowest $V_2C$ compositions that can be obtained under the respective conditions and correspond to respective temperatures of about 1580 and 1530°. This shows that the vanadium extraction and X-ray analysis methods are valid so long as the heating temperature is kept below this region.

The results of Schönberg,[10] and Gurevich and Ormont[3] indicate that the phase boundary should lie at $VC_{0.37}$ and $VC_{0.41}$, respectively. In neither case was the temperature range given over which these results should apply, although Schönberg did state that he heated at 1900°. His results therefore are placed on Fig. 1 at the breakaway temperature. Nevertheless, this discrepancy can be understood if the techniques used are considered. Schönberg obtained his value by plotting lattice parameter *vs.* composition. Three points were used to define the slope in the single-phase region even though the lattice parameter of one of these points was not significantly different from the value obtained when vanadium metal was present. Allowing for reasonable errors in lattice parameters and analysis, his data can be made consistent with the work reported here. Gurevich and Ormont did not use this technique but their samples were reported to contain a large amount of oxygen, up to 5.6 wt. %. Apparently no effort was made to correct for this impurity. Most early work on this system, of which there is a considerable amount, is invalid for this very reason, as Gurevich and Ormont have stated so well in their paper.

**ζ-Phase.**—Samples having a composition within the two-phase field showed additional lines in the

TABLE III

SUMMARY OF CRITICAL SAMPLES

| Final compn. C/V | V + C, wt. % | Impurities, wt. % | Heating temp., °C. | Heating time, hr. | X-Ray phases |
|---|---|---|---|---|---|
| 0.43 ± 0.01 | 97.99 | 1.0% Fe, 500 p.p.m. Si | 1954 melted | | V + $V_2C$ |
| .43 ± .01 | 99.1 | 0.2% Fe, 500 p.p.m. Si, 100 p.p.m. Cr | 1302 | 62 | V + $V_2C$ |
| .457 ± .004 | 98.96 | 0.11% N, 0.70% O 0.2% Fe | 1433 | 6 | V + $V_2C$ |
| .462 ± .006 | 98.91 | 0.13% N, 0.94% O | 1300 | 24 | V + $V_2C$ |
| | | | 1400 | 23 | $V_2C$ |
| .478 ± .004 | 99.25 | 0.12% N | 1100 | 72 | $V_2C$ |
| .48 ± .01 | 99.01 | 0.10% Fe, 10 p.p.m. N, 200 p.p.m. Si | 1300 | 114 | $V_2C$ |
| .49 ± .004 | 99.11 | 0.11% N | 1300 | 23 | $V_2C$ |
| .505 ± .004 | 98.48 | 0.15% N | 1300 | 12 | $V_2C$ + VC |

| Combined carbon C/V | V + C, wt. % | Impurities, p.p.m. | $a_0$, Å. | Temp., °C. | Time, hr. | Free C, wt. % |
|---|---|---|---|---|---|---|
| 0.88 | 99.92 | 300 Fe | 4.1663 ± 0.0006 | 1027 | 200 | 5.87 |
| .86 | 100.09 | ... | 4.1662 ± .0003 | 1340 | 30 | 4.37 |
| .87 | 99.81 | 270 O 140 N 500 Fe | 4.1660 ± .0008 | 1431 | 18 | 5.76 |
| .86 | 99.83 | 130 N | 4.1665 ± .0001 | 1925 | 65 | 3.35 |
| .87 | 99.78 | ... | 4.1664 ± .0006 | 2085 | 1 | 1.44 |
| .86 | 99.84 | ... | 4.1639 ± .0023 | 2148 | 1 | 0.00 |
| .85 | 99.67 | 300 O 500 Fe | 4.1633 ± .0005 | Melted in He | | 0.12 |
| .84 | 98.66 | 205 N | 4.168 ± .001 | Arc melted in Ar | | 3.08 |

| Combined carbon, C/V | V + C, wt. % | Impurities, p.p.m. | $a_0$, Å. | Temp., °C. | Time, hr. | X-Ray phases |
|---|---|---|---|---|---|---|
| 0.72 | | | 4.1305 | 1348 | 22 | VC + $V_2C$ |
| .722 | 99.7 | 393 N 80 O 400 Fe | 4.1288 ± 0.0005 | 1370 | 14.5 | VC + $V_2C$ |
| .73 | 99.1 | 1200 N 4800 O | 4.1350 ± .0006 | 1100 | 23 | VC |
| .75 | 99.5 | 500 O | 4.1352 ± .0004 | 1340 | 69 | VC |

powder patterns besides those due to VC and $V_2C$. These are listed in Table IV. In addition, there is a break in the lattice parameter *vs.* heating temperature curve (Fig. 3) at 1344° suggesting the formation of another phase below this temperature. Samples heated above this temperature also contained this phase, presumably because of its formation during cooling. However, heating the same $VC_{0.69}$ sample for 90 hr. at 1235° and 141 hr. at 850° or a different sample of the same composition at 1190° for 68 hr. did not bring about equilibrium. This observation certainly will warrant further study. It is sufficient at this time to observe that the powder pattern produced by this phase is very similar to that produced by the zeta-phase reported by Lesser and Brauer[14] in the Ta–C system and is definitely not the face-centered-cubic $\delta$-phase reported by Gurevich and Ormont. The possibility that the $\zeta$-phase is impurity-induced has not been eliminated. A hypothetical relationship between the phases in this region is shown in Fig. 1. Because this phase is so tentative, no effort has been made to modify the phase boundaries in this region. Incorporation of the zeta-phase is meant to summarize, graphically, the experimental observations, not to state a conclusion.

**VC-Phase.**—The region in which VC is stable as a single phase begins at $VC_{0.60}$ at the peritectic temperature and approaches $VC_{0.74}$ at lower temperatures. The position of this boundary lies to the right of the two-phase point at $VC_{0.72}$ and to the left of the single-phase point at $VC_{0.75}$. The position of the phase boundary also has been made consistent with Fig. 3 and 4. Above 1420° the phase boundary is drawn as a dashed line because the VC composition existing at the heating temperature cannot be retained by cooling *in vacuo*. This is demonstrated as follows (Fig. 3): Two-phase samples of indicated composition were heated *in vacuo* for the indicated times. Upon cooling, the lattice parameter of the VC-phase was found to be a function of heating temperature. Three other samples were heated to higher temperatures, two were cooled *in vacuo* and the other in He, as indicated in Fig. 3. By placing their lattice parameter on the figure it is possible to determine at what temperatures equilibrium ceased to be maintained, thus the breakaway temperature. Figure 3 also provides a sensitive criterion of whether a material contains

(14) R. Lesser and G. Brauer, *Z. Metallk.*, **49**, 622 (1958).

TABLE IV

POWDER PATTERN OF THE ZETA-PHASE

| Line | A[a] | B[b] | C[c] | D[d] | E[e] | $\sin^2\theta$ | I | Phase | *hkl* |
|---|---|---|---|---|---|---|---|---|---|
| 1 | 16.28 | ... | 17.50 | ... | 16.90 | 0.08248 | VVF | *f* | |
| 2 | 17.86 | 17.91 | 17.90 | 17.84 | 17.87 | .09416 | F | $V_2C$ | 100 |
| 3 | 18.11 | 18.07 | 18.12 | 18.39 | 18.10 | .09652 | VVF | *f* | |
| 4 | 18.92 | 18.90 | 18.87 | 18.84 | 18.89 | .10481 | VS | VC | 111 |
| 5 | 19.69 | 19.67 | 19.65 | 19.64 | 19.66 | .11319 | M | *f* | |
| 6 | 20.52 | 20.52 | 20.52 | 20.44 | 20.52 | .12287 | S | $V_2C$ | 101 |
| 7 | 21.24 | 21.22 | 21.22 | 21.24 | 21.23 | .13112 | M | *f* | |
| 8 | 21.97 | 21.95 | 21.92 | 21.89 | 21.94 | .13961 | VS | VC | 200 |
| 9 | 22.77 | 22.80 | 22.15 | 22.29 | 22.62 | .14793 | VF | *f* | |
| 10 | 24.35 | 24.37 | 24.40 | 24.44 | 24.39 | .17053 | F | *f* | |
| 11 | 25.60 | ... | 25.57 | ... | 25.57 | .18629 | VF | *f* | |
| 12 | 27.13 | 27.16 | 27.12 | 27.09 | 27.13 | .20795 | MW | $V_2C$ | 102 |
| 13 | 29.61 | 29.66 | 29.60 | 29.54 | 29.60 | .24398 | F | *f* | |
| 14 | 31.94 | 31.91 | 31.87 | 31.89 | 31.91 | .27941 | VVS | VC | 220 |
| 15 | 34.20 | 34.21 | 34.17 | 34.19 | 34.19 | .31578 | F | *f* | |
| 16 | 36.22 | 36.22 | 36.24 | 36.27 | 36.24 | .34948 | MW | $V_2C$ | 103 |
| 17 | 37.45 | 37.49 | 37.50 | ... | 37.49 | .37042 | F | *f* | |
| 18 | 38.32 | 38.24 | 38.20 | 38.19 | 38.22 | .38276 | S | VC | 311 |
| 19 | 38.70 | 38.74 | 38.65 | 38.69 | 38.70 | .39093 | W | *f* | |
| 20 | 38.95 | 38.97 | 38.95 | 38.94 | 38.95 | .39519 | MW | $V_2C$ | 112 |
| 21 | 39.48 | 39.47 | 39.50 | 39.49 | 39.49 | .40442 | F | $V_2C$ | 201 |
| 22 | 39.83 | 39.84 | 39.82 | 39.84 | 39.83 | .41025 | F | *f* | |
| 23 | 40.33 | 40.27 | 40.22 | 40.29 | 40.30 | .41834 | W | VC | 222 |

[a] $VC_{0.69}$ heated at 1540° for 1.25 hr. [b] Same sample heated at 1235° for 90 hr. [c] Same sample heated at 850° for 141 hr. [d] $VC_{0.67}$ heated at 1440° for 21 hr. [e] Weighted average of four films. [f] Zeta phase. Only lines which appeared on two films are included. Copper $K\alpha_1$(Ni filtered) radiation was used.

VC or VC + $V_2C$. All homogeneous, pure two-phase samples which have obtained equilibrium will fall on the line, single-phase samples will fall to the right of the line as does $VC_{0.75}$, and material which is not at equilibrium will be found in the region left of the line. The results of Schönberg,[10] when placed at the breakaway temperature, agree fairly well at this phase boundary. Schnell,[15] using pure materials heated at 1900°, placed the phase boundary at $VC_{0.74}$.

The VC–C phase boundary, rather unexpectedly, lies near $VC_{0.88}$ rather than at $VC_{1.00}$ as has been assumed in the past. This is sufficiently unusual that a clear summary of the evidence is called for. The following points are advanced to support this conclusion:

1. Six samples in which free carbon was detected by analysis were used to determine this boundary. One sample was heated for 200 hr. and another was melted. As can be seen from Table III, none of the materials has a composition higher than $VC_{0.88}$. These values are placed on Fig. 1 at the composition of the VC-phase as determined from chemical analysis.

2. The constant melting temperature between $VC_{0.85}$ (the VC-phase composition after melting) and $VC_{1.2}$ (the highest composition investigated) requires that two solid phases be present at the melting temperature.

3. Two samples were analyzed after they were melted, one in an arc furnace and the other as a plug using induction heating. The total conversion to the liquid phase and the rapid quenching after melting gives the arc melted sample particular importance, in that such treatment should hasten the reaction with carbon.

4. The presence of impurities might be blamed for this phenomenon. When analyzed, the amount

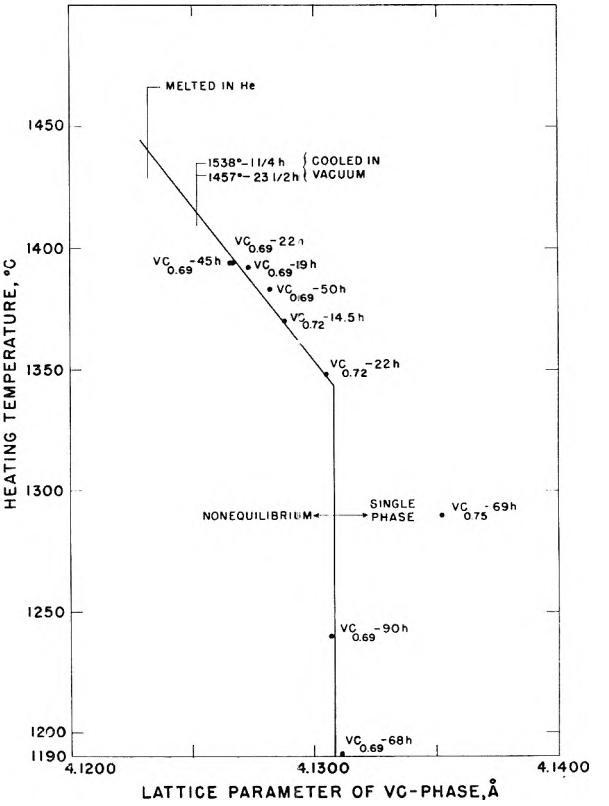


Fig. 3.—Relationship between heating temperature and the lattice parameter of the VC-phase.

(15) W. D. Schnell, "Carbonitride of Vanadium," Inaugural Dissertation, University of Freiburg, Freiburg im Breisgau, Germany, 1960.

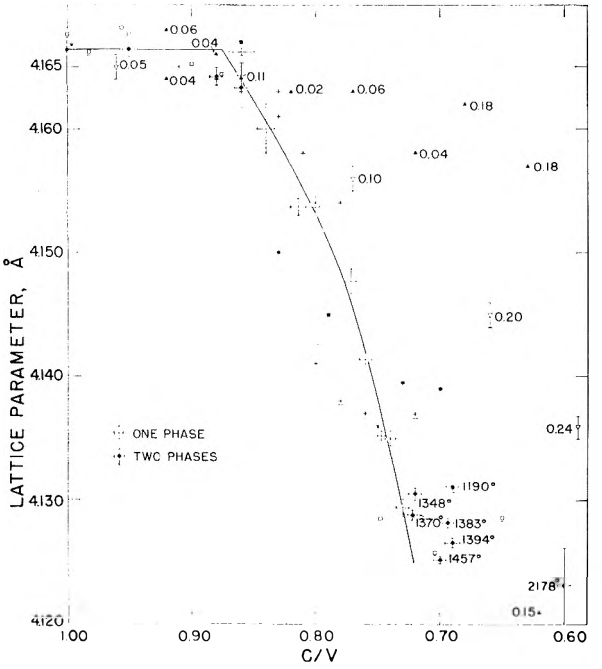


Fig. 4.—Lattice parameter of VC as a function of composition: ×, Schönberg[10]; ●, Ôsawa and Ôya[21]; ▲, Gurevich and Ormont[3], O/V molar ratio shown; ■, Dawihl and Rix[22]; ▽, Krainer and Konopicky[23], O/V ratio shown; □, single phase, ▣, two phase, Schnell[15]; +, ϵ-phase, ±, δ-phase, Alyamovskii, *et al.*[24]; * note: average of four values beyond $VC_{1.0}$.

of the major impurities (oxygen, nitrogen, iron, and silicon) was too low to have the necessary effect. Furthermore, the summation of V + C, even under the worst conditions, does not deviate sufficiently from 100% to allow undetected impurities or analytical errors to be blamed.

5. All recent investigators, except Schönberg,[10] have reported lattice parameters, within experimental error, of 4.166 Å. (see Fig. 4). Thus, there is no inconsistency in suggesting that a composition higher than $VC_{0.88}$ has never been prepared in spite of many reports to the contrary.

Schönberg[10] found that free carbon always was present in samples over $VC_{0.8}$ and that a large excess was needed to produce $VC_{0.96}$. He assumed that the inability to reach the 1:1 ratio was caused by slow reaction rates. In view of the limit at $VC_{0.88}$, it is probable that errors in the analysis for free carbon aggravated by its large excess (40 wt. %) were responsible for the high reported composition. Meerson and Krein,[16] while studying the formation of VC from $V_2O_3$ and carbon, could not obtain compositions higher than $VC_{0.90-0.92}$. Zhelankin, *et al.*,[17] during a study of the same reaction, obtained $VC_{0.96}$, for which a lattice parameter of 4.1663 Å. was reported.

Schnell,[15] after examining his data in light of Schönberg's conclusions, gave $VC_{0.92}$ as the upper limit of the phase boundary. An average maximum lattice parameter of 4.167 Å. can be calculated from his data.

VC melts peritectically at 2650° rather than having a melting point maximum as is true of NbC and TaC. The early values were obtained so long ago and under conditions that a host of impurities could have been present. Ruff and Martin,[18] by melting compositions between 1.15 and 19.1% C, obtained a steep rise from the eutectic to a flat maximum at 2750° for $VC_{1.0}$. Friederich and Sittig,[19] using VC prepared from $V_2O_3$ and C, claimed 2830°. The other melting points which they report are generally higher than the presently accepted values. Engelke, *et al.*,[20] using arc melting techniques, recently reported a value of 2780°. Their failure to allow for the difference in spectral emissivity between the metals used to calibrate the temperature scale and the carbide can account for this high value.

**Lattice Parameter Determinations.**—The relationship between the lattice parameter of the VC-phase and composition is shown in Fig. 4. Included is the work of Schönberg,[10] Ôsawa and Ôya[21], Gurevich and Ormont,[3] Schnell,[15] Dawihl and Rix,[22] Krainer and Konopicky,[23] and Alyamovskii, *et al.*[24] Schönberg reported a lattice parameter of 4.182 Å. for a composition of $VC_{0.96}$ which is not shown but which is clearly in error. This value has never been duplicated and is, it is interesting to note, very near the value obtained if the present curve is extrapolated to $VC_{1.00}$. Gurevich and Ormont, because they were interested in the V–C–O system, analyzed for oxygen. The O/V-molar ratio is shown beside their points. There seems to be no clear dependence on the amount of oxygen, but their lattice parameters approach our values at high carbon contents. This same trend is followed by the data of Krainer and Konopicky.[23] As is the case with the NbC system, the presence of oxygen or nitrogen will cause the $a_0$ values to fall to the right of the curve. The more carbon present, the easier oxygen or nitrogen can be eliminated. For this reason there is good agreement in the high carbon region in spite of the reported high oxygen values. The X-ray density is 5.644 g./cm.$^3$ at $VC_{0.88}$ and 5.628 g./cm.$^3$ at $VC_{0.73}$ with a minimum of 5.611 g./cm.$^3$ at $VC_{0.78}$. NbC also shows a minimum at this same composition.[25]

The lattice parameters of $V_2C$ have been measured at both phase boundaries. These are shown in Table V with the values obtained by others. The values for $a_0$ agree amazingly well between the investigators. However, the values for $c_0$ show no consistency. Schönberg's conclusion that the $c/a$ ratio is constant is not borne out when the arithmetical error in his value is corrected. In fact,

(16) G. A. Meerson and O. E. Krein, *Zh. Neorg. Khim.*, **5**, 1924 (1960).

(17) V. I. Zhelankin, V. S. Kutsev, and B. F. Ormont, *ibid.*, **3**, 1237 (1958).

(18) O. Ruff and W. Martin, *Z. angew. Chem.*, **25**, 39 (1912).

(19) E. Friederich and L. Sittig, *Z. anorg. allgem. Chem.*, **144**, 169 (1925).

(20) J. L. Engelke, F. A. Halden, and E. P. Farley, WADC-TR-59-654, Feb., 1960, 39 pp.

(21) A. Ôsawa and M. Ôya, *Sci. Rept. Tôhoku Imp. Univ.*, **19**, 95 (1930). The values of Ôsawa and Ôya have been converted to Å. and recomputed using an extrapolation to $\theta = 90°$ by the Cohn method. The VC-phase was designated $V_4C_3$ in their paper.

(22) W. Dawihl and W. Rix, *Z. anorgm. allge. Chem.*, **244**, 191 (1940).

(23) H. Krainer and M. Konopicky, *Berg- und Hüttenmänn. Monatsh. Montan. Hochschule Leoben*, **92**, 166 (1947).

(24) S. I. Alyamovskii, P. V. Geld, and I. I. Matveenko, *Zh. Strukt. Khim.*, 445 (1961).

(25) C. P. Kempter, E. K. Storms, and R. J. Fries, *J. Chem. Phys.*, **33**, 1 (1960).

where he shows an increase in $c/a$ the trend is, according to this work, in the other direction.

**The Melting Point of Vanadium Metal.**—The melting point of the powdered metal, prepared as described earlier, was determined in the same manner as the carbide samples. Each melting point was obtained by heating a $^3/_8 \times {}^3/_4$ in. plug, in which a $0.040 \times {}^1/_4$ in.-hole had been drilled for temperature measurements. The temperature was kept about 30° below the melting point for about 10 min., until the pressure had dropped below $1 \times 10^{-5}$ torr. After the window was cleaned and the system reëvacuated, the temperature was raised rapidly until the hole filled with liquid. At the melting point the temperature remained constant before the hole filled, allowing an accurate determination. Reproducibility was better than 4°. Before melting, the lattice parameter was 3.0335 ± 0.0005 Å., somewhat higher than the 3.0240 ± 0.0003 Å. value reported by James and Straumanis.[26] Presumably, this was due to the presence of oxygen and nitrogen. The impurity contents of the original two batches of metal are listed in Table I. The effect of the more abundant impurities on the melting point was determined in order that corrections could be made. The results of these studies are summarized in Table VI.

TABLE V

COMPARISON OF LITERATURE VALUES FOR THE LATTICE PARAMETERS OF $V_2C$

| Investigator | V + $V_2C$ | VC + $V_2C$ |
|---|---|---|
| Present work | $a_0$ = 2.8855 ± 0.0005 Å. | 2.9020 ± 0.0005 Å. |
| | $c_0$ = 4.5705 ± 0.0005 | 4.5770 ± 0.0010 |
| | $c/a$ = 1.584 | 1.577 |
| Gurevich and Ormont[8] | $a_0$ = 2.880 | 2.902 |
| | $c_0$ = 4.553 | 4.573 |
| | $c/a$ = 1.581 | 1.576 |
| Schönberg[19] | $a_0$ = 2.881 | 2.906 |
| | $c_0$ = 4.547 | 4.597 |
| | $c/a$ = 1.578 | 1.582 |
| Schnell[15] | $a_0$ = 2.884 | 2.904 |
| | $c_0$ = 4.568 | 4.588 |
| | $c/a$ = 1.584 | 1.580 |
| Ôsawa and Ôya[21] | $a_0$ = 2.862 | |
| | $c_0$ = 4.554 | |
| | $c/a$ = 1.591 | |

TABLE VI

| Sample no. | Iron | Silicon | Nitrogen | Oxygen | Melting temp., °C.[a] |
|---|---|---|---|---|---|
| | p. p. m. | | | | |
| 1 | 1000 | 500 | 1200 | 5,100 | 1887 |
| 2 | 100 | 900 | 775 | 3,300 | 1895 |
| | | | | | 1891 |
| 3 | 100 | 900 | 1250 | 3,300 | 1892 |
| 4 | 100 | 900 | ~1250 | 8,700 | 1895 |
| 5 | 100 | 900 | ~1250 | 15,000 | 1895 |
| 6 | 100 | 1800 | ~1250 | 8,700 | 1900 |

[a] Uncorrected melting point = 1894° (average of samples 2, 3, 4, and 5).

The nitrogen and oxygen contents were increased by adding VN and $V_2O_5$. Neither of these impurities caused a change in the melting point. It is assumed that the treatment prior to melting removed essentially all of the oxygen and nitrogen. According to the results of Seybolt,[27] if all of the oxygen in sample no. 2 remained at the melting point, the melting temperature would have been lowered by about 30°.

Sufficient Si metal powder was added to bring the Si content to 1800 p.p.m. This produced a 6° increase, which gives a −0.67°/100 p.p.m. Si correction factor, assuming of course that the effect is linear over this range. Nothing can be concluded from this experiment concerning the solidus in the V–Si system. Such a small amount of Si might interact with the other impurities to produce an anomalous effect.

If the Si correction is applied to sample no. 1 and the remaining error blamed on the Fe, a +0.44°/100 p.p.m. Fe correction factor is obtained.

By averaging the samples in which the Si and Fe were constant and applying the appropriate correction, a melting point of 1888 ± 10° is obtained for pure vanadium metal. The bulk of the error is due to uncertainties in the temperature calibration.

This value can be compared to a determination by Adenstedt, *et al.*,[28] who reported a value of 1900 ± 25°. Although their metal was pure in other respects, it contained sufficient tungsten to be seen metallographically. D. J. McPherson, in a discussion of this paper, reported a melting point of 1920° for the same material that Adenstedt used. Wilhelm, *et al.*,[29] obtained 1860° during a study of the Nb–V system. However, the value they obtained for the melting point of Nb is about 50° lower than the presently accepted value of 2468°,[30] leading one to suspect that the reported V melting temperature is also low. Oriani and Jones[31] reported a value of 1919 ± 2° for a metal having a purity of 99.8–99.9% V. Because no detailed statement of the impurities was given, it is impossible to evaluate this determination. Williams,[32] during a study of the V–Zr system, obtained a melting point of 1860°. However, the metal contained sufficient carbon to lower the melting temperature by about 20°.

## Discussion

VC is not unique among the group Va carbides in having a homogeneity range that does not extend to the 1:1 atomic ratio. The phase boundary in the Nb–C system apparently lies at $NbC_{0.99}$.[33] However, the extent to which VC deviates is rather unusual.

The wide homogeneity range may be thought of as resulting from a substraction type lattice caused by a random absence of carbon atoms in the basic f.c.c. metal structure. With this view the 1:1 ratio is significant only because it represents the composition when all the lattice sites are filled, which is not necessarily the phase boundary. The actual phase boundary will be determined by the

(26) W. J. James and M. E. Straumanis, *Z. physik. Chem.*, **29**, 134 (1961).

(27) A. U. Seybolt and H. T. Sumsion, *Trans. AIME*, **197**, 292 (1953).

(28) H. L. Adenstedt, J. R. Pequignot, and J. M. Raymer, *Trans. ASM*, **44**, 990 (1952).

(29) H. A. Wilhelm, O. N. Carlson, and J. M. Dickinson, *J. Metals*, **6**, 915 (1954).

(30) T. H. Schofield, *J. Inst. Metals*, **85**, 372 (1956–1957).

(31) R. A. Oriani and T. S. Jones, *Rev. Sci. Instr.*, **25**, 248 (1954).

(32) J. T. Williams, *Trans. AIME*, **203**, 345 (1955).

(33) E. K. Storms and N. H. Krikorian, *J. Phys. Chem.*, **64**, 1471 (1960).

relative stabilities of carbon in VC and in the graphite lattice, as the composition of the VC-phase changes. The paper by Anderson[34] should be consulted for a more detailed discussion of this phenomenon.

## Summary

The V–VC system contains the following important features: (1) a eutectic temperature of 1630 ± 15° between $VC_{0.09}$ (2.08 wt. % C) and $VC_{0.33}$ (7.22 wt. % C); (2) a peritectic temperature of 2165 ± 25° between $VC_{0.56}$ (11.66 wt. % C) and $VC_{0.60}$ (12.39 wt. % C); (3) a peritectic temperature of 2650 ± 35° extending from $VC_{0.85}$ (16.69 wt. % C) to at least $VC_{1.2}$; (4) a range of homogeneity of $V_2C$ between $VC_{0.47}$ (9.97 wt. % C) and $VC_{0.50}$ (10.54 wt. % C) at 1100°; (5) a range of homogeneity of VC between $VC_{0.73}$ (14.68 wt. % C) and $VC_{0.87}$ (17.02 wt. % C) at 1100°; (6) evidence for an additional phase in the region between $VC_{0.50}$ and $VC_{0.74}$ below 1344°; (7) preferential evaporation of vanadium from all compositions studied; and (8) in addition, the melting point of pure vanadium metal has been determined to be 1888 ± 10°.

**Acknowledgment.**—We gratefully acknowledge the support of Dr. Melvin G. Bowman during the course of this work. Thanks are due Mr. C. G. Heasly and Mr. M. H. Peek for the analytical work, and Mrs. Mary Jane Jorgensen for reading the X-ray diffraction patterns.

(34) J. S. Anderson, National Physical Laboratory Symposium #9, Vol. II, Paper 7A, 1959.

# SOLID SOLUTION STUDY OF SOME POST-TRANSITION METAL TELLURIDES OF THE ROCK SALT STRUCTURAL TYPE

BY R. MAZELSKY AND M. S. LUBELL

*Westinghouse Research Laboratories, Beulah Road, Churchill Borough, Pittsburgh 35, Pennsylvania*

*Received February 8, 1962*

A solid solution study was made of the pseudo-binary systems $(1 - x)TlSbTe_2$–$xTlBiTe_2$, $(1 - x)MTe$–$(x/2)TlBiTe_2$, $(1 - x)MTe$–$(x/2)TlSbTe_2$ where M = Sn and Pb. Limits of solid solution were determined by means of X-ray powder photography. A phase diagram of the $SnTe$–$TlSbTe_2$ system has been proposed from cooling curves and powder X-ray data. The bond type of these post-transition metal tellurides is discussed on the basis of covalent bonding, the most likely configuration being $p^3d^3$.

## Introduction

With the increase of interest in binary semiconductors, an appreciable amount of effort has been expended on materials of the rock-salt structural type. Of particular interest are the compounds of the post-transition group IV elements with selenium and tellurium, *i.e.*, germanium, tin, and lead tellurides and selenides. Assuming that tellurium in these materials is dinegative, germanium, tin, and lead must be in a +2 oxidation state.

It was, therefore, a logical extension to prepare ternary compounds, with the cations having an average valence of +2. Wernick, Geller, and Benson[1] studied six pseudo-binary systems consisting of the systems $AgSbSe_2$, $AgSbTe_2$, $AgBiSe_2$, and $AgBiTe_2$. A valence of +3 was assumed for antimony and bismuth and rock-salt related structures were observed for all the stable compositions.

Recently, Hockings and White[2] reported two similar materials; $TlBiTe_2$ and $TlSbTe_2$. These were characterized as having a rhombohedral structure with the cations ordered in the layers perpendicular to the "*c*" direction of the hexagonal cell.

In this paper, some materials of the rock-salt type were investigated, both by themselves and in solid solutions. Three pseudo-binary systems were examined—$(1 - x)TlSbTe_2$–$xTlBiTe_2$, $(1 - x)$-$MTe$–$(x/2)TlBiTe_2$, and $(1 - x)MTe$–$(x/2)Tl$-$SbTe_2$, where M = Sn and Pb.

(1) J. W. Wernick, S. Geller, and K. E. Benson, *Phys. Chem. Solids*, **2/3**, 240 (1958).

(2) E. F. Hockings and J. G. White, *Acta Cryst.*, **14**, 328 (1961).

**Preparation.**—All the elements in the preparation of the compounds had a purity of 99.999% or better with respect to metallic impurities. Unless otherwise indicated, all materials were prepared by modified powder metallurgical techniques. This entailed placing correct proportions of the appropriate elements in a Vycor tube and evacuating the tube. The tube then was sealed and the contents melted in a resistance furnace. While molten, the contents of the tube were mixed manually at frequent intervals over a 4–5-hr. period. The capsule and its contents were air-quenched and the ingot removed. The ingot then was ground into a powder and pressed at 40 to 50 t.s.i. into a pellet. The pellet was placed in a Vycor capsule and evacuated, sealed, and sintered over a 16 to 20-hr. period at a temperature that was roughly 85 to 90% of its melting point.

**X-Ray.**—Powder photographs of all materials were taken with $CoK\alpha$ radiation using a camera with 114.6 mm. diameter. Lattice parameters were determined from high angle reflections.

$TlSbTe_2$ and $TlBiTe_2$ and solid solutions of the two yielded powder photographs with broad line widths. It was found that a 4-day anneal at 200° resulted in satisfactory photographs.

The system $TlSb_{1-x}Bi_xTe_2$ showed a complete range of solid solution in the range $x = 0.0$–$1.0$. The data were indexed on the basis of a hexagonal cell. The reflections observed statisfied the conditions $(-h+k+l = 3n)$ for a rhombohedral lattice and the rhombohedral parameters were obtained from the equations

$$a_R = \frac{1}{3}\left[3a^2_H + c_H{}^2\right]^{1/2}$$

$$\sin \alpha/2 = \frac{3a_H}{2\left[3a_H{}^2 + c_H{}^2\right]^{1/2}}$$

The data are shown in Table I for the system $TlSb_{1-x}Bi_xTe_2$.

TABLE I

LATTICE PARAMETERS AND RHOMBOHEDRAL ANGLES FOR THE SYSTEM $TlSb_{1-x}Bi_xTe_2$

| $x$ | $a$ (Å.) | $\alpha$ |
|---|---|---|
| 0.0 | 8.177 | 31° 30′ |
| .1 | 8.176 | 31° 32′ |
| .2 | 8.161 | 31° 45′ |
| .5 | 8.159 | 31° 49′ |
| .75 | 8.143 | 32° 0′ |
| 1.0 | 8.139 | 32° 10′ |

The lattice parameters and rhombohedral angles for the systems $Pb_{1-x}Tl_{x/2}Bi_{x/2}Te$ and $Pb_{1-x}Tl_{x/2}Sb_{x/2}Te$ are shown in Table II. The samples used for the X-ray analysis were slowly cooled to room temperature to minimize quenching phenomena. For ease of comparison with the rock-salt structure of PbTe, a rhombohedral pseudo-cell was chosen for $TlSbTe_2$ and $TlBiTe_2$ in which the rhombohedral cell edge is essentially equal to the "$a$" edge of the cubic cell and the rhombohedral angle is near 90°.

TABLE II

LATTICE PARAMETERS AND RHOMBOHEDRAL ANGLES FOR THE SYSTEMS

$(1 - x)PbTe-(x/2)Tl(Sb,Bi)Te_2$

| | $(1 - x)PbTe-(x/2)TlBiTe_2$ | | $(1 - x)PbTe-(x/2)TlSbTe_2$ | |
|---|---|---|---|---|
| $x$ | $a$ (Å.) | $\alpha$ | $a$ (Å.) | $\alpha$ |
| 0.0 | 6.459 | 90° | 6.459 | 90° |
| .25 | 6.463 | 90° | 6.448 | 90° |
| .60 | 6.469 | 90° | 6.431 | 90° |
| .70 | 6.469[a] | 90° | 6.431[a] | 90° |
| .80 | 6.474[b] | 88° 44′ | | |
| .90 | 6.475 | 88° 42′ | 6.412 | 87° 12′ |
| 1.00 | 6.477 | 88° 15′ | 6.412 | 87° 12′ |

[a] Two phase—cubic phase parameters. [b] Two phase—rhombohedral phase parameters.

It was observed that a continuous range of solid solution at room temperature does not exist, a two-phase region occurring between the rhombohedral to cubic transformation. The limits of the range of solution are estimated by assuming that when the cubic or rhombohedral phase has no further change in lattice parameter, the solid solution limit has been reached. In this manner, $Pb_{1-x}Tl_{x/2}Bi_{x/2}Te$ is found to be cubic between $x = 0.0$ and $x = 0.62$ and rhombohedral between $x = 0.89$ and $x = 1.0$. The rhombohedral phase boundary in $Pb_{1-x}Tl_{x/2}Sb_{x/2}Te$ could only be estimated. For $x = 0.9$ the powder photograph showed a few weak lines indicative of the cubic phase. The rhombohedral phase field thus apparently is quite narrow, perhaps in the range $x = 0.95$–$1.0$. The cubic phase field encompasses the range $x = 0.0$–$0.62$.

Using X-ray powder methods, the systems $Sn_{1-x}Tl_{x/2}Bi_{x/2}Te$ and $Sn_{1-x}Tl_{x/2}Sb_{x/2}Te$ were examined. The results are shown in Table III. The cubic phase exists between $x = 0.00$ and $x = 0.72$ for the former and $x = 0.00$ and $x = 0.42$ for the latter, the rhombohedral phase limits being $x = 0.88$–$1.0$ and $x = 0.75$–$1.0$, respectively. It is of interest to note that an extrapolation of the rhombohedral angle to 90° coincided with the edge of the cubic phase field at room temperature as determined from lattice parameters.

TABLE III

LATTICE PARAMETERS AND RHOMBOHEDRAL ANGLES FOR THE SYSTEM

$(1 - x)SnTe-(x/2)Tl(Sb, Bi)Te_2$

| | $(1 - x)SnTe-(x/2)TlBiTe_2$ | | $(1 - x)SnTe-(x/2)TlSbTe_2$ | |
|---|---|---|---|---|
| $x$ | $a$ (Å.) | $\alpha$ | $a$ (Å.) | $\alpha$ |
| 0.0 | 6.320 | 90° | 6.320 | 90° |
| .10 | 6.334 | 90° | | |
| .20 | | | 6.334 | 90° |
| .50 | 6.388 | 90° | 6.356[a] | 90° |
| .60 | 6.405 | 90° | | |
| .70 | 6.422 | 90° | 6.389[b] | 88° 20′ |
| .80 | 6.425[a] | 90° | | |
| .80 | 6.456[b] | 88° 40′ | | |
| .85 | | | 6.397 | 87° 48′ |
| .90 | 6.458 | 88° 40′ | | |
| 1.00 | 6.477 | 88° 15′ | 6.412 | 87° 12′ |

[a] Two phase—cubic phase parameters. [b] Two phase—rhombohedral phase parameters.

An examination was made of the system SnTe–$TlSbTe_2$ to determine the general shape of the phase diagram. Cooling curves were taken to find the melting temperatures. The solid points on Fig. 1 are the thermal arrests observed. The solid phase fields as a function of temperature were estimated from quench experiments on powdered samples of various compositions. The identifications were made by X-ray powder diffraction photographs. A eutectic composition was observed at approximately 90% $Tl_{0.5}Sb_{0.5}Te$. Contrary to the data reported by Hockings and White,[2] thermal arrests were observed below the melting point—one at 465° and another at 405°. A high temperature X-ray picture of $TlSbTe_2$ at 420°, however, showed no phase change. The variance between these data and ref. 2 may in part be due to the method of preparation of the sample. $TlSbTe_2$ was prepared stoichiometrically by powder metallurgical methods rather than by the Bridgman method. The material formed from the melt may differ somewhat from the stoichiometric composition. The observed thermal arrests in that case could be due to additional phases being present.

**Electrical Measurements.**—Measurements of the Seebeck coefficient of pressed and sintered samples of $TlSbTe_2$ and $TlBiTe_2$ gave values of +70 and −70 μv./deg., respectively. In both cases, this indicated a fairly large extent of non-stoichiometry and therefore a correspondingly high vacancy concentration. Large carrier concentrations also were indicated from the low Hall coefficients observed, the values being in the range of 0.30–0.35 cm.$^3$/coul. From carrier concentrations estimated from Hall measurements, and assuming one carrier per vacancy, the vacancy concentration calculates out at around 0.1 atom %. However, the nature of the vacancies is not clear. Houston, *et al.*,[3] report that tin telluride crystallizes with excess tellurium, the resulting carriers having a concentra-

(3) B. B. Houston, R. F. Bis, and E. Guber, *Bull. Am. Phys. Soc.*, [2] 6, 436 (1961).

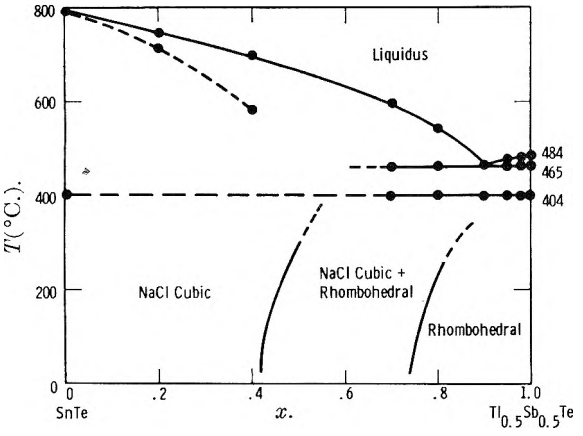


Fig. 1.—$Sn_{1-x}Tl_{x/2}Sb_{x/2}Te$ proposed phase diagram—temperature *vs.* composition parameter $x$.

tion in the range of $10^{20}$/cc. The Seebeck coefficient of $SnTe_{1+x}$ is in the range of +30 $\mu$.v/deg. Germanium telluride is similar to SnTe. It has a composition of $GeTe_{1.025}$. This has been verified by phase diagram work and chemical analysis.[4] Hall data from which carrier concentrations were calculated give excellent agreement with carrier concentrations calculated on the above stoichiometry and assuming two carriers per excess tellurium.[5] Lead telluride appears to be the exception. It has a Seebeck coefficient in excess of +300 $\mu$v./deg. with the attendant low carrier concentration.

## Discussion

Using measurements of the Seebeck and Hall coefficients, it was established that of the materials under discussion, only lead telluride forms with a nearly stoichiometric composition. In the binary materials, germanium and tin tellurides, the carrier concentration may be immediately related to the vacancy concentration of the cations (due to excess tellurium in the lattice). With the ternary materials ($TlSbTe_2$ and $TlBiTe_2$) the data are insufficient to determine which element is responsible for the vacancies. (Interstitial sites also must be considered.) Furthermore, since $TlSbTe_2$ has a positive Seebeck coefficient and $TlBiTe_2$ a negative one, the type of non-stoichiometry in each material is most likely of a different kind. In addition, the Hall measurements would indicate that only 0.1 atom % deficiency of one of the constituents (based on one carrier only per vacancy) is sufficient to provide enough carriers to agree with experiment. These resulting impurities are in too small an amount to be observed by X-ray methods.

Measurements of the Seebeck coefficients of the various solid solutions indicate that the vacancy concentration inherent in $TlBiTe_2$ and $TlSbTe_2$ is carried along into the solid solution. The Seebeck coefficient decreases in a regular manner as increasing amounts of $TlSbTe_2$ and $TlBiTe_2$ are dissolved in PbTe.

Within the homogeneity range of solid solution the lattice parameter behaves ideally, *i.e.*, there is a linear dependence of lattice parameter with composition. It is of particular interest to note the coincidence of the rhombohedral angle extrapolated to 90° and the limit of the cubic phase field as determined from the variation in lattice parameter—in spite of the fact that the extrapolation is made across a wide two-phase region.

As a consequence of the apparent ideal behavior of the solid solutions, it appears likely that an equation can be written for the lattice parameter *vs.* composition curve. For the system $M_{(1-x)}Tl_{(x/2)}N_{(x/2)}Te$, it would have the form $2(1-x)r_M + xr_{Tl+N} + 2r_{Te} = a$ when M = Sn, Pb and N = Sb and Bi, and $r$ is the radius. The implication is that the gross effect of the size of (Tl + Sb) and (Tl + Bi) is a constant and the lattice parameter changes linearly with the concentration of (Tl + Sb) and (Tl + Bi) in SnTe and PbTe.

On Table IV are listed interatomic distances calculated from Pauling's covalent single bond octahedral radii, ionic radii, and the distance reported by several investigators for the different materials. Interatomic distances for PbTe, SnTe, and GeTe were estimated from the experimentally determined lattice parameters. Bond numbers were calculated from $D(n) = D(1) - 0.6 \log n$, where $D(n)$ is the observed interatomic distance, $D(1)$ is the single covalent bond length, and $n$ is the bond number. Qualitatively, the observed bond distances are intermediate between the covalent and ionic distance, and aside from a few exceptions, the bond order for all these tellurides is in the range of $^1/_2$. The exceptions are Pb–Te in lead telluride which seems primarily ionic, and Bi–Te[I] in $Bi_2Te_3$, which is primarily covalent. It is of interest to note that the Bi–Te and Sb–Te interatomic distances in $TlBiTe_2$ and $TlSbTe_2$ are of the same order of magnitude as in $Bi_2Te_3$ and $Sb_2Te_3$.

The bond distances discussed all have been calculated on the basis of octahedral bonds, most likely of the type $sp^3d^2$ since the lower lying "d" shells are all filled. This orbital configuration requires twelve electrons. The binary tellurides, (Pb,Sn,Ge)Te, as well as $Tl_{1/2}Sb_{1/2}Te$ and $Tl_{1/2}Bi_{1/2}Te$, have a total of 10 electrons available for bond formation, only $^5/_6$ of the electron requirements being satisfied. The resulting weakening of the covalent bond then could account for the increased interatomic distances observed. However, the presence of unfilled orbitals in this configuration would lead one to expect metallic or semimetallic behavior. The indications are that all of the above materials are semiconductors with forbidden energy gaps in the range of 0.5 e.v. or less. Furthermore, if the bonds were of this type, a predominantly covalent bond would be expected. This is not observed.

An alternative picture is described by Krebs[6] for PbS, which takes into account the fact that the group IV elements behave as group II elements. In other words, Ge, Sn, Pb behave as if two electrons are available for bond formation. Similarly, Sb and Bi would have three electrons and Tl one electron for bond formation with the result that all

(4) J. P. McHugh and W. A. Tiller, *Trans. Met. Soc. AIME*, **218**, 187 (1960).

(5) R. W. Ure, Jr., R. Bowers, and R. C. Miller, "Properties of Elemental and Compound Semiconductors," ed. by H. C. Gatos, Interscience Publ., New York, N. Y., 1960, pp. 245–257.

(6) H. Krebs, *Physica*, **20**, 1125 (1954).

these materials (including Te) have a filled "s" shell which does not enter into the bonding scheme. On this basis, six "p" bonds are formed with the six electrons available from the elements or half the number required to fill the six "p" orbitals.

TABLE IV

INTERATOMIC DISTANCES

| Material | Exp. inter. atom. dist. | Empirical ionic IAD[7] | Octahedral constant IAD[8] | Bond number |
|---|---|---|---|---|
| PbTe | 3.33 | 3.42 | 3.02 | 0.32 |
| SnTe | 3.15 | 3.33 | 2.97 | .50 |
| GeTe | 2.99 | 3.14 | 2.78 | .45 |
| $TlSbTe_2$[2] | | | | |
| Tl–Te | 3.30 | 3.61 | 3.05 | .39 |
| Sb–Te | 3.11 | 3.13[a] | 2.92 | .48 |
| $TlBiTe_2$[2] | | | | |
| Tl–Te | 3.30 | 3.61 | 3.05 | .39 |
| Bi–Te | 3.19 | 3.21[a] | 3.03 | .54 |
| $Bi_2Te_3$[9] | | | | |
| Bi–Te[I] | 3.12 | 3.21[a] | 3.03 | .71[b] |
| Bi–Te[II] | 3.22 | 3.21[a] | 3.03 | .48 |
| $Sb_2Te_3$[10] | | | | |
| Sb–Te[I] | 3.06 | 3.13[a] | 2.92 | .59 |
| Sb–Te[II] | 3.16 | 3.13[a] | 2.92 | .40 |

[a] Estimated values for $Bi^{+3}$ and $Sb^{+3}$. [b] Based on octahedral radii. It is believed[7] that this is actually a "p" bond, in which case the bond number is less.

As a result a resonating picture was proposed. If "p" bonds are involved, longer interatomic distances and a large amount of ionic character would be observed. The bond numbers calculated on Table I do indeed show a large ionic contribution. Since the bond numbers were calculated for octahedral $sp^3d^2$ bonds, and since the "p" bonds do not extend as far from the nucleus as the $sp^3d^2$ hybrid, there will be less overlap between the cation and anion "p" orbitals and only a weak covalent bond will be formed. Therefore, an appreciable amount of ionic character would be expected and the electrons would be distributed predominantly near the anion. If the electrons are situated in this manner, the metallic conductivity expected from a half-filled bond orbital would not occur. The difficulty of this representation would be that, because of small amount of overlap, low electronic mobilities would be expected. The "p" type mobility for PbTe is in the range of 800 cm./volt. The mobilities of GeTe and SnTe are lower, near 100 cm./volt, but this low value probably is due to their high carrier concentration.

A third possibility would be $p^3d^3$ bonding. This would result in a trigonal antiprism which can be looked at as a distorted octahedron. If all the electrons available in the outer shells were used, "s" electrons would be available and an $sp^3d^2$ hybrid probably would be formed. Assuming a filled "s" shell with "p" electrons only being used for bond formation, the $p^3d^3$ orbitals would be only half-filled. This latter representation gives bond numbers of the correct magnitude and is a tempting representation. In order to avoid the metallic conduction implicit in unfilled orbitals a resonating structure similar to that proposed for $p^3$ bonding would be required. The large $p^3d^3$ orbitals would be expected to show greater overlap as compared with $p^3$ orbitals. In addition, the strength of the bonds would be comparable to the $sp^3d^2$. Therefore, the bond type would be less ionic in $p^3d^3$ as compared with $p^3$ and rather higher mobilities would be expected. It is felt that $p^3d^3$ hybridization is the most likely configuration for these materials.

Although the lattice parameters appear to behave simply at room temperature, high temperature data, at least in the SnTe–$TlSbTe_2$ system, are quite complex. For the proposed phase diagram in Fig. 1, certain features of the system are apparent. A eutectic composition at 465° exists at the composition 90$TlSbTe_2$–10SnTe. The amount of the $TlSbTe_2$ that can be dissolved in SnTe while retaining the cubic structure increases with temperature. However, due to the errors inherent in quench experiments with subsequent X-ray analysis, it is difficult to be certain of the exact temperatures at which the effect occurs. Finally, with increasing $TlSbTe_2$ the structure changes from cubic to rhombohedral through a two-phase mixture of the two, at least at low temperatures. At higher temperatures the nature of the phases indicated from cooling curves is not known although the liquidus curve has been well defined.

**Acknowledgment.**—The authors wish to thank W. E. Kramer for his assistance with the experiments and also to thank R. Jones and B. Kagle for the powder photographs. We appreciate valuable discussions with Drs. F. L. Carter and R. C. Miller.

This work was supported by the U. S. Navy, Bureau of Ships, contract No. NOBS-84317.

(7) L. Pauling, "The Nature of the Chemical Bond," 3rd ed., Cornell Univ. Press, Ithaca, N. Y., Chapt. 13, 1960.

(8) Reference 7, Chapt. 7.

(9) J. R. Drabble and C. H. L. Goodman, *J. Phys. Chem. Solids*, **5**, 142 (1958).

(10) S. U. Airapetyants and B. A. Efimova, *Zh. Tekh. Fiz.*, **28**, 8, 1768 (1958).

# THE RELATIVE VOLATILITIES OF THE SYSTEM $H_2O^{17}$–$H_2O^{16}$

By J. L. Borowitz

*Israel Atomic Energy Commission, Rehovoth, Israel, and The Weizmann Institute of Science, Rehovoth, Israel*

*Received February 9, 1962*

The relative volatility of the system $H_2O^{17}$–$H_2O^{16}$ was determined at absolute pressures of 100 and 260 mm. The experiments were carried out in a distillation column with production.

## Introduction

The relative volatility, $\alpha$, for a binary mixture is defined by the equation

$$\alpha = \frac{n}{1-n} \Big/ \frac{N}{1-N}$$

where $n$ and $N$ are the mole fractions of one of the components in the vapor phase and in the condensed phase, respectively.

Measurements of the relative volatility for the system $H_2O^{18}$–$H_2O^{16}$ have been made by many workers, using different techniques. The results until 1957 were summarized by Dostrovsky and Raviv.[1] Thode, Smith, and Walkling[2] determined the relative volatility of $H_2O^{17}$–$H_2O^{16}$ at two pressures, using a distillation column.

This paper reports measurements of the relative volatility of $H_2O^{17}$–$H_2O^{16}$ made at two more pressures. The method used was similar to that of Dostrovsky and co-workers[3] for $O^{18}$ and is based on the relationship between enrichment and production.

**Theory.**—The equation connecting enrichment and production in a distillation column, as given by Dostrovsky, Gillis, Llewellyn, and Vromen[3] is

$$q = \frac{\alpha p/(\alpha-1) + l}{\alpha p/(\alpha-1) + [1/\alpha(1+p)] \exp[-\nu(\alpha - 1 + \alpha p)]} \tag{1}$$

where

- $q$ is the enrichment in the reboiler, *i.e.*, the steady-state concn. of isotope in the reboiler divided by the concn. in the feed
- $\alpha$ is the relative volatility
- $L$ is the liquid flow rate down the column (l./day)
- $l$ is the vapor flow rate up the column (l. liquid/day)
- $P = L - l$ is the rate of withdrawal of enriched water from the reboiler (l./day)
- $p = P/l$
- $\nu$ is the number of theoretical plates in the column

As there are two unknowns in this equation, *viz.*, $\nu$ and $\alpha$, at least two experiments with different values of $p$ are required to solve the equation for them and more than two usually are done. Equation 1 is transcendental, and thus difficult to solve. A convenient method of solution is given by Lehrer[4]; thus we write

$$\nu(\alpha - 1 + \alpha p) = \Omega \tag{2}$$

and rearrange eq. 1

$$e^{\Omega} = (q_\infty - 1)q/(q_\infty - q) \tag{3}$$

where

$$\left.\begin{aligned} q_\infty &= 1 + 1/\alpha^* p \\ \text{and } \alpha^* &= \alpha/(\alpha - 1) \end{aligned}\right\} \tag{4}$$

Equation 3 may be rewritten

$$a + bp - L\Omega = 0 \tag{5}$$

where

$$a = L\nu(\alpha - 1) \tag{6}$$

and

$$b = \alpha^* a \tag{7}$$

and we thus have a linear equation in two unknowns, $a$ and $b$.

Using eq. 3 and an assumed value for $\alpha$, $\Omega$ may be calculated from the experimental values of $p$ and $q$; $a$ and $b$ may be determined from the results of two or more experiments by substituting $L$, $p$, and $\Omega$ in eq. 5. The ratio between them then may be used to check whether the assumption for $\alpha$ is correct. The following procedure therefore was used. The enrichment in the reboiler, $q$, was measured for various values of $p$. Using an assumed value for $\alpha$, $a$ and $b$ were computed by the method of least squares. The assumed value for $\alpha$ was checked using eq. 7. If the value found from eq. 7 was not in close agreement with that assumed, the computation was repeated with a different value of $\alpha$. This method of successive approximation was described by Lehrer.[4] The probable error was calculated from the residual, $\Delta$, of each experiment

$$\Delta = a + bp - L\Omega$$

(1) I. Dostrovsky and A. Raviv, "Proceedings of the Symposium on Isotope Separation," North-Holland Publishing Co., Amsterdam, 1958, p. 337.

(2) H. G. Thode, S. R. Smith, and F. O. Walkling, *Can. J. Res.*, **22B**, 127 (1944).

(3) I. Dostrovsky, J. Gillis, D. R. Llewellyn, and B. H. Vromen, *J. Chem. Soc.*, 3578 (1952).

(4) Y. Lehrer, Ph.D. Thesis, The Hebrew University, Jerusalem, 1961 (in Hebrew), pp. 81–82.

TABLE I[a]

| Exp. no. | Liquid flow rate, l./day: Measured | λ | σ | Total | Produc. (l./day) | Period of equil. for $O^{18}$, days | Enrich. of $O^{18}$ in boiler $q$ | Calcd. $q$ ($O^{18}$) | Period of equil. for $O^{17}$, days | Enrich. of $O^{17}$ in boiler ($Q$) | Calcd. $Q$ ($O^{17}$) | Remarks |
|---|---|---|---|---|---|---|---|---|---|---|---|---|
| 1 | 173 ± 4 | 17 ± 2 | 15 | 205 | 0.6 | 12 | 2.57 | 2.57 | 5 | 1.77 | 1.77 | Absolute pressure |
| 2 | 173 ± 4 | 17 ± 2 | 15 | 205 | .3 | 9 | 3.49 | 3.45 | 4 | 2.06 | 2.07 | in condenser 260 |
| 3 | 173 ± 4 | 17 ± 2 | 15 | 205 | .2 | 26 | 4.04 | 3.98 | 10 | 2.24 | 2.23 | mm., temp., 73° |
| 4 | 173 ± 4 | 17 ± 2 | 15 | 205 | .1 | 6 | 4.64 | 4.71 | 5 | 2.42 | 2.42 | |
| 5 | 151 ± 4 | 17 ± 2 | 7 | 168 ± 6 | .7 | 10 | 2.45 | 2.45 | 5 | 1.72 | 1.72 | Absolute pressure |
| 6 | 151 ± 4 | 17 ± 2 | 7 | 168 ± 6 | .5 | 8 | 2.82 | 2.82 | 5 | 1.86 | 1.86 | in condenser 100 |
| 7 | 151 ± 4 | 17 ± 2 | 7 | 168 ± 6 | .25 | 10 | 3.64 | 3.64 | 5 | 2.12 | 2.12 | mm., temp., 52° |

[a] The pressure drop across the column (between reboiler and condenser) was 75 mm. in the first series and 60 mm. in the second.

TABLE II

| Pressure, mm. | System | $\alpha$ | $\nu$ | $a$ | $b$ |
|---|---|---|---|---|---|
| 260 | $H_2O^{16}$-$H_2O^{18}$ | 1.0055 ± 0.0004 | 329 ± 11 | 372 ± 12 | 68800 ± 4200 |
| 100 | $H_2O^{16}$-$H_2O^{18}$ | 1.0070 ± .0001 | 244 ± 2 | 304 ± 2.5 | 41720 ± 450 |
| 260 | $H_2O^{16}$-$H_2O^{17}$ | 1.0030 ± .0001 | 327 ± 6 | 201 ± 3.6 | 69500 ± 1200 |
| 100 | $H_2O^{16}$-$H_2O^{17}$ | 1.0039 ± .0001 | 240 ± 2.5 | 164.2 ± 0.8 | 41970 ± 180 |

according to the method given by Margenau and Murphy[5]; $\alpha$ and $\nu$ were calculated from $a$ and $b$ using eq. 6 and 7. As a further check, the value of $q$ was calculated for each experiment from the computed values of $\alpha$ and $\nu$. The results are shown in Table I.

## Experimental

The column was a 100-mm. diameter copper tube, 5.5 m. high, fitted with a steam heated flash reboiler and a two-stage condenser. For the first experiment (at 260 mm. absolute pressure) the column was packed to a height of 5.25 m. with 1/8 in. diameter copper Dixon rings, surface oxidized. In the second experiment the height of the packing was 4 m. There was a two-inch layer of glass wool lagging around the column and reboiler to reduce heat losses. The additional flow in the column due to condensation of vapor because of the remaining heat losses was estimated by passing steam at atmospheric pressure through the column so that a constant rate of condensation, approximately equal to the working flow rate, was kept up in the condenser. This condensate left the system. The steam entered the column through the reboiler which was kept at just over 100° in order to reduce the wetness of the steam as far as possible. After waiting some time for steady conditions to be attained, the water condensing in the column and making its way down to the bottom was collected and measured. This rate of condensation was 17 ± 2 l./day, or about 10% of the measured flow rate.

The flow rate was estimated by measuring the quantity of distillate collected every hour, and was adjusted to 2/3 of the flooding rate of the packing. Distilled natural water was used as feed. The above rate of condensation due to heat losses λ, as well as the rate of condensation of vapor by the feed water σ, which was calculated from the temperature, was added to the measured flow rate according to ref. 6. Values are given in Table I.

The vacuum in the condenser was kept constant within ±10 mm. by a manostat. Production was taken in equal parts spread over the day; thus, if 240 cc. per day was taken, it would be taken in 12 two-hourly portions of 20 cc. each. Analyses were by mass spectrometer. Equilibrium was assumed to have been attained with respect to each of the isotopes if the concentration in the reboiler remained constant for more than 4 consecutive days.

(5) H. Margenau and G. M. Murphy, "The Mathematics of Physics and Chemistry," D. Van Nostrand, New York, N. Y., 1943, pp. 500–502.

(6) I. Dostrovsky, J. Gillis, D. R. Llewellyn, and B. H. Vromen, *J. Chem. Soc.*, 3520 (1952).

## Results

The values of the variables measured are given in Table I. The figures for the enrichments for each experiment are the averages of the analyses obtained for the period of equilibrium of the experiments. Table II was calculated from these results.

## Discussion

The values for $\alpha_{O^{18}}$ measured by previous workers using distillation methods, as summarized by Dostrovsky and Samuel[7], are represented approximately by the formula

$$\ln \alpha = 0.0206 - 5.81/T$$

where $T$ is the absolute temperature. The value found here at 260 mm. agrees with that calculated using this formula within the experimental error. At 100 mm. the result differs from the formula by just the experimental error. The value of $\nu$ is seen not to be significantly different for $H_2O^{18}$ and $H_2O^{17}$ at the same pressure.

Bigeleisen[8] has published a statistical-mechanical treatment of the vapor pressure ratios of isotopic species, where it is shown that the ratio of the vapor pressures can be expressed as a product of the difference in the reciprocal masses of the isotopic atoms and a difference in force constants, thus

$$\ln (P'/P) = (24N)^{-1} (\hbar/kT)^2 \sum_{i=1}^{3nN} (\mu_i' - \mu_i)(a_{ii} - b_{ii})$$

where $P'$ and $P$ are the vapor pressures of the lighter and heavier isotopic molecules, respectively, at the temperature $T$.

$N$ is Avogadro's number
$\hbar = h/2\pi$ where $h$ is Planck's constant
$k$ = Boltzmann's constant

(7) I. Dostrovsky and D. Samuel, Fig. IIb in "The Isotopes of Oxygen," in press.

(8) J. Bigeleisen, *J. Chem. Phys.*, 34, 1489 (1961) (eq. 3.13)

TABLE III

| Temp., °C. | $\alpha_{O^{17}}$ | $\alpha_{O^{18}}$ | $(\alpha_{O^{17}} - 1)/(\alpha_{O^{18}} - 1)$ | |
|---|---|---|---|---|
| 52 | 1.0039 ± 0.0001 | 1.0070 | 0.558 ± 0.022 | |
| 58 | 1.0033 ± .0002 | 1.0063 | .525 ± .031 | Thode, *et al.* |
| | 1.0040 ± .0002 | 1.0070 | | Thode, *et al.* cor. so that $\alpha_{O^{18}}$ corresponds to formula |
| 67 | 1.0026 ± .0002 | 1.0056 | .465 ± .035 | Thode, *et al.* |
| | 1.0033 ± .0002 | 1.0063 | | Thode, *et al.* cor. so that $\alpha_{O^{18}}$ corresponds to formula |
| 73 | 1.0030 ± .0001 | 1.0055 | .527 ± .058 | |

$n$ is the number of atoms in the molecule
$\mu_i', \mu_i$ are the reciprocal masses of the $i$th atom, for the lighter and heavier isotope, respectively
$a_{ii}, b_{ii}$ are the Cartesian force constants for the displacement of the $i$th atom in the condensed and gaseous phases, respectively

If the force constants are the same for the isotopes, the ratio of $(\alpha - 1)$ for $O^{17}$ and $O^{18}$ will simply be given by

$$(\alpha - 1)_{O^{17}} \Big/ (\alpha - 1)_{O^{18}} = \left(\frac{1}{16} - \frac{1}{17}\right) \Big/ \left(\frac{1}{16} - \frac{1}{18}\right) = 0.529$$

In Table III the results for $O^{17}$ are compared with the results of Thode, *et al.*, and with the values of $\alpha_{O^{18}}$ at the corresponding temperatures. Thode, *et al.*, actually measured the ratio $(\alpha_{O^{17}} - 1)/(\alpha_{O^{18}} - 1)$ and in the table the $\alpha_{O^{17}}$ values are given as originally published, using the results of Lewis and Cornish[9] for $\alpha_{O^{18}}$ as a standard. These values also have been recalculated using $\alpha_{O^{18}}$, as given by the formula, as a standard, in order to make direct comparison with the present results possible.

The experimental errors in all the measurements are, however, very large, so that the present results differ barely significantly from Thode's. All that can be said about the change in $(\alpha - 1)$ with temperature is that it takes place in the right direction.

The ratio $(\alpha - 1)_{O^{17}}/(\alpha - 1)_{O^{18}}$ is not significantly different from 0.529 in the experiments at 58 and 73° only. However, considering that the formula for $\alpha_{O^{18}}$ is an approximate formula only, and the large experimental errors in the results for $O^{17}$, the agreement between the average of the four values for the ratio, and the theoretical results, *viz.*, 0.519 with a standard deviation of 0.038, and 0.529, respectively, is satisfactory.

**Acknowledgment.**—Thanks are expressed to Dr. Y. Lehrer and Professor I. Dostrovsky for valuable discussions. The coöperation of the staff of the Israel Atomic Energy Commission and the Heavy Oxygen Plant at the Weizmann Institute of Science is gratefully acknowledged.

(9) G. N. Lewis and R. E. Cornish, *J. Am. Chem. Soc.*, **55**, 2616 (1933).

# CARATHÉODORY'S PRINCIPLE AND THE THERMOKINETIC POTENTIAL IN IRREVERSIBLE THERMODYNAMICS

BY JAMES C. M. LI

*Edgar C. Bain Laboratory for Fundamental Research, United States Steel Corporation Research Center, Monroeville, Pennsylvania*

*Received February 10, 1962*

Carathéodory's principle of the integrability of a Pfaffian differential equation is applied to non-equilibrium systems to establish a thermokinetic potential for the steady state. Such a potential can only decrease with time in all natural processes. Examples on viscous flow, heterogeneous heat conduction, heterogeneous diffusion, consecutive chemical reactions, and a simple radiation heating are used to demonstrate that it is this potential, not the rate of entropy production, which becomes a minimum at the steady state with adjustable variables. In the Appendix the problem of cyclic processes is briefly discussed and it is shown how a small perturbation can cause the system to spiral into the steady state, consistent with the existence of a thermokinetic potential for such a kinetic system.

## Introduction

The second law of thermodynamics was not put on a formal axiomatic basis until Carathéodory[1-3] pointed out that the existence of the entropy function is equivalent to the hypothesis of the existence of inaccessible states in the neighborhood of any arbitrary state along an adiabatic path. Briefly, Carathéodory's approach is as follows; the first-law description of an adiabatic process is simply

$$dE + \delta w = 0 \qquad (1)$$

where $dE$ is the increase of internal energy of the system with $E$ being a state variable and $w$, the work done by the system on the surroundings, not being a state variable. To express $\delta w$ in terms of state variables, advantage is taken of the generally accepted experience that the full capacity of the system to do work in passing from one state to another is never realized on account of the omnipresence of frictional and friction-like processes

(1) C. Carathéodory, *Math. Ann.*, **67**, 355 (1909); *Sitzber. preuss. Akad. Wiss. Physik.-math Kl.*, 39 (1925).

(2) I. N. Sneddon, "Elements of Partial Differential Equations," McGraw-Hill Book Co., Inc., New York, N. Y., 1957, p. 33.

(3) M. Born, *Physik Z.*, **22**, 218, 249, 282 (1921); H. A. Buchdahl, *Am. J. Phys.*, **17**, 44, 212 (1949); **23**, 65 (1955); L. A. Turner, *ibid.*, **28**, 781 (1960).

$$\delta w \leq P\,dV + \ldots \qquad (2)$$

Thus for any actual adiabatic process, the change of state of the system must obey the inequality

$$dE + P\,dV + \ldots \geq 0 \qquad (3)$$

Carathéodory's principle states that the Pfaffian differential equation represented by the equality in eq. 3 is integrable if, and only if, in the neighborhood of any state described by the variables ($E$, $V$, . . .), there exist states which cannot be reached from the given state through an ideal adiabatic path [eq. 3 with equality]. When this inaccessibility is taken as an axiom, eq. 3 is integrable, and an integrating factor (which turns out to be simply $1/T$) can be found from a known system such as an ideal gas. After multiplying by $1/T$, the left-hand side of eq. 3 becomes a total differential and the new state function can be called the entropy, $S$. Thus, we arrive at the second law of thermodynamics

$$dS \geq 0 \qquad (4)$$

Except for the mathematical formalism and the simple axiomatic nature of the approach, the foregoing procedure received little attention mainly because of the fact that the second law of thermodynamics was developed earlier on engineering and physical grounds and was already generally accepted. However, such a procedure would be very useful in problems where the physical development is not yet available. One such problem is the thermodynamic description of a non-equilibrium steady state. It is intended in the following to follow Carathéodory's procedure and to establish a function, the thermokinetic potential, for the steady state. A brief account of this approach has been reported previously[4] as an alternative method of arriving at the thermokinetic potential.

**Second-Law Inequality.**—As we saw in the foregoing procedure for the development of the second law of thermodynamics, we need an inequality, eq. 3, among the state variables, which generally is true for a certain process. To find such an inequality among non-equilibrium state variables, it turns out that the second-law inequality is useful. This latter inequality arises from the fact that if a system is in stable equilibrium when isolated by itself, the stable equilibrium will still prevail when two such identical systems are isolated together. In particular, any virtual transfer of a conservative quantity, $\alpha$, (matter, energy, charge, etc.) between the two identical systems will decrease the entropy, namely

$$dS = dS + dS' = \frac{\partial S}{\partial \alpha}\,d\alpha + \frac{1}{2}\frac{\partial^2 S}{\partial \alpha^2}(d\alpha)^2 + \ldots$$

$$+ \frac{\partial S'}{\partial \alpha'}\,d\alpha' + \frac{1}{2}\left(\frac{\partial^2 S'}{\partial \alpha'^2}\right)(d\alpha')^2 + \ldots \leq 0 \qquad (5)$$

where the prime quantities belong to the second system. Now since

$$d\alpha = -\,d\alpha' \qquad (6)$$

we have

$$\frac{\partial^2 S}{\partial \alpha^2} \leq 0 \qquad (7)$$

required by the second law of thermodynamics for a stable equilibrium system. For two or more variables, the second-law inequality is simply

$$\sum_i \sum_j \frac{\partial^2 S}{\partial \alpha_i\,\partial \alpha_j}\,d\alpha_i\,d\alpha_j \leq 0 \qquad (8)$$

or that the second-order derivatives form a negative definite matrix. Now let us consider a non-equilibrium system by bringing together two slightly different systems. Since the two systems are now different, transfer of conservative quantities between them may take place naturally. This is described by the fluxes

$$J_i = \frac{d\alpha_i'}{dt} = -\frac{d\alpha_i}{dt} \qquad (9)$$

The entropy change accompanying each such transfer is defined as the thermodynamic force

$$X_i = \frac{\partial S'}{\partial \alpha_i'} - \frac{\partial S}{\partial \alpha_i} \qquad (10)$$

We now can examine the quantity

$$\sum_i J_i \frac{dX_i}{dt} = \sum_i \frac{d\alpha_i'}{dt} \sum_j \left( \frac{\partial^2 S'}{\partial \alpha_i'\,\partial \alpha_i'} \frac{d\alpha_j'}{dt} - \frac{\partial^2 S}{\partial \alpha_i\,\partial \alpha_j} \frac{d\alpha_j}{dt} \right) = \sum_i \sum_j \frac{\partial^2 S'}{\partial \alpha_i'\,\partial \alpha_j'} \frac{d\alpha_i'}{dt} \frac{d\alpha_j'}{dt} +$$

$$\sum_i \sum_j \frac{\partial^2 S}{\partial \alpha_i\,\partial \alpha_j} \frac{d\alpha_i}{dt} \frac{d\alpha_j}{dt} \qquad (11)$$

A comparison between eq. 8 and 11 indicates that if the two systems we brought together to form a non-equilbrium system can be assumed to be stable equilibrium systems when isolated separately, we obtain the following inequality[5] for all natural processes

$$\sum_i J_i\,dX_i \leq 0 \qquad (12)$$

**Thermokinetic Potential.**—Before we go on to apply Carathéodory's principle, let us examine the inequality, eq. 12. It states that the thermodynamic forces can decrease only by virtue of the fluxes induced by them when the system is isolated. It thus is only a more rigorous way of stating the Le Chatelier principle for non-equilibrium systems, namely that the effects always take place in a direction so as to moderate the causes. It is to be noted that due to possible interactions among the various causes and effects, eq. 12 states that each individual force may not decrease, and may increase at the expense of larger decreases of other forces. Although the original Le Chatelier principle was intended only for perturbations in an equilibrium

(4) J. C. M. Li, *J. Appl. Phys.*, **33**, 616 (1962).

(5) For systems with mechanical equilibrium and time independent boundary conditions, such an inequality has been shown to be valid by P. Glansdorff and I. Prigogine, *Physica*, **20**, 773 (1954).

system, the foregoing derivation of eq. 12 indicates that the principle is valid even when the system is far from the equilibrium state as long as the irreversible changes can be considered to take place only between the equilibrium parts. This restriction merely asserts the possibility of a thermodynamic description of the state variables at each point in a non-equilibrium system, and seems to be a prerequisite for any macroscopic theory of irreversible processes.

Now when the two systems that we brought together to form a non-equilibrium system are isolated together, eq. 12 will be valid at all times until finally the two systems become one equilibrium system when eq. 12 becomes an equality. Since the fluxes are unique functions of the forces and the forces depend only on the thermodynamic state of each system, which in turn depends only on the amount of fluxes, the natural path from the non-equilibrium state to the equilibrium state is described by a monotonically decreasing function of the nature

$$\mathfrak{F}(t) = \int_{\infty}^{t} \sum_i J_i \frac{dX_i}{dt} dt \qquad (13)$$

For a given initial non-equilibrium system, this function has a unique value at each time if the integral is convergent. The integral will be convergent if $J$ is a well behaved increasing function of $X$ and does not contain terms such as $X^{-1}$. Since this function can only decrease with time in all natural processes, it plays the role of a kinetic potential and can be called the thermokinetic potential of the non-equilibrium system. It also measures the extent of non-equilibrium or the "distance" for the non-equilibrium state to the equilibrium state.

Instead of isolating the two systems together so that the final state is an equilibrium state, we also can apply some external constraints to maintain fixed some of the state variables in each system. For example, we can constrain the temperature of each system to be at constant but different values. This can be done so that all the irreversible changes between the two systems take place as if the two systems were left alone together at any moment. Equation 12 thus still is valid at any time $t$, but the system finally goes to a steady state. Before it reaches the steady state, the path again can be described by the monotonically decreasing function

$$\mathfrak{F}(t) - \mathfrak{F}^0 = \int_{\infty}^{t} \sum_i J_i \frac{dX_i}{dt} dt \qquad (14)$$

where $\mathfrak{F}^0$ is the thermokinetic potential of the steady state defined by eq. 13 for $t = 0$ when the steady state is isolated and left alone.

Different external constraints will give different final steady states. Each steady state will have a unique thermokinetic potential defined by eq. 13. It is possible to change the external constraints on a steady state so that the new steady state has the same thermokinetic potential as the original steady state. Since the thermokinetic potential is a measure of the extent of off-equilibrium, it describes also the dynamic behavior of the non-equilibrium state. An external process which changes the non-equilibrium state but maintains the thermokinetic potential can be called an isodynamic process. Such a process also can be described by eq. 12 with the equality sign.

**Carathéodory's Principle.**—We now can proceed to state a hypothesis for the non-equilibrium system similar to that of Carathéodory for the equilibrium system.[6] Since any steady state, when isolated, will decrease its thermokinetic potential by changing to a slightly different state, we may try to propose that arbitrarily near a given non-equilibrium state described by $(X_1, X_2 \ldots)$ there exist states which cannot be reached by an isodynamic process defined by eq. 12 with the equality sign. According to Carathéodory, eq. 12 then can be integrated after introducing a suitable integrating factor. To find such an integrating factor, we can examine the partial derivatives

$$\frac{\partial J_i}{\partial X_j} = L_{ij} \qquad (15)$$

If the integrating factor which is applicable to any non-equilibrium state is applicable also at the equilibrium state, we have only to examine these partial derivatives at the equilibrium state. At the equilibrium state, they are found to obey the Onsager relations

$$L_{ij} = L_{ji} \qquad (16)$$

Without using the microscopic reversibility, eq. 16 can be considered as an experimental finding just to indicate that the integrating factor can be unity.[7]

We have now constructed a new function which depends only on the non-equilibrium state and can be called the thermokinetic potential

$$d\mathfrak{F} = \sum_i J_i \, dX_i \qquad (17)$$

The difference between eq. 17 and 14 is that in eq. 17 the path of integration is now immaterial. We can calculate the change of thermokinetic potential by eq. 17 from one state to another, not necessarily along the natural path indicated by eq. 14. In fact, an explicit expression for the function $\mathfrak{F}$ can be found when the flux $J_i$ can be expanded into a power series of $X_j$ around the equilibrium state

$$J_i = \sum_j L_{ij} X_j + \frac{1}{2} \sum_j \sum_k L_{ijk} X_j X_k + \ldots \qquad (18)$$

Equation 17 can be integrated if all the $L$'s are constants and are completely symmetric, namely

$$L_{ij} = L_{ji} \qquad (19)$$

$$L_{ijk} = L_{jik} = L_{jki} = \ldots \qquad (20)$$

Then we have

(6) It is to be noted that the Carathéodory principle is a mathematical principle and to use it for the second law of thermodynamics, we have to assume the existence of inaccessible states along the adiabatic path. Similarly, to use it for the non-equilibrium states we have to postulate an analogous assumption. The consequences of these assumptions do not follow directly from Carathéodory's principle and have to be tested by experiments.

(7) The integrating factor may not be unity if eq. 16 does not hold in some cases.

$$\mathfrak{F} = \frac{1}{2!}\sum_i\sum_j L_{ij}X_iX_j + \frac{1}{3!}\sum_i\sum_j\sum_k L_{ijk}X_iX_jX_k + \ldots \quad (21)$$

It is worth mentioning here that eq. 12 always can be integrated if there are only two forces,[2] and therefore for a bi-variant non-equilibrium system, a thermokinetic potential can be defined without Carathéodory's principle. For three or more forces, either of the following two assumptions is needed to ascertain the existence of the thermokinetic potential: (1) the existence in the neighborhood of any non-equilibrium state of states inaccessible by an isodynamic process, or (2) complete symmetry of phenomenological coefficients.[4] The existence of the thermokinetic potential implies also the existence of a stable steady state. The problem of the cyclic processes in which the system oscillates or rotates around the steady state will be discussed in the Appendix.

The relation between the thermokinetic potential and the rate of entropy production has been discussed previously.[4] It has been shown that it is the minimum thermokinetic potential, not the minimum rate of entropy production, which characterizes a steady state. In the following we shall illustrate the interrelationship between these two minimizations by a few specific examples.

**Viscous Flow.**—When the phenomenological equations are linear and with constant coefficients, the thermokinetic potential reduces to exactly one-half of the rate of entropy production. We shall illustrate this with the example of viscous flow. Let the pressure of the viscous fluid at the ends of a uniform pipe be fixed at $P_1$ and $P_2$, respectively. The problem is to find the pressure distribution along the length of the pipe at the steady state. For a viscous liquid, the rate of flow at any point along the pipe is proportional to the pressure gradient

$$J = -k\frac{dP}{d\xi} \quad (22)$$

where $\xi$ is the distance along the pipe, and the thermodynamic force at this point is, when the temperature is kept constant at $T$

$$X = -\frac{V}{T}\frac{dP}{d\xi} \quad (23)$$

For incompressible fluids the specific volume $V$ is also a constant and it is seen from eq. 22 and 23 that the phenomenological equation (between the flux and the force) is linear and with constant coefficients. In this special case, the entropy production for any pressure distribution is simply

$$\dot{S} = \Sigma J_iX_i = \frac{kV}{T}\int_1^2\left(\frac{dP}{d\xi}\right)^2 d\xi \quad (24)$$

and the variational solution to minimize the above integral is simply

$$\frac{dP}{d\xi} = \text{constant} \quad (25)$$

which, of course, is a correct result. Now the change of thermokinetic potential from one pressure distribution to another is

$$d\mathfrak{F} = \Sigma J_i\,dX_i = \frac{kV}{T}\int_1^2\left(\frac{dP}{d\xi}\right)d\left(\frac{dP}{d\xi}\right)d\xi \quad (26)$$

Integrating from the equilibrium state, in which $dP/d\xi = 0$ everywhere, we have

$$\mathfrak{F} = \frac{kV}{2T}\int_1^2\left(\frac{dP}{d\xi}\right)^2 d\xi \quad (27)$$

A comparison between eq. 24 and 27 confirms that the thermokinetic potential is in this case exactly one-half of the rate of entropy production and therefore the condition of minimum thermokinetic potential also is given by eq. 25, which is the correct solution.

**Heterogeneous Heat Conduction.**—When the phenomenological equations are non-linear, or with variable coefficients, or both, the thermokinetic potential is different from one-half the rate of entropy production. It is only the former which becomes a minimum at the steady state. We shall demonstrate this by a few examples.

Let two slabs of similar dimension but of different material be put into thermal contact. The temperature of the external surface of the first slab is kept at $T_1$ and that of the second slab is kept at $T_2$. For simplicity, the temperature distribution within each slab will be assumed linear. The problem is to find at the steady state the temperature, $T$, of the surface of contact of the two slabs. We shall first try to minimize the rate of entropy production. The flux within each slab is proportional to the temperature difference

$$J_1 = k_1(T_1 - T) \quad (28)$$

$$J_2 = k_2(T - T_2) \quad (29)$$

with the corresponding forces

$$X_1 = \frac{1}{T} - \frac{1}{T_1} \quad (30)$$

$$X_2 = \frac{1}{T_2} - \frac{1}{T} \quad (31)$$

The rate of entropy production thus is

$$\dot{S} = J_1X_1 + J_2X_2 = k_1\left(\frac{T_1}{T} + \frac{T}{T_1}\right) + k_2\left(\frac{T_2}{T} + \frac{T}{T_2}\right) - 2(k_1 + k_2) \quad (32)$$

which becomes a minimum at

$$T = \sqrt{T_hT_a} \quad (33)$$

where $T_h$ and $T_a$ are the following weighted harmonic and arithmetic means of $T_1$ and $T_2$

$$\frac{k_1 + k_2}{T_h} = \frac{k_1}{T_1} + \frac{k_2}{T_2} \tag{34}$$

and

$$T_a = \frac{k_1T_1 + k_2T_2}{k_1 + k_2} \tag{35}$$

The temperature in eq. 33 becomes simply the geometric mean of $T_1$ and $T_2$ when $k_1 = k_2$, which is obviously a wrong result.

We now can try to minimize the thermokinetic potential. The change of thermokinetic potential from one interfacial temperature to another is simply

$$d\mathfrak{F} = J_1dX_1 + J_2dX_2$$
$$= [k_1T_1 + k_2T_2 - (k_1 + k_2)T][-dT/T^2) \tag{36}$$

which indicates that the thermokinetic potential is a minimum at

$$T = T_a \tag{37}$$

This is the correct result and reduces to $(T_1 + T_2)/2$ when $k_1 = k_2$ as it should. Equation 36 can be integrated and the thermokinetic potential relative to the steady state is

$$\Delta\mathfrak{F} = (k_1 + k_2)\left(\frac{T_a}{T} + \ln\frac{T}{T_a} - 1\right) \tag{38}$$

which easily can be verified to be positive for all values of $T/T_a$ except $T = T_a$, the steady state value, where $\Delta\mathfrak{F}$ is zero by definiton. Since both the harmonic and the geometric mean approach the arithmetic mean when $T_1$ approaches $T_2$, the condition for minimum rate of entropy production approaches that for the minimum thermokinetic potential when the deviation from equilibrium is small.

**Heterogeneous Diffusion.**—In a similar arrangement as in the case of heterogeneous heat conduction, let the concentration at the external surfaces of the two slabs be kept at $C_1$ and $C_2$, respectively. The problem is to find the concentration, $C$, at the interface in the steady-state isothermal diffusion. Again we shall first try to minimize the rate of entropy production. The fluxes and the forces in the two slabs are

$$J_1 = D_1(C_1 - C) \tag{39}$$
$$J_2 = D_2(C - C_2) \tag{40}$$
$$X_1 = \ln(C_1/C) \tag{41}$$
$$X_2 = \ln(C/C_2) \tag{42}$$

Therefore the rate of entropy production is simply

$$\dot{S} = J_1X_1 + J_2X_2$$
$$= D_1(C_1 - C)\ln\frac{C_1}{C} + D_2(C - C_2)\ln\frac{C}{C_2} \tag{43}$$

and is a minimum at

$$C = \frac{D_1C_1 + D_2C_2}{D_1\left(1 - \ln\frac{C_1}{C}\right) + D_2\left(1 - \ln\frac{C_2}{C}\right)} \tag{44}$$

which is obviously a wrong result for the steady state.

Now the change of thermokinetic potential with respect to the interfacial concentration is

$$d\mathfrak{F} = J_1dX_1 + J_2dX_2$$
$$= [D_1C_1 + D_2C_2 - (D_1 + D_2)C](-dC/C) \tag{45}$$

The thermokinetic potential has thus a minimum at the correct arithmetic mean concentration

$$C_a = \frac{D_1C_1 + D_2C_2}{D_1 + D_2} \tag{46}$$

and has a value which is always higher than that of the steady state by

$$\Delta\mathfrak{F} = (D_1 + D_2)C_a\left(\frac{C}{C_a} + \ln\frac{C_a}{C} - 1\right) \tag{47}$$

similar to eq. 38. Here it is seen again that eq. 44 approaches eq. 46 when the deviation from equilibrium is small.

**Consecutive Chemical Reactions.**—The foregoing two examples can be considered as linear phenomenological equations with variable coefficients. Let us examine a case of non-linear phenomenological equations. The fluxes and forces for the following first-order chemical reactions

$$A \underset{\leftarrow}{\overset{J_1}{\rightarrow}} B \underset{\leftarrow}{\overset{J_2}{\rightarrow}} C \tag{48}$$

are

$$J_1 = k_1A - k_1'B \tag{49}$$
$$J_2 = k_2B - k_2'C \tag{50}$$
$$X_1 = \frac{\mu_A - \mu_B}{T} = \frac{\mu_A^0 - \mu_B^0}{T} + R\ln\frac{A}{B} \tag{51}$$
$$X_2 = \frac{\mu_B - \mu_C}{T} = \frac{\mu_B^0 - \mu_C^0}{T} + R\ln\frac{B}{C} \tag{52}$$

The rate of entropy production is thus

$$\dot{S} = J_1X_1 + J_2X_2$$
$$= (k_1A - k_1'B)\frac{\mu_A - \mu_B}{T} + (k_2B - k_2'C)\frac{\mu_B - \mu_C}{T} \tag{53}$$

and has, when the concentrations of $A$ and $C$ are kept constant, a minimum at

$$B = \frac{RT(k_1A + k_2'C)}{k_1'(\mu_B - \mu_A + RT) + k_2(\mu_B - \mu_C + RT)} \tag{54}$$

which again is not the correct result.

On the other hand, the change of thermokinetic potential with respect to $B$ is

$$\frac{d\mathfrak{F}}{dB} = \frac{R}{B}(k_2B - k_2'C + k_1'B - k_1A) \quad (55)$$

which indicates that the thermokinetic potential has a minimum at

$$B^* = \frac{k_1A + k_2'C}{k_1' + k_2} \quad (56)$$

This is a correct result for the steady state, as one can easily verify by equating $J_1$ and $J_2$ and solving for $B$. It again is seen that eq. 54 approaches eq. 56 when the deviation from the equilibrium is small, namely, when $\mu_A$, $\mu_B$, and $\mu_C$ are close to each other. Integration of eq. 55 gives

$$\Delta\mathfrak{F} = (k_1' + k_2)B^*\left(\frac{B}{B^*} + \ln\frac{B^*}{B} - 1\right) \quad (57)$$

relative to the steady state. The surprisingly similar results of eq. 38, 47, and 57 may indicate a characteristic form of the thermokinetic potential for this type of problem.

**Radiation Heating.**—Another interesting nonlinear example is used by Klein[8] to illustrate that the state of minimum entropy production does not agree with the steady state. He considers a system of $N$ non-interacting particles each of which has two energy states, 0 and $\epsilon$. The system is subjected to radiation whose quanta have energy $\epsilon$ by transition from one state to another with the transition probability $b$ per unit time in both directions. The system also can interact with a heat bath at temperature $T$ with a transition probability $a$ per unit time for the upward transition and $a\alpha$ per unit time for the downward transition. The problem is to find the steady state distribution of the particles in each energy state. For any given distribution, let $p_1$ and $p_2$ be the fraction of particles in the lower and upper states, respectively. In the phenomenological languages, the quantum flux received by the system from radiation is

$$J_1 = Nb(p_1 - p_2) \quad (58)$$

and that rejected by the system to the heat bath is

$$J_2 = Na(\alpha p_2 - p_1) \quad (59)$$

The corresponding thermodynamic forces are the entropy increases associated with each quantum transfer

$$X_1 = k\ln\frac{p_1}{p_2} \quad (60)$$

and

$$X_2 = k\ln\frac{p_2}{p_1} + \frac{\epsilon}{T} \quad (61)$$

(8) M. J. Klein, "A Note on the Domain of Validity of the Principle of Minimum Entropy Production" in "Transport Process in Statistical Mechanics," edited by I. Prigogine Interscience Publishers, Inc., New York, N. Y., 1958, p. 311.

The rate of entropy production thus is

$$\dot{S} = J_1X_1 + J_2X_2$$
$$= Nk\left[b(p_1 - p_2)\ln\frac{p_1}{p_2} + a(\alpha p_2 - p_1)\left(\ln\frac{p_2}{p_1} + \frac{\epsilon}{kT}\right)\right] \quad (62)$$

which agrees with the result obtained by Klein.[8] The state which gives the minimum rate of entropy production does not agree with the steady state. This part is fully discussed by Klein and will not be repeated here.[9] On the other hand, the change of thermokinetic potential with respect to a change of distribution is

$$d\mathfrak{F} = J_1dX_1 + J_2dX_2$$
$$= Nk[b(p_1 - p_2) - a(\alpha p_2 - p_1)]\frac{dp_1}{p_1p_2} \quad (63)$$

which indicates that the thermokinetic potential is a minimum at

$$p_1^0 = \frac{a\alpha + b}{a\alpha + a + 2b} \quad (64)$$

This agrees with the steady-state distribution calculated by Klein by requiring that $dp_1/dt = 0$. Equation 63 can be integrated and the thermokinetic potential relative to the steady state is

$$\Delta\mathfrak{F} = Nk(a\alpha + a + 2b)\left[p_1^0\left(\ln\frac{p_1^0}{p_1} + \frac{p_1}{p_1^0} - 1\right) + p_2^0\left(\ln\frac{p_2^0}{p_2} + \frac{p_2}{p_2^0} - 1\right)\right] \quad (65)$$

which has been written in a form similar to eq. 38, 47, and 57 to show that $\Delta\mathfrak{F}$ is always positive. Equation 65 does not agree with the function proposed by Klein and Rosenbaum,[8] although they are quite similar to each other.

**Acknowledgment.**—The author wishes to thank Drs. L. S. Darken and R. A. Oriani of this Laboratory for valuable discussions.

## Appendix

**Cyclic Processes.**—The assumption of the existence of a thermokinetic potential implies the existence of a stable steady state with respect to variations of adjustable or unprescribed variables. However, the natural path through which a system approaches the steady state may not be straight or direct but may be cycling in a spiral manner. In some extreme cases the situation may be such that the system actually returns to the original state in one cycle. This

(9) One interesting feature of Klein's analysis is the fact that the rate of entropy production goes through a minimum before the system reaches the steady state This happens also in the case of heat conduction where a slab, initially at $T_1$, is heated by maintaining one surface at $T_2$ and another at $T_1$. The entropy production first decreases, goes through a minimum, then increases to the steady state value. The state of mininum entropy production does not give a linear temperature distribution in the slab, as has been shown by Cahn and Mullins.[10]

(10) J. W. Cahn and W. W. Mullins, Discussion of the paper by J. S. Kirkaldy "Theory of Diffusional Growth in Solid-Solid Transformations," AIME Symposium on the Decomposition of Austenite by Diffusional Processes, to be published by AIME.

is the cyclic process discussed by Prigogine and Balescu.[11] As an example, a system contains two species A and B which vary according to the rate laws

$$\frac{dA}{dt} = -A(B - \epsilon_1) \quad (66)$$

$$\frac{dB}{dt} = B(A - \epsilon_2) \quad (67)$$

The natural path of the state of the system can be described by a point in the $A$, $B$ space, which rotates counterclockwise and actually forms a closed loop around the point ($\epsilon_2$, $\epsilon_1$). The situation is, of course, highly unstable, since any small perturbation will change the loop into a spiral. To complete the thermodynamic analysis of this problem, Prigogine and Balescu[8] approximated the above rate laws by the following set of chemical reactions

$$A + M \rightleftarrows 2A \quad (68)$$

$$A + B \rightleftarrows 2B \quad (69)$$

$$B + M \rightleftarrows M' \quad (70)$$

with the following fluxes and corresponding forces

$$J_1 = \epsilon_1'MA - k_1A^2 \quad X_1 = \ln(\epsilon_1'M/k_1A) \quad (71)$$

$$J_2 = AB - k_2B^2 \quad X_2 = \ln(A/k_2B) \quad (72)$$

$$J_3 = \epsilon_2'MB - k_3M' \quad X_3 = \ln(\epsilon_2'MB/k_3M') \quad (73)$$

When $M$ and $M'$ are kept constant such that $\epsilon_1'M = \epsilon_1$ and $\epsilon_2' M = \epsilon_2$ and $k_1$, $k_2$, and $k_3$ are very small, it is seen that these chemical reactions approach the rate laws of eq. 66 and 67. However, small perturbations due to the reverse reactions will change the steady-state point ($\epsilon_2$, $\epsilon_1$) to

$$A = \epsilon_2 + k_2B - k_3\frac{M'}{B} \quad (74)$$

$$B = \epsilon_1 - k_1A + k_2\frac{B^2}{A} \quad (75)$$

For simplicity, let us examine the case where the new ($\epsilon_2^0$, $\epsilon_1^0$) becomes

$$\epsilon_2^0 = \epsilon_2 + k_2(B - \epsilon_1) \quad (76)$$

$$\epsilon_1^0 = \epsilon_1 \quad (77)$$

(11) I. Prigogine and R. Balescu, *Bull. classe sci. Acad. roy. Belg.*, **42**, 256 (1956); also in "Transport Processes in Statistical Mechanics," Proceedings of International Symposium, Brussels, Aug., 1956, edited by I. Prigogine, Interscience Publishers, Inc., New York, N. Y., 1958, p. 343.

This gives the new rate laws

$$\frac{dA}{dt} = -A(B - \epsilon_1) \quad (78)$$

$$\frac{dB}{dt} = B[A - \epsilon_2 - k_2(B - \epsilon_1)] \quad (79)$$

This will cause the state of the system to spiral into the steady state, as can be seen from

$$\frac{(dB/dA)_{new}}{(dB/dA)_{old}} = 1 - k_2\frac{B - \epsilon_1}{A - \epsilon_2} \quad (80)$$

so that the slope is less negative in the first and third quadrants but more positive in the second and fourth quadrants and for a counterclockwise motion this means spiraling into the origin ($\epsilon_2$, $\epsilon_1$). Now with such a perturbation a stable state requires the inequality

$$J_1dX_1 + J_2dX_2 + J_3dX_3 = (B - \epsilon_1)dA - [A - \epsilon_2 - k_2(B - \epsilon_1)]\,dB \leq 0 \quad (81)$$

This is equivalent to the following inequality in terms of polar coördinates ($r$, $\theta$) relative to the steady state ($\epsilon_2$, $\epsilon_1$)

$$k_2\,d\ln r - \frac{1 - k_2\sin\theta\cos\theta}{\sin^2\theta}\,d\theta \leq 0 \quad (82)$$

Equation 82 can be integrated and the following positive angle can be defined as the thermokinetic potential of the system

$$\mathfrak{F} = \tan^{-1}\left[k_2\ln r + \cot\theta + \frac{k_2}{2}\ln\sin^2\theta\right] \quad (83)$$

The inequalities (81) and (82) demand that $\mathfrak{F}$ decreases with time for a natural process. This can be achieved either by rotating counterclockwise around the steady state ($\epsilon_2$, $\epsilon_1$) or by reducing $r$. Without the perturbation required by a positive $k_2$, the system cannot reach the steady state even though the thermokinetic potential can still decrease with time by increasing $\theta$. But with the perturbation, the system can now spiral into the steady state by reducing $r$. Very near the steady state, the spiraling nature can be illustrated for the case of $\epsilon_1 = \epsilon_2$

$$\frac{d\ln r}{d\theta} = -\frac{k_2}{1 - k_2\cot\theta + \cot^2\theta} \quad (84)$$

It is seen that $r$ decreases with counterclockwise rotation for any small positive $k_2$.

The foregoing example is really a very rare situation. The purpose of the discussion here is only to show that the possibility of a cyclic process does not rule out the existence of a thermokinetic potential for such a kinetic system.

# TRACER STUDIES ON THE OXIDATION OF LEAD(II) BY HYDROGEN PEROXIDE[1]

BY U. AGARWALA, M. ANBAR, AND HENRY TAUBE

*George Herbert Jones Laboratory of the University of Chicago, Chicago, Ill.*

*Received February 12, 1962*

In the reaction of $H_2O_2$ with Pb(II) in alkaline solution, only partial oxidation of Pb(II) to Pb(IV) takes place. Tracer studies show that over a considerable range of conditions, the oxygen content of the $PbO_2$ component of the solid is derived entirely from the $H_2O_2$, and that of the PbO component from the solvent. With permonoacetate as oxidizing agent, the extent of oxygen transfer from the oxidizing agent is much less. Pb(II) can be leached from the solid by acid without bringing about complete exchange of $PbO_2$ with solvent. When Pb is oxidized by $H_2O_2$ in alkali, the peroxide oxygen content of the solid exceeds that which is equivalent to the $PbO_2$.

Little work has been done on the mechanism of formation of metal oxides (or hydrous oxides) by the action of oxidizing agents or on the mechanism of reduction of such oxides. For many of the reactions, the stoichiometry is hard to define, and for most of them, significant kinetic data are not obtainable. But even for systems which are intractable in these respects, tracer studies often can be made, and the results of these studies may constitute the most important experimental evidence bearing on the mechanism of the reactions. In this paper we report the results of one such study made using $O^{18}$ as a tracer in the oxidation of Pb(II) by $H_2O_2$ in alkaline solution.

**Method.**—In a typical experiment, $H_2O_2$ in solution with enriched water was added with vigorous stirring to the alkaline solution containing Pb(II) in water of the same isotopic enrichment as that carrying the oxidizing agent. The reaction takes place immediately on mixing. The product precipitate was collected, washed with water of the isotopic composition of the reaction mixture, dried *in vacuo* at 80–90°, then at 150° for several hours more. A part of the precipitate was analyzed for the content of lead (using the $PbMoO_4$ method) and for the content of Pb(IV) (using oxalate as reducing agent). A part was subjected to isotopic analysis using the Anbar and Guttman[2] method to convert the contained oxygen to $CO_2$.

Atmospheric $CO_2$ vitiates the experiments, and precautions were taken to keep contamination by it to a minimum. The alkali was treated so as to render it "carbonate-free"; the solutions, while alkaline, were kept under a blanket of $CO_2$-free $N_2$.

As will be noted from the report of results which follows, the oxidation of Pb(II) to Pb(IV) is in no case complete, even when a large excess of oxidizing agent is used. Furthermore, the extent of oxidation is variable from experiment to experiment so that a simple formula cannot be assigned to the product. It is not easy to decide using ordinary physico-chemical tools whether a mixture of phases is present, or whether a solution of $PbO_2$ in PbO is formed. No lines are observed when a sample of the dry powder is subjected to examination by X-rays, but only diffuse bands, and it must be concluded that the crystals, whatever their finer structure, are very small. The last traces of water are difficult to remove; a typical product which contains, for example, 40–60% $PbO_2$ retains approximately 2 to 3% of water after drying at room temperature.

The isotopic compositions throughout are reported as enrichment ratios; $E$:$E$ is defined as the isotopic ratio in the sample under investigation compared to that of a standard sample of normal isotopic composition.

## Results

In Table I are shown the results of a series of related experiments on the reaction of Pb(II) with $H_2O_2$.

(1) This study was begun by M.A. in 1955, and the observations have been refined and extended by U.A.

(2) M. Anbar and S. Guttman, *J. Appl. Rad. Isotopes*, **5**, 233 (1959).

TABLE I

TRANSFER OF OXYGEN IN THE REACTION OF $H_2O_2$ WITH Pb(II)

Concentrations are recorded for the mixed solutions before reaction; $E$ of the solvent is in the range 2.3 to 2.5; $E$ of $H_2O_2$ is 1.00

| A ($Pb(NO_3)_2$) | B (NaOH) | C ($H_2O_2$) | Order of mixing | % $PbO_2$ | E of product Obsd. | E of product Calcd.[a] |
|---|---|---|---|---|---|---|
| 0.08 | 1.5 | 0.5 | C to A + B | 58.5 | 1.31 | 1.35 |
| .045 | 0.6 | .10 | C to A + B | 56.1 | 1.32 | 1.39 |
| .08 | 1.0 | .5 | C to A + B | 42.9 | 1.66 | 1.63 |
| .05[b] | 0.3 | .16 | C to A + B | 61.5 | 1.40 | 1.30 |
| .05[b] | .3 | .16 | C to A + B | 53.1 | 1.50 | 1.41 |
| .05 | .4 | .18 | C − B to A | 34.9 | 2.04 | 1.65 |
| .06 | .5 | .18 | C − B to A | 32.8 | 1.97 | 1.64 |

[a] Assuming that all and only the oxygen in $PbO_2$ is derived from $H_2O_2$. Since the $PbO_2$-oxygen content is assumed to be of normal isotopic composition, and the PbO being derived from the solvent contains enriched oxygen, the values of $E_{calcd.}$ are obtained from the expression: (atom fraction $PbO_2$-oxygen) + $E_{solv.}$ (atom fraction PbO-oxygen) where $E_{solv.}$ is the enrichment ratio of the solvent. [b] In these experiments, the bulk of the Pb(II) was present initially as a precipitate.

In the first three experiments of Table I the peroxide-oxygen content of the solid corresponds very closely to that contained in $PbO_2$. Even in the next two experiments in which hydrous PbO was the principal form in which the reducing agent was initially present so that the reaction involves the transformation of one solid to another, the peroxide-oxygen content still corresponds fairly closely to that of $PbO_2$. But in the last two experiments, in which alkaline $H_2O_2$ was added to $Pb(NO_3)_2$ which had not been made alkaline, the extent of transfer of peroxide oxygen is much diminished.

In all of the experiments reported in Table I the oxidizing agent, $H_2O_2$, was added to the liquid containing Pb(II). When the reverse order of mixing is used there is copious decomposition of the peroxide, and even when the $H_2O_2$ is used in high excess and remains in excess for much of the reaction, the $PbO_2$ content of the solid product is small. In two experiments, in each of which a solution of $Pb(NO_3)_2$ was added to a solution initially 1.5 $M$ in $H_2O_2$ and 0.60 $M$ in NaOH, the percentages of $PbO_2$ in the solid after filtering, washing, and drying were 24 and 37%. The experiments did not agree in the peroxide-oxygen content of the solid; in one case it corresponded to more than the $PbO_2$ content, and in the other to less.

When concentrated $H_2O_2$ is added to the plum-

bite solution, the formation of a black-brown precipitate appears to be instantaneous, but with dilute $H_2O_2$ different stages of the reaction can be discerned. A brownish white precipitate is first formed at the point of contact of the solutions and then rapidly darkens. When $Pb(OAc)_2$ rather than $Pb(NO_3)_2$ is used to make up the plumbite solution, the separate reaction stages are more strikingly displayed. Using again a dilute solution of $H_2O_2$, a white precipitate is observed to form at the point of contact of the solutions, and this precipitate then darkens. The tracer result obtained when the plumbite is made up from $Pb(OAc)_2$ is not as clean cut as it is when $Pb(NO_3)_2$ is used. Thus in an experiment done adding $H_2O_2$ to a solution initially 1.2 $M$ in NaOH and 0.08 $M$ in $Pb(OAc)_2$, the $PbO_2$ content of the product was found to be 55.6% with $E = 1.31$. This value of $E$ is to be compared to $E = 1.50$ calculated assuming that only and all the oxygen in the $PbO_2$ part of the product is derived $H_2O_2$, and to $E = 2.67$ for the solvent.

When the reaction of $H_2O_2$ with Pb(II) takes place in a medium alkaline enough (>3 $M$ NaOH) so that Pb(IV) remains in solution and $PbO_2$ is later precipitated by acidifying, the solid that is formed has an isotopic composition within 1% of that of the solvent. This result was obtained using $NH_4Cl$ to acidify the solution. When acetic acid is used, some acetate-oxygen appears in the product.

An experiment was done to learn whether $PbO_2$-oxygen is retained when the incompletely oxidized solid formed in the reaction of Pb(II) in alkali with $H_2O_2$ is leached with acid. The solid used in this experiment was the product obtained in experiment 3 of the table. The material of average $E = 1.66$ was treated at 50° with 0.5 $M$ $HNO_3$ in 2.6-fold enriched water. The resulting black solid was filtered, washed, and dried, then chemical and isotopic analyses were made. The content of $PbO_2$ had risen to 85.6% and the value of $E$ to 1.94, still far from the equilibrium value of 2.60, but also far from the value of 1.14 calculated assuming that the $PbO_2$ portion undergoes no exchange.

The attempts to oxidize PbO with $H_2O_2$ in alkaline solution did not lead to a useful tracer result because the extent of oxidation was in every case too small, at most 3 to 4%. However, other observations were made in the course of these experiments which do seem worth reporting. No measurable exchange was observed between commercially prepared PbO and water in a period of time of 18 hr. But when PbO is used which is freshly prepared (the hydroxide was precipitated at room temperature and the solid was heated at 180–190° for 5 hr. and 500° for 1 hr.) the exchange was much more rapid. With this solid using enriched water of $E = 2.85$, the value of $E$ rose from 1.00 to 1.88 after 1 hr. and to 1.95 after 2 hr. When the experiment was repeated but with $H_2O_2$ present at ~1 $M$ and NaOH at ~0.7 $M$, the value of $E$ rose to only 1.35 after about 1 hr. of contact.

When permonoacetate is the oxidizing agent, the transfer of oxygen to the lead oxide is much less than it is for $H_2O_2$. In an experiment in which permonoacetate was added to a solution 0.08 $M$ in Pb(II) and 1 $M$ in NaOH, the solid oxide was found to contain 32.2% $PbO_2$. The value of $E$ for the oxide was found to be 2.60. This is to be compared with $E$ for the solvent as 2.85, and $E$ calculated, assuming all and one-half of the $PbO_2$ oxygen to be derived from the permonoacetate as 1.98 and 2.41, respectively.

The oxidation of lead metal by alkaline hydrogen peroxide proceeds rapidly but again with incomplete oxidation of Pb to Pb(IV). One such reaction was carried out, and isotopic and chemical analyses were performed on the solid product. They showed that the composition of the product can be expressed by the formula $PbO_2 \cdot 0.60PbO \cdot 0.83PbO^*$, where O and O* represent peroxide and solvent oxygen, respectively.

Some oxygen tracer experiments also were done on the oxidation of PbS to $PbSO_4$. Using 3 $M$ $H_2O_2$ as the oxidizing agent in three experiments, one done with commercial PbS, and the other two with the freshly prepared material, the number of oxygens for each $SO_4^{-2}$ formed which originated in the peroxide was found to be 3.10, 3.09, and 3.08. With alkaline $OCl^-$ as oxidizing agent (3 $M$ NaOCl, 1 $M$ NaOH), 1.0 oxygen for each $SO_4^{-2}$ was found as originating in the oxidizing agent.

## Discussion

The major result obtained in this study is that in the reaction of plumbite with $H_2O_2$ all of the oxygen in the $PbO_2$ part of the solid is derived from the oxidizing agent. The Pb(II) makes special use of the peroxide oxygen, and keeps it distinct from other oxygen with which it is in contact. The reaction thus has some similarity to that of $H_2O_2$ with sulfite[3] or nitrite[4] in acid, and it can be understood in a similar way. An $HO_2^-$ or $O_2^{-2}$ group coordinated to $Pb^{++}$ rearranges, presumably making use of the free electron pair which the cation has, just as the formation of $SO_4^{-2}$ can be imagined as

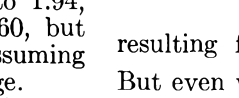

resulting from a rearrangement of $HOO{:}\ddot{\underset{\ddot{}}{S}}{:}O^-$. But even when this much is admitted, two rather different mechanisms remain for serious consideration and cannot be distinguished on the basis of present evidence. One is that a peroxide phase of formula $Pb(II)O_2$ first precipitates and then rearranges to $PbO_2$; if this is the case, the preference of $PbO_2$ for peroxide-oxygen is not a matter of oxidation mechanism but of stability of the Pb(II)-$O_2$ phase. The other is that $PbO_2$ is laid down directly from Pb(II) and $H_2O_2$ as they come into contact on the solid. The essential difference is that by the first mechanism Pb(II) in being oxidized is in contact only with peroxide oxygen, while by the second mechanism, it excludes other oxygen and selects peroxide oxygen in the act of being oxidized. It is not clear how this distinction can be made, unless perhaps it proves possible to identify the $Pb(II)O_2$ stage directly as part of the reaction sequence. That a peroxy-containing phase may form first in some systems is indicated by the observations made with $Pb(OAc)_2$. The white precipitate first formed may be a mixed peroxide–

(3) J. Halperin and H. Taube, *J. Am. Chem. Soc.*, **74**, 380 (1952).
(4) M. Anbar and H. Taube, *ibid.*, **76**, 6243 (1954).

acetate of Pb(II). Taking the observations with plumbite made up from $Pb(NO_3)_2$ and $Pb(OAc)_2$ together, it seems likely that a peroxy-containing phase forms first in both systems, and the distinction between the two mechanisms devolves on the question: is the solid phase $Pb(II)O_2$, or does it contain ions such as $OH^-$ and $OAc^-$ in addition to $OOH^-$?

The extent of transfer from $CH_3CO_3^-$ to lead oxide corresponds to less than one oxygen for each $PbO_2$ formed. The qualitative difference from the reaction with $H_2O_2$ is not surprising, because the rearrangement mechanism which leads to two peroxide oxygens for each Pb(IV) would require $CH_3CO^+$ to be removed from the peroxide. The fact that the transfer is less than one oxygen for each molecule of oxidizing agent may mean that the reaction can take place partly by electron transfer, and constitutes an aspect of the work calling for further investigation.

The observation that most of the PbO can be leached from the solid without bringing $PbO_2$ into complete isotopic equilibrium with the solvent suggests that Pb(IV) is not homogeneously distributed throughout the solid but that it constitutes a separate phase though it may be extremely finely dispersed.

Special attention should be directed to the observations on the oxidation of Pb metal. The peroxide oxygen content of the product is well in excess of that associated with Pb(IV). This shows that the first stage of the oxidation, which presumably takes Pb to Pb(II), does not proceed entirely by an "electrolytic" mechanism, because in large part the very oxygen that is released by the oxidizing agent is incorporated into the solid, even a part of that corresponding to the PbO component. In view of the exchange between PbO and water observed in other experiments, the value reported as the peroxide-oxygen content of the solid is a lower limit on that actually transferred, and the extent of transfer may well be almost 100%.

The observations made thus far on the oxidation of PbS provide little basis for comment. Although transfer of oxygen is only partial, both with $H_2O_2$ and $OCl^-$, the extent of transfer corresponds rather closely to simple stoichiometry for the isotopic course of the reaction. It will be interesting to learn whether the stoichiometry is the accidental result of competition between exchange and transfer, or whether it is something more nearly intrinsic and as such is preserved over a considerable range of conditions.

**Acknowledgment.**—This work was supported by the Office of Naval Research under Contract Nonr-2121(16).

# STANDARD ELECTROMOTIVE FORCE OF THE CELL $H_2$; HBr($m$), AgBr; Ag FROM 0 TO 50°

BY HANNAH B. HETZER, R. A. ROBINSON, AND ROGER G. BATES

*Solution Chemistry Section, National Bureau of Standards, Washington 25, D. C.*

*Received February 12, 1962*

The standard electromotive force of the cell Pt; $H_2$ (G, 1 atm.), HBr($m$), AgBr; Ag from 0 to 50° has been redetermined in an effort to resolve a discrepancy appearing in the literature. Thermal silver–silver bromide electrodes were used, and the molality of hydrobromic acid varied from 0.005125 to 0.10085. The activity coefficient at 0, 25, and 50° and the relative partial molal heat content of hydrobromic acid at 25° have been derived from the measurements. The results are in satisfactory accord with the earlier work of Harned, Keston, and Donelson[3] but do not confirm the later values of Harned and Donelson[4] and of Owen and Foering[5] which are themselves in substantial agreement. The activity coefficients derived from three separate studies agree well, suggesting that the differences in standard potential may be attributed to differences among electrodes prepared in different ways.

## Introduction

The hydrogen–silver chloride cell has been used successfully in this Laboratory to study the ionization behavior of a number of weak nitrogenous bases.[1] In order to obtain accurate results, it is sometimes necessary to apply corrections for the solubility of silver chloride in the buffer solutions and to prevent, by mechanical means, the diffusion of silver to the hydrogen electrode. In order to study amines which form unusually stable complexes with silver ion, it was deemed advisable to substitute the silver–silver bromide electrode for the silver–silver chloride electrode, silver chloride being about fifteen times more soluble than silver bromide. Although the standard potential of the silver–silver bromide electrode has been the subject of several careful studies, the reported values differ by as much as 0.37 mv. and it is not clear which set of data should be considered the most reliable.

Keston[2] studied the hydrogen–silver bromide cell at 25° only and found $E^0$ to be 0.0711 abs. v. Harned, Keston, and Donelson (H, K, and D)[3] studied the same cell from 0 to 60° with solutions of hydrobromic acid varying in concentration from 0.003 to 0.2 $m$. From their results at 25°, $E^0$ is found to have a value of 0.07105 abs. v.

The results of Harned and Donelson,[4] on the other hand, for the same cell containing 0.1 $m$ hydrobromic acid with added lithium bromide at 0 to 60°

(1) See, for example, R. G. Bates and G. D. Pinching, *J. Res. Natl. Bur. Std.*, **42**, 419 (1949); R. G. Bates and H. B. Hetzer, *J. Phys. Chem.*, **65**, 667 (1961); and H. B. Hetzer and R. G. Bates, *ibid.*, **66**, 308 (1962).

(2) A. S. Keston, *J. Am. Chem. Soc.*, **57**, 1671 (1935).

(3) H. S. Harned, A. S. Keston, and J. G. Donelson, *ibid.*, **58**, 989 (1936).

(4) H. S. Harned and J. G. Donelson, *ibid.*, **59**, 1280 (1937).

TABLE I

ELECTROMOTIVE FORCE OF THE CELL Pt; $H_2$(G, 1 ATM.), HBr($m$), AgBr; Ag FROM 0 TO 50° (IN V.)

| $m$ | 0° | 5° | 10° | 15° | 20° | 25° | 30° | 35° | 40° | 45° | 50° |
|---|---|---|---|---|---|---|---|---|---|---|---|
| 0.005125 | 0.33291 | 0.33592 | 0.33865 | 0.34129 | 0.34368 | 0.34594 | 0.34804 | 0.35004 | 0.35189 | 0.35359 | 0.35521 |
| .005140 | .33268 | .33566 | .33843 | .34110 | .34349 | .34582 | .34782 | .34981 | .35172 | .35337 | .35496 |
| .007617 | .31471 | .31735 | .31978 | .32209 | .32420 | .32611 | .... | .... | .... | .... | .... |
| .010021 | .... | .... | .... | .... | .... | .31265 | .... | .... | .... | .... | .... |
| .010065 | .30209 | .30454 | .30681 | .30882 | .31070 | .31238 | .31399 | .31529 | .31664 | .31777 | .31880 |
| .012389 | .29279 | .29500 | .29703 | .29894 | .30065 | .30229 | .30354 | .30488 | .30603 | .30706 | .30789 |
| .015158 | .28366 | .28577 | .28761 | .28931 | .29084 | .29225 | .29347 | .29454 | .29552 | .29624 | .29689 |
| .019876 | .27162 | .27344 | .27516 | .27663 | .27787 | .27898 | .28005 | .28098 | .28172 | .28228 | .28275 |
| .02533 | .... | .... | .... | .... | .... | .26718 | .... | .... | .... | .... | .... |
| .03006 | .25325 | .25482 | .25613 | .25726 | .25825 | .25901 | .25976 | .26020 | .26072 | .26098 | .26112 |
| .03041 | .25247 | .25400 | .25533 | .25649 | .25744 | .25825 | .25897 | .25950 | .25991 | .26018 | .26033 |
| .03999 | .24025 | .24165 | .24271 | .24353 | .24429 | .24492 | .24537 | .24566 | .24589 | .24596 | .24575 |
| .04974 | .23045 | .23170 | .23264 | .23343 | .23407 | .23449 | .23479 | .23497 | .23499 | .23486 | .23450 |
| .04980 | .... | .... | .... | .... | .... | .23426 | .... | .... | .... | .... | .... |
| .05030 | .... | .... | .... | .... | .... | .23385 | .... | .... | .... | .... | .... |
| .06015 | .22188 | .22284 | .22364 | .22428 | .22473 | .22498 | .22514 | .22519 | .22501 | .22471 | .22429 |
| .06586 | .21773 | .21871 | .21945 | .21996 | .22036 | .22063 | .22066 | .22054 | .22036 | .22007 | .21963 |
| .06985 | .21529 | .21614 | .21679 | .21726 | .21758 | .21778 | .21780 | .21773 | .21741 | .21708 | .21656 |
| .07578 | .21155 | .21325 | .21296 | .21337 | .21360 | .21382 | .21367 | .21351 | .21319 | .21283 | .21224 |
| .08048 | .20894 | .20969 | .21026 | .21064 | .21085 | .21093 | .21085 | .21064 | .21026 | .20979 | .20919 |
| .09035 | .20356 | .20432 | .20482 | .20512 | .20524 | .20524 | .20506 | .20478 | .20432 | .20382 | .20316 |
| .10082 | .19886 | .19943 | .19982 | .20003 | .20006 | .19994 | .19970 | .19934 | .19883 | .19821 | .19745 |
| .10085 | .19886 | .19945 | .19983 | .19996 | .20001 | .19993 | .... | .... | .... | .... | .... |

lead to $E^0 = 0.07133$ at 25°. The latter value is in good agreement with $E^0 = 0.07131$ abs. v. derived by Owen and Foering[5] from studies (at 5 to 40°) of hydrogen–silver bromide cells containing potassium bromide solutions buffered with borax. Thermal silver bromide electrodes were used in the two latter studies, whereas H, K, and D studied electrodes of both the thermal and electrolytic types. No consistent differences between the two types of electrode were found. A still higher value, 0.0716 abs. v. at 25°, has been reported by Towns, Greeley, and Lietzke.[6]

The standard electromotive force of the hydrogen–silver bromide cell now has been redetermined from 0 to 50° by means of e.m.f. measurements using hydrobromic acid solutions varying in concentration from 0.005125 to 0.10085 $m$. The silver bromide electrodes were of the thermal type. The standard potential at 25° was found to be 0.07106 abs. v. The activity coefficient of hydrobromic acid in aqueous solutions at molalities less than 0.1 and temperatures from 0 to 50° has been obtained, and the relative partial molal heat content of hydrobromic acid in these solutions at 25° has been derived.

## Materials and Procedures

A reagent-grade solution of hydrobromic acid containing about 48% by weight HBr was distilled twice from a little red phosphorus. The middle half of the distillate was collected. The azeotropic concentration is 47.8% by weight HBr at 1 atm.[7] This solution was diluted to about 0.1 $M$ and was preserved in a large Pyrex bottle shielded from the light. The concentration of this stock solution was determined gravimetrically by weighing silver bromide. The analysis was repeated during the series of measurements as well as after the work was completed. No significant change was detected.

The silver–silver bromide electrodes were of the thermal type, formed by heating at 550° a paste consisting of 10% by weight of silver bromate and 90% silver oxide. Two coats of paste were applied, and each was heated for 10 min. at 550° to effect complete decomposition. The finished electrodes, light gray in color, were roughly spherical and about 5 mm. in diameter. Before use, each set of electrodes was intercompared in 0.05 $M$ hydrobromic acid from which oxygen had been removed by bubbling hydrogen. After an initial aging period of a few hours, electrodes agreed among themselves to better than 0.05 mv. Electrodes prepared by decomposition at 580° likewise displayed the same potentials as those prepared at 550° after initial equilibrium had been obtained.

The silver bromate was recrystallized twice from hot water. The preparation of the silver oxide and of the platinum–hydrogen electrodes has been described elsewhere.[8]

The cells were also of a type earlier described.[9] The solutions were prepared by the weight dilution of the stock solution with water which, in equilibrium with the air, had a conductance of 0.7 to 0.8 $\times 10^{-6}$ ohm$^{-1}$ cm.$^{-1}$. The solutions were de-aerated with bubbling hydrogen before the cells were filled.

The e.m.f. usually was measured at 25° at the beginning, in the middle, and at the end of each run. The mean difference between the first and second readings was 0.07 mv., whereas that between the second and third readings at 25° was 0.06 mv. Each e.m.f. value recorded in Table I is the mean of two pairs of electrodes in the same cell. Observed values of the e.m.f. have been corrected to a hydrogen partial pressure of 1 atm.

## Results

In order to reduce the e.m.f. data to a straight-line function of $m$, from which the standard potential could be obtained accurately, the quantity $E^{0\prime}$ was computed from each value of the e.m.f. recorded in Table I.

(5) B. B. Owen and L. Foering, *J. Am. Chem. Soc.*, **58**, 1575 (1936).

(6) M. B. Towns, R. S. Greeley, and M. R. Lietzke, *J. Phys. Chem.*, **64**, 1861 (1960).

(7) D. T. Ewing and H. A. Shadduck, *J. Am. Chem. Soc.*, **47**, 1901 (1925).

(8) R. G. Bates, "Electrometric pH Determinations," John Wiley and Sons, Inc., New York, N. Y., 1954, pp. 166 and 206.

(9) R. G. Bates and S. F. Acree, *J. Res. Natl. Bur. Std.*, **30**, 129 (1943).

$$E^{0\prime} \equiv E^0 - 2k\beta m = E + 2k \log m - 2k\left[\frac{A\sqrt{m}}{1 + Ba^*\sqrt{m}}\right] \quad (1)$$

In this equation, $A$ and $B$ are constants of the Debye–Hückel theory,[10] $a^*$ is the ion-size parameter, $\beta$ is the slope of the extrapolation line, and $k$ is written for $2.3026RT/F$. The value of $R$ was taken to be 8.31467 j. deg.$^{-1}$ mole $^{-1}$ (1.98725 defined cal. deg.$^{-1}$ mole $^{-1}$), $F$ to be 96,495.4 coulombs equiv.$^{-1}$, and $T$ to be $t$ (°C.) + 273.150. This form of extrapolation function, which utilizes the two-parameter form of the Debye-Hückel equation, was found to be more suitable than that used by H, K, and D (which employs the limiting law) or that suggested by MacInnes,[11] inasmuch as an extrapolation line of considerably smaller slope was obtained.

Several values of $a^*$ were tried, and the standard deviation of the individual points from the line was used as a guide to the proper choice.[12] The most suitable value was found to be 4.4 Å. for the entire temperature range. This is also the value most consistent with the activity coefficients of hydrobromic acid.[3] The plots of $E^{0\prime}$ (calculated with $a^* = 4.4$ Å.) as a function of $m$ at 0, 25, and 50° are shown in Fig. 1.

The values of the standard potential ($E^0$) obtained by the method of least squares are summarized in Table II, together with the corresponding values of $\sigma_i$, the standard deviation of the intercept. Figure 1 and the data of H, K, and D show that the values of $E^{0\prime}$ fall slightly above the straight line at $m$ greater than about 0.1. Consequently, the points at $m = 0.10082$ and $m = 0.10085$ were not included in the least-squares treatment.

TABLE II

STANDARD ELECTROMOTIVE FORCE ($E^0$) OF THE CELL $H_2$; HBr($m$), AgBr; Ag FROM 0 TO 50°

| $t$ | This investigation, v. | $\sigma_i$, mv. | H, K, and D,[3] v. |
|---|---|---|---|
| 0 | 0.08128 | 0 04 | 0.08130 |
| 5 | .07961 | .04 | .07958 |
| 10 | .07773 | .04 | .07773 |
| 15 | .07572 | .04 | .07563 |
| 20 | .07349 | .04 | .07342 |
| 25 | .07106 | .03 | .07105 |
| 30 | .06856 | .04 | .06847 |
| 35 | .06585 | .04 | .06577 |
| 40 | .06310 | 05 | .06294 |
| 45 | .06012 | 04 | .05999 |
| 50 | .05704 | .04 | .05689 |

The value of $E^0$ (in v.) is given as a function of $t$ (in °C.) by

$$E^0 = 0.07109 - 4.87 \times 10^{-4}(t - 25) - 3.08 \times 10^{-6}(t - 25)^2 \quad (2)$$

The average difference between the "observed" values of $E^0$ and those calculated by eq. 2 at the 11 temperatures is 0.03 mv.

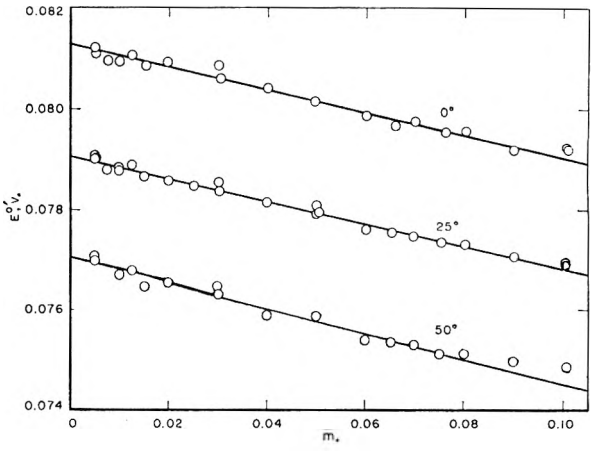


Fig. 1.—Plots of $E^{0\prime}$ as a function of $m$ at 0, 25, and 50°. The best straight line was established by least-squares methods, using only the points at $m < 0.1$.

Table II also lists the standard potentials obtained by H, K, and D,[3] corrected to abs. v. The results obtained by Harned and Donelson[4] and by Owen and Foering[5] at 5 to 30° are from 0.2 to 0.3 mv. higher than those found in this investigation. At 40°, the results of all four investigations are in substantial agreement. Above 40°, the values of $E^0$ found by Harned and Donelson are lower than those found in the present work.

**Derived Quantities.**—Values of $\gamma_\pm$, the mean ionic molal activity coefficient of hydrobromic acid at 0, 25, and 50°, were calculated by the equation

$$-\log \gamma_\pm = \frac{E - E^0}{2k} + \log m \quad (3)$$

and are given in Table III. The relative partial molal heat content ($\bar{L}_2$) of hydrobromic acid (in cal. mole$^{-1}$) at 25° was computed from the temperature coefficient of log $\gamma_\pm$. It is included in Table III where, for purposes of comparison, also are listed the comparable values of $\gamma_\pm$ and $\bar{L}_2$ obtained by H, K, and D.[3] In general, the agreement between the results of the two investigations may be said to be most satisfactory.

## Discussion

Although most of the cells used by Harned and Donelson contained 0.01 $m$ hydrobromic acid and different amounts of lithium bromide, one cell contained 0.01 $m$ hydrobromic acid only. Harned, Keston, and Donelson used cells containing only hydrobromic acid, and in one cell the concentration was also 0.01 $m$. The results of Harned and Donelson between 0 and 35° are uniformly about 0.3 mv. higher than those of H, K, and D. The two results agree at 45°, but that of Harned and Donelson is 0.19 mv. lower than that of H, K, and D at 50°. This difference is reflected in the extrapolated standard potentials. There may, therefore, have been some difference in the method of preparing the silver–silver bromide electrodes.

The data of Owen and Foering agree with those of Harned and Donelson and, between 5 and 35°, are higher than those of H, K, and D and those

(10) R. A. Robinson and R. H. Stokes, "Electrolyte Solutions," 2nd Ed., Academic Press, Inc., New York, N. Y., 1959, Appendix 7.1.

(11) D. A. MacInnes, "The Principles of Electrochemistry," Reinhold Publ. Corp., New York, N. Y., 1939, p. 184.

(12) R. G. Bates and V. E. Bower, *J. Res. Natl. Bur. Std.*, **53**, 283 (1954).

TABLE III

ACTIVITY COEFFICIENTS OF HBr AT 0, 25, AND 50°; $\bar{L}_2$ AT 25°

| | $\gamma_\pm$ (0°) | | $\gamma_\pm$ (25°) | | $\gamma_\pm$ (50°) | | $\bar{L}_2$ (25°), cal. mole$^{-1}$ | |
|---|---|---|---|---|---|---|---|---|
| $m$ | a | b | a | b | a | b | a | b |
| 0.005 | 0.932 | 0.932 | $0.929_5$ | $0.929_5$ | 0.926 | 0.926 | 44 | 47 |
| .01 | .910 | .910 | .906 | .906 | .902 | .902 | 61 | 64 |
| .02 | .884 | .883 | .879 | .879 | $.873_5$ | .873 | 81 | 85 |
| .05 | .845 | .843 | .838 | .838 | .831 | .829 | 118 | 124 |
| .07 | .832 | .. | .823 | ... | $.815_5$ | .. | 136 | .. |
| .10 | $.816_5$ | .812 | .808 | .805 | .797 | .794 | 168 | 163 |

[a] This investigation. [b] Data of Harned, Keston, and Donelson.[3] Values at 50° were interpolated from data at 45 and 60°.

reported in this paper. Again, the only explanation we can advance for the difference is an unsuspected difference in the method of preparing the electrodes.

It has been proposed[13] that the silver–silver chloride electrode be standardized by measuring the potential of the cell: $H_2$; 0.01 *m* HCl, AgCl; Ag at 25° and using $\gamma_\pm$(0.01 *m* HCl) = 0.904. Although the standard potentials of the silver–silver bromide electrode of H, K, and D and those now reported do not agree with those of Harned and Donelson, all three sets of measurements lead to $\gamma_\pm$(0.01 *m* HBr) = 0.906 at 25°; thus the silver–silver bromide electrode can be similarly standardized in the 0.01 *m* solution of hydrobromic acid.

(13) R. G. Bates, E. A. Guggenheim, H. S. Harned, D. J. G. Ives, G. J. Janz, C. B. Monk, J. E. Prue, R. A. Robinson, R. H. Stokes, and W. F. K. Wynne-Jones, *J. Chem. Phys.*, **25**, 361 (1956).

# RATE OF DECOMPOSITION OF AZOMETHANE IN A SHOCK TUBE

BY GEORGES CHILTZ,[1] CARL F. ATEN, JR., AND S. H. BAUER

*Department of Chemistry and the Graduate School of Aeronautical Engineering, Cornell University, Ithaca, New York*

*Received February 15, 1962*

The pyrolysis of azomethane was studied in a shock tube over the temperature range 800–1300°K. Concentrations of the azomethane of 1–3% in argon were used. The rate of decomposition in the incident shock region was followed spectrophotometrically at λ 338 mμ. It was estimated that under shock conditions the depletion of the reactant *via* a chain mechanism was negligible compared to that due to the unimolecular decomposition. Due to the exothermicity of the over-all reaction (products, $N_2$ and $C_2H_6$), only *average* rate constants could be evaluated from the recorded oscilloscope traces. These were found to fall well within the extrapolations of the two most recent low-temperature studies, based on a strict Arrhenius temperature dependence.

## Introduction

The thermal decomposition of azomethane often is cited as a classical example of a gaseous unimolecular reaction. In 1927, Ramsperger reported[2] an activation energy of 51.2 kcal./mole for this decomposition. His later experimental results gave a rate constant $k^\infty = 3.13 \times 10^{16} \exp(-52{,}500/RT)$. A value close to this one is still accepted.[3-5] No one has succeeded in studying this decomposition at a sufficiently low pressure to detect the transition to the collision-limited regime. Recently, however, this decomposition has been added to the already large list of "unimolecular" processes which proved to be more complex than indicated. Steel and Trotman-Dickenson[6] found for the rate constant $k^\infty = 10^{15.7} \exp(-51{,}200/RT)$ but emphasized that a chain reaction occurs simultaneously with the unimolecular process. At 560°K. and 60 mm. pressure, the rate of decomposition due to the radical chain is approximately equal to the unimolecular rate. That a chain is involved is inherently plausible. Since the initial products of the decomposition are methyl radicals, these not only can associate with each other but also may attack the residual azomethane. This secondary reaction of azomethane can be suppressed by the addition of radical inhibitors, such as nitric oxide, propylene, and toluene. Such an experiment has been reported by Forst and Rice.[7] They found log $k^\infty = 17.3 - 55{,}400/(2.303RT)$. A comparison of the two most recent studies is given in Fig. 1. The temperature range covered in the above investigations is 500–600°K.

Due to the rather high preëxponential factor, it has been proposed that the fragmentation step is a simultaneous fission of the two N–$CH_3$ bonds. The $\Delta H_0^0$ expected for such a process is approximately 15.7 kcal. as compared with the observed activation energy of around 53 kcal. and an over-all $\Delta H_0^0$ of −67.6 kcal. for the production of ethane and nitrogen.

It is of interest to study the thermal decomposition of azomethane at temperatures above 600°K. for several reasons. Although the detailed mechanism for the radical chain has not

(1) Meurice Institute of Technology, Brussels.

(2) H. C. Ramsperger, *J. Am. Chem. Soc.*, **49**, 912, 1495 (1927); **50**, 123 (1928).

(3) (a) O. K. Rice and D. V. Sickman, *J. Chem. Phys.*, **4**, 239, 242, 508 (1936); (b) E. W. Ribbett and C. Rubin, *J. Am. Chem. Soc.*, **59**, 1537 (1937).

(4) M. Page, H. O. Pritchard, and A. F. Trotman-Dickenson, *J. Chem. Soc.*, 3878 (1953).

(5) M. H. Jones and E. W. R. Steacie, *J. Chem. Phys.*, **21**, 1018 (1953).

(6) C. Steel and A. F. Trotman-Dickenson, *J. Chem. Soc.*, 975 (1959).

(7) W. Forst and O. K. Rice, Abstr. No. 118, Div. Phys. Chem., 139th National Meeting, ACS, St. Louis, Mo., March, 1961.

been established, one can readily formulate a simple sequence of reactions which provides a framework for semi-quantitative estimates. One result of such an analysis is that at 800°K. the extent of decomposition of the azomethane due to the radical attack is expected to be only 1% of the unimolecular decomposition. This follows from the lower activation energy for the chain reaction, which was assumed to be 35 kcal. as compared with the considerably higher value for the unimolecular process. Secondly, extension of the observed temperature range for the unimolecular step hopefully would provide a more precise value for the activation energy. The most crucial objective is the measurement of the rate constant over a large range of temperatures to establish the validity of a strict Arrhenius temperature dependence. In turn, this would provide a measure of the relative efficiency for decomposition as a function of the energy which a molecule possesses above the lower limit required for dissociation. It has been established[8] that a temperature independent preëxponential factor implies that the probability for dissociation is

$$k_E = 0 \qquad \text{if } E < E_a$$

$$k_E = Ap(E - E_a)/p(E) \qquad \text{if } E > E_a$$

where $p(E)$ is the weight factor for molecular energy states.

Recently, it has been reported by Lee[9] on the basis of a single-pulse shock tube study of the decomposition of azomethane that the activation energy was 47 kcal. Replotting of the points taken from Lee's tables gave a value closer to 43 kcal., as shown in Fig. 1, and a rate which is somewhat above the extrapolated value of Steel and Trotman-Dickenson. The temperature regime covered in the work reported in this communication begins at about the upper temperature used by Lee and extends to approximately 1300°K.

## Experimental

**Materials.**—The azomethane was prepared by the method of Renaud.[10] The product, as collected, contained a number of impurities which were difficult to separate by distillation at low temperatures. The infrared spectrum showed an absorption band at 12.6 $\mu$ due to $CCl_4$; chloroform was detected in the mass spectrum. A modification of the procedure which involved a careful purification of the intermediate dimethylhydrazine dihydrochloride did give a product which after fractionation in a LeRoy still[11] showed none of these impurities. The column was maintained at −150°, at which temperature the total vapor pressure of the impure preparation was about 400 $\mu$. The impurities were condensed in a trap maintained at liquid nitrogen temperature, and the distillation was continued until the pressure dropped to 50 $\mu$, at which time the column was heated to −25° for the distillation of the bulk of the azomethane. The final spectrum of our product was like that reported by Pierson, *et al.*,[12] with the exception of the band at 12.6 $\mu$ which our sample did not show.

The argon used was as supplied by the Matheson Company; nitrogen and helium used as driver gases were supplied by the Air Reduction Company.

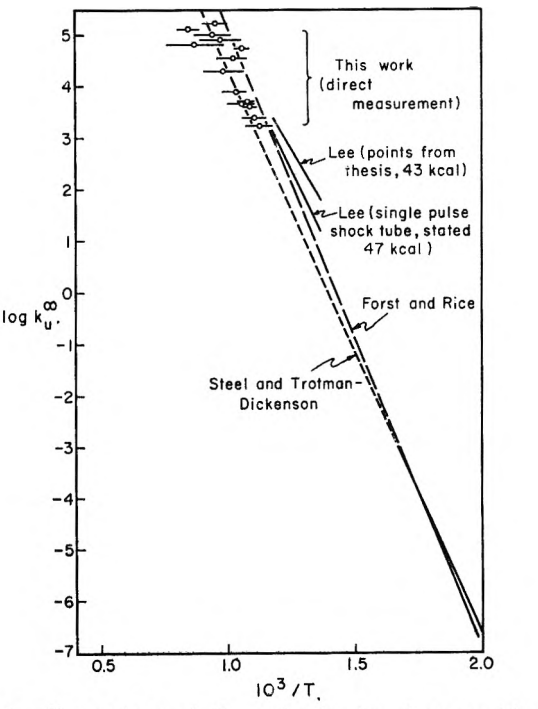


Fig. 1.—Comparison of the unimolecular decomposition rate constants as a function of the temperature.

**Apparatus.**—The shock tube with a square experimental section, 3.5 cm. on a side, was 3.4 m. long. Shock velocities were measured with two piezoelectric gages, 46 cm. apart, one on each side of the observation windows. The transit time of the shock between the two gages was recorded with a Universal Eput and Timer, Model 7360, Beckman. The piezoelectric gages were shock mounted according to the directions recommended by Knight.[13] The first of the gages also triggered the oscilloscope for recording the transmitted light intensities.

The observation windows were of Vycor glass, 2.5 cm. thick with 6 cm. diameter. An Osram mercury lamp, HBO-107, was used with a combination of a Bausch and Lomb interference filter (centered on 338 m$\mu$) and Corning Glass filter No. 5850. The slit system was set up to provide a 0.5-mm. wide parallel beam of light which was monitored with an IP28 photomultiplier tube, the output of which was recorded on a Tektronix No. 535 oscilloscope. The transmission region of the filters and the absorption band of the azomethane are shown in Fig. 2.

The experimental section of the shock tube was evacuated through a diffusion pump and liquid nitrogen cooled traps to a pressure of 2–5 $\times$ $10^{-5}$ mm. The leak rate was less than 1 $\mu$ per min. A dilute solution of azomethane in argon was introduced into the driven section to the desired pressure from a tank in which the mixture was prepared and thoroughly stirred prior to use. The shocks were initiated by pressure bursts from mixtures of helium and nitrogen of a range of compositions required to provide the desired shock speeds.

**Calculations.**—The thermodynamic functions for azomethane were calculated on the basis of the rigid rotor, simple harmonic oscillator approximation according to a machine program set up by Sitney and modified by Duff.[14] The enthalpy and free energy functions then were expressed in polynomial form.

$$\frac{H_T^0 - H_0^0}{RT} = a + bT + cT^2 + dT^3 + eT^4$$

(8) N. B. Slater, "Theory of Unimolecular Reactions," Cornell Univ. Press, Ithaca, N. Y., 1959, pp. 25–28.

(9) W. E. Lee, Ph.D. Thesis, Ohio State Univ., 1959.

(10) R. Renaud and L. C. Leitch, *Can. J. Chem.*, **32**, 545 (1954).

(11) D. J. LeRoy, *Can. J. Res.*, **32**, 492 (1950).

(12) R. H. Pierson, A. N. Fletcher, and E. St. Clair Gantz, *Anal. Chem.*, **28**, 1218 (1956).

(13) H. T. Knight, *Rev. Sci. Instr.*, **29**, 174 (1958).

(14) L. R. Sitney, PUBCO-I, IBM 704 Code, issued May 8, 1959 by the Los Alamos Scientific Laboratory, LA-2278.

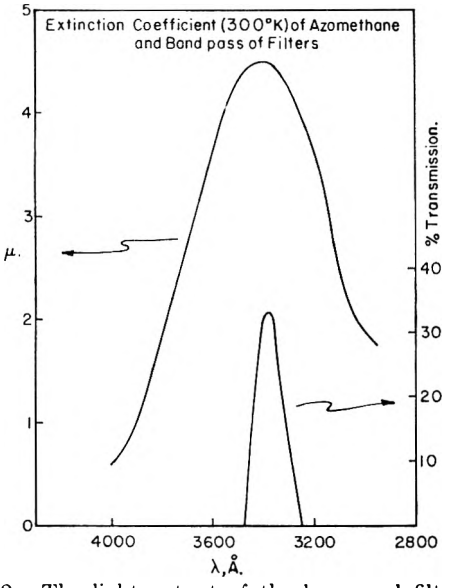


Fig. 2.—The light output of the lamp and filter combination, as a function of the wave length, compared with the absorption coefficient of the azomethane.

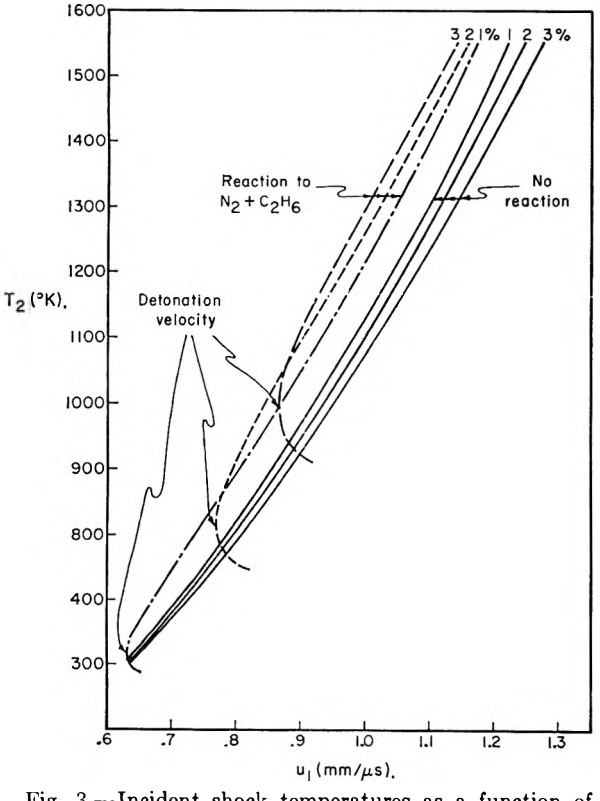


Fig. 3.—Incident shock temperatures as a function of the incident shock speed for various concentrations of azomethane in argon.

$$\frac{F_T^0 - H_0^0}{RT} = a(1 - \ln T) - bT - \frac{cT^2}{2} - \frac{dT^3}{3} - \frac{eT^4}{4} - k$$

The coefficients, $a$–$k$, were obtained by least squares fitting of the computed functions over the temperature range 50–2000°K. These coefficients are given in Table I.

TABLE I

THERMODYNAMIC FIT COEFFICIENTS FOR AZOMETHANE

| | |
|---|---|
| $a = 3.6294120$ | $d = -1.0832205 \times 10^{-8}$ |
| $b = 3.0098154 \times 10^{-3}$ | $e = 2.3809214 \times 10^{-12}$ |
| $c = 1.4217475 \times 10^{-5}$ | $k = 1.207981 \times 10^{+1}$ |

The molecular parameters required for the computation of the thermodynamic functions were obtained as follows. The interatomic distances and angles were taken from the table by H. J. M. Bowen, *et al.*[15] The methyl groups were assumed to be like those in methyl cyanide, and rotational barriers of 2 kcal./mole were postulated, similar to that reported for *trans*-butene-2. The vibrational frequencies for azomethane are given by West and Killingsworth.[16] The torsional frequency about the N=N bond was assumed to be similar to that for the C=C bond in *trans*-butene-2.[17]

The heat of formation of azomethane was estimated from the heat of combustion of azoisopropane.[18] It was assumed that the heats of reaction for the two steps are equal. Since the $\Delta H^0_{0f}$

$$(CH_3)_2HC{-}N_2{-}CH(CH_3)_2 \longrightarrow 2(CH_3)_2CH + N_2$$

$$CH_3{-}N_2{-}CH_3 \longrightarrow 2CH_3 + N_2$$

for $CH_3$, $(CH_3)_2CH$, and azoisopropane are 33.4, 21.9, and 30.2 kcal./mole, respectively, it follows that the heat of formation of gaseous azomethane is 51.2 kcal./mole at 0°K. A previous estimate[19] based on the same data for azoisopropane but analyzed in a different manner led to a heat of formation for this compound of 43.2 kcal./mole. Due to an error in transcription, the value used for the shock speed computations was 47.3; correction would alter the computed temperatures only slightly, since very dilute mixtures were run.

In order to compute the shock temperature from the incident shock speed, it is necessary to specify the composition of the gas behind the shock front. For our purposes, two limiting conditions were imposed. In the first, it was assumed that no reaction occurred behind the shock front, and in the second it was assumed that the system reached equilibrium with respect to the azomethane, ethane, and nitrogen. Clearly, other reactions do occur but to a minor extent. Since we used low concentrations of the azomethane, these assumptions are justified for estimating the final shock temperatures. Figure 3 summarizes the results of the computations based on these two assumptions for three concentrations of azomethane in argon. Note that the curves in which reaction was allowed attain a lower limiting shock speed which is the detonation velocity; the lower portions are the imaginary solutions for the speed, which

(15) H. J. M. Bowen, *et al.*, "Tables of Interatomic Distances and Configuration in Molecules and Ions," Special Publication No. 11, The Chemical Society, London, 1958.

(16) W. West and R. B. Killingsworth, *J. Chem. Phys.*, **6**, 1 (1938).

(17) J. E. Kilpatrick and K. S. Pitzer, *J. Res. Natl. Bur. Std.*, **37**, 166 (1946).

(18) G. E. Coates and L. E. Sutton, *J. Chem. Soc.*, 1187 (1948).

(19) M. Page, H. O. Pritchard, and A. F. Trotman-Dickenson, *ibid.*, 3878 (1953).

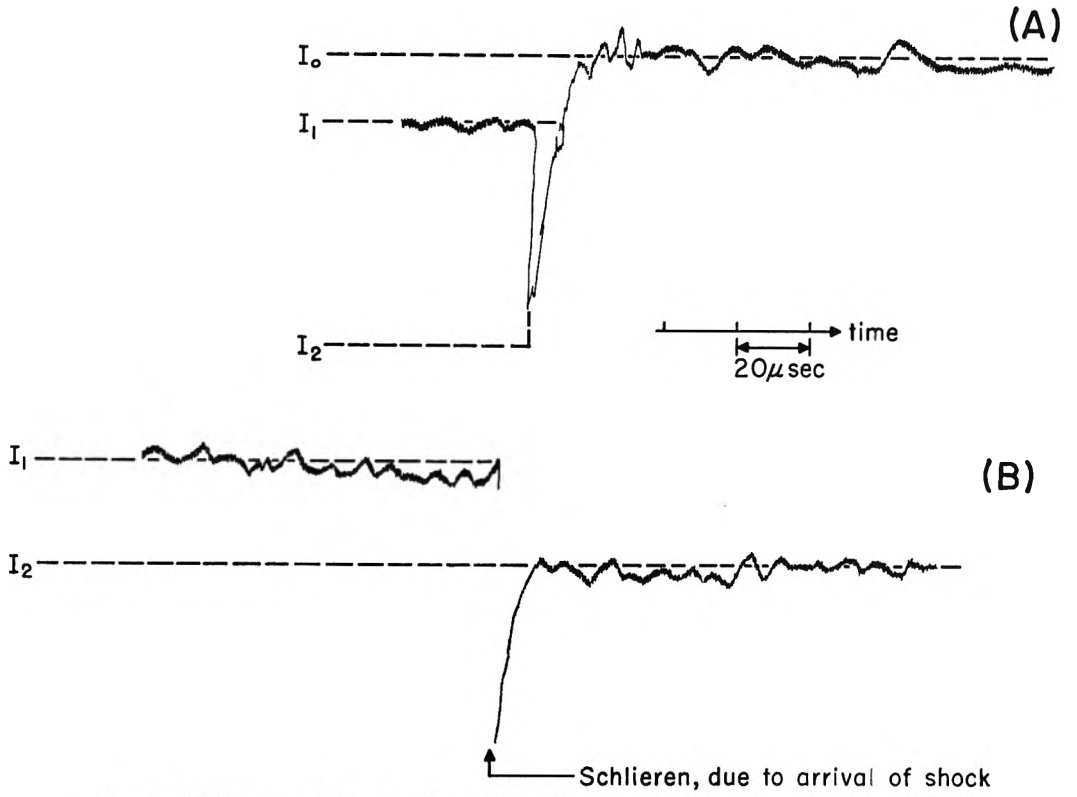


Fig. 4.—Light transmission records: (A) for $T_{shock} > 1000°K.$, (B) for $T_{shock} < 800°K.$

also are given by the machine program (R. E. Duff).

The effective extinction coefficient for azomethane as a function of temperature was estimated from the light absorption records as recorded immediately after passage of the shock front. Figure 4 shows the appearance of two such records: (A) is typical for shock temperatures greater than 1000°K. in which the reaction occurred very rapidly, and (B) shows the oscilloscope output for shock temperatures less than 800°K., in which the reaction was so slow that it is barely detectable during the time interval of observation. In the case of the fast reaction, the record provides a value for $(I_0 - I_1)$, where $I_0$ is the lamp intensity when there is no absorbing sample, while $I_1$ is the intensity transmitted at the initial concentration of azomethane (room temperature). The recorded magnitudes of $I_0$ check the assumption that none of the products formed during this period absorb in the wave length region of the filters. When the reaction was slow, a value of $(I_1 - I_2)$ was obtained, where $I_2$ is the intensity reduced by absorption due to the hot azomethane under the shock conditions, prior to reaction. In Fig. 5, the extinction coefficient, defined by $\mu = 1/cl \times \log (I_0/I)$, in which $c$ is in moles/liter and $l$ is in centimeters, is plotted as a function of the temperature, for the band pass of the filter as characterized in Fig. 2. The shock temperatures used for the abscissa were computed for the case of "no reaction." The room temperature value is an average over ten points ($4.8 \pm 0.4$ compares favorably with $\mu = 4.5$ given by Ramsperger for 3380 Å.). Although there is considerable scatter in the data due to the presence

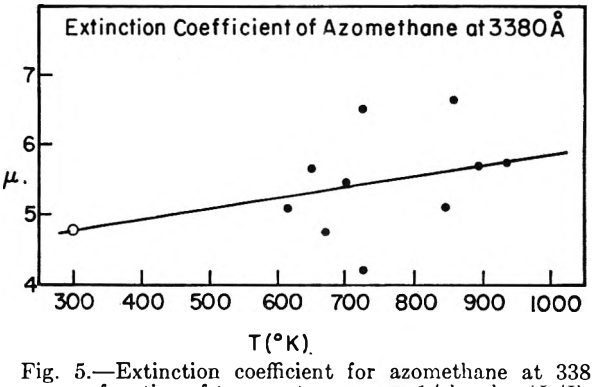


Fig. 5.—Extinction coefficient for azomethane at 338 mμ, as a function of temperature: $\mu \equiv 1/cl \times \log (I_0/I)$; $c$ is in moles/l., and $l$ is in cm.

of irregularities in the light intensity at the shock front and some confusion with small deflections of the light beam due to schlieren effects, it is nevertheless clear that the extinction coefficient rises somewhat with temperature. The best straight line through the ten points which were recorded was used in the following analysis.

**Reaction Rate Constants.**—For shock temperatures between the extremes illustrated in Fig. 4, it was possible to deduce an average dissociation rate constant. To obtain such an average, it was assumed that the reaction was first order in azomethane. Then, for a given value of the absorption coefficient and concentration corresponding to the initial conditions behind the shock, as calculated from the incident shock speed, a series of transmission curves were calculated for a sequence of assumed values of $k^{\infty}$. The observed curves were

TABLE II

RATE CONSTANTS FOR SELECTED DENSITIES AND TEMPERATURES

| Azomethane, % | $\rho_2^a/\rho_1$ | Concn. (mole l.$^{-1}$)$^b$ Total × $10^2$ | AZM × $10^4$ | $T_i$,$^c$ °K. | $T_f$,$^d$ °K. | log $k^\infty$, sec.$^{-1}$ | |
|---|---|---|---|---|---|---|---|
| 1.73 | 3.38 | 4.41 | 7.63 | 1105 | 1250 | 5.08 | |
| 5.02 | 3.81 | 7.29 | 36.6 | 1005 | 1315 | 4.81 | |
| 5.06 | 3.80 | 7.35 | 37.2 | 980 | 1300 | 5.04 | |
| 2.28 | 3.27 | 4.37 | 9.96 | 981 | 1148 | 5.01 | |
| 1.99 | 3.20 | 6.28 | 12.49 | 950 | 1100 | 4.30 | |
| 2.51 | 3.29 | 6.58 | 16.51 | 945 | 1120 | 4.90 | |
| 1.24 | 3.04 | 6.16 | 7.64 | 930 | 1025 | 3.85 | |
| 1.59 | 3.04 | 4.05 | 6.43 | 925 | 1042 | 4.55 | |
| 0.63 | 2.90 | 3.92 | 2.47 | 919 | 970 | 4.74 | |
| 1.80 | 3.09 | 6.43 | 11.56 | 890 | 1022 | 3.85 | |
| 0.71 | 2.93 | 6.00 | 4.26 | 900 | 960 | 3.70 | |
| 1.46 | 3.04 | 6.27 | 9.16 | 895 | 1000 | 3.70 | |
| 0.54 | 2.98 | 6.53 | 3.53 | 900 | 940 | 3.60 | |
| 1.02 | 2.90 | 5.88 | 5.99 | 865 | 940 | 3.40 | |
| 0.96 | 2.87 | 5.83 | 5.60 | 845 | 920 | 3.23 | |
| 1.28 | 2.61 | 5.36 | 6.86 | 700 | .. | 2.08 | These were the first |
| 1.25 | 2.68 | 5.40 | 6.75 | 725 | .. | 2.17 | two runs made |

[a] Total density behind shock before reaction occurred. [b] Initial concentrations behind the shock before reaction occurred. [c] Initial temperature behind shock before reaction occurred. [d] Equilibrium temperature behind shock, for the reaction $H_3CNNCH_3 \rightleftarrows C_2H_6 + N_2$.

matched with the calculated curves and the value of $k^\infty$ interpolated for the best over-all match. The values of the rate constants estimated in this manner are listed in Table II for a range of concentrations of azomethane in argon. For each run, the incident shock temperature and the final shock temperature are given as read from the curves in Fig. 3. The logarithms of these rate constants were plotted in Fig. 1 against the reciprocal of the average temperatures, with the lengths of the arrows indicating the total range between the incident and the final temperatures.

In evaluating the significance of the above reaction rate constants, two effects should be considered. As noted, the heating of the gas by the reaction during the time of observation of any one shock was sufficiently large, so that it cannot be ignored. We would have preferred to work with lower concentrations of the azomethane in the argon so as to reduce the rise in temperature during the shock. However, for concentrations less than those indicated, the absorption is too small to permit the measurement of concentration changes from optical densities. Thus, we are forced to accept rate constants which in each case are an average over the temperature from that immediately behind the shock front to the final equilibrium value. Since the primary reaction which occurs in the gas after passage of the shock is the decomposition of the azomethane and the association of methyls to form ethane (with very little material channeled into side reactions by the chain mechanism) and since heating is due primarily to the recombination of the two radicals, which is much faster than the decomposition step, it follows that the rate constant as evaluated above is indeed an average over the temperature range indicated by the two extremes plotted in Fig. 3. Regrettably, the signal to noise ratio is not sufficiently good to permit us to estimate rate constants as a function of time behind the shock front and thus to correct for the temperature change.

In addition to the self-heating behind the shock, there is a decrease in density which could affect the calculation of the rate constant in two ways. First, the decrease in light absorption at intermediate times was due partly to the decrease in density rather than to the reduction in absorber concentration by decomposition. This leads to a value of $k^\infty$ which is too large. Second, the relation between the reaction time and the observed time (behind the shock) depends on the density changes, since $t_{\text{reaction}} = t_{\text{obsd}}\rho/\rho_1$, where $\rho$ is the density behind the shock and $\rho_1$ the initial density. In calculating $k^\infty$, the value of $\rho$ was taken as that before reaction, so that it was too large for subsequent times. Values of $t_{\text{reaction}}$ also were too large, leading to values of $k^\infty$ which were too small. In a particular case, the change in density could have affected the value of log $k^\infty$ by 0.1 if one considered only one of the effects mentioned above. In the same shock, the temperature increased by 145°K., which made log $k^\infty$ uncertain by 1.0. Since these two factors on the density affect $k^\infty$ in opposite directions and since each is small compared with the heating, they were not considered further.

The values obtained in this study as plotted in Fig. 1 generally fall between the extrapolations of the two recent low temperature experiments (Steel and Trotman-Dickenson, and Forst and Rice). The low temperature data had to be corrected for the radical chain mechanism or run under conditions in which the radical chains were inhibited by the addition of scavengers. These two studies agree very well on the value of the rate constants but give activation energies of 51.2 and 55.4 kcal., respectively. Although the scatter in our results is rather large due to the uncertainty in the temperature, it is still correct to state that within the accuracy of all the data the rate constant

for the decomposition of azomethane follows an Arrhenius expression over approximately twelve decades. The combination of the low temperature data and our results indicate that the best value for the activation energies lies somewhere between 51.2 and 55.4 kcal., with a value of 53 kcal. preferred.

**Acknowledgments.**—This work was supported by the AFOSR, Mechanics Division, under Contract AF49(638)-716. Sincere thanks are given to Dr. R. E. Duff (LASL) for computing the thermodynamic functions of azomethane and for furnishing the IBM program for the shock temperature computations. We also thank Mr. Paul Marrone (CAL) for supervising the shock speed computations. Frequent consultations with Professor E. L. Resler, Jr., on the design and construction of the shock tube are acknowledged with sincere thanks.

# THE HYDROGENOLYSIS OF DICYCLOPROPYLMETHANE ON PLATINUM CATALYSTS

BY JOHN NEWHAM AND ROBERT L. BURWELL, JR.[1]

*Department of Chemistry, Northwestern University, Evanston, Illinois*

*Received February 16, 1962*

The hydrogenolysis of dicyclopropylmethane (A) has been studied in a flow reactor at 52°, $H_2/A = 16$, on coprecipitated platinum–alumina, two impregnated platinum–aluminas, platinum–pumice, and platinum–charcoal. Compound A hydrogenolyzes to butylcyclopropane (B) and isobutylcyclopropane (C). B further hydrogenolyzes to heptane (D) and 2-methylhexane (E); C to E and 2,4-dimethylpentane (F). The ratios B/C in the first reaction and D/E in the second are about $^1/_6$ and E/F in the third is about $^1/_{15}$, but there is some variation from catalyst to catalyst. Over half of the sequence A → B → D + E proceeds directly to D + E by a surface reaction which intercepts the formation of vapor phase B. The surface reaction is much less prominent in the sequence A → C → E + F. A very active impregnated platinum–alumina was investigated in three mesh sizes, 60–100, 40–60, and 20–40. The first behaved normally but the third gave much less C and a large initial ratio F/C. This behavior is diagnostic of large concentration gradients in the catalyst pores. The very active platinum–charcoal gave even more extreme behavior. The extreme cases of diffusional control do not agree very well with a model which assumes cylindrical pores. This matter and the effect of channelling upon selectivity are discussed.

On transition metal catalysts, cyclopropanes undergo ring-opening hydrogenolysis at rates intermediate between those of hydrogenation of olefins and those of isotopic exchange between alkanes and deuterium. Alkylcyclopropanes open in two ways

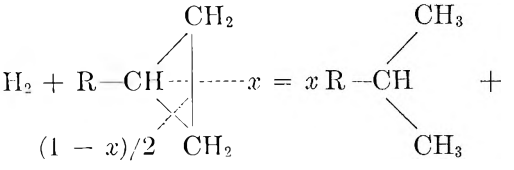

$$(1 - x)\ \text{R-CH}_2\text{CH}_2\text{CH}_3 \quad (1)$$

but $x$ is much larger than $(1 - x)$.[2,3]

Consider now the hydrogenolysis of dicyclopropylmethane (A). It should hydrogenolyze into two products each of which would further hydrogenolyze in two ways as shown in Fig. 1. The quantities $x$, $y$, and $z$ express the probabilities that cleavage occurs between the unsubstituted positions.

The concentrations of B and C must be greater in the catalyst pores than in the bulk vapor phase if there is to be net conversion of A into B and C, *i.e.*, if B and C are to flow from the catalyst pores into the bulk vapor phase.[4,5] If such gradients are a substantial fraction of the concentrations of B and C, then the concentrations of B and C will be substantially greater inside the catalyst pores than outside. Judged only from analysis of the vapor phase, some A will seem to be converted directly into D, E, and F without proceeding through vapor phase, *i.e.*, through desorbed B and C as intermediates. In an extreme case of diffusional control, the dependence of concentrations with distance from the end of a cylindrical pore is shown in Fig. 2. For simplicity, B and C are considered to behave identically.

An analogous situation has been reported recently[6] for hydrogenation of 3,3-dimethyl-1,4-pentadiene.

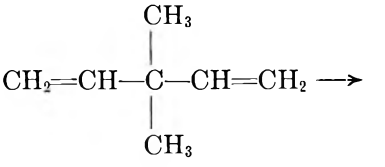

(A)

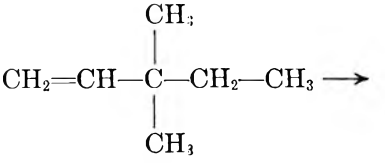

(B(+ C))

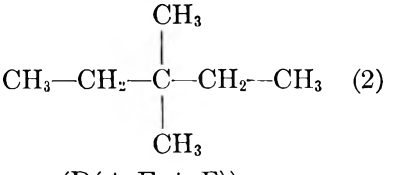

(2)

(D(+ E + F))

(1) To whom queries concerning this paper should be addressed.

(2) For reviews dealing with the rather extensive literature on this subject see (a) B. B. Corson, "The Chemistry of Petroleum Hydrocarbons," edited by B. T. Brooks, C. E. Boord, S. S. Kurtz, Jr., and L. Schmerling, Reinhold Publ. Corp., New York, N. Y., 1955, Vol. III, pp. 298–307; (b) A. L. Liberman, *Usp. Khim.*, **30**, 564 (1961).

(3) G. C. Bond and J. Newham, *Trans. Faraday Soc.*, **56**, 1501 (1960).

(4) (a) A. Wheeler, "Catalysis," edited by P. H. Emmett, Vol. II, Chapt. 2, Reinhold Publ. Corp., New York, N. Y., 1955.

(5) E. Wicke, *Z. Elektrochem.*, **60**, 774 (1956).

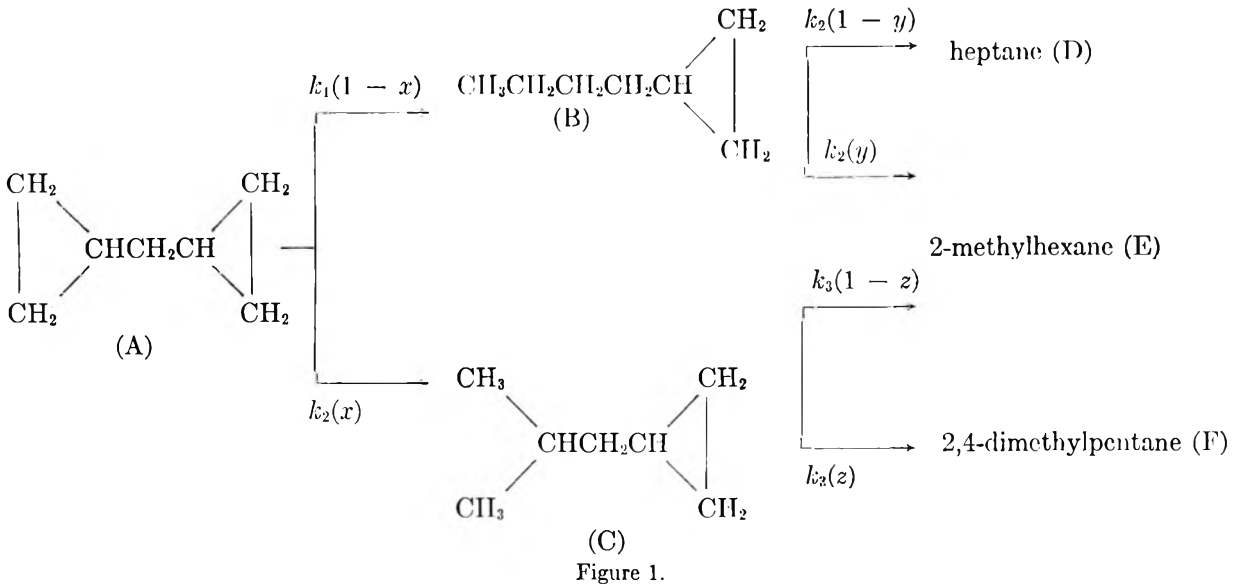


Figure 1.

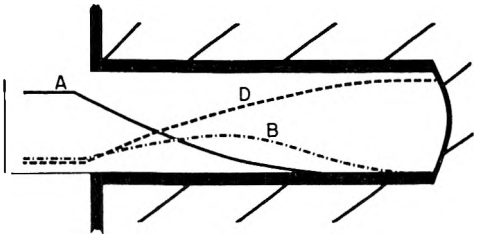


Fig. 2.—Schematic representation of concentration variation with penetration into a pore for the reaction A → B → D. Concentrations are plotted in the direction of the arrow.

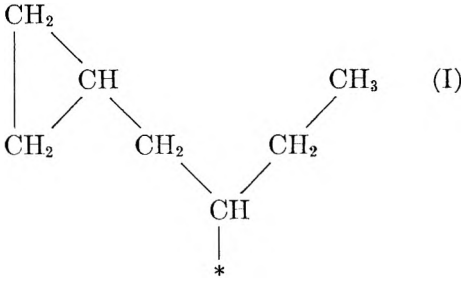


(I)

Of that portion of A which reacts, the fraction, $\alpha$, is considered to form D directly, the fraction, $1 - \alpha$, to form B. Of course, the D which appears to be formed directly is actually formed *via* the desorbed intermediate B in the catalyst pores. The degree of diffusional control is measured by $\alpha$ or alternatively by $(D/B)_{\text{initial}}$ where $D$ and $B$ are the hydrocarbon fractions of D and B. If diffusional control is negligible, $\alpha = 0$ and no D appears initially. Thus, the degree of diffusional control is diagnosed from measurement of the composition of the bulk vapor phase and without recourse to measurements of rate constants, diffusion coefficients, catalyst geometry, etc.

The incursion of serious concentration gradients into the scheme of Fig. 1 will change the rate constant for formation of B to $k_1(1 - \alpha)(1 - x)$ and that for C to $k_1(1 - \beta)(x)$. Two different diffusional control terms are necessary if $k_2 \neq k_3$. For a given value of $k_1$, $\alpha$ will increase as $k_2/k_1$ increases, *i.e.*, the faster the relative rate of reaction of B, the greater its chance of further hydrogenation before it escapes from a pore.

At some stage the conversion of A into B will involve an adsorbed intermediate such as I. This may desorb as B or it might react perhaps *via* other intermediates to open the second ring without preliminary desorption (see paper II). Such a process would appear to increase $\alpha$ and perhaps to change the value of $y$. Double-opening reactions might perhaps be avoided by employing dicyclopropylpropane.

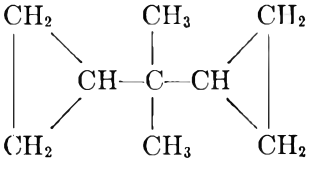


(II)

The *gem*-dimethyl group insulates the two cyclopropyl groups against certain kinds of interactions. However, we report here an investigation of the hydrogenolysis of the species without the *gem*-dimethyl group, dicyclopropylmethane. It is much more accessible and its lower boiling point permits one to study the reaction at lower temperatures without encountering dew point problems. Further, interaction of the type suggested has not been studied and could be of mechanistic interest.

A particular reason for investigating the test of diffusional control employing dicyclopropylmethane is the following. In the case previously studied, eq. 2, the olefin is strongly adsorbed. Relative to hydrogen, cyclopropanes cover the surface sparsely.[3] It appeared desirable to extend our test of diffusional control to this kinetically quite different situation.

Paper I of this series reports the hydrogenolysis on several supported platinum catalysts. Paper II reports the reaction on nickel catalysts.

(6) R. Ciola and R. L. Burwell, Jr., *J. Phys. Chem.*, **65**, 1158 (1961).

## Experimental

**Materials.**—Butylcyclopropane was prepared by interaction of zinc–copper couple, methylene iodide, and 1-hexene in ethyl ether.[7] Following fractionation it was chromatographically pure. Dicyclopropylmethane was prepared by the Wolff–Kishner reduction of dicyclopropyl ketone (Aldrich Chemical Co.).[8] The infrared spectrum closely matched that provided by Professor Harold Hart. Despite careful fractionation, we could not eliminate two impurities detectable by gas chromatography. One was 0.2% of butylcyclopropane. Mass spectroscopy indicated that the other, present to 0.7%, had the same molecular weight as dicyclopropylmethane. It reacted much more rapidly than dicyclopropylmethane and was absent after the hydrogenolysis of the first few tenths of dicyclopropylmethane. It was very probably a cyclopropylbutene with the same carbon skeleton as butylcyclopropane and, most likely, 4-cyclopropylbutene.

**Catalysts.**—**Platinum-I** consisted of platinum-on-alumina powder (Baker and Co., lot no. 2728) which was pelleted, crushed, and sieved to 60–100 mesh. **Platinum-II** (20–40 mesh), **Platinum-III** (40–60 mesh), and **Platinum-IV** (60–100 mesh) were prepared as follows. Hard alumina pellets (Harshaw Chemical Co.) were crushed and sieved. Equal weights of 20–40, 40–60, and 60–100 material were combined and stirred into a solution of 0.03 *M* chloroplatinic acid. The mix was maintained at 75° for 3 hr. After drying at 110°, the material was resieved. The catalyst is estimated to contain 2% platinum.

A 12% platinum-on-charcoal catalyst, **Platinum-VII**, was prepared by a similar impregnation of 20–40 mesh activated charcoal. **Platinum-VIII**, platinum-on-pumice, was similarly prepared. Pumice (20–40 mesh) was treated with hot concentrated sulfuric acid containing 10% nitric acid, exhaustively washed, and then dried. It was impregnated with a 0.05 *M* chloroplatinic acid solution. Its estimated platinum content was 1%.

**Platinum-VI**, a 2% coprecipitated platinum–alumina, was made by adding ammonia to a solution of chloroplatinic acid and aluminum nitrate. The precipitate was washed with 1% ammonium nitrate solution dried at 110°, heated gradually to 750° over a period of 3 hr., and maintained there for 1 hr. The 20–40 mesh portion was employed.

We are indebted to Mr. R. F. Waters of the Whiting Research Laboratories of the American Oil Company for the determination of pore diameter distributions on two of our catalysts by analysis of nitrogen adsorption data.[9]

| | Pt-II | Pt-VI |
|---|---|---|
| Surface area, m.²/g. | 76 | 125 |
| Pore volume, cc./g. | 0.255 | 0.296 |
| Av. pore diameter, Å. | 133 | 94.5 |

In the plot of fraction of the pore volume in pores of a given size *vs.* pore diameter, Pt-II exhibited two maxima, one at 85 Å., the other at 195 Å., and a minimum at 135 Å. The relative values at 85, 135, and 195 Å. were 0.0112, 0.0058, and 0.0092. Pt-VI showed a single maximum at 110 Å. down to one-half at 70 and 155 Å.

Catalysts were reduced *in situ* in hydrogen flowing at about 20 cc. per minute. The temperature was raised to 450° and maintained there for 8 hr. With Platinum I, the terminal temperature was 300°.

**Apparatus.**—A hydrogen–dicyclopropylmethane mixture whose molar ratio was 16 ± 1 was passed over the catalyst maintained in most cases at about 52°. The partial pressure of hydrocarbon was established in a thermostated helix through which was passed a hydrogen–hydrocarbon mixture obtained by bubbling hydrogen through previously deoxygenated hydrocarbon at a temperature about 15° above that of the helix. Electrolytic hydrogen (Matheson) was passed over hot copper gauze, through calcium chloride and Linde Molecular Sieve 4A, and then bubbled through liquid sodium–potassium alloy.

Since complete hydrogenolysis of dicyclopropylmethane liberates about 70 kcal. per mole of hydrocarbon, temperature control posed problems. The catalyst chamber was of 10-mm. internal diameter tubing. A thermocouple well ran down the center of the tubing. After the reactor vessel was completed, the outer walls were reduced to about half their original thickness by treatment with aqueous hydrofluoric acid. The catalyst chamber was thermostated in a water bath at temperatures of 55° or below. At higher temperatures an air bath was employed. In most cases about 0.1 g. of catalyst gave the desired conversions but heat liberation in such a small volume led to large temperature rises. Accordingly, the catalyst was uniformly distributed in about 4 g. of 60–80 mesh glass beads. Temperature rises in the thermocouple well were then small, although we have no information as to possible temperature profiles within individual catalyst particles.

Table I presents the weights of catalysts and beads employed.

TABLE I

CATALYST SAMPLES EMPLOYED

| Catalyst | Sample | Wt. of catalyst, g. | Wt. of glass beads, g. |
|---|---|---|---|
| Pt-I | C | 0.014 | 4.00 |
| | D | .030 | 4.20 |
| Pt-II | A | .120 | 4.01 |
| | B | .056 | 4.53 |
| | C | .020 | 4.32 |
| Pt-IV | A | .049 | 4.20 |
| | B | .051 | 4.30 |
| | C | .012 | 4.32 |
| Pt-VI | A | .308 | 4.21 |
| | B | .601 | 4.22 |
| Pt-VII | A | .057 | 4.26 |
| | B | .023 | 4.37 |
| | C | .009 | 4.36 |
| Pt-VIII | C | 1.389 | 0.0 |
| | D | 5.078 | 0.0 |

**Analysis.**—Products of runs were trapped at −78° and analyzed by gas chromatography on an Aerograph chromatograph employing a 5-m. column of 2,2′-oxydipropionitrile on firebrick. Identifications of all products were made by comparison with authentic compounds except for isobutylcyclopropane and propylcyclopropane. Internal chemical evidence provides strong evidence for these assignments.

## Results and Discussion

**Results in the Absence of Serious Concentration Gradients.**—Results with coprecipitated Pt-VI at 52° are shown in Fig. 3. Conversions below 50% refer to Pt-VI-A, those above, to Pt-VI-B. If hydrogenolysis is first order in dicyclopropylmethane (A)[3]

$$k_1 = (L/\text{wt.}) \ln (A_0/A) \qquad (3)$$

where $L$ is the flow rate of A in mmoles/hr., the weight is that of the actual catalyst in mg., $A$ is the mole fraction of A in the hydrocarbon portion, and $A_0$ is its initial value. On this basis, $k_1$ for the four runs on Pt-VI-A was 0.0085 ± 0.005 and that for the two runs on Pt-VI-B at lower conversions was 0.015 ± 0.006. Different conversions were obtained by variation in $L$.

If the kinetic forms for hydrogenolysis of the mono- and dicyclopropyl species are identical, then[6]

$$B = (1 - \alpha)(1 - x)\frac{k_1}{k_1 - k_2}\left[A_0^{(k_1-k_2)/k_1} A^{k_2/k_1} - A\right] + B_0 \left(A_0^{-k_2/k_1}\right) A^{k_2/k_1} \qquad (4)$$

(7) H. E. Simmons and R. D. Smith *J. Am. Chem. Soc.*, **81**, 4256 (1959).

(8) H. Hart and O. E. Curtis, Jr., *ibid.*, **78**, 112 (1956).

(9) C. G. Shull, *J. Am. Chem. Soc.*, **70**, 1405 (1948).

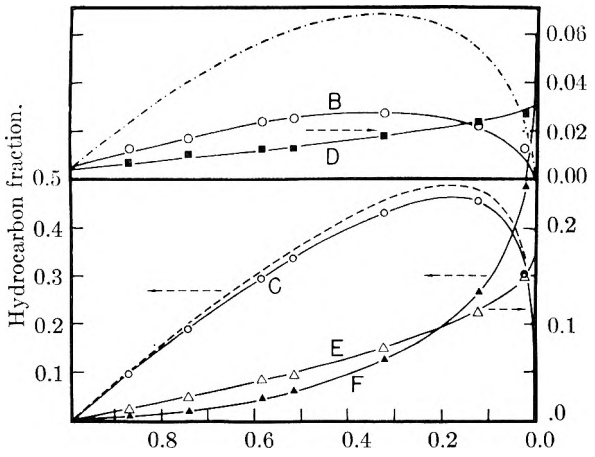


Fig. 3.—Results for Pt-VI.

$$C = (1 - \beta)\, x \frac{k_1}{k_1 - k_3} \left[A_0^{(k_1 - k_3)/k_1} A^{k_3/k_1} - A\right] \quad (5)$$

The $C_0$ term is omitted in (5) since $C_0$ is zero in our experiments. The other quantities are defined in Fig. 1 and the introduction. $D$, $E$, and $F$ may be computed from the sets ($A$, $B$, $C$, $x$, $y$, $z$); for example, $F = z[x(A_0 - A) - C]$.

We assume that the 0.7% of impurity believed to be cyclopropylbutene hydrogenates immediately to 0.3% B and 0.4% D. The ratio is chosen to give the best fit to the data but it is in line with that reported for hydrogenation of cyclopropyl olefins.[10] Thus, $A_0$ is 0.991, $B_0$ is 0.005, and $D_0$ is 0.004. Owing to their small magnitudes, $B$ and $D$ are more affected by these corrections than are $C$, $E$, and $F$.

We first judge from the data the values of $A$ and $C$ at which $dC/dA = 0$. The value of $A$ fixes $k_1/k_3$ and $C$ then fixes $x(1-\beta)$. The terms $k_1/k_2$ and $(1-x)(1-\alpha)$ are found similarly. These parameters establish $B$ and $C$ as functions of $A$. As shown in Fig. 3, the fit is excellent. The remaining parameters are determined by trial and error adjustment to fit $D$, $E$, and $F$. In most cases, although not with Pt-VI, the values of $D$, $E$, and $F$ at $A = 0$, $B = 0$, $C = 0$ were measured experimentally. Such data provide two equations which depend only upon $x$, $y$, and $z$.

The values of the parameters for Fig. 3 are given in Table II. The number of parameters is large but the amount of data to be fitted is much larger. We estimate that the rate constant ratios are accurate to within 10% and $x$, $y$, $z$, $\alpha$, and $\beta$, to within 0.02.

There is clearly little diffusional control in the sequence, A → C → E + F, as judged either by the small value of $\beta$ or by the very small initial ratio, $F/C$. On the contrary, $\alpha$ is large for the sequence, A → B → D + E. This may be seen also from the rather large initial ratio of $E/B$ since initially almost all E comes from this sequence.

In Fig. 3, we have plotted $B$ and $C$ as broken lines for $\alpha$ and $\beta = 0$. The initial divergences between these curves and the observed curves represent initial formation of $D$, $E$, and $F$.

Why is $\alpha$ so much larger than $\beta$? The greater reactivity of B than C ($k_2/k_3 = 2.5$) is hardly sufficient to cause such a large change in the degree of diffusional control.

As described in the introduction, the value of $\alpha$ is determined by two factors, the degree of diffusional control and the fraction of the sequence, A → B → D + E, which proceeds directly from A to D + E as a surface reaction. Although we cannot eliminate the presence of a very small amount of diffusional control, the large value of $\alpha$ must result mainly from a much greater incursion of the double-opening reaction in A → D + E than in A → E + F.

As will be shown in paper II, in almost any mechanism for the hydrogenolysis of dicyclopropylmethane, the adsorbed species which just precede desorbed B and C are monoadsorbed species like I (introduction). There will be differences in detail between the species which might well lead the double-opening reaction to intercept the formation of B to a greater extent than C. In particular, the position of adsorption in the adsorbed butylcyclopropane generated by initial opening of the first ring can be closer to the remaining cyclopropyl ring than in the case of isobutylcyclopropane.

Pt-I gave results very similar to those of Pt-VI and a similar analysis gives an equally good fit to the data. The optimum values of the parameters are listed in Table II. The catalytic activity of Pt-I was about ten times that of Pt-VI. With both samples $k_1$ started at 0.12 and declined about 40% during the course of four runs.

A competitive hydrogenolysis was run on a mixture of dicyclopropylmethane and butylcyclopropane under conditions such that about one-half of the former compound was converted. The results lead to $k_1/k_2 = 1.3 \pm 0.1$. The rather large uncertainty results from the problem in how to treat the B which results from hydrogenolysis of A. The measured value is consistent with that which gives the best fit to the data (see Table II).

TABLE II

VALUES OF THE PARAMETERS FOR THE VARIOUS CATALYSTS

| Catalyst | $k_1/k_2$ | $k_1/k_3$ | $x$ | $y$ | $z$ | $\alpha$ | $\beta$ | Initial $k_1$[a] |
|---|---|---|---|---|---|---|---|---|
| Pt-I | 1.2 | 2.5 | 0.81 | 0.78 | 0.88 | 0.81 | 0.037 | 0.12 |
| Pt-IV | 1.4 | 2.5 | .80 | .79 | .92 | .754 | .079 | 1.0 |
| Pt-VI | 1.3 | 3.2 | .84 | .84 | .96 | .619 | .056 | 0.01 |
| Pt-VII | ? | ? | .875 | .85 | .96 | ? | .6[b] | 1.0 |
| Pt-VIII[c] | 1.3 | 3.0 | .93 | .83 | .97 | .40 | .17 | 0.0004 |

[a] Approximate initial activity, $k_1$ from eq. 3, mmoles/hr./mg. of catalyst. [b] Approximate value for catalyst at initial activity. [c] Values of lower precision because the conversions were not carried far enough to get $k_1/k_2$ and $k_1/k_3$ very accurately.

Pt-I-A and Pt-I-B were much larger samples of catalyst which gave 100% conversions at the largest practical space velocity. We attempted sufficiently to reduce the activity of Pt-I-B by sintering in hydrogen. The attempt failed but we did observe that the fraction of F increased steadily with sintering temperature. As reduced at 280°, Pt-I-B gave for $D$, $E$, and $F$: 0.036, 0.243, 0.721; after sintering at 500°, 0.028, 0.219, 0.754; after sintering at 590°,

(10) B. A. Kazanskiĭ, M. Yu. Lukina, and A. I. Malyshev, *Izv. Akad. Nauk SSSR. Otd. Khim. Nauk*, 1399 (1956).

0.019, 0.194, 0.786; at 650°, 0.020, 0.156, 0.824. As reduced at 280°, Pt-I-A gave 0.045, 0.249, 0.706 and the data on Pt-I-C and Pt-I-D lead to 0.042, 0.245, and 0.713. The consistency at the lower temperature of reduction is good. Reduction of Pt-I-C and Pt-I-D at 450°, the temperature used for the other catalysts, would have given values of $x$, $y$, and $z$ closer to those for Pt-VI for which $D$, $E$, and $F$ were 0.0305, 0.170, and 0.800.

We attempted to study hydrogenolysis on 0.010-in. platinum wire but we were unable to get significant activity with 3.50 g. Catalyst VIII, 1% platinum-on-pumice, is probably the closest to unsupported platinum of any catalyst which we studied since pumice has the lowest surface area by far of any support which we used. As shown in Table II, it had the largest preference for cleaving between the two unsubstituted positions (the largest values of $x$, $y$, and $z$) of any of our catalysts. Bond and Newham[3] reported that hydrogenolysis of methylcyclopropane on a similar catalyst at 50° gave 5% butane, a very similar result.

We doubt that the degree of diffusional control was significant on Pt-VIII. The support has much larger pores than the aluminas. The catalyst was of low activity, only about 0.11 that of Pt-VI and 0.001 that of Pt-I for both of which diffusional control is very small. Further, the catalytic activity declined substantially from run to run. The extreme variation was from 0.00047 to 0.000048. All points fell on the same smooth curves. Had there been a moderate degree of diffusional control for the most active Pt-VIII, there hardly could have been any for the least active. Further, $k_1/k_3$, $x$, $z$, and $\beta$ all seem independent of $k_1$.

**Results in the Presence of Serious Concentration Gradients.**—Thus, in catalysts I, VI, and VIII, the finite values of $\alpha$ and $\beta$ seem to derive from the double-opening reaction direct to D, E, and F and not from substantial concentration gradients in the pores. However, the incursion of diffusional control is clearly evident in the sequence Pt-II, Pt-III, and Pt-IV. These impregnated aluminas differed only in particle size, 20–40, 40–60, and 60–100 mesh.

Pt-IV and Pt-VII were nearly ten times as active as Pt-I, the next most active catalyst. Results for Pt-IV are shown in Fig. 4 and Table III and the parameters are given in Table II. The behavior of Pt-IV is similar to that of Pt-I, Pt-VI, and Pt-VIII. The scatter of the points in Fig. 4 is somewhat worse than for the catalysts discussed before this. In particular, the values of $C$ for runs A4 and A5 (at $A = 0.60$ and 0.804) lie above the computed line. The catalytic activity in these runs had declined to but 10% of the original. This suggests that a small amount of diffusional control may be involved in the sequence A → C → E + F.

We cannot explain the origin of these declines in activity which were observed on all catalysts except Pt-VI. Marked decline in activity such as that between runs A3 and A4 in Pt-IV usually occurred when the catalyst stood in hydrogen between runs for overnight or longer. Perhaps solution of hydrogen in platinum is involved.

Results for Pt-II are shown in Fig. 5 and Table III. Although the points might appear to be a scatter diagram at first glance, $x$, $y$, and $z$ are the same as on Pt-IV. That is, the observed values of $D$, $E$, and $F$ are in excellent agreement with those computed from the experimental values of $A$, $B$, and $C$ *via* the relations

$$D = 0.004 + (1 - y)\,[0.005 + (0.991 - A)(1 - x) - B]$$

$$F = z\,[(0.991 - A)x - C]$$

$$E = 1 - A - B - C - D - F$$

Further, the runs of lowest activity, B5, B6, B7, and B8, fit a line of $\beta = 0.132$ which is not much different from the line of $\beta = 0.079$ of Pt-IV in Fig. 4. In runs B7 and B8, the feed contained small amounts of 2-methylthiophene (for which

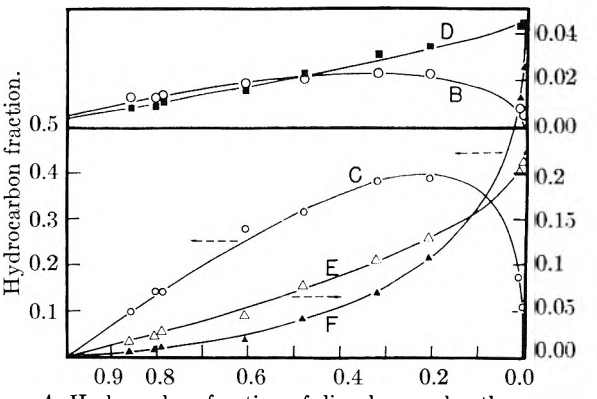


Fig. 4.—Results for Pt-IV.

TABLE III

HYDROGENOLYSIS OF DICYCLOPROPYLMETHANE ON IMPREGNATED PLATINUM–ALUMINA CATALYSTS, Pt-II AND Pt-IV, AT 52°

| Run | Flow rate $A$, mmoles/hr. | Activity[a] | $A$[b] | $B$ | $C$ | $D$ | $E$ | $F$ |
|---|---|---|---|---|---|---|---|---|
| | | | Pt-II (20–40 mesh) | | | | | |
| A1 | 7.5 | ... | 0.000 | 0.000 | 0.007 | 0.044 | 0.246 | 0.703 |
| B1 | 6.1 | 0.25 | .102 | .009 | .167 | .042 | .186 | .494 |
| B2 | 12.7 | .25 | .326 | .016 | .254 | .029 | .121 | .253 |
| B3 | 24.1 | .27 | .532 | .014 | .220 | .021 | .079 | .133 |
| B4 | 8.5 | .17 | .319 | .018 | .290 | .029 | .115 | .229 |
| B5 | 39.0 | .13 | .820 | .011 | .116 | .010 | .023 | .019 |
| B6 | 6.9 | .086 | .494 | .018 | .298 | .022 | .073 | .094 |
| B7 | 7.1 | .060 | .615 | .020 | .235 | .017 | .052 | .061 |
| B8 | 6.9 | .014 | .887 | .012 | .072 | .006 | .013 | .010 |
| B9 | 3.0 | ... | .990 | .004 | .003 | .0015 | .0005 | .0004 |
| C1 | 24.5 | .71 | .554 | .010 | .139 | .020 | .083 | .195 |
| C2 | 56.9 | .71 | .772 | .007 | .084 | .010 | .042 | .084 |
| | | | Pt-IV (60–100 mesh) | | | | | |
| A1 | 8.6 | ... | .003 | .005 | .108 | .045 | .212 | .628 |
| A2 | 43.7 | .64 | .481 | .021 | .315 | .023 | .077 | .084 |
| A3 | 24.2 | .56 | .322 | .023 | .381 | .031 | .105 | .139 |
| A4 | 10.2 | .10 | .608 | .019 | .278 | .016 | .044 | .035 |
| A5 | 26.1 | .11 | .805 | .013 | .140 | .009 | .021 | .011 |
| B1 | 16.9 | 1.5 | .011 | .008 | .172 | .043 | .201 | .564 |
| B2 | 33.1 | 1.01 | .208 | .023 | .389 | .035 | .129 | .216 |
| C1 | 24.9 | 0.47 | .789 | .014 | .140 | .011 | .026 | .019 |
| C2 | 39.3 | .47 | .860 | .013 | .097 | .008 | .015 | .008 |

[a] $k_1$, in eq. 3. [b] The analyses ignore any cyclopropylbutene impurity.

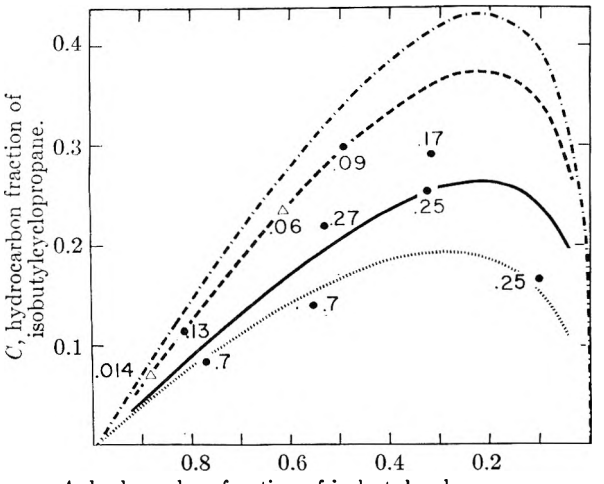


Fig. 5.—Results for Pt-II. The upper three curves are plots of equation 5 with (from the top down) $\beta = 0.00, 0.132$, and 0.39. The lowest curve represents eq. 6. The numbers give activities.

we thank Professor F. G. Bordwell) chosen as a poison because its boiling point is nearly the same as A.

As the activity of the catalyst increases, the observed values of $C$ lie more and more below the line of $\beta = 0.132$ as may be most clearly seen in the sequence C1, B3, B6, which lies at $A$ equal to about 0.5. The amount of C formed about doubles as the activity drops from 0.7 to 0.09. The same effect is seen in the sequence, B2, B4, at $A = 0.3$.

It appears then, that an activity of about 0.1 is marginal for diffusional control on this 20–40 mesh catalyst. At higher activities, serious concentration gradients develop in the catalyst interstices.

The behavior of the cyclopropylbutene impurity is further indicative of the intrusion of serious concentration gradients. Thus, on Pt-VIII, for which diffusional control is negligible, the cyclopropylbutene had disappeared by $A = 0.95$, but, in run C2 of Pt-II, about 70% of the impurity remained when $A = 0.86$. Similarly on Pt-VII, B3, about 55% impurity remained at $A = 0.75$. On the considerably poisoned Pt-II, B8, however, less than 10% of the impurity remained at $A = 0.89$, confirming our suggestion that diffusional control is small in the least active runs on Pt-II.

Serious concentration gradients lower the values of $C$ at any given $A$ and the degree of lowering increases with increasing conversion (decreasing $A$). Consider the sequence of nearly constant activity, B1, B2, B3. Point B3 ($A = 0.53$) lies on a line of $\beta = 0.32$; B2 ($A = 0.33$) on $\beta = 0.39$; and B1 ($A = 0.1$) on $\beta = 0.58$. Thus, as should be expected,[6] eq. 5 fails increasingly at larger conversions. A correct equation should not only lower $C$ but would move the value of $A$ at which $C$ maximizes to larger values of $A$.

Wheeler[4a] has derived an equation valid for large concentration gradients for first-order reactions on catalysts with cylindrical pores which assumes the following form for our application.

$$C = \frac{k_1}{k_1 - k_3} x \left[A^{\sqrt{k_1/k_1}} - A\right] \text{ for } A_0 = 1 \quad (6)$$

The effect of diffusional control is introduced *via* change in the exponent in eq. 5 from $k_3/k_1$ to $\sqrt{k_3/k_1}$ rather than by prefixing $(1 - \beta)$. If, however, the value of $\beta$ for the runs of lowest activity, B5–B8, results entirely from the double opening reaction, the right-hand side of eq. 6 should be multiplied by $(1 - 0.132)$. The resulting equation is plotted in Fig. 5. Although the points C1 and C2 lie somewhat below the line, it is a step in the correct direction since the value at which $C$ maximizes is shifted to higher values of $A$. However, as shown by the sequence B1, B2, B3, an even more rapid fall of $C$ is needed at higher conversions.

The same general trends are observed in plots of $B$ *vs.* $A$. However, the small values of $B$ and the problem of how to treat the impurity makes the interpretation of the data for $B$ more difficult.

The 40–60 mesh Pt-III shows the phenomena of Fig. 5 but in a lesser degree. At $k_1$ less than 0.3, observed values of $C$ fall on the line of Fig. 4. The decline in $C$ at larger values of $k_1$ is shown by the following sets of $k_1$, $A$, and $C$: low, 0.31, 0.385; 0.50 0.307, 0.336; 0.95, 0.319, 0.274; 1.25, 0.301, 0.257. The first set is taken from the curve for $C$ in Fig. 4 and is that expected for no diffusional control.

**The Effect of Temperature.**—Catalyst Pt-III was employed for a cursory examination of the effect of temperature upon the composition of the heptane product. At 90°, $x$ seemed essentially unchanged at 0.80 but $y$ and $z$ were decreased to 0.63 and 0.60, respectively (compare Pt-IV at 52° in Table II). At 72°, the average between the values at 52 and 90° seemed to apply. At 142°, the reduction in $y$ and $z$ leads 2-methylhexane to be the principal product as with nickel (see paper II). At complete reaction, the approximate composition is $D = 0.14$, $E = 0.52$, and $F = 0.35$. Correspondingly, if one compares a run at 52° with one at higher temperatures and if $A$ and $k_1$ are the same at both temperatures, then $C$ is lower at the higher temperature and, since the $k_1$'s are the same, not because of increased diffusional control.

The change in $y$ and $z$ unaccompanied by change in $x$ indicates an increased incursion of the double-opening reaction and a much increased tendency for this reaction to open a bond in the second ring adjacent to the side chain. Thus, the two total reactions, A → C → E + F and A → E + F no longer give the same ratio of $E$ to $F$ and the treatment valid at 52° will fail. Presumably, one could employ the treatment used for Ni-I in paper II but we had too little data to test this.

**Platinum–Charcoal.**—Table IV presents results on platinum–charcoal, catalyst VII. Values of $D$, $E$, and $F$ are fairly well computed from the experimental values of $A$, $B$, and $C$ and the values of $x$, $y$, and $z$ given in Table II.

A detailed analysis would require data on catalyst so fine that diffusional control was negligible since otherwise $k_1/k_2$ and $k_1/k_3$ are unobtainable. However, it seems clear that very serious concentration gradients existed within the pores of Pt-VII. This assumption is consistent with the following considerations. The catalyst is very active and charcoal is well known to be characterized by very small pores. About 55% of the cyclopropylbutene re-

mained unreacted at 25% conversion of the dicyclopropylmethane (Table IV, B3). The runs on catalyst which had lost activity gave somewhat larger amounts of C (compare runs A2 and A5 or runs B3 and C1 in Table IV). The maximum yield of C is only about 11%. Thus, in a plot of $C$ *vs.* $A$, the maximum is much lowered and shifted to larger values of $A$ (speaking in terms of Fig. 5). The degree of diffusional control exceeds that of runs C1 and C2 of Pt-II.

One may compute $\beta$ for the least active Pt-VII catalysts, C2 and C3, from $1.04F/C$.[6] The factor, 1.04, allows for the small amount of E which accompanies F as the reaction product of C. This ratio is 0.9 and the derived value of $\beta$ is 0.47. For run B3, the estimated value of $\beta$ is 0.6.

TABLE IV

HYDROGENOLYSIS OF DICYCLOPROPYLMETHANE ON PLATINUM–CHARCOAL (Pt-VII) AT 50°

| Run | Flow rate A, mmoles/hr. | Activity[a] | $A$[b] | $B$ | $C$ | $D$ | $E$ | $F$ |
|---|---|---|---|---|---|---|---|---|
| A1 | 7.6 | .. | 0.016 | 0.000 | 0.025 | 0.020 | 0.132 | 0.809 |
| A2 | 35.4 | 0.89 | .238 | .004 | .101 | .019 | .101 | .537 |
| A3 | 63.3 | .91 | .437 | .008 | .110 | .017 | .081 | .346 |
| A4 | 49.6 | .78 | .406 | .006 | .113 | .019 | .089 | .366 |
| A5 | 15.3 | .42 | .210 | .006 | .117 | .019 | .109 | .539 |
| B1 | 9.6 | .78 | .156 | .003 | .081 | .019 | .110 | .631 |
| B2 | 43.6 | .94 | .605 | .008 | .107 | .010 | .049 | .220 |
| B3 | 71.0 | .88 | .749 | .008 | .083 | .007 | .028 | .125 |
| C1 | 17.9 | .61 | .733 | .009 | .101 | .006 | .026 | .125 |
| C2 | 53.6 | .30 | .948 | .006 | .021 | .002 | .005 | .018 |
| C3 | 20.0 | .15 | .931 | .008 | .028 | .002 | .006 | .024 |

[a] $k_1$, in eq. 3. [b] The analyses ignore any cyclopropylbutene impurity.

Since we do not know $k_1/k_3$, we cannot directly test eq. 6. However, the data lie well below the plot of eq. 6 with any reasonable value of $k_1/k_3$, *i.e.*, $k_1/k_3 > 1.4$.

**The Model for Porous Catalysts.**—The model from which eq. 6 is derived is based upon cylindrical pores. If alumina supports consist of agglomerated spheroids whose radius is about 50 Å., the interstices would consist of a series of small chambers interconnected by smaller orifices. Consider a simplified, extreme form of such a system in which catalytically active surface lines the interior of cavities which open to the bulk gas phase through small holes. Let us apply this to the reaction A → B → D. In a steady state, the cavity acts as a stirred flow reactor

$$-\mathrm{d}n_A/\mathrm{d}t = \mathfrak{K}(A - A')$$

where $\mathrm{d}n_A/\mathrm{d}t$ represents the rate of flow of A from the cavity into the gas steam, $A'$ is the hydrocarbon fraction in the cavity, and $\mathfrak{K}$ involves the Knudsen diffusion coefficient of A, the orifice size, and a coefficient to convert $A$ into $C_A$ (we assume that the hydrogen is in large excess). Similar forms apply to B and D and we can assume that the same value of $\mathfrak{K}$ applies to all hydrocarbon species.

Further

$$\mathfrak{K}(A - A') - k_1SA' = 0 \text{ and } \mathfrak{K}(B - B') - k_2SB' + k_1SA' = 0$$

Here $k_1$ is the rate constant of the first step per cm.$^2$ of surface and $S$ is the area of the inside of the cavity. Then

$$\frac{-\mathrm{d}n_A}{\mathrm{d}t} = \frac{\mathfrak{K}k_1SA}{\mathfrak{K} + k_1S}$$

$$\frac{-\mathrm{d}n_B}{\mathrm{d}t} = \frac{\mathfrak{K}k_2SB}{\mathfrak{K} + k_2S} - \left(\frac{\mathfrak{K}}{\mathfrak{K} + k_1S}\right)\left(\frac{\mathfrak{K}}{\mathfrak{K} + k_2S}\right)k_1SA$$

One cavity produces a change in $A$

$$\Delta A = \frac{\mathrm{d}n_A/\mathrm{d}t}{L} = -\frac{A}{L}\left(\frac{\mathfrak{K}k_1S}{\mathfrak{K} + k_1S}\right)$$

where $L$ is the feed rate of A.

In a tube packed with a large number of cavities

$$-\mathrm{d}A = \frac{A(\mathfrak{K}k_1S)}{L(\mathfrak{K} + k_1S)}\,\mathrm{d}N$$

where $N$ is the number of cavities. A similar form applies to $\mathrm{d}B$. Then

$$\mathrm{d}B/\mathrm{d}A = \left(\frac{\mathfrak{K} + k_1S}{\mathfrak{K} + k_2S}\right)\left(\frac{k_2S}{k_1S}\right)\frac{B}{A} - \frac{\mathfrak{K}}{\mathfrak{K} + k_2S}$$

Whence

$$B = \frac{k_1}{k_1 - k_2}\left[A^{\frac{k_2}{k_1}\left[1 + \frac{k_1S - k_2S}{\mathfrak{K} + k_2S}\right]} - A\right] \text{ for } A_0 = 1 \qquad (7)$$

Equation 7 is valid for all degrees of diffusional control and reduces to an equation of the form of 4 and 5 when $\mathfrak{K}$ is large. As $\mathfrak{K}$ decreases, the position of maximum $B$ moves to larger $A$ and the maximum value of $B$ is lowered. Equation 7 has, therefore, an effect rather similar to that of eq. 6 even though the model is quite different. Although the correct model probably would be somewhat intermediate between the model of Wheeler and one with a network of cavities some of which are blind,[11] it is evident that lowering of the concentration of the intermediate and increase in the value of $A$ at which it maximizes will attend almost any type of intrusion of serious concentration gradients.

The variability and complexity of actually occurring situations would appear to prevent the derivation of any generally valid and mechanistically significant equation. We suggest, therefore, that it often will be useful to employ a mechanistically neutral formulation, to examine the low conversion region for the system A → B → D, and to represent severity of concentration gradients by $\alpha$ or by $(D/B)_{in}$. Further, equations like 6 and 7 upon expansion at low conversions reduce to ones of the type of 4 and 5. For example, the plot of eq. 5 with $\beta = 0.47$ in Fig. 5 gives a curve which

(11) The observed deactivation of our catalysts during runs or the deliberate poisoning in runs B7, B8, and B9 of Pt-II might have led to a case of poisoned pore mouths.[4] This model would somewhat resemble the model of eq. 7. In fact, however, decline in activity causes the results to approach the behavior characteristic of low concentration gradients. Thus, the deactivation and the poisoning seem to reduce the catalytic activity rather uniformly throughout the catalyst particles.

essentially duplicates that of eq. 6 for $A$ from 1.0 to about 0.75.

**Channelling.**—Consider the system A → C → F under conditions such that concentration gradients in the catalyst pores are negligible. The occurrence of channelling in flow through the catalyst bed will introduce a new type of concentration gradient in the plane perpendicular to the direction of flow and many of the characteristics of diffusional control will reappear.

Suppose, for example, that the flow is divided into two streams which remix at the end of the bed and let the compositions of the two streams just before mixing be $A',C'$ and $A'',C''$. If we are employing Pt-VI, both compositions will lie on the line $C$ *vs.* $A$ in Fig. 3. The composition after mixing, $A,C$, will be on the line joining $A',C'$ and $A'',C''$ and it will lie below the line $C$ *vs.* $A$. This will be the general result of channelling as it was of diffusional control.

However, if conversion is so low that the most converted stream still lies on the initial linear section of $C$ *vs.* $A$, *i.e.*, $A$ greater than about 0.8, then the effect of channelling will be very small. That is, channelling will not ordinarily affect $(C/A)_{in}$ but concentration gradients in catalyst pores will.

Since $C$ closely follows eq. 5 for the less active catalysts, channelling in our experiments was small or negligible.

**Conclusion.**—We believe that the techniques described in this paper constitute in appropriate cases a very powerful technique for characterizing the presence or absence of various types of concentration gradients. Furthermore, this work reëmphasizes the importance of establishing the absence of significant concentration gradients in any catalytic study aimed at mechanism. For example, had one had only our results on platinum–charcoal, one might well have concluded that 2,4-dimethylpentane was a *major initial* product in the hydrogenolysis of dicyclopropylmethane whereas it is, in fact, a very minor one.

This work also emphasizes that it frequently is easier to elucidate mechanistic details on a complicated system than on a simple system. The simultaneous occurrence of the reactions A → B → D + E and A → C → E + F permitted us to characterize the relative contributions of the double-opening reaction and of concentration gradients rather clearly. In a simpler reaction in which only one of these reactions occurred, this would have been much more difficult. However, as paper II will show, complications can become excessive.

**Acknowledgment.**—This work was supported by the Air Force Office of Scientific Research (Directorate of Chemical Sciences).

# THE HYDROGENOLYSIS OF DICYCLOPROPYLMETHANE ON NICKEL CATALYSTS

BY JOHN NEWHAM AND ROBERT L. BURWELL, JR.[1]

*Department of Chemistry, Northwestern University, Evanston, Illinois*

*Received February 16, 1962*

This paper deals with the hydrogenolysis of dicyclopropylmethane (A) on nickel–silica, reduced nickel oxide, and nickel wire at 55° in a flow reactor. Diffusional control was negligible. Results differ in two major ways from those on platinum (paper I), a much increased yield of 2-methylhexane (E) and the intrusion of demethanation. E amounts to about 70% of the final heptane product which indicates that cleavage of the first and of the second rings occurs preferentially in opposite locations and, therefore, with some difference in mechanism. The double ring opening reaction *via* a surface reaction intercepts the formation of desorbed isobutylcyclopropane (C) to a much greater extent than on platinum. The large yield of E results from predominant cleavage of a bond adjacent to the side chain during the opening of the second ring. The mechanism of ring opening is discussed with the tentative conclusion that the initial ring opens *via* formation of 1,3-diadsorbed 2-substituted cyclopropane either by direct reaction of physically adsorbed A or from 1-monoadsorbed 2-substituted cyclopropane. The adsorbed species formed in this reaction either desorb or further react to open the second ring before desorption. About 10% of the initial ring cleavage leads to demethanation by breaking two bonds in the cyclopropyl ring. The effect of temperature upon selectivities is much smaller than on platinum.

This paper reports the results of the hydrogenolysis of dicyclopropylmethane on three nickel catalysts, nickel–silica, reduced nickel oxide, and nickel wire.

## Experimental

The apparatus and techniques were the same as reported in paper I.[2] The procedures for gas chromatography were also the same except that four new products were present of which hexane, 2-methylpentane, and pentane were assigned by comparison with authentic samples and propylcyclopropane, on the basis of internal chemical evidence.

Nickel I consisted of 0.1 g. of 60–100 mesh nickel–kieselguhr (Harshaw Chemical Company) diluted with about 4.5 g. of 60–80 mesh glass beads. Nickel II was prepared from nickel nitrate *via* the carbonate and oxide[3]; 1.01 g. of 60–100 mesh material was mixed with 3 g. of glass beads. Nickel wire of a reported purity of 99.95% (United Mineral and Chemical Corporation) and of a diameter of 0.01 in. was made into helices of about 2 mm. diameter. These were packed in a tube parallel to its axis and the gaps between the helices were largely filled with thin glass rods. Ni-III-A weighed 10.2 g.; Ni-III-B, 23 g. Ni-III-A was treated with oxygen for 1 hr. at 600° and then reduced in hydrogen at 450°. The catalytic activity of the resulting material was very low. The oxidation–reduction sequence was repeated seven times more after which the nickel wire had substantial catalytic activity at 50°. The wire now had a matte appearance. Ni-III-B was treated with hydrogen at 450° for 8 hr. but it displayed no catalytic activity at up

(1) To whom queries about this paper should be directed.

(2) J. Newham and R. L. Burwell, Jr., *J. Phys. Chem.*, **66**, 1431 (1962).

(3) H. C. Rowlinson, R. L. Burwell, Jr., and R. H. Tuxworth, *ibid.*, **59**, 226 (1955).

TABLE I

HYDROGENOLYSIS OF DICYCLOPROPYLMETHANE ON NICKEL CATALYSTS[a]

| Run | $L$[b] | $A$ | $B$ | $C$ | $G$ | $D$ | $E$ | $F$ | $H$ | $MP$ | $P$ |
|---|---|---|---|---|---|---|---|---|---|---|---|
| | | | | | | Ni-I | | | | | |
| C2 | 9.6 | 0.000 | 0.000 | 0.020 | 0.000 | 0.067 | 0.518 | 0.153 | 0.110 | 0.110 | 0.022 |
| C3 | 3.5 | .086 | .015 | .098 | .046 | .077 | .449 | .070 | .081 | .055 | .013 |
| C4[c] | 13.2 | .514 | .016 | .107 | .016 | .029 | .263 | .021 | .026 | .007 | .001 |
| | | | | | | ( .032) | ( .267) | ( .017) | ( .026) | ( .005) | ( .000) |
| C5[c] | 7.1 | .289 | .015 | .128 | .019 | .047 | .400 | .049 | .058 | .014 | .001 |
| | | | | | | ( .046) | ( .401) | ( .050) | ( .060) | ( .013) | ( .001) |
| C6[c] | 37.4 | .823 | .009 | .036 | .006 | .013 | .095 | .007 | .009 | .002 | .000 |
| | | | | | | ( .014) | ( .094) | ( .008) | ( .009) | ( .002) | ( .000) |
| C7[c] | 23.0 | .775 | .011 | .049 | .007 | .018 | .115 | .008 | .015 | .002 | .000 |
| | | | | | | ( .017) | ( .120) | ( .007) | ( .012) | ( .003) | ( .000) |
| E5 | 4.8 | .715 | .022 | .103 | .013 | .019 | .109 | .007 | .010 | .001 | .000 |
| E4[d] | 4.6 | | .706 | | | .035 | .228 | | .030 | | |
| E3[e] | 27 | .231 | .397 | .032 | .008 | .040 | .244 | .016 | .029 | .001 | .000 |
| | | | | | | Ni-II | | | | | |
| B1 | 3.6 | .242 | .001 | .083 | .023 | .097 | .357 | .114 | .047 | .034 | .001 |
| B2 | 13.5 | .910 | .009 | .035 | .003 | .007 | .031 | .002 | .003 | .000 | .000 |
| B3 | 2.3 | .197 | .017 | .156 | .020 | .098 | .348 | .097 | .037 | .031 | .000 |
| B4 | 6.1 | .540 | .019 | .143 | .016 | .052 | .175 | .023 | .023 | .009 | .000 |
| B5 | 3.0 | .603 | .017 | .162 | .016 | .030 | .133 | .018 | .015 | .007 | .000 |
| B6 | 5.2 | .851 | .008 | .066 | .003 | .011 | .051 | .004 | .004 | .001 | .000 |
| B10[f] | 3.7 | .007 | .000 | .003 | .000 | .131 | .519 | .187 | .076 | .074 | .001 |

[a] At 55°. [b] $L$ is flow rate in mmoles/hr. of A. The molar ratio $H_2$/A was 17. $A$ is the mole fraction of dicyclopropylmethane in the product; $B$, that of butylcyclopropane; $C$, isobutylcyclopropane; $D$, heptane; $E$, 2-methylhexane; $F$, 2,4-dimethylpentane; $G$, propylcyclopropane; $H$, hexane; $MP$, 2-methylpentane; $P$, pentane. [c] Values in parentheses are those computed as described in the text. [d] Feed hydrocarbon was butylcyclopropane. [e] A mixture of A and B 0.423/0.577 was fed. [f] At 76°.

to 200°. It then was treated with oxygen at 620° for 4 hr. and reduced in hydrogen at 450° for 8 hr. This material was active at 120°.

**Competitive Hydrogenolysis of Dicyclopropylmethane and Cyclopropane or Butylcyclopropane on Ni-I.**—In an experiment with cyclopropane, 0.3% of this compound reacted, 40% of dicyclopropylmethane. Thus, the latter compound reacts about 200 times as fast as cyclopropane. The result with butylcyclopropane is given in run E3, Table I.

## Results and Discussion

The nickel catalysts differ from the platinum catalysts[2] in two conspicuous ways: at 55°, much larger amounts of 2-methylhexane are made than on platinum; a demethanation reaction accompanies ring cleavage to give products not observed with platinum: propylcyclopropane, hexane, 2-methylpentane, and pentane.

**Catalyst Ni-I.**—These features may be seen in Table I for Ni-I, nickel–kieselguhr. Ni-I-C was reduced in hydrogen at 450°. Its activity being far too great, it was sintered in hydrogen at 620° for 1 hr. after run C2. The activity was then in a convenient range. Ni-I-E was similarly sintered after run E1. Runs C1 and E1 gave results almost identical with C2. Ni-I-D behaved anomalously. After initial reduction at 450°, its activity was no greater than that of C and E after sintering. Probably it had been incompletely reduced. It gave less 2-methylpentane and 2,4-dimethylpentane and more heptane than Ni-I-C and Ni-I-E.

Except possibly in runs C1, C2, and E1, there were no serious concentration gradients in the catalyst pores. First, as may be seen from runs C6 and C7, $(F/C)_{in}$ is small (see Table I for symbols, also paper I, "Results in the presence of serious concentration gradients"). Further, as with the less active platinum catalysts, the 0.7% cyclopropylbutene disappeared at low conversions of dicyclopropylmethane. Similar considerations apply to Ni-II and Ni-III.

As shown in Table I, hexane and 2-methylpentane were found in all runs and pentane was observed in all runs at higher conversions. In addition, one more species was observed which appears to be an initial product (see the runs at lowest conversion, C6 and C7) and which further reacts to disappear from the final products. Gas chromatographically, its relationship to the hexanes is much like that of butylcyclopropane to heptanes. It hardly can be other than propylcyclopropane, the further demethanation of which generates the pentane and the hydrogenolysis of which generates some of the hexane and 2-methylpentane.

Previous investigations of the hydrogenolysis of cyclopropanes on nickel catalysts appear to have overlooked the occurrence of the demethanation reaction[4] and not surprisingly since they anteceded the availability of gas chromatography. The occurrence of the demethanation reaction accords with the well known tendency of nickel toward hydrogenolysis. It should be emphasized that the demethanation accompanies the opening of the ring since alkanes are not hydrogenolyzed under these conditions.[3]

2-Methylhexane constitutes about 70% of the final *heptane* product on these catalysts, a rather puzzling result since it implies that one ring is preferably opened at *a*, the other, at *b*

(4) For example, R. Van Volkenburgh, K. W. Greenlee, J. M. Derfer, and C. E. Boord, *J. Am. Chem. Soc.*, **71**, 172 (1949); N. Kishner, *J. Russ. Phys. Chem. Soc.*, **45**, 957 (1913).

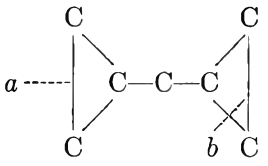


Thus, to some degree, the mechanism of opening the second ring must differ from that of opening the first.

We cannot present such a detailed analysis of the reactions on nickel as we did with platinum. A full unravelling of such a complicated reaction would require much more experimental data than we attempted to collect. Other complications *vis-a-vis* platinum are that the selectivity ratios change with time and with declining activity on the nickel catalysts and differ much more from sample to sample of the same batch of nickel catalyst, presumably because of the greater effect of minor differences in the reduction regime. Thus, as may be seen in comparing runs C2 and C3 of Ni-I in Table I, sintering results in a decline in the relative degree of the demethanation reaction. Further decline occurred between C3 and C4 although the catalyst received no additional treatment.

The sequence C4–C7 seems reasonably coherent and to involve only a small decline in activity. These runs are reasonably well reproduced by the following model. The symbols are defined in Table I. Values computed from the parameters of the model and the experimental values of $A$, $B$, $C$, and $G$ are entered in parentheses in Table I. Despite the excellence of the agreement with the observed values, in such a complicated system we cannot be sure that this model is unique although it does appear plausible.

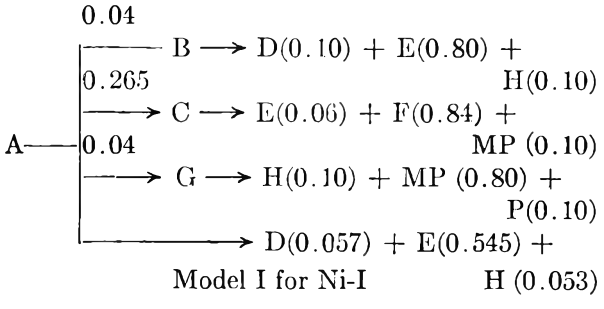


Model I for Ni-I

Eliminating demethanation, the results on Pt-I, Pt-IV, Pt-VI, and Pt-VIII could be expressed similarly although additionally $B$ and $C$ are given as functions of $A$ for platinum.

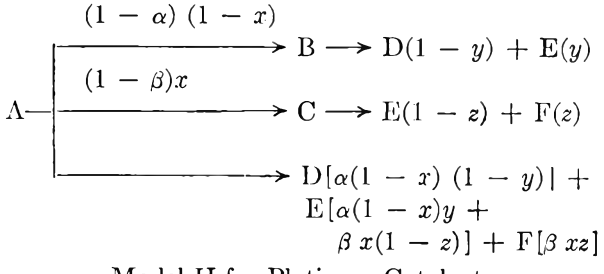


Model II for Platinum Catalysts

With Pt-VI, for example, in the last line one gets: D(0.016) + E(0.085) + F(0.045).

In both Models I and II, the last line can be interpreted as further reaction of those species adsorbed in the initial ring cleavage with resulting opening of the second ring before desorption. With platinum, a plausible set of parameters can be chosen such that the last line can be combined with the first two by treating it as a short-circuiting of B and C, *i.e.*, the composition of the products from the double-opening reaction is the same as that which results from the two-step reaction. We have not seen how to do this with the nickel catalysts, *i.e.*, the numbers on the last line of Model I are additional arbitrary parameters.

In Model I, since F does not appear on the last line, F is not an initial product. The model assumes that the second ring opening always leads to cleavage of a bond adjacent to the side chain of the remaining cyclopropyl ring. It would be possible, of course, to readjust the parameters to add a small amount of F to the last line. With platinum, however, it is impossible to choose any set of parameters which permits F on the last line to be zero. Even if all of the C which is made is converted to F ($z = 1$), F still would be too small. This conclusion could only be circumvented if concentration gradients existed in the pores during runs with all platinum catalysts such that observed values of $C$ were reduced below the ideal, *i.e.*, if the observed value of $\beta$ were almost entirely determined by diffusion control. Since this appears unlikely, one must conclude that the double-opening reaction on nickel is much more likely to result in cleaving the remaining ring adjacent to the side chain. This difference between the two catalysts may be a function of temperature. At temperatures of 90° and above with platinum, the values of $y$ and $z$ are much smaller than those of $x$, probably because the surface reaction on platinum increasingly favors the cleavage of the residual ring at a bond adjacent to the side chain.

In Model I, ring opening is diverted into demethanation 10% of the time if one considers that the hexane in the last line results from a surface reaction which intercepts the formation of propylcyclopropane. This makes hexane an initial product whereas 2-methylpentane is not. The initial yield of 2-methylpentane like that of dimethylpentane is certainly small if not zero. This implies that little of the surface reaction diverts to demethanation; otherwise nearly 10% of the 2-methylhexane formed in the surface reaction would be diverted to 2-methylpentane.

**Mechanism.**—Enough is known about the cleavage of cyclopropanes to encourage speculation about its mechanism but not enough to establish the mechanism with any certainty. It seems desirable to list possible mechanisms systematically as is done in Table II.[5]

Reactions 2–7 of monoadsorbed cyclopropane can be duplicated with diadsorbed as exemplified by reaction 6′. Some of the reactions written in two steps might be concerted. For example, reaction 1 might be written without intermediate formation of 1,3-diadsorbed propane.[5]

(5) For previous discussion of the mechanism of this reaction, see G. C. Bond and J. Newham, *Trans. Faraday Soc.*, **56**, 1501 (1960).

TABLE II

POSSIBLE REACTIONS OF CYCLOPROPANE[a]

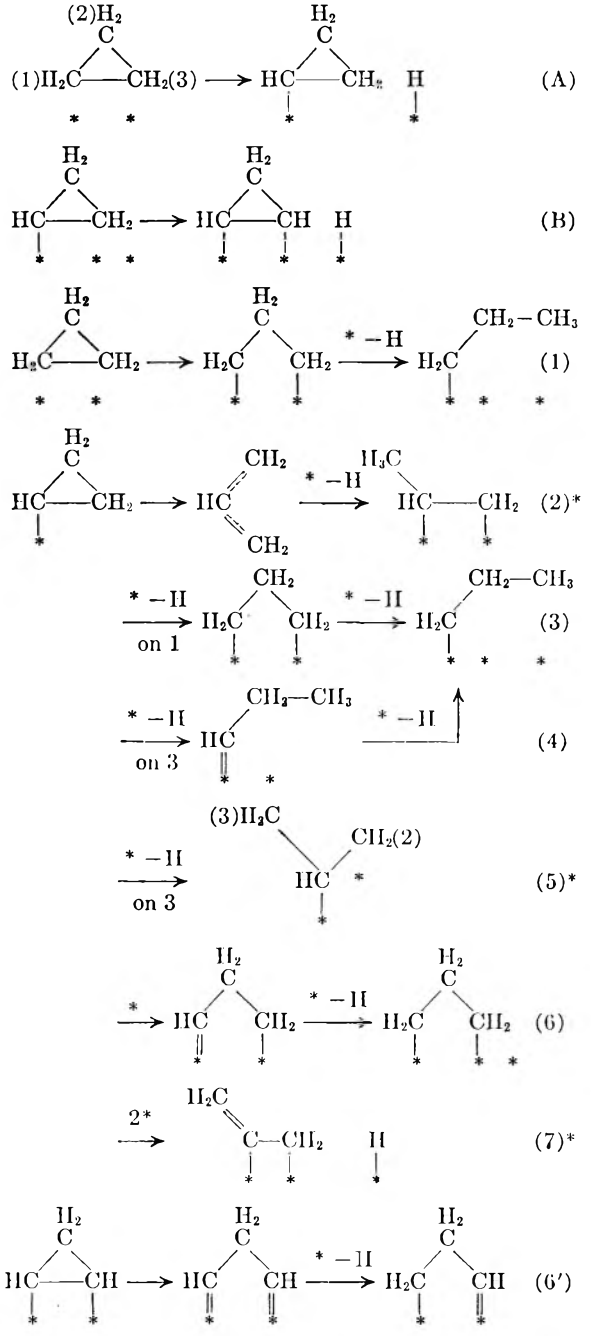


[a] In reactions 2–7, the bond opposite the position of adsorption is cleaved in reactions 2, 5, and 7 (these are marked with asterisks) whereas a bond adjacent to the position of adsorption is cleaved in 3, 4, and 6.

Reaction 1 has a homogeneous analogy. Cyclopropane reacts with platinum(IV) halides[6] to form the chloride-bridge polymer of

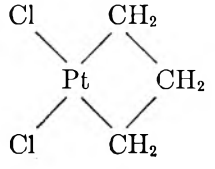

(6) D. M. Adams, J. Chatt, R. G. Guy, and N. Sheppard, *J. Chem. Soc.*, 738 (1961).

Such reactions, unknown for ordinary carbon–carbon bonds, would be favored in cyclopropane by the much reduced bond dissociation energy. Thus, $\Delta H$ for the hydrogenolysis of cyclopropane is $-37.6$ kcal., for ethane, $-15.6$.[7]

In reaction 2, the plane of adsorbed allyl is taken as parallel to the catalyst surface. The compound, $(C_3H_5PdCl)_2$, very probably has this structure.[8] Alternatively, the adsorbed species might resemble that reported[8] for a cobalt complex. It would be

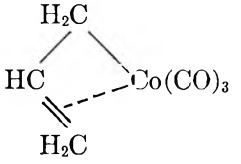

interesting to ascertain the structure of the reaction product of cyclopropylmagnesium halide (which, like dicyclopropylmercury, has a normal structure[9]) with phosphine-complexed platinum halides.

The other adsorbed species all have some plausibility. The mono- and *vic*-diadsorbed propanes at the extreme right of reactions 1 and 2 are the conventional intermediates in isotopic exchange of alkanes and in hydrogenation of olefins.[10,11] The diadsorbed propane will react with *–H to form a monoadsorbed propane which will either revert to diadsorbed propane or react with *–H to form desorbed propane.

Although 1,3-diadsorbed alkanes[3,12–14] and the *gem*-diadsorbed species[11] of reactions 4 and 6 appear to be of relatively high energy, their formation would be coupled with cleavage of a cyclopropane carbon–carbon bond. The species of reaction 7 is that presumed to be formed initially in the hydrogenation of allene.

Reaction A is an established reaction. Anderson and Kemball[15] report that cyclopropane and deuterium form deuteriocyclopropanes and deuteriopropanes at about equal rates on evaporated rhodium film at $-100°$. At 50° on rhodium, platinum, palladium, and iridium supported on pumice, the rate of formation of deuteriocyclopropanes, while finite, is much smaller than that of deuteriopropanes.[16] Further, the exchanged cyclopropanes are mostly di- and trideuterio- and this supports the occurrence of reaction B.

(7) J. W. Knowlton and F. D. Rossini, *J. Res. Natl. Bur. Std.*, **43**, 113 (1949). American Petroleum Institute, Research Project 44, "Selected Values of Properties of Hydrocarbons and Related Compounds," Table 1p.

(8) G. E. Coates, "Organometallic Compounds," 2nd edition, Methuen and Co., Ltd., London, 1960, pp. 305 and 340. G. Wilkinson, "Advances in the Chemistry of Coördination Compounds," edited by S. Kirschner, The Macmillan Co., New York, N. Y., 1961, p. 60.

(9) G. F. Reynolds, R. E. Dessy, and H. H. Jaffé, *J. Org. Chem.*, **23**, 1217 (1958).

(10) R. L. Burwell, Jr., *Chem. Rev.*, **57**, 895 (1957).

(11) C. Kemball, *Advan. Catalysis* **11**, 223 (1959).

(12) R. L. Burwell, Jr., and W. S. Brigge, *J. Am. Chem. Soc.*, **74**, 5096 (1952).

(13) C. Kemball, *Trans. Faraday Soc.*, **50**, 1344 (1954).

(14) R. L. Burwell, Jr., B. K. C. Shim, and H. C. Rowlinson, *J. Am. Chem. Soc.*, **79**, 5142 (1957).

(15) J. R. Anderson and C. Kemball, *Proc. Roy. Soc.* (London), **A226**, 472 (1954).

(16) J. Addy and G. C. Bond, *Trans. Faraday Soc.*, **53**, 368, 383, 388 (1957).

Thus, all of these intermediates are plausible to some degree and there is the fearsome possibility that each may be significant at least with certain substituted cyclopropanes and under some particular set of conditions.

It is easier to judge the plausibility of intermediates than of the reactions which form them. Many of the reactions involve rather extensive rearrangement of structure, rotations of the methylene groups as well as bond angle changes. For example, in the first step of reaction 2, the atoms all must move into one plane. The plausibility of this is difficult to judge since we know neither the geometry of the surface, the actual nature of the surface sites (the * is a symbol of ignorance, not of knowledge), nor the spatial distribution of the surface orbitals. Indeed, we know very little about the intermediate stages of even reaction A[14] which is fundamental to the interaction between hydrogen and hydrocarbons on metallic surfaces. However, on the surfaces of metals there are probably a number of unfilled orbitals variously directed. These can interact with the various intermediate stages so as much to reduce the activation energies over what would exist in the absence of a metallic surface.

The initiating reactions of Table I are A and 1. Since dicyclopropylmethane and butylcyclopropane react about 100 times faster than cyclopropane on Ni-I at 55°, the actual reactant in these steps is probably in a preëquilibrium physically adsorbed state, a suggestion also made by Bond and Addy.[16]

Of available data, the following probably are of particular mechanistic significance.

A. Alkylcyclopropanes predominantly cleave opposite the position of substitution.

B. 1,1-Dialkylcyclopropanes cleave much more slowly than alkylcyclopropanes and 1,1,3,3-tetraalkylcyclopropanes cleave even more slowly.[17] Opposing reports on the nature of the products from 1,1-dialkylcyclopropanes have been made.[17,18]

C. Phenylcyclopropane cleaves much more readily[19] than alkylcyclopropanes and only to give *n*-propylbenzene.[20]

D. Both *cis*- and *trans*-1,2-diphenylcyclopropane undergo hydrogenolysis on palladium to give 1,3-diphenylpropane exclusively. The *trans* reacts 2–3 times as fast as the *cis*. Phenylcyclopropane reacts a little faster than the *cis*.[21]

E. 1,1-Diphenylcyclopropane reacts much more slowly than the 1,2-diphenylcyclopropanes.[21]

F. At room temperature with Adams platinum oxide, and glacial acetic acid as solvent, the bicyclopentane gives cyclopentane as the only product.[22] Ordinary alkylcyclopropanes would be inert under these conditions.

The major effects of most substituents upon the ease of the cleavage of an adjacent bond in the cyclopropyl ring probably are two: electron delocalization in the transition state which facilitates cleavage; steric interaction of the substituent with the surface which retards cleavage. For comparative purposes, the effect of the substituents upon the relevant bond dissociation energies is a useful approximation to the first effect. Thus, in datum F, the bond which opens has much the lowest bond dissociation energy and the ordinary direction of cleavage (datum A) is not followed.

Consider reaction 1 with a substituent at carbon atom 1 in the numbering of reaction A, Table II. From bond dissociation energies, both alkyl and phenyl should facilitate rupture of bond 1–2 but the effect of phenyl should be much larger. Both alkyl and phenyl would retard by steric interaction. Data A and C would require that steric interaction dominate with alkyl, electron delocalization with phenyl. This is plausible and also is reflected in the ready hydrogenolysis of benzyl alcohol to toluene.

In reactions 2–7 the substituent will affect both initial cleavage of a carbon–hydrogen bond and subsequent cleavage of a carbon–carbon bond. Phenyl will facilitate cleavage of the 1–2 carbon–carbon bond no matter whether initial adsorption is at position 1 or 2 but phenyl will only facilitate initial adsorption at position 1. In view of datum C, reactions 2, 5, and 7 (those marked with an asterisk) are unlikely at least with phenylcyclopropane.

The effect of an alkyl substituent at carbon-1 upon reaction A is problematic. In an acyclic alkane, carbon–hydrogen cleavage probably would occur at the most substituted carbon atom (*i.e.*, the analog of carbon-1).[23] However, the hybridization in the orbitals employed in the carbon–hydrogen bond in cyclopropane is closer to $sp^2$ than to $sp^3$ and, consequently, the electronegativity of the carbon atoms is greater than in acyclic alkanes. If the transition state in reaction A has much carbanion character, the hydrogen atom at the less substituted position will cleave preferentially.[24] If 1-monoadsorbed 1-alkylcyclopropane is favored, datum A requires predominant involvement of the asterisked reactions 2, 5, and 7, *i.e.*, the opposite of those required with phenylcyclopropane. If alkyl depresses adsorption at position 1, the direction of cleavage depends upon the balance between facilita-

(17) R. G. Kelso, K. W. Greenlee, J. M. Derfer, and C. E. Boord, *J. Am. Chem. Soc.*, **77**, 1751 (1955); **74**, 287 (1952); R. W. Shortridge, R. A. Craig, K. W. Greenlee, J. M. Derfer, and C. E. Boord, *ibid.*, **70**, 946 (1948). Temperatures of 180 to 250° were necessary on a nickel–kieselguhr catalyst, although we find that hydrogenolysis of butylcyclopropane is fast on a similar catalyst at 55°. Data such as these must be used with caution since the adventitious presence of traces of poison can vitiate any conclusions. The only safe conclusions are those obtained in competitive experiments.

(18) Ya. M. Slobodin, V. I. Grigor'eva, and Ya. E. Shmulyakovskiĭ, *Zh. Obshch. Khim.*, **23**, 1480 (1953). On nickel–kieselguhr at 150°, 1 atm., no 1,1-dimethylcyclopropane opens between atoms 2 and 3. At 180° on nickel–kieselguhr at high pressures of hydrogen, cleavage occurs only at this bond (ref. 17, last paper). Preliminary isomerization to olefin may be involved in the first example.

(19) A. A. Balandin and M. L. Khidekel, *Dokl. Akad. Nauk SSSR*, **123**, 83 (1958).

(20) B. A. Kazanskiĭ, M. Yu. Lukina, and I. L. Safonova, *Izv. Akad. Nauk SSSR, Otd. Khim. Nauk*, 102 (1958).

(21) B. A. Kazanskiĭ, M. Yu. Lukina, and I. L. Safonova, *Dokl. Akad. Nauk SSSR*, **130**, 322 (1960).

(22) R. Criegee and A. Rimmelin, *Ber.*, **90**, 414 (1957).

(23) T. I. Taylor, "Catalysis," Vol. V., edited by P. H. Emmett, Reinhold Publ. Corp., New York, N. Y., 1957, pp. 323 and 334.

(24) For a review of these considerations see R. L. Burwell, Jr., A. B. Littlewood, M. Cardew, G. Pass, and C. T. H. Stoddart, *J. Am. Chem. Soc.*, **82**, 6272 (1960).

tion by reduced bond dissociation energy and retardation by steric interaction. If the latter effect dominates, reactions 3, 4, and 6 are acceptable although the incursion of steric hindrance into reaction 4 is somewhat harder to understand than in reactions 3 and 6.

We suggest then, very tentatively, that reactions 1 and 3 or 6 are primarily involved. Reactions 3 and 6 are closely related, since the first step of reaction 3 is merely a concerted form of the first two steps of reaction 6. Reactions 3′ and 6′ are possible alternatives.

Let us now consider the reaction in which both rings of dicyclopropylmethane open during one period of adsorption. A species such as the following will be formed consequent to opening of the first ring.

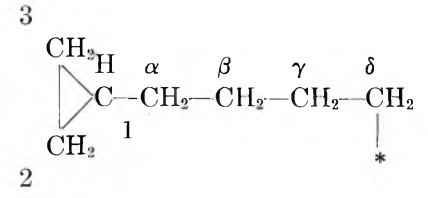


The sequence, δ-monoadsorbed, γ,δ-diadsorbed, γ-monoadsorbed, β,γ-diadsorbed, etc., can transfer the position of monoadsorption to any other position, and, in particular, to position 1, where reactions 3 or 6 could open the second ring. In addition, a side-chain monoadsorbed species can react as in reaction A or 1 of Table II to form, for example

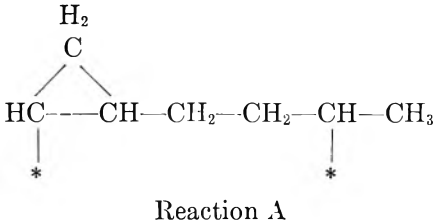


Reaction A

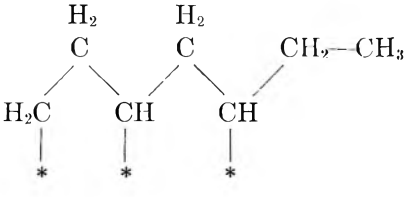


Reaction 1

Quite probably, all of these reactions occur simultaneously and we do not see how to predict product ratios *a priori*. Models do, however, indicate that reaction 1 would preferably cleave bond 1–2 in α- and β-monoadsorbed and probably bond 2–3 in α- and δ-monoadsorbed. The observed differences between nickel and platinum could depend upon rather minor differences in the rates of the elementary reactions. In particular, the greater prevalence of double-opening on nickel could result from a greater relative rate of the migration of the position of adsorption on the side chain.

In the demethanation reaction, two of the bonds in the cyclopropane ring are cleaved, either in two steps or in one concerted step. It is important to note that negligible amounts of pentane are formed from butylcyclopropane. Thus, the bonds cleaved are those shown by the full line below, not the dotted line

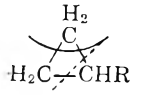


Further, since the relative yield of the demethanation reaction on nickel declines with time, special sites probably are involved and perhaps those with particular geometry such as sites at steps which would permit concerted cleavage of two bonds.

**Ni-II and Ni-III.**—The results with reduced nickel oxide, Ni-II (Table I), and nickel wire, Ni-III, resembled those with nickel–silica, Ni-I, in major features. The composition of the products at complete reaction is similar (compare run B10 of Ni-II with C2 of Ni-I) both in regard to demethanation and the high yield of 2-methylhexane (E).

As may be seen from runs B2 and B6 of Ni-II, the initial yield of isobutylcyclopropane (C) is 0.43 as compared with 0.265 for Ni-I as shown in Model I. Correspondingly, the yields of the double-opening reaction (last line of Model I) for Ni-II are only 0.7 those for Ni-I. Since the final yield of E is about the same on the two catalysts, the fraction of C converted to E must be much larger with Ni-II, 0.4 to 0.5 *vs.* 0.06. Yet in the initial cleavage on Ni-II, isobutylcyclopropane heavily predominates over butylcyclopropane. The results for Ni-II are internally less consistent than with Ni-I or any of the platinum catalysts of paper I. This may be seen in comparing runs B4 and B5. B5 gives a much lower yield of D, E, and H. The results with Ni-II seem unsuitable for the kind of treatment given with the other catalysts because of changes in selectivity either with time or with conversion.

At 55°, the initial product composition on nickel wire was almost the same as that on Ni-II. The catalyst was of low area and of low activity and its activity declined rapidly with use. Activity was restored by an oxidation–reduction sequence. Since conversions were not carried beyond 20% reaction of dicyclopropylmethane, one cannot test models of the type of Model I.

Nickel wire was chosen as a catalyst which was *a priori* unlikely to involve serious concentration gradients. The initial value of F/C was less than 0.05, which supports this expectation. Further, in a run in which only 1.5% of A had reacted, the cyclopropylbutene impurity had slightly more than half disappeared.

Nickel-III was packed into the catalyst tube in the form of parallel helices. Since one might worry about channelling, after several runs on Ni-III-B, the catalyst was removed, cut into single-turn helices, repacked in the reactor, and reactivated. It gave the same product distribution as before.

Runs were made on Ni-III-A at 37 and 52°, on Ni-III-B at 125°. The effect of temperature upon product distribution was small, much smaller than on platinum (paper I). With increasing temperature, the yield of products involving initial cleav-

age adjacent to the side chain rises, *i.e.*, less C, more B and D. There is also a small increase in demethanation (more G).

**Acknowledgment.**—This work was supported by the Air Force Office of Scientific Research (Directorate of Chemical Sciences).

# THE THERMODYNAMIC PROPERTIES OF 2-BUTANOL

BY NEIL S. BERMAN AND JOHN J. MCKETTA

*Department of Chemical Engineering at The University of Texas, Austin, Texas*

*Received February 17, 1962*

The vapor heat capacity and latent heat of vaporization of 2-butanol have been determined experimentally. A model of an equilibrium mixture of monomers, dimers, and tetramers was used to select constants of an equation of state to fit the heat capacity data and total gas imperfection calculated from the Clapeyron equation. Molecular structure, spectroscopic information, and the vapor heat capacity data were used to evaluate barriers to internal rotation and compute tables of thermodynamic functions.

As part of a program to study the properties of oxygenated hydrocarbons, the vapor heat capacity of 2-butanol has been measured experimentally in a pressure range of one-fourth to five-fourths atmospheres and a temperature range of 365.15 to 455.15°K. The heat of vaporization has been determined along with the vapor pressure over the pressure range from one-fourth to five-fourths atmospheres. A model of an equilibrium mixture of monomers, dimers, and tetramers was used to correlate the heat capacity data and the total gas imperfection calculated from the Clapeyron relation. Molecular structure, spectroscopic information from the literature, and vapor heat capacity data were used to evaluate the barriers to internal rotation. Tables of thermodynamic functions for this compound are presented at selected temperatures from 0 to 1000°K.

## Experimental

**Physical Constants and Definitions.**—Calculations in this work are based on the 1956 Atomic Weights,[1] the values of the fundamental physical constants reported by Rossini, *et al.*,[2] and the definitions: 0°C. = 273.15°K. and 1 cal. = 4.1840 abs. joules. Temperatures are on the defined International Temperature Scale.

**The Material.**—The sample of 2-butanol was supplied by the Celanese Corporation of America. It was purified from Eastman Kodak secondary butyl alcohol by multiple fractional distillation using a 1-in. 90 tray Oldershaw column. Purity by gas chromatography was found to be 99.92%. This material was further distilled in a 1.2-m. column packed with glass rings and vacuum distilled into receivers for introduction into the apparatus. The boiling range of the final distillate was less than 0.005° at atmospheric pressure. No significant changes in the color or boiling point of the compounds were noted in the course of the determinations reported.

**The Apparatus.**—The apparatus used to measure the vapor heat capacities, heats of vaporization, and vapor pressures was the flow calorimeter used by Pennington,[3] Mathews,[4] and Nickerson[5] and the same type described by Waddington, *et al.*,[6] and Pitzer[7] with modifications discussed by McCullough, *et al.*[8] The three-way solenoid valve used in the previous research was replaced with a pair of two-way valves for the heat of vaporization determinations.

**Vapor Pressure.**—Vapor pressures of 2-butanol were obtained from the flow data at five pressures between one-fourth and five-fourths atmospheres. The values shown in Table I are based upon the average of at least eight experimental measurements.

TABLE I

EXPERIMENTAL VAPOR PRESSURES AND LATENT HEAT OF VAPORIZATION OF 2-BUTANOL

| Temp., °K. | Pressure, mm. | $\Delta H_v$, cal./mole |
|---|---|---|
| 339.91 | 189.78 | 10824 |
| 355.20 | 379.63 | 10350 |
| 365.10 | 568.46 | 10014 |
| 372.49 | 754.70 | 9753 |
| 378.49 | 937.63 | — |

$$\log p = 7.14472 - \frac{1129.08}{165.26 + t} \qquad (1)$$

Where $p$ is in mm. and $t$ in °C. The accuracy uncertainty of this equation is estimated as ±0.5 mm. The normal boiling point of 99.54° compares favorably with the values of 99.529° by Brunel[9] and 99.52–99.55° by Parks, *et al.*[10]

**The Heat of Vaporization.**—Latent heats of vaporization of 2-butanol were measured at pressures of 1/4, 2/4, 3/4, and 4/4 atmosphere at saturation temperatures. The latent heats can be represented by the equation

$$\Delta H_v = 1092.15(225.30 - t)^{0.45282} \qquad (2)$$

where $\Delta H_v$ is in cal./mole and $t$ in °C. It is estimated that the accuracy uncertainty of this equation is not greater than ±0.15% in the range 66.5 to 100°. Experimental results are presented in Table I.

**The Vapor Heat Capacity.**—The vapor heat capacity of 2-butanol was measured at selected pressures from 1/4 to 5/4 atmospheres and at temperatures from 365.15 to 455.15°K. The experimental results are presented in Table II. The accuracy uncertainty of these data is at least ±0.3%. Figure 1 presents a plot of these data and the calculated heat capacities.

Direct heat capacity measurements have been made by Sinke and DeVries[11] from 375 to 437°K. and a pressure of 750 mm. Jatkar and Lakshminarsyanan[12] deduced the heat

(1) E. Wichers, *J. Am. Chem. Soc.*, **78**, 3235 (1956).

(2) F. D. Rossini, F. T. Gucker, H. L. Johnston, L. Pauling, and G. W. Vinal, *ibid.*, **74**, 2699 (1952).

(3) R. E. Pennington and K. A. Kobe, *ibid.*, **79**, 300 (1957).

(4) J. F. Mathews and J. J. McKetta, *J. Phys. Chem.*, **65**, 758 (1961).

(5) J. K. Nickerson, K. A. Kobe, and J. J. McKetta, *ibid.*, **65**, 1037 (1961).

(6) (a) G. Waddington, S. S. Todd, and H. M. Huffman, *J. Am. Chem. Soc.*, **69**, 22 (1947); (b) G. Waddington and D. R. Douslin, *ibid.*, **69**, 2275 (1947).

(7) K. S. Pitzer, *ibid.*, **63**, 2413 (1941).

(8) J. P. McCullough, D. W. Scott, R. E. Pennington, I. A. Hossenlopp, and G. Waddington, *ibid.*, **76**, 4791 (1954).

(9) R. F. Brunel, *ibid.*, **45**, 1334 (1923).

(10) G. S. Parks, S. B. Thomas, and D. W. Light, *J. Chem. Phys.*, **4**, 64 (1936).

(11) G. C. Sinke and T. DeVries, *J. Am. Chem. Soc.*, **75**, 1815 (1953).

(12) S. K. K. Jatkar and D. Lakshminarsyanan, *Chem. Abstr.*, **41**, 1901c (1947); *J. Indian Inst. Sci.*, **28A**, 1 (1946).

TABLE II

VAPOR HEAT CAPACITY OF 2-BUTANOL IN CALORIES PER MOLE DEGREE

| | Temp., °K. | | | | | |
|---|---|---|---|---|---|---|
| | 365.15 | 383.15 | 401.15 | 419.15 | 437.15 | 455.15 |
| $C_p$ ($^5/_4$ atm. abs.) | | | 35.83 | | | 37.74 |
| $C_p$ ($^4/_4$ atm. abs.) | | 35.48 | 35.30 | 35.84 | 36.73 | 37.64 |
| $C_p$ ($^3/_4$ atm. abs.) | | 34.43 | 34.83 | 35.60 | 36.54 | 37.56 |
| $C_p$ ($^2/_4$ atm. abs.) | 33.57 | 33.67 | 34.41 | 35.38 | 36.38 | |
| $C_p$ ($^1/_4$ atm. abs.) | 32.23 | 33.13 | 34.11 | 35.22 | | |
| $A$[a] | 2.801 | 1.815 | 1.217 | 0.842 | 0.598 | 0.433 |
| $C$[b] | 5.312 | 1.093 | 0.257 | 0.068 | 0.020 | 0.007 |
| $C_p^0$ (exptl.) | 31.48 | 32.63 | 33.81 | 34.95 | 36.08 | 37.20 |
| $C_p^0$ (by equation) | 31.47 | 32.64 | 33.80 | 34.95 | 36.08 | 37.21 |
| $C_p^0$ (calcd.) | 31.50 | 32.66 | 33.81 | 34.94 | 36.06 | 37.13 |

[a] Parameter in eq. 6, cal./mole °K. atm. [b] Parameter in eq. 6, cal./mole °K. atm.$^3$.

capacity from sonic velocity measurements. These results are presented for comparison in Fig. 2 after correction to zero pressure.

### Correlation of the Effects of Gas Imperfection

**Hydrogen Bonding in Alcohols.**—Thermodynamic and spectroscopic studies of various alcohols have shown that two or four molecules tend to associate with the formation of a weak chemical bond. Fox and Martin[13] suggested that polymers with more than four monomer units were unlikely and that the cyclic tetramer was the major polymeric species beyond the dimer. Weltner and Pitzer,[14] Kretschmer and Wiebe,[15] and Mathews[4] all found that heat capacity could be correlated best by assuming an equilibrium mixture of dimers, tetramers, and monomers. Correlation of the results of the measurement of the intensity of absorption bands in the 2.5 to 3.2 $\mu$ region of the infrared by Gove[16] led to the same assumptions.

**Gas Imperfection of Associated Molecules.**—The model of an equilibrium mixture of monomers, dimers, and tetramers can be used to derive an equation of state in the form

$$V = RT/p + B + Dp^2 \qquad (3)$$

$$B = -b - RT \exp(\Delta F_2/RT) \qquad (4)$$

$$D = -3RT \exp(\Delta F_4/RT) \qquad (5)$$

where effects other than those due to association are grouped in the constant $b$. From the relationship between heat capacity and the equation of state

$$C_p = C_p^0 + Ap + Cp^3 \qquad (6)$$

$$A = \frac{\Delta H_2^2}{RT^2} \exp(\Delta F_2/RT) \qquad (7)$$

$$C = \frac{\Delta H_2^2}{RT^2} \exp(\Delta F_4/RT) \qquad (8)$$

Equations 6, 7, and 8 were used to correlate the experimental heat capacity data on 2-butanol to give the parameters in Table II and the curves

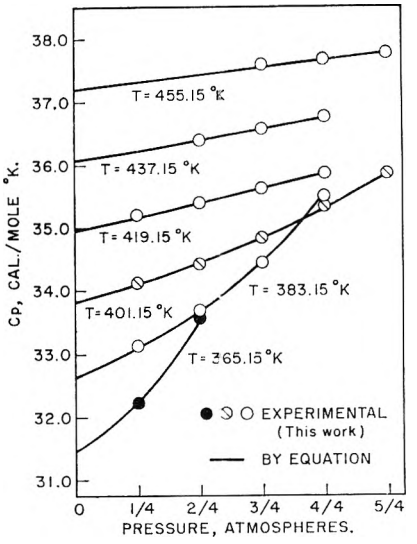


Fig. 1.—Vapor heat capacity of 2-butanol as a function of pressure.

in Fig. 1. The experimental data can be represented within a maximum deviation of ±0.12% by

$$A = \frac{282.0}{T^2} \exp(2625/T) \quad \text{cal./mole atm. °K.} \qquad (9)$$

$$C = \frac{1.266 \times 10^{-8}}{T_2} \exp(11559/T) \quad \text{cal./mole atm.}^3 \text{ °K.} \qquad (10)$$

when

$$C_p^0 = 5.533 + 0.07687T - 1.598 \times 10^{-5}T^2 \qquad (11)$$

From the constants of eq. 9 and 10 the entropies and heats of formation of the dimers and tetramers are

$\Delta S_2$ = 21.4 e.u. $\Delta S_4$ = 74.7 e.u.

$\Delta H_2$ = 5250 cal./mole $\Delta H_4$ = 23118 cal./mole

Deviations from ideal gaseous behavior ($V - RT/p$) were calculated from the Clapeyron equation and the vapor pressure and heats of vaporiza-

(13) J. J. Fox and A. E. Martin, *Trans. Faraday Soc.*, **36**, 897 (1940).

(14) W. Weltner, Jr., and K. S. Pitzer, *J. Am. Chem. Soc.*, **73**, 2606 (1951).

(15) C. B. Kretschmer and R. Wiebe, *ibid.*, **76**, 2579 (1954).

(16) J. L. Gove, Ph.D. Dissertation, Pennsylvania State University, 1957.

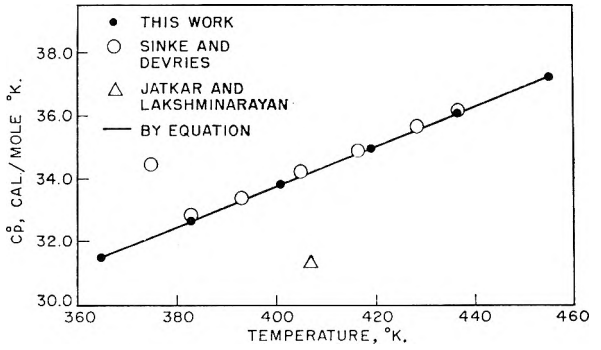


Fig. 2.—Ideal vapor heat capacity of 2-butanol.

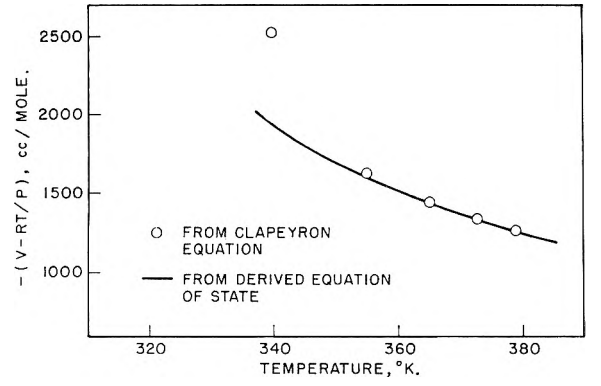


Fig. 3.—Total gas imperfection of 2-butanol for the saturation curve.

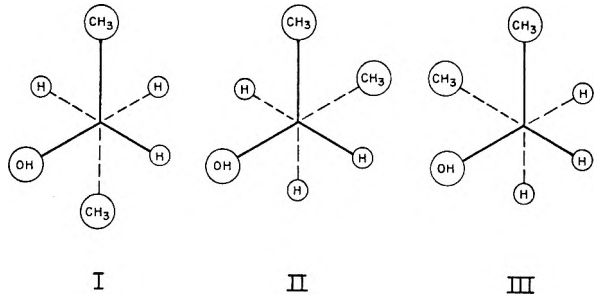


Fig. 4.—The rotational conformations of 2-butanol.

tion found in this work. The results of these calculations are shown in Fig. 3. The smooth curve in this illustration was obtained by setting $b$ equal to 480. Then the parameters $B$ and $D$ in eq. 3 become

$$B = -480 - 1.690 \times 10^{-3} T \exp(2625/T), \text{ cc./mole} \quad (12)$$

$$D = -1.1738 \times 10^{-14} T \exp(11559/T), \text{ cc./mole atm.}^2 \quad (13)$$

The large deviation at the lowest temperature may indicate that $b$ should be some function of temperature. $PVT$ data at low temperatures would be necessary to develop an equation that can be extended outside of the range of this work.

## Calculation of the Thermodynamic Properties of 2-Butanol

The thermodynamic properties in the ideal gaseous state were calculated from molecular data. Preliminary steps in this procedure include calculation of the kinetic energy matrix for rotation and assignment of the normal vibrational frequencies.

**Rotational Constants.**—The 2-butanol molecule $CH_3CH_2C^*HOHCH_3$ has an asymmetric carbon atom (marked with the asterisk) and therefore exists as a $d$ and an $l$-form. Hindered rotation about the C–C* bond results in the three rotational isomers shown in Fig. 4. In this figure the molecules are viewed along the C–C* axis, and it is assumed that these isomers are more stable than the "eclipsed" forms. (That is, the configurations in Fig. 4 correspond to the minima of the potential energy curve as a function of azimuthal angle.)

Bernstein and Pederson[17] have measured the specific rotation of 2-butanol as a function of temperature to determine the equilibrium concentrations of the isomers and the heats of isomerization. Their results in the liquid phase are corrected for association by dilution in a non-polar solvent, and a solvent correction is derived from rotation measurements in different solvents. This treatment yields an approximation for the gaseous state. They also conclude that I and II in Fig. 4 have the lowest energy, each of the same magnitude. McCullough, *et al.*,[18] used a similar assumption in the study of the thermodynamic properties of 2-butanethiol.

The product of the principal moments of inertia and the reduced moments of the rotating tops were calculated for conformation I using the formalized procedure of Kilpatrick and Pitzer.[19] The bond distances and angles in 2-butanol were taken to be the same as those of 1-propanol as used by Mathews.[4] Bond lengths for C–H, C–C, C–O, O–H are 1.09, 1.54, 1.43, and 0.96 Å., respectively. Bond angles are tetrahedral except for C–O–H which was taken as 110°. The kinetic energy matrix $[D]$ for internal rotation becomes

$$[D] = \begin{bmatrix} 3.0369 & 0.0299 & 0.3516 & 0.1567 \\ 0.0299 & 0.7952 & -0.5272 & -0.0299 \\ 0.3516 & -0.5272 & 18.2320 & 0.7124 \\ 0.1567 & -0.0299 & 0.7124 & 3.0369 \end{bmatrix}$$

If the off diagonal elements are neglected, the reduced moments are $5.043 \times 10^{-40}$ g. cm.$^2$ for

TABLE III

SKELETAL BENDING FREQUENCIES OF 2-BUTANOL, CM.$^{-1}$

| Conformation | | | |
|---|---|---|---|
| I | II | III | Obsd.[20] |
| | | 467 | |
| 450 | | 450 | 500 |
| | 435 | | 469 |
| 405 | | 400 | 435 |
| | 395 | | 410 |
| 370 | 370 | | 382 |
| 230 | 250 | | 274 |
| | | 190 | |

(17) H. J. Bernstein and E. E. Pederson, *J. Chem. Phys.*, **17**, 885 (1949).

(18) J. P. McCullough, H. L. Finke, D. W. Scott, R. E. Pennington, M. E. Gross, J. F. Messerly, and G. Waddington, *J. Am. Chem. Soc.*, **80**, 4786 (1958).

(19) J. E. Kilpatrick and K. S. Pitzer, *J. Chem. Phys.*, **17**, 1064 (1949).

TABLE IV

SELECTED SPECTRA AND THE VIBRATIONAL ASSIGNMENT

| Infrared, cm.$^{-1}$ | | | Raman, cm.$^{-1}$ | | | |
|---|---|---|---|---|---|---|
| Vapor[23a] | Liquid in $CCl_4$ and $CS_2$ [24] | Fig. 5[20] | [25b] | [26c] | Fundamental | Conformation I designation |
| 3682w | 3401 | | | | 3682 | O–H stretch |
| 2980s | 2959 | | 2972 (8) | | 2980 (6) | C–H stretches |
| 2943s | 2924 | | 2928 (10) | | 2943 (2) | |
| 2891s | 2865 | | 2874 (7) | | 2891 (1) | |
| | | | | 1537 (0.008) | | |
| 1459m | 1456 | | 1450 (6) | 1445 ( .120) | 1450 (5) | C–H bends |
| 1394m | 1403 | | | | 1394 | COH bend |
| | 1376 | | | | 1380 (2) | C–H bend |
| | | | 1350 (1) | 1357 ( .038) | 1350 | CH wag |
| | 1314 | | | | 1314 | CH wag |
| | 1290 | | 1298 (1) | 1299 ( .028) | 1290 | $CH_2$ twist |
| 1241m | 1250 | | | | 1250 | $CH_2$ wag |
| | | | | 1210 ( .012) | | |
| 1145w | 1147 | | | 1155 ( .026) | 1145 | C–C stretch |
| 1128w | 1116 | | 1108 (3) | 1113 ( .062) | 1110 | $CH_3$ rock |
| 1080m | | | | | 1080 | $CH_3$ rock |
| 1040vw | | | | | | |
| 1026vw | 1031 | | 1030 (2) | 1034 ( .040) | 1034 | C–O stretch |
| 992m | 992 | | 990 (2) | 994 ( .075) | 992 | $CH_3$ rock |
| | 969 | | | | 970 | C–C stretch |
| 920m | 912 | | 909 (3) | 914 ( .043) | 912 | $CH_3$ rock |
| 907m | | | | | | |
| 886w | | | | | | |
| | 820 | | 820 (6) | 823 ( .087) | 820 | C–C stretch |
| | 794 | | | | | |
| | 777 | | 780 (4) | 779 ( .058) | 780 | $CH_2$ rock |
| 722w | | | | 723 ( .011) | | |
| | | 497 | 500 (5) | 501 ( .052) | 500 | CCO bend |
| | | 438 | 437 (1) | 435 ( .028) | 435 | CCO bend |
| | | 386 | 383 (1) | 382 ( .017) | 382 | CCC bend |
| | | 274 | | | 274 | CCC bend |

[a] Relative intensities are indicated by vw = very weak, w = weak, m = medium, and s = strong. [b] Relative intensities are indicated by numbers opposite the frequencies. [c] Absolute intensities are indicated by the scattering coefficients opposite the frequencies.

the $CH_3$ tops, $1.320 \times 10^{-40}$ g. cm.$^2$ for the OH top, and $30.271 \times 10^{-40}$ for the skeletal rotation. The product of the principal moments of inertia is $7910 \times 10^{-117}$ g.$^3$ cm.$^6$.

**Vibrational Assignment.**—Four of the internal degrees of freedom of 2-butanol can be attributed to internal rotations leaving 35 others due to vibrations. As an aid to assigning the skeletal bending frequencies, some infrared data in the range 250–650 cm.$^{-1}$ were obtained from Union Carbide Chemicals Company[20] and an analysis of the skeletons of several simpler alcohols was made using the method described for 2-methylbutane[21] and the tabulations of Wilson, *et al.*[22] Force constants were selected to give agreement with the observed frequencies of ethanol and propane. The results in Table III do not show good agreement with the observed frequencies of 2-butanol; however, they were sufficient to assign the strongest absorptions shown in Fig. 5 to the I conformation.

The vibrational assignments along with selected infrared[20,23,24] and Raman[25,26] data are presented in Table IV. This assignment is only schematic. The C–C stretches were assigned by comparing the results from the approximate normal coördinate analysis. The 820, 970, and 1140 cm.$^{-1}$ lines assigned to 2-butanol appeared in 1-propanol, 971 cm.$^{-1}$, and 2-propanol near 820 and 1140 cm.$^{-1}$. The various carbon–hydrogen motions were as-

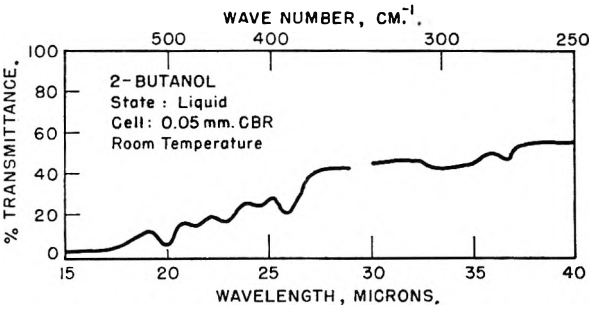


Fig. 5.—The infrared spectra of 2-butanol 39.

(20) Private communication.

(21) D. W. Scott, J. P. McCullough, K. D. Williamson, and G. Waddington, *J. Am. Chem. Soc.*, **73**, 1707 (1951).

(22) E. B. Wilson, Jr., J. C. Decius, and P. C. Cross, "Molecular Vibrations," McGraw–Hill Book Co., Inc., New York, N. Y., 1955.

(23) J. R. Quinan and S. E. Wiberley, *Anal. Chem.*, **26**, 1762 (1954).

(24) A.P.I. Research Project 44, Catalog of Infrared Spectral Data, Serial Numbers 431 and 750.

(25) K. W. F. Kohlrausch, "Ramanspektren," Akademische Verlagesellschaft Becker und Erler, Kom.-Ges., Leipzig, 1943.

(26) W. Braun, D. Spooner, and M. Fenske, *Anal. Chem.*, **22**, 1074 (1950).

TABLE V

THERMODYNAMIC PROPERTIES IN THE IDEAL GASEOUS STATE[a]

| Temp., °K. | $C_p^0$, cal./mole, °K. | $S^0$, cal./mole, °K. | $(H_T^0 - H_0^0)/T$, cal./mole, °K. | $-(F_T^0 - H_0^0)/T$, cal./mole, °K. | $-\Delta H_f^0$, kcal./mole | $\Delta F_f^0$, kcal./mole | log $K_f^0$ |
|---|---|---|---|---|---|---|---|
| 0 | 0 | 0 | 0 | 0 | 62.86 | −62.86 | Infinite |
| 273.15 | 24.46 | 83.66 | 16.57 | 67.03 | 69.35 | −48.93 | 39.19 |
| 298.15 | 27.08 | 85.81 | 17.39 | 68.42 | 69.84 | −46.94 | 34.46 |
| 300.00 | 27.20 | 85.98 | 17.44 | 68.53 | 69.87 | −46.79 | 34.14 |
| 400 | 33.70 | 94.78 | 20.71 | 74.07 | 71.64 | −38.29 | 20.96 |
| 500 | 39.70 | 103.01 | 23.92 | 79.09 | 73.09 | −28.98 | 12.69 |
| 600 | 44.72 | 110.74 | 26.97 | 83.76 | 74.25 | −19.26 | 7.04 |
| 700 | 49.02 | 117.99 | 29.82 | 88.17 | 75.16 | − 9.06 | 2 84 |
| 800 | 52.68 | 124.80 | 32.46 | 92.34 | 75.83 | 1.50 | −0.40 |
| 900 | 55.88 | 131.20 | 34.90 | 96.33 | 76.30 | 12.33 | −2.99 |
| 1000 | 58.62 | 137.26 | 37.14 | 100.14 | 76.60 | 23.39 | −5.11 |

[a] To retain internal consistency some of the values in this table are given to more decimal places than are justified by their absolute accuracy.

signed with the aid of the work on 2-butanethiol by McCullough.[18] Although the heat capacities calculated with this vibrational assignment are in agreement with experiment, much controversy exists on the vibrational modes. Mathews[4] summarizes some of the discussion on the O–H bend and the C–O stretch, and his conclusions are used in this work. A recent analysis of the infrared spectra of methanol by Falk and Whalley[27] also places the O–H bend in the 1300–1400 cm.$^{-1}$ region.

**Internal Rotation.**—Internal rotational contributions to the thermodynamic properties come from the two methyl rotations, the hydroxyl rotation, and the rotation about the central C–C bond. Simple threefold cosine type barriers to internal rotation were assumed for the methyl and hydroxyl groups. Values of barrier heights selected were 3100 and 4000 cal./mole for the methyl rotations as in 2-butanethiol,[18] and 800 cal./mole for the hydroxyl rotation as in other alcohols.[4,28]

The contributions from the rotation about the central bond were calculated as those for a simple threefold barrier of height 2150 cal./mole plus the contribution due to "conversion" of molecules from the I and II conformations to the III form. The latter values were obtained from a consideration of the equilibrium between isomers[29] using Bernstein and Pederson's[17] equation for the equilibrium constant representing the conversion of I to III or II to III

$$K = 1.43 \exp(-803/RT) \qquad (14)$$

The restricted rotor contributions to the thermodynamic properties were taken from the tables of Pitzer and Gwinn[30] and the extension of these tables by Li and Pitzer.[31] The barrier height 2150 cal./mole was selected to give the best fit to the experimental heat capacity data. Table II presents a comparison between the calculated and experimental heat capacities. The maximum deviation is 0.22% and the average deviation 0.09%.

**Thermodynamic Functions.**—The vibrational assignment, product of principal moments of inertia, reduced moments of inertia of internal rotating groups, barriers to internal rotation, and the equilibrium between rotational isomers discussed above were used to compute the values of the thermodynamic functions of 2-butanol at selected temperatures between 0 and 1000° K., and are presented in Table V.

The standard heat, standard free energy, and common logarithm of the equilibrium constant for the formation of 2-butanol from the elements also are tabulated.

$$4C(\text{graphite}) + 5H_2(g) + {}^1/_2O_2(g) = 2\text{-}C_4H_9OH(g) \qquad (15)$$

The value of the heat of combustion of 2-butanol reported by Skinner and Snelson[32] (635.91 ± 0.22 kcal./mole) and the values of the heats of formation of water and carbon dioxide[33] were used to compute the heat of formation of 2-butanol at 298.15°K. Table V, the heat of formation at 298.15°K., and the thermodynamic functions of hydrogen, carbon, and oxygen[33] were used to compute the remainder of the table.

(27) M. Falk and E. Whalley, *J. Chem. Phys.*, **34**, 1554 (1961).
(28) G. M. Barrow, *ibid.*, **20**, 1739 (1952).
(29) K. S. Pitzer, *ibid.*, **5**, 473 (1937).
(30) K. S. Pitzer and W. D. Gwinn, *ibid.*, **10**, 428 (1942).
(31) J. C. Li and K. S. Pitzer, *J. Phys. Chem.*, **60**, 466 (1956).
(32) H. A. Skinner and A. Snelson, *Trans. Faraday Soc.*, **56**, 1776 (1960).
(33) D. D. Wagman, J. E. Kilpatrick, W. S. Taylor, K. S. Pitzer and F. D. Rossini, *J. Res. Natl. Bur. Std.*, **34**, 143 (1945).

# THE DIPOLE MOMENT AND MAGNETIC SUSCEPTIBILITY OF DECABORANE[1]

BY RUDOLPH S. BOTTEI AND A. W. LAUBENGAYER

*Department of Chemistry, Cornell University, Ithaca, New York*

*Received February 21, 1962*

The dipole moment of decaborane has been determined by measuring the dielectric constants of benzene, cyclohexane, and carbon disulfide solutions. The data have been treated by the Debye method and by the method proposed by Guggenheim. The dipole moment varies from 3.17 in carbon disulfide to 3.62 in benzene. The magnetic suspectibility of decaborane has been determined by the Gouy method. Decaborane is diamagnetic; its gram molar susceptibility is $-116 \pm 1.5 \times 10^{-6}$.

## Introduction

In a previous communication,[2] we reported the dipole moment of decaborane, $B_{10}H_{14}$, as determined from measurements of the dielectric constants of benzene solutions and calculated by the Debye method. In this paper, additional data for benzene solutions are reported, as well as data for cyclohexane and carbon disulfide solutions. The dipole moment has been calculated by the Debye method and by the method proposed by Guggenheim.[3] The magnetic susceptibility of $B_{10}H_{14}$ as determined by the Gouy method also is reported.

## Experimental

**Purification of Solvents.**—Benzene, Baker C.P., was dried with sodium, distilled, and fractionally crystallized four times, each time freezing out about two-thirds of the benzene and pouring off the remainder. It then was fractionally distilled over sodium through a 1-m. Schneider column. The middle fraction was redistilled and a new fraction that boiled at 79.5–79.8° (uncorrected) was collected. The purified benzene was stored over sodium for a week before it was used ($d^{25}$ 0.87360, lit. 0.87360[4] and 0.87366[5]; $n^{25}D$ 1.4980, lit. 1.4981[6]).

Cyclohexane, Matheson C.P., was treated in the same way as benzene. The final fraction collected had a boiling point of 79.8–80.1° (uncorrected). The purified cyclohexane was stored over sodium ($d^{25}$ 0.77385, lit. 0.77383[7] and 0.77389[8]; $n^{25}D$ 1.4236, lit. 1.42354[8]).

Carbon disulfide, Baker and Adamson C.P., was purified by two methods. One method[9] involved extensive treatments with potassium permanganate solution, mercury, and mercury(II) sulfate solution, followed by distillation in a nitrogen atmosphere. The carbon disulfide obtained was unsatisfactory. When decarborane was added to it, the decaborane was dispersed and a very cloudy liquid was produced. Carbon disulfide then was purified by first distilling over ceresin wax.[10] A middle fraction was distilled over phosphorus pentoxide in a nitrogen atmosphere. The purified material was stored in a brown bottle over phosphorus pentoxide and kept in the dark. Its purity was checked by determination of its critical solution temperature (c.s.t.) in methyl alcohol; 80.24% $CS_2$ c.s.t. 35.45°, lit. 35.4°,[10,11] 85.32% $CS_2$, c.s.t. 35.56°, lit. 35.6°.[10,11]

Methyl alcohol, Baker and Adamson C.P., was dried with magnesium and distilled over sulfanilic acid[12] ($d^{25}$ 0.7865, lit. 0.7866[13]).

**Purification of Decaborane.**—Decaborane was purified by sublimation under high vacuum at room temperature, m.p. 99.6–99.7°, lit. 99.6–99.7.[14]

**Preparation of Solutions.**—The solvents were distilled under high vacuum at room temperature from a suitable drying agent into weighed flasks. The flasks containing solvent were stored in a desiccator and reweighed just prior to the preparation of solutions.

The sublimator, containing purified decaborane under high vacuum, was opened in a drybox through which dry nitrogen had been passed for at least 1 hr. The drybox was equipped with a glass bulb through which liquid nitrogen was passed to condense the last traces of moisture before opening the sublimator.

Decaborane was put into weighed screw-cap vials which were removed from the drybox and reweighed. After the vials were returned to the drybox, dry nitrogen again was passed through it for about 45 min. The last traces of moisture were removed as previously described. The caps then were removed from the vials and the vials slipped into flasks containing weighed solvent. The flasks were well shaken to ensure that all of the decaborane had dissolved and the solutions were homogeneous. The solutions were transferred to the dielectric cell using a special siphoning apparatus so that there was very little exposure to air during the transfer.

**Measurements.**—The dielectric constants of the solutions were measured at 25.0 ± 0.02°, using a heterodyne beat oscillator operated at a frequency of 1.57 Mc. The dielectric constants at 25° of the solvents used were taken to be: benzene, 2.2750,[15] cyclohexane, 2.015,[16] and carbon disulfide, 2.634.[17]

Refractive indices for the sodium-D line were measured at 25 ± 0.10° with an Abbe refractometer (Bausch and Lomb).

Densities of solutions were determined after the dielectric constants of the solutions had been measured. Measurements were made using standard Ostwald–Sprengel pycnometers which were calibrated at 25° with pure standard water.[18] The pycnometers were thermostated for about 15 hr. in a well stirred water bath regulated at 25 ± 0.002°. To standardize the effect of the adsorption of moisture, the pycnometers were wiped with a moist chamois and remained in the balance case for 20 min. before each weighing. A tare was treated in the same way. After the initial weighing, the weight was rechecked after 10 min. more to ensure that thermal equilibrium had been attained. Weights calibrated

(1) Taken in part from a thesis submitted by R. S. B. in partial fulfillment of the requirements for the M.S., September, 1952, Cornell University.

(2) A. W. Laubengayer and R. Bottei, *J. Am. Chem. Soc.*, **74**, 1618 (1952).

(3) E. A. Guggenheim, *Trans. Faraday Soc.*, **47**, 573 (1951).

(4) A. L. Olsen and E. R. Washburn, *J. Am. Chem. Soc.*, **57**, 303 (1935).

(5) D. R. Simonsen and E. R. Washburn, *ibid.*, **68**, 235 (1946).

(6) A. V. Few and J. W. Smith, *J. Chem. Soc.*, 753 (1949).

(7) G. Scatchard, S. E. Wood, and J. M. Mochel, *J. Am. Chem. Soc.*, **61**, 3206 (1939).

(8) A. F. Forziati, A. R. Glasgow, Jr., C. B. Willingham, and F. D. Rossini, *J. Res. Natl. Bur. Std.*, **36**, 129 (1946).

(9) D. L. Hammick and J. Howard, *J. Chem. Soc.*, 2915 (1932).

(10) E. C. McKelvey and D. H. Simpson, *J. Am. Chem. Soc.*, **44**, 108 (1922).

(11) Interpolated values.

(12) W. Herold and K. L. Wolf, *Z. physik. Chem.*, **12B**, 182 (1931).

(13) H. T. Briscoe and W. T. Finehart, *J. Phys. Chem.*, **46**, 387 (1952).

(14) A. Stock, "Hydrides of Boron and Silicon," Cornell University Press, Ithaca, N. Y., 1933.

(15) A. S. Brown, P. M. Levin, and E. W. Abrahamson, *J. Chem. Phys.*, **19**, 1226 (1951).

(16) M. A. Govinda Rau and B. N. Narayanaswamy, *Proc. Indian Acad. Sci.*, **1**, 14 (1934).

(17) M. G. Malone and A. L. Ferguson, *J. Chem. Phys.*, **2**, 99 (1934).

(18) A. Weissberger, "Physical Methods of Organic Chemistry," Vol. I, Interscience Publishers, Inc., New York, N. Y., 1945, p. 256.

according to the method of Richards were used. For each weighing, the pressure, temperature of the balance case, and the humidity were recorded. Densities were calculated as shown in Weissberger, page 275. No vapor correction was necessary because the gas space above the liquid in the capillary arms of the pycnometers was kept free of vapor by making them long and narrow. A correction was made for the buoyancy effect of air. The densities were reproducible to $\pm 1 \times 10^{-5}$.

The magnetic susceptibility was determined by the Gouy method, using a solution of $NiCl_2$ whose volume susceptibility was $6.208 \times 10^{-6}$ as a standard. The apparatus and method of measurement have been described by Conroy and Sienko.[19] The sample of decaborane was packed in the same precision bore Pyrex tube that was used in the calibration. The packing was done in a drybox through which dry nitrogen was passed for 1 hr. The tube was sealed with a Lucite cap to protect the sample from moisture. The height of the same was measured with a cathetometer. The change of weight of the sample with changes in field strength was determined at the same temperature at which the calibration was made. The usual precautions were taken to ensure thermal equilibrium was attained and that a dry nitrogen atmosphere surrounded the sample throughout the measurements. Two sets of measurements were made on the same sample.

**Calculations.**—Polarizations at infinite dilution, ${}_0P_2$, were calculated by the Debye method and by the Guggenheim method.[3]

In the Debye method, ${}_0P_2$ was corrected for electronic polarization, $P_E$, and atomic polarization, $P_A$. The sum of $P_E$ and $P_A$ was assumed to be 1.15 times $MR_D$, the molar refraction for the D-sodium line, which for $B_{10}H_{14}$ was 46 ± 1. The dipole moment was calculated by the usual equation

$$\mu = 0.0128 \times 10^{-18} [({}_0P_2 - 1.15MR_D)T]^{1/2}$$

where $T$ is the absolute temperature.

In the Guggenheim method,[20] the data $\epsilon - \epsilon_1/W$, where $\epsilon$ is the dielectric constant of solution, $\epsilon_1$, that of the solvent, and $W$ is the weight fraction of the solute, were plotted against $W$ and the best value of $[(\epsilon - \epsilon_1)/W]_{w\to 0}$ was estimated. Likewise, the best value of $[(n^2 - n_1^2)/W]_{w\to 0}$, where $n$ is the refractive index of the solution and $n_1$ that of the solvent, was estimated. The value of $[(n^2 - n_1^2)/W]_{w\to 0}$ was subtracted from $[(\epsilon - \epsilon_1)/W]_{w\to 0}$ to obtain $(\Delta/W)_{w\to 0}$, where $\Delta$ is equal to $[(\epsilon - \epsilon_1) - (n^2 - n_1^2)]$. Polarizations at infinite dilution were calculated using the equation

$${}_0P_2 = \frac{3}{(E+2)^2}\frac{M_2}{d_1}\left(\frac{\Delta}{W}\right)_{W\to 0}$$

here $M_2$ is the molecular weight of the solute and $d_1$ is the density of the solvent. Polarizations at infinite dilution were corrected for atomic polarization (0.15 $P_E$) and the dipole moment was calculated in the usual manner.

TABLE I

MOLE FRACTIONS AND MOLAR POLARIZATIONS OF $B_{10}H_{14}$—DEBYE METHOD

| Mole fraction | Molar polarization |
|---|---|
| In benzene | |
| $0.0071345$ | 307.4 |
| $.0073878$ | 306.2 |
| $.0078698$ | 304.3 |
| $.014133$ | 297.5 |
| $.017660$ | 293.3 |
| $.018691$ | 290.4 |
| | ${}_0P_2 = 315.3$ |
| In cyclohexane | |
| $0.0037279$ | 291.0 |
| $.0093958$ | 287.7 |
| $.0094486$ | 286.3 |
| $.011287$ | 286.6 |
| $.014205$ | 287.9 |
| $.021043$ | 291.1 |
| | ${}_0P_2 = 288.0$ |
| In carbon disulfide | |
| $0.0024542$ | 256.9 |
| $.0048692$ | 262.9 |
| $.0085013$ | 259.6 |
| $.0095470$ | 262.8 |
| $.010818$ | 257.5 |
| | ${}_0P_2 = 259.0$ |

## Results

The molar polarizations of $B_{10}H_{14}$ as determined by the Debye method are listed in Table I. In Table II are listed the data for the calculation of the dipole moment by the Guggenheim method. The dipole moments of $B_{10}H_{14}$ are listed in Table III.

Decaborane is diamagnetic; the gram molar susceptibility is $-116 \pm 1.5 \times 10^{-6}$.

TABLE II

EXPERIMENTAL DATA AND CALCULATED MOLAR POLARIZATION OF $B_{10}H_{14}$—GUGGENHEIM METHOD

| $W$ | $\epsilon$ | $\frac{\epsilon - \epsilon_1}{W}$ | $n$ | $\frac{n^2 - n_1^2}{W}$ |
|---|---|---|---|---|
| In benzene | | | | |
| 0 | 2.2750 | | 1.4980 | |
| $0.011127$ | $2.40736$ | 11.899 | 1.4989 | 0.242 |
| $.011520$ | $2.41223$ | 11.910 | 1.4989 | .234 |
| $.012268$ | $2.42222$ | 12.011 | 1.4990 | .245 |
| $.021662$ | $2.53054$ | 11.795 | 1.4998 | .249 |
| $.021954$ | $2.53819$ | 11.887 | 1.4998 | .240 |
| $.027533$ | $2.60466$ | 11.701 | 1.5002 | .240 |
| $.028964$ | $2.61931$ | 11.987 | 1.5503 | .238 |
| $\left(\frac{\epsilon - \epsilon_1}{W}\right)_{W\to 0} = 12.12$ | | | $\left(\frac{n^2 - n_1^2}{W}\right)_{W\to 0} = 0.24$ | |
| | | | ${}_0P_2 = 272.7$ | |
| In cyclohexane | | | | |
| 0 | 2.015 | | 1.4236 | |
| $0.0054087$ | $2.0605$ | 8.412 | .... | ... |
| $.013597$ | $2.1354$ | 8.856 | 1.4254 | 0.382 |
| $.013673$ | $2.1354$ | 9.806 | 1.4255 | .397 |
| $.016319$ | $2.1596$ | 8.860 | 1.4258 | .380 |
| $.020512$ | $2.1995$ | 8.994 | 1.4264 | .390 |
| $.030223$ | $2.2962$ | 9.304 | 1.4274 | .397 |
| $\left(\frac{\epsilon - \epsilon_1}{W}\right)_{W\to 0} = 8.33$ | | | $\left(\frac{n^2 - n_1^2}{W}\right)_{W\to 0} = 0.39$ | |
| | | | ${}_0P_2 = 233.2$ | |
| In carbon disulfide | | | | |
| 0 | 2.634 | | 1.6235 | |
| $0.0039371$ | $2.6975$ | 16.133 | 1.6231 | −0.432 |
| $.0077999$ | $2.7556$ | 15.595 | 1.6226 | − .385 |
| $.013588$ | $2.8503$ | 15.519 | 1.6221 | − .338 |
| $.015250$ | $2.8786$ | 16.041 | 1.6219 | − .341 |
| $.017266$ | $2.9117$ | 16.085 | 1.6217 | − .349 |
| $\left(\frac{\epsilon - \epsilon_1}{W}\right)_{W\to 0} = 16.12$ | | | $\left(\frac{n^2 - n_1^2}{W}\right)_{W\to 0} = -0.45$ | |
| | | | ${}_0P_2 = 225.0$ | |

(19) L. E. Conroy and M. J. Sienko, *J. Am. Chem. Soc.*, **74**, 3250 (1952).

(20) This method is most advantageous since densities need not be determined.

TABLE III

DIPOLE MOMENTS OF $B_{10}H_{14}$

| Solvent | Debye method | Guggenheim method |
|---|---|---|
| Cyclohexane | 3.39 ± 0.02 D. | 3.36 ± 0.02 D. |
| Benzene | 3.62 ± .02 D. | 3.61 ± .03 D. |
| Carbon disulfide | 3.17 ± .03 D. | 3.26 ± .04 D. |

## Discussion

The dipole moments as calculated by both methods are in rather good agreement. There is no correlation between the dipole moment and the dielectric constant of the solvent in which the dipole moment was measured. It was, therefore, not possible, as originally planned, to use the equation proposed by Smyth[21] for the ratio of the dipole moment in solution to that of the gas. The high value of the dipole moment has been rationalized by molecular orbital treatment[22] of boron hydride structures using a three-center-bond approximation.

Although it has been reported that $B_{10}H_{14}$ is quite stable to oxidation and hydrolysis by moist air at room temperature, preliminary experiments showed that even short exposure to moist air led to variable results. Molar polarizations were always greater for solutions prepared using $B_{10}H_{14}$ which had been exposed to moist air than for those prepared as described in the Experimental part of this paper. The longer the exposure, the greater was the molar polarization. The extent of reaction, however, was very small, because if $B_{10}H_{14}$ which had been exposed to moist air for a short time was sublimed, the amount of nonsublimable residue from a charge of about 2 g. was barely enough for a melting point determination. The amount of residue increased with increased exposure, but it was never very much. The residue was orthoboric acid as determined from its melting point, microscopical observation, and X-ray powder pattern. The increased polarity probably is due to a rather rapid surface reaction which introduces the very polar OH group into the $B_{10}H_{14}$ molecule.

If the diamagnetic atomic susceptibility of boron is taken to be $-6.7 \times 10^{-6}$ [23] and that of hydrogen as $-2.93 \times 10^{-6}$,[24] the calculated gram molar susceptibility is $-108 \times 10^{-6}$. The difference between the experimental and calculated values probably is due to the value that has been assumed for hydrogen. The value used is for a singly-bonded hydrogen and probably will not hold for the four bridge-bonded hydrogens. The calculated value would be in closer agreement with the experimental value if a constitutive correction for this bonding were available.

(21) W. P. Conner, R. P. Clarke, and C. P. Smyth, *J. Am. Chem. Soc.*, **64**, 1379 (1942).

(22) W. B. Eberhardt, B. Crawford, Jr., and W. N. Lipscomb, *J. Chem. Phys.*, **22**, 989 (1954).

(23) L. Klemm, *Z. Elektrochem.*, **45**, 434 (1939).

(24) P. W. Selwood, "Magnetochemistry," Interscience Publishers, Inc., New York, N. Y., 1943, p. 52.

# AN INFRARED STUDY OF THE CHEMISORPTION OF ETHYLENE ON ALUMINUM OXIDE

BY P. J. LUCCHESI, J. L. CARTER, AND D. J. C. YATES

*Esso Research and Engineering Company, Linden, New Jersey*

*Received March 1, 1962*

An infrared study of the adsorption of ethylene on aluminum oxide shows several interesting features about the nature, orientation, and reactivity of the adsorbed species. On some oxides, room temperature adsorption leads to the slow formation of ethyl groups $S-CH_2CH_3$ (S is a surface site). The formation of $C_2H_5$ involves self-hydrogenation, as the oxide contributes no hydrogen. The surface species reacts with hydrogen at 450° to give $CH_4$, $C_2H_6$, and $C_3H_8$ in the gas phase. In contrast, on another crystallographically similar oxide, ethylene adsorption leads to the formation of $S-CH_2CH_2-S$. This species reacts with hydrogen at 450° to yield first $S-CH_2CH_3$ and then gaseous $C_2H_6$. The results are discussed in terms of their significance in the general problem of elucidating the nature of the chemisorption and catalytic hydrogenation of ethylene on aluminum oxides. No chemisorption of ethylene was found to occur on silica at room temperature.

## Introduction

The advent of the infrared method for studying the adsorption of gases on solids has provided a new tool for probing the details of catalysis. This method can give direct information about the nature and orientation of the adsorbed species. A fairly substantial literature has developed on this subject, and has been reviewed recently.[1,2]

One of the catalytic reactions that has been studied in some detail is the hydrogenation of ethylene. A central problem has been the elucidation of the details of ethylene chemisorption on various surfaces. Data on nickel films[3,4] showed that some form of dissociative acetylenic complex was formed. The following reactions could have occurred

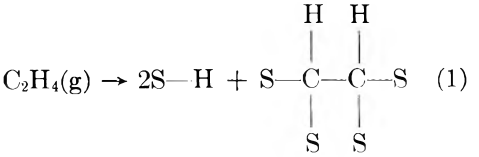

$$C_2H_4(g) \rightarrow 2S{-}H + S{-}\underset{\displaystyle S}{\overset{\displaystyle H}{C}}{-}\underset{\displaystyle S}{\overset{\displaystyle H}{C}}{-}S \quad (1)$$

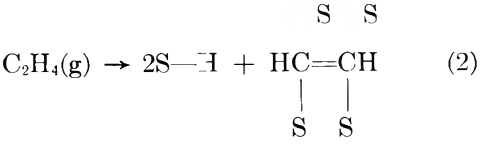

$$C_2H_4(g) \rightarrow 2S{-}H + HC{=}CH \quad (2)$$

where the symbol S denotes a surface site, and S–C a surface to carbon bond. No choice could be

(1) R. P. Eischens and W. A. Pliskin, *Advan. Catalysis*, **10**, 2 (1958).

(2) V. Crawford, *Quart. Rev.* (London), **14**, 378 (1960).

(3) O. Beeck, *Discussions Faraday Soc.*, **8**, 118 (1950).

(4) G. I. Jenkins and E. K. Rideal, *J. Chem. Soc.*, 2490 (1955).

made between eq. 1 and 2 from the classical adsorption studies. The chemisorbed hydrogen, S–H, then was thought to react with gas phase $C_2H_4$, to give[3,4] chemisorbed ethyl groups S–$CH_2CH_3$. This is part of the so-called "self-hydrogenation" of ethylene, a reaction that has received considerable attention. On evaporated palladium films,[5] ethylene was observed to self-hydrogenate to ethane, by a path which was postulated to involve the formation of acetylenic residues, S–H, and subsequent reactions between this hydrogen and adsorbed ethylene. Similar self-hydrogenation has been found for several other metals. Some evidence has been presented[4] that associative adsorption can occur

$$C_2H_4(g) \rightarrow \begin{matrix} H_2C & -- & CH_2 \\ | & & | \\ S & & S \end{matrix} \qquad (3)$$

The associative species can be clearly differentiated from the dissociative species by their infrared spectra. Using nickel supported on silica, Eischens and Pliskin[1,6] showed that, on hydrogen-covered nickel, the chemisorbed ethylene is mostly in the associative form. On hydrogen-free nickel, dissociative adsorption occurred. The spectra indicated that the carbons in the acetylenic complex were saturated, as in eq. 1. Adsorbed ethyl groups also were found from the self-hydrogenation of the ethylene. Similar self-hydrogenation of $C_2H_4$ also has been reported[7] on evaporated rhodium films.

We have been interested in the nature of chemisorption of hydrocarbons by oxides, such as alumina, as these surfaces are important in many catalytic processes. For example, the chemisorption of ethylene on alumina seems not to have been studied in detail, and yet it represents a system of great interest. The reactions of hydrocarbons catalyzed by the so-called "acidic" oxides generally are rationalized by theories concerning the properties of carbonium ions. Since such species are not normally involved in discussing the elementary reactions of hydrocarbons on metals, a comparison between oxides and metals for simple adsorbents is of interest. Infrared studies have shown that ethylene is chemisorbed at room temperature on alumina. On some aluminas, ethyl groups are formed, and on others, associative adsorption occurs. The rate of formation of these groups is quite slow, making their detection by conventional methods difficult. Spectroscopic identification of the surface species formed has been supplemented by analysis of the product formed after hydrogenation, and by the changes this hydrogenation produced in the adsorbed species.

## Experimental

**Materials.**—Two sources of alumina were used. Most of the work was done with one prepared by heating a $\beta$-trihydrate for 4 hr. at 600°. The trihydrate was prepared from aluminum alcoholate. This alumina gave an $\eta$-alumina X-ray diffraction pattern[8] and had a BET surface area of 295 m.²/g. The impurities were Fe, Si, Mg, Cu, and Ca, and in all cases their concentrations were less than 0.1%. This oxide is referred to in the text as (A)$Al_2O_3$.

Another alumina also was made from a $\beta$-trihydrate. This was prepared by reacting aluminum with aqueous HCl to form $AlCl_3$, then precipitating the product with $NH_3$. After heating for 4 hr. at 600°, this material gave an X-ray diffraction pattern characteristic of $\eta$-alumina, and had a surface area of 190 m.²/g. The impurities B, Fe, Si, Mg, Cu, and Ca were present in concentrations less than 0.1%. This alumina is referred to as (B)$Al_2O_3$.

The silica used was Cabosil HS5 and was supplied by the Cabot Company, Boston. The surface area was 340 m.²/g. and was prepared by the high temperature hydrolysis of silicon tetrachloride.

The ethylene was supplied by the Matheson Co. and was stated to be 99.5% pure. Deuterioethylene ($C_2D_4$) was supplied by the Volk Radiochemical Co., Chicago, and was found to be 99.7% pure. Deuterium was obtained from the General Dynamics Corp. of San Carlos, California, and was found to be 99.5% pure. It was dried by passing it through a liquid nitrogen trap.

**Sample Preparation.**—The first step consisted of grinding the alumina in an agate mortar to a very fine powder, which reduces losses due to light scattering. The powder then was pressed[9] into a thin flake by pressing the powder in a 2.5-cm. die at 15,000 lb./in.². A portion of the resulting flake, about 2.0 × 0.7 cm. in size, was used for the experiments. The "thickness" of the flakes used was about 0.02–0.03 g./cm.².

**Apparatus.**—The cell was a dual cell, one end having barium fluoride windows, 2 cm. apart, attached with Glyptal cement to a Pyrex tube. For experiments in the 1000–650 cm.$^{-1}$ region, sodium chloride windows were used. The other end of the cell was made of fused silica, joined with a silica-to-Pyrex seal. The cell could be rotated on a greased cone joint to slide the sample from the silica end, after treatments at high temperatures, to the window end. The window end could be removed, for inserting samples, by means of a waxed cone joint. Before the wide tube was sealed on, a slot 5 mm. wide was cut in the end of the main tube to permit infrared radiation to pass through the cell. The volume of the cell to its stopcock was 32.3 cm.³, and the volume of manometer and connecting tube was 106.6 cm.³.

The vacuum system consisted of a mechanical backing pump, a metal oil-diffusion pump, and a trap cooled with solid carbon dioxide. Dynamic vacuums of about $10^{-7}$ mm. were recorded by the Veeco (Alpert type) ionization gage.

A Beckman IR-7 double-beam grating spectrometer was used, with two mirror systems providing two external foci. The cell was placed at one of these, and wire gauzes were put in the other beam to balance the energy in the two beams. The alumina transmitted about 30% of the incident radiation from 1000–2000 cm.$^{-1}$, decreasing at higher wave numbers quite markedly. At 4000 cm.$^{-1}$, about 10% was transmitted. Wider slits than normal were used to compensate for these losses. The slit widths (in mm.) and resolution (in cm.$^{-1}$) used in the main regions of interest are given in Table I. Schedule A refers to that used for the silica samples and B that used for the alumina samples.

**Procedure.**—After insertion in the cell the sample was evacuated and heated slowly to 600°, evacuation being continued until the pressure was $5 \times 10^{-6}$ mm. The sample then was cooled to room temperature and the background spectrum recorded. The ethylene then was admitted to the cell and the spectrum recorded. The spectrum again was recorded at various intervals up to 8 days. At certain times the ethylene was removed by evacuation at room temperature and the spectrum of the adsorbed species recorded. Details of the deuteration procedure have been given elsewhere.[9]

## Results and Interpretation

**Adsorption on (A)$Al_2O_3$.**—After adding ethylene at room temperature to a sample of (A)$Al_2O_3$, the system was allowed to stand for 1 hr. The spec-

(5) S. J. Stephens, *J. Phys. Chem.*, **62**, 714 (1958).

(6) W. A. Pliskin and R. P. Eischens, *J. Chem. Phys.*, **24**, 482 (1956).

(7) H. L. Pickering and H. C. Eckstrom, *J. Phys. Chem.*, **63**, 512 (1959).

(8) J. W. Newsome, H. W. Heiser, A. S. Russell, and H. C. Stumpf, "Alumina Properties," The Aluminum Company of America, Pittsburgh, Pa., 1960.

(9) D. J. C. Yates and P. J. Lucchesi, *J. Chem. Phys.*, **35**, 243 (1961).

TABLE I

SLIT PROGRAM

| Frequency (cm.$^{-1}$) | A Slit width (mm.) | A Resolution (cm.$^{-1}$) | B Slit width (mm.) | B Resolution (cm.$^{-1}$) |
|---|---|---|---|---|
| 1250 | 0.80 | 1.2 | 1.78 | 2.7 |
| 1300 | .65 | 1.1 | 1.45 | 2.5 |
| 1350 | .54 | 1.0 | 1.20 | 2.2 |
| 1400 | .51 | 1.0 | 1.15 | 2.3 |
| 1450 | .48 | 1.0 | 1.08 | 2.4 |
| 1500 | .46 | 1.1 | 1.02 | 2.4 |
| 2800 | 1.00 | 4.2 | 2.00 | 8.4 |
| 2900 | 0.80 | 3.3 | 1.55 | 7.0 |
| 3000 | .63 | 3.1 | 1.25 | 6.2 |
| 3100 | .55 | 2.9 | 1.07 | 5.8 |
| 3200 | .47 | 2.7 | 0.91 | 5.4 |
| 3300 | .41 | 2.5 | 0.78 | 5.0 |
| 3400 | .41 | 2.6 | 0.78 | 5.2 |
| 3500 | .40 | 2.8 | 0.78 | 5.6 |
| 3600 | .40 | 2.9 | 0.78 | 5.8 |
| 3700 | .45 | 3.5 | 0.86 | 7.0 |
| 3800 | .53 | 4.4 | 1.10 | 9.1 |
| 3900 | .62 | 5.5 | 1.20 | 11.0 |
| 4000 | .73 | 6.7 | 1.40 | 13.4 |

trum then was run, and no bands could be seen other than those due to the gaseous $C_2H_4$ in the cell. After standing for 24 hr., bands due to adsorbed molecules were found (Fig. 1) at 2970, 2932, 2880, 1465, and 1383 cm.$^{-1}$. These bands were not affected by evacuating the $C_2H_4$ from the system at room temperature. No bands were observed that were attributable to C≡C or C=C bonds, or to acetylenic or vinyl CH bonds. The possible presence of CH bonds in structures containing only one hydrogen on each carbon could not be verified, as this absorption frequency is overlapped by the observed bands. Table II gives suggested assignments of the observed bands which seem reasonable based on published correlations.[10] The symmetrical $CH_2$ stretching vibration, normally observed in bulk materials[10] at 2853 cm.$^{-1}$, was observed only as a shoulder of the 2880 cm.$^{-1}$ band. From this, it is likely that the adsorbed species is an alkane derivative structure $S–(CH_2)_nCH_3$, where S denotes a surface site. Certainly the value of $n$ is not 4 or more, as no band was found near 720 cm.$^{-1}$ in the spectrum of the adsorbed species. A strong band in this region has been found in all hydrocarbon chains containing 4 or more directly linked $CH_2$ groups.[10]

TABLE II

| Vibration | Frequency range (in cm.$^{-1}$) found in satd. bulk hydrocarbons[10] | Frequency (in cm.$^{-1}$) of bands of adsorbed $C_2H_4$ |
|---|---|---|
| Asymm. CH stretch in $CH_3$ | 2962 ± 10 | 2970 |
| Asymm. CH stretch in $CH_2$ | 2926 ± 10 | 2932 |
| Symm. CH stretch in $CH_3$ | 2872 ± 10 | 2880 |
| Asymm. CH bending in $CH_3$ | 1450 ± 20 | 1465 |
| CH bending in $CH_2$ | 1465 ± 20 | |
| Symm. CH bending in $CH_3$ | 1375 ± 5 | 1383 |

Two methods have been used to determine the number of $CH_2$ groups per $CH_3$ group. This can be done spectroscopically by the ratio of the absorbances (log 1/transmission) of the bands at 2970 cm.$^{-1}$ (due to the $CH_3$ group) and that at 2932 cm.$^{-1}$ (the $CH_2$ group). The experimental values for adsorbed ethylene are compared in Table III with other values for liquid ethyl bromide[11] and those determined in this work, using slit widths as given in Table I. Other paraffins also were adsorbed on the same sample of alumina, and the absorbance ratios obtained also are given in the table. It is of interest to note that these paraffins were only weakly adsorbed on this alumina. The adsorbed butane is of particular interest, as its spectrum in the CH stretching region was very similar indeed to that of adsorbed ethylene, but it could all be desorbed rapidly by evacuation at room temperature. The above evidence indicates that the $CH_3/CH_2$ ratio is unity in the species formed by the chemisorption of ethylene. The simplest way to obtain this ratio is by the presence of an ethyl group, most probably attached in the configuration $S–CH_2CH_3$.

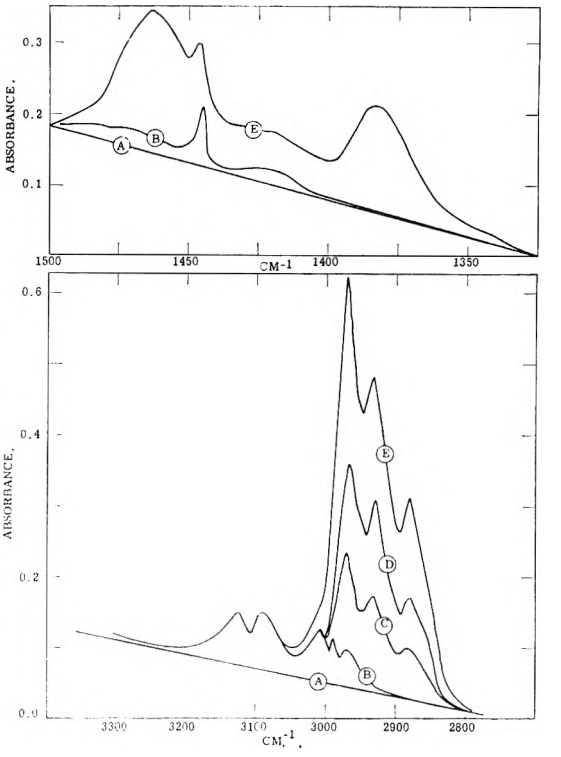


Fig. 1.—(A) Background spectrum of (A)$Al_2O_3$ after evacuation at 600°; (B) immediately after adding 6.8 cm. of ethylene at room temperature; (C) after 20 hr.; (D) after 4 days; (E) after 8 days. Bands centered at 3105, 2989, and 1443 cm.$^{-1}$ are due to gaseous ethylene.

The second way of determining the $CH_3/CH_2$ ratio is by examining the chemical properties of the adsorbed species. After evacuating gaseous ethylene from the cell, 37 cm. of hydrogen was added, and the cell stopcock closed. After heating at 200° for 48 hr., some rearrangement of the adsorbed species had taken place, as shown by the growth of a CH stretching band at 3020 cm.$^{-1}$. Bands of frequencies higher than 3000 cm.$^{-1}$ are found in unsaturated hydrocarbons.[10] Heating at

(10) L. J. Bellamy, "The Infrared Spectra of Complex Molecules," Second Ed., Methuen and Co. Ltd., London, 1958.

(11) L. H. Little, N. Sheppard, and D. J. C. Yates, *Proc. Roy. Soc.* (London), **A259**, 242 (1960).

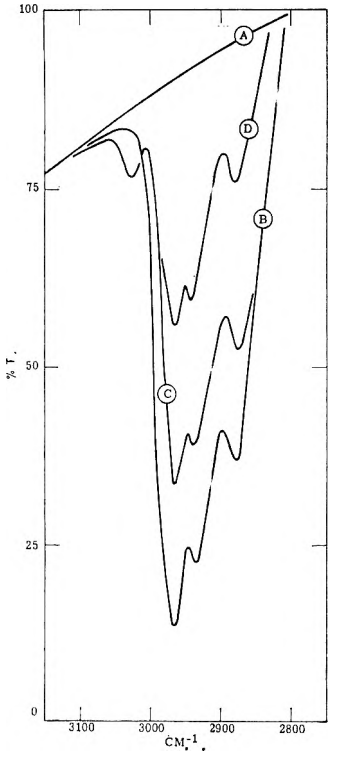


Fig. 2.—(A) Background spectrum of (A)$Al_2O_3$ after evacuation at 600°; (B) after the formation of chemisorbed ethyl groups; (C) after hydrogen treatment (37 cm.) for 1.5 hr. at 450°; (D) after hydrogen treatment for 18 hr. at 450°.

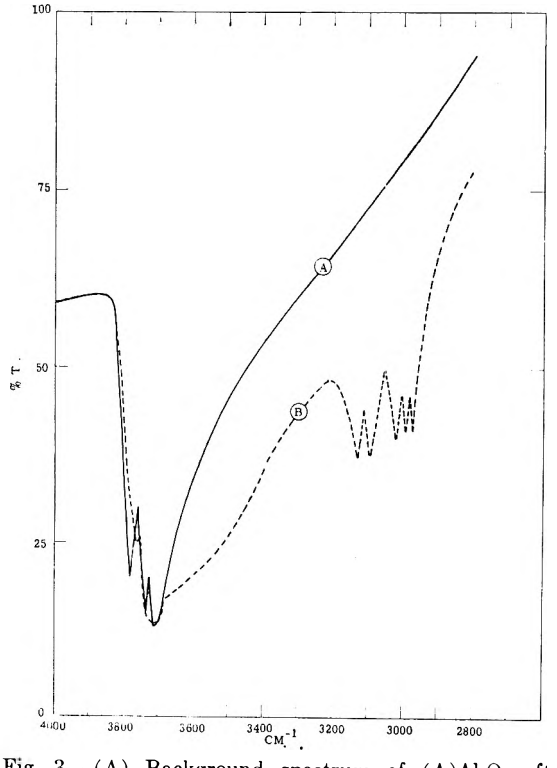


Fig. 3.—(A) Background spectrum of (A)$Al_2O_3$ after evacuation at 600°; (B) immediately after adding 7 cm. of ethylene at room temperature.

350° for 1.5 hr. had little more effect, but the same time at 450° hydrogenated quite a number of the adsorbed species (Fig. 2c). After 18 hr. at 450°, most of the adsorbed species had reacted (Fig. 2d). Then the gas in the cell was expanded into a side arm cooled to liquid nitrogen temperature. Mass spectrographic analysis of this gas gave the mole percentage composition: $H_2$, 97.63; $CH_4$, 1.13; $C_2H_6$, 0.80; $C_3H_8$ 0.38; $n$-$C_4H_{10}$, 0.04. This gives an approximate mole ratio of 3:2:1 for $CH_4$, $C_2H_6$, and $C_3H_8$. These figures indicate that the value of $n$ in the adsorbed alkyl chain (S–$(CH_2)_nCH_3$) is two or less.

TABLE III

| Absorbance ratio, $CH_3/CH_2$ (from 2970 and 2932 cm.$^{-1}$ bands) | Species |
|---|---|
| 1.36 | Adsorbed $n$-$C_4H_{10}$ |
| 1.26 | Adsorbed $n$-$C_5H_{12}$ |
| 0.82 | Adsorbed $n$-$C_7H_{16}$ |
| 1.35 | Liquid $C_2H_5Br$ (this work) |
| 1.31 | Liquid $C_2H_5Br$ (from ref. 11) |
| 1.33 | Chemisorbed $C_2H_4$ |

We were not able to find mild enough conditions of hydrogenation to give only the expected $C_2H_6$ in the gas phase. However, it has been found that ethylene chemisorbs on the platinum–alumina system giving an adsorbed species similar to that discussed above. These adsorbed species hydrogenate at lower temperatures than used in this work, and the resulting product was predominantly ethane. The formation of $CH_4$ and $C_3H_8$, observed after hydrogenating in this work at 450°, thus is ascribed to reactions between chemisorbed ethyl groups and $H_2$. It is possible that $CH_4$ (gas) and S–$CH_3$ are formed from S–$CH_2CH_3$ and $H_2$. The remaining S–$CH_3$ groups then may react with ethylene to form adsorbed propyl groups, and eventually propane. Alternatively, one may visualize the combination of S–$CH_3$ and S–$CH_2CH_3$ to yield propane, and a reaction between S–$CH_3$ and $H_2$ to give $CH_4$.

It is well known that alumina and other oxides contain surface OH groups at the outgassing conditions used here. These give three adsorption bands at 3785, 3740, and 3710 cm.$^{-1}$. It also is possible that the alumina could contain hydrogen, as so-called "water of constitution," that is not, for some reason, observable in the infrared spectrum. The formation of ethyl groups from $C_2H_4$ requires the addition of hydrogen, and it is important to determine whether the solid contributes hydrogen, or whether the reaction proceeds by self-hydrogenation.

Figure 3 shows that, after the adsorption of ethylene, the 3785 cm.$^{-1}$ band is markedly reduced in intensity, and also gives a general lowering of transmission between 3700 and 3200 cm.$^{-1}$. This indicates that weak hydrogen bonding is taking place between the adsorbent and the surface hydroxyl groups.

In one experiment, the surface OH groups all were converted to OD groups. Adding $C_2H_4$ to this sample, under the same conditions as used for undeuterated alumina, gave chemisorbed S–$CH_2$–$CH_3$ species with, however, no bands due to CD bonds (Fig. 4). This rules out the possibility that the S–$CH_2CH_3$ was formed from $C_2H_4$ and a hydrogen atom donated by a surface hydroxyl group.

However, a very small number of OH bands were produced although no C–D bands were observed. This hydrogen could have been provided by the $C_2H_4$.

On adsorbing pure $C_2D_4$ on a fully deuterated surface, only C–D bands were seen in the chemisorbed species. This makes it very unlikely that the hydrogen for the formation of S–$C_2H_5$ comes from a source within the alumina that is not visible in the infrared spectrum. The chemisorbed species made in this experiment gave three bands in the C–D stretching region similar in intensity distribution to those in the C–H stretching region from $C_2H_4$ adsorbed on undeuterated alumina. The species are presumed to be S–$CD_2CD_3$, but positive identification is difficult because few data are available on deuterio-ethyl compounds.

Finally, in one experiment, the surface hydroxyl groups were removed by evacuation at 1000° for 15 min. The resulting alumina was found, by X-ray analysis, to be $\theta$- rather than $\eta$-form.[8] The adsorption of $C_2H_4$ on this surface gave the same spectrum as obtained with the $\eta$-alumina evacuated at 600°.

We conclude, therefore, that at room temperature ethylene chemisorbs on (A)$Al_2O_3$, giving chemisorbed ethyl groups. The hydrogen is not donated by the alumina, the process being one of self-hydrogenation.

**Adsorption on (B)$Al_2O_3$.**—Both the above aluminas gave the same species after the chemisorption of ethylene, despite their crystallographic differences. However, the adsorption of ethylene on another $\eta$-alumina ((B)$Al_2O_3$) showed surprising differences between this alumina and the (A)$Al_2O_3$ discussed in the previous section.

On (B)$Al_2O_3$, the adsorption of ethylene is quite rapid at room temperature. Within 15 min. after admitting the gas, the spectrum reveals an adsorbed species (Fig. 5) which contains no $CH_3$, vinyl C–H, C≡C, or C=C groups. The only bands found were at 2928, 2855, and 1468 cm.$^{-1}$. In bulk saturated hydrocarbons, correlations[10] show that the band due to the asymmetrical $CH_2$ stretching mode is found at 2926 ± 10 cm.$^{-1}$, and that due to symmetrical stretch at 2853 ± 10 cm.$^{-1}$. The $CH_2$ deformation mode is found at 1465 ± 20 cm.$^{-1}$. These assignments are in excellent agreement with the bands observed when $C_2H_4$ is chemisorbed on (B)$Al_2O_3$. Since no bands were observed in the 800–700 cm.$^{-1}$ region, the –$CH_2$– chain of the chemisorbed species contains 3 or less $CH_2$ groups.[10]

In order to determine the length of the –$CH_2$– chain, the samples were heated in hydrogen (10 cm. pressure) at various temperatures, after removing gaseous ethylene from the cell. No changes were noted after heating for 10 min. at several temperatures below 300°, and at 300°. At 450°, after 20 min., a considerable fraction of the adsorbed species was removed. Some of them had been converted into an adsorbed species whose spectrum (Fig. 6c) was identical with that observed at room temperature after adding $C_2H_4$ to (A)$Al_2O_2$. We suggest that this spectrum indicates that the structure S–$CH_2CH_3$ is present.

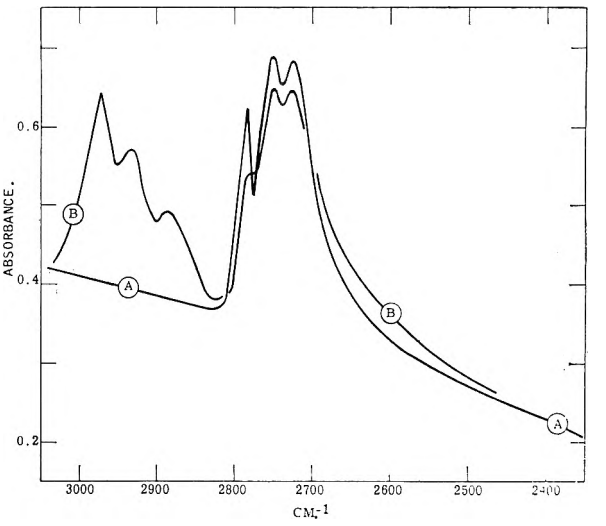


Fig. 4.—(A) Background spectrum of (A)$Al_2O_3$ after deaeration at 600°; (B) after the addition of $C_2H_4$ forming chemisorbed $C_2H_5$ groups.

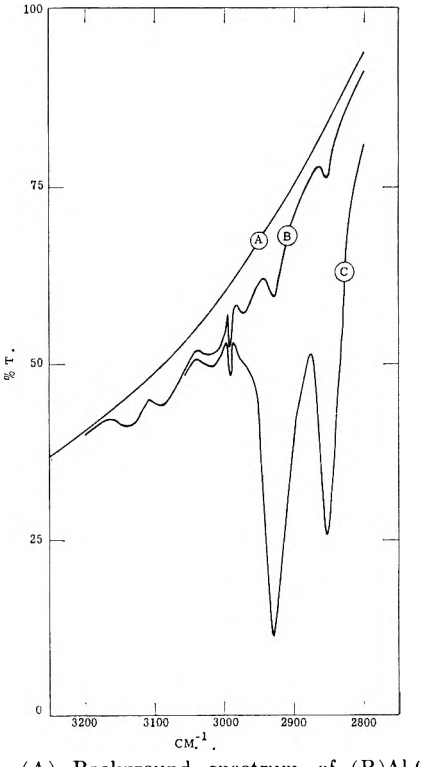


Fig. 5.—(A) Background spectrum of (B)$Al_2O_3$ after evacuation at 600°; (B) immediately after the addition of 6.3 cm. of ethylene at room temperature; (C) after 20 hr. under the same conditions.

In another experiment, the chemisorbed ethylene was treated with 30 cm. of hydrogen at 450° for 20 min. All adsorbed species were removed by this treatment. Since no adsorption bands were obtained by examining the gas in the cell, the products were present in a low concentration. The products were transferred, by a cold trap, to a flame ionization detector type of vapor fractometer. The hydrocarbon content of this gas was 92 mole % ethane and 8 mole % *n*-butane.

We conclude that the room temperature adsorption of ethylene on (B)$Al_2O_3$ is a relatively

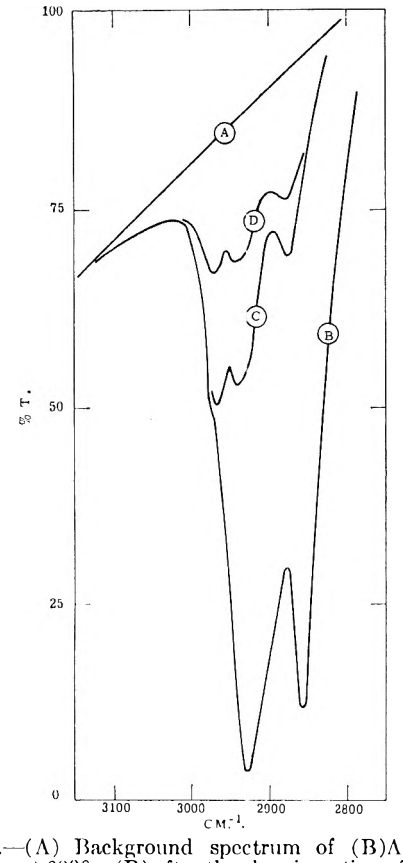


Fig. 6.—(A) Background spectrum of (B)$Al_2O_3$ after evacuation at 600°; (B) after the chemisorption of ethylene; (C) after hydrogen treatment (10 cm.) for 20 min. at 450°; (D) after hydrogen treatment for 10 min. at 500°.

rapid process leading predominantly to the formation of the chemisorbed species S–$CH_2CH_2$–S. It should be remarked at this point that the sequence

$$\text{S–CH}_2\text{–CH}_2\text{–S} \xrightarrow{H_2} \text{S–CH}_2\text{CH}_3 \xrightarrow{H_2} \text{CH}_3\text{CH}_3(g)$$

one in which all the intermediates were observed on (B)$Al_2O_3$, would seem to offer at least one path for the hydrogenation of $C_2H_4$ as catalyzed by alumina. It is not, of course, claimed that this is the only mechanism of ethylene hydrogenation on alumina, but only that all the steps have been observed on at least one type of alumina.

**Adsorption on Silica.**—After evacuating a Cabosil sample at 600°, ethylene at 7 cm. pressure was added. Neither physically nor chemically adsorbed ethylene was detected in a spectrum run soon after this addition. After standing until the next day, the spectrum still showed only gaseous ethylene. Hence at pressure of the order of 10 cm., after standing at room temperature for 24 hr., no adsorption of ethylene could be detected on silica.

## Discussion

Much progress has been made in understanding hydrocarbon reactions catalyzed by acidic oxides, by the use of carbonium ion mechanisms. Presumably, one of the ways in which such ions can be formed over acidic oxide involves the protonation of olefins by the catalyst. However, when ethylene is chemisorbed on alumina, under the conditions used here, such protonation apparently does not occur. Although no further details can be given without invoking several new assumptions, it seems clear that one of the paths by which ethylene is chemisorbed on alumina involves a two-site adsorption, forming S–$CH_2CH_2$–S. This is similar to the associative form of the chemisorption of ethylene on metals (eq. 3).

In contrast with (B)$Al_2O_3$, (A)$Al_2O_3$ forms chemisorbed ethyl groups from ethylene. The experiments with the latter alumina when deuterated show that self-hydrogenation occurs to give the S–$CH_2CH_3$ groups. In other words, the hydrogen used in the ethyl group formation is derived from the ethylene and not from the alumina or its surface OH or OD groups. This hydrogen (S–H) is most probably derived *via* the formation of some type of adsorbed $C_2H_2$ complex, as shown in eq. 1. Whether or not the formation of S–$CH_2CH_2$–S groups is a precursor of the formation of this acetylenic complex we do not know. Certainly no bands corresponding to the species S–$CH_2CH_2$–S were observed on (A)$Al_2O_3$ in the initial stages of the chemisorption of $C_2H_4$. It also is possible that the hydrogen formed in eq. 1 reacts with the alumina to generate (irreversibly) OH groups. In addition to the data in this paper, unpublished work in this Laboratory has shown that hydrogen can react with alumina to form surface OH groups.

Finally, it is important to repeat that the essential ingredients for a plausible mechanism of the hydrogenation of ethylene over alumina seem to be available from this study. That is, the intermediates have been observed directly on at least one acidic aluminum oxide.

$$\text{S–CH}_2\text{CH}_2\text{–S} \xrightarrow{H_2} \text{SCH}_2\text{CH}_3 \xrightarrow{H_2} \text{C}_2\text{H}_6(g)$$

**Acknowledgments.**—The authors wish to acknowledge the contribution of Dr. R. O. Steiner for his valuable suggestions during the early stages of this work. Special thanks also are due to Dr. H. Ladenheim, who contributed the sensitive gas chromatographic analyses described in the text.

# ELECTRONIC SPECTRA OF OLEFINS ADSORBED ON SILICA–ALUMINA CATALYSTS

BY HARRY P. LEFTIN AND W. KEITH HALL

*Mellon Institute, Pittsburgh, Penna.*

*Received March 2, 1962*

The spectra of 1,1-diphenylethylene and of α-methylstyrene adsorbed on silica–alumina and of acidic solutions of these olefins have been obtained. In addition to bands in the 400-mμ region, assigned to the classical carbonium ions, bands of uncertain origin were observed at longer wave lengths. The kinetic behavior of these systems was studied spectroscopically. These results, coupled with observations of the effects of oxidizing agents on the rates, indicate that the long wave length bands stem from intermediates formed during the oxidation of the olefin and that radical ions may be involved. Consideration of the available data leads to the conclusion that the long wave length bands arise from intramolecular, rather than charge-transfer transitions, as was previously supposed.

## Introduction

The visible spectrum of 1,1-diphenylethylene (DPE), adsorbed on the surface of a silica–alumina catalyst, has been found[1-3] to consist of two principal bands at 423 and 607 mμ. The first of these has been attributed to the methyldiphenylcarbonium ion[1-5] formed by addition of a proton or of a Lewis acid to the double bond. The other band is of uncertain origin. It may be supposed, however, that it is characteristic of a definite unstable intermediate formed by reaction of the olefin with the catalyst surface.

Evans, Jones, and Thomas[4] and Lavrushin[5] observed similar behavior with DPE in acidic solutions. They found that while DPE in concentrated $H_2SO_4$ yielded only the classical carbonium ion band, in sulfuric acid–acetic acid mixtures[5] and in benzene solution with trichloroacetic acid,[4] both the 423 and 607 mμ bands appeared. This work recently has been confirmed and extended by Grace and Symons.[6]

Since most reactions of olefins over silica–alumina catalysts have been explained by mechanisms involving only classical carbonium ion intermediates, knowledge of the surface species responsible for the long wave length band may prove to be of considerable theoretical interest to catalytic chemists. We have noted earlier[1,7a] that it has most of the attributes of an ion radical. It is the purpose of the present paper to present the detailed results of our investigations into the nature of this species.

## Experimental

**Equipment and Procedures.**—The optical cells and techniques employed for measurement of the electronic spectra of chemisorbed species have been described elsewhere.[3,7b] Spectra were obtained by transmission with a Beckman Model DK-1 recording spectrophotometer using quartz optical cells in conjunction with a high vacuum system of conventional design. Where catalysts were used, they were mounted as thin, fairly transparent platelets on quartz racks which positioned them inside the optical cells.

The catalyst samples were calcined at 500° in a stream of dried oxygen for 16 to 24 hr. before being placed into the optical cells. After sealing the cells directly to the vacuum line, the catalyst samples were evacuated for 1 hr., calcined in oxygen for 24 hr., evacuated for 24 hr., all at 500°, and then sealed off under vacuum. The organic reagent to be adsorbed was separately purified and sealed under vacuum in a separate compartment attached to the optical cell through a break-off seal. It was transferred to the catalyst through the vapor phase. Generally, the total amount of substrate used was only sufficient to provide for coverage of about $5 \times 10^{12}$ sites/cm.$^2$ of catalyst surface; this was the number of Lewis acid sites measured earlier.[7b] When, after the band intensities had become nearly time-independent, it was desired to treat the adsorbed species with another reagent such as $H_2O$, $NH_3$, $BF_3$, or HF, a stopcock was sealed to the cell through a second break-off seal previously provided for that purpose.

Comparative experiments were made using several solvent systems. For the purpose of the kinetic measurements, the reaction vessel consisted of two compartments separated by a break-off seal. Solutions containing olefin and solutions containing the active acid reagent were separately degassed at −195° and sealed off. After equilibrating at 25 ± 0.5°, these solutions were vigorously mixed to initiate the reaction and the rates were monitored spectrophotometrically. Spectra of the products of the reaction of alkali metals with olefins were measured using evacuated cells of similar design.

**Catalysts.**—The same transparent highly active[8] high-purity silica–alumina (DSA-1) and silica gel (DGS-4) catalysts used in earlier work[3,7] were employed; they had surface areas of 278 and 550 m.$^2$/g., respectively.

**Reagents.**—All reagents were commercial samples which were further purified until their spectra showed no bands due to impurities. Wherever comparison was possible, these and other physical properties were in good agreement with reported data.

Aldrich Chemical Co. 1,1-diphenylethylene was redistilled under reduced pressure and dried over calcium hydride ($n^{20}$n 1.6008). The 1,1-diphenylethane (Beacon Chemical Co.) was vacuum distilled and the distillate percolated through columns of silica gel and activated alumina. Eastman White Label α-methylstyrene (α-MS) was redistilled and dried over calcium hydride. The cumene was an API standard sample which was further purified by the method of Plank and Nace.[9]

Triphenylethylene and tetraphenylethylene (Aldrich Chemical Co.) were recrystallized from suitable solvents; the purified materials melted at 67.5 to 68.9° and 224.6 to 226.9°, respectively. Perylene and anthracene were fluorescent grade, obtained from the same source, and used without further purification.

Samples of the linear dimer (1,1,3,3-tetraphenylbutene-1) and of the cyclic dimer (1,1,3-triphenyl-3-methylindan) of 1,1-diphenylethylene were prepared by the method of Schoepfle and Ryan.[10] The former melted at 111 to 112° and the latter at 143.6 to 144.8°. The oxidation dimer (1,1,4,4-tetraphenylbutadiene) from the Aldrich Chemical Co. was used without further purification.

(1) H. P. Leftin and W. K. Hall, *J. Phys. Chem.*, **64**, 382 (1960).

(2) A. N. Webb, *Actes Congr. Intern. Catalyse, 2e, Paris*, **1**, 1289 (1961).

(3) H. P. Leftin, *J. Phys. Chem.*, **64**, 1714 (1960).

(4) A. G. Evans, P. M. S. Jones, and J. H. Thomas, (a) *J. Chem. Soc.*, 1824 (1954); (b) 104 (1957).

(5) V. F. Lavrushin, *Zh. Obshch. Khim.*, **26**, 2697 (1954).

(6) J. A. Grace and M. C. R. Symons, *J. Chem. Soc.*, 958 (1959).

(7) (a) H. P. Leftin and W. K. Hall, *Actes Congr. Intern. Catalyse, 2e, Paris*, **1**, 1307 (1961); (b) *ibid.*, **1**, 1353 (1961).

(8) W. K. Hall, D. S. MacIver, and H. P. Weber, *Ind. Eng. Chem.*, **52**, 421 (1960).

(9) C. J. Plank and D. M. Nace, *ibid.*, **47**, 2374 (1955).

(10) C. S. Schoepfle and J. D. Ryan, *J. Am. Chem. Soc.*, **52**, 4021 (1930).

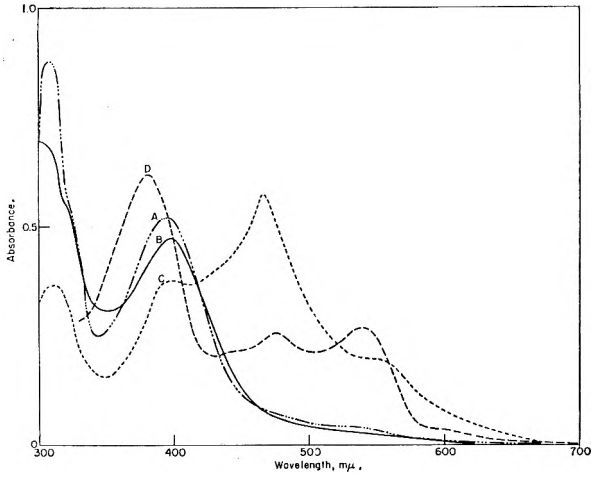


A. $C_6H_5(CH_3)C{=}CH_2$ in $H_2SO_4$
B. $C_6H_5CH(CH_3)_2$ on DSA-1
C. $C_6H_5(CH_3)C{=}CH_2$ on DSA-1
D. $C_6H_5(CH_3)C{=}CH_2$ in $(CH_3O)_2SO_2$

Fig. 1.—Spectra of hydrocarbons adsorbed on silica–alumina and dissolved in $H_2SO_4$ and in $(CH_3O)_2SO_2$ with added $H_2SO_4$.

**Solvents and Solutions.**—Unless otherwise noted, solvents of C.P. or A.R. quality were used as received. Dimethyl sulfate, freshly distilled over $K_2CO_3$, afforded solutions of the olefins which were transparent in the visible region. These solutions remained colorless for periods of weeks if stored *in vacuo*. Color developed slowly upon exposure to the atmosphere and quite rapidly upon addition of as little as 0.01% of concentrated $H_2SO_4$.

Acetic acid, monochloroacetic acid, dichloromethane, benzene, and tetrahydrofuran all afforded colorless solutions of the olefins. The tetrahydrofuran was distilled under vacuum into a mixture of benzophenone and potassium metal. It then was redistilled from the potassium ketyl solution into an evacuated storage bulb containing Na–K alloy.

## Results

**Spectra of Adsorbed Species.**—When the catalyst platelets were exposed to limited amounts of the phenylated hydrocarbons using high vacuum techniques, absorption bands developed more and more slowly until the spectra became nearly invariant with time. With the olefins, the bands formed readily at room temperature, but with 1,1-diphenylethane and cumene, temperatures of 100 and 320°, respectively, were required.

In Fig. 1, the spectra of cumene (curve B) and of α-methylstyrene (curve C) adsorbed on silica–alumina are compared with those of α-methylstyrene solutions in concentrated sulfuric acid (curve A) and in $(CH_3O)_2SO_2$–$H_2SO_4$ (curve D). As previously demonstrated,[7b] silica–alumina abstracts hydride ions from tertiary aliphatic carbon atoms, to form the corresponding carbonium ions. Thus, the band at 395 mμ can readily be assigned to the dimethylphenylcarbonium ion.

Analogous results were obtained with 1,1-diphenylethane and 1,1-diphenylethylene, respectively. On the silica–alumina surface, the methyldiphenylcarbonium ion was formed from the former,[7b] while a corresponding band appeared (at 423 mμ) in the spectrum of the latter.[3] It cannot be decided from the present data whether the species responsible for this band (in the case of the olefin) was the proton or, as suggested by Webb,[2] the Lewis acid adduct.

When the olefins were dissolved in concentrated $H_2SO_4$, these same carbonium ions were formed by proton addition.[11–14] Provided care was taken to avoid reaction between these ions and excess olefin during the solution process,[6] only the bands for the classical carbonium ions were obtained. When, however, these olefins were adsorbed on a silica–alumina catalyst or dissolved in weakly acidic media, additional bands appeared in the spectra at about 607 mμ with DPE (Fig. 2) and at 470 and 570 mμ with α-MS. The absence of these long wave length bands in the spectra obtained with the related saturated hydrocarbons indicates that the unknown entities cannot be formed by a simple equilibrium rearrangement of the classical carbonium ions, as has been suggested previously.[4] A simple interpretation is that excess olefin is required. Evidence in support of this was provided by the observation that only the 423-mμ carbonium ion band was formed on silica–alumina at very low DPE coverages. Contrary to the finding of Webb,[2] both bands always were formed at higher coverages, whether or not the DPE was distilled from $P_2O_5$ (or $CaH_2$).

A catalyst platelet was prepared by pressing finely ground Houdry S-65 catalyst to 18,000 p.s.i. In order to obtain sufficient transmission, the sample was immersed in a solution of DPE in $CCl_4$. The most intense band formed was at 423 mμ. Additional bands appeared at 570 and 607 mμ. The former had the greater intensity and may be due to an additional species formed from DPE. Alternatively, it may arise through some reaction with the solvent.

The spectrum from DPE adsorbed on silica gel (DGS-4) was identical with that of the parent hydrocarbon in non-acidic solvents, indicating that the olefin was physically adsorbed. On the admission of about 1 cc. (NTP) of anhydrous HF, bands at 426 and 595 mμ developed rapidly, the latter being considerably more intense. Similar results were obtained when the olefin was adsorbed on silica gel and treated with $BF_3$.

The molar extinction coefficient for the methyldiphenylcarbonium ion was determined in sulfuric acid; in agreement with Grace and Symons,[6] a value of $3.1 \times 10^4$ l. mole$^{-1}$ cm.$^{-1}$ was obtained. For the 607-mμ absorption, Beer's law was not obeyed, so that only minimum values of the extinction coefficient could be obtained. In our work, these fell between $5 \times 10^3$ and $2.2 \times 10^4$ l. mole$^{-1}$ cm.$^{-1}$. We therefore concur with the opinion of Grace and Symons[6] that the value for the long wave length band is at least as great, and possibly greater, than that for the carbonium ion.

The effect of water vapor and ammonia on the spectrum of the DPE–silica–alumina complex is shown in Fig. 2. On exposure to a small amount of

(11) N. C. Deno, J. J. Jaruzelski, and A. Schriesheim, *J. Org. Chem.*, **19**, 155 (1954).

(12) V. Gold, B. W. V. Hawes, and F. L. Tye, *J. Chem. Soc.*, 2167 (1952).

(13) A. G. Evans, *J. Appl. Chem.* (London), **1**, 240 (1951).

(14) D. E. O'Reilly and H. P. Leftin, *J. Phys. Chem.*, **64**, 1555 (1960).

water vapor at room temperature, the classical carbonium ion band was virtually eliminated, while the long wave length absorption band was unaffected (compare curves 1 and 2). On subsequent evacuation for 5 min. at 25°, the band due to the carbonium ion was partially restored (curve 3). The reversibility of this process was demonstrated (curves 4 and 5) where it also is shown that the band at 607 mμ is not affected by a large excess of $H_2O$. Both bands were completely eliminated by exposure to excess ammonia. These data emphasize that the entity responsible for the 607-mμ absorption is independent of the carbonium ion, as the concentration of the latter can be varied at will without affecting the concentration of the former. The behavior of the carbonium ion band closely resembled that presented earlier[7b] for the triphenylcarbonium ion formed from triphenylmethane.

A few measurements were made of the rates of development of the 423 and 607 mμ bands on catalyst surfaces. These were sufficient to demonstrate: (a) that the 423-mμ band always was detected first and (b) that when the amount of olefin exposed to the catalyst was severely limited, only the 423-mμ peak appeared.

**Kinetic Studies in Oxidizing Media.**—Evans and co-workers[4,13] have shown that both bands appear in DPE–sulfuric acid–acetic acid solutions. Unfortunately, the properties of this solvent are such that rapid dimerization occurs and the total concentration of ionic species remains low. A mixture of monochloroacetic acid, acetic acid, and sulfuric acid gave better results. Data obtained from a typical experiment using this ternary system are presented in Fig. 3. Initially, the concentrations of the classical carbonium ion and of the 607-mμ species increased simultaneously. After about 30 hr., both approached their maximum intensity, but while the former remained constant or increased extremely slowly, the latter decreased in concentration until after about 240 hr. the system reached a metastable state that remained invariant for at least 1000 hr. When only the data for the first 40 min. were plotted (see insert on Fig. 3), it became evident that while the intensity of the 423-mμ band increased linearly with time, the time dependence of the 607-mμ band was approximately parabolic. This behavior is consistent with the view[4b] that the initial rate of formation of the 607-mμ species depends upon the concentration of the classical carbonium ion. The fall-off in concentration beyond the maximum may correspond to any of a variety of reactions including the formation of neutral dimeric species. It further was observed that the initial rate of formation of both species increased strongly with increasing sulfuric acid and with olefin concentration.

The effect of trace amounts of oxidizing agents on the kinetic behavior was investigated. Selenic acid, peroxydisulfuric acid, and potassium ferricyanide were selected for the following reasons: (a) selenic acid has only twice the acid strength of sulfuric acid, yet its oxidation potential is greater by a factor of five[15]; (b) peroxydisulfuric acid is

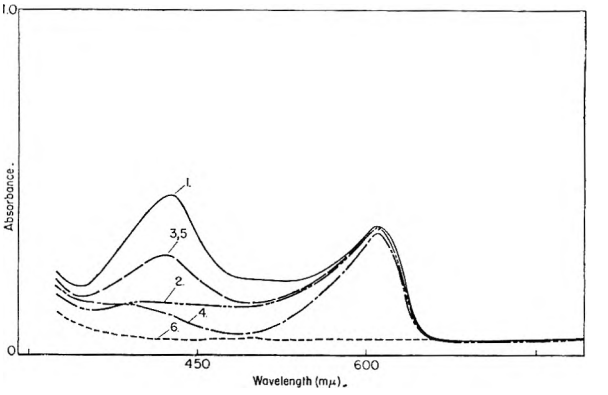


1. Initial Spectrum
2. & 4. $H_2O$ added
3. & 5. Evacuated
6. $NH_3$ added

Fig. 2.—Effect of $H_2O$ and $NH_3$ on spectrum of $(C_6H_5)_2C{=}CH_2$ ($1.3 \times 10^{-4}$ cc. NTP) adsorbed on silica–alumina. The curves are identified as follows: (1) initial spectrum; (2) spectrum after adsorbing 0.16 cc. NTP of $H_2O$ on dry plate (area ~10 m.²); (3) evacuated for 5 min. at 30°; (4) cell filled with 20 mm. of $H_2O$ vapor; (5) cell evacuated for 10 min. at 30°; (6) cell filled with 200 mm. of $NH_3$.

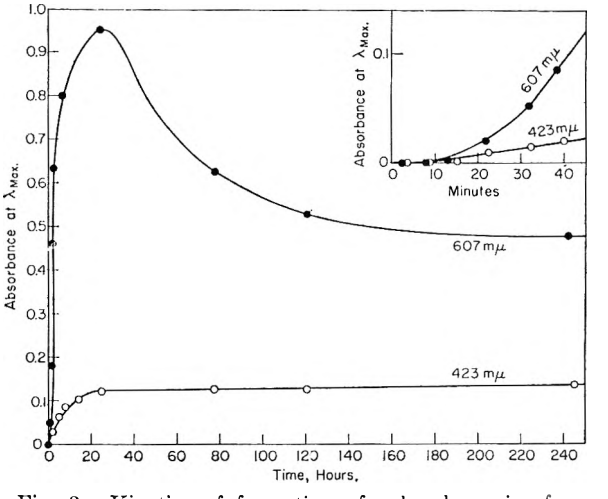


Fig. 3.—Kinetics of formation of colored species from $(C_6H_5)_2C{=}CH_2$ in a ternary solvent system, *viz.*, 2.96 *M* $ClCH_2COOH$ in $CH_3COOH$ plus 15% $H_2SO_4$. The hydrocarbon concentration was $1.02 \times 10^{-4}$ *M* in the combined solvent.

similar in these respects[16a]; and, finally, (c) potassium ferricyanide is a good oxidizing agent which usually involves the transfer of only a single electron.[16b] These data, presented in Fig. 4, show that with the addition of as little as 0.15% $H_2SeO_4$, the same over-all kinetic pattern was obtained but the entire process required only 30 min. as compared to over 250 hr. for the experiment of Fig. 3. For direct comparison, the uncatalyzed process for the same acid concentration (15% $H_2SO_4$) and for a higher acid concentration (22.5% $H_2SO_4$) are shown (Fig. 4). It can be seen that the vastly increased rate cannot result from the small increase in acid strength of the medium attending

(15) N. V. Sidgwick, "The Chemical Elements and Their Compounds, Vol. II, Clarendon Press, Oxford, 1950, p. 975 f.

(16) W. M. Latimer and J. H. Hildebrand, "Reference Book on Inorganic Chemistry," The Macmillan Co., New York, N. Y., 1940 (a) pp. 243–251; (b) p. 395.

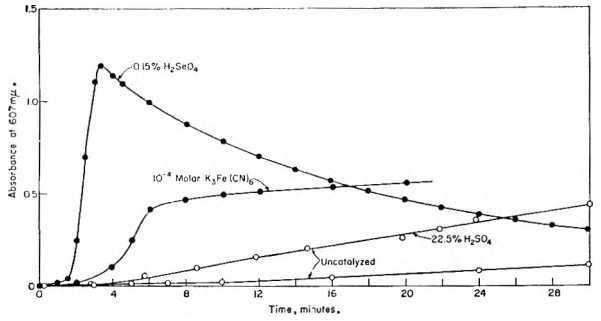


Fig. 4.—Comparison of kinetics of formation of 607 mμ species when catalyzed by small amounts of oxidizing agents to uncatalyzed reaction. In all cases, the same ternary solvent system shown in Fig. 3 was used except for one instance where the concentration of $H_2SO_4$ was increased to 22.5%. The olefin concentration was $4.62 \times 10^{-4}$ *M*.

the addition of the $H_2SeO_4$. Similar results were obtained with peroxydisulfuric acid. More striking, however, was the fact that the addition of as little as $1 \times 10^{-4}$ mole/l. of $K_3Fe(CN)_6$ also strongly catalyzed the process. These results indicate that the species exhibiting the 607-mμ band is an intermediate in an oxidation process involving the olefin. The facts that the band develops on the catalyst surface and that its formation in solution is catalyzed by an electronic oxidizing agent (*e.g.*, $K_3Fe(CN)_6$) restrict the types of oxidation possible. These considerations led to the idea that the entity in question might be a cation radical (positive radical ion).[1]

Repeated experiments were made with trifluoroacetic acid, vacuum distilled from anthrone into a solution of the olefin dissolved in $CaH_2$-dried, spectroscopically pure benzene. In agreement with the work of Evans,[4] both bands appeared, demonstrating that the species responsible may form in the absence of any known oxidizing agent other than the methyldiphenylcarbonium ion. This is in accord with the result obtained when the olefin was adsorbed on silica gel and exposed to gaseous anhydrous HF. As with the catalyst–olefin system, no e.p.r. absorption could be found for these solutions.

Both the 423-mμ and the long wave length (at 595 mμ) bands appeared when $SbCl_5$ was added to $CH_2Cl_2$ solutions of DPE. These solutions were quite unstable, but the kinetic behavior appeared to follow the same pattern as in the mixed acid solutions, *i.e.*, the blue color developed rapidly and then faded. A single strong sharp e.p.r. line, having a width of less than 10 gauss, centered at $g = 2.00$ was obtained from this system, but the spin concentration did not always appear to be related to the blue color. When $CCl_4$ was substituted for $CH_2Cl_2$, a deep blue paramagnetic complex precipitated. A sample of this precipitate, dissolved in $CH_2Cl_2$, also exhibited a strong e.p.r. signal. A blank consisting of 10% (by vol.) $SbCl_5$ in $CH_2Cl_2$ showed no resonance.

**Reaction of DPE with Alkali Metals.**—In work reported earlier,[1] it was found that when DPE was treated with lithium, sodium, potassium, or even calcium in tetrahydrofuran, the solutions first became blue and then turned to a deep red. These were found to be paramagnetic and the paramagnetism correlated roughly with the blue color. The red and the blue solutions appeared to be stable and interconvertible, the color depending upon whether excess metal or excess DPE was present. Thus, if additional potassium was added to a blue solution, it became red (475 mμ); the blue color (615 mμ) could be restored by the addition of more 1,1-diphenylethylene. As similar behavior had been reported previously[17,18] for stilbene (1,2-diphenylethylene), and since, in this case, the dark green color was attributed to the paramagnetic species $(C_6H_5CH{=}CHC_6H_5)^-$ and the red color to the diamagnetic ion $(C_6H_5CH{=}CHC_6H_5)^=$, it was suggested that corresponding species were responsible for our results with 1,1-diphenylethylene. More recent experiments have revealed that the 615-mμ band appears in these solutions when some samples of DPE, but not when others, are used. Freshly distilled samples produced only the 475-mμ band. As it was determined that these deteriorate noticeably within a few days, it must be concluded that the band at 615 mμ may be due to an ion formed from a decomposition product of DPE. If it is due to the monomeric radical ion, as previously suggested,[1] then it is not clear why the dinegative (475-mμ) ion forms exclusively in some cases, but not in others. We so far have not been able to resolve this question satisfactorily.

**Spectra of Possible Reaction Products.**—Dimethyl sulfate solutions of the linear and cyclic dimers of 1,1-diphenylethylene initially showed no absorption in the visible region. Color developed rapidly, however, following the addition of trace amounts of $H_2SO_4$. The cyclic dimer solution developed a single broad band at about 495 mμ in contradistinction to the work of Evans and coworkers,[4b] who found no bands in the visible region with benzene–trichloroacetic acid solutions of this compound. As might have been predicted, solutions of the linear dimer (1,1,3,3-tetraphenylbutene-1) rapidly developed the same two spectral peaks obtained from the monomeric olefin. It cannot be decided from this observation whether this result indicates a rapid depolymerization of the dimer in the acidic medium, or whether the absorption bands can be obtained directly from the dimer.

The oxidation dimer 1,1,4,4-tetraphenylbutadiene reacted rapidly with $H_2SO_4$ in the ternary solvent mixture to give an intensely blue solution. The spectrum from this solution, however, was composed of a broad band at 715 and a stronger band at 560 mμ. The spectrum of its potassium complex in tetrahydrofuran solution was very similar, having bands at 583 and 715 mμ. Although the behavior of this dimer is similar to that of DPE, it can be seen that they are otherwise unrelated.

Benzophenone is one of the more likely impurities that might be present in DPE, as it is an oxidation product of the olefin. Benzophenone, in the ternary solvent mixture, does not give a

(17) D. E. Paul, D. Lipkin, and S. I. Weissman, *J. Am. Chem. Soc.*, **78**, 116 (1956).

(18) G. J. Hoijtink and P. H. van der Meij, *Z. physik. Chem.*, **20**, 1 (1959).

blue solution, even with added selenic acid. However, the potassium ketyl in tetrahydrofuran exhibited a single broad absorption band at 710 mμ.

Evans and co-workers[4,13] have considered some of these and other possibilities and have concluded that the 607-mμ band is not related to any expected reaction product. Our results tend to corroborate this view.

## Discussion

The results presented herein can be qualitatively explained if it is assumed that the species responsible for the 607-mμ absorption band, obtained from adsorbed DPE, is formed during the oxidation of the olefin. In a number of ways our data are inconsistent with the assignment[2,4] of this band to a charge-transfer complex, involving the interaction of the proton of a weak acid with the olefinic double bond. Evidence in support of these statements is listed below.

**Oxidation Hypothesis.**—(1) The fact that excess olefin is necessary to obtain the long wave length band may be taken as evidence that the 607-mμ species can be formed through reaction of a carbonium ion with an olefin molecule.

(2) The kinetic behavior shown in Fig. 3 supports this view and, in addition, is typical of a free radical oxidation process. Although insufficient kinetic data were obtained for detailed analysis, certain characteristics of the mechanism are evident, *viz.*, (a) the initial rate of formation of the 607-mμ species is proportional to the carbonium ion concentration, and (b) the former is destroyed by subsequent reactions. The first of these items is in agreement with the findings of Evans[4b] and the first and second with those of Aalbersberg[19] for DPE in the $C_6H_6$–$CF_3COOH$ and polynuclear aromatic hydrocarbons in the $BF_3$–$CF_3COOH$–$H_2O$–$O_2$ systems, respectively. Aalbersberg writes (for 9-bromoanthracene)

$$\frac{d(\text{cation radical})}{dt} = k_1(\text{carbonium ion}) - k_2(\text{cation radical}) \quad (1)$$

an equation which describes the principal features of our results if it is supposed that the 607 mμ band stems from the species: $[(C_6H_5)_2C{=}CH_2]^+$.

(3) Trace amounts of oxidizing agents strongly accelerate these processes, as shown in Fig. 4. Although these effects are not entirely understood, they may be rationalized in terms of a reaction sequence analogous to one suggested by Symons,[20] *i.e.*

$$(C_6H_5)_2C{=}CH_2 + H^+ \rightleftharpoons (C_6H_5)_2\overset{\oplus}{C}{-}CH_3 \quad (2)$$

$$(C_6H_5)_2\overset{\oplus}{C}CH_3 + (C_6H_5)_2C{=}CH_2 \rightleftharpoons (C_6H_5)_2\dot{C}CH_3 + [(C_6H_5)_2C{=}CH_2]^+ \quad (3)$$

$$(C_6H_5)_2\dot{C}CH_3 + 4H_2SO_4 \longrightarrow [(C_6H_5)_2C{=}CH_2]^+ + 2H_3C^+ + SO_2 + 3HSO_4^- \quad (4)$$

where it is understood that both the carbonium ion and the cation radical may be removed by additional reactions to form stable products such as the cyclic dimer of DPE. These considerations led to the suggestion[1] that the 607-mμ band corresponded to an ion radical.

(4) The ability of the silica–alumina surface to act as an oxidizing agent already is well established; it can abstract hydride ions from phenylated alkanes[7b] and it can oxidize polynuclear aromatic hydrocarbons to their corresponding radical ions.[21–23] Moreover, it is known that the oxidation state of the surface is in some way involved in these processes.[21] In agreement with eq. 4, it is known that $SO_2$ is evolved when olefins are treated with sulfuric acid.[24,25] Hence, the oxidation involves transfer of oxygen. The possibility exists that silica–alumina also supplies oxygen atoms.

**Shortcomings of the Charge-Transfer Complex Hypothesis.**—(1) It offers no explanation for the kinetic effects nor for the effects of oxidizing agents noted above.

(2) The data strongly support the view that the species responsible for the 607-mμ band is formed by reaction of a DPE molecule with its carbonium ion. They appear to be inconsistent with the suggestion of Evans, *et al.*,[4] that the carbonium ion rearranges into the new species. It should be noted that Evans' assignment[4] was derived by a process of elimination.

(3) The effects of water, shown in Fig. 2, demonstrate that the 423 and 607 mμ bands are due to two independent species. Webb,[2] in accord with Evans' hypothesis, assumed that the long wave length band originated from a charge-transfer complex involving the olefin and an OH group of the catalyst surface. Since the intensity of the 607-mμ band does not increase as the 423-mμ band decreases, we believe that the hydrogen associated with hydrated Lewis acid sites is not responsible for its formation. Moreover, since the spectrum of DPE on high area silica gel is identical with that of the parent olefin, Webb's suggestion that surface hydroxyl groups are the source of the pi bonding protons also seems very unlikely; were this the case, a decided difference in hydrogen bonding ability between the hydrogen atoms of silica and silica–alumina would be required. The available evidence does not support this view.[26,27] Webb's interpretation was backed by the observation that the formation of the long wave length band on the catalyst surface appeared

(19) W. I. Aalbersberg, Thesis, Free University of Amsterdam, 1960.

(20) A. Carrington, F. Dravnieks, and M. C. R. Symons, *J. Chem. Soc.*, 947 (1959).

(21) W. K. Hall, *J. Cat.*, **1**, 53 (1962).

(22) J. J. Rooney and R. C. Pink, *Proc. Chem. Soc.*, 70, 142 (1961).

(23) D. M. Brouwer, *Chem. Ind.* (London), 177 (1961).

(24) V. F. Lavrushin, D. N. Kursanov, and V. N. Setkina, *Dokl. Akad. Nauk SSSR*, **97**, 265 (1954).

(25) J. Gonzales-Vidal, E. Kohn, and F. A. Matsen, *J. Chem. Phys.*, **25**, 181 (1956).

(26) M. R. Basila, Abstracts of Papers presented at the 141st National Meeting, American Chemical Society, Washington, D. C., March, 1962.

(27) W. K. Hall, H. P. Leftin, and D. E. O'Reilly, to be published.

to be favored by "added-back" water. Our results show that when water is added to a system where both species are present, carbonium ions are preferentially desorbed. Hence, if $H_2O$ were added first, one might expect to obtain only the long wave length band.

(4) The observation of the species in some solutions of DPE, when treated with alkali metals, appears to have no explanation in terms of pi complex theory.

(5) Grace and Symons[6] noted a similarity between the behavior of 1,1-diphenylethylene and diphenylmethanol in strong and weakly acidic media and pointed out that there is no way of deriving a complex of the type suggested by Evans from the latter compound. On the other hand, such a similarity might be expected to result from an oxidation process.

(6) The band appeared in systems which are substantially free of hydrogen, *e.g.*, anhydrous $AlCl_3$[2] and in the present work when DPE was adsorbed on silica gel and treated with $BF_3$. In these instances, as with a number of other systems,[19,28] the formation of a proton-containing complex such as postulated by Webb[2] and by Evans[4] is very unlikely.

(7) On more general grounds, a wave length of 607 m$\mu$ is too long to correspond to a charge-transfer complex of the benzene–iodine type. Buckles and co-workers[29] showed that tetra-*p*-methoxyphenylethylene interacts with a number of electron acceptors to form blue solutions ($\lambda_{max}$ 575 m$\mu$) which slowly turn yellow on standing. This band had the high molar extinction coefficient ($\sim 10^4$) typical of those observed in the present work. The systems forming this band with the olefin included: $H_2SO_4$ in $CH_3COOH$, $CF_3COOH$ in $CCl_4$, $BF_3$ in $CH_2Cl_2$, $PCl_5$ in $CCl_4$, and finally, of particular interest here, the halogens including $I_2$ in $ClCH_2CH_2Cl$. The wave length of the maximum was quite insensitive to the acceptor molecule used, as observed for DPE in the present and related work.[4,6] It also is known[6] that styrene forms bands at 435 and 615 m$\mu$ in $H_2SO_4$ and in $H_2SO_4$–$CH_3COOH$ mixtures, respectively. It may be inferred, therefore, that these three olefins all form similar complexes from which the long wave length bands arise. McConnell, Ham, and Platt[30] showed that the frequency of transitions of CT complexes with $I_2$ form a linear correlation with the ionization potential of the donor molecule. Recent ionization potential measurements[31] yielded values of 9.0 and 8.8 for styrene and DPE, respectively. Accordingly, their CT complexes (with $I_2$) would be expected[30] to provide bands in the 310 to 330 m$\mu$ region. Moreover, the work of Hastings, Franklin, Schiller, and Matsen[32] suggests that bands in the 600-m$\mu$ region cannot be expected from this system; this would require a much stronger acceptor molecule, *e.g.*, tetracyanoethylene.[33]

(8) Charge-transfer theory offers no explanation for the appearance of a band at nearly the same wave length in a wide variety of systems, *i.e.*, in dimethyl sulfate, in sulfuric acid–acetic acid mixtures, in benzene–$CF_3COOH$ solutions, in the $CH_2Cl_2$–$SbCl_5$, and in tetrahydrofuran–alkali metal systems, as well as adsorbed on silica–alumina or on silica gel with $BF_3$ or HF. It is a well known consequence of charge-transfer theory that the frequency of the transition varies appreciably with both the donor and acceptor.[34] This observation indicates that, regardless of the nature of the species, the band arises from an intramolecular transition, rather than one of the charge-transfer type.

**Concluding Remarks.**—The nature of the species responsible for the 607-m$\mu$ absorption band formed from adsorbed DPE is of considerable interest as it may correspond to an ionic intermediate not previously considered in the catalytic literature. Evidence that such intermediates may exist is to be found in several places. Taft and co-workers[35] have studied the mechanism of the hydration of isobutene and the reverse reaction in dilute acid solutions and have been forced to the conclusion that all of their kinetic results cannot be rationalized by the assumption of a single carbonium ion intermediate. They advanced the idea that the missing entity is a pi complex or possibly a hydrated carbonium ion. Haag and Pines[36] and Lucchesi[37] also have used the pi complex concept to explain the excess (above equilibrium) production of *cis*-butene-2 over the *trans*-isomer in the isomerization of butene-1. These studies are of particular interest in view of the fact that Webb[2] has found spectral evidence of complexes formed from butene-2 adsorbed on silica–alumina analogous to those reported here for 1,1-diphenylethylene and $\alpha$-methylstyrene.

The kinetic evidence (Fig. 3 and 4) is readily understood in terms of eq. 1-4, suggesting that the 607-m$\mu$ band is due to a cation radical. The free radical formed in (3) is a powerful electron and/or hydrogen atom donor. Step (4) is one of several possible reactions. It can be seen, therefore, that cation radicals may be formed according to (3) even in the absence of strong oxidizing agents so long as excess olefin is present in the system. Hence, they could form on the surface of silica gel when treated with anhydrous HF yet not form when the same olefin is dissolved in liquid HF (for the same reason that only the carbonium ion forms in concentrated $H_2SO_4$). On the other hand, as shown by (4), the formation will be favored by the presence of an oxidizing agent, affording a qualitative explanation for our results. Repeated attempts to prevent the formation of the

(28) W. I. Aalbersberg, G. J. Hoijtink, E. L. Mackor, and W. P. Weijland, *J. Chem. Soc.*, 3049, 3055 (1959).

(29) R. E. Buckles, R. E. Erickson, J. D. Snyder, and W. B. Person, *J. Am. Chem. Soc.*, **82**, 2444 (1960).

(30) H. L. McConnell, J. S. Ham, and J. R. Platt, *J. Chem. Phys.*, **21**, 66 (1953).

(31) G. F. Crable, Gulf Research & Development Company, private communication.

(32) S. H. Hastings, J. L. Franklin, J. C. Schiller, and F. A. Matsen, *J. Am. Chem. Soc.*, **75**, 2900 (1953).

(33) H. Kuroda, M. Kobayashi, M. Kinoshita, and S. Takemoto, *J. Chem. Phys.*, **36**, 457 (1962).

(34) R. Foster, *Tetrahedron*, **10**, 96 (1960).

(35) R. W. Taft, Preprints, Petroleum Division ACS, General Papers, Vol. 5, 133, March, 1960; *J. Am. Chem. Soc.*, **82**, 4729 (1960).

(36) W. O. Haag and H. Pines, *ibid.*, **82**, 2488 (1960).

(37) P. J. Lucchesi, D. L. Baeder, and J. P. Longwell, *ibid.*, **81**, 3235 (1959).

blue (607 mμ) species in $C_6H_6$–$CF_3COOH$ mixtures failed, even though great care was taken to remove all possible oxidizing agents. Yet, Aalbersberg[19,28] produced the spectra of the cation radicals of the polynuclear aromatic hydrocarbons in liquid HF and in aqueous $CF_3COOH$ saturated with $BF_3$ when these were contacted with air; only the proton adducts were formed in the absence of oxygen. All these results are consistent with eq. 1–4 and with the requirement that the 607-mμ species be an intermediate formed by the oxidation of the olefin.

Recently, it has been unambiguously demonstrated that cation radicals do form on the surface of silica–alumina catalysts when the substrate is one of the closely related polynuclear aromatic hydrocarbons, such as perylene or anthracene.[21–23] From the quantum mechanical point of view, anthracene and 1,1-diphenylethylene are closely related molecules. Their electronic spectra should be closely similar and this also should apply to their carbonium ions and to their radical ions. These relationships have been noted elsewhere.[6,12,21] The strong band at 720 mμ of the radical ion of anthracene has been justified by quantum mechanical calculations.[38–41] Both anthracene and 1,1-diphenylethylene are alternant polynuclear aromatic hydrocarbons. Hence, the strong theoretical support for the existence of the polynuclear aromatic radical ions also favors the view that the aryl olefins should behave similarly, and in many ways they do.

Repeated attempts to observe the paramagnetism expected for the radical ion of DPE by the e.p.r. technique, both in acidic solutions[6,20,21] and with catalysts,[21,22] have failed. This is an admittedly serious shortcoming, particularly as the radical ion of anthracene can be readily identified in the same systems. However, it is generally recognized that the inability to observe paramagnetism by the e.p.r. technique does not prove its absence. As the observation of an e.p.r. signal from adsorbed DPE (on a different silica–alumina catalyst) has recently been reported by another Laboratory,[42] this interpretation must remain a definite possibility.

It now is known that the oxidation state of the silica–alumina surface influences its ability to generate ion radicals from the polynuclear aromatic hydrocarbons[21,43] and it was pointed out[21] that oxygen atoms may be involved in the process. In the interpretation of our data, the possibility that the 607-mμ species includes an atom of oxygen cannot be overlooked. Buckles, *et al.*,[29] found that, in the presence of traces of $H_2O$, the corresponding pinacolone was formed in 22% yield when tetra-*p*-methoxyethylene was treated with a slight excess of $Cl_2$ in dilute solution in dichloroethane. On the other hand, the olefin could be quantitatively recovered from the same blue ($\lambda_{max}$ = 575 mμ) solutions by the addition of Cu powder. Moreover, Webb[2] contended that traces of $H_2O$ were essential for the formation of the 607-mμ band from DPE. Thus, although it is not yet possible to assign the long wave length bands observed with aryl olefins to a particular species, the rough outlines of some previously unsuspected chemistry of surfaces have been made apparent.

**Acknowledgment.**—This work was sponsored by the Gulf Research & Development Co. as part of the research program of the Multiple Fellowship on Petroleum. Thanks are due to Dr. A. J. Saraceno at Gulf Research and Development Co. for making the e.p.r. measurements.

(38) G. J. Hoijtink and W. P. Weijland, *Rec. trav. chim.*, **76**, 836 (1957).

(39) A. A. Verrijn-Stuart and E. L. Mackor, *J. Chem. Phys.*, **27**, 826 (1957).

(40) D. E. Paul, D. Lipkin, and S. I. Weissman, *J. Am. Chem. Soc.*, **78**, 116 (1946).

(41) T. L. Chu, G. E. Pake, D. E. Paul, J. Townsend, and S. I. Weissman, *J. Phys. Chem.*, **57**, 504 (1953).

(42) J. Turkevich, 140th National Meeting of the American Chemical Society, Division of Colloid and Surface Chemistry, Chicago, Illinois, September 3–8, 1961.

(43) J. K. Fogo, *J. Phys. Chem.*, **65**, 1919 (1961).

# INFRARED SPECTRA OF CO, $CO_2$, $O_2$, AND $H_2O$ ADSORBED ON SILICA-SUPPORTED IRON[1]

BY GEORGE BLYHOLDER AND LAURENCE D. NEFF

*Chemistry Department, University of Arkansas, Fayetteville, Arkansas*

*Received March 5, 1962*

The infrared spectra of CO, $CO_2$, $O_2$, and $H_2O$ adsorbed on silica-supported iron at 20 and 180° have been obtained. Chemisorbed CO and gas phase CO are in dynamic equilibrium at 180°. Chemisorbed CO gives bands at 4.95, 5.05, and 5.3 $\mu$. Upon adsorption at 20°, $CO_2$ dissociates into chemisorbed CO and an oxide ion. Both $O_2$ and $H_2O$ displace chemisorbed CO from the surface but do not give any bands themselves. At 180° adsorbed $O_2$ gives a spectrum which is characteristic of iron oxide. At 180° adsorbed water apparently completely dissociates since it gives no OH band. While $CO_2$ gives no evidence of physical adsorption at 20°, at 180° it gives a band at 4.3 $\mu$ which is tentatively assigned as physically adsorbed $CO_2$. Either $CO_2$ or a mixture of CO and $O_2$ when heated to 180° give a surface complex with a band at 6.5 $\mu$. This complex is tentatively assigned a carboxylate type structure.

## Introduction

The study of the adsorption of gases on metals has provided many interesting results. The great majority of studies have been volumetric or kinetic in nature. These data do not directly furnish information about the structure of adsorbed species so there has been much speculation on this point. Infrared spectroscopy has proven to be one of the most powerful tools for determining chemical structure. Eischens[2] and co-workers have demonstrated the feasibility of applying infrared techniques to the study of adsorbed species on metals. The reader is referred to reference 2 for a review of the literature on the infrared spectra of molecules adsorbed on non-metal as well as metal adsorbents. Studies of the infrared spectra of CO chemisorbed on a variety of metals have been reported,[2-4] as have also studies of simple hydrocarbons and $CO_2$ on nickel. The only infrared study dealing with iron is that of Eischens,[2] which gives the spectrum of CO chemisorbed on supported iron at 35° and the change in the chemisorbed CO band upon addition of a small quantity of oxygen.

In order to gain insight into the nature of iron as a chemisorber and indirectly as a catalyst, we thought it would be interesting to look at the spectra of a variety of gases chemisorbed on iron. We therefore are reporting herein the infrared spectra obtained when silica-supported iron is exposed to CO, $CO_2$, $O_2$, and $H_2O$. We also have investigated the effect of changing the temperature from 20 to 180° upon the nature of the interaction of these gases.

## Experimental

**Purification of Gases.**—Carbon monoxide (C.P. grade) and hydrogen were obtained from the Matheson Co., Inc. Oxygen was removed from the hydrogen by passing the gas over copper turnings at 420°. The hydrogen used for the reduction process was dried, after passing over the hot copper turnings, by passing it through a cold trap cooled to −77° using an acetone–Dry Ice mixture. The hydrogen used for experimental purposes was passed over hot copper turnings to remove the oxygen present and then dried by passing the gas through a cold trap cooled with liquid nitrogen. After drying, the hydrogen was passed through an activated charcoal (C. R. Fischer Scientific Co.) trap cooled with liquid air. Iron carbonyl and other impurities were removed from the carbon monoxide by passing the gas through a trap cooled with liquid nitrogen and then through an activated charcoal trap cooled with liquid nitrogen.

The gases used for the experimental studies were stored, after purification, in 2-l. glass bulbs. These bulbs were evacuated to 0.001 $\mu$ pressure for 8–10 hr. before being filled with the gas.

The charcoal was "re-activated" before each use by pumping on it while heated to 300° for 18–24 hr. At the end of the heating period, the pressure inside the charcoal trap was 0.001 $\mu$. The activated charcoal then was cooled *in vacuo* before use.

The oxygen and $CO_2$ were supplied by the Matheson Company. They were purified by passing through a trap cooled with liquid air. The oxygen was collected in a cold trap and then distilled into the storage bulbs. The $CO_2$ which was collected in the cold trap was distilled while being evacuated to remove the volatile materials present in the sample. After this was accomplished, the $CO_2$ was distilled into a storage bulb.

The $H_2O$ was twice distilled and passed through a 5-ft. ion-exchange column.

**Cell.**—The cell used is shown in Fig. 1. It is of such design that the reaction is carried out *in situ*. It is basically a 10-cm. gas cell, equipped with two side arms. The side arms have 10/30 standard taper ground glass outer joints for attaching the cell to the vacuum system. The cell windows used were sodium chloride. The cell is equipped with a heater about the middle.

As can be seen from Fig. 1, the ends of the cell are equipped with cooling coils. This allows the center of the cell to be heated to 500° without allowing the ends of the cell to become hot enough to permit the sealing grease to flow onto the windows. Cold water is circulated through these cooling coils during the reduction procedure.

Using temperatures of 180° or less, the heater will hold the temperature to ±5°. At higher temperatures, about 400°, the heater will only hold the temperature to ±15°. However, at the higher temperature, the 15° variance makes little difference as this occurs at temperatures considerably above those at which the disk starts to reduce. The temperature gradient between the outside of the cell wall and the center of the disk at temperatures less than 200° is 27° at the maximum. However, at reduction temperatures, about 380° inside, the temperature gradient is 100°.

The windows were secured to the cell using Dow Corning High-Vacuum grease. The grease was thickened by mixing approximately 600 mg. of silica into approximately 3 g. of the grease. The resulting grease will hold a vacuum well and will not flow over the salt windows on heating.

The samples were held in a holder as shown in Fig. 1. The cell as well as the sample holder is constructed from Pyrex glass. The sample was placed between the ground surfaces and the pieces of the holder secured together using 18 gage nichrome wire. After the sample was placed in the holder and the holder assembled, the assembly was placed in the cell and held in position using a small spring. This kept the sample holder from moving while inside the cell. The holder held the sample in a vertical position in the cell

(1) This work was supported in part by a grant from the Research Corporation. Acknowledgment is made to the donors of the Petroleum Research Fund, administered by the American Chemical Society, for partial support of this research.

(2) R. P. Eischens and W. A. Pliskin, *Advan. Catalysis*, **10**, 1 (1958).

(3) R. P. Eischens, W. A. Pliskin, and S. A. Francis, *J. Chem. Phys.*, **22**, 1986 (1954).

(4) (a) A. C. Yang and C. W. Garland, *J. Phys. Chem.*, **61**, 1504 (1957); (b) J. T. Yates, Jr., and C. W. Garland, *ibid.*, **65**, 617 (1961).

during reduction and while the cell was in position on the spectrophotometer.

A Perkin-Elmer Model 21 double beam infrared spectrophotometer was used with a sodium chloride prism. A "differential" technique was used in the studies. This was done by placing identical samples in the instrument, one in each beam, and then using one of the samples for experimental purposes. By operating the instrument in such a manner, the background spectrum due to a single sample was automatically compensated for. Also the differential technique allowed the cells to be heated to 200° in the beam of the spectrophotometer. If a differential technique were not used, the emitted radiation from the hot sample would have interfered greatly with the absorption spectrum, *i.e.*, there also would be an emission spectrum recorded. But, since both beams contained samples, the emitted radiation was automatically compensated for. By using 10-cm. gas cells, the cells could fit into the sample compartment in a special cell holder. Using such an arrangement it was not necessary to deflect the beam with mirrors from its "normal" path.

**Adsorbent Preparation.**—The iron was supported on silica. The silica (Cab-O-Sil H 35) was a gift of the G. L. Cabot Company of Boston. The surface area of the support, as supplied by the manufacturer, is 300–350 $m.^2/g.$ The mean particle size of the silica is about 200 Å. The silica-supported iron was prepared by the reduction of a mixture of silica with iron(III) nitrate, reagent grade, obtained from J. T. Baker Chemical Company. The final result is 10% Fe by weight.

The silica support was covered with the desired metal as follows. An aqueous solution containing 1 g. of the metal was prepared. The amount of water used was enough to produce a thin slurry when 9 g. of the silica was added to it. The resulting slurry was stirred until a homogeneous mixture was obtained. This then was placed on watch glasses and allowed to dry. Upon drying, the samples were ground to a fine consistency using an agate mortar and pestle.

After grinding, 100 mg. of the sample was pressed into a disk, 2.54 cm. in diameter, using a pressure of 8000 p.s.i. Before pressing, the samples were dried in an oven at 120° for 10–20 min. If they are not dried long enough, they will adhere to the surface of the die and cannot be removed whole. The die also is warmed slightly before pressing.

**Reduction and Adsorption Procedure.**—The sample, after being pressed, was placed in the sample holder. The holder was secured with wires and then placed within the cell. After the sample was in place, the ground surfaces were covered with a thin coat of the specially prepared silicone grease to assure a vacuum-tight seal. After the grease was applied, the windows were placed on the cell, and the whole cell evacuated on the vacuum system. After evacuation (which took 6–9 hr. to assure complete evacuation and removal of any contaminants), hydrogen, at 1 atm. pressure, was passed through the purification system, into the vacuum system, and then through the cell. The initial flow rate was about 500 ml./min. After the hydrogen was allowed to flow for 1–2 min. the heating coils were warmed up to about 280°. This flow rate and temperature were used for about the first hour. After the first hour, the flow rate was reduced to about 100 ml./min. and the temperature increased to about 320°. Then after another 2 hr. the flow rate was reduced to 20–50 ml./min. and the temperature increased to 380°. This process was continued for about 15 hr. After the reduction process was completed, the sample was cooled in a hydrogen atmosphere and then evacuated. After cooling, the cells were completely evacuated, removed from the vacuum system, and then placed in the spectrophotometer. After this was accomplished, a vacuum system for handling gases was attached to the sample cell *via* a movable arm. Then a background spectrum of the two samples was recorded using the "differential" technique described earlier. Because the silica only transmits infrared radiation from 2.5 to 7.6 $\mu$, only this range can be used. After the background spectrum was recorded, the gas was introduced into the cell.

The gas was introduced to a clean iron sample while the sample was at 20°. Spectra were recorded immediately on introduction of the gas to the cell, and again about 30 min. later. After the second spectrum was recorded, the cells were heated to 180° with the gas samples in the cells. After a 6–7 hr. heating period had elapsed, spectra again were recorded.

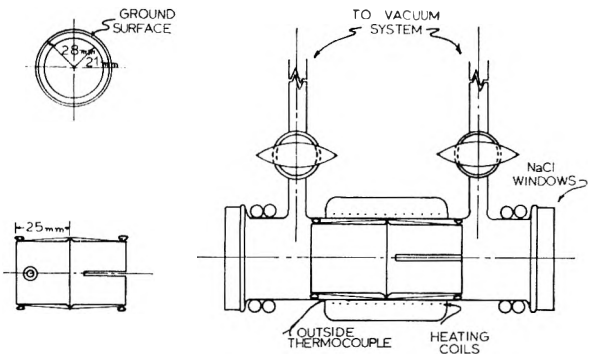


Fig. 1.—*In situ* cell and sample holder.

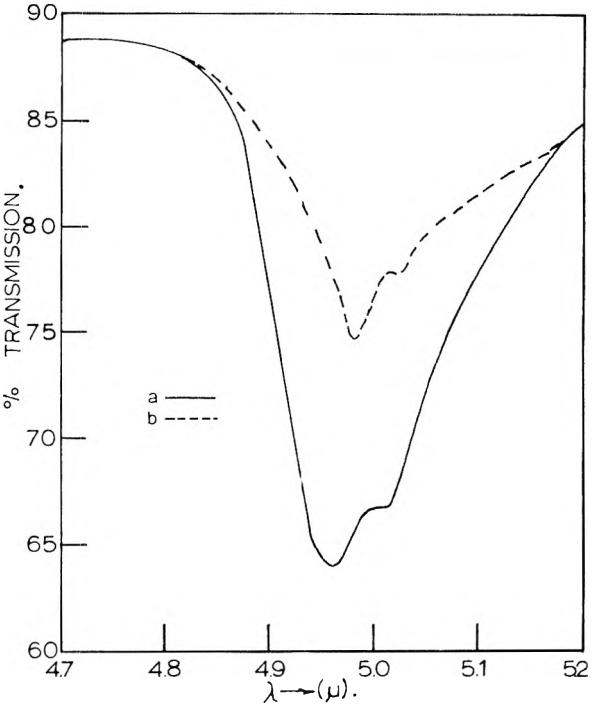


Fig. 2.—CO chemisorbed on silica-supported iron at (a) 25° and (b) 150°.

## Results

**CO Chemisorption.**—The spectra of CO chemisorbed on iron can be seen in Fig. 2. The spectrum (a) corresponds to CO chemisorbed on iron while the sample was at 20°. Spectrum (b) corresponds to CO chemisorbed on iron with the sample temperature at 150°. On a clean surface at 20° the size of the chemisorbed peak is independent of the pressure of CO present in the cell. However, on an iron surface at 180°, the size of the chemisorbed CO band depends on the pressure of gas present and at lower pressures the band centers at longer wave lengths. This can be seen in Fig. 3, where spectra a, b, c, d, and e correspond to CO pressures of 20, 12.5, 5, 2, and 1 cm., respectively. The shift goes from 4.94 $\mu$ at 20 cm. pressure to 5.05 $\mu$ at 1 mm. pressure. The bands at 4.61 and 4.73 $\mu$ are due to gas phase CO.

At 180°, the amount of CO on the surface is a function of the pressure and is reversible. A plot of $p/v$ *vs.* $p$, where $p$ is the gas phase CO pressure and $v$ is the amount of CO adsorbed as measured by

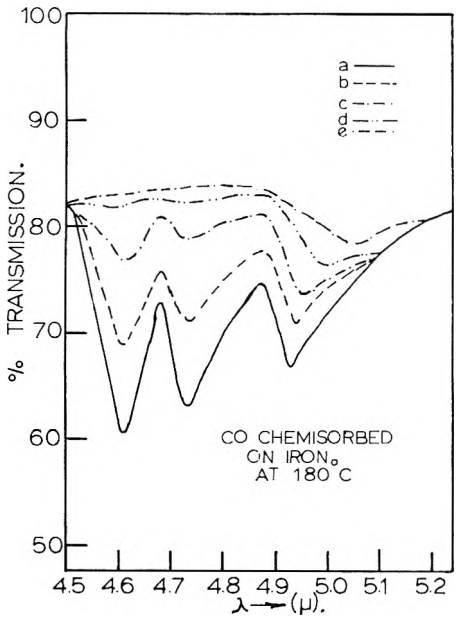


Fig. 3.—CO chemisorbed on silica-supported iron at 180° as a function of pressure: (a) 20 cm. of CO; (b) 12.5 cm.; (c) 5 cm.; (d) 2 cm.; (e) 1 cm.

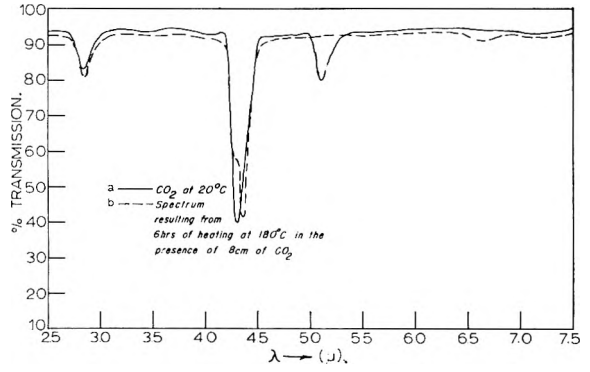


Fig. 4.—Spectra with 8 cm. of $CO_2$ in cell with silica-supported iron: (a) 20°; (b) after 6 hr. of heating at 180°.

the integrated intensity of the chemisorbed CO band, gives a straight line.

Sometimes, the CO band has a broad shoulder on the long wave length side, indicating a band centered at 5.3 μ.

**$CO_2$ Chemisorption.**—Figure 4 shows the spectra recorded when 8 cm. of $CO_2$ was added to a cell containing a clean iron surface. When the $CO_2$ was first placed in a cell a peak at 5.1 μ was observed in addition to that due to gas phase $CO_2$ at 4.23 μ. This is shown in spectrum (a), which was recorded 30 min. after the gas was admitted to the cell at 20°. The peak at 5.1 μ appears to correspond to a chemisorbed CO peak of about 50% of that observed when CO is admitted to a clean iron surface, which probably means that about 50% of the surface normally covered with CO was covered. Spectrum (b) denotes the spectrum recorded after the iron sample had been heated to 180° for 6 hr. in the presence of 8 cm. of $CO_2$. The peak at 4.23 μ had changed shape somewhat, and the peak due to chemisorbed CO, at 5.1 μ, disappeared. A small broad peak was observed at 6.5 μ after heating. This remained upon evacuation while the sample was at 180°. Nothing else was observed.

**$O_2$ Chemisorption.**—1 cm. of $O_2$ was added to a clean iron surface. The resulting spectra are shown in Fig. 5, where (a) denotes the spectrum recorded 30 min. after the gas was admitted to the cell at 20°. Only the band at 2.8 μ which is part of the background was observed. Spectrum (b), which was recorded after 6 hr. of heating at 180° with 1 cm. of $O_2$ present in the cell, shows bands at 4.75, 5.5, and 6.5 μ. These bands remained when the sample was evacuated hot.

**Interaction of CO and $O_2$.** When 8 cm. of CO was added to an iron sample and heated to 180° for 6 hr., no band changes occurred.

Figure 6 denotes the spectra obtained when 8 cm. of CO and 5 cm. of $O_2$ were added to the cell. The CO was added first to the iron at 20° to obtain spectrum (a). Then the oxygen was added. The chemisorbed CO peak disappeared but no other changes were observed while the sample was at 20°. Then the sample was heated to 180° for 6 hr. with 8.7 cm. of CO and 5 cm. of $O_2$ present in the cell. The resulting spectrum is shown as spectrum (b). After the heating period of 6 hr. a peak at 6.42 μ was observed. After the spectrum was recorded, the cell was evacuated for several minutes and another spectrum recorded. Nothing new was observed and the peak at 6.42 μ remained.

**Chemisorption of $H_2O$ and $H_2$.**—When 1 cm. of water vapor was added to the cold iron catalyst, large bands appeared at 2.9 and 6.14 μ. A background spectrum recorded prior to the introduction of the water vapor showed a small peak at 2.48 μ due to OH on the silica. When the sample was heated to 180° for 6 hr., with the water vapor present in the cell, the spectrum corresponded exactly to the background spectrum. That is to say, the bands at 2.9 and 6.14 μ disappeared and only the one band at 2.84 μ remained unchanged in intensity. The reason this band did not show up when the water vapor was added to the cold iron is assumed to be due to its being "masked" by the large –OH band at 2.9 μ. After the spectrum was recorded, upon heating the sample for 6 hr. in the presence of 1 cm. water vapor, the cell was evacuated hot and another spectrum recorded. The resulting spectrum corresponded to the original background spectrum.

An experiment was carried out using 1 cm. of water vapor and 14 cm. of $H_2$. The gases were introduced to an iron sample. Then, with the gases present in the cell, the sample was heated to 180° for 6 hr. Nothing was observed to be different from the results obtained upon heating with water vapor alone in the cell, as described in the preceding paragraph. When a sample with CO chemisorbed on it was exposed to 10 mm. of water vapor at room temperature, the band for chemisorbed CO immediately disappeared.

**Adsorption on Pure Silica Disk.**—Hydrogen, 14 cm., was added to a cell which contained a sample of the support material. This was heated for 4 hr. at 180°. No increase in the OH band at 2.8 μ was noted in the spectra.

A mixture of 8 cm. of CO and 14 cm. of hydrogen was added to a freshly prepared silica sample. This was heated for 6 hr. at 180°. No interaction

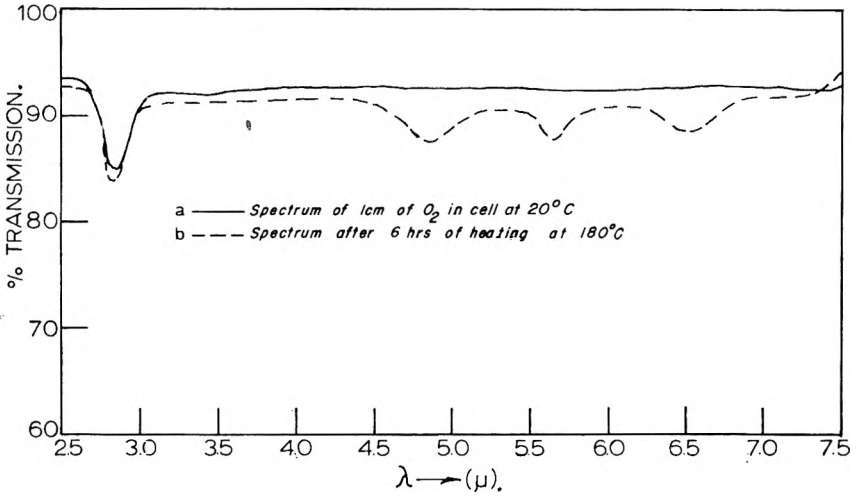


Fig. 5.—Spectra with 1 cm. of $O_2$ in cell with silica-supported iron: (a) 20°; (b) after heating for 6 hr. at 180°.

between the hydrogen and CO was observed from the spectrum.

## Discussion

**CO Chemisorbed on Iron.**—Eischens[2] observed a band at 5.1 $\mu$ with a shoulder at 4.95 $\mu$. He attributed the 5.1 $\mu$ band to CO chemisorbed in a linear structure, Fe—C≡O. Eischens suggested that the 4.95 $\mu$ band might be due to iron carbonyl or to a weakly chemisorbed form of linear CO. These assignments are made by analogy to the spectra of $Fe(CO)_5$. On the basis of the spectra from 2 to 30 $\mu$ of CO chemisorbed on iron suspended in oil, Blyholder[5] assigns, in general agreement with Eischens, the 5.1 $\mu$ band to CO chemisorbed in a linear structure, Fe=C=O. Comparison of Fig. 3 with Eischens' spectra reveals that the relative intensities of the two peaks observed are just reversed.

If the two bands between 4.95 and 5.1 $\mu$ are regarded as arising from basically the same structure, *i.e.*, linear Fe–C–O, which is our belief, then the question is presented as to whether the two bands are due to interactions of chemisorbed CO molecules with each other or are due to surface heterogeneity. If interactions are responsible we expect one band at low coverages located between the two bands found at high coverages. The spectra do not support this position. We therefore attribute the two bands to adsorption on two different types of sites or regions. Since two definite bands are produced, the regions are internally reasonably homogeneous. It seems reasonable to associate these regions with different crystal faces. Since the reduction procedure to produce the supported iron samples used here and Eischens' procedure are different, the relative development of crystal faces may well be different. This would account for the difference in relative intensities of the two observed bands between our work and Eischens'.

While Fig. 3 indicates that the CO responsible for the 4.95 $\mu$ band is less strongly held than the CO giving the longer wave length band, the fact that the spectrum of chemisorbed CO at 150° in Fig. 2 has the same shape, although the band intensity is reduced, as the band at 25° indicates

(5) G. D. Blyholder, *J. Chem. Phys.*, **36**, 2036 (1962).

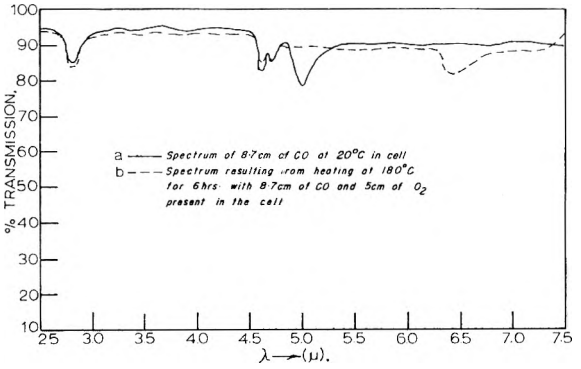


Fig. 6.—Interaction of $O_2$ and CO: (a) spectrum with 8.7 cm. of CO in cell with silica-supported iron at 20°; (b) spectrum after addition of $O_2$ and heating for 6 hr. at 180° with 8.7 cm. of CO and 5 cm of $O_2$ in cell.

that the CO giving the 4.95 $\mu$ band is quite strongly held. This is in contrast to Eischens' suggestion that the band at 4.95 $\mu$ is due to weakly held CO. The sizes of the bands at room temperature are independent of pressure and they are stable to evacuation of the cell for several days.

The band at 5.3 $\mu$ was not obtained by Eischens. In general Eischens has interpreted bands in this region as due to bridge type structures, $\begin{matrix} M \\ \diagdown \\ \quad >C=O \\ \diagup \\ M \end{matrix}$.

While this is a possible assignment, the possibility of CO chemisorbing by forming a $\pi$-complex should not be overlooked. Our data do not distinguish between these possibilities at present. As the sample is heated the band at 5.3 $\mu$ is the first to go, indicating that this band represents the least stable CO species on the surface. The relative instability of this complex also can be inferred from the difficulty in obtaining a sufficiently clean surface to form this species. At least we presume that lack of cleanliness of the surface is the reason we do not always obtain the band at 5.3 $\mu$. Although he does not specifically state how he reduces his iron samples, Eischens describes a batch type reduction process for general use. We suspect that because it is easier to remove the last traces of impurities with a flow system than with a batch system, Eischens did not obtain a band at 5.3 $\mu$ because of

surface contamination. We have found active iron samples much more difficult to prepare than nickel samples.

At 180° once about 1/4 of the surface is covered with CO, as judged by the assumption that the chemisorbed CO band at 20° represents complete coverage, the amount of CO chemisorbed is a function of the pressure and is readily reversible. It is concluded from this that the surface and gas phases are in rapid dynamic equilibrium at 180°. In plotting the relationship between the amount of CO chemisorbed at 180° and the gas phase CO pressure, $p/v$, where $v$ is the amount adsorbed, plotted *vs.* $p$ gives a straight line indicating that a Langmuir isotherm is followed for pressures between 5 and 50 cm. This indicates that as the surface coverage goes from about 1/4 to 3/4, the heat of adsorption is constant and the type of surface site reacting is not changing. The coverage of the first quarter of the surface is not so readily reversible and the heat of adsorption presumably is greater than for the subsequent adsorption.

**Adsorbed $CO_2$.**—Figure 4 shows that as well as a large band at 4.25 $\mu$ due to gas phase $CO_2$ when $CO_2$ is added to the cell at 20°, a band appears at 5.1 $\mu$. This band is attributed to chemisorbed CO. This indicates that even at 20°, $CO_2$ is chemisorbed on a clean iron surface by dissociation to CO and presumably an adsorbed oxygen atom. Nothing else shows up in the spectrum at 20°.

When the cell, which is open to the manifold of the vacuum system with 8 cm. of $CO_2$ in it, is heated to 180°, several changes occur. The chemisorbed CO desorbs due to the negligible partial pressure of CO in the gas phase. Since the cell is open to the manifold, when the cell is heated the concentration of $CO_2$ in the cell is reduced to about 2/3 its value at 20°. This results in the gas phase band for $CO_2$ being reduced. A new band at 4.3 $\mu$ appears. Since this band is so close to the gas phase band and it disappears on evacuation of the cell, it is attributed to adsorbed $CO_2$. Comparison of the intensity of the 4.25 $\mu$ band obtained at 20° to that at 180° reveals that there is little if any contribution to this band from adsorbed $CO_2$. The appearance of adsorbed $CO_2$ at 180° when there is none at 20° was not expected. This fact and the perturbation of the band suggests that there is an appreciable activation energy for formation of the adsorbed species.

In addition to these bands at 180° a band at 6.6 $\mu$ also appears. Investigating the spectrum of CO chemisorbed on supported nickel, Eischens[2] assigned bands at 6.5 and 7.2 $\mu$ to a carboxylate type structure with the carbon attached to a nickel atom. While we observed only one band, comparison of the relative intensities of the two bands reported by Eischens indicates that the longer wave length band could well be too weak to be observed in our spectrum. Since $CO_2$ does dissociate at least partially on an iron surface at room temperature, the possibility of the 6.6 $\mu$ band being due to an iron oxide formation must be considered. Figure 5 shows that while $O_2$ does interact at 180° with iron to produce a band at 6.5 $\mu$ it also produces bands at 5.5 and 4.75 $\mu$. On the assumption that production of one oxide band without the others is unlikely, we tentatively assign the 6.6 $\mu$ band to a carboxylate type structure of $CO_2$ chemisorbed on iron.

**Chemisorbed $O_2$.**—When $O_2$ is placed in a cell at 20° no absorption bands are observed. The fact that $O_2$ displaces chemisorbed CO indicates that it does adsorb on the surface. While most organic peroxides[6] absorb around 9 $\mu$, the relationship of the frequency of an organic peroxide to a surface peroxide complex is not clear. Thus the fact that we observed no bands in the 2 to 7.5 $\mu$ region does not eliminate peroxide type structures. When the cell was heated to 180° for 6 hr. with oxygen in it, bands developed at 4.7, 5.5, and 6.5 $\mu$. We attribute these to iron oxide formation on the basis of having observed[7] bands at 4.75 and 6.6 $\mu$ for disks of pressed $\alpha$-$Fe_2O_3$ and $Fe_3O_4$.

**Interaction of CO and $O_2$.**—Upon addition of a few microns of $O_2$ to chemisorbed CO on iron, Eischens found that the band at 5.1 $\mu$ disappeared and a new band appeared at 4.7 $\mu$ which is close to the frequency of gas phase CO. Eischens does not report on the stability of the 4.7 $\mu$ band. When we added 5 cm. of $O_2$ to a cell at 20° already containing 8.7 cm. of CO and therefore a chemisorbed CO band at 5.1 $\mu$, the band at 5.1 $\mu$ immediately disappeared and no other bands appeared. This indicates that under the conditions of our experiment with an excess of $O_2$ present, CO is displaced from the surface and even though 8.7 cm. of gas phase CO is present, it does not chemisorb.

When the cell with 8.7 cm. of CO and 5 cm. of $O_2$ is heated to 180° for 6 hr. a band at 6.5 $\mu$ develops. In accordance with our spectra obtained with $CO_2$ in the cell, this band also is tentatively assigned to a carboxylate type structure. At any rate, as might be expected, heating CO and $O_2$ in the cell produces the same surface complex as heating $CO_2$ in the cell. This complex is quite tightly bound to the surface as evacuation of the cell at 180° produces no change in the 6.5 $\mu$ band.

**$H_2O$ Adsorption.**—When water vapor is present in the cell at 20° the only bands appearing are at 6.2 and 3 $\mu$, which presumably are due to physically adsorbed water, as these bands disappear on heating. The appearance of the O–H stretching frequency at 3.0 $\mu$ rather than 2.75 $\mu$ indicates interaction of the OH group of the adsorbed water. Hydrogen bonding seems to us to be the most likely explanation of the shift from 2.75 $\mu$ for a free OH group. No OH band for adsorbed hydroxyl groups was observed after the cell was heated. We thought $H_2O$ might dissociate completely to leave oxygen atoms on the surface and so we added $H_2$ to the gas phase with the thought that this might produce more surface OH. No increase in the OH band region was observed.

The lack of observation of a band which can be ascribed to adsorbed water leads to the question of whether it interacts at all. The fact that chemisorbed CO is displaced by water at 20° means that water does adsorb on the surface. This fact coupled with the lack of observation of an OH band

(6) L. J. Bellamy, "The Infrared Spectra of Complex Molecules," Methuen and Co. Ltd., London, 1958.

(7) G. Blyholder and E. A. Richardson, paper in preparation.

indicates that when $H_2O$ adsorbs at 180° it completely dissociates on the iron surface.

In summary, it appears for the compounds investigated that oxygen, except where it can form multiple bonds with carbon, tends to dissociate from its compounds to presumably form oxide ions on the metal surface. Water dissociates so as to leave no OH groups on the surface. Oxygen adsorbs to form an oxide lattice at 180°. $CO_2$ dissociates on a clean surface at 20° to form chemisorbed CO and presumably an oxide ion. CO shows no tendency to dissociate, even at 180° where chemisorbed and gas phase CO are in dynamic equilibrium. On the basis of several bands appearing for chemisorbed CO, the surface is presumed to have a heterogeneity consisting of several regions which are reasonably homogeneous within themselves.

# THERMODYNAMIC CONSTANTS FOR HYDROGEN BOND FORMATION IN THE CHLOROFORM–BENZENE–CYCLOHEXANE SYSTEM

BY CLIFFORD J. CRESWELL AND A. L. ALLRED

*Department of Chemistry, Northwestern University, Evanston, Illinois*

*Received March 5, 1962*

The association of chloroform and benzene has been investigated in the temperature range 25–75° by nuclear magnetic resonance spectroscopy. The equilibrium constant at 25° is $1.06 \pm 0.30$ $(m.f.)^{-1}$ and the enthalpy and entropy of association are $-1.97 \pm 0.35$ kcal. $mole^{-1}$ and $-6.5 \pm 0.5$ cal. $mole^{-1}$ $deg.^{-1}$, respectively. A system involving the solvent cyclohexane and a low, fixed concentration of chloroform was chosen to minimize contributions from solvent effects to chemical shifts. The chemical shift ($\delta_{benzene\cdots chloroform} - \delta_{chloroform}$) due to hydrogen bond formation is $1.91 \pm 0.40$ p.p.m. From a comparable investigation of the association of chloroform and triethylamine, values of the equilibrium constant at 25°, enthalpy, entropy, and ($\delta_{triethylamine\cdots chloroform} - \delta_{chloroform}$) at 25° are $4.2 \pm 0.2$ $(m.f.)^{-1}$, $-4.15 \pm 0.20$ kcal. $mole^{-1}$, $-11.0$ cal. $mole^{-1}$ $deg.^{-1}$, and $-1.48$ p.p.m., respectively.

## Introduction

This paper reports the investigation of the extent of hydrogen bond formation between chloroform and benzene. The association of chloroform with various bases has been demonstrated by vapor pressure measurements,[1] dielectric polarization,[2] solubilities,[3,4] heats of mixing,[5] ultrasonic absorption,[6] infrared spectroscopy,[7–9] change of volume upon mixing,[10] nuclear magnetic resonance (n.m.r.),[11–13] freezing point diagrams,[12] and $PVT$ behavior.[14] For additional references and discussion concerning hydrogen bonding by chloroform, see reference 15. Evidence for the specific interaction of chloroform with benzene includes heats of mixing,[16] enhancement of the intensity of infrared absorption due to the C–D stretch of chloroform-*d*,[8] and the n.m.r. chemical shift of chloroform dissolved in benzene.[12,17] Hydrogen bonding involving electron-donating $\pi$-orbitals is discussed elsewhere.[18]

The general low-field shift in proton magnetic resonance spectra due to hydrogen bonding has been recognized for over a decade,[19,20] and theoretical interpretations of the hydrogen bond shift have been given elsewhere.[21] However, when compounds, including chloroform, having a propensity for hydrogen bond formation are dissolved in aromatic solvents, a high-field shift of the resonance of the donor proton is observed.[12,17,22–24] This high-field shift, which is opposite to the chemical shift of protons known to be involved in hydrogen bond formation in other types of systems, can be attributed to the magnetic anisotropy of benzene and other aromatic compounds. The anisotropy arises from the induced circulation of $\pi$ electrons[25,26] and produces a secondary field which opposes the applied field in the vicinity of the symmetry axis of benzene and augments the field near the edge of the ring. The relative contributions to the high-field shift by specific hydrogen bonds, by "statistical" positioning of the solute between aromatic planes, and by

(1) E. Beckman and O. Faust, *Z. physik. Chem.*, **89**, 247 (1914).
(2) D. P. Earp and S. Glasstone, *J. Chem. Soc.*, 1709 (1935).
(3) M. J. Copley, G. F. Zellhoefer, and C. S. Marvel, *J. Am. Chem. Soc.*, **60**, 1337 (1938).
(4) J. H. Hildebrand and R. L. Scott, "Solubilities of Non-electrolytes," Reinhold Publ. Corp., New York, N. Y., 1950.
(5) W. Gordy and S. C. Stanford, *J. Chem. Phys.*, **9**, 204 (1941).
(6) R. Parshad, *Indian J. Phys.*, **16**, 1, 307 (1942).
(7) G. M. Barrow and E. A. Yerger, *J. Am. Chem. Soc.*, **76**, 5247 (1954).
(8) C. M. Huggins and G. C. Pimentel, *J. Chem. Phys.*, **23**, 896 (1955).
(9) R. C. Lord, B. Nolin, and H. D. Stidham, *J. Am. Chem. Soc.*, **77**, 1365 (1955).
(10) L. A. K. Staveley, W. I. Tupman, and K. R. Hart, *Trans. Faraday Soc.*, **51**, 323 (1955).
(11) C. M. Huggins, G. C. Pimentel, and J. N. Shoolery, *J. Chem. Phys.*, **23**, 1244 (1955).
(12) L. W. Reeves and W. G. Schneider, *Can. J. Chem.*, **35**, 251 (1957).
(13) G. J. Korinek and W. G. Schneider, *ibid.*, **35**, 1157 (1957).
(14) J. D. Lambert, J. S. Clarke, J. F. Duke, C. L. Hicks, S. D. Lawrence, D. M. Morris, and M. G. T. Shone, *Proc. Roy. Soc.* (London), **249A**, 414 (1959).
(15) G. C. Pimentel and A. L. McClellan, "The Hydrogen Bond," Freeman, San Francisco, 1960, p. 197.
(16) M. Tamres, *J. Am. Chem. Soc.*, **74**, 3375 (1952).
(17) A. A. Bothner-By and R. E. Glick, *J. Chem. Phys.*, **26**, 1651 (1957).
(18) (a) Ref. 15, p. 202; (b) M. L. Josien and G. Sourisseau, "Hydrogen Bonding," ed. by D. Hadzi, Pergamon Press, New York, N. Y., 1959, pp. 129–137.
(19) U. Liddel and N. F. Ramsey, *J. Chem. Phys.*, **19**, 1608 (1951).
(20) J. T. Arnold and M. G. Packard, *ibid.*, **19**, 1608 (1951).
(21) W. G. Schneider, H. J. Bernstein, and J. A. Pople, *ibid.*, **28**, 601 (1958).
(22) A. D. Cohen and C. Reid, *ibid.*, **25**, 790 (1956).
(23) T. Schaefer and W. G. Schneider, *ibid.*, **32**, 1218 (1960).
(24) J. C. Davis, Jr., and K. S. Pitzer, *J. Phys. Chem.*, **64**, 886 (1960).
(25) L. Pauling, *J. Chem. Phys.*, **4**, 673 (1936).
(26) J. A. Pople, *ibid.*, **24**, 1111 (1956).

other solvent effects discussed below, have not been established previously.[27,12,17]

For the reaction

$$CHCl_3 + C_6H_6 \rightleftharpoons Cl_3CH \cdots C_6H_6 \quad (1)$$

the equilibrium constant in mole fraction units is

$$K = \frac{C(s + A + B - C)}{(A - C)(B - C)} \quad (2)$$

where $C$ is the number of moles of complex formed, $s$ is the number of moles of inert solvent, in this case cyclohexane, $A$ is the initial number of moles of chloroform, and $B$ is the initial number of moles of benzene. The observed proton chemical shift, $\delta_{obsd}$ is given by the expression

$$\delta_{obsd} = \frac{C}{A}\delta_{complex} + \frac{A - C}{A}\delta_{free} \quad (3)$$

(comparable with equations in references 11 and 28) in which $C/A$ and $(A - C)/A$ are the fractions of complexed and free chloroforms, respectively, and in which $\delta_{complex}$ and $\delta_{free}$ are the chemical shifts of chloroform in the complex and of unassociated chloroform, respectively.

The difference between chemical shifts of molecules in solution and those of isolated gas molecules can be expressed in terms of the screening constant, $\sigma_{solvent}$, due to the presence of the solvent. In a recent paper, Buckingham, Schaefer, and Schneider[29] attributed $\sigma_{solvent}$ to contributions from the bulk magnetic susceptibility of the medium $\sigma_b$, the magnetic anisotropy of the solvent molecules $\sigma_a$, the van der Waals forces between solute and solvent $\sigma_w$, and the polar effect $\sigma_E$ according to the equation

$$\sigma_{solvent} = \sigma_b + \sigma_a + \sigma_w + \sigma_E \quad (4)$$

In addition to these physical effects, chemical association, for example hydrogen bonding, can contribute to $\delta_{obsd}$. For the determination of the extent of hydrogen bond formation by n.m.r., the contributions to $\sigma_{solvent}$ must be eliminated or compensated for.

## Experimental

**Chemicals.**—Chloroform was washed with concentrated sulfuric acid, dilute sodium hydroxide, and ice water.[30] The chloroform then was dried over potassium carbonate and distilled shortly before use (b.p. 61.0°).

Thiophene-free benzene and cyclohexane were distilled three times through a Vigreux column and dried over sodium wire (b.p. 80.0° and 81.3°).

Triethylamine was distilled from acetic anhydride, dried with activated alumina, and distilled three times under reduced pressure.[30] The triethylamine then was stored over potassium hydroxide and was redistilled just before use (b.p. 89.4°).

Tetramethylsilane was obtained from Anderson Chemical Company.

Dimethylacetylene, shown by mass spectrometry to be very pure, was donated by Mr. E. Meyer of this department.

**N.m.r. Measurements.**—All n.m.r. spectra were observed with a Varian Associates, Inc., high-resolution spectrometer operating at 60 Mc. The 5-mm. o.d. Pyrex sample tubes were filled to a height of approximately 7 cm. Chemical shift measurements were made by the side-band technique with a standard deviation of approximately 0.008 p.p.m. Chemical shifts are reported in p.p.m., a negative shift indicating resonance at an applied field lower than that required for the reference. Careful thermostating of samples to within ±0.2° was achieved with an instrument designed by Dr. D. DeFord and built by J. Palmer.[31]

## Results and Discussion

In Table I and Fig. 1 are presented the chemical shifts $\delta_{obsd}$ of chloroform, 0.015 mole fraction, in solutions with various ratios of moles of cyclohexane to moles of cyclohexane plus moles of benzene, $s/(s + B)$. A low, fixed concentration of chloroform was chosen to avoid the effects of self-association of chloroform. The plot, Fig. 1 of ref. 12, of $\delta_{obsd}$ for chloroform as a function of concentration in cyclohexane demonstrates the absence of observable hydrogen bonding between chloroform molecules at the concentration of 0.015 mole fraction. Recently,[32] the equilibrium constant for the self-association of chloroform was reported to be 0.16 ± 0.006 (m.f.)$^{-1}$. We have observed a comparable association of chloroform with carbon tetrachloride.

TABLE I

OBSERVED CHEMICAL SHIFTS OF CHLOROFORM IN SOLUTIONS CONTAINING 0.015 MOLE FRACTION CHLOROFORM, $s$ MOLES OF CYCLOHEXANE, AND $B$ MOLES OF BENZENE

| $\frac{s}{s + B}$ | $\delta_{obsd}$. (p.p.m.; reference: cyclohexane) 25.5° | 35.0° | 43.5° | 59.0° | 74.5° |
|---|---|---|---|---|---|
| 1.00 | −5.65 | −5.65 | −5.65 | −5.65 | −5.65 |
| 0.90 | −5.47 | .... | −5.50 | −5.52 | −5.54 |
| .75 | −5.28 | −5.30 | −5.32 | −5.35 | −5.40 |
| .50 | −5.05 | −5.09 | −5.12 | −5.17 | −5.20 |
| .25 | −4.88 | −4.91 | −4.94 | −5.03 | −5.07 |
| .10 | −4.81 | −4.84 | −4.89 | −4.95 | −4.99 |
| .02 | −4.78 | −4.82 | .... | .... | .... |
| $K$ | 1.30 | 1.20 | 1.08 | 0.93 | 0.82 |

Rearrangement of equation 3 gives

$$\delta_{obsd} = \frac{C}{A}(\Delta) + \delta_{free} \quad (5)$$

where $\Delta$ is the hydrogen bond shift ($\delta_{complex} - \delta_{free}$). For assumed values of $K$, the fraction $C/A$ can be evaluated from eq. 2. The plot of $\delta_{obsd}$ as a function of $C/A$ is a straight line only for the correct $K$. After determining $K$ to within 0.10 (m.f.)$^{-1}$, $\Delta$ and $\delta_{free}$ can be obtained from the slope and intercept, respectively. Values of $K$ at various temperatures are presented in Table I. At each temperature, $\Delta$ is $1.56_2$, $\delta_{complex}$ is $-4.08_8$, and $\delta_{free}$ is −5.65 p.p.m., within experimental error.

The importance of the various contributions to $\sigma_{solvent}$ and reasons for the choice of the chloroform–benzene–cyclohexane system will be considered next. It is sufficient to choose a system in which the magnitudes of the contributions of $\sigma_{solvent}$

(27) R. E. Glick and D. F. Kates, *J. Phys. Chem.*, **62**, 1469 (1958).

(28) H. S. Gutowsky and A. Saika, *J. Chem. Phys.*, **21**, 1688 (1953).

(29) A. D. Buckingham, T. Schaefer, and W. G. Schneider, *ibid.*, **32**, 1227 (1960).

(30) A. Weissberger, "Techniques of Organic Chemistry," Vol. 7, Interscience Publishers, New York, N. Y., 1949.

(31) J. Palmer, "Studies of Hydrogen Isotope Exchange in Transition Metal Amine Complexes," Thesis, Northwestern University, 1960.

(32) C. F. Jumper, M. T. Emerson, and B. B. Howard, *J. Chem. Phys.*, **35**, 1911 (1961).

to $\delta_{complex}$ and $\delta_{free}$ have the same value at each concentration studied. That is, the resonances of the reference, the free chloroform, and the hydrogen-bonded chloroform must be affected to the same extent in a given sample, and the field at each hydrogen nucleus being observed must change by the same amount when the composition of the solvent is varied.

The effect of bulk magnetic susceptibility, $\sigma_b$, can be eliminated readily for a series of solutions of different concentrations by using an internal reference, cyclohexane in the present case.

Buckingham, Schaefer, and Schneider[29] demonstrated a linear correlation between the proton shift ($\delta_{solution} - \delta_{gas}$) of methane and the heat of vaporization at the boiling point of the solvent for thirteen solvents with small or zero magnetic anisotropies. The heat of vaporization at the boiling point of the pure solvent should be an indirect measure of the van der Waals interaction energy between the solvent and a given solute at dilute concentrations and, therefore, also proportional to $\sigma_w$.[29] Since the heats of vaporization of cyclohexane and benzene at their boiling points are 7.18 and 7.34 kcal./mole,[33] respectively, the effects of the van der Waals interactions with the dilute chloroform and with the reference, cyclohexane, should be approximately constant over the concentration range from almost pure cyclohexane to almost pure benzene.

The contribution, $\sigma_a$, due to the magnetic anisotropy of the solvent, should be approximately constant for solute molecules of the same shape. Since the shapes of chloroform and cyclohexane differ, the following experiments were designed to ascertain the importance of the shape of the solute in benzene–cyclohexane solutions. The proton resonance shift, $\delta_{solute-C_6H_{12}}$, was determined for differently-shaped inert molecules at concentrations of 0.01 mole fraction in solutions varying in concentration from 0.99 mole fraction benzene and 0 mole fraction cyclohexane to 0 mole fraction benzene and 0.99 mole fraction cyclohexane. Over this range of concentrations, $\delta_{(solute-C_6H_{12})}$ increased 0.04 p.p.m. for spherically-shaped tetramethylsilane and decreased 0.05 p.p.m. for linearly-shaped dimethylacetylene. The small variations of both $\delta_{(Si(CH_3)_4-C_6H_{12})}$ and $\delta_{(CH_3C\equiv CCH_3-C_6H_{12})}$ were linear with concentration. The magnitude of $\delta_{(solute-C_6H_{12})}$, for the tertiary hydrogen of isobutane which has a shape comparable with that of chloroform, could not be measured accurately in the isobutane–cyclohexane–benzene system due to overlapping of peaks. However, there is no variation of $\delta_{\underline{H}C(CH_3)_3-Si(CH_3)_4}$ with concentration in solutions containing 0.04 mole fraction of isobutane, 0.01 mole fraction of tetramethylsilane, benzene, and carbon tetrachloride, with the concentration of benzene ranging from 0 to 0.95 mole fraction. Therefore, it is concluded that the contributions of $\sigma_a$ to the chemical shifts of chloroform and of the reference, cyclohexane, do not differ by more than 0.04 p.p.m. No corrections were made for this small effect. However, the benzene–chloroform complex differs from other molecules discussed above due to the proton in the hydrogen bond being near the center of the complex and therefore probably being less affected by the magnetic anisotropy of benzene. Consider the resonance frequencies of free chloroform, cyclohexane, and complexed chloroform first in a solution containing 0.015 mole fraction (m.f.) chloroform, 0.015 m.f. benzene, and 0.97 m.f. cyclohexane, and then in a solution containing 0.015 m.f. chloroform, 0.97 benzene, and 0.015 cyclohexane. Even after corrections for magnetic susceptibilities, the resonance frequencies of free chloroform and of cyclohexane are greater in the latter solution, but the difference between the frequencies should remain approximately constant. On the other hand, the resonance frequency of the complex *may* not increase as much as that of cyclohexane and thus $\delta_{complex-C_6H_{12}}$ would vary with concentration. The maximum effect on the calculated equilibrium constant of different contributions of $\sigma_a$ was estimated as follows. The difference of the solution shifts of methane in benzene and in cyclohexane is 0.41 p.p.m. (Table I, ref. 29) after correction for magnetic susceptibilities. With the assumptions that the magnetic anisotropy of benzene would shift the resonance frequencies of both dilute free chloroform and dilute cyclohexane to a higher field by 0.41 p.p.m., and that the high field shift of dilute complex would be only one-fourth of this amount, the observed frequencies should be given by the equation

$$\delta_{obsd.} = \frac{C}{A}\left[\delta_{complex} + (0.75)(-0.41)\left(\frac{B}{s+B}\right)\right] + \left(\frac{A-C}{A}\right)\delta_{free} \quad (6)$$

With eq. 6, the calculated and observed average frequencies match if $K = 0.83$ at 25.5° with $\delta_{complex} = -3.394$ p.p.m. This result increases somewhat the uncertainty of the above calculations. The values $\delta_{complex} = -3.74 \pm 0.40$ and $K_{25°} = 1.06 \pm 0.30$ (m.f.)$^{-1}$ appear reasonable.

The polar effect, $\sigma_E$, arises from neighboring polarized solvent molecules which produce an electric field at the polar solute and therefore a change in electronic structure and nuclear screening. The magnitude of $\sigma_E$ is given[34] approximately by

$$\sigma_E = -2 \times 10^{-12}\,[(\epsilon - 1)/(2\epsilon + 2.5)](\mu \cos\phi/\alpha) - 10^{-18}\,[(\epsilon - 1)/(2\epsilon + 2.5)]^2\,(\mu^2/\alpha^2) \quad (7)$$

where $\epsilon$ is the dielectric constant of the solvent, $\mu$ is the permanent dipole moment of the solute molecule, $\phi$ is the angle between the permanent dipole moment of the solute and the X–H bond, and the polarizability, $\alpha$, of the solute is assumed to be $[(n^2 - 1)/(n^2 + 2)]r^3$ in which $n$ and $r$ are the refractive index and average radius, respectively. The contribution of $\sigma_E$ to the chemical shift of cyclohexane is, of course, zero. The magnitude of $\sigma_E$ is −0.043 p.p.m. for chloroform at infinite dilution in benzene and is −0.038 p.p.m. for chloroform

(33) R. R. Dreisbach, "Physical Properties of Chemical Compounds," American Chemical Society, Washington, D. C., 1955.

(34) A. D. Buckingham, *Can. J. Chem.*, **38**, 300 (1960).

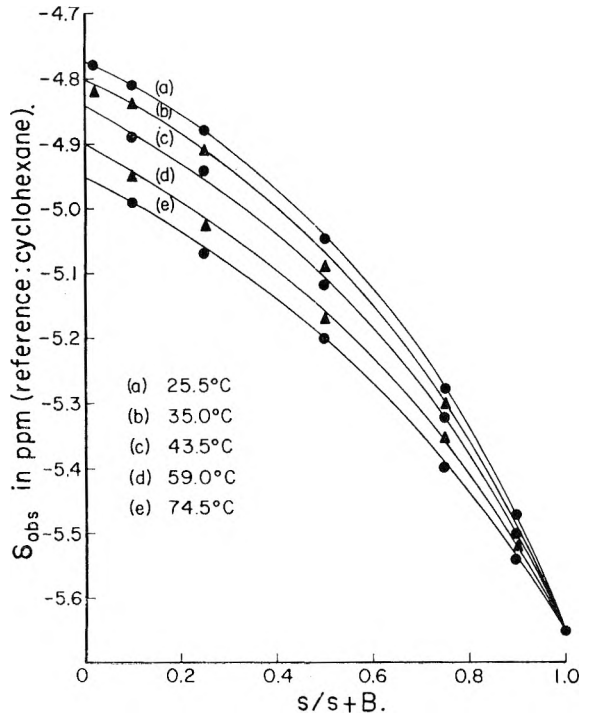


Fig. 1.—Chemical shift of the chloroform proton resonance, $\delta_{obsd}$, as a function of the ratio of moles of cyclohexane to moles of cyclohexane plus moles of benzene, $s/(s + B)$, at several temperatures.

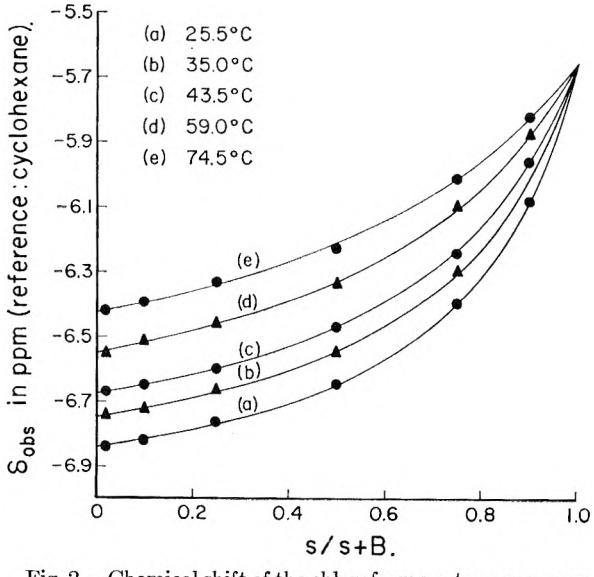


Fig. 2.—Chemical shift of the chloroform proton resonance, $\delta_{obsd}$, as a function of the ratio of moles of cyclohexane to moles of cyclohexane plus moles of triethylamine, $s/(s + B)$, at several temperatures.

at infinite dilution in cyclohexane, using eq. 7, 1.02 $\times 10^{-18}$ e.s.u. for $\mu$, +1 for cos $\phi$, and 2.28 and 2.02 for $\epsilon$ of benzene and cyclohexane, respectively. The calculated change in $\sigma_E$ in going from cyclohexane to benzene as the solvent is 0.005 p.p.m. and within experimental error; therefore, no correction for $\sigma_E$ is required for the chloroform–benzene–cyclohexane system.

**Thermodynamic Constants.**—The slope of a log $k$ *vs.* $1/T$ plot gives $\Delta H = -1.97 \pm 0.35$ kcal. mole$^{-1}$. A total uncertainty of 0.35 kcal. mole$^{-1}$ is assigned since comparable calculations using eq. 6 led to a value differing by 0.15 kcal. mole$^{-1}$. For $K_{25°} = 1.06$ (m.f.)$^{-1}$, $\Delta S$ is $-6.5 \pm 0.5$ cal. mole$^{-1}$ deg.$^{-1}$.

In view of the association of chloroform and benzene, it is reasonable that the use of benzene, instead of cyclohexane or carbon tetrachloride, as a solvent in the study of hydrogen bond formations leads to appreciably smaller magnitudes of $K$ and $\Delta H$.[35] It is concluded that benzene cannot be employed as an "inert" solvent in investigations of hydrogen bonding.

**The Chloroform–Triethylamine–Cyclohexane System.**—The association of chloroform and triethylamine also was investigated by the above procedure. The concentration of chloroform was 0.015 mole fraction and cyclohexane was the solvent in all of the samples. In Table II and in Fig. 2 are presented the observed chemical shifts for various concentrations, $s/(s + B)$. The equilibrium constants calculated from a linear plot of $\delta_{obsd}$ as a function of $C/A$ also are presented in Table II. At 25°, the chemical shift of the chloroform–triethylamine complex is −7.13 p.p.m. relative to cyclohexane, and the hydrogen bond shift, $\Delta$, is $-1.48 \pm 0.04$ p.p.m. The hydrogen bond shift decreased monotonically with increasing temperature and was approximately −1.27 p.p.m. at 74.5°.

TABLE II

OBSERVED CHEMICAL SHIFTS OF CHLOROFORM IN SOLUTIONS CONTAINING 0.015 MOLE FRACTION CHLOROFORM, $s$ MOLES OF CYCLOHEXANE, AND $B$ MOLES OF TRIETHYLAMINE

| $\frac{s}{s + B}$ | $\delta_{obsd}$. (p.p.m.; reference, cyclohexane) 25.5° | 35.0° | 43.5° | 59.0° | 74.5° |
|---|---|---|---|---|---|
| 1.00 | −5.65 | −5.65 | −5.65 | −5.65 | −5.65 |
| 0.90 | −6.08 | .... | −5.96 | −5.87 | −5.82 |
| .75 | −6.39 | −6.29 | −6.24 | −6.09 | −6.01 |
| .50 | −6.64 | −6.54 | −6.47 | −6.33 | −6.23 |
| .25 | −6.76 | −6.66 | −6.60 | −6.46 | −6.33 |
| .10 | −6.82 | −6.70 | −6.65 | −6.51 | −6.39 |
| .02 | −6.84 | −6.74 | −6.67 | −6.55 | −6.42 |
| $K$ | 4.20 | 3.50 | 3.10 | 2.10 | 1.60 |

From the plot of log $K$ as a function of $1/T$, $\Delta H$ is $-4.15 \pm 0.20$ kcal. mole$^{-1}$. With $K_{25°}$ expressed as (m.f.)$^{-1}$, $\Delta S$ is −11.0 cal. mole$^{-1}$ deg.$^{-1}$. Barrow and Yerger[7] reported the equilibrium constant, 0.36 l./mole, from an investigation by infrared absorption of the association of chloroform-*d* and triethylamine in carbon tetrachloride. The present value, $4.2 \pm 0.2$ (m.f.)$^{-1}$ or $0.51 \pm 0.02$ l./mole, should be higher than the value obtained with carbon tetrachloride as the solvent, due to the interaction, mentioned above, of chloroform and carbon tetrachloride. Huggins, Pimentel, and Shoolery[11] reported $K_{28°} = 3.0 \pm 1.0$ (m.f.)$^{-1}$ and $\Delta H = -4$ kcal. mole$^{-1}$ (−23° to +28°) from n.m.r. observations of association in the two-component system, chloroform–triethylamine. The agreement is satisfactory.

**Acknowledgment.**—C. J. C. wishes to acknowledge that this investigation was carried out during the tenure of a Predoctoral Fellowship from the Division of General Medical Sciences, United States Public Health Service.

(35) See data in Appendices B and C, ref. 15.

# PHOTOCHEMICALLY-INDUCED OXIDATION OF ARSENITE: EVIDENCE FOR THE EXISTENCE OF ARSENIC(IV)

BY MALCOLM DANIELS

*Radioisotope Applications Division, Puerto Rico Nuclear Center, Rio Piedras, P. R., and Chemistry Department, University of Puerto Rico, Rio Piedras, P. R.*

*Received March 7, 1962*

Hydrogen peroxide has been photolyzed by 2537 Å. radiation in the presence of arsenite ion under conditions of complete radical scavenging. In the absence of oxygen, hydrogen peroxide is consumed and arsenate formed in equivalent amounts which show an exponential dependence on the duration of photolysis, $\phi_i(-H_2O_2) = 0.55$, $\phi_i(As(V)) = 0.47$. When oxygen is added to the system, consumption of hydrogen peroxide ceases, formation of arsenate becomes linear with time and the quantum yield effectively doubles, $\phi_i(As(V))_{O_2}/\phi(As(V)_{O_2-free} = 1.9$. It is shown that these results are evidence for the existence of an intermediate oxidation state of arsenic, As(IV), which is capable of reacting with oxygen to form a peroxy radical $As(IV)\cdot O_2$. Implications concerning the photolysis of $H_2O_2$ are discussed.

## Introduction

Previous investigation of the radiation chemistry of arsenite solution[1] gave results which were interpreted in terms of a transitory intermediate oxidation state, As(IV), capable of reaction with oxygen. It obviously was desirable to get further evidence from an independent method to support this postulate. Accordingly oxidation of arsenite has been initiated by OH radicals generated by the photolysis of hydrogen peroxide solutions under suitably chosen conditions, and the effect of oxygen on the course of the reaction has been investigated.

## Experimental

(i) **Apparatus.**—Photolyses were carried out in a fused quartz vessel of the type previously described,[2] such that solutions could be readily degassed without contamination. A 550-w. Hanovia low pressure mercury arc supplied from a Ferranti voltage stabilizer was used in most of the work. The radiation, chiefly 1849 and 2537 Å., was condensed and filtered by a cobalt–nickel filter solution[3] in a spherical quartz flask and the photolysis vessel was cooled by a centrifuged blower. Under these conditions, no 1849 Å. radiation reached the photolysis vessel. Chemical actinometers were compared using a Mineralight lamp.

(ii) **Actinometry.**—Both the monochloroacetic acid[4] and ferrioxalate[5] systems were used as chemical actinometers.

Intensity of incident light was determined under conditions of complete absorption, giving the value $0.96 \times 10^{-4}$ einstein/l./min. From this the fraction of light absorbed by the peroxide–arsenite mixture was found to be 5.3%. Optical density of the mixture was calculated from literature values for $\epsilon(H_2O_2)$[6] of 19.6.

In view of uncertainties in the quantum yield of the monochloroacetic acid actinometer,[4,7] the incident light was redetermined by the ferrioxalate method. Using $\phi_{2537} = 1.20$ for the latter,[5] agreement was obtained between the two methods if $\phi_{Cl^-} = 0.25$, this being a short extrapolation of the results of Smith, Leighton, and Leighton to 19° (the temperature of the photolyses).

(iii).—Reagents and preparation of solutions were as previously described.[1] 90% unstabilized $H_2O_2$ (Laporte) was suitably diluted with triple-distilled water. The procedure for degassing before photolysis, and the collection of gases afterwards, has been described,[2] as have the analytical methods.[1] Gas analysis was carried out on a Metropolitan Vickers M.S.2 mass spectrometer.

## Results

Conditions in which unambiguous results could be obtained were limited by properties of the system. Thus, to eliminate chain decomposition of hydrogen peroxide and to facilitate efficient scavenging of OH radicals by arsenite, the hydrogen peroxide concentration was kept low. The arsenite concentration, however, was limited by thermal reaction with hydrogen peroxide. Preliminary experiments on arsenite–peroxide mixtures showed the following concentrations to be stable for several hours at room temperature, and they were used in all subsequent experiments.

$$(H_2O_2)_0 = 200\ \mu M,\ (As(III))_0 = 2\ mM,$$
$$H_2SO_4 = 0.1\ N$$

It was essential to be certain that chemical reactions should be ascribable only to light absorbed by the hydrogen peroxide. Consequently the absorption spectrum of arsenite in acid solution was measured, and showed no appreciable absorption above 2200 Å., in agreement with Goldfinger and von Schweinitz.[8] As a further check, acid arsenite solutions alone were irradiated in the presence and absence of oxygen. In no case was any chemical reaction observed. Accordingly it was demonstrated that the presence of hydrogen peroxide was necessary for photolysis to occur.

(i) **Photolysis in the Absence of Oxygen.**—Results for oxygen-free solutions are shown in Fig. 1. Hydrogen peroxide was consumed and arsenate formed in equivalent amounts. At any one time, the sum of arsenate formed and peroxide consumed is constant, indicating that no other product is formed. This was checked by carrying out gas analyses and a typical gas analysis after 60 min. was

| | | |
|---|---|---|
| $N_2$ | 24% | Total gas = 14 μmoles |
| $O_2$ | 20% | |
| $CO_2$ | 54% | |
| $H_2$ | 0% | |

Accordingly the stoichiometry is simply

$$H_2O_2 + As(III) \longrightarrow H_2O + As(V)$$

As would be expected for such a small fractional light absorption, change of concentrations is an

(1) M. Daniels and J. Weiss, *J. Chem. Soc.*, 2467 (1958).
(2) T. Rigg and J. Weiss, *J. Chem. Phys.*, **20**, 1144 (1952).
(3) M. Kasha, *J. Opt. Soc. Am.*, **38**, 929 (1948).
(4) R. N. Smith, P. A. Leighton, and W. G. Leighton, *J. Am. Chem. Soc.*, **61**, 2299 (1939).
(5) C. A. Parker, *Proc. Roy. Soc.* (London), **A235**, 518 (1956).
(6) W. C. Schumb, C. N. Satterfield, and R. L. Wentworth, "Hydrogen Peroxide," A. C. S. Monograph, 1955.
(7) L. Kuchler and H. Pick, *Z. physik. Chem.*, **B45**, 116 (1940).
(8) P. Goldfinger and G. von Schweinitz, *ibid.*, **B19** 219 (1932).

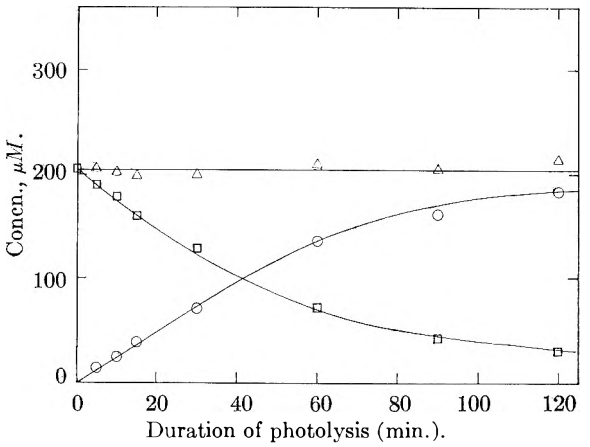


Fig. 1.—Photolysis of oxygen-free arsenite–peroxide mixtures: □, $H_2O_2$; ○, As(V); △ = $\Sigma H_2O_2$ + As(V).

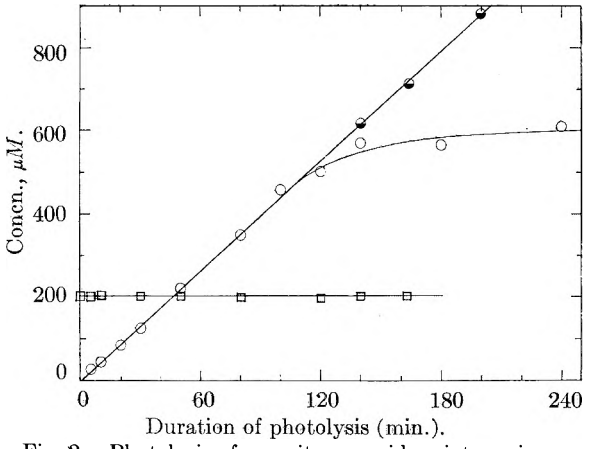


Fig. 2.—Photolysis of arsenite–peroxide mixtures in presence of oxygen: ○, As(V) (air-saturated); ◒, As(V) (oxygen-saturated); □, $H_2O_2$.

exponential function of the time of photolysis, $-d(H_2O_2)/dt = k_{Abs.}$ and in very dilute solution $I_{Abs.} \simeq I_0 \epsilon c l$, so that $-d \ln(H_2O_2)/dt = kI_0\epsilon l$. From the initial slopes, the following quantum yields were obtained

$$\phi_i(-H_2O_2) = 0.55 \quad \phi_i(As(V)) = 0.47$$

(ii) **Photolysis in the Presence of Oxygen.**—When photolysis of the mixture is carried out using air-equilibrated solutions ($[O_2]_0 \sim 255$ $\mu M$) the behavior changes completely. No hydrogen peroxide is consumed at all, although its presence has been shown to be necessary for oxidation to occur. Arsenate formation is now a linear function of time and occurs at an increased rate compared to the $O_2$-free case until available oxygen has been consumed.

Results for As(V) and $H_2O_2$ in air-equilibrated solutions obtained after approximately 120 min. were rather erratic and it is suggested that this is due to continued absorption of $O_2$ from the gas phase above the photolyzed solution. These results therefore are not considered in the discussion. That the change in slope is indeed due to oxygen consumption was shown by photolyzing oxygen saturated solutions ($[O_2]_0 \sim 1250$ $\mu M$) when the initial rate was maintained well past the previous point of inflection. Furthermore, at this point the arsenate concentration is 530 $\mu M$—approximately double the initial oxygen concentration of air-equilibrium solution. Accordingly, the over-all process and stoichiometry now follows the equation

$$O_2 + 2As(III) \longrightarrow 2As(V)$$

with the quantum yield $\phi(As(V))_{O_2} = 0.9$. The results are shown in Fig. 2.

## Discussion

**A. Photolysis of Oxygen-Free Solutions.**—It is now satisfactorily established[9-11] that under suitable conditions of high light intensity and low concentration, hydrogen peroxide can be photolyzed in a non-chain manner, at a quantum yield $\phi(-H_2O_2)$ of 1.0 at room temperature. The commonly accepted mechanism accounting for this is the reaction sequence (1)–(3) (consideration of an alternative

$$H_2O_2 \longrightarrow 2OH \qquad (1)$$

$$OH + H_2O_2 \longrightarrow H_2O + HO_2 \qquad (2)$$

$$2HO_2 \longrightarrow H_2O_2 + O_2 \qquad (3)$$

formulation is given below), which infers that the primary quantum yield $\phi_p(-H_2O_2)$ is 0.5. This value is the same as that reported here for photolyses in oxygen-free solution. In view of the evidence from radiation chemistry[1] that arsenite reacts readily with OH radicals, together with the evidence presented here for complete scavenging of OH radicals (*i.e.*, absence of $O_2$ formation), it is suggested that the behavior in oxygen-free solution can be satisfactorily represented by reaction 1 fol-

$$OH + As(III) \longrightarrow H_2O + As(IV) \qquad (4)$$

$$2As(IV) \longrightarrow As(III) + As(V) \qquad (5)$$

lowed by (4) and (5), noting that existence of the intermediate oxidation state As(IV) again is presumed. This will lead to $\phi_i(-H_2O_2) = \phi_i(As(V)) = 0.5 = \phi_p(-H_2O_2)$, in reasonable agreement with the values reported here. It also should be noted that reactions 4 and 5 are utilized in accounting for the radiation chemistry of oxygen-free solution.[12] However, in itself this no proof of the existence of As(IV); this arises from consideration of the effect of oxygen.

**B. Photolysis of Oxygenated Solutions.**—It has been shown (see Results) that peroxide is necessary for oxidation of arsenite to occur when oxygen is present. Clearly then, as there is no net consumption of peroxide, it must be regenerated in the course of the secondary reactions. Furthermore, as oxygen has no effect on the photolysis of peroxide alone, such secondary reactions must involve the arsenic species, and as neither arsenite nor arsenate react with oxygen at this pH, it must be concluded that the only other possible species, As(IV), is the reactive entity. In the presence of oxygen, then, it is suggested that reaction 4 is suc-

(9) J. P. Hunt and H. Taube, *J. Am. Chem. Soc.*, **74**, 5999 (1952).
(10) J. L. Weeks and M. S. Matheson, *ibid.*, **78**, 1273 (1956).
(11) J. H. Baxendale and J. A. Wilson, *Trans. Faraday Soc.*, **53**, 344 (1957).
(12) M. Daniels, *J. Phys. Chem.*, **66**, 1475 (1962).

ceeded by formation of a peroxy radical according to

$$As(VI) + O_2 \longrightarrow As(IV)\cdot O_2 \qquad (6)$$

the relevant structures being represented as

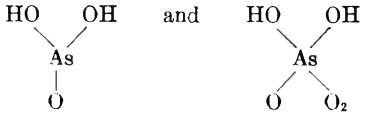


As the quantum yield is not changed by increasing the oxygen concentration fivefold, it seems that reaction 6 is 100% effective in the present conditions.

Subsequent reactions of As(IV) are not so clear. On the basis of the present work we cannot distinguish between the following two modes of reaction.

$$As(IV)\cdot O_2 \longrightarrow As(V) + HO_2 \qquad (7a)$$

followed by reaction 3, or

$$2As(IV)\cdot O_2 \longrightarrow 2As(V) + H_2O_2 + O_2 \qquad (7b)$$

and indeed distinction is irrelevant for the present purpose. Both of these reactions lead to the regeneration of $H_2O_2$ together with a doubling of the quantum yield of arsenate compared to the $O_2$-free solution (experimentally $\phi_i(As(V))_{O_2}/\phi_i(As(V))_{O_2\text{-free}} = 1.9$) and it is concluded then that reactions 1, 4, 6, and 7 give an adequate account of the behavior of oxygenated solution.

It is hoped to obtain further evidence concerning reaction 7 from two sources: (a) rapid reaction whether the peroxy radical disappears by either first-order or second-order kinetics, and (b) the kinetics of the radiation-induced chain reaction[1,13] having reaction 7 as termination steps should show either first power or half power intensity dependence, respectively.

(13) M. Daniels, communication in preparation.

At the beginning of this discussion an alternative mechanism for the photolysis of hydrogen peroxide was mentioned and it is appropriate to consider the implications of this now. On the basis of oxygen fractionation experiments it was pointed out by Hunt and Taube[9] that the net primary step of photolysis may be

$$H_2O_2 \longrightarrow (HO + OH) \longrightarrow H_2O + O \qquad (8)$$

followed under non-chain conditions by

$$O + O \longrightarrow O_2 \qquad (9)$$

In this case, then, the primary quantum yield is identical with the observed quantum yield of 1.0. Arsenite would be expected to be a ready scavenger for oxygen atoms, according to

$$As(III) + O \longrightarrow As(V) \qquad (10)$$

so that if photolysis followed this pattern, then according to the evidence and arguments presented above, arsenate should be formed at a quantum yield of 1.0 in oxygen-free solution. Further, as arsenite should (according to (10)) proceed directly in a one-step reaction to arsenate, oxygen should have no effect on the quantum yield. Neither of these expectations is fulfilled, and it is concluded that the results reported here are evidence against the photolysis of hydrogen peroxide producing kinetically significant quantities of freely diffusing oxygen atoms.

**Acknowledgments.**—This work was carried out at King's College, Newcastle-on-Tyne, Argonne National Laboratory, Argonne, Illinois, and University College of the West Indies, Kingston, Jamaica. Thanks are due to Professor J. Weiss, for encouragement and interest while the major part of the experimental work was carried out and to A.E.R.E. (Harwell) for support and permission to publish.

# THE RADIATION CHEMISTRY OF ARSENITE. PART II. OXYGEN-FREE SOLUTION

BY MALCOLM DANIELS

*Radioisotope Applications Division, Puerto Rico Nuclear Center, Rio Piedras, P. R., and Chemistry Department, University of Puerto Rico, Rio Piedras, P. R.*

*Received March 7, 1962*

Irradiation of oxygen-free solutions of arsenite at pH 2.7 produced hydrogen and arsenate in small, equivalent amounts. $G(H_2) = 0.45$, $G(As(V)) = 0.48$. Hydrogen peroxide was not formed. Irradiation of oxygen-free mixtures of arsenite and hydrogen peroxide showed increased formation of arsenate and consumption of hydrogen peroxide. $G$-values increased with the ratio $(H_2O_2)_0/(As(III))_0$ to the limiting values of $G(As(V)) = 3.3$ and $G(-H_2O_2) = 2.8$. The hydrogen yield is unaffected and no oxygen is formed. Results are interpreted in terms of an intermediate oxidation state As(IV), and competition between arsenite and hydrogen peroxide for H atoms.

## Introduction

Previous work[1] on the radiation chemistry of the arsenite system concerned the effect of pH in oxygenated solutions, and showed, not surprisingly, that oxidation was the major process. The present work, which was a natural continuation, was aimed at determining (1) whether net oxidation or reduction of arsenite would take place in the absence of oxygen, (2) the yields of the "molecular products" $H_2$ and $H_2O_2$, (3) the mode of reaction of the primary radicals H and OH and the secondary radical As(IV).

(1) M. Daniels and J. Weiss, *J. Chem. Soc.*, 2467 (1958).

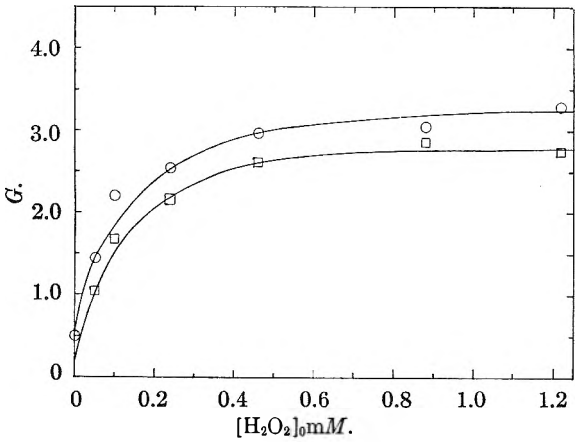


Fig. 1.—Rate of formation of arsenate and rate of consumption of $H_2O_2$ as a function of concentration of $H_2O_2$ added prior to irradiation: ○, $G(As(V))$; □, $G(-H_2O_2)$; $(As(III))_0$ = 1 m$M$, pH 2.7.

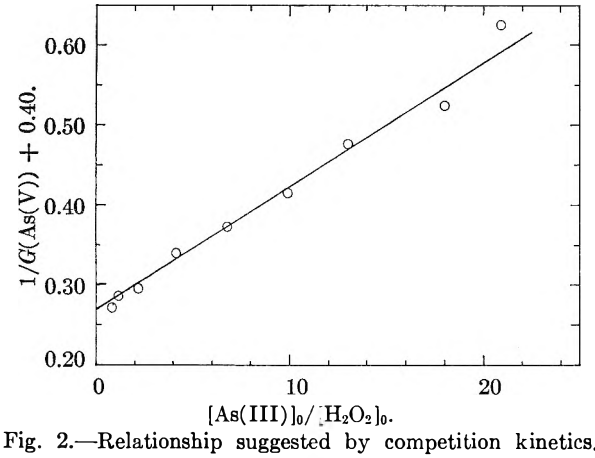


Fig. 2.—Relationship suggested by competition kinetics.

## Experimental

All experimental techniques have been described previously.[1,2] With one exception all experiments were at pH 2.7, obtained by neutralizing an alkaline solution of arsenious oxide with $H_2SO_4$. The radiation source was 200-kv. X-rays, unfiltered at a dose rate of $1.81 \times 10^{20}$ e.v./l./min., measured by the Fricke dosimeter.

## Results

The only products detectable after irradiation of 1 m$M$ arsenite were hydrogen gas and arsenate, both in low yield. Linear yield–dose curves were obtained, and a typical gas analysis was

| | |
|---|---|
| $H_2$ | 94.4% |
| $O_2$ | 0.6% |
| $N_2$ | 4.5% |
| $CO_2$ | 0.5% |

on a gas volume of 5 $\mu$moles. The rates of formation were $G(H_2) = 0.45$, $G(As(V)) = 0.48$ and stoichiometry thus was satisfied. No hydrogen peroxide could be detected, even after prolonged irradiation ($3.2 \times 10^{22}$ e.v./l.), although it would be thermally stable toward arsenite at this pH. The absence of hydrogen peroxide suggested that it was concerned in the reactions leading to arsenate formation, and to test this, oxygen-free mixtures of arsenite and hydrogen peroxide were irradiated. The rate of arsenate formation was found to be increased, and at the same time hydrogen peroxide was consumed. Yield–dose curves were linear up to 30% conversion and $G(As(V))$ was always greater than $G(-H_2O_2)$. Results obtained for 1 m$M$ arsenite on varying the initial peroxide concentration from 0.05 to 1.2 m$M$ are shown in Fig. 1. $G$-values increase rapidly with peroxide concentration, however, reaching limiting values of $G(As(V)) = 3.3$ and $G(-H_2O_2) = 2.8$. Mass spectrometric analysis of gases at $0.46 \times 10^{-3}$ $M$ $H_2O_2$ showed the absence of oxygen and gave hydrogen as the only product. Typical analyses are

| | | |
|---|---|---|
| $H_2$ | 98.02% | 97.33% |
| $O_2$ | 0.42% | 1.29% |
| $N_2$ | 0.76% | 1.27% |
| $CO_2$ | 0.2% | 0.1% |

The yield of hydrogen was linear with dose and identical with that found in the absence of hydrogen peroxide, $G(H_2) = 0.45$. Schwarz, Losee, and Allen[3] with $Co^{60}$ $\gamma$-rays, report $G(H_2) = 0.45$ from 2 m$M$ arsenite at pH 10.4 and Fricke and Hart[4] report a similar yield with X-rays, independent of pH from 2 to 11. In a single experiment carried out here at pH 12.6 a result was obtained slightly higher than at pH 2.7, namely 0.48.

Under limiting yield conditions, satisfactory oxidation–reduction balance is obtained, in that

$$G(H_2) + G(-H_2O_2) = G(As(V))$$

Experiments also were carried out with arsenite concentrations ranging from 0.1 to 2.0 m$M$. All results on arsenite–peroxide mixtures are gathered together and presented in Fig. 2.

## Discussion

The low rate of formation of arsenate in the absence of added hydrogen peroxide is not surprising as the two primary radicals formed by radiolysis of water (generally considered to be H and OH) have opposing chemical effects. It has been shown[2] that OH radicals can oxidize arsenite to As(IV), a transitory oxidation state, and this is in accordance with previous studies of the radiation chemistry[1]

$$OH + As(III) \longrightarrow H_2O + As(IV) \quad (1)$$

As the measured rate of formation of hydrogen gas corresponds to that expected for "molecular product," it is reasonable to assume that the H atoms react in a reducing manner (the pH was chosen to avoid possible complications of $H_2^+$ formation and yet remain in the region of thermal stability of arsenite–peroxide mixtures). Furthermore, as reduction to arsenic can occur under certain conditions[5] the reaction of H atoms is written as

$$H + As(III) \longrightarrow As(II) + H^+ \quad (2)$$

Reaction of these two arsenic species means that

(2) M. Daniels, *J. Phys. Chem.*, **66**, 1473 (1962).

(3) H. Schwarz, A. Losee, and A. O. Allen, *J. Am. Chem. Soc.*, **76**, 4693 (1954).

(4) H. Fricke and E. J. Hart, *J. Chem. Phys.*, **3**, 596 (1935).

(5) M. Daniels, unpublished observations.

the two radicals H and OH largely cancel each other.

$$As(II) + As(IV) \longrightarrow 2As(III) \qquad (3)$$

The small yield of arsenate which is observed undoubtedly is connected with the non-appearance of "molecular yield" hydrogen peroxide and the slight excess of H atoms over OH radicals.[6] It is suggested that reaction of H atoms with arsenite is slow and that the arsenite does not protect the molecular yield peroxide against attack by the H atoms.

$$H + H_2O_2 \longrightarrow H_2O + OH \qquad (4)$$

Subsequent reactions of the As(IV) by

$$2As(IV) \longrightarrow As(III) + As(V) \qquad (5)$$

quantitatively accounts for the results obtained in the absence of added hydrogen peroxide and infers that $G(H_2O_2) = 0.96$. Values similar to this are reported for other systems using 200 kv. X-rays.[7,8]

This suggestion was tested by adding hydrogen peroxide prior to irradiation, in order to favor reaction 4 relative to reaction 2, with results which have been described above. The limiting rates are readily understood if reaction 2 (and hence also 3) is eliminated at high ratios of $H_2O_2$/As(III), for then

$$G(As(V)) = 1/2\ (gH + gOH)$$

and

$$G(-H_2O_2) = gH - gH_2O_2$$

Taking the above value for $g(H_2O_2)$ gives $g(H) = 3.75$ and $g(OH) = 2.8$. For pH 2.7 the figures are higher than expected, but there are unfortunately few well documented results for the variation of radical yields with pH using 200 kv. X-rays.

(6) A. O. Allen, *Radiation Res.*, **1**, 85 (1954).

(7) G. R. A. Johnson and J. Weiss, *Proc. Roy. Soc.* (London), **A340**, 189 (1957).

(8) J. D. Backhurst, G. R. A. Johnson, H. Scholes, and J. Weiss, *Nature*, **183**, 176 (1959).

Incidentally, the existence of limiting yields allows the possible reaction (6) to be discounted, as it would

$$As(IV) + H_2O_2 \longrightarrow As(V) + OH \qquad (6)$$

lead to a chain sequence. If the stationary state approximation, or its equivalent,[9] is applied to eq. 1–5, then the expression describing the competition kinetics is readily derived as

$$\frac{1}{G(As(V)) + 1/2\ (gH - gOH)} = \frac{1}{g(H)} + \frac{1}{gH}\frac{k_2}{k_4}\frac{(As(III))_0}{(H_2O_2)_0}$$

Figure 2 shows that this satisfactorily accounts for the experimental results. Internal consistency is shown by evaluation of $gH = 3.70$ from the intercept, and the ratio of the rate constants for reactions 2 and 4 then is obtained as

$$\frac{k_4}{k_2} \simeq 5 \times 10^{-2}$$

This bears out the suggestion above that reaction of H atoms with arsenite is slow, and comparison with results for the nitrite system[9] shows that the differences between the two may be largely ascribed to the differing rates of reaction with H atoms, *viz.*

$$\frac{k_H + NO_2}{k_H + As(III)} \sim 10$$

However, the pH difference between the nitrite and arsenite work must not be ignored and it may be that the reducing species (here designated H) are not the same in the two systems.

**Acknowledgments.**—This work was carried out at King's College, Newcastle-on-Tyne. Thanks are due to Professor J. Weiss for encouragement and interest while the major part of the experimental work was carried out and to A.E.R.E. (Harewell) for support and permission to publish.

(9) H. Schwartz and A. O. Allen, *J. Am. Chem. Soc.*, **77**, 1324 (1955).

# THE DETERMINATION OF SUBLIMATION EQUILIBRIA BY DIFFERENTIAL THERMAL ANALYSIS

BY MEYER M. MARKOWITZ AND DANIEL A. BORYTA

*Foote Mineral Co., Research and Engineering Center, Chemicals Division, Route 100, Exton, Pennsylvania*

*Received March 7, 1962*

A controlled-pressure d.t.a. method has been used to determine the solid–vapor characteristics of ammonium chloride as a function of temperature. The results obtained agree favorably with those previously derived by a static method. The data from the present study were used in the computation of the free energy, entropy, and average enthalpy of dissociation of ammonium chloride over the temperature range 230.2–338.2°.

## Introduction

The pressure–temperature relationships involving the vaporization of pure solids cannot be easily determined by visual observations as can many fusion and boiling phenomena. Accordingly, it is the intent to describe in this paper the use of differential thermal analysis (d.t.a.) in the determination of univariant sublimation equilibria and to illustrate in some detail the utility of such data in the specific case of ammonium chloride. The method described here essentially stems from the dynamic thermal analysis approach of Ramsay and

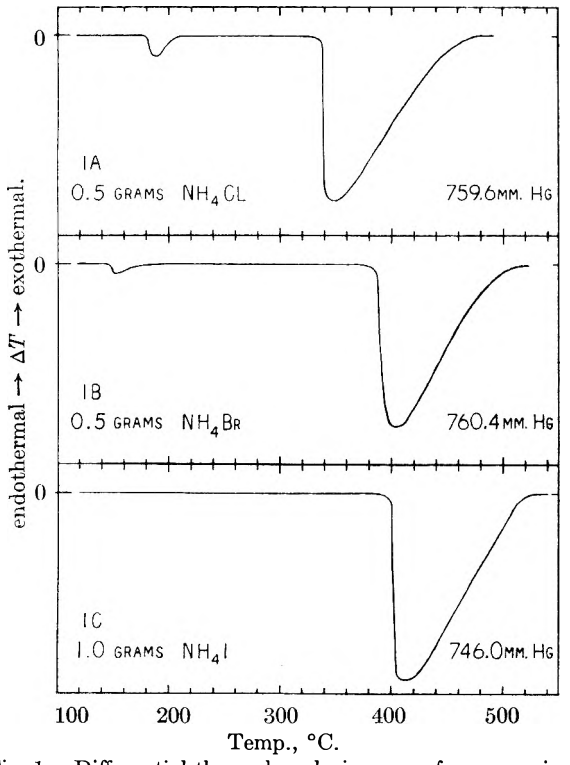


Fig. 1.—Differential thermal analysis curves for ammonium chloride, bromide, and iodide at atmospheric pressure.

Young,[1] who observed the temperature halts occasioned by subliming materials.

## Equipment and Procedures

D.t.a. experiments were performed in a system which permitted control of the pressure of the gaseous environment in which the sample was heated. The cylindrical aluminum heating block containing two symmetrically-placed holes for the sample and reference test tubes was held in a small crucible furnace (Furnace Type FD 101, Hoskins Mfg. Co., Detroit, Mich.). The current to the furnace was controlled by a motorized variable transformer which afforded essentially linear heating rates.[2] The instrumentation and arrangement of the thermocouples have been described previously.[3] Ignited alumina was used as the reference material.

The experimental sample was contained in a small test tube provided with two side arms. This assembly was connected to a suitable vacuum line. The Chromel–Alumel thermocouple was inserted into the sample through a glass well fitted to the test tube by a standard taper joint. The pressure in the system was maintained at the desired level by a mercury manostat to ±0.1 mm. (Cartesian Manostat No. 6A, Manostat Corp., New York 13, N. Y.). Absolute pressures in mm., corrected to 0°, were measured with a manometer to ±0.1 mm. (Manometer No. 10709, Manostat Corp.). All runs were performed in an argon atmosphere to prevent any possibility of air oxidation of the solid sample or of its vapors. At atmospheric pressure, a small flow of argon (50 cc./min. at ambient conditions) was passed through the system. Prior to evacuation and study under reduced pressures, the system was thoroughly flushed with argon.

D.t.a. runs were performed at atmospheric pressure on reagent grade ammonium chloride, bromide, and iodide at a heating rate of 3.5°/min. (Fig. 1). A sequence of determinations at this same heating rate but at varying pressures was made on ammonium chloride. The temperatures and pressures corresponding to the endotherms recorded during these latter experiments are listed in Table I. All samples were premixed with 0.5 g. of ignited alumina so as to avoid leaving a bare sample thermocouple after sublimation of the ammonium salt was complete. In each case the appropriate d.t.a. temperature (*i.e.*, extrapolated peak temperature) was derived from the point of intersection of the two extended straight lines drawn from the sides of the well defined endotherm indicative of crystallographic transition or of sublimation.[4,5]

## Results

In Fig. 1, the initial small, low temperature endotherms observed for ammonium chloride and bromide at atmospheric pressure correspond to the known crystallographic transitions from the cesium chloride to the sodium chloride structures.[6,7] These endotherms were determined to be reversible upon repeated cooling and heating cycles. The values determined in the present study for these transition temperatures are 186.3 ± 0.5° (average of 19 runs on $NH_4Cl$) and 146.3 ± 0.6° (average of 10 runs on $NH_4Br$). The corresponding values reported in the earlier literature are 184.3°[8] and 137.8°,[8] respectively, for ammonium chloride and bromide. Ammonium iodide undergoes a similar transformation at −17.6°.[6-8]

Some experiments were performed on ammonium chloride and bromide to determine the possible influence of heating rates on the observed d.t.a. transition temperatures. No strong dependency was found in this regard with either material, though there was a trend to somewhat lower observed transition temperatures as the heating rate was lowered. Ideally, it would appear that the true equilibrium transition temperature should be measured at zero heating rate.[9] However, at the present time the extrapolation of transition temperatures obtained at finite heating rates to a zero heating rate cannot be reliably made.

The atmospheric pressure sublimation temperatures found for ammonium chloride, bromide, and iodide are 338.2° at 759.6 mm., 395.2° at 760.4 mm., and 403.6° at 746.0 mm., respectively. These values are in good agreement with those reported in the literature[10] at the cited pressures, namely, 337.8° ($NH_4Cl$), 394.6° ($NH_4Br$), and 404.0° ($NH_4I$). Table I contains a summary of the d.t.a. data obtained with ammonium chloride as heated at 3.5°/min. under the indicated pressures of argon. Comparison of these data with equilibrium vapor pressure results as determined by a static method[10] shows good concordance. Consideration of the relative simplicity and ease of operation of the d.t.a. technique point to its utility as a means for the characterization of sublimation equilibria. The relatively short residence time of appreciable concentrations of the sample vapors in the high temperature zone of the furnace reduces the tendency toward gas-phase decomposition into nitrogen, hydrogen, and free halogen.[11,12] In long

(1) W. Ramsay and S. Young, *Phil. Trans.*, **177**, 96 (1886).
(2) M. M. Markowitz, D. A. Boryta, and G. Capriola, *J. Chem. Educ.*, **38**, 96 (1961).
(3) M. M. Markowitz, *J. Phys. Chem.*, **62**, 827 (1958).
(4) R. T. Smyth, *J. Am. Ceram. Soc.*, **34**, 221 (1951).
(5) D. A. Vassallo and J. C. Harden, *Anal. Chem.*, **34**, 132 (1962).
(6) A. F. Wells, "Structural Inorganic Chemistry," Second Ed., Oxford Press, 1950, p. 245.
(7) H. A. Levy and S. W. Peterson, *J. Am. Chem. Soc.*, **75**, 1536 (1953).
(8) P. W. Bridgman, *Proc. Am. Acad.*, **52**, 136 (1916/1917).
(9) M. M. Markowitz, J. E. Ricci, and P. F. Winternitz, *J. Am. Chem. Soc.*, **77**, 3482 (1955).
(10) A. Smith and R. P. Calvert, *ibid.*, **36**, 1363 (1914).
(11) A. T. Larson and R. L. Dodge, *ibid.*, **45**, 2918 (1923).

duration static vapor pressure determinations such effects can lead to abnormally high vapor pressures and thus spurious results if appropriate corrections are not made.[13,14]

TABLE I

VARIABLE PRESSURE D.T.A. DATA FOR THE SUBLIMATION OF AMMONIUM CHLORIDE

| Pressure, mm. | Transition temp., °C. | Sublimation temp., °C. |
|---|---|---|
| 759.6 | 186.8 | 338.2 |
| 394.5 | 185.2 | 315.0 |
| 294.0 | 185.8 | 306.5 |
| 191.5 | 185.8 | 290.8 |
| 102.5 | 186.2 | 271.0 |
| 48.7 | 185.8 | 249.6 |
| 24.8 | 185.8 | 230.2 |

## Discussion

Ammonium chloride,[15,16] like the bromide[17] and the iodide,[18] is known to be completely dissociated in the vapor phase as per: $NH_4X(solid) \rightarrow NH_3(gas) + HX(gas)$, where X = Cl, Br, or I. Accordingly, the vaporization of ammonium chloride represents a dissociation process for which the standard free energy change and the equilibrium constant can be readily computed from the experimentally determined sublimation pressures.[13] Thus, $\Delta F^0_{diss.} = -RT \ln K_p$, $K_p = p_{NH_3}p_{HCl}$, and $p_{NH_3} = p_{HCl} = P_{NH_4Cl}/2$, where $P_{NH_4Cl}$ refers to the sublimation pressure of ammonium chloride. Consequently, $\Delta F^0_{diss.} = -RT \ln(P^2_{NH_4Cl}/4)$ and $K_p = P^2_{NH_4Cl}/4$. Now, $d \ln K_p/dT = 2\, d \ln P_{NH_4Cl}/dT = \Delta H^0_{diss.}/RT^2$ or $d \ln P_{NH_4Cl}/dT = \Delta H_{subl.}/RT^2$, where $\Delta H^0_{diss.} = 2\Delta H_{subl.}$. Accordingly, the slope of the straight line obtained by plotting log $P_{NH_4Cl}$ *vs.* $1/T$ is equal to $-\Delta\bar{H}_{subl.}/2.303R$, where $\Delta\bar{H}_{subl.}$ is the average value of the enthalpy of sublimation (or $^1/_2\ \Delta\bar{H}^0_{diss.}$) over the temperature range covered. Furthermore, $\Delta F^0_{diss.} = \Delta\bar{H}^0_{diss.} - T\Delta S^0_{diss.}$, and $\Delta F^0_{NH_4Cl,\ formn.} = -\Delta F^0_{diss.} + \Delta F_{NH_3,\ formn.} + \Delta F^0_{HCl,\ formn.}$, so that the standard entropy of dissociation and free energy of formation of ammonium chloride at the various temperatures indicated in Table I also can be calculated. The composite results of such computations are given in Table II.

At the transition temperature of 186.3°, the free energies of both crystalline forms of ammonium chloride are, of course, equal, and the standard free energy of formation of ammonium chloride at this temperature has been computed to be −33.8 kcal./mole, with a corresponding vapor pressure of 4.0 mm. Both $\Delta H^0_{diss.}$ and $\Delta S^0_{diss.}$ remain virtually constant over the temperature range covered (230.2–338.2°). It thus is apparent that the increasing tendency of ammonium chloride to vaporize as the temperature is raised is related to the increasing magnitude of the $T\Delta S^0_{diss.}$ term in the free energy equation. This effect forms the thermodynamic basis for the thermal decompositions of many materials at elevated temperatures.[19]

TABLE II

SOME THERMODYNAMIC PROPERTIES OF AMMONIUM CHLORIDE AS OBTAINED FROM D.T.A. DATA

$$\log P_{NH_4Cl} = -4795.5/T + 9.7291$$

$$\Delta H^0_{diss.} = 38.40 \text{ kcal./mole } NH_4Cl$$

| Temp., °C. | $\Delta F^0_{diss.}$, kcal./mole | $\Delta S^0_{diss.}$, e.u. | $\Delta F^0_{NH_4Cl,\ formn.}$, kcal./mole | $K_p$ |
|---|---|---|---|---|
| 338.2 | 1.69 | 60.1 | −20.8 | 0.250 |
| 315.0 | 3.15 | 59.9 | −22.8 | .0674 |
| 306.5 | 3.79 | 59.7 | −23.6 | .0374 |
| 290.8 | 4.64 | 59.8 | −24.9 | .0159 |
| 271.0 | 5.83 | 59.8 | −26.6 | .00455 |
| 249.6 | 7.15 | 59.8 | −28.5 | .00103 |
| 230.2 | 8.24 | 59.9 | −30.1 | .000266 |

It is of interest to note that the crystallographic transition temperature of ammonium chloride remains substantially constant (Table I) despite an approximate 30-fold variation in external pressure. The change in transition temperature with pressure, $dT/dp$, is given by the Clapeyron–Clausius equation.[20] Thus, for ammonium chloride the coefficient $dT/dp$ was computed to have a value of but 0.079°/atm.[21,22] In the present investigation, however, the effect of decreasing transition temperature with decreasing pressure is too small to be measured accurately.

As substantially ionic solids[6,7,22] the ease of concomitant vaporization and dissociation of the ammonium halides is unique. From the d.t.a. curves of Fig. 1, it may be seen that the relative stabilities of these ammonium salts increase in the order $NH_4Cl < NH_4Br < NH_4I$, which is consistent with the relative strengths of the halogen acids.[23] The enthalpies of dissociation of the ammonium halides are rather similar[24] and give no indication of the observed sequence of stability (42.3, 44.9, and 43.5 kcal./mole at 25° for $NH_4Cl$, $NH_4Br$, and $NH_4I$, respectively). However, the sublimation pressure determinations are ultimately direct measurements of the free energies of dissociation and thus of the thermal stabilities of these materials.[25,26]

(12) M. Bodenstein, *Z. physik. Chem.*, **13**, 56 (1894).
(13) G. Feick, *J. Am. Chem. Soc.*, **76**, 5658 (1954).
(14) F. M. G. Johnson, *Z. physik. Chem.*, **65**, 36 (1909).
(15) W. H. Rodebush and J. C. Michalek, *J. Am. Chem. Soc.*, **51**, 788 (1929); *Proc. Natl. Acad. Sci. U.S.*, **14**, 131 (1928).
(16) H. Braune and S. Knoke, *Z. physik. Chem.*, **135**, 49 (1928).
(17) A. Smits and R. Purcell, *J. Chem. Soc.*, 2936, 2944 (1928).
(18) R. H. Purcell, *ibid.*, 275 (1929).
(19) G. W. MacWood and F. H. Verhoek, *J. Chem. Educ.*, **38**, 334 (1961).
(20) A. Findlay, "The Phase Rule and Its Applications," D. N. Campbell, ed., Eighth Edition, Dover Publications, New York, N. Y., 1938, pp. 22–26.
(21) F. D. Rossini, D. D. Wagman, W. R. Evans, S. Levine, and I. Jaffe, "Selected Values of Chemical Thermodynamic Properties," National Bureau of Standards Circular 500, U. S. Government Printing Office, Washington, D. C., 1952.
(22) W. Hueckel, "Structural Chemistry of Inorganic Compounds," Elsevier Publishing Co., New York N. Y., 1950, pp. 665–666.
(23) C. A. Vanderwerf, "Acids, Bases and the Chemistry of the Covalent Bond," Reinhold Publ. Corp., New York, N. Y., 1961, pp. 50–54.
(24) N. W. Luft, *Ind. Chemist*, **31**, 502 (1955).
(25) H. C. Brown, M. D. Taylor, and M. Gerstein, *J. Am. Chem. Soc.*, **66**, 431 (1944).
(26) H. C. Brown, H. Bartholomay, and M. D. Taylor, *ibid.*, **66**, 435 (1944).

# ENRICHMENT OF OXYGEN-18 BY THE CHEMICAL EXCHANGE OF NITRIC OXIDE WITH NITRIC ACID SOLUTIONS[1]

BY S. C. SAXENA AND T. I. TAYLOR

*Chemistry Department, Columbia University, New York, N. Y.*

*Received March 8, 1962*

The rapid exchange of oxygen-18 between nitric oxide and nitric acid solutions occurs with a single stage enrichment factor of 1.020 ± 0.002 in approximate agreement with calculations from spectroscopic data. Since oxygen-18 concentrates in the gas phase, the use of this system required the conversion of nitric oxide to water and nitric acid. This was accomplished by partial decomposition of the nitric oxide in an arc, and reaction of the remainder with hydrogen to form water. The water extracted $NO_2$ from the gas stream to form nitric acid of the desired concentration. Some of the characteristics of the exchange reaction were investigated during the operation of exchange columns for the concentration of oxygen-18. For 8 *M* nitric acid, the height equivalent to a theoretical plate (H.E.T.P.) increases approximately linearly with flow rates above 60 mg. atoms of O/min.-cm.$^2$. At 25° and a flow rate of 85 mg. atoms of O/min.-cm.$^2$, the maximum over-all separation was obtained for 6 *M* $HNO_3$. Although the rate of the exchange reaction increases with increasing acid concentration, the value of $(\alpha - 1)$ decreases so that $(\alpha - 1)$/H.E.T.P. is maximum for 6 *M* $HNO_3$. The over-all separation was not greatly affected when the temperature was increased from 25 to 60°, indicating that the product of the transfer coefficient and $(\alpha - 1)$ is approximately constant. With a decrease in temperature, the decrease in the transfer coefficient was not compensated by an increase in $(\alpha - 1)$, so that the over-all separation decreased when the temperature was lowered to 0°. Cohen's theoretical equations for the increase in isotope concentration with time were used to analyze the operation of the exchange column and to determine the ratio of hold-up at the reflux end to the hold-up in the column. The optimum operating conditions for the system were selected and a comparison was made with other methods of concentrating oxygen-18. The exchange system described here appears to be somewhat more favorable than the distillation of water, but not as promising as the low temperature distillation of nitric oxide.

## Introduction

A variety of methods for separating the isotopes of oxygen have been investigated including absorption, chemical exchange, diffusion, electrolysis, fractional distillation, thermal diffusion, etc.[2,3] The most successful of these have been the thermal diffusion of oxygen[4,5] and the fractional distillation of water,[6,7] carbon monoxide,[8] or nitric oxide.[9] Although chemical exchange methods have been successful for the separation of the isotopes of a number of the lighter elements, no satisfactory exchange reaction has been found for the isotopes of oxygen. Among the exchange reactions investigated,[3] the one between carbon dioxide and water[10-15] has been of particular interest because of its relatively large enrichment factor, 1.038 at 25°. Unfortunately, the exchange reaction between carbon dioxide and water is slow, and until a satisfactory catalyst is found this exchange reaction will not be very useful for producing high concentrations of oxygen-18.

The exchange reaction between nitric oxide and nitric acid has been used to prepare 99.9% nitrogen-15,[16,17] and since this exchange must involve water, oxygen-18 exchange between nitric acid solutions must also occur rather rapidly. Preliminary measurements of Taylor and Clarke[18] on the enrichment of oxygen-18 appeared promising, and in this paper we give the results of our further reasearch on the system.

**Enrichment Factors.**—Although enrichment factors have been calculated for a number of exchange reactions involving the isotopes of oxygen,[10,19] values were not available for several exchange reactions involving the oxides and oxy-ions of nitrogen. Taylor and Clarke[18] calculated a number of these at 25°, and the calculations reported here extend them and Urey's table[19] to include NO, $NO_2$, $NO_3^-$, and $NO_2^-$ at several temperatures. The methods of Urey[19] and Bigeleisen and Mayer[20] were used to calculate the partition function ratios and the enrichment factors from spectroscopic data. The frequencies used for $N^{14}O^{16}$, $N^{14}O_2^{16}$, $N^{14}O_2^{16-}$, and $N^{14}O_3^{16-}$ were those summarized by Begun and Fletcher[21] and the frequencies for $H_2O^{16}$ and $H_2O^{18}$ were those given by Urey.[19] Vibrational frequencies for the isotopic molecules with oxygen-18 were calculated from the equations given by Herzberg,[22] assuming the validity of the

(1) This research was supported in part by a grant from the U. S. Atomic Energy Commission.

(2) G. M. Begun, "Isotope Separation and Isotope Exchange, a Bibliography with Abstracts" ORNL-2852, Office of Technical Services, Department of Commerce, Washington, D. C., 1958.

(3) D. Samuel and P. F. Steckel, "Bibliography of the Stable Isotopes of Oxygen," Pergamon Press, Inc., New York, N. Y., 1959.

(4) K. Clusius, G. Dickel, and E. W. Becker, *Naturwiss.*, **31**, 210 (1943).

(5) K. Clusius and G. Dickel, *Z. physik. Chem.*, **193**, 274 (1944).

(6) I. Dostrovsky and A. Raviv, "Proceedings of the International Symposium on Isotope Separation," North-Holland Publishing Co., Amsterdam, Netherlands, 1958, p. 336. References to earlier work on the distillation of water are given in this paper.

(7) M. Thurkauf, A. Narten, and W. Kuhn, *Helv. Chim. Acta*, **43**, 989 (1960).

(8) H. London, "Proceedings of the International Symposium on Isotope Separation," North-Holland Publishing Co., Amsterdam, Netherlands, 1958, p. 331.

(9) K. Clusius, K. Schleich, and M. Vecchi, *Helv. Chim. Acta*, **44**, 343 (1961).

(10) H. C. Urey and L. J. Greiff, *J. Am. Chem. Soc.*, **57**, 321 (1935).

(11) L. A. Webster, M. H. Wahl, and H. C. Urey, *J. Chem. Phys.*, **3**, 129 (1935).

(12) M. Cohn and H. C. Urey, *J. Am. Chem. Soc.*, **60**, 679 (1938).

(13) G. A. Mills and H. C. Urey, *ibid.*, **62**, 1019 (1940).

(14) A. F. Reid and H. C. Urey, *J. Chem. Phys.*, **11**, 403 (1943).

(15) W. T. Boyd and R. R. White, *Ind. Eng. Chem.*, **44**, 2202 (1952).

(16) W. Spindel and T. I. Taylor, *J. Chem. Phys.*, **23**, 981 (1955); **24**, 626 (1956).

(17) T. I. Taylor and W. Spindel, "Proceedings of the International Symposium on Isotope Separation," North-Holland Publishing Co., Amsterdam, Netherlands, 1958, p. 158.

(18) T. I. Taylor and J. C. Clarke, *J. Chem. Phys.*, **31**, 277 (1959).

(19) H. C. Urey, *J. Chem. Soc.*, 562 (1947).

(20) J. Bigeleisen and M. G. Mayer, *J. Chem. Phys.*, **15**, 261 (1947).

(21) G. M. Begun and W. H. Fletcher, *ibid.*, **33**, 1083 (1960).

(22) G. Herzberg, "Infrared and Raman Spectra of Polyatomic Molecules," D. Van Nostrand Co., Inc., New York, N. Y., 1946.

TABLE I

ENRICHMENT FACTORS FOR OXYGEN EXCHANGE OF WATER AND OXIDES AND OXY-IONS OF NITROGEN

| $\left[\frac{NO^{18}}{NO^{16}}\right]$ | $\left[\frac{NO_2^{18}}{NO_2^{16}}\right]^{1/2}$ | $\left[\frac{NO_3^{18-}}{NO_3^{16-}}\right]^{1/3}$ | $\left[\frac{H_2O^{18}}{H_2O^{16}}\right]_l$ | $\left[\frac{NO_2^{18-}}{NO_2^{16-}}\right]^{1/2}$ | $\left[\frac{H_2O^{18}}{H_2O^{16}}\right]_g$ | $T$, °C |
|---|---|---|---|---|---|---|
| 1.1103 | 1.1030 | 1.0979 | 1.0888 | 1.0825 | 1.0770 | 0 |
| 1.0982 | 1.0903 | 1.0847 | 1.0780 | 1.0719 | 1.0694 | 25 |
| 1.0880 | 1.0798 | 1.0740 | 1.0710 | 1.0632 | 1.0630 | 50 |
| 1.0810 | 1.0727 | 1.0667 | 1.0642 | 1.0573 | 1.0584 | 70 |
| 1.0000 | 1.0066 | 1.011 | 1.020 | 1.026 | 1.031 | 0 |
| | 1.0072 | 1.012 | 1.019 | 1.025 | 1.027 | 25 |
| | 1.0076 | 1.013 | 1.017 | 1.023 | 1.024 | 50 |
| | 1.0077 | 1.013 | 1.016 | 1.022 | 1.021 | 70 |
| | 1.0000 | 1.0046 | 1.013 | 1.019 | 1.024 | 0 |
| | | 1.0052 | 1.011 | 1.017 | 1.020 | 25 |
| | | 1.0054 | 1.0091 | 1.016 | 1.016 | 50 |
| | | 1.0056 | 1.0080 | 1.015 | 1.014 | 70 |
| | | 1.000 | 1.0084 | 1.014 | 1.019 | 0 |
| | | | 1.0062 | 1.012 | 1.014 | 25 |
| | | | 1.0036 | 1.010 | 1.010 | 50 |
| | | | 1.0023 | 1.0089 | 1.0078 | 70 |
| | | | 1.0000 | 1.0058 | 1.011 | 0 |
| | | | | 1.0057 | 1.0080 | 25 |
| | | | | 1.0065 | 1.0067 | 50 |
| | | | | 1.0065 | 1.0055 | 70 |
| | | | | 1.0000 | 1.0051 | 0 |
| | | | | | 1.0023 | 25 |
| | | | | | 1.0002 | 50 |
| | | | | | 0.9990 | 70 |

$\left[\frac{Q_1}{Q_2}\right]^{1/n}$

valence force method.[23] Calculated values of the partition function ratios along with the enrichment factors at temperatures 0, 25, 50, and 70° are recorded in Table I. The partition function ratios for liquid water were generated from those of gaseous water by multiplying the partition functions of the latter by the ratio of the vapor pressures of $H_2O^{16}$ and $H_2O^{18}$. The vapor pressure ratios were calculated at each temperature according to the formula given by Urey.[19]

Because of the complexity of the system NO–$HNO_3$–$H_2O$, the computed values of the enrichment factors will not apply exactly. When nitric oxide and solutions of nitric acid are equilibrated, several ionic and molecular species result. The gas phase contains NO, $NO_2$, $N_2O_3$, $N_2O_4$, $H_2O$, $HNO_3$, and $HNO_2$, while the liquid phase, in addition to $HNO_3$ and $H_2O$, contains NO, $NO_2$, $N_2O_3$, $N_2O_4$, $HNO_2$, $H_3O^+$, $NO_3^-$, and $NO_2^-$. The equilibrium amounts of these species depend on temperature, gas pressure, and concentration of the acid.[24] It is conventional, therefore, to determine experimentally an effective single stage enrichment factor, $\alpha$, defined as

$$\alpha = \frac{(O^{18})/(O^{16})\ \text{gas}}{(O^{18})/(O^{16})\ \text{liquid}} \qquad (1)$$

where the symbols in parentheses refer to the atom fractions of the isotopic species in the two phases. This $\alpha$ is a weighted mean of the enrichment factors for exchanges between various species. Since according to Table I, the enrichment factor which is most favorable for enriching oxygen-18 in the gas phase is the one between nitric oxide and water, and as the concentration of the other compounds increases with acid concentration, one would expect $\alpha$ to fall with increasing acid molarity at the same temperature and pressure.

The enrichment factor, $\alpha$, was determined by equilibrating nitric oxide with 25 ml. of nitric acid in a flask (1200 ml.) at room temperature (25°), and at one atmosphere pressure. The nitric acid was added to the flask and, after the solution was frozen, the flask was evacuated. To out-gas the nitric acid, the flask was warmed to room temperature and evacuated again after freezing the solution. This procedure was repeated two to three times. Nitric oxide then was added with continuous shaking of the flask to saturate the solution at atmospheric pressure. The flask was turned on its side and rotated with a motor for 24 hr. or more at room temperature to ensure complete isotopic equilibration. Samples of the oxides of nitrogen from the gas phase were taken directly in a discharge tube for decomposition into $N_2$ and $O_2$ for mass spectrometric determination of the 32/34 ratio. A sample of the liquid phase was analyzed after decomposition in a similar discharge tube.[25] Values of $\alpha$ calculated according to eq. 1 are summarized in Table II, along with the composition of the gas phase for several concentrations of nitric acid. These values are in approximate agreement with the theoretical calculations from spectroscopic data and the preliminary value of 1.020 ± 0.002

(23) S. C. Saxena, D. N. Bhatnagar, and S. Ramaswamy. Details of the calculations for the molecules of interest here along with others will be published elsewhere.

(24) E. Abel, H. Schmid, and H. Stein-Wein, *Z. Elektrochem.*, **36**, 692 (1930).

(25) T. I. Taylor, to be published elsewhere.

reported by Taylor and Clarke[18] for 6 $M$ $HNO_3$ at 25° and 1 atm. pressure.

TABLE II

ENRICHMENT FACTORS FOR THE EXCHANGE OF NITRIC OXIDE WITH NITRIC ACID SOLUTIONS AT 25° AND ONE ATMOSPHERE GAS PRESSURE

| Nitric acid concn., $M$ | 4.1 | 6.2 | 8.0 | 9.7 |
|---|---|---|---|---|
| Volume of acid phase, ml. | 25.0 | 25.0 | 25.0 | 25.0 |
| Volume of gas phase, ml. | 1135 | 1135 | 1135 | 1135 |
| Composition of gas phase: | | | | |
| Mole % NO | 95.4 | 95.7 | 94.2 | 80.7 |
| Mole % $NO_2$ | 0.53 | 1.7 | 4.5 | 10.3 |
| Mole % $N_2O_4$ | 0.02 | 0.21 | 1.4 | 7.4 |
| Mole % $H_2O$ | 2.6 | 2.2 | 1.9 | 1.6 |
| Mole % $HNO_2$ | 1.3 | 0.2 | .. | .. |
| Mole % $HNO_3$ | .. | .. | .. | 0.03 |
| Atom % O in NO | 93.9 | 93.1 | 84.9 | 62.5 |
| Atom % O in $NO_2 + N_2O_4$ | 1.1 | 4.4 | 13.4 | 36.3 |
| Enrichment factor, $\alpha$ | 1.028 ±0.004 | 1.020 ±0.003 | 1.018 ±0.003 | 1.015 ±0.003 |

## Experimental

The exchange column used in these investigations was made of glass, 145 cm. long, 13 mm. inside diameter, and packed with No. 3012 stainless "Helipak" column packing. Previous experiments on the concentration of nitrogen-15 in packed columns, bubble cap columns, and bubble plate columns showed that "Helipak" gave the highest separations. Since the exchange systems for nitrogen-15 and oxygen-18 are similar in many respects, the same packing was used. A relatively small diameter was selected for the column so that a wide range of flow rates could be run with the same reflux equipment.

The column had a concentric jacket through which water was circulated at the desired temperature from a conventional thermostatically controlled bath. The feed to the column was a stream of waste gases, from another column enriching nitrogen-15, and is described in detail by Spindel and Taylor.[16,17] The feed consisted of a mixture of mostly nitric oxide and other oxides of nitrogen in a proportion determined by the equilibrium composition (Table II) of the gas phase in contact with the nitric acid in the nitrogen-15 column at that temperature, pressure, and concentration. The column can, of course, be fed with the oxides of nitrogen from other sources.

These nitrogen oxides rise countercurrently against the nitric acid in the column and exchange mostly according to the reaction

$$NO^{16}(g) + H_2O^{18}(liq.) \xrightarrow{HNO_3} NO^{18}(g) + H_2O^{16}(liq.)$$

The exchange here is rather complex because the gas and liquid phases consist of several ionic and molecular species as mentioned previously. A mobile equilibrium among the various species undoubtedly provides the mechanism for rapid isotope exchange between the major components, nitric oxide and water. For reflux, the nitrogen oxides at the top of the column must be converted into water and nitric acid without any loss or addition of oxygen. Various designs were tried for the reflux system and after considerable experimentation and experience, it was found that the following method worked satisfactorily.

A part of the nitric oxide was decomposed into $N_2$ and $O_2$ by means of an electric discharge between platinum electrodes using a neon-sign transformer. The $O_2$ reacts with some of the excess NO to form $NO_2$. This was absorbed to form nitric acid according to the equation $3NO_2 + H_2O \rightarrow 2HNO_3 + NO$ as the gases passed countercurrently to water in a short section of a packed column. The concentration of the nitric acid so produced and hence the amount of nitric oxide to be decomposed was adjusted by the arc size and voltage. A photocell was used to monitor the concentration of $NO_2$ in the gas stream.

The remainder of the nitric oxide was reacted with hydrogen to form water according to the reaction $2NO + 2H_2 \rightarrow 2H_2O + N_2$. This reaction occurred on a roll of stainless steel screen about 3 in. long in the front section of a stainless steel tube, 1¾ in. diameter and 28 in. long. After the reaction was started at 700–800°, the heat evolved was sufficient to maintain the reaction without a furnace. The small amount of ammonia formed was decomposed on a 6 in. section of stainless steel wire cloth at 800–900° in the back section of the same stainless steel tube. Most of the water was condensed from the gas stream by condensers cooled to about 0°. The remainder of the water was recovered and returned to the column by means of molecular sieve adsorbents. Two glass tubes, each filled with 10 to 15 g. of type 5A Molecular Sieve adsorbents, were connected in parallel so that one could be used while the other was being regenerated by backflushing with dry nitrogen. A timer with microswitches connected to solenoid valves and heaters automatically controlled this operation. Since it was found[18,26] that the molecular sieve adsorbents exchange with oxygen-18 water at the temperature of regeneration (200–250°), the quantity used was reduced to a minimum. This exchange constitutes a holdup at the top of the column and reduces the rate of build-up of oxygen-18 to the steady state.

The effluent nitric acid was collected and titrated from time to time so that adjustments could be made to maintain the same acid concentration at the top and bottom of the column. The volume of acid collected per minute was used to calculate the flow rate of oxygen in the column. Gas samples of enriched NO were taken from the top of the column and decomposed into oxygen and nitrogen in a discharge tube. A mass spectrometer[27] with a single collector was used to determine the 32/34 ratio in the oxygen of the samples. Samples of the gas fed to the bottom of the column were analyzed in the same way. Since the 32/34 ratio in the feed gas was practically the same as that in tank oxygen, the latter was used as a reference for calculating the over-all separations.

The procedure adopted for making a run was essentially the same for all experiments. The temperature of the column was adjusted to the desired value and the column was flooded slowly with an auxiliary supply of nitric acid of the concentration to be maintained in the column during the run. After the column was flooded, the flow of auxiliary nitric acid was adjusted to the operating rate and maintained at this rate while the column was drained and while the reflux system was started. To start the reflux system, the whole system was flushed with nitrogen, the furnaces were preheated, the molecular sieve system was turned on, and then the appropriate flow of hydrogen was established. The feed gases from the nitrogen-15 system were admitted and after nitric acid started to drip from the refluxer, the flow from the auxiliary supply of nitric acid was stopped. This procedure maintained the proper wetting of the packing in the column. For operational convenience, all of the experiments were carried out at atmospheric pressure.

## Results and Discussion

Although there is some similarity between the exchange reactions for the nitrogen-15 system[16,17] and the oxygen-18 system described here, the differences between the two systems influence the optimum operating conditions. This arises principally because the oxygen of both the water and the oxygen compounds of nitrogen must exchange rapidly with the gas phase. Also, as seen from Tables I and II, high concentrations of nitric acid reduce the effective enrichment factor per stage. Consequently, it was necessary to evaluate the effect of the various parameters on the over-all separation, including flow rate, acid concentration, and temperature. The results of a number of experiments for this purpose are summarized in Table III.

**Effect of Flow Rate.**—The over-all separation, $S_\infty$, in a multistage fractionation column such as the one used for these studies, operating under total reflux, is given by Cohen[28] as

(26) S. C. Saxena and T. I. Taylor, details to be published.

(27) A. O. C. Nier, *Rev. Sci. Instr.*, **11**, 212 (1940); **18**, 398 (1947).

(28) K. Cohen, "The Theory of Isotope Separation," McGraw-Hill Book Co., Inc., New York, N. Y., 1951, Chapters 3 and 7; see also *J. Chem. Phys.*, **8**, 588 (1940).

TABLE III

SUMMARY OF OVER-ALL SEPARATIONS AS A FUNCTION OF ACID CONCENTRATION, FLOW RATE, AND TEMPERATURE IN A COLUMN 1.3 CM. I.D. AND 145 CM. LONG PACKED WITH NO. 3012 STAINLESS STEEL HELIPAK COLUMN PACKING

| Run no. | Approx. $HNO_3$ concn., moles/l. | Temp., °C. | Flow rate, ml. nitric acid/min. | Flow rate, $L$, mg.-atoms O/min.-cm.$^2$ | Over-all sep. $S_\infty$ | $\alpha$ | H.E.T.P., cm. |
|---|---|---|---|---|---|---|---|
| II-O | 4 | 25 | 1.81 | 83.4 | 1.34 | 1.028 | 13.7 |
| III-O | 4 | 60 | 1.89 | 86.4 | 1.34 | | |
| VII-O | 6 | 25 | 1.36 | 64.7 | 1.87 | 1.020 | 4.6 |
| VII-O | 6 | 25 | 1.42 | 67.6 | 1.86 | | 4.6 |
| VI-O | 6 | 0 | 1.77 | 84.2 | 1.51 | | 7.0 |
| VI-O | 6 | 25 | 1.78 | 84.7 | 1.73 | | 5.2 |
| VI-O | 6 | 60 | 1.77 | 84.2 | 1.63 | | 5.9 |
| W-O | 8 | 25 | 0.85 | 41.9 | 2.00 | 1.018 | 3.7 |
| W-O | 8 | 45 | 0.86 | 42.6 | 2.12 | | 3.4 |
| W-O | 8 | 70 | 0.85 | 41.8 | 2.14 | | 3.4 |
| V-O | 8 | 25 | 1.30 | 64.0 | 1.86 | | 4.2 |
| U-O | 8 | 25 | 1.74 | 85.7 | 1.52 | | 6.2 |
| X-O | 8 | 25 | 2.12 | 104.4 | 1.44 | | 7.1 |
| IV-O | 10 | 25 | 1.50 | 76.0 | 1.53 | 1.015 | 5.1 |
| IX-O | 13.7 | 22 | 1.80 | 94.6 | 1.31 | ... | .. |

$$\ln S_\infty = \frac{kZ(\alpha - 1)}{L} \qquad (2)$$

for systems in which $\alpha$ is near 1. Here $Z$ is the length of column and $L$ is the flow rate. The coefficient $k$ occurs in the equations for the rate of transfer of desired isotope across the interface per unit length of column and its form depends upon the rate determining process. This may be the rate of attainment of isotope equilibrium or the rate of diffusion through the fluid boundary layers.

If the interfacial concentrations for the diffusion limited case do not differ appreciably from the concentrations in the body of the fluid, the rate of transfer $T$ for both cases is[28]

$$T = -k[n(1 - N) - \alpha N(1 - n)] \qquad (3)$$

where $k = k'cC$ for the reaction limited case and $1/k = B/DC\sigma + b/dc\sigma$ for the diffusion limited case. In these equations $N$, $C$, $B$, and $D$ are, respectively, the mole fraction of desired isotope, the concentrations of reacting species in the liquid phase, the thickness of the liquid film, and the diffusion coefficient in the liquid. The lower case letters refer to the same quantities for the gas phase, $\sigma$ is the area of interface per unit length of column, and $k'$ is the rate constant for the exchange reaction.

Since $\ln S_\infty/(\alpha - 1)$ is the number of plates, $s$, in the column, it follows from eq. 2 that $kZ/L$ may be identified with $s$ so that H.E.T.P. $= L/k$. Thus, for conditions to which eq. 2 and 3 apply, a plot of H.E.T.P. *vs.* $L$ should be a straight line if $\alpha$ and $Z$ are constant and $k$ does not change significantly with flow rate. For the limited range of flow rates normally used for isotope separation, these conditions apply and the plot for both of the rate-limiting processes should be a straight line for a given acid concentration.

A plot of H.E.T.P. *vs.* flow rate for 8 $M$ $HNO_3$ is shown in Fig. 1. The flow rates in mg.-atoms of O/min. were evaluated from measurements of the volume and concentration of effluent nitric acid as well as from measurements on the gas stream fed to the column. The total moles of nitrogen oxides fed to the column per minute was known from the flow of nitric acid fed to the nitrogen-15 column. A Cary spectrophotometer was used to determine the concentration of $NO_2$ so that the flow rate of the gas phase in mg.-atoms of O/min. could be calculated.

The results shown in Fig. 1 indicate that the H.E.T.P. increases approximately linearly with flow rate above about 60 mg.-atoms of O/min.-cm.$^2$. At low flow rates, improper wetting of packing may cause an increase in H.E.T.P. and at high flow rates, one would expect a departure from linearity because of turbulence and flooding. On the basis of the results of these experiments, flow rates from 60 to 85 mg.-atoms of O/cm.$^2$-min. were selected for measurements on the influence of the other variables. These flows represent a compromise between over-all separation and the transport or time to reach a steady state. Comparison of the results for 6 and 8 $M$ $HNO_3$ (Table III) at a flow rate of about 85 mg.-atoms of O/cm.$^2$-min., where the values of H.E.T.P. are, respectively, 5.2 and 6.2 cm., indicates that the optimum flow may be higher for 6 $M$ than for 8 $M$ $HNO_3$.

**Effect of Acid Concentration.**—Little information is available on the kinetics and mechanism of oxygen-18 exchange between NO and water in solutions of nitric acid. Bunton, Halevi, and Llewellyn[29] have studied the exchange of oxygen-18 between nitric acid and water. The rate was markedly dependent upon the concentration of nitrous acid. In the absence of nitrous acid, no appreciable exchange occurred below about 40 mole % $HNO_3$. Above this concentration, the exchange was rapid.

In our system, in which nitric oxide is in equilibrium with nitric acid, other oxides of nitrogen and nitrous acid (Table II) are continuously present to catalyze the exchange. As the concentration of nitric acid increases, the concentration of the higher oxides of nitrogen increases and presumably also the rate of exchange. But, as shown from the calculated values of the enrichment factors (Table I), $\alpha$ for NO and $NO_3^-$ is appreciably smaller than that for NO and $H_2O$. Furthermore, the increase in $NO_2$ in the gas phase will further decrease $\alpha$. Thus, even though an increase in acid concentration may increase the rate of exchange and give a shorter H.E.T.P., the decrease in $\alpha$ may be sufficient to decrease the over-all separation. Since the over-all separation, $S$, is given by $S = e^{s(\alpha-1)}$ and since the number of stages, $s$, in a length of column $Z$ is $s = Z/\text{H.E.T.P.}$, we desire to known the acid concentration for which $(\alpha - 1)/\text{H.E.T.P.}$ is a maximum. This can be obtained from measurements of the over-all separation as a function of acid concentration, keeping the other parameters

(29) C. A. Bunton, E. A. Halevi, and D. R. Llewellyn, *J. Chem. Soc.*, 4913 (1952).

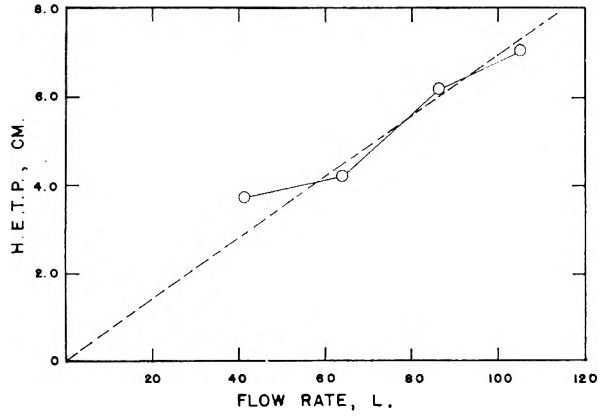


Fig. 1.—Effect of flow rate on the over-all separation for 6 and 8 $M$ $HNO_3$.

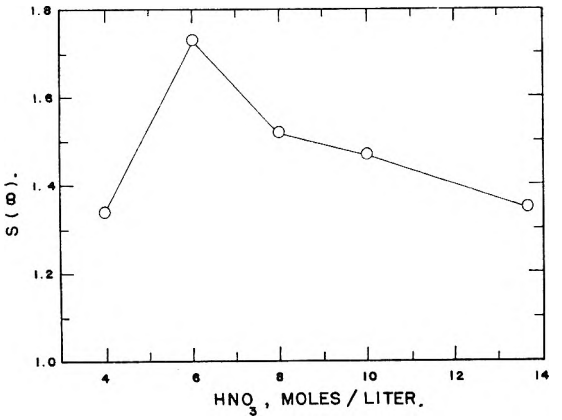


Fig. 2.—Over-all separation as a function of acid concentration at approximately 25° and a flow rate of approximately 85 mg.-atoms of O/cm.²-min.

constant, such as flow rate, temperature, length, column packing, etc.

In Fig. 2, the over-all separation at steady state and total reflux, $S_\infty$, is plotted against acid concentration for approximately the same flow rate (85 mg.-atoms of O/cm.²-min.) and temperature (25°). For the 10 and 13.7 $M$ $HNO_3$, a small correction to the values in Table III was made assuming the validity of eq. 2. A maximum in the over-all separation occurs at about 6 $M$ $HNO_3$. The separation falls rather rapidly for more dilute solutions, probably because of a low exchange rate resulting in a small value for the phase transfer constant, $k$ (eq. 2 and 3). At the higher acid concentrations, the over-all separation decreases owing to a decrease in $\alpha$. At other temperatures and pressures, the optimum acid concentration for high over-all separation may change because the values of $\alpha$ and $k$ may be affected differently.

**Effect of Temperature.**—From eq. 2, the steady state separation depends upon the product $k(\alpha - 1)$. Since an increase in temperature decreases $\alpha$ (Table I) and usually increases $k$, the effect of an increase in temperature is determined by the relative magnitudes of these two opposing effects. The experimental results for the effect of temperature on the over-all separation with 6 $M$ $HNO_3$ at a flow rate of approximately 85 mg.-atoms of O/cm.²-min. are shown in Fig. 3. At 25°, the over-all separation is slightly higher than at 60°, but the separation dropped from 1.73 to 1.51 when the temperature was lowered to 0°. Apparently, any increase in $\alpha$ is more than compensated for by a decrease in $k$. In another experiment with 6 $M$ $HNO_3$ at a flow rate of 65 mg.-atoms of O/cm.²-min. (Table III), the over-all separation did not change significantly when the temperature was increased from 25 to 45°.

For 8 $M$ $HNO_3$, the over-all separations increased slightly as the temperature was increased from 25 to 45° and 75° (Table III). No significant change in over-all separation was observed for 4 $M$ $HNO_3$ when the temperature was increased from 25 to 60°. Any decrease in $\alpha$ with increase in temperature apparently is balanced by an increase in $k$. The above results show that the system is not very sensitive to temperature changes in the range from 25 to 75°. Thus it is not necessary to control the temperature closely and, for convenience, the system can be operated at room temperature.

**Approach to Steady State.**—An important property of a system for separating isotopes is the rate of approach to the steady state. A comparison of the experimental behavior of the system with that predicted from theory enables one to check or to determine some of the important constants such as $\alpha$, the hold-up, or the flows. Estimates of the hold-up in the reflux system at the product end of the exchange column indicated that it probably was responsible for the relatively slow rate of approach to the steady state. Since the hold-up was difficult to measure and since the extent of oxygen-18 exchange with the molecular sieve adsorbents and the catalyst for decomposition of $NH_3$ was uncertain, the effective hold-up in the reflux system was evaluated by comparison with theory.

Cohen[28] has derived theoretical equations that give the increase in mole fraction of desired isotope as a function of the time of operation of a fractionating column such as ours. The feed end (bottom) was maintained at a constant mole fraction, $N_0$, of the desired isotope by supplying fresh material continuously, but there was an appreciable hold-up, $H_r$, gram-atoms of O, at the product end (top). The value of $\alpha$ is small and the extent of separation was not great, so that the mole fraction $N$ of oxygen-18 in the feed and in the product was always small compared to 1, *i.e.*, $N << 1$. For this case, when the column is operated at total reflux, the fundamental partial differential equation is written as

$$\lambda \frac{\partial N}{\partial t} = \frac{\partial^2 N}{\partial s^2} - (\alpha - 1) \frac{\partial N}{\partial s} \qquad (4)$$

where $N$ is the mole fraction of isotope in the $s$th stage at time $t$; $\lambda$ is the processing time per stage and is given by the hold-up per stage, $H$, divided by the flow rate, $L$.

For the boundary conditions mentioned above, the solution to eq. 4 can be put in the form[28]

$$\frac{N_t}{N_0} = S_\infty - A(S_\infty - 1)e^{-Bt/\lambda s^2} \qquad (5)$$

where $N_t$ is the mole fraction of oxygen-18 at time $t$, at the product end; $N_0$ is the mole fraction of oxygen-18 in the feed; $s$ is the number of stages in the column; and $S_\infty$ is the over-all separation at steady state with no product withdrawals. The constants $A$ and $B$ are functions of $(\alpha - 1)s$ and $K/\lambda s$, where $K$ is the hold-up $H_T$ at the product end of the column divided by the flow, $L$. Thus $K/\lambda s$ is the ratio of the hold-up at the product end of the column to the hold-up in the column. This is the quantity we desire to determine.

Tables of the values for the functions $A$ and $B$ are given[28] for several values of $(\alpha - 1)s$ and $K/\lambda s$ which apply to times $t > \lambda s^2/10$. However, for application to our experiment, it was necessary to solve Cohen's equations[30] for values of $K/\lambda s$ greater than those given in his tables. The results of the calculations are plotted in Fig. 4 along with the experimental results for run V-O (Table III) for which the hold-up in the column was 2.2 g.-atoms of oxygen. The upper part of Fig. 4 is obtained from eq. 5 in the form

$$-\ln\left(S_\infty - \frac{N_t}{N_0}\right) = -\ln A(S_\infty - 1) + Bt/\lambda s^2 \qquad (6)$$

In this plot the slopes of the straight lines are $B/\lambda s^2$ and the intercepts are $-\ln A(S_\infty - 1)$.

A comparison of the experimental results with the theoretical curves indicates that $K/\lambda s$ was approximately 1. That is, the effective hold-up in the reflux system was about the same as the hold-up in the column. This is somewhat higher than our estimates of 0.7 to 0.8 for $K/\lambda s$. A more rapid approach to the steady state could be achieved by some alterations in the design of the reflux system which would reduce the hold-up.

**Optimum Operating Conditions.**—A summary of the operating conditions and the performance of the column for two acid concentrations that appear to be most favorable is presented in Table IV. We conclude from our experiments that the use of approximately 6 $M$ $HNO_3$ at room temperature (25°) at a flow rate of 85 mg.-atoms of O/cm.$^2$ are about the optimum operating requirements for small packed columns. Higher pressures than 1 atm. perhaps would improve the performance, but the optimum acid concentration may be somewhat different.

When high enrichment is a major consideration, the use of 8 $M$ $HNO_3$ at 25 or 50° at a lower throughput would be advantageous. This concentration has the additional advantage of being an acid concentration that also gives good results for the concentration of nitrogen-15. Thus, with 8 $M$ $HNO_3$, the two systems could conveniently be used in series to produce both nitrogen-15 and oxygen-18. If the nitrogen-15 column were operating with 10 $M$ $HNO_3$, the waste gas stream also could be used directly with acceptable results. Alternatively, a part of the $NO_2$ and $N_2O_4$ in the gas stream could be removed by cooling it to the appropriate temperature (10 to 15°), or by passing it concurrently with a controlled flow of water through a short packed column.

(30) Reference 28, p. 46, equations 3.24–3.28.

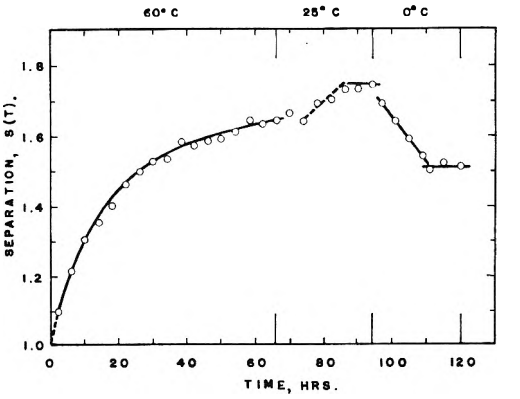


Fig. 3.—Effect of temperature on the over-all separation for 6 $M$ $HNO_3$ at a flow rate of approximately 85 mg.-atoms of O/cm.$^2$-min.

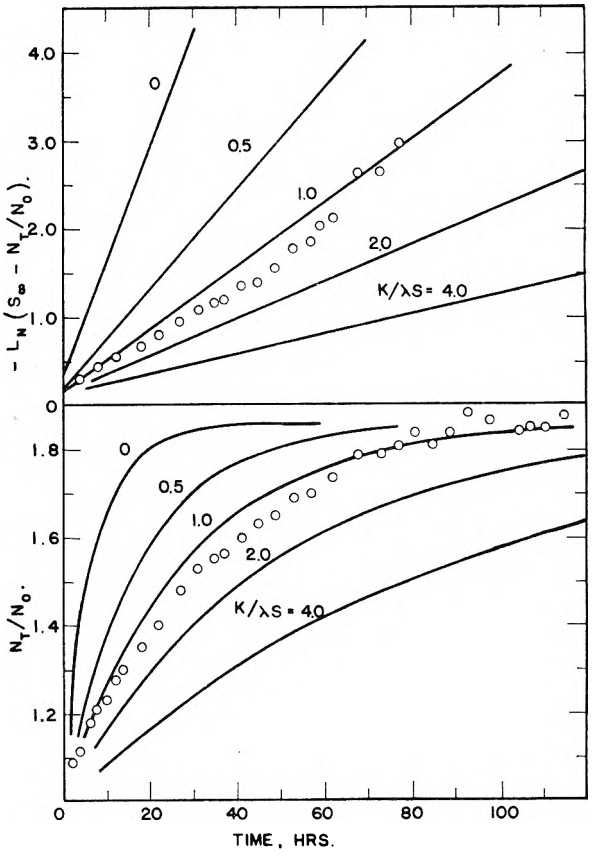


Fig. 4.—Effect of hold-up in the reflux system on the approach to the steady state.

## Comparison with Other Methods

**Chemical Exchange.**—The results of experiments by Boyd and White[15] on the oxygen-18 exchange between carbon dioxide and water, using ammonia as a catalyst, indicate that the exchange rate was too slow for practical use of the method. At a flow rate of 50.3 mg.-atoms of O/min.-cm.$^2$, they obtained an over-all separation of 2.58 or an H.E.T.P. of 16.5 cm. in a 22-ft. column, 1 in. i.d., filled with Fenske helices. At about the same flow rate (42.5 mg.-atoms of O/min.-cm.$^2$) in a column filled with Helipak, the H.E.T.P. was 3.4 cm. for the NO–$HNO_3$ exchange system. Allowing for a factor of two to three[17] for the H.E.T.P.

Table IV

Summary of Operating Conditions and Performance of Columns for Enriching Oxygen-18 for Two Favorable Nitric Acid Concentrations

| Item | 6 *M* $HNO_3$ | 8 *M* $HNO_3$ |
|---|---|---|
| Column length, cm. | 145 | 145 |
| Column diameter, cm. | 1.3 | 1.3 |
| Packing, stainless steel rectangular spirals 0.035 in. × 0.070 in., No. 3012 | Helipak | Helipak |
| Temp., °C. | 25 | 50 |
| Feed to $N^{15}$ column, mmoles $HNO_3$/min. | 96.0 | 50.6 |
| Compn. of gas stream column, approx. % $NO_2$ (as $NO_2 + N_2O_4$) | 1.9 | 7.2 |
| Hydrogen flow to refluxer, mmoles $H_2$/min. (~20% excess) | 135 | 68 |
| Nitric acid flow in the column, ml./min. | 1.78 | 0.86 |
| Throughput, *L*, mg.-atoms of O/min.-cm.$^2$ | 84.7 | 42.6 |
| Period (63% of equilibrium) approx., hr. | 30 | 48 |
| Hold-up in column, g.-atoms of O | 2.1 | 1.9 |
| Over-all separation, $S_\infty$ | 1.73 | 2.12 |
| Enrichment factor, $\alpha$ | 1.020 | 1.018 |
| Stages, *s* | 28 | 42 |
| H.E.T.P., cm. | 5.2 | 3.4 |
| Processing time in column, min./stage | 0.67 | 0.8 |

difference between the two packings the NO–$HNO_3$ exchange is significantly more favorable for the concentration of oxygen-18 than the $CO_2$–$H_2O$ exchange. However, work in progress on the catalysis of the $CO_2$–$H_2O$ exchange may improve its performance.

**Distillation of Water.**—At the present time, the distillation of water[6,7] is the principal process used for the preparation of high concentrations of oxygen-18. The system described by Dostrovsky and Raviv[6] is a four-section tapered enriching cascade with a total length of 38.5 m. and a straight stripping section of 19 m. We have operated our exchange columns at about the same flow rates as those in the smaller sections of their cascade so that an approximate comparison can be made. Their distillation columns were filled with Dixon type packing, which is at least equivalent to Helipak used in our columns.

In Table V, a number of comparisons are listed for the exchange and distillation systems. The number of stages, $s_{min}$, required for total reflux and no product withdrawal is given by $S = \alpha^{s_{min}}$. For a system without a stripping section, the minimum interstage flow to product ratio was calculated from the equation[17]

$$\frac{L_{min}}{P} = \frac{N_P[1 + (\alpha - 1)(1 - N_0)] - N_0}{(\alpha - 1)N_0(1 - N_0)} \quad (7)$$

where *L* is the minimum interstage flow in g.-atoms of oxygen per unit time; *P* is the withdrawal rate of product in g.-atoms of oxygen per unit time; $N_0$ is the mole fraction of oxygen-18 in the feed material; $N_p$ is the mole fraction of oxygen-18 in the product; and $\alpha$ is the enrichment factor. Thus, to produce 90% oxygen-18 by our exchange process

Table V

Comparison of the Exchange of Nitric Oxide with 8 *M* Nitric Acid and Distillation Methods for the Preparation of 1 Gram of Oxygen-18 per Day at 90% Concentration in a Square Cascade Consisting of a Single Column

| | NO–$HNO_3$ Exchange | $H_2O$ Distillation | NO Distillation |
|---|---|---|---|
| Over-all separation, *S* | 4400 | 4400 | 4400 |
| Enrichment factor, $\alpha$ | 1.018 | 1.0064 | 1.039 |
| H.E.T.P. (cm.) | 3.4 | 1.0 | 1.79 |
| Minimum no. of stages ($s_{min.}$) | 470 | 1315 | 219 |
| Length of column for $s_{min.}$ (m.) | 16.0 | 13.1 | 5.7 |
| $L_{min.}/P$ | 25,000 | 69,000 | 12,000 |
| Interstage flow, $L_{min.}$ (mg.-atom O/min.) | 1070 | 2960 | 514 |
| Flow per cm.$^2$ (mg.-atoms O/min.-cm.$^2$) | 40 | 40 | 29 |
| Minimum area of column (cm.$^2$) | 27 | 74 | 18 |
| Minimum volume of column (l.) | 430 | 970 | 103 |
| Processing time, $\lambda = H/L$ (min./stage) | 0.8 | 0.24 | 0.37 |
| Relative equilibrium time | 1 | 2.3 | 0.10 |

from feed material of the normal abundance of 0.204% oxygen-18, the interstage flow required at the feed point is at least 25,000 times the product withdrawal rate. This is for maximum transport when an infinite number of stages is provided. Usually about twice the minimum number of stages is used in an actual system, and because of losses, fluctuations, etc., the flow or area of column is usually about 30% greater than the calculated minimum. Furthermore, a tapered cascade is used rather than a single column, to which the comparisons in Table V apply.

For two systems, the relative equilibrium times vary approximately as $\lambda/(\alpha - 1)^2$ where $\lambda$ is the processing time per stage. If the two systems have the same flow per cm.$^2$ and the same hold-up per cm.$^3$ of packing, the relative equilibrium times (or sizes of systems) vary approximately as H.E.T.P./$(\alpha - 1)^2$. This factor is about 2.3 in favor of the NO–$HNO_3$ exchange system relative to the distillation of water. However, because of the relatively larger H.E.T.P., a longer column is needed for the chemical exchange system, but by catalysis it may be possible to improve the system in this respect.

The relative costs for producing oxygen-18 by distillation of water and chemical exchange have not been estimated, but the corrosive nature of the NO–$HNO_3$ system requires more expensive materials of construction. Furthermore, the cost of chemicals undoubtedly is greater for the exchange system than the cost of heat or refrigeration for a properly designed distillation system. The chemical cost for the exchange system relative to the value of the products is somewhat reduced when nitrogen-15 and oxygen-18 are produced in an integrated system. The nitrogen-15 system would require nitric acid for feed and sulfur dioxide for reflux. Rather than converting the oxides of nitrogen to nitric acid for a stripping section in the

nitrogen-15 system, they would be used as feed material to the oxygen-18 system, which then requires hydrogen for reflux. Thus, the integrated system requires nitric acid, sulfur dioxide, and hydrogen as raw materials, from which one obtains nitrogen-15 and oxygen-18 in approximately the ratio of the values of $(\alpha - 1)$, or 0.055 to 0.018, *i.e.*, 3 to 1. The by-products are sulfuric acid and nitrogen gas.

An evaluation of the chemical exchange relative to the distillation of water for the production of large quantities of nitrogen-15 and oxygen-18 would require rather complete cost analysis. However, for the preparation of quantities of these isotopes normally used for research and for tracers in chemical and biological processes, considerations of the equilibrium time and the size of the system may be as important as the cost of chemicals relative to the cost of heat or refrigeration.

**Distillation of Nitric Oxide.**—Since the completion of the work for this paper, Clusius, Schleich, and Vecchi[9] have obtained some encouraging results on the low temperature distillation of nitric oxide for the concentration of both nitrogen-15 and oxygen-18. Even at the present stage of development, the results summarized in Table V show that the length of the column, the interstage flow, the volume of the column, and the relative equilibrium time all are significantly better for NO distillation than for the distillation of water or chemical exchange. Apparently, the technical difficulties of operating the low temperature distillation columns continuously and at controlled temperatures have been solved. The comparisons in Table V emphasize the importance of high values for the enrichment factor, $\alpha$, and small values for H.E.T.P.

**Acknowledgments.**—The important contributions of Mr. Heiko Ohlenbusch and Mr. Jerome Schupack for aid in setting up and operating the isotope separation columns are gratefully acknowledged. Mr. Jerry Goodisman aided when the columns were in continuous operation, and Mr. Vincent G. Saltamach maintained the mass spectrometer and helped with the isotope analyses.

# THE DEPENDENCE OF THE ELECTROLYTIC HYDROGEN–DEUTERIUM SEPARATION FACTOR ON THE ELECTRODE POTENTIAL

BY GERALD P. LEWIS[1] AND PAUL RUETSCHI

*The Electric Storage Battery Company, The Carl F. Norberg Research Center, Yardley, Pennsylvania*

*Received March 14, 1962*

The influence of the electrode potential on the cathodic hydrogen–deuterium separation factor was determined with potentiostatic experiments. Additional variables studied were electrode materials, temperature, and surface roughness (porous *vs.* smooth electrodes). The separation factor $S$ was found to pass through a maximum as increasingly negative electrode potentials were applied. The maximum for $S$ occurred at a different potential for each electrode material. In the decreasing region at high negative potentials, the influence of the individual electrode material on $S$ decreased, and the data for all electrodes merged and could be represented by a single line with a scatter of only 25%. The porous electrodes gave separation factors 10 to 100% smaller than the smooth electrodes. The separation factor decreased with increasing temperature by about 1% per °C. in the range 30 to 50°.

## Introduction

The electrolytic separation factor $S$ for the hydrogen isotopes is defined as the H/D ratio in the evolved gas divided by the H/D ratio in the electrolyte. Many investigators[2–7] have studied the effect of electrode material, temperature, current density, and the nature and concentration of the electrolyte on the separation factor. It was found that $S$ was dependent on all of the above variables. However, the exact nature of the dependence on each variable has not been agreed upon, with the exception of the temperature dependence, where $S$ is found to decrease as the electrolysis temperature is increased. Generally, the electrode materials were placed in two classes: high overvoltage materials such as lead and mercury with separation factors in the range 3 to 4, and low overvoltage materials such as silver and platinum with values of $S$ around 6. These two classes were thought to correspond to two different mechanisms of hydrogen evolution—the "slow discharge mechanism" controlling in the first case and the "recombination mechanism" controlling in the latter case. Farkas and Horiuti[8,9] first showed that the chemical exchange reaction $HD + H_2O \rightleftarrows HDO + H_2$ influences the measured separation factor. At room temperature, the thermodynamic equilibrium value for $S$ is 3.7. Electrodes with highly catalytic surfaces usually give separation factors close to the equilibrium value during electrolysis, indicating that equilibrium between the adsorbed gas on the electrodes and the electrolyte is almost completely established.

Vielstich[10] showed that the separation factor for a given electrode material is a function of the applied electrode potential, and that $S$ reaches a maximum and then decreases. This dependence does not by itself relate $S$ and the current density, since only under carefully controlled conditions can a repro-

(1) Submitted in partial fulfillment for the degree of Doctor of Philosophy in Chemical Engineering at the Polytechnic Institute of Brooklyn.

(2) R. P. Bell, *J. Chem. Phys.*, **2**, 135 (1934).

(3) J. H. Wolfenden and H. F. Walton, *Trans. Faraday Soc.*, **34**, 436 (1938).

(4) F. P. Bowden and H. F. Henyon, *Nature*, **135**, 105 (1935).

(5) G. Ogden and C. Bawn, *Trans. Faraday Soc.*, **30**, 432 (1934).

(6) K. Czike and P. Csayni, *Magy. Kem. Folyoirat*, **61**, 385 (1955).

(7) B. E. Conway, *Proc. Roy. Soc.* (London), **256**, 128 (1960).

(8) A. Farkas, *Trans. Faraday Soc.*, **33**, 552 (1937).

(9) J. Horiuti and M. Polanyi, *Nature*, **132**, 931 (1933).

(10) W. Vielstich and H. Schuchardt, *Z. Elektrochem.*, **63**, 1014 (1959).

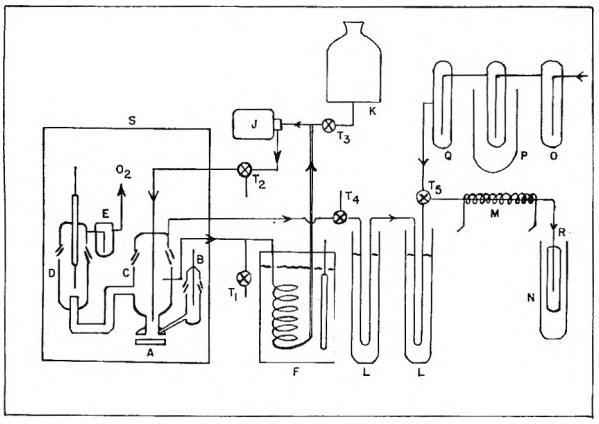


Fig. 1.—Schematic of apparatus for separation factor determinations: A, test electrode; B, Hg/HgO reference electrode; C, hydrogen compartment; D, oxygen compartment; E, valve; F, water bath; I, coils; J, pump; K, feed bottle; L, Dry Ice–acetone trap; M, catalyst tube; N, ice water trap; O, $CaCl_2$ trap; Q, magnesium perchlorate trap; R, sampling tube; S, constant temperature box; T, stopcocks.

ducible Tafel relationship between current density and potential be established. The present investigation was initiated to establish more fully the dependence of $S$ on the electrode potential, and also the dependence of $S$ on other variables previously studied by earlier workers.

## Experimental

**Analysis of $D_2O$ Mixtures.**—The deuterium determination was carried out by infrared analysis in the liquid state as described by Guant.[11] The instrument used was a Perkin-Elmer Model 21 double beam spectrometer. The maximum deuterium concentration measured was 0.8 wt. % $D_2O$. Samples of higher concentrations were diluted to this range. A differential analysis using a 0.2-mm. $CaF_2$ cavity cell in the sample beam, and a $CaF_2$ variable path length cell in the reference beam was carried out, in order to observe the 3.98 $\mu$ HDO band in a liquid sample of over 99% $H_2O$. Standard samples purchased from Isomet Corporation were used for the calibration curves. Calibration curves of optical density *vs.* concentration were taken each time a group of samples was analyzed. By calibrating the instrument during each analysis, the effects of temperature and instrument drift were eliminated. The maximum deviation from the least squares calibration line was 1%.

**Preparation of Materials.**—Six smooth and two porous electrode materials were investigated. Smooth platinum and palladium foils were obtained from Engelhard Industries, and were of 99.9% purity. They were etched in aqua regia and degreased prior to placement in the test cell. Nickel foil was obtained from Exmet Co., and silver foil from Handy and Harman. Both were of 99.9% purity. Lead foil was obtained from the National Lead Co. and was of 99.99% purity. All these electrodes were etched in dilute nitric acid and degreased prior to each use. The porous electrodes were mixtures of nickel, silver, and palladium powders, and nickel, silver, and palladium-coated carbon powders. They were pressed into disks about 1/8 in. thick and sintered at elevated temperatures in hydrogen. The mercury electrode was prepared by covering silver foil with triple-distilled mercury. The electrolyte used was 6 $N$ KOH, prepared from triple-distilled water and Fisher Certified reagent grade KOH pellets. The electrolyte contained 2 wt. % $D_2O$, on a KOH free basis. $D_2O$ of 99.5 wt. % purity, purchased from Isomet Corporation, was used to make up the electrolyte solutions.

**Experimental Apparatus.**—The separation factor was obtained by measurement of the deuterium concentration of the electrolyte and that of the evolved gas. The evolved gas was completely oxidized catalytically with oxygen to form water, and the water was then analyzed. A schematic diagram of the apparatus is shown in Fig. 1. A two-compartment cell was used to prevent oxygen from contacting the hydrogen electrode. The evolved hydrogen gas was passed through two Dry Ice–acetone traps to remove entrained electrolyte and was then sent to the catalyst chamber. Air, filtered and dried by successive traps of calcium chloride, Dry Ice–acetone, and magnesium perchlorate, was passed into the catalyst chamber in excess of that needed for complete combination. The catalyst was 3% platinum on alumina pellets, purchased from Engelhard Industries. The catalyst chamber was maintained at 300° by heating tape. The water vapor produced was collected in a trap immersed in ice water. The electrolyte, 6 $N$ KOH, was preelectrolyzed between platinum electrodes at 100 ma./l. for 48 hr. prior to each experiment. The electrolyte was circulated continually by a polyethylene pump. The electrode was clamped against a circular opening in the bottom of the cell, and the electrolyte impinged onto the electrode through a nozzle tip located 1 cm. above the electrode. This provided excellent convection at the electrode surface. The electrolyte flowed through Pyrex coils immersed in a thermostatically regulated water bath to provide constant temperature. In addition, the cells and the reference electrode were placed in a constant temperature airbox. The entire apparatus was constructed of Teflon and Pyrex. Six current densities were used: 5, 10, 20, 50, 100, and 200 ma./cm.$^2$. The measurements were made on two sizes of electrodes, 1 and 10 cm.$^2$, such that only three currents of 50, 100, and 200 ma. had to be employed. A run was completed after a liquid sample of 0.1 cc. of water was collected. Fresh catalyst was inserted into the catalyst chamber after each run. Nitrogen was flushed through the electrolyte after each run in a given series to remove the dissolved hydrogen and deuterium produced during the previous run.

**Effect of Catalyst.**—During the course of the experiments, it was found that the quantity of catalyst used and the length of time over which the sample was collected influenced the results on deuterium concentration in the sample. Special experiments showed that for the same inlet hydrogen–deuterium mixture, the deuterium concentration of the liquid sample produced varied by 50% depending on the quantity of catalyst present. Even though the catalyst was flushed with dry air at 350° over prolonged periods of time before the run, adsorbed moisture must have been present which then exchanged with the water formed by the reaction of hydrogen and deuterium with the inlet oxygen. The results subsequently were corrected for this effect. The necessary corrections were obtained by experiments using standardized hydrogen–deuterium gas mixtures, supplied and analyzed by the Matheson Co. These known mixtures were oxidized over the catalyst, and the catalyst conditions which gave an H/D value for the liquid equal to that of the inlet gas were established.

**Additional Measurements.**—The electrode potential was measured with a Hewlett-Packard Model 412A vacuum tube voltmeter of 1% accuracy, against a Hg/HgO reference electrode in the 6 $N$ KOH electrolyte. The potential of this reference electrode against a reversible hydrogen electrode in 6 $N$ KOH was −932 mv. at 30°, and −924 mv. at 50°. A Luggin capillary hole, intersecting the side wall of the cell, was used to eliminate ohmic drop in the measurements.

**Accuracy of Results.**—The over-all accuracy of the measured factors is about 10%. The main source of error was the moisture in the recombining catalyst. The accuracy of the potential measurements was ±15 mv.

## Results

The results of the cathodic separation factor measurements are presented in Fig. 2–9 in the form of curves of separation factors *vs.* half cell potentials of the test electrodes, at temperatures of 30 and 50°. A maximum in the separation factor is clearly indicated in all the curves. Most curves also show a second maximum. For some of the electrodes, the ascending portion of the curve could not be observed because the current densities applied had to be kept at relatively high values in order to produce enough sample in a reasonable period of time. However, since the separation factor at open circuit

(11) J. Guant, *Spectrochim. Acta*, **8**, 57 (1956).

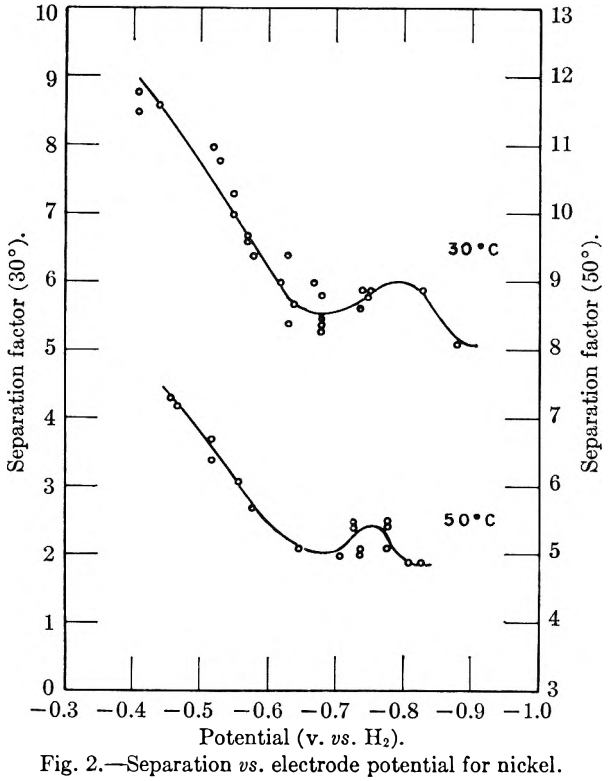


Fig. 2.—Separation *vs.* electrode potential for nickel.

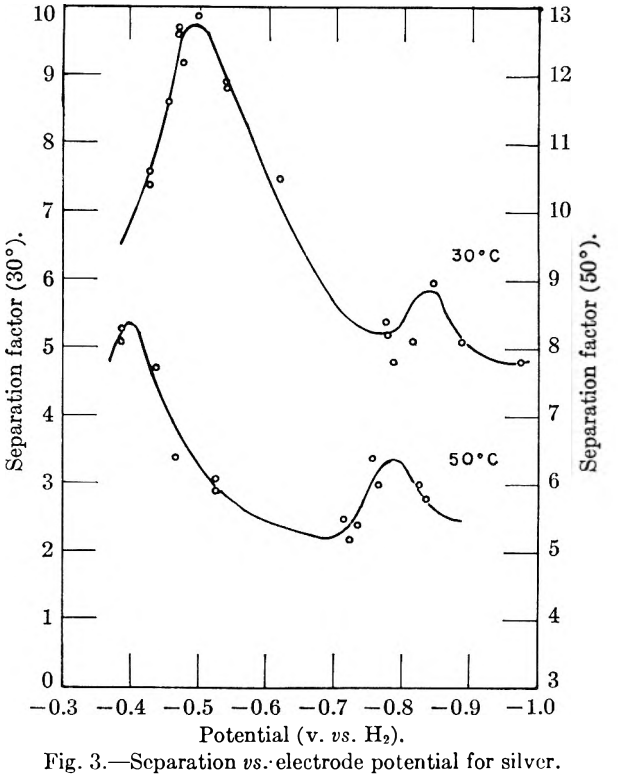


Fig. 3.—Separation *vs.* electrode potential for silver.

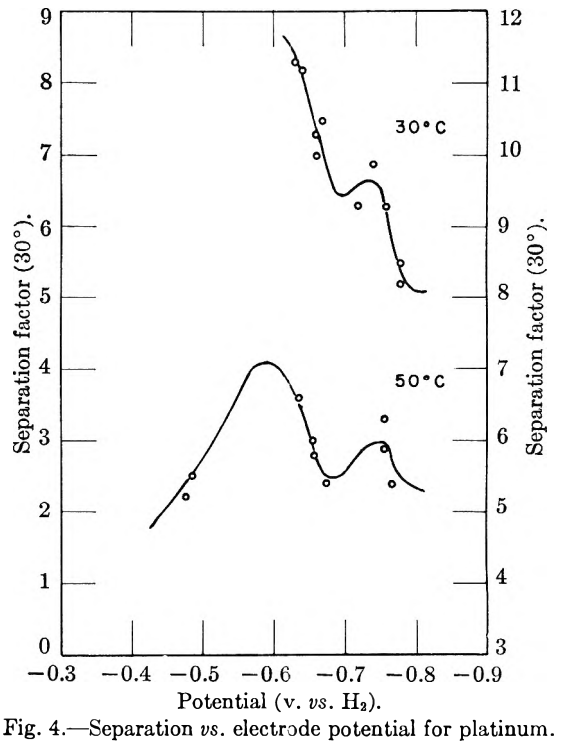


Fig. 4.—Separation *vs.* electrode potential for platinum.

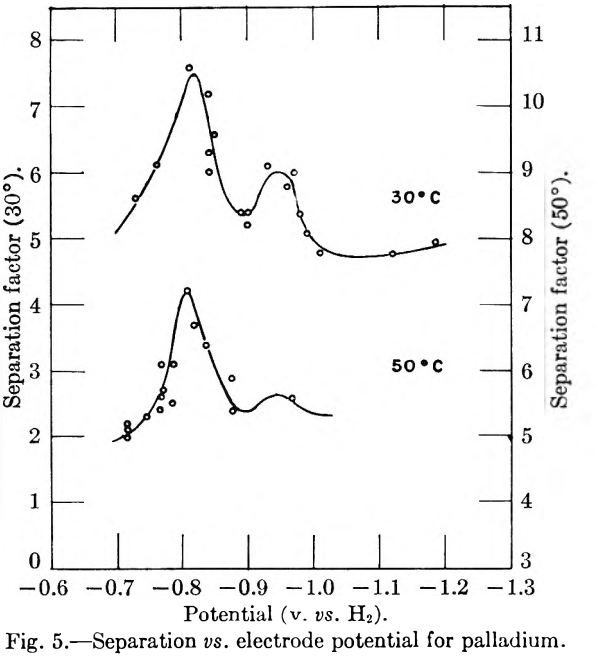


Fig. 5.—Separation *vs.* electrode potential for palladium.

is 3.7 (at 25°), which is the equilibrium constant for the exchange reaction, the separation factor must rise from this value.

Efforts were made to collect a sample only after a constant potential had been reached, which was usually after several hours of current flow. However, the potential of each electrode material at a constant current was not reproducible for different electrodes of the same material. Different potentials were thus measured for two runs at the same current density. The electrodes became roughened and cathodic corrosion was observed during the course of the electrolysis. In spite of all efforts, in some cases the potential of the electrode varied during the run, and an average potential had to be computed. The separation factor was, of course, always an average value for the run, which lasted from 3 to 12 hr., depending on the applied current. In several instances, successive runs were made on the same electrode at the same constant current, and the potentials were different

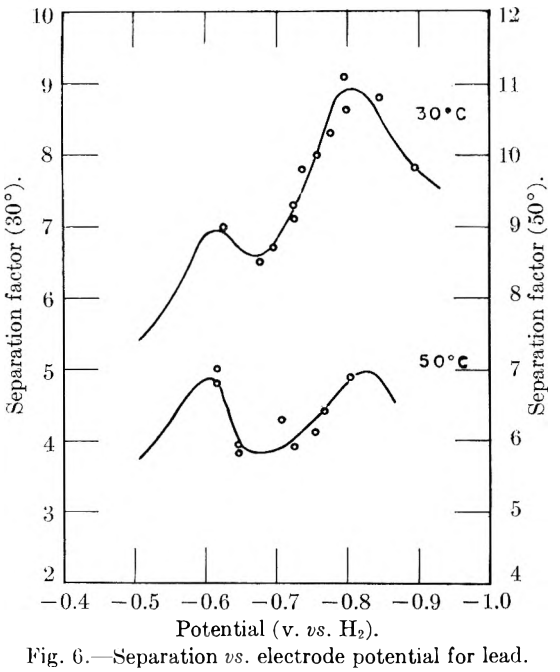


Fig. 6.—Separation *vs.* electrode potential for lead.

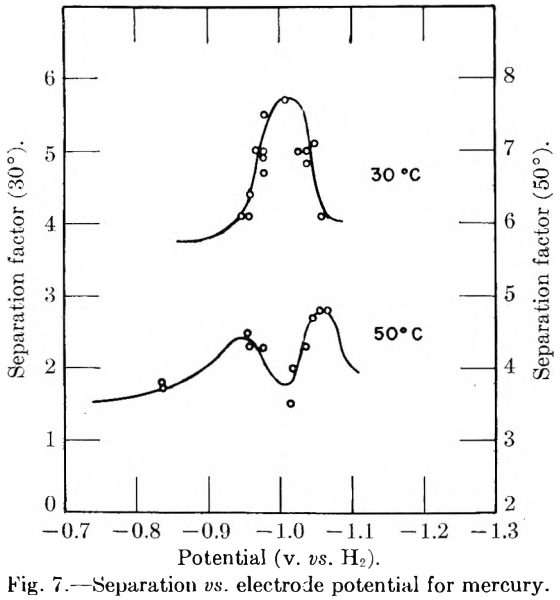


Fig. 7.—Separation *vs.* electrode potential for mercury.

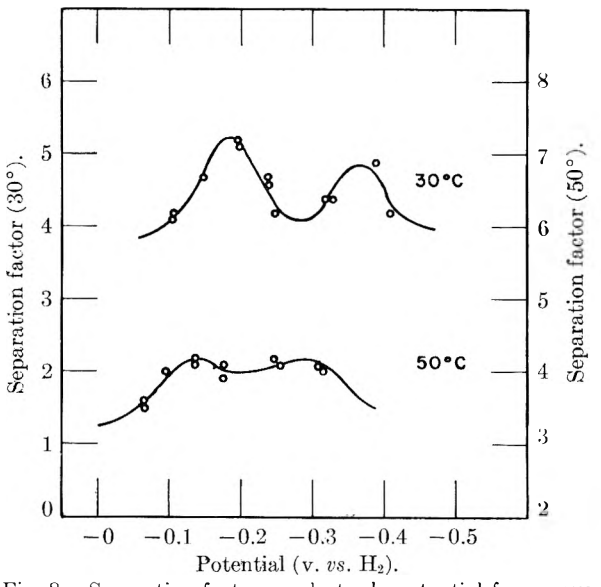


Fig. 8.—Separation factor *vs.* electrode potential for porous sintered Ni–Ag–Pd–C electrode.

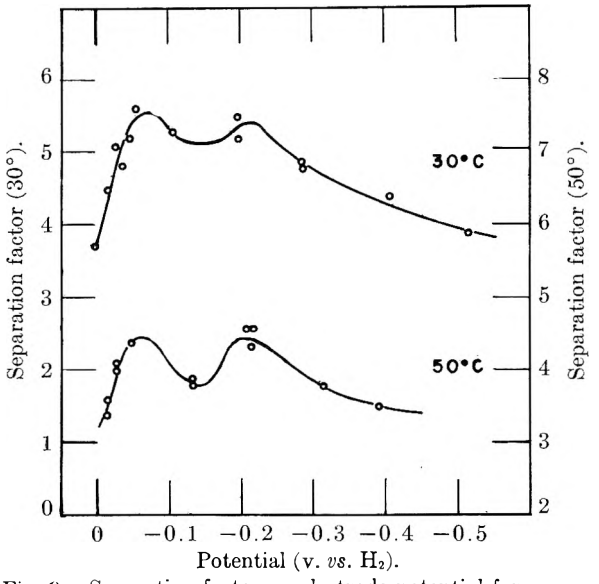


Fig. 9.—Separation factor *vs.* electrode potential for porous sintered Ni–Ag–Pd electrode.

for each run. During the first run the potential continually increased toward more negative values, and during the second run the potential had reached a steady value. The average potential for the first run was in some cases more than 100 mv. less negative than the steady potential of the second run. Significantly, the measured separation factors also differed for the two runs. The data therefore clearly indicated that the separation factor is a function of the electrode potential rather than the current flowing through the electrode. Differences in electrode surface roughness, or electrode contamination, thus will produce different potentials at the same current density, and so will give correspondingly different separation factors. Different current densities on the same electrode material, which in some cases resulted in equal electrode potentials, gave identical separation factors. Successive runs, where the electrode potential remained constant, gave values of $S$ differing by less than 3%.

Measurements close to the reversible hydrogen potential were possible with the porous electrodes even at relatively high current densities. This is because the true area of the porous electrodes was extremely large, resulting in low actual current densities. The reproducibility of the potential and the separation factors was better on the porous electrodes than on the smooth electrodes.

## Discussion

The following conclusions can be drawn from the data (Fig. 2–9) on cathodic hydrogen–deuterium separation factors.

1. The separation factor is a function of the cathode material and cathode potential.

2. The separation factor will rise from a value around 3.7 at open circuit to a maximum, and it

will then decrease as the potential of the electrode is made more negative.

3. The potential at which the first maximum in separation factor occurs is dependent on the electrode material. Those materials with low hydrogen overvoltages have the maximum occurring at −1.3 to −1.5 volts *vs.* Hg/HgO. High overvoltage electrodes such as mercury show a maximum separation factor around −1.9 volts *vs.* Hg/HgO. Nickel has the maximum for $S$ at the lowest potential. Then follow silver, platinum, palladium, lead, and mercury, respectively, in order of increasing negative potential.

4. The separation factor for all electrodes is lowered by 15–20% for a temperature increase from 30 to 50°. This is about 1% per °C.

5. Porous metal electrodes give separation factors 10 to 100% smaller than smooth electrodes.

6. The influence of the individual electrode material on the separation factor is diminished in the potential region negative to the maxima, and the data for all electrodes can be represented by a single curve with a scatter of about 25%.

An idealized representation of the data is shown in Fig. 10. Using this ideal picture, the following general explanation can be given for the dependence of the separation of the hydrogen isotopes by electrolysis, on the electrode potential, on the type of electrode surface, and on the temperature of electrolysis. When the electrode is maintained at an open circuit potential, the rates of the forward and backward electrochemical reactions are equal, and $S$ is approximately 3.8. As current is applied and the potential is made more negative, the rate of the forward electrochemical reaction will increase. Since hydrogen discharges faster than deuterium, the adsorbed gas on the electrode and the evolved gas become increasingly poorer in deuterium. At low overvoltages the backward electrochemical reaction is still important, and the separation factor therefore is less than that obtained from measurements in the Tafel overvoltage region. The low values of the separation factors in the vicinity of the reversible potential are due in part to a chemical exchange reaction between HDO in the electrolyte and hydrogen-rich gas adsorbed on the electrode, $HDO + H_2 \rightleftarrows HD + H_2O$. This exchange can take place on the electrode at sites where the electrode potential is inoperative or only partially operative.

As the potential is made more negative the rate of the electrochemical backward reaction becomes negligible. However, the chemical exchange reaction still can proceed at surface sites covered with gas bubbles or located in pores and cracks into which the negative electrode potential does not penetrate. The effect of the exchange reactions is to lower the separation factors even in potential regions where the backward electrochemical reaction can be expected to be very small. This reduces the maximum of the separation factor curve, explaining the low values for the porous electrodes.

In general, gas evolution will not start until the potential is sufficiently negative to activate the surfaces. This means that the bonds to anions and water dipoles must be weakened so that hydrogen

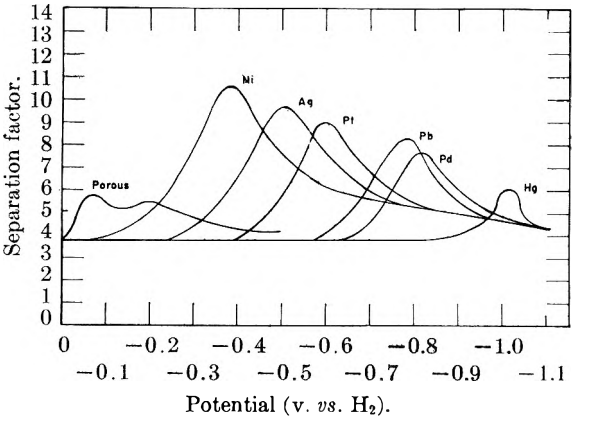


Fig. 10.—Idealized dependence of separation factors *vs.* electrode potentials for various electrodes at 30°.

and deuterium can be discharged. Electrochemical separation cannot take place and the separation factor will remain undefined, but theoretically close to the equilibrium value, until a certain quantity of current flows. The double layer of high overvoltage materials consists of strongly adsorbed foreign species, at voltages only slightly negative to the reversible potential, and discharge and adsorption of hydrogen is limited. The higher the overvoltage characteristics of the electrode, which are determined by the relative adsorption energies of reacting and foreign species,[12,13] the more negative the potential must be before appreciable discharge takes place. On the mercury electrode, therefore, the separation factor does not start to rise until a potential of 1.8 v. negative is reached.

At a characteristic potential, which is different for each electrode material, the surface coverage of the electrode by adsorbed protons and deuterons becomes sufficient to force the ions to be discharged at energetically less favorable surface sites. The ions moving toward the electrode then are neutralized by electrons which move through the covered electrode–solution interface. The specific influence of the adsorption sites (which determines which isotope will discharge) is decreased considerably at these high surface coverages. Hydrogen then will not be discharged as preferentially relative to deuterium, as when discharge takes place primarily on a "bare" electrode surface. The separation factor decreases, therefore, from the maximum value, as the potential is made more negative. The increased coverage of the electrode surface has the effect of making all electrode materials look similar to oncoming ions. Consequently, the rates of hydrogen and deuterium ion discharge will not be strongly dependent on the electrode material in the extreme negative potential region where the separation factors decrease. The separation factors then should tend to merge in this region for all electrode materials, and this result was indeed confirmed experimentally.

The data on porous electrodes can be explained by the same reasoning. The high internal sur-

(12) P. Ruetschi and P. Delahay, *J. Chem. Phys.*, **23**, 195 (1955).
(13) P. Ruetschi, *J. Electrochem. Soc.*, **106**, 9 (1959).

face area, however, shifts the data to lower separation factor values and lower potentials. Since the porous electrodes can discharge ions at very low potentials, the backward electrochemical reaction rate is quite high, and the separation factors are correspondingly lower. In addition, the internal surface roughness, which results in a highly catalytic surface and unequal potential distribution over the true area, increases the rate of the chemical exchange at sites where the potential is inoperative, to the extent that the maximum separation factor on the porous electrodes is less than 6 in all instances. The general shape of the curve of separation factor *vs.* potential for porous electrodes is the same as for smooth electrodes. The existence of two maxima in the separation factor curves seem to correspond to the presence of two energetically different adsorption or reaction sites at two different degrees of surface coverage.

The decrease in separation factor with increasing temperature is due to both the lower hydrogen overvoltage and the lower exchange reaction equilibrium constant at the higher temperature. The thermodynamic equilibrium constant is lowered by 13% as the temperature is increased from 30 to 50°. This decrease is close to the total percentage decrease in $S$ observed experimentally over the same temperature range. The overvoltage difference between hydrogen and deuterium ion discharge decreases slightly with increasing temperature. The shape of the separation factor *vs.* potential curve remains the same at increased temperature with a lower maximum for $S$, which is shifted to less negative potentials.

# MASS SPECTROMETRIC STUDY OF THE VAPORIZATION OF THE TITANIUM–BORON SYSTEM[1]

BY P. O. SCHISSEL[2a] AND O. C. TRULSON[2b]

*Parma Research Laboratory, Union Carbide Corp., Cleveland, Ohio*

*Received March 16, 1962*

A mass spectrometer has been used with Knudsen cells to study the vaporization of the titanium–boron system. The pressures of Ti(g) and B(g) have been determined over several condensed phases and yield $\Delta H^0_{298} = 430$ kcal./mole and $\Delta H^0_{298} = -52$ kcal./mole for the heats of vaporization and formation of $TiB_2$, respectively. Thermodynamic functions for TiB(s) have been obtained.

## Introduction

Brewer and Haraldsen[3] have summarized thermodynamic information on some refractory borides and have made qualitative estimates of heats of formation based on the relative stabilities of boron-containing compounds at high temperatures. They mention the experimental difficulties associated with borides and suggest vapor pressure measurements as a promising approach to the evaluation of thermodynamic quantities. Vapor pressure measurements on elemental boron have been made by Chupka,[4] Thorn,[4] Schissel and Williams,[5] and Akishin, *et al.*,[6] who find values in agreement for the heat of sublimation near $\Delta H_0^0 = 130$ kcal./mole.

The qualitative observations of Brewer and Haraldsen[3] indicate a heat of formation for $TiB_2$(s) near −72 kcal./mole; this value is confirmed by Samsonov.[7] However, mass spectrometric determinations of partial vapor pressures by Schissel and Williams[5] showed $TiB_2$ to be more volatile than would correspond to $\Delta H_f^0 = -72$ kcal./mole, leading to a value of about −32 kcal./mole instead; the congruent vaporization of the Ti–B system as used by Searcy, *et al.*,[8] provided bounds for the relative electron impact ionization cross sections for titanium and boron vapor and substantiated the conclusions of Schissel and Williams; and a high temperature calorimetric measurement by Lowell and Williams[9] resulted in $\Delta H_f^0 = -50 \pm 5$ kcal./mole.

A mass spectrometer was employed in the present work with Knudsen effusion cells where the pressures of titanium and boron vapor were determined from rates of effusion. The vaporization of $TiB_2$ was studied under several experimental conditions: (1) $TiB_2$ with excess boron added, (2) $TiB_2$, and (3) $TiB_2$ with excess titanium added. The results of each set of measurements were used to compute the heat of vaporization of $TiB_2$, and current thermodynamic data were used to obtain the heat of formation at 298°K.

**Apparatus.**—The mass spectrometer, similar to that developed by Inghram and co-workers,[10] was a 60° sector instrument of 12 in. radius, differentially pumped by two 5-l./sec. ion-getter vacuum pumps.[11] Electron bombardment was used to heat the Knudsen cells in an arrangement similar to that of Chupka and Inghram.[12] A movable shutter interposed between the cell and the electron-impact ionization

(1) This work was accomplished with ARPA support under AOMC Contract DA-30-069-ORD-2787.

(2) (a) Union Carbide Corporation, Parma Research Laboratory; (b) Union Carbide Research Institute.

(3) L. Brewer and H. Haraldsen, *J. Electrochem. Soc.*, **102**, 399 (1955).

(4) JANAF Interim Thermochemical Tables, The Dow Chemical Co., Midland, Michigan, December 31, 1960.

(5) P. O. Schissel and W. S. Williams, *Bull. Am. Phys. Soc.*, Ser. II, **4**, No. 3 (1959).

(6) P. A. Akishin, O. T. Nikitin, and L. N. Gorokov, *Dokl. Akad. Nauk SSSR*, **129**, 1075 (1959).

(7) G. V. Samsonov, *J. Applied Chem.* (USSR), **28**, 975 (1955).

(8) A. W. Searcy, W. S. Williams, and P. O. Schissel, *J. Chem. Phys.*, **32**, 957 (1960).

(9) C. E. Lowell and W. S. Williams, *Rev. Sci. Instr.*, in press.

(10) M. G. Inghram and R. J. Hayden, National Academy of Sciences and National Research Council, Publication 311 (1954).

(11) Varian Associates, 611 Hansen Way, Palo Alto, California.

(12) W. A. Chupka and M. G. Inghram, *J. Phys. Chem.*, **59**, 100 (1955).

source was used to distinguish neutral species from background non-condensable molecules of the same mass. The energy of the ionizing electrons was continuously adjustable from 5 to 150 e.v. for appearance potential measurements. The main detector[13] was a twenty-stage electron multiplier employing Be–Cu dynodes. Provision was also made to collect the ion beam directly on an adjustable plate which could be moved in and out of the line of the ion beam The output from each collector was measured with an electrometer and recorded continuously on a strip-chart recorder.

Temperature measurements were made with a Leeds and Northrup disappearing-filament optical pyrometer sighted into small holes (0.030 in. diam., 0.060 in. deep) in the sides of the Knudsen cells. The pyrometer was calibrated against a standard lamp certified by the National Bureau of Standards to be accurate to ±7° at the highest temperatures employed in this study. An auxiliary check was made against a pyrometer calibrated by the National Bureau of Standards and no systematic differences were noted. The calibration error therefore was taken to be ±7°. The temperature correction for the sight window was determined before and after all data were taken. The estimated total error was ±20° for the work with boron added to $TiB_2$ and ±10° for the remaining measurements. Because of the high emissivity of graphite and since the temperatures were measured by sighting in holes in the graphite, no emissivity corrections were necessary. Further tests on the temperature measurements showed the above statement to be correct, and further that temperature gradients in the cell were small. In an auxiliary vacuum system two pyrometers were simultaneously sighted on a tungsten ribbon filament to obtain their relative calibration. The Knudsen cell then was placed at the same position as the tungsten ribbon with one pyrometer sighted into the temperature measuring hole in the side of the cell and the second pyrometer sighted into the Knudsen effusion hole. At the temperatures used in the experiments for which third law calculations were made in this study no systematic difference could be measured, but at the very lowest temperatures (1700°K.), attained only during measurements pertaining to the second law treatment of the vaporization of boron, a temperature difference was noted but never exceeded 14°.

**Procedure and Results.**—The phase diagram shown by Brewer and Haraldsen[3] for the Ti–B–C system indicates the expected mutual stabilities of the various phases. This diagram was used to determine suitable crucible materials for the systems which were studied. For the experimental situations discussed below, the phase systems are identified by the sample materials initially loaded in the crucible. Subsequent X-ray analyses of the samples after heating showed partial conversion to other phases, particularly in the boron- and titanium-rich cases. The experimental results are discussed in the light of the X-ray observations made at room temperatures after the runs.

$TiB_2$(s) + B(s).—X-Ray analysis of an aliquot part of the $TiB_2$ and boron powdered samples showed no detectable impurities, and spectroscopic analysis showed 0.1% iron, 0.1% silicon, and smaller amounts of chromium and other metals. The samples were run in a $B_4C$ crucible ($^{11}/_{32}$ in. diam., $^{11}/_{16}$ in. long, $^{1}/_{32}$ in. wall thickness) which was contained in a graphite outer jacket ($^{15}/_{16}$ in. diam., 1-$^{1}/_{4}$ in. long, $^{1}/_{8}$ in. wall thickness). Two $B_4C$ crucibles were made by heating graphite crucibles in the presence of boron. The first crucible was used to demonstrate the complete boronization of the graphite; the second was used for the experimental runs. Both crucible and jacket had rectangular orifices 4.5 mm. long and 0.75 mm. wide which provided a ratio of orifice area to sample area of $\sigma_A \cong 0.04$ (sample area means gross exposed powder area, not the microscopic area which may make the effective $\sigma_A$ smaller).

After the sample was loaded, the Knudsen cell was heated slowly to the temperature at which a shutter effect was observed on $Ti^{48}$ and $B^{11}$. (These isotopic signals were used for all the measurements, whereas signals at other isotopic positions were used only to confirm the identification of the species.) During the preliminary outgassing period, gaseous titanium oxide and boron oxide species were observed, but disappeared completely after several hours of heating. No data were taken until signals obviously characteristic of the oxide species had disappeared and appearance-potential measurements indicated that the B and Ti signals resulted solely from the elemental gases.

Data were taken on the temperature dependence of the boron signal and were plotted according to the Clausius–Clapeyron relation to obtain the heat of sublimation of boron, $\Delta H_T^0$. Four experimental runs of this type were made. The results for $\Delta H_T^0$ in kcal./mole obtained chronologically are: 130.2 ± 4.4 at 1962°K., 128.4 ± 1.2 at 2085°K., 133.0 ± 2.2 at 2072°K., and 132.6 ± 1.5 at 2121°K., where the errors are the statistical errors determined from least square analyses, and the temperatures are the average mid-range temperatures of the individual runs. Tabulated data[4] were used to reduce the $\Delta H_T^0$ values to $\Delta H_0^0$ with the results $\Delta H_0^0$ = 130.8 ± 5.1, 129.3 ± 2.7, 133.8 ± 3.4, and 133.5 ± 2.9 kcal./mole. The final error assignments were obtained from the statistical combination of random errors from the least squares analyses and from the instrumental uncertainty in the absolute temperature (fractional error in $\Delta H_T^0 = 2(\Delta T/T)$, as described by Trulson, *et al.*[14] A powder pattern X-ray analysis of the sample after the runs showed strong $TiB_2$ lines and no boron lines. While the boron lines were weak even at the start, it is possible that all free boron was lost during the course of heating. Nevertheless, the average of the above second law values, 131.9 kcal./mole, is only slightly higher than mass spectrometric determinations using the third law[4–6] and is in excellent agreement with recently tabulated data.[4] Therefore, computations in this section will utilize the tabulated data for the vapor pressure of boron.

The titanium pressure was determined relative to the boron pressure from

$$P_{Ti} = P_B \frac{I_{Ti}\, T_{Ti}}{I_B\, T_B} \frac{(\sigma i S)_B}{(\sigma i S)_{Ti}} \qquad (1)$$

where $P$ denotes the partial pressure, $I$ the relative collected ion current, $\sigma$ the cross section for ionization of neutral species, $T$ the temperature, $i$ the isotopic abundance correction factor, and $S$ the electron multiplier conversion factor. The ionization cross sections computed by Otvos and Stevenson[15] were used, and the multiplier conversion efficiencies were determined directly for both boron and titanium signals. The relative ion signals were measured at the same temperature. Electron bombardment energies ranging from 15 to 60 e.v. were used, but always were normalized to 40 e.v. by means of appearance-potential data of relative signal intensity *vs.* electron energy taken when the signals were large.

The boron and titanium pressures were used to obtain the equilibrium constant $K$ for the reaction $TiB_2(s) \rightarrow Ti(g) + 2B(g)$. The free energy change was computed ($\Delta F_T^0 = -RT \ln K$), and the heat of vaporization was obtained from

$$\Delta H^0_{298} = \Delta F^0_T + T\left(-\frac{\Delta F^0_T - \Delta H^0_{298}}{T}\right)_{Ti(s)\rightarrow Ti(g)} + 2T\left(-\frac{\Delta F^0_T - \Delta H^0_{298}}{T}\right)_{B(s)\rightarrow B(g)} \qquad (2)$$

where tabulated[4] free energy functions for Ti and B were used, and free energy functions for $TiB_2$(s) were assumed equal to those for Ti(s) + 2B(s), which assumption is equivalent to assuming $\Delta C_p$ and $\Delta S$ are zero for the solid–solid reaction. Walker, *et al.*,[16] have shown that $\Delta C_p \simeq 0$ up to 700°. The heat of formation of $TiB_2$(s) was computed from $\Delta H^0_{298}$ and the tabulated[4] heats of sublimation of boron and titanium.

Data used to compute the heat of vaporization of $TiB_2$ are given in section 1 of Table I. Ten determinations of $P_{Ti}$ relative to $P_B$ were made over a temperature range of approximately 200°K. The table gives the equilibrium constant, free energy change, and heat of vaporization of $TiB_2$(s). The average heat of vaporization at 298°K. is

(13) Nuclide Analysis Associates, Box 752, State College, Pennsylvania.

(14) O. C. Trulson, D. E. Hudson, and F. H. Spedding, *J. Chem. Phys.*, in press.

(15) J. W. Otvos and D. P. Stevenson, *J. Am. Chem. Soc.*, **78**, 546 (1956).

(16) B. E. Walker, C. T. Ewing, and R. R. Miller, *J. Phys. Chem.*, **61**, 1682 (1957).

TABLE I

CALCULATION OF THE HEAT OF VAPORIZATION AND HEAT OF FORMATION OF $TiB_2$(s)

| System before heating | | $T$ (°K.) | $-\log P_B$ | $-\log P_{Ti}$ | $-\log K$ | $\Delta F_T^0$ (kcal./mole) | $\Delta H^0_{298}$ (kcal./mole) | | $-\Delta H_f^0$ (kcal./mole) | |
|---|---|---|---|---|---|---|---|---|---|---|
| B + $TiB_2$ in $B_4C$ | 1 | 2244 | | 8.47 | 18.92 | 194.3 | 427.5 | | 49.8 | |
| | | 2296 | | 8.46 | 18.33 | 192.6 | 430.9 | | 53.2 | |
| | | 2347 | | 8.26 | 17.62 | 189.2 | 432.6 | | 54.9 | |
| | | 2357 | | 8.44 | 17.69 | 190.8 | 435.2 | | 57.5 | |
| | | 2382 | | 7.97 | 16.98 | 185.0 | 432.0 | | 54.2 | |
| | | 2398 | | 7.96 | 16.81 | 184.4 | 432.9 | | 55.2 | |
| | | 2408 | | 7.74 | 16.50 | 181.8 | 431.2 | | 53.5 | |
| | 2 | 2306 | | 8.40 | 18.16 | 191.7 | 431.1 | | 53.3 | |
| | | 2462 | | 7.38 | 15.64 | 176.2 | 431.0 | | 53.3 | |
| | 3 | 2411 | | 7.56 | 16.29 | 179.7 | 429.5 | | 51.8 | |
| | | | | | | | | 431.4 | | Av. 53.7 ± 0.7 |
| $TiB_2$ in C | 4 | 2192 | 6.54 | 7.19 | 20.27 | 203.3 | 431.4 | | 53.7 | |
| | | 2185 | 6.62 | 7.11 | 20.36 | 203.5 | 430.9 | | 53.2 | |
| | 5 | 2353 | 5.14 | 6.31 | 16.60 | 178.7 | 422.7 | | 45.0 | |
| | 6 | 2246 | 6.20 | 7.12 | 19.52 | 200.6 | 434.1 | | 56.3 | |
| | | 2246 | 6.22 | 7.00 | 19.44 | 199.8 | 433.2 | | 55.5 | |
| | | 2246 | 6.13 | 7.04 | 19.30 | 198.4 | 431.8 | | 54.1 | |
| | | 2278 | 5.78 | 6.83 | 18.40 | 191.8 | 428.3 | | 50.6 | |
| | | 2278 | 5.73 | 6.78 | 18.23 | 190.1 | 426.6 | | 48.9 | |
| | | 2278 | 5.77 | 6.79 | 18.33 | 191.1 | 427.6 | | 49.9 | |
| | | 2310 | 5.57 | 6.83 | 17.97 | 189.9 | 429.7 | | 52.0 | |
| | | | | | | | | 429.6 | | Av. 51.9 ± 1.1 |
| Ti + $TiB_2$ in C | 7 | 2271 | 6.22 | 6.02 | 18.46 | 191.8 | 427.7 | | 50.0 | |
| | | 2269 | 6.18 | 6.21 | 18.56 | 192.7 | 428.4 | | 50.7 | |
| | | 2269 | 6.11 | 6.29 | 18.51 | 192.1 | 427.9 | | 50.1 | |
| | | 2307 | 5.93 | 6.21 | 18.06 | 190.6 | 430.1 | | 52.4 | |
| | | 2063 | 7.61 | 7.92 | 23.15 | 218.5 | 433.7 | | 56.0 | |
| | | 2107 | 7.04 | 7.59 | 21.68 | 209.0 | 428.6 | | 50.9 | |
| | | 2272 | 6.01 | 6.44 | 18.45 | 191.8 | 427.8 | | 50.1 | |
| | 8 | 2276 | 5.96 | 6.55 | 18.47 | 192.4 | 428.8 | | 51.0 | |
| | 9 | 2266 | 6.61 | 5.35 | 18.56 | 192.5 | 427.9 | | 50.2 | |
| | 10 | 2340 | 6.11 | 4.96 | 17.18 | 183.9 | 426.7 | | 49.0 | |
| | | 2327 | 6.05 | 5.37 | 17.47 | 186.0 | 427.5 | | 49.7 | |
| | | | | | | | | 428.6 | | Av. 50.9 ± 0.7 |

431.4 ± 5.9 kcal./mole, and the heat of formation is −53.7 ± 5.9 kcal./mole.

**$TiB_2$ in Graphite.**—A crucible fabricated from "National" TSX graphite was used with a $TiB_2$ powdered sample. The knife-edged circular orifice in the crucible lid was 0.75 mm. in diameter to give $\sigma_A \leq 5 \times 10^{-3}$. In a preliminary run the crucible was heated empty to the highest temperatures anticipated for the $TiB_2$ measurements to demonstrate that no boron background impurity signals were present. The $TiB_2$ sample was then loaded with a 5-mg. silver calibration charge and heated to approximately 1100°, where the silver charge was allowed to vaporize completely. This method of calibration has been described by Chupka and Inghram.[12] The pressures of titanium and boron were determined from ion intensity data taken at higher temperatures according to the relation

$$P_x = \frac{I_x}{K_{Ag}} \frac{T}{(\sigma i S)_x} \frac{(\sigma i S)_{Ag}}{} \qquad (3)$$

where $I_x$ denotes the relative ion current for species x (titanium or boron), $T$ the cell temperature, and $(\sigma iS)$ as described in eq. 1. The constant $K_{Ag}$ represents the effective sensitivity constant (the collected charge per effused neutral particle) for the mass spectrometer determined from the silver calibration measurements.

The relative intensities of the boron and titanium signals were observed to increase slowly with time at fixed crucible temperature. Since boron already had the higher partial pressure, this further increase would be paradoxical if titanium and boron only were present. However, equilibration with carbon, while having little effect on the integral free energy for the reaction, $TiB_2(s) \rightarrow Ti(g) + 2B(g)$, can change the partial molal free energies of the titanium and boron markedly. In other terms, the equilibrium constant should remain nearly unchanged when carbon is added while the partial pressures may change significantly.

Equilibrium constants and integral free energies of evaporation were calculated by the third law method outlined in eq. 2. Ten determinations of $P_{Ti}$ and $P_B$ were made over $TiB_2$ in graphite and are given in Table I, section 2. These results yield $\Delta H^0_{298} = 429.6 \pm 5.4$ kcal./mole for the vaporization of $TiB_2$ and $\Delta H^0_{298} = -51.9 \pm 5.4$ kcal./mole for the heat of formation.

**Ti + $TiB_2$.**—Excess titanium was added to the graphite crucible containing the $TiB_2$ sample used in the runs described above. The crucible was heated for several hours above the melting point of titanium to allow complete reaction, and subsequent X-ray analysis of the sample showed $TiB_2$ only, while the inside of the crucible lid showed C and TiC. Additional titanium was added and the heating process was repeated; again the reaction occurred but at a much slower rate. A third loading of titanium was added with a weighed amount of silver. A silver calibration was performed at 1100° and was in agreement (~10%) with other calibrations. The vapor pressure of solid titanium was determined from eq. 3: at 1842°K., $P_{Ti} = 1.0 \times 10^{-6}$ atm.; at 1858°K., $P_{Ti} = 1.6 \times 10^{-6}$ atm.; and at 1722°K., $P_{Ti} = 1.1 \times 10^{-7}$ atm. These results are in excellent agreement with tabulated data[4] and are used to confirm the ionization cross sections computed by Otvos and Stevenson[15] for titanium. While Ti(s) cannot be in equilibrium with C, TiC, and $TiB_2$, it is assumed the reaction rate was sufficiently slow after the crucible had been previously exposed to titanium at much higher temperatures to sustain the pressure

over solid titanium though the pressure of pure titanium was not sustained over the more reactive liquid. This assumption is corroborated by the observation that even after the second loading of titanium, a plot of ln $P_{Ti}$ *vs.* $1/T$ taken before the titanium was melted yielded a heat of sublimation of titanium only 7 kcal. larger than given in the JANAF tables.

Below the melting point of titanium, the boron signal could not be observed, but at higher temperatures both signals were measured. At the higher temperatures the reaction of titanium again became evident, since the vapor pressure (which was determined after each of the three successive titanium loadings) of liquid titanium could not be maintained, although the pressure exceeded that to be expected over TiC + C.

The pressure data are given in section 3 of Table I, and unlike the previous results, were not obtained at a fixed position in the phase diagram. As excess titanium was added, different phases formed, and X-ray analyses showed TiC + C + $TiB_2$ after the first heating and TiC + TiB (orthorhombic) + $TiB_2$ after the final heating. The effect of the additional titanium manifests itself in a 20-fold increase in titanium pressure at 2300°K., as inspection of the values of $P_{Ti}$ in section 3 of Table I will show, and corresponds to the formation of TiB. Titanium diboride was always present and each set of pressures gives consistent values for its heat of vaporization. Results for eleven sets of data give an average heat of vaporization for $TiB_2$ of 428.6 ± 5.3 kcal./mole and a heat of formation of −50.9 ± 5.3 kcal./mole. The pressures from run No. 10 of Table I, taken in the TiC–TiB–$TiB_2$ region of the phase diagram, yield for the reaction TiB(s) → Ti(g) + B(g), log $K_{2340}$ = −11.07, $\Delta F^0_{2340}$ = 118.5 kcal./mole, and $\Delta H^0_{298}$ = 279 kcal./mole. The associated heat of formation of TiB(s) at 298°K. is −34 kcal./mole.

**Summary.**—Data from all the experimental points given in Table I can be used to plot the equilibrium constant for the vaporization of $TiB_2$. A least squares analysis of a plot of ln $K$ *vs.* $1/T$ yields $\Delta H^0_{2287}$ = 424 ± 14 kcal./mole and $\Delta H^0_{298}$ = 435 kcal./mole, in excellent internal agreement with the third law computations. This result is independent of any assumptions regarding ionization cross sections.

Searches for Ti–B gaseous species were negative; for example, at 2426°K., $P_{TiB(g)}$ was less than $10^{-9}$ atm. during the B + $TiB_2$ runs. Similar bounds for other simple combinations occurred and, in general, extended sweeps through mass 600 indicated no species to ~1% of the B(g) signal. A search for $B_2$(g) was negative and indicated $P_{B_2}$ was less than $4 \times 10^{-9}$ atm. at 2316°K. over B + $TiB_2$. This bound is not low enough to test the tabulated data.[4]

Some impurity signals were observed. In addition to the oxide species which volatilized, elemental Fe(g) and Cr(g) impurities were observed and never completely disappeared. During the final runs where excess titanium was added, the pressure of Cr(g) was comparable to Ti(g) even though spectroscopic analysis showed the Ti(s) to contain no Cr. It is presumed that chromium borides in the $TiB_2$ at trace levels were converted to titanium borides and excess chromium. The rather high impurity level of Cr on the inside of the lid corroborates this assumption.

Some unexplained signals occurred at the mass 32 through 37 positions which appeared by every test to be legitimate neutral species leaving the cell during the work with B + $TiB_2$ in $B_4C$. It is believed they are not related to the Ti–B system but are possibly gaseous B–C species.

In all the previous results, the net experimental error assignment comprised the random uncertainties obtained as the standard deviation of the means compounded with the instrumental uncertainties obtained from the estimated errors in the temperature and vapor pressures. The temperature error has been discussed above; the pressure error was determined from uncertainties in the relative ionization cross sections and in the measured relative multiplier gains for the several species. The internal agreement among the second and third law measurements by Chupka,[4] the third law measurements by Schissel and Williams,[5] and the second law data herein presented on the sublimation of boron, shows that the relative cross sections $\sigma_B/\sigma_{Ag}$ predicted by Otvos and Stevenson[15] are in error by less than ±50%. Assuming that the tabulated data[4] on titanium are correct, the pressure determinations on titanium in this study show the relative cross sections $\sigma_{Ti}/\sigma_{Ag}$ to be in error by less than ±50%, and thus the ratio $\sigma_B/\sigma_{Ti}$ is known to at least a factor of two. These observations are consistent with those of Searcy, *et al.*,[8] for the free surface vaporization of $TiB_2$. The multiplier response for Ag, B, and Ti was measured in this work with an uncertainty of ±10%. All thermodynamic results taken from tabulated data were assumed to be without error.

## Discussion

Partial pressures of titanium and boron have been determined over condensed phases of the Ti–B–C system for several regions of the phase diagram. The first set of measurements was made in the region $TiB_2$–$B_4C$–B, where boron and $TiB_2$ powders were used in a $B_4C$ crucible. The second set of measurements was made with $TiB_2$ powder loaded in a graphite crucible, ostensibly along the line $TiB_2$–C in the phase diagram. The third set of measurements was made with titanium metal added to the $TiB_2$ powder in the graphite crucible used for the second set of measurements. Results for the heat of vaporization and formation of $TiB_2$ are in excellent agreement, giving an average $\Delta H^0_{298}$ = 429.8 kcal./mole and an average $\Delta H^0_{298}$ = −52.1 kcal./mole, respectively.

As discussed by Brewer and Haraldsen[3] the observation that $TiB_2$(s) is stable in graphite bounds the stability of $TiB_2$ relative to TiC. Using the data of Humphrey[17] for TiC, one finds $\Delta H_f^0(TiB_2) \leq -44$ kcal./mole, while the data of Fujishiro and Gokcen[18] would yield $\Delta H_f^0(TiB_2) \leq -31.3$ kcal./mole. Brewer and Haraldsen state that the heats of formation of titanium borides should be about −36 kcal./mole of boron. The agreement between this result and that of Samsonov[7] for $TiB_2$ apparently is fortuitous, since Samsonov used the value −66 kcal./mole for the heat of formation of $B_4C$ in disagreement with the value used by Brewer and Haraldsen and with recently tabulated values.[4] The present results for $TiB_2$ do not agree with $\Delta H_f^0$ = −72 kcal./mole.

The measurements of Schissel and Williams[5] yield $\Delta H_f^0 \cong -32$ kcal./mole for $TiB_2$. These mass spectrometric measurements were made with a mixture of boron and $TiB_2$ powders contained in a

(17) G. L. Humphrey, *J. Am. Chem. Soc.*, **73**, 2261 (1951).

(18) S. Fujishiro and N. A. Gokcen, *J. Phys. Chem.*, **65**, 161 (1961).

$TiB_2$ crucible which was held in a tungsten outer jacket. The boron pressure determinations are in agreement with the data of this report although the titanium pressure was anomalously high. The discrepancy in the titanium pressure is believed to be due to titanium vapor escaping from the region between the $TiB_2$ cell and the tungsten jacket, possibly enhanced by reaction with the tungsten, thus leading to erroneous heats of vaporization and formation of $TiB_2$. In a recent experiment with a high temperature calorimeter, Lowell and Williams[9] obtained $\Delta H_f^0 = -50 \pm 5$ kcal./mole for $TiB_2$, in agreement with the result of the present investigation.

The question of vaporization coefficients has not been systematically investigated, but the values of $\sigma$ for the two cells were different by one decade and resulted in a statistically insignificant difference in the $TiB_2$ values.

The observation that TiB is found with $TiB_2$ after samples of the appropriate composition range are heated does not preclude the possibility that TiB is stable over a limited temperature range only. However, for TiB(s) to be unstable at low temperatures relative to Ti(s) and $TiB_2$(s), the heat of the reaction $Ti(s) + TiB_2(s) \rightarrow 2TiB(s)$ must be positive.[19] The value found in this research is $-16$ kcal./mole. TiB may be unstable at some temperatures relative to decomposition to $TiB_2$ plus a titanium rich phase, however. If, as suggested by Hansen and Anderko,[20] TiB decomposes at temperatures above about 2330°K., by the reaction $3TiB(s) \rightarrow Ti_2B(s) + TiB_2(s)$, a few of these measurements may have been made for $Ti_2B$ and $TiB_2$ mixtures. However, $\Delta F$ must be small for the decomposition reaction near the transition point, and no significant error is introduced by the assumption that TiB was the phase present with $TiB_2$.

**Acknowledgment.**—The authors wish to thank Dr. R. Goton for preparing the $B_4C$ crucibles and C. E. Lowell for the X-ray analyses. Several helpful discussions with Prof. A. W. Searcy are greatly appreciated.

(19) A. W. Searcy in "Proceedings of Second International High Temperature Symposium," Asilomar, California (Oct. 1959), McGraw-Hill Book Co., Inc., New York, N. Y., 1960.

(20) M. Hansen and K. Anderko, "Constitution of Binary Alloys," McGraw-Hill Book Co., Inc., New York, N. Y., 1958.

# KINETICS OF THE HYDROLYSIS OF ACETAL IN N-METHYLPROPIONAMIDE–WATER AND N,N-DIMETHYLFORMAMIDE–WATER SOLVENTS AT 20, 25, 30, AND 40°

BY RICHARD K. WOLFORD AND ROGER G. BATES

*Solution Chemistry Section, National Bureau of Standards, Washington 25, D. C.*

*Received March 17, 1962*

Rate constants for the acid-catalyzed hydrolysis of acetal in the binary solvent mixtures N-methylpropionamide–water and N,N-dimethylformamide–water have been obtained as a function of solvent composition and temperature. There is a marked decrease in the second-order rate constant when either amide is added to the aqueous solvent. The energy of activation remains essentially constant in the temperature range 20 to 30° but manifests an unexplained complex behavior in the 30 to 40° range. The decrease in rate when the aqueous solvent is enriched with either amide appears to follow the Winstein Y solvent parameter but shows no simple relationship with the change of dielectric constant of the bulk solvent. The various factors which may influence the rate of the reaction as the solvent composition is altered are discussed. Qualitatively it seems likely that the abrupt drop in rate of the acid-catalyzed reaction reflects to a large degree a decreased proton energy level resulting from the addition of relatively basic amide species.

## Introduction

The effect of a change in composition of a binary solvent mixture on the acid-catalyzed hydrolysis of acetal has been studied at different temperatures and acid concentrations. The reaction

$$CH_3CH(OC_2H_5)_2 + H_2O \longrightarrow CH_3CHO + 2C_2H_5OH$$

was chosen for several reasons: it has been studied many times in aqueous solution,[1,2] the hydrolysis reaction does not affect the acidity or ionic strength of the solution, the uncatalyzed hydrolysis is negligible, and the reaction appears to be catalyzed only by hydrogen ion.

The non-aqueous constituents of the aqueous binary solvent mixtures were N-methylpropionamide and N,N-dimethylformamide. The dielectric constants of these compounds (172.2 and 36.71, respectively, at 25°)[3] indicate a high degree of solvent polarity. The study of rate processes in amide–water mixtures may be expected to throw some added light on the structure of the solvent and the nature of specific solvation or "solvent sorting" around a charged ion.

The kinetics of a few reactions already have been investigated[4,5] using the pure amides and their mixtures as solvents. Studies dealing with the basicities of the amides have been published,[6,7] while proton magnetic resonance techniques have

(1) J. N. Brønsted and W. F. K. Wynne-Jones, *Trans. Faraday Soc.*, **25**, 59 (1929).

(2) L. K. J. Tong and A. R. Olson, *J. Am. Chem. Soc.*, **65**, 1704 (1943).

(3) G. R. Leader and J. F. Gormley, *ibid.*, **73**, 5731 (1951).

(4) S. D. Ross and M. M. Labes, *ibid.*, **79**, 4155 (1957).

(5) L. R. Dawson, J. E. Berger, and H. C. Eckstrom, *J. Phys. Chem.*, **65**, 986 (1961).

(6) R. J. L. Martin and I. H. Reece, *J. Chem. Soc.*, 4697 (1960).

(7) A. R. Goldfarb, A. Mele, and N. Gutstein, *J. Am. Chem. Soc.*, **77**, 6194 (1955).

provided information on proton exchange rates[8–10] and hydrolysis rates[11] for the pure amides and aqueous acid solutions of the amides. The extensive conductivity studies of Dawson, Sears, and their co-workers in amide solvents have been summarized elsewhere.[12]

## Experimental

The rate of reaction was followed by observing the change in volume of the solution by a dilatometric procedure.[2] The dilatometer consisted essentially of a Pyrex tube (1 cm. i.d.) shaped into the form of a helix. The helix was approximately 20 cm. high and 9 cm. wide and terminated at the top in a Pyrex tube (5 mm. i.d.) 7.5 cm. in length. This smaller tube was connected to a 7.5-cm. length of capillary tubing (1 mm. i.d.), and this in turn was connected to a piece of smaller capillary tubing (0.5 mm. i.d.) 30 cm. in length. The total volume of the dilatometer was approximately 90 ml. A vessel in which the components of the reaction were mixed and another smaller vessel containing mercury were attached to the bottom of the helix by means of a three-way stopcock. The complete assembly was immersed in a water bath maintained to within ±0.001°. Only the capillary tubes projected above the surface of the bath liquid. After the components of the reaction were mixed in the side vessel and forced into the dilatometer, an amount of mercury sufficient to seal the dilatometer was forced in. All solutions were made up by weight, and the concentration of each constituent in the solution was determined in terms of the total weight of all constituents. The density obtained at the end of the reaction allowed a calculation of molar concentrations to be made.

N-Methylpropionamide was prepared from propionic acid (Eastman White Label) and methylamine (Matheson Company). The reaction mixture was heated to eliminate water and then fractionally distilled through an efficient column to give a product that had a conductivity less than $1 \times 10^{-6}$ ohm$^{-1}$ cm.$^{-1}$. Eastman White Label N,N-dimethylformamide was used without purification; its conductivity was less than $1 \times 10^{-6}$ ohm$^{-1}$ cm.$^{-1}$. Conductivity water was used for all experiments. Acetal (Eastman White Label) was dried over calcium chloride, decanted, treated with sodium hydroxide pellets, and finally distilled in a spinning-band still.

For several experiments, the progress of the reaction was followed by analyzing the mixture for acetaldehyde content, using a modification of the method of Siggia and Maxcy.[13] In addition to providing a check on the dilatometric procedure, this analysis also confirmed the stoichiometry of the reaction.

## Results

The rate $v$ of the reaction is

$$v = k_1 c_A = k_2 c_A c_{H^+} \qquad (1)$$

where $c_A$ is the molar concentration of acetal, $c_{H^+}$ the stoichiometric molar concentration of hydrochloric acid, $k_1$ the pseudo first-order rate constant in sec.$^{-1}$, and $k_2$ the second-order (or catalytic) rate constant in l. mole$^{-1}$ sec.$^{-1}$. Experimental data were obtained by noting the liquid height in the capillary as a function of time. To obtain the rate constants $k_1$, these data were treated by the methods suggested by Guggenheim[14] or Swinbourne.[15]

Table I lists pertinent data for the hydrolysis of acetal in aqueous hydrochloric acid and in solutions of hydrochloric acid in solvent mixtures composed of water and N-methylpropionamide at 20, 25, 30, and 40°. As the amide content increases, $k_2$ decreases rapidly. The mole fraction of the amide was maintained at a constant value for selected ex-

TABLE I

RATES OF HYDROLYSIS OF ACETAL IN AQUEOUS HYDROCHLORIC ACID–N-METHYLPROPIONAMIDE (NMP) SOLUTIONS AT VARIOUS TEMPERATURES

| Mole % NMP | Density (g. ml.$^{-1}$) | $c$(acetal) (moles l.$^{-1}$) | $10^3 c_{HCl}$ (moles l.$^{-1}$) | $10^3 k_1$ (sec.$^{-1}$) | $k_2$ (l. mole$^{-1}$ sec.$^{-1}$) |
|---|---|---|---|---|---|
| | | | $t$ = 20° | | |
| 0 | 0.997 | 0.069 | 0.990 | 0.777 | 0.785 |
| 5.43 | .997 | .067 | 4.252 | .928 | .218 |
| 13.9 | .997 | .070 | 11.57 | .682 | .0589 |
| 20.4 | .994 | .071 | 30.19 | .847 | .0280 |
| 33.6 | .983 | .072 | 103.6 | .947 | .00914 |
| 52.1 | .966 | .073 | 167.6 | .568 | .00339 |
| | | | $t$ = 25° | | |
| 0 | 0.996 | *a* | *a* | *a* | 1.462[a] |
| 0 | .996 | 0.076 | 0.800 | 1.182 | 1.48[b] |
| 3.51 | .995 | .066 | 1.878 | 1.172 | 0.624 |
| 8.04 | .996 | .045 | 0.957 | 0.267 | .279 |
| 8.04 | .996 | .045 | 3.176 | .875 | .278 |
| 8.04 | .996 | .045 | 2.554 | .699 | .274 |
| 14.8 | .994 | .064 | 9.202 | .935 | .102 |
| 23.9 | .987 | .064 | 19.43 | .785 | .0404[b] |
| 24.3 | .986 | .045 | 6.450 | .230 | .0357 |
| 24.3 | .986 | .045 | 12.44 | .449 | .0361 |
| 24.3 | .986 | .045 | 23.55 | .839 | .0356 |
| 43.4 | .969 | .057 | 81.04 | .728 | .00898 |
| 53.8 | .960 | .065 | 91.97 | .505 | .00549 |
| | | | $t$ = 30° | | |
| 0 | 0.995 | 0.047 | 0.3415 | 0.924 | 2.706 |
| 0 | .995 | .047 | .4763 | 1.285 | 2.698 |
| 0 | .995 | .047 | .6824 | 1.848 | 2.708 |
| 3.61 | .993 | .059 | .847 | 0.962 | 1.136 |
| 9.60 | .992 | .061 | 1.748 | .695 | 0.398 |
| 14.7 | .990 | .073 | 4.413 | .768 | .174 |
| 20.9 | .985 | .063 | 8.710 | .787 | .0904 |
| 31.3 | .975 | .073 | 22.57 | .832 | .0368 |
| 35.7 | .972 | .053 | 27.7 | .740 | .0267[c] |
| 35.9 | .972 | .053 | 27.7 | .720 | .0260[d] |
| 42.5 | .965 | .071 | 54.54 | .977 | .0179 |
| 53.8 | .956 | .065 | 92.28 | .933 | .0101 |
| | | | $t$ = 40° | | |
| 1.96 | 0.989 | 0.070 | 0.251 | 1.263 | 5.04 |
| 7.13 | .987 | .069 | .869 | 1.351 | 1.56 |
| 10.0 | .986 | .070 | 1.006 | 0.948 | 0.943 |
| 13.6 | .983 | .072 | 1.641 | .878 | .535 |
| 19.0 | .979 | .072 | 2.605 | .787 | .302 |
| 25.9 | .972 | .074 | 5.302 | .948 | .179 |
| 29.1 | .969 | .065 | 9.237 | 1.325 | .143 |
| 37.9 | .960 | .071 | 11.44 | 0.860 | .0752 |
| 46.8 | .952 | .070 | 12.82 | .598 | .0467 |

[a] 14 experiments, $10^3 c_{HCl}$ varied from 0.448 to 1.026, $10^3 k_1$ varied from 0.658 to 1.49, $c$(acetal) varied from 0.045 to 0.092. Standard deviation for $k_2$ is 0.011. [b] Bisulfite titration. [c] Acetic acid added 0.0870 mole l.$^{-1}$. [d] Acetic acid added 0.174 mole l.$^{-1}$.

(8) H. S. Gutowsky and C. H. Holm, *J. Chem. Phys.*, **25**, 1228 (1956).

(9) A. Berger, A. Loewenstein, and S. Meiboom, *J. Am. Chem. Soc.*, **81**, 62 (1959).

(10) M. Takeda and E. O. Stejskal, *ibid.*, **82**, 25 (1960).

(11) A. Saika, *ibid.*, **82**, 3540 (1960).

(12) R. A. Robinson and R. H. Stokes, "Electrolyte Solutions," Butterworths Scientific Publications, London, 2nd Ed., 1959, pp. 167–168.

(13) S. Siggia, "Quantitative Organic Analysis *via* Functional Groups," John Wiley and Sons, Inc., New York, N. Y., 2nd Ed., 1954, p. 21.

(14) E. A. Guggenheim, *Phil. Mag.*, **2**, 538 (1926).

(15) E. S. Swinbourne, *J. Chem. Soc.*, 2371 (1960).

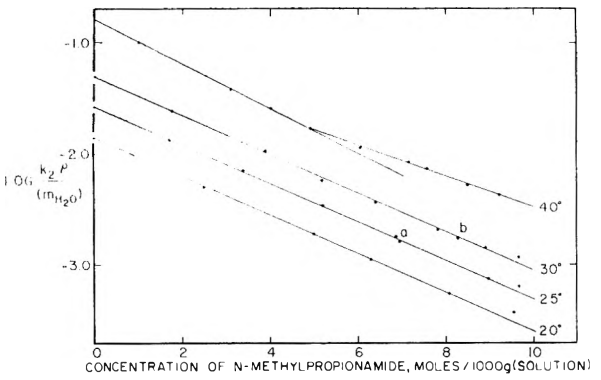


Fig. 1.—Log $(k_2\rho/m_{H_2O})$ as a function of $m_{NMP}$ in mixtures of aqueous hydrochloric acid and N-methylpropionamide at 20, 25, 30, and 40°: point a, bisulfite titration; point b, acetic acid added.

periments at 25°, and it can be seen that eq. 1 describes the rate behavior for these solutions. Two experiments (indicated in Table I) show that the presence of acetic acid at different concentrations exerts a negligible effect upon the rate. This observation suggests the absence of general acid catalysis. Data for the hydrolysis of acetal in aqueous hydrochloric acid–N,N-dimethylformamide solutions are given in Table II.

TABLE II

RATES OF HYDROLYSIS OF ACETAL IN AQUEOUS HYDROCHLORIC ACID–N,N-DIMETHYLFORMAMIDE (DMF) SOLUTIONS AT 25°

| Mole % DMF | $10^3 c_{HCl}$ (moles l.$^{-1}$) | $10^3 k_1$ (sec.$^{-1}$) | $k_2$ (l. mole$^{-1}$ sec.$^{-1}$) |
|---|---|---|---|
| 2.71 | 0.7806 | 0.686 | 0.879 |
| 5.28 | .7765 | .493 | .635 |
| 5.28 | .7765 | .490 | .631 |
| 5.28 | 1.551 | 1.017 | .656 |
| 5.28 | 1.551 | 1.000 | .645 |
| 8.20 | 1.571 | 0.677 | .431 |
| 12.3 | 1.569 | .406 | .259 |
| 22.7 | 7.405 | .757 | .1022 |
| 40.0 | 27.66 | .962 | .0348 |
| 40.0 | 14.61 | .515 | .0352 |
| 40.0 | 20.71 | .748 | .0361 |
| 43.7 | 7.561 | .228 | .0302 |
| 48.5 | 39.98 | 1.05 | .0263 |
| 55.7 | 41.33 | 1.085 | .0263 |

The value of $k_2$ obtained in this work for aqueous hydrochloric acid solutions may be compared with other values reported in the literature. Tong and Olson have summarized the latter.[2] A bisulfite titration procedure gave $k_2 = 68.5$ l. mole$^{-1}$ min.$^{-1}$, while dilatometric methods have yielded $k_2 = 84$, 76.5, 78, and 82 l. mole$^{-1}$ min.$^{-1}$. The present paper reports $k_2 = 87.6$ by the dilatometric method and 88.8 l. mole$^{-1}$ min.$^{-1}$ by bisulfite titration.

The change in rate with the change in solvent composition may be expressed conveniently by

$$\log (k_2\rho/m_{H_2O}) = \log (k_2\rho/m_{H_2O})_{aq} - sm_{NMP} \quad (2)$$

for solvents where $0 \leq m_{NMP} < 9$ (*i.e.*, from 0 mole % amide to about an equimolar mixture of amide and water). The symbol $m$ designates the solvent composition in moles of N-methylpropionamide or water per 1000 g. of solution and $\rho$ is the density of the solution in g. ml.$^{-1}$. Plots of log $(k_2/c_{H_2O})$ as a function of $c_{H_2O}$ are linear ($c_{H_2O}$ is the concentration of water in moles l.$^{-1}$). Figure 1 is a plot of equation 2 for the four temperatures. The following values for the slope $(-s)$ were obtained by a least squares treatment of the data: 0.173 (20°), 0.172 (25°), 0.174 (30°), 0.197 (40°, $m_{NMP} < 5$), and 0.138 (40°, $m_{NMP} > 5$). The diameters of the circles correspond to an uncertainty of ±2% in $k_2$.

When log $(k_2\rho/m_{H_2O})_{aq}$ for aqueous hydrochloric acid solutions is plotted against $1/T$ a good straight line results, and the slope gives an activation energy, $\Delta E$, of 21.6 kcal. mole$^{-1}$. Other workers have reported $\Delta E = 21.7$[16] and 21 kcal. mole$^{-1}$.[17] Considering the probable experimental errors in the rate constant and the fact that the slopes of eq. 2 are nearly identical for 20, 25, and 30°, the value 21.6 ± 0.4 kcal. mole$^{-1}$ is reported as the activation energy in this temperature range for acetal hydrolysis in solvent mixtures containing from 0 to about 50 mole % N-methylpropionamide. By combining eq. 2 for 30 and 40° with the Arrhenius equation, an approximate $\Delta E$ in this temperature range can be determined as a function of solvent composition. The values obtained are 22.2, 19.9, 18.3, 17.8, 19.4, 20.6, 22.6, and 23.8 kcal. mole$^{-1}$ for solutions containing 0, 5, 10, 15, 20, 25, 35, and 45 mole % N-methylpropionamide, respectively.

## Discussion

The foregoing data for the activation energy make it appear that $\Delta E$ is essentially unchanged over a considerable range of solvent composition in the range 20 to 30°, yet passes through a minimum as the aqueous solvent is enriched with the amide in the range 30 to 40°. Many investigators have attached significance to "isodielectric activation energies" determined for mixtures of equal dielectric constant.[18,19] The dielectric constants of mixtures of N-methylpropionamide and water at 20, 25, 30, and 40° have been determined recently in this Laboratory. The values at 25° are given to within one dielectric constant unit by

$$D_0 = 78.3 + 21.47x - 36.1x^2 + 111.8x^3 \quad (3)$$

where $x$ is the mole fraction of the amide.[20] They are plotted in Fig. 2 which shows, as well, the abrupt drop of $k_2$ as amide is added to the solution.

The smooth curves of log $(k_2\rho)$ as a function of $1/D_0$ at 20, 25, and 30° have a positive slope and intersect at $D_0 = 85$. It appears that isodielectric activation energies are positive for $D_0 > 85$ and negative for $D_0 < 85$. Although theoretical equations based largely on electrostatic considerations[21] of ion–neutral molecule reactions predict the rate

(16) M. Kilpatrick and E. F. Chase, *J. Am. Chem. Soc.*, **53**, 1732 (1931).

(17) R. Leimu and R. Vuorinen, *Ann. Acad. Sci. Fennicae*, **AII**, No. 19 (1946).

(18) W. J. Svirbely and J. C. Warner, *J. Am. Chem. Soc.*, **57**, 1883 (1935).

(19) E. A. Braude, *J. Chem. Soc.*, 443 (1944).

(20) T. B. Hoover, unpublished results, National Bureau of Standards.

(21) A. A. Frost and R. G. Pearson, "Kinetics and Mechanism," John Wiley and Sons, Inc., New York, N. Y., 1953, p. 137.

behavior in an approximate fashion for N-methylpropionamide–water mixtures, it is evident that the experimental results cannot be accounted for by this means alone. An attempt therefore was made to identify other factors that may influence the change in reaction rate with solvent composition.

1. Hyne[22] recently has proposed a model based on the difference in solvation of the initial and transition states of a reaction due to specific solvation by the more polar constituent of a binary solvent mixture. Activation energy extrema as the component of poorer solvating power is added are explained for reactions where passage to a transition state results in either charge delocalization (sulfonium salt solvolyses, $\Delta E$ maximum) or charge intensification (many organic halide solvolyses, $\Delta E$ minimum). The generally accepted mechanism for acetal hydrolysis[23–25] consists of a fast preëquilibrium between acetal, hydronium ion, and the protonated form of acetal, followed by a rate-determining unimolecular step

$$[CH_3CH(OC_2H_5)_2]H^+ \rightleftharpoons CH_3\overset{\delta+}{C}HOC_2H_5 \xrightarrow{k} (CH_3CHOC_2H_5)^+ + HOC_2H_5 \quad (4)$$

It appears that there is ample evidence that the solvating power of water is greater than that of the amide. For example, it has been found[4] that the solvolysis of *t*-butyl halides is unexpectedly slow in pure N-methylpropionamide and in N,N-dimethylformamide, even slower than one would expect after allowing for a reasonably reduced solvating power. A maximum might be expected in $\Delta E$ based on eq. 4, whereas a minimum actually is found for the temperature range 30 to 40° as amide is added to the solvent mixture.

2. If, on the other hand, the solvation capacity were to increase with amide content, then the qualitative Ingold theory of solvent effects would predict a slight decrease in rate with increasing solvent polarity for a mechanism such as eq. 4. The observed drop in rate is extremely severe when either amide is added to the aqueous mixture (Fig. 2), although one causes an increase and another a decrease in the dielectric constant. Among others who have considered solvation effects, Brown and Hudson[26] have found the rate of certain SN1 solvolyses to be independent of the concentration of non-polar constituent and also have found stoichiometric relations between rate and the concentration of the more polar constituent. Figure 2 compares the hydrolysis rates in the two amide–water mixtures and illustrates the greater effect caused by the N-methylamide.[27]

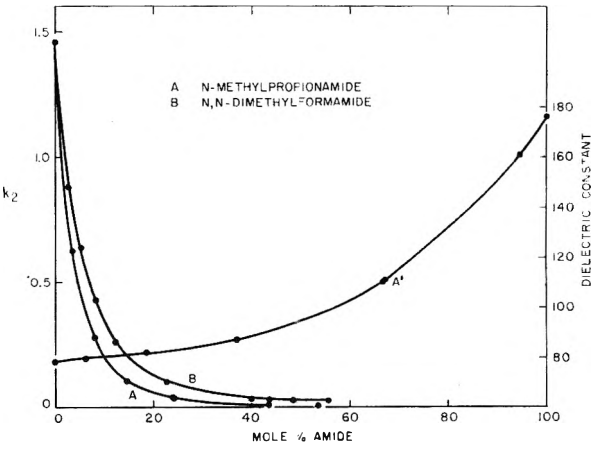


Fig. 2.—Dielectric constant (A′) and $k_2$(A,B) as a function of mole % amide for amide–water solvents at 25°.

3. The internal structure of the solvent also must be considered in any attempt to explain rate behavior when solvent composition is varied.[28] When N,N-dimethylformamide or N-methylpropionamide is added to water, heat is evolved, signifying an interaction between amide and water molecules. The stability of the H-bond between amide molecules in water is small.[29] The infrared spectra for the N-methylacetamide–water mixtures up to amide concentrations of 7 or 8 *M* (essentially the same range of amide concentrations used for the rate studies) show that amide dimers or higher aggregates essentially do not exist, and this situation persists as long as enough water molecules are available to occupy the basic sites of the amide molecule. The viscosity maximum in N,N-dimethylacetamide–water mixtures also is indicative of stronger amide–water attractions than amide–amide attractions.[30]

4. Winstein's[31] values of Y are a measure of the ionizing power of the solvent and, hence, may be a useful index of solvent effects. Values of Y for both N-methylpropionamide and N,N-dimethylformamide have been estimated.[4] Based on certain organic halide solvolysis rates, Y for water as a solvent is a little greater than +3, whereas that for both of the amides is approximately −3.5. If the value of Y decreases with increasing amide content, a close parallelism may exist between the value of Y and the observed decrease in rate, in spite of the fact that the dielectric constant is increasing for the N-methylamide–water and decreasing for the N,N-dimethylamide–water mixture.

5. It is possible that the fundamental cause of the large decrease in rate is to be found in a reduction of the average energy level of protons as amide is added to the aqueous solvent. It is convenient here to regard the primary medium effect as composed of electrostatic and chemical terms.[32] As a

(22) J. B. Hyne, *J. Am. Chem. Soc.*, **82**, 5129 (1960).
(23) F. A. Long and M. A. Paul, *Chem. Rev.*, **57**, 935 (1957).
(24) M. M. Kreevoy and R. W. Taft, *J. Am. Chem. Soc.*, **77**, 3146 (1955).
(25) E. Whalley, *Trans. Faraday Soc.*, **55**, 798 (1959).
(26) D. A. Brown and R. F. Hudson *J. Chem. Soc.*, 3352 (1953).
(27) The viscosity of N-methylpropionamide is about 4.5 times that of water while that for N,N-dimethylformamide is slightly less than that for water. From a consideration of the kinetic results it would appear that viscosity changes do not have an important effect on the rate behavior.
(28) E. Tommila and A. Nieminen, *Acta Chem. Scand.*, **9**, 989 (1955).
(29) I. M. Klotz and J. S. Franzen, *J. Am. Chem. Soc.*, **82**, 5241 (1960).
(30) R. C. Petersen, *J. Phys. Chem.*, **64**, 184 (1960).
(31) A. H. Fainberg and S. Winstein, *J. Am. Chem. Soc.*, **78**, 2770 (1956).
(32) R. W. Gurney, "Ionic Processes in Solution," McGraw-Hill Book Co., Inc., New York, N. Y., 1953, chapter 7.

first approximation the effect of coulombic terms can be estimated by the Born treatment, whereas the change of solvent basicity and solvating power are the most important chemical factors. If the effective ionic radii are assumed to be unchanged as the solvent composition is altered, the Born treatment predicts that a decreased ionic free energy will result from an increase in the dielectric constant. Increased basicity of the solvent will have a similar effect.

Unfortunately, no measurements of primary medium effects in mixtures of water and N-methylpropionamide have been made. However, the standard potential of the cell: Pt, $H_2$; HCl($m$), AgCl; Ag in N-methylacetamide at 40° has been determined recently by Dawson and co-workers.[33] On the mole-fraction scale, their results give $E^0_N = +0.064$ v., as compared with $E^0_N = -0.005$ v. for the same cell with pure water as the solvent. The primary medium effect is therefore negative and $\log f^m_{HCl} = -0.557$.

(33) L. R. Dawson, R. C. Sheridan, and H. C. Eckstrom, *J. Phys. Chem.*, **65**, 1829 (1961).

The free energy of hydrochloric acid (and presumably also the "availability" of protons) therefore decreases as the solvent is enriched with N-methylpropionamide. It is impossible to say whether this effect is entirely electrostatic or whether a part of it is to be attributed to an increased average basicity of the solvent. Nevertheless, both N-methylpropionamide and N,N-dimethylformamide produce a decrease in rate in spite of their different effects on the dielectric constant of the mixtures. It therefore would seem that the change of basicity is the predominant factor. At any rate, the result should be a decreased amount of the protonated form of acetal and a consequent decrease in the rate of the reaction.

This explanation is consistent with the qualitative success of the Y values as an index of the rate behavior, while no simple relationship between rate and dielectric constant appears to exist.

**Acknowledgments.**—The authors are indebted to Dr. R. T. Leslie and Mr. E. C. Kuehner for the distillation of the acetal.

# THEORIES OF FUSED SALT SOLUTIONS

BY GEORGE E. BLOMGREN

*Parma Research Laboratory, Union Carbide Corporation, Parma 30, Ohio*

*Received March 17, 1962*

The current status of theory and experiment in the field of fused salt solutions is discussed. An application of regular solution theory is shown to be inadequate to explain recent experimental results on silver salt solutions. A derivation of a regular solution theory for ternary solutions, which is more general than earlier theories, is given and, although available experimental data are of solutions too dilute for the additional terms in the theory to have a sensible effect, some of the limitations of the application of regular solution theory are clearly shown by the derivation. Finally, a molecular theory of dilute fused salt solutions is given which is found to be in semiquantitative agreement with measured heats of solution. No satisfactory extension of the theory to concentrated solutions was found.

## I. Introduction

In recent years a considerable amount of interest has been shown in the thermodynamic and mechanical properties of fused salt solutions.[1] Advances in the techniques of handling materials at high temperatures have enabled reasonably precise measurements to be made on mixtures of fused salts which, even in the simplest cases, show some deviations from ideal behavior.

Fused salts have an advantage over non-ionic liquids in that, for materials for which reversible electrodes can be constructed, the electromotive force of a solution can be measured. The e.m.f. is related to the partial molar free energy of the measured component, and the temperature dependence of the e.m.f. is related to the partial molar entropy of that component. The properties of the other component in a binary solution can be obtained from the same data by well known methods. This technique has been successfully applied by several workers[2-6] to various silver salts mixed with group I and II salts. Alternatively, the excess partial molar free energy may be obtained from phase diagram studies.[8]

Thermal properties of fused salt solutions have not received much attention in the past, except in phase diagram studies, but recent developments in high temperature calorimetry should lead to increasing interest in this type of measurement. Most notable of recent work in this field are the measurements of the heat of solution of alkali metal nitrates by Kleppa and Hersh[7] and the measurements of alkali halide solutions by Aukrust, Björge, Flood, and Forland.[8]

Measurements of molar volumes of fused salt solutions have often been carried out in conjunction with electrical conductivity measurements in order to obtain equivalent conductivities. Since the excess volume has not been the main concern, many of these determinations are not very precise,

(1) For reference to recent work see G. E. Blomgren and E. R. Van Artsdalen, "Annual Review of Physical Chemistry," Vol. 11, Annual Reviews, Inc., Palo Alto, Calif., 1960, pp. 273–306.

(2) J. H. Hildebrand and E. J. Salstrom, *J. Am. Chem. Soc.*, **54**, 4257 (1933), and references cited therein.

(3) R. W. Laity, *ibid.*, **79**, 1849 (1957).

(4) K. H. Stern, *J. Phys. Chem.*, **60**, 679 (1956).

(5) M. B. Panish, F. F. Blankenship, W. R. Grimes, and R. F. Newton, *ibid.*, **62**, 1325 (1958).

(6) M. B. Panish, R. F. Newton, W. R. Grimes, and F. F. Blankenship, *ibid.*, **63**, 668 (1959).

(7) O. J. Kleppa and L. S. Hersh, *J. Chem. Phys.*, **34**, 351 (1961).

(8) E. Aukrust, B. Björge, H. Flood, and T. Forland, *Ann. N. Y. Acad. Sci.*, **79**, 831 (1960), Art. 11.

but some of the better measurements show interesting results. For example, Van Artsdalen and Yaffe[9] showed that, even for many simple alkali halide mixtures, there are small, but definite positive deviations from ideal volume behavior. Byrne, Fleming, and Wetmore[10] measured the $AgNO_3$–$NaNO_3$ system and observed large positive excess volumes.

The theoretical development of molten salt solutions has met with some success in correlating some of the excess properties. Hildebrand and Salstrom[2] successfully applied the zeroth-order regular solution theory to explain the excess partial molar free energy of AgBr in various metal bromide solutions. Temkin[11] developed an ideal solution theory to deal with more complicated mixtures. Flood, Forland, and Grjotheim[12] extended the zeroth-order regular solution theory to systems involving two cations and two anions. This theory was further developed by Blander and Braunstein to the first-order or quasi-chemical approximation.[13,14] All of the theories mentioned above have relied on a rigid lattice model for the liquid solution, as does the work in this paper. It may seem at first that the representation of a liquid salt solution by a crystalline lattice would be grossly inadequate, since the coulombic forces are long range and might be expected to change radically from the solid to the liquid phase and vary greatly from one liquid to another. It is observed, however, that heats of fusion for salts are not exceptionally large compared to the over-all lattice energy of the solid (about 3–5% for many salts). This must mean that the coulombic energy does not change greatly on fusion, since this is by far the largest contribution to the lattice energy, even though long range ordering can no longer be present. Thus, in a calculation of excess properties, the lattice approximation may not be too severe. The restriction of rigidity, *i.e.*, that the ions are fixed to their lattice sites, may be more serious. Both entropy and volume effects, and to some extent the free energy, are difficult to explain on this basis. The discussion of specific theories which follows will bring out this point more clearly.

## II. Regular Solution Theories

**A. Binary Solutions.**—Binary solutions are taken to mean solutions with a common anion (cation) and two different cations (anions). The early studies of Hildebrand and Salstrom[2] on (Ag–M)Br solutions showed the excess partial molar free energy to be independent of temperature to within the experimental uncertainty of the data. This implies that the excess entropy of the solutions is zero, and one might expect the zeroth approximation of regular solution theory[15] to apply. Thus, one considers an anion lattice of fixed dimension and allows the cations to be mixed on the cation lattice. The mixing of the cations will be determined by a single interaction energy parameter, $\omega$, which is defined as

$$\omega = \omega_{AB} - \frac{1}{2}(\omega_{AA} + \omega_{BB}) \qquad (1)$$

where $\omega_{AB}$, $\omega_{AA}$, and $\omega_{BB}$ are the interaction energies of an A–B pair, an A–A pair, and a B–B pair, respectively, and A and B stand for $Ag^+$ and $M^+$. An ideal solution results from $\omega = 0$ and deviations from ideality are described in terms of intermolecular pairwise interactions of cations, which, in salts, are next nearest neighbors. The excess partial molar free energy is given in this approximation by

$$\bar{F}_A^E = n_B^2\omega \text{ or } \bar{F}_1^E = n_2^2\omega \qquad (2)$$

where $n_B$ is the cation fraction of B and $n_2$ is the mole fraction of the salt 2. By plotting the measured values of $F_1^E$ *vs.* $n_2^2$, Hildebrand and Salstrom[2] found good linear plots of the data for LiBr, NaBr, KBr, and RbBr mixed with AgBr, and the slopes of the lines gave values for $\omega$. This approach is phenomenological in the sense that no attempt is made to deduce the magnitude of $\omega$ from molecular properties.

More recent measurements have been made on the similar systems (Li–Ag)Cl[6] and (Na–Ag)Cl[5] by Panish, *et al.* Wider temperature ranges were studied for these materials and analysis of the temperature coefficients of the e.m.f. consistently gives positive partial molar entropies of AgCl, although the precision is not good. Application of the regular solution theory to these systems shows that the interaction energy $\omega$ does not remain constant on determining the best straight line at various temperatures. Table I shows the agreement of the experimental results of $\bar{F}_1 - \bar{F}_i$ with the calculated $n_2^2\omega$. Although there is considerable scatter in the data, it is clear that a single temperature independent interaction energy cannot be used to describe the systems. It is also possible to calculate excess partial molar entropy from the partial molar entropies given by Panish, *et al.*,[5,6] from the relation

$$\bar{S}_1^E = \bar{S}_1 - \bar{S}_1^i = \bar{S}_1 + R \log n_1 \qquad (3)$$

These values are also given in Table I. It should be noted that the values are all positive. Thus it would be of little use to attempt to extend the regular solution theory with any of the order–disorder theories such as the quasi-chemical theory[15] or the expansion method of Kirkwood,[16] since these extensions would lead to negative values of the excess partial molar entropy and would result in poor agreement with experiment. In any event, these corrections to the regular solution theory are small since the interaction energy is not large compared to $RT$.

It would appear, from the few systems studied so far, that the behavior of fused (Ag–M)X systems is

(9) E. R. Van Artsdalen and I. S. Yaffe, *J. Phys. Chem.*, **59**, 118 (1955).

(10) J. Byrne, H. Fleming, and F. E. W. Wetmore, *Can. J. Chem.*, **30**, 922 (1952).

(11) M. Temkin, *Acta Physicochim. URSS*, **20**, 411 (1945).

(12) H. Flood, T. Forland, and K. Grjotheim, *Z. anorg. allgem. Chem.*, **276**, 289 (1954).

(13) M. Blander, *J. Phys. Chem.*, **63**, 1262 (1959).

(14) M. Blander and J. Braunstein, *Ann. N. Y. Acad. Sci.*, **79**, 838 (1960), Art. 11.

(15) See, for example, R. Fowler and E. A. Guggenheim, "Statistical Thermodynamics," Cambridge University Press, New York, N. Y., 1939, Chapter VIII.

(16) J. G. Kirkwood, *J. Phys. Chem.*, **43**, 97 (1939).

TABLE I

PARTIAL MOLAR EXCESS FREE ENERGIES AND ENTROPIES FOR (Ag–Li)Cl AND (Ag–Na)Cl SOLUTIONS[a]

(Ag–Li)Cl[6]

| | 600° ω = 2240 cal./mole | | 700° ω = 2140 cal./mole | | 800° ω = 2060 cal./mole | | 900° ω = 1940 cal./mole | | |
|---|---|---|---|---|---|---|---|---|---|
| $n_1$ | $\bar{F}_1^E$(obsd.) | $\bar{F}_1^E$(calcd.) | $\bar{F}_1^E$(obsd.) | $\bar{F}_1^E$(calcd.) | $\bar{F}_1^E$(obsd.) | $\bar{F}_1^E$(calcd.) | $\bar{F}_1^E$(obsd.) | $\bar{F}_1^E$(calcd.) | $\bar{S}_1^E$(e.u.)(obsd.) |
| 0.0286 | 2.14 | 2.12 | 2.05 | 2.02 | 1.95 | 1.95 | 1.85 | 1.83 | 1.16 |
| .105 | 1.74 | 1.79 | 1.74 | 1.72 | 1.73 | 1.65 | 1.74 | 1.55 | 0.16 |
| .191 | 1.39 | 1.46 | 1.39 | 1.40 | 1.38 | 1.35 | 1.36 | 1.27 | .29 |
| .238 | 1.20 | 1.30 | 1.18 | 1.24 | 1.14 | 1.20 | 1.10 | 1.13 | .46 |
| .252 | 1.18 | 1.25 | 1.14 | 1.20 | 1.17 | 1.15 | 1.08 | 1.08 | .52 |
| .585 | 0.30 | 0.38 | 0.30 | 0.37 | 0.24 | 0.35 | 0.23 | 0.33 | .46 |
| .815 | .02 | .08 | .04 | .07 | .05 | .07 | .04 | .07 | .13 |
| .905 | − .05 | .02 | .01 | .02 | .05 | .02 | .06 | .02 | − .20 |
| 1.000 | 0 | 0 | 0 | 0 | 0 | 0 | 0 | 0 | 0 |

(Ag–Na)Cl[5]

| | 700° ω = 1120 cal./mole | | 800° ω = 940 cal./mole | | 900° ω = 750 cal./mole | | |
|---|---|---|---|---|---|---|---|
| $n_1$ | $\bar{F}_1^E$(obsd.) | $\bar{F}_1^E$(calcd.) | $\bar{F}_1^E$(obsd.) | $\bar{F}_1^E$(calcd.) | $\bar{F}_1^E$(obsd.) | $\bar{F}_1^E$(calcd.) | $\bar{S}_1^E$(e.u.)(obsd.) |
| 0.0313 | .. | .. | 0.91 | 0.88 | 0.77 | 0.70 | 1.48 |
| .0978 | .. | .. | .76 | .76 | .66 | .61 | 1.10 |
| .209 | .. | .. | .62 | .59 | .43 | .47 | 0.75 |
| .351 | 0.46 | 0.47 | .34 | .39 | .20 | .31 | 1.36 |
| .505 | .28 | .27 | .23 | .23 | .10 | .18 | 0.74 |
| .615 | .08 | .17 | .01 | .14 | − .06 | .11 | .57 |
| 1.000 | 0 | 0 | 0 | 0 | 0 | 0 | 0 |

[a] Subscript 1 = AgCl.

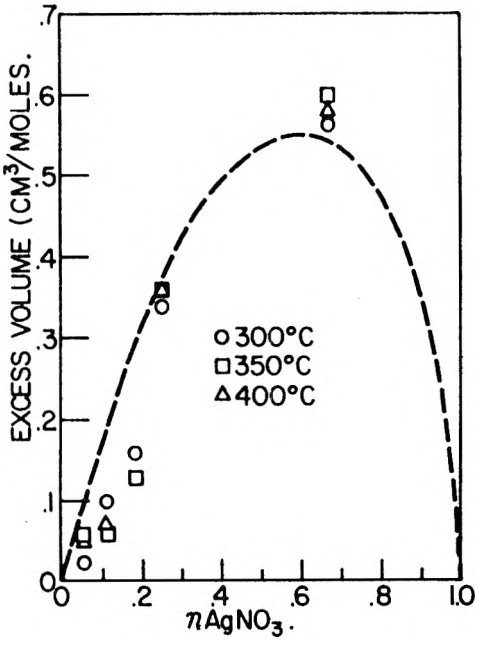


Fig. 1.—Excess volume in the (Ag–Na)$NO_3$ system as a function of mole fractions of $AgNO_3$.

fairly insensitive to the nature of the anion and that the trends in the behavior with respect to the other cation are apparently independent of the anion. This can be seen in Table II, where the interaction energies from regular solution theory are compared for various bromide, chloride, and nitrate solutions.

Another measurement of interest concerning silver salt solutions is the density determination of (Ag–Na)$NO_3$ solutions by Byrne, Fleming, and Wetmore.[10] The result of converting these measurements into excess volume quantities is shown in Fig. 1. The system shows a rather large positive excess volume, and since the regular solution theory assumes a geometric mean for the volume behavior and the ideal volume is given by an arithmetic mean, the excess volume predicted by regular solution theory is of the opposite sign from the observed and is much too small.

The disagreement of excess entropy and volume quantities with regular solution theory for silver salt solutions is not unexpected. This situation is often encountered in non-electrolyte solutions and is generally explained[17] in terms of effects arising from the dependence of particle oscillations on the surroundings, which is entirely ignored in the regular solution theory. This sort of explanation, however, presupposes some knowledge of the intermolecular interactions in the system and, at least in the case of silver salts, very little is known about these interactions. Thus, silver salts are poor examples from the theoretical point of view, although they are very good ones from the experimental electrochemical point of view.

TABLE II

INTERACTION ENERGIES FROM REGULAR SOLUTION THEORY FOR SILVER SALT SOLUTIONS

| | M | | | |
|---|---|---|---|---|
| | Li | Na | K | Rb |
| ω (Ag–M)Br[3] | 1880 | 1050 | −1480 | −2580 |
| ω (Ag–M)Cl | 1940–2240[6] | 750–1100[5] | ∼−1000[4] | |
| ω (Ag–M)$NO_3$[3] | | 840 | | |

Thermal measurements probably are the best means of determining thermodynamic excess properties of simple salts such as the alkali halides, for

(17) See I. Prigogine, "The Molecular Theory of Solutions," Interscience Publishers, Inc., New York, N. Y., 1957.

which some hope exists for a molecular theory of solutions. The recent work of Kleppa and Hersh[7] extends the above phenomenological approach, including first-order correction to the regular solution theory, in order to explain their heat of solution data on alkali nitrate solutions. An asymmetry in the heat of solution *vs.* mole fraction curve remains and is empirically taken into account. All of the heats are negative, however, while the heats of the corresponding solid solutions are all positive. A possible explanation of this phenomenon will be discussed in a later section.

**B. Ternary Solutions.**—Ternary or reciprocal salt solutions will be taken to mean solutions of three salts involving two different cations and two different anions. Blander and Braunstein[13,14] have developed a theory based on the quasi-chemical approximation which is applicable to dilute solutions, but this theory can be developed in more general terms to include interactions not considered by those authors for application to concentrated solutions. In this discussion the notation of Fowler and Guggenheim[15] will be largely followed. First of all, the interactions to be considered will be limited to first neighbors (cation–anion interactions) and second neighbors (cation–cation and anion–anion interactions). Thus we can write a table of numbers of pairs and energies for any given configuration of the system where $z_1$ is the first coördination number of a cation or anion, $z_2$ is the second coördination number of a cation or anion, A and B are the two cations, C and D are the anions, $N_A$ is the number of A ions, and $\omega_{AC}/z_1$, etc., are the (short range) interaction energies per AC, etc., pair for given and fixed interionic separations. The results are given in Table III. The total energy of the configuration is given

TABLE III

DEFINITIONS FOR PAIR INTERACTIONS FOR TERNARY SALT SOLUTIONS

| Pair | No. of pairs | Energy per pair | Total energy of pairs |
|---|---|---|---|
| AC | $z_1X_1$ | $-\omega_{AC}/z_1$ | $-X_1\omega_{AC}$ |
| AD | $z_1(N_A - X_1)$ | $-\omega_{AD}/z_1$ | $-(N_A - X_1)\omega_{AD}$ |
| BC | $z_1(N_C - X_1)$ | $-\omega_{BC}/z_1$ | $-(N_C - X_1)\omega_{BC}$ |
| BD | $z_1(N_B - N_C + X_1)$ | $-\omega_{BD}/z_1$ | $-(N_B - N_C + X_1)\omega_{BD}$ |
| AA | $^1/_2z_2(N_A - X_2)$ | $-\omega_{AA}/z_2$ | $-^1/_2(N_A - X_2)\omega_{AA}$ |
| BB | $^1/_2z_2(N_B - X_2)$ | $-\omega_{BB}/z_2$ | $-^1/_2(N_B - X_2)\omega_{BB}$ |
| AB | $z_2X_2$ | $-\omega_{AB}/z_2$ | $-X_2\omega_{AB}$ |
| CC | $^1/_2z_2(N_C - X_3)$ | $-\omega_{CC}/z_2$ | $-^1/_2(N_X - X_3)\omega_{CC}$ |
| DD | $^1/_2z_2(N_D - X_3)$ | $-\omega_{DD}/z_2$ | $-^1/_2(N_D - X_3)\omega_{DD}$ |
| CD | $z_2X_3$ | $-\omega_{CD}/z_2$ | $-X_3\omega_{CD}$ |

by the sum of the terms of the last column of Table III, as

$$W = -N_{AD}\left(\omega_{AD} + \frac{1}{2}\omega_{AA} + \frac{1}{2}\omega_{BB}\right) - N_{BC}\left(\omega_{BC} + \frac{1}{2}\omega_{BB} + \frac{1}{2}\omega_{CC}\right) - N_{BD}\left(\omega_{BD} + \frac{1}{2}\omega_{BB} + \frac{1}{2}\omega_{DD}\right) + X_1\omega_1 + X_2\omega_2 + X_3\omega_3 \quad (4)$$

where

$$N_{AD} = N_A,\ N_{BC} = N_C \text{ and } N_{BD} = N_B - N_C \quad (5)$$

are the number of molecules of the salt AD, etc., added to the mixture, since any concentration of the ions A, B, C, and D can be specified by mixtures of the salts AD, BC, and BD. By definition

$$\omega_1 = -(\omega_{AC} + \omega_{BD} - \omega_{AD} - \omega_{BC})$$
$$\omega_2 = -\left(\omega_{AB} - \frac{1}{2}\omega_{AA} - \frac{1}{2}\omega_{BB}\right)$$
$$\omega_3 = -\left(\omega_{CD} - \frac{1}{2}\omega_{CC} - \frac{1}{2}\omega_{DD}\right) \quad (6)$$

It is clear from eq. 4 that the system has been described in terms of short range interaction only and the long range coulomb forces have not been introduced. If the molar volumes of the pure salts are equal and if there is no volume change in the system on mixing, there will be no change in the lattice constant on mixing and the coulomb part can be added on, since

$$N\omega_C = (N_{AD} + N_{BC} + N_{BD})\omega_C$$

where $N$ is the total number of molecules in the system (half the number of ions) and $\omega_C$ is the coulomb energy of a system of point charges. Then eq. 4 becomes

$$W = N_{AD}\chi_{AD} + N_{BC}\chi_{BC} + N_{BD}\chi_{BD} + X_1\omega_1 + X_2\omega_2 + X_3\omega_3 \quad (7)$$

where $\chi_{AD}$, etc., are the lattice energies of the pure salts defined by

$$\chi_{AD} = \omega_C - \left(\omega_{AD} + \frac{1}{2}\omega_{AA} + \frac{1}{2}\omega_{BB}\right)$$
$$\chi_{BC} = \omega_C - \left(\omega_{BC} + \frac{1}{2}\omega_{BB} + \frac{1}{2}\omega_{CC}\right)$$
$$\chi_{BD} = \omega_C - \left(\omega_{BD} + \frac{1}{2}\omega_{BB} + \frac{1}{2}\omega_{DD}\right) \quad (8)$$

The configurational part of the partition function is given by

$$\Omega(T) = \frac{1}{N_A!N_B!N_C!N_D!}\int\cdots\int e^{-W/kT}\,(d\tau_A)^{N_A}\,(d\tau_B)^{N_B}\,(d\tau_C)^{N_C}\,(d\tau_D)^{N_D} = \frac{\exp\left[(\chi_{AD}N_{AD} + \chi_{BC}N_{BC} + \chi_{BD}N_{BD})/kT\right]}{N_A!N_B!N_C!N_D!} \times \int\cdots\int e^{-(X_1\omega_1 + X_2\omega_2 + X_3\omega_3)/kT} \times (d\tau_A)^{N_A}\,(d\tau_B)^{N_B}\,(d\tau_C)^{N_C}\,(d\tau_D)^{N_D} \quad (9)$$

where eq. 7 has been substituted for $W$ and the symbol $(d\tau_A)^{N_A}$ is defined as

$$(d\tau_A)^{N_A} = \prod_{r=1}^{N_A}(dx_A\,dy_A\,dz_A)_r$$

and the integrations for A and B are carried out over the cation space and those for C and D over the anion space. Some interesting results are obtained from the condition

$$\omega_1 = \omega_2 = \omega_3 = 0$$

Equation 9 becomes

$$\Omega(T) = \frac{\exp[(\chi_{AD}N_{AD} + \chi_{BC}N_{BC} + \chi_{BD}N_{BD})/kT]}{N_A!N_B!N_C!N_D!} \times \int\cdots\int (d\tau_A)^{N_A} (d\tau_B)^{N_B} (d\tau_C)^{N_C} (d\tau_D)^{N_D}$$

$$= \frac{\exp[(\chi_{AD}N_{AD} + \chi_{BC}N_{BC} + \chi_{BD}N_{BD})/kT]}{N_A!N_B!N_C!N_D!} (V_{cat})^{N_A + N_B} (V_{An})^{N_C + N_D} \quad (10)$$

where $V_{cat}$ and $V_{An}$ are the volumes of the cation and anion space, respectively, defined by

$$V_{cat} = N_A v_A + N_B v_B$$

$$V_{An} = N_C v_C + N_D v_D$$

where $v_A$, etc., are the ionic free volumes. If the ionic free volumes are not very different, the relations

$$(V_{cat})^{N_A + N_B} = (N_A + N_B)^{N_A + N_B} v_A^{N_A} v_B^{N_B}$$

$$(V_{An})^{N_C + N_D} = (N_C + N_D)^{N_C + N_D} v_C^{N_C} v_D^{N_D} \quad (11)$$

are nearly true. From Stirling's approximation

$$(N_A + N_B)^{N_A + N_B} = e^{N_A + N_B} (N_A + N_B)!$$

$$(N_C + N_D)^{N_C + N_D} = e^{N_C + N_D} (N_C + N_D)! \quad (12)$$

Substituting eq. 11, 12, and 5 into eq. 10

$$\Omega(T) = \frac{(N_A + N_B)!}{N_A!N_B!} \frac{(N_C + N_D)!}{N_C!N_D!} \times [(v_A + v_D)e^2 e^{\chi_{AD}}]^{N_{AD}} \times [(v_B + v_C)e^2 e^{\chi_{BC}}]^{N_{CB}} [(v_B + v_D)e^2 e^{\chi_{BD}}]^{N_{BD}} \quad (13)$$

where the last three terms of the product are conventional free volume terms for the pure salts, AD, BC, and BD. Thus, the free energy of solution and entropy of solution are given by

$$\Delta A = \Delta S = N_A kT \ln \frac{N_A}{N_A + N_B} + N_B kT \ln \frac{N_B}{N_A + N_B} + N_C kT \ln \frac{N_C}{N_C + N_D} + N_D kT \ln \frac{N_D}{N_C + N_D} \quad (14)$$

The partial molar free energy of solution is given by

$$\Delta\bar{A}_{AD} = N_{Av} \frac{\partial \Delta A}{\partial N_{AD}} = RT \ln n_A n_D \quad (15)$$

where $N_{Av}$ is Avogadro's number. Equations 14 and 15 give the same results as the Temkin[11] model for the ideal solution. For the general case where none of $\omega_1$, $\omega_2$, or $\omega_3$ is equal to zero, new quantities $\bar{\bar{X}}_i$ can be defined for mathematical convenience by the equation

$$e^{-(\bar{\bar{X}}_1\omega_1 + \bar{\bar{X}}_2\omega_2 + \bar{\bar{X}}_3\omega_3)} \int\cdots\int \prod_A (d\tau_A)^{N_A} = \int\cdots\int e^{-(X_1\omega_1 + X_2\omega_2 + X_3\omega_3)/kT} \prod_A (d\tau_A)^{N_A} \quad (16)$$

From the left hand side of eq. 16 the free energy of solution is given by

$$\Delta A = kT \sum_A N_A \ln \frac{N_A}{N} + \bar{\bar{X}}_1\omega_1 + \bar{\bar{X}}_2\omega_2 + \bar{\bar{X}}_3\omega_3 \quad (17)$$

By differentiating both sides of eq. 16 with respect to temperature, we find

$$\bar{\bar{X}}_1\omega_1 + \bar{\bar{X}}_2\omega_2 + \bar{\bar{X}}_3\omega_3 - T\left(\omega_1 \frac{\partial \bar{\bar{X}}_1}{\partial T} + \omega_2 \frac{\partial \bar{\bar{X}}_2}{\partial T} + \omega_3 \frac{\partial \bar{\bar{X}}_3}{\partial T}\right) = \bar{X}_1\omega_1 + \bar{X}_2\omega_2 + \bar{X}_3\omega_3 \quad (18)$$

where by definition

$$\bar{X}_1 \int\cdots\int e^{-(X_1\omega_1 + X_2\omega_2 + X_3\omega_3)/kT} \prod_A (d\tau_A)^{N_A} = \int\cdots\int X_1 e^{-(X_1\omega_1 + X_2\omega_2 + X_3\omega_3)/kT} \prod_A (d\tau_A)^{N_A} \quad (19)$$

Equation 18 can be simplified to

$$\omega_1 \frac{\partial(\bar{\bar{X}}_1/T)}{\partial(1/T)} + \omega_2 \frac{\partial(\bar{\bar{X}}_2/T)}{\partial(1/T)} + \omega_3 \frac{\partial(\bar{\bar{X}}_3/T)}{\partial(1/T)} = \omega_1\bar{X}_1 + \omega_2\bar{X}_2 + \omega_3\bar{X}_3 \quad (20)$$

Equation 20 can be integrated to give an equation for the $\bar{\bar{X}}_i$, if an approximate expression for the $\bar{X}_i$ can be given. An obvious solution occurs if three separate quasi-chemical conditions are used.[15] This will not be quite correct, since the mixing of cations will be influenced by the cation–anion interaction and the anion–anion interaction and so on, but the approximation may not be too severe. Thus, we have

$$\frac{\bar{X}_1(N_B - N_C + \bar{X}_1)}{(N_A - \bar{X}_1)(N_C - \bar{X}_1)} = e^{-\omega_1/z_1kT} \quad (a)$$

$$\frac{\bar{X}_2^2}{(N_A - \bar{X}_2)(N_B - \bar{X}_2)} = e^{-\omega_2/z_2kT} \quad (b)$$

$$\frac{\bar{X}_3^2}{(N_C - \bar{X}_3)(N_D - \bar{X}_3)} = e^{-\omega_3/z_2kT} \quad (c) \quad (21)$$

We could have set the left hand side of any or all of eq. 21 equal to unity and obtained the zeroth or regular solution result. We proceed to integrate eq. 20. Since

$$\frac{\bar{\bar{X}}_i}{T} \longrightarrow 0 \text{ as } \frac{1}{T} \longrightarrow 0$$

we have, on changing the partial to total differentials

$$\omega_1 \frac{\bar{\bar{X}}_1}{T} + \omega_2 \frac{\bar{\bar{X}}_2}{T} + \omega_3 \frac{\bar{\bar{X}}_3}{T} = \int_0^{1/T} \omega_1 \bar{X}_1 \mathrm{d}\left(\frac{1}{T}\right) + \int_0^{1/T} \omega_2 \bar{X}_2 \mathrm{d}\left(\frac{1}{T}\right) + \int_0^{1/T} \omega_3 \bar{X}_3 \mathrm{d}\left(\frac{1}{T}\right) \quad (22)$$

The integrations on the right hand side of eq. 22 have already been done, the first by Blander and Braunstein[14] and the second and third are the standard quasi-chemical integrations.[15] Performing the integrations and substituting the result into eq. 17 gives the free energy of solution. Differentiating with respect to $N_{AD}$ gives the partial molar free energy of solution

$$\overline{\Delta A}_{AD} = RT \ln n_A n_D + z_1 RT \ln \left[\frac{(1 - \bar{X}_1/N_A)}{n_D}\right] + z_2 RT \ln \left[\frac{\beta_2 + n_A - n_B}{n_A(\beta_2 + 1)}\right] + z_2 RT \ln \left[\frac{\beta_3 + n_D - n_C}{n_D(\beta_3 + 1)}\right] = RT \ln \alpha_{AD} \quad (23)$$

where $n_A$, etc., are the ion fractions and

$$\beta_2 = \left[1 + \frac{4N_A N_B(e^{\omega_2/z_2 kT} - 1)}{(N_A + N_B)^2}\right]^{1/2}$$

$$\beta_3 = \left[1 + \frac{4N_C N_D(e^{\omega_3/z_2 kT} - 1)}{(N_C + N_D)^2}\right]^{1/2} \quad (24)$$

and the activity coefficient is given by

$$\gamma_{AD} = \left[\frac{(1 - \bar{X}_1/N_A)}{N_D}\right]^{z_1} \left[\frac{\beta_2 + n_A - n_B}{n_A(\beta_2 + 1)}\right]^{z_2} \times \left[\frac{\beta_3 + n_D - n_C}{n_D(\beta_3 + 1)}\right]^{z_2} \quad (25)$$

Equation 25 can be applied to a system studied by Hill, Braunstein, and Blander,[18] the system $NaNO_3$–$AgNO_3$–NaCl. Here the cation–cation interaction energy has been determined by Laity[3] in the binary system. However, since concentration cells of the type

$$\mathrm{Ag} \left| \begin{matrix} \mathrm{AgNO_3}(n'_{Ag}) \\ \mathrm{NaNO_3} \end{matrix} \right\| \begin{matrix} \mathrm{AgNO_3}(n_{Ag}) \\ \mathrm{NaNO_3} \\ \mathrm{NaCl} \end{matrix} \left| \mathrm{Ag} \right.$$

were used, where $n'_{Ag}$ is nearly equal to $n_{Ag}$, the second term makes a negligible correction to the activity coefficient as obtained from the first term by itself. The third term is also near unity, since the system is very dilute in $Cl^-$ ion and the activity coefficient sought is for the nitrate. To show this, in the zeroth approximation the third term in eq. 25 is given by

$$\exp(\omega_3 n^2_{BC}) = \exp(\omega_3 n^2_{NaCl})$$

which gives for any reasonable energy, and a concentration of NaCl to about $10^{-3}$ mole fraction, a contribution of very nearly unity. It would be interesting to test eq. 25, but unfortunately no system has yet been studied for which the equation would be applicable.

Although experimental information is lacking for testing the results of the theoretical development of this section, some insight into some of the approximations involved in applying the conventional lattice theories to molten salt solutions has been gained. It has been shown that, in order to use a theory of nearest neighbor or next nearest neighbor lattice statistics, the molar volumes of the pure liquids and all solutions must have the same value, or else serious difficulties are encountered with the coulomb energy. This result is valid for binary as well as ternary solutions. It also has been shown that the use of concentration cells of the above type with nearly equal silver ion concentrations on either side fortuitously simplifies the theoretical analysis of the data.

## III. Molecular Theory of Simple Salt Solutions

It was mentioned in the Introduction that the heat of solution is an interesting property of solutions. This is particularly so from a theoretical point of view. The oscillations of particles in the lattice and the changes which take place in solution affect the excess entropy and volume properties to a much greater degree than the heat of solution. In fact, if one uses a simple square well for the particle potential energy, no effect is manifested in the heat of solution.[17] Thus the rigid lattice model can be applied with greater confidence to the heat of solution than to the other properties.

Blander[19] recently has calculated the effect on the coulomb potential of one molecule of solute in a linear chain of solvent molecules, implicitly assuming a hard sphere repulsion. While the model gives results in qualitative agreement with experiment, it is difficult to extend it to two or three dimensions and, of course, indicates nothing about the effect of short range repulsive forces.

Another approach to the problem is to extend the solid solution theory of Durham and Hawkins[20] to the case of liquid solutions. The only difference between the model of the liquid and the solid is the magnitude of the lattice constant. Hence, we can apply the theory directly by choosing appropriate lattice constants for the solutions.

The (Li–K)Cl system was chosen for the calculation for several reasons. First, there are already some crude measurements of the heat of solution in the literature[8] with which semiquantitative comparisons can be made. The densities of the entire solution range have been accurately measured by Van Artsdalen and Yaffe[9] and the molar volume has been found to be a linear function of concentration to within experimental error. Also, the interionic potential constants for the pure liquids are known from the work of Mayer and Huggins,[21–23]

(18) D. G. Hill, J. Braunstein, and M. Blander, *J. Phys. Chem.*, **64**, 1038 (1960).

(19) M. Blander, *J. Chem. Phys.*, **34**, 697 (1961).

(20) G. S. Durham and J. A. Hawkins, *ibid.*, **19**, 149 (1951).

(21) J. E. Mayer, *ibid.*, **1**, 270 (1933).

(22) M. L. Huggins and J. E. Mayer, *ibid.*, **1**, 643 (1933).

(23) M. L. Huggins, *ibid.*, **5**, 143 (1937).

and those for the Li–K interactions can be easily calculated.

The Durham and Hawkins theory[20] is conceptually straightforward. It considers that, for example, in a solution of a large and a small cation, an average lattice spacing is obtained which lies between the extremes of the pure liquid lattice spacings. Hence, one would expect that an anion which lies between a large cation and a small cation would not be in a position of minimum potential energy at the lattice site, but would rather be displaced toward the small cation. In the calculation, one can consider all configurations of cations around anions and calculate the displacements and displacement energies at the potential energy minima, and by making the assumption of random mixing, calculate the probabilities of each configuration. The sum of the energy–probability products gives the change in energy due to the relaxation of the anions from lattice sites to positions of minimum potential energy and this quantity is subtracted from the energy calculated for the unrelaxed lattice. It was found that for the solid solutions[20] only the repulsive energy was large enough and varied rapidly enough to make a significant contribution to the displacement energy. The following is a calculation based on the same model for a liquid (Li–K)Cl solution.

The equations for calculating the unrelaxed lattice energy are eq. 11, 12, and 13 of Durham and Hawkins.[20] The potential constants used are summarized in Table IV. The Li–K dipole–dipole constant was calculated according to the method of Mayer[21] and the (Li–K) dipole–quadrupole constant was taken as the geometric mean of the (Li–Li) and (K–K) values. The (Cl–Cl) dipole–dipole and dipole–quadrupole constants were taken as the arithmetic mean of the two pure solutions. The repulsion term is of an exponential form with constants given by Huggins.[23] The energy of solution, which, in a region of low vapor pressure, is nearly the same as the heat of solution, is given by

$$\Delta H = \Delta E = E_s - n_{LiCl} E_{LiCl} - n_{KCl} E_{KCl}$$

TABLE IV

POTENTIAL CONSTANTS FOR (Li–K)Cl SOLUTIONS

1 = $Li^+$, 2 = $K^+$, 3 = $Cl^-$

Dipole–dipole[21]

$C_{11} = 0.073$, $C_{12} = 1.61$, $C_{22} = 24.3$, $C_{13} = 2.0$, $C_{23} = 48$, $C_{33} = 118 \times 10^{-60}$ erg cm.$^6$

Dipole–quadrupole[21]

$d_{11} = 0.03$, $d_{12} = 0.85$, $d_{22} = 24$, $d_{13} = 2.4$, $d_{23} = 73$, $d_{33} = 236 \times 10^{-76}$ erg cm.$^8$

Repulsive radii[23]

$r_1 = 0.570$, $r_2 = 1.235$, $r_3 = 1.435$ Å., $a = 3.00$ Å.$^{-1}$

Cation–anion distance

$r_{LiCl} = 2.909$, $r_{KCl} = 3.437$ Å.

For a 40–60 mole % (Li–K)Cl solution, we calculate

$$\Delta H = -172.10 + 0.4(192.90) + 0.6(164.23) = 3.60 \text{ kcal./mole}$$

where the cation–anion distance $\bar{r} = 3.246$ Å. was obtained by linear interpolation of the molar volume curve.[9] The displacements and displacement energies for repulsion only then were calculated for each configuration and these results are summarized in Table V, where the notation of configurations is the same as Durham and Hawkins'.[20] The total displacement energy is calculated to be 2.16 kcal. and subtracting this from the unrelaxed heat of solution gives $\Delta H = 1.44$ kcal. The experimental value of the heat of solution is, however, approximately −0.6 kcal. and thus disagrees in both sign and magnitude with the calculated value. The effect of the coulomb force has not yet been considered and this may be considerable since the displacements are relatively large (values for the solid solution[20] are about $0.03\ \bar{r}$, whereas our displacements are of the order of $0.1\ \bar{r}$). Durham and Hawkins[20] considered the coulomb effect for anions displaced individually with all other ions at normal lattice positions and found the effect to be negligible. This effect is also calculated to be small for the liquid solution. However, the neglect of coulomb interactions among displaced particles is not really justified, especially with large displacements, since on the average the chloride ions will be slightly closer to each lithium ion, and therefore to each other, and slightly farther from each other around the potassium ions. The effect of cation displacements also could be considerable in the presence of large anion displacements. Both of these effects are difficult to account for in concentrated solutions, but the situation is considerably simplified in the dilute solution.

In a dilute solution (taken as 1 mole % LiCl for this calculation), the probability of two lithium ions lying close together is very small. Hence, the lithium ions and their environments can be treated as being independent. In general, then, one would expect that the environment of each lithium ion should be somewhat contracted about the lithium, as shown in Fig. 2. It is likely that first neighbor displacements will not be sufficient to describe the system, and for this calculation we will consider first through fourth neighbor displacements. The program for the calculation is to calculate the first neighbor displacements from repulsive interactions, then the second neighbor ones with the first already displaced, and so on through the fourth neighbors. This has been done using the same repulsion constants as for the concentrated solution and an average anion–cation distance from the molar volume curve of $\bar{r} = 3.4322$ Å., with the result that the first neighbor displacement is $0.13\bar{r}$ with an energy of $-0.055 \times 10^{-12}$ erg, second and third neighbor displacements are negligible (less than $0.005\bar{r}$), and the fourth neighbor displacement is $0.10\bar{r}$ with an energy of $-0.038 \times 10^{-12}$ erg. The probability factor is now given approximately by $6n_{Li} = 0.06$ for both the first and fourth neighbors, so that the total relaxation energy is $-0.006 \times 10^{-12}$ erg. The energy of solution for the unrelaxed lattice is calculated to be $+0.010 \times 10^{-12}$ erg, where $c_{33}$ and $d_{33}$ are now taken as the values for pure KCl,[21] *i.e.*, $c_{33} = 124.5 \times 10^{-60}$ erg cm.$^6$

TABLE V

DISPLACEMENT ENERGIES FOR 40–60 MOLE % (Li–K)Cl SOLUTION

| | A | | | B | | C |
|---|---|---|---|---|---|---|
| | $5Li^+$ $1K^+$ | $5K^+$ $1Li^+$ | $3Li^+$ $3K^+$ | $4Li^+$ $2K^+$ | $4K^+$ $2Li^+$ | $3K^+$ $3Li^+$ |
| Displacement | $x' = 0.15\bar{r}$ $y' = z' = 0$ | $0.098\bar{r}$ 0 | $0.123\bar{r}$ 0 | $x' = y' = 0.11\bar{r}$ $z' = 0$ | $0.14\bar{r}$ 0 | $x' = y' = z' = 0.12\bar{r}$ |
| Energy ($\Delta B$) $10^{12}$ ergs | −0.140 | −0.085 | −0.107 | −0.182 | −0.232 | −0.294 |
| Probability ($P$) | 0.037 | 0.187 | 0.166 | 0.111 | 0.249 | 0.111 |
| $P\Delta B$ | −0.0058 | −0.0160 | −0.0177 | −0.0202 | −0.0578 | −0.0326 |

$\sum P\Delta B = -0.1501 \times 10^{-12}$ erg $= -2.160$ kcal.

and $d_{33} = 250 \times 10^{-76}$ erg cm.$^8$, and the calculation is the same as for the concentrated solution. The coulomb effect can be considered in two parts; the energy of displacement of the individual ions with respect to the rest of the (fixed) lattice, and the interactions among the displaced ions. The first part can be calculated by using the well known theta-transformation of Ewald[24] to obtain the potential at the displaced position, subtracting the energy of interaction of an ion at the lattice site with one of the same sign at the displaced position, and subtracting the lattice energy of the ion at the lattice site. Thus for an anion

$$E_- = (-e)V_E(x', y', z') - (x'^2 + y'^2 + z'^2)^{-1/2}e^2/\bar{r} - (-1.7476)e^2/\bar{r} \quad (26)$$

and for a cation

$$E_+ = eV_E(x', y', z') - (x'^2 + y'^2 + z'^2)^{-1/2}e^2/\bar{r} - (1.7476)e^2/\bar{r} \quad (27)$$

where $V_E$ is the Ewald potential. A similar problem has been treated by Dienes[25] and, in fact, it is possible to use his eq. 6 to calculate the Ewald potential. It should be noted that the factor 8 in the first term is an error and should be deleted. Performing this calculation and noting that there are six anions and six cations displaced for each lithium ion we get the result

$$\Delta E_{c_1} = [6(-0.0011) + 6(-0.0006)](e^2/\bar{r})n_{LiCl} = -0.0102(e^2/\bar{r})n_{LiCl} \quad (28)$$

The second part of the coulomb interaction is done by calculating the difference between the energy of a pair of displaced ions and the energy of the pair when only one is displaced. Reference to Fig. 2 shows that in the 3-dimensional lattice there are 12 pairs of the 1–4 type, 3 pairs of 2–4 type, 6 pairs of 8–4 type, 6 pairs of 8–2 type, 24 pairs of the 8–1 type, 3 pairs of the 8–6 type and 12 pairs of the 8–5 type. The calculation is straightforward and only the result will be given

$$\Delta E_{c_2} = -0.1161(e^2/\bar{r})n_{LiCl} \quad (29)$$

The total coulomb energy is given by eq. 28 and 29 as

$$\Delta E_c = -0.008 \times 10^{-12} \text{ erg}$$

The calculated heat of mixing thus is

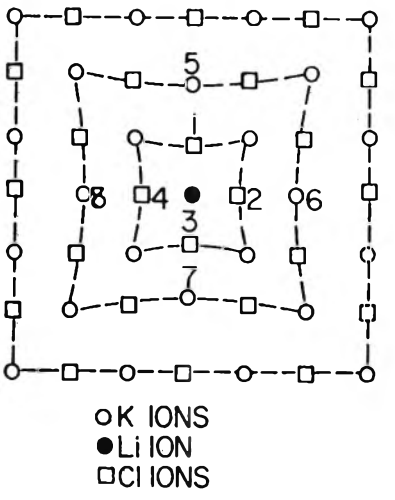


Fig. 2.—Ion displacements in the dilute solutions.

$$\Delta H = \Delta E = (0.010 - 0.006 - 0.008) \times 10^{-12} \text{ erg} = -0.004 \times 10^{-12} \text{ erg} = -0.06 \text{ kcal./mole}$$

A crude comparison with experiment is possible. The heat of solution[8] of (Li–K)Cl at $n_{LiCl} = 0.5$ is about twice as large as that of the corresponding nitrate system.[7] The interpolation formula of Kleppa and Hersh[7] gives for the nitrate system at $n_{LiNO_3} = 0.01$

$$\Delta H = -0.02 \text{ kcal. (Li–K)}NO_3$$

If it can be assumed that the chloride system is still twice as large as the nitrate system, then the estimated experimental heat of solution for the chloride system is

$$\Delta H \sim -0.04 \text{ kcal. (Li–K)Cl}$$

The agreement between the calculated value and the estimated experimental value is as good as can be expected, and at least the signs agree. There are several points which have been neglected in the theoretical calculation. The effects of other short range forces have not been considered, nearest neighbors only have been used to determine the potential energy minima, coulomb interactions between groups of displaced ions around different lithium ions have not been considered, and the effect of the coulomb energy on changing the displacements has not been calculated. It is felt that these corrections, however, probably would be small. The results of this section show that the calculation of heats of solution of fused salts based on the rigid

(24) P. P. Ewald, *Ann. Physik*, **64**, 253 (1921).
(25) G. J. Dienes, *J. Chem. Phys.*, **14**, 620 (1948).

lattice model can give qualitative agreement with experiment only if the complicated interplay between short range repulsive forces and long range coulomb forces is taken into account.

Two alternatives remain for the calculation of the heats of more concentrated fused salt solutions. The rigid lattice model can be retained, and simplifying assumptions which would allow a calculation of the coulomb energy can be sought, or the rigid lattice model can be abandoned, either by the introduction of a large concentration of vacancies or by the use of a radial distribution function theory. Either of these approaches is likely to be difficult.

### IV. Conclusions

The standard order–disorder theory was shown to present some rather difficult conceptual problems when applied to fused salt solutions primarily because interactions are limited to nearest neighbors, while the interactions in the ionic medium must extend to large distances. This does not invalidate the order–disorder approach, but does place some rather severe restrictions on it. Also, as was to be expected, the excess entropy and volume characteristics of the fused salt solutions which have been discussed are in almost total disagreement with the predictions of order–disorder theory.

An attempt was made to calculate heats of fused salt solutions from existing knowledge of interionic interactions using a rigid lattice model. The theory was applied with semiquantitative success to the dilute solution, but could not be extended to more concentrated regions.

---

# THEORY OF FUSED SALTS[1]

BY DONALD A. MCQUARRIE

*Department of Chemistry, University of Oregon, Eugene, Oregon*[1a]

*Received March 17, 1962*

The Lennard-Jones–Devonshire theory of liquids has been applied in a straightforward manner to systems of fused salts. Because of the long-range coulombic potential, the calculations must be extended to include all neighboring shells, but this problem is resolved by the natural occurrence of the Madelung constant. An interesting result is that the Coulomb potential does not influence the motion of an ion directly, and so a molten salt may be approximated as a fluid of hard spheres in certain cases. The derived partition function is used to calculate several thermodynamic quantities for fused salts. An equation of state is derived which obeys the law of corresponding states for fused salts and from this the reduced critical constants of alkali halides are obtained. The treatment has been carried out only for the halides of lithium, sodium, potassium, and rubidium, but is easily extended to include other salts.

## I

In this article we shall apply the Lennard-Jones–Devonshire theory of liquids[2] to fused salts. It will be shown that a straightforward application of their theory is possible in spite of the long-range coulombic potential.

The most rigorous treatment of fused salts has been given by Stillinger, Kirkwood, and Wojtowicz.[3] They used the theory of distribution functions and derived the usual set of integral equations which, in their case, determines the fused salt ion distributions. It is interesting to note that the superposition approximation has not been used in their work, and a less restrictive hypothesis has been used in its place. Their treatment is quite formal.[4]

Carlson, Eyring, and Ree[5] have applied the recent theory of significant structures to fused salts with success. In this theory, a partition function is constructed by identifying three significant structures in the liquid state. These are (1) solid-like degrees of freedom, (2) degrees of freedom arising from the possible position degeneracy of the solid, and (3) gas-like degrees of freedom. This is not rigorous but has a certain intuitive appeal. Recently an interesting criticism of this theory (and all other solid-like theories of the liquid state) has been published by Hildebrand.[6] Blomgren has extended the significant structure theory and has applied it to fused salts.[7]

The advantage to using the Lennard-Jones–Devonshire theory is that it is fairly easy to produce numerical results and that Kirkwood has given this theory a firm statistical mechanical foundation.[8] This cell or cage model of liquids should be applicable to fused salts since it requires a central molecule to be surrounded by its neighbors, "smeared" over the surface of a spherical shell whose radius is equal to the distance between the central molecule and its neighbors. In fused salts, the force between nearest neighbors is of the order of a hundred times stronger than that between rare gas molecules, to which the theory has been most extensively applied. It was found in reference 3 that a given ion is surrounded on the average by concentric shells of alternating charge, similar to that of the corresponding ionic crystal. This is exactly the model required by an applica-

(1) Supported in part by a research grant from the National Science Foundation.

(1a) Department of Chemistry, Michigan State University, East Lansing, Michigan.

(2) J. E. Lennard-Jones and A. F. Devonshire, *Proc. Roy. Soc.* (London), **A163**, 53 (1937); **A165**, 1 (1938).

(3) F. H. Stillinger, J. G. Kirkwood, and P. J. Wojtowicz, *J. Chem. Phys.*, **32**, 1837 (1960).

(4) For a discussion of the theory of molecular distribution functions, see T. L. Hill, "Statistical Mechanics," McGraw-Hill Book Co., Inc., New York, N. Y., 1956, Chap. 6.

(5) C. M. Carlson, H. Eyring, and T. Ree, *Proc. Natl. Acad. Sci.*, **46**, 333 (1960).

(6) J. H. Hildebrand and G. Archer, *ibid.*, **47**, 1881 (1961).

(7) G. E. Blomgren, *Ann. N. Y. Acad. Sci.*, **79**, 781 (1960).

(8) J. G. Kirkwood, *J. Chem. Phys.*, **18**, 380 (1950).

tion of the Lennard-Jones–Devonshire theory. This "smeared on the average" concept is the same as that encountered in the familiar Debye–Hückel theory.

The theory is essentially a theory of the solid state made applicable to the liquid state by introducing a disordered effect due to thermal motion. Each molecule instead of vibrating around a lattice site is now allowed to move freely in the cell formed by its first neighbors. The entropy of an actual liquid would be higher than that calculated from this model, since each molecule is confined to its cell. Additional entropy can be introduced into this model by the inclusion of a suitable term in the partition function. This problem, called the communal entropy problem, is discussed elsewhere.[4,9]

The only deviations that we shall make from the simple Lennard-Jones–Devonshire theory is to consider a two component system (the positive ions and negative ions), and an extension to include shells of further neighbors. Buehler, Wentorf, Hirschfelder, and Curtiss[10] considered second and third shells in a numerical tabulation of several important functions of the Lennard-Jones–Devonshire theory using a 6–12 potential. Thermodynamic properties are not greatly affected by the inclusion of higher shells when a 6–12 potential is used, but we must consider all shells, since the $1/r$ coulombic potential decreases so slowly.

In section II we shall derive an explicit expression for the canonical ensemble partition function, in section III we shall derive several thermodynamic quantities from this partition function and calculate entropies of fusion and vaporization and critical points for some 1–1 salts, and section IV will be a discussion of these results.

## II

For simplicity we shall consider only 1–1 type salts, but an extension to include others follows immediately. Since the Lennard-Jones–Devonshire theory is actually a modified theory of the solid state, we shall begin with a partition function, $Q$, for a two-component lattice and show how this may be modified to correspond to the liquid state

$$Q(N_+, N_-, T) = q_+(T)^{N_+} q_-(T)^{N_-} \sum_{N_{+-}, N_{+-,-}, \ldots} g(N_+, N_-, N_{+-}, N_{+-,-}, \ldots) e^{-w/kT} \quad (1)$$

where $q_\pm(T)$ is the partition function of a $\pm$ ion situated at a lattice site, $N_\pm$ is the number of $\pm$ ions, $g$ is the number of ways $N_+$ positive ions and $N_-$ negative ions can be arranged on a lattice such that there are $N_{+-}$ positive and negative ions as first neighbors, $N_{+-,-}$ as second neighbors, etc., and where

$$W = N_{++}u_{++} + N_{--}u_{--} + N_{+-}u_{+-} + \ldots \quad (2)$$

$u$ is the coulombic potential between two ions situated at appropriate lattice sites. We assume that all the sites are occupied and that the positive and negative ions are distributed as in the crystal. This is the point at which we could consider the existence of holes in fused salts. We shall not do this, however, but shall discuss this point later. This makes $g$ equal to two and

$$W = N_+(c_1u_1 + c_2u_2 + \ldots) \quad (3)$$

where $c_j$ is the number of j-nearest neighbors and $u_j$ is the potential between j-neighbors. In order to apply this to liquids, we consider the particle not to be restricted to a lattice site but allowed to move in a volume bounded by its first neighbors. To allow for disorder due to the thermal agitation, the neighbors are considered to be uniformly distributed over the surface of a sphere. We also include a factor for the communal entropy. The partition function now becomes

$$Q(N_+,N_-,T) = \frac{2}{N_+!N_-!}\left[\frac{v_f}{\Lambda_+^3}\right]^{N_+}\left[\frac{v_f}{\Lambda_-^3}\right]^{N_-} \exp\left(-\frac{N}{2}\frac{\varphi(0;v)}{RT}\right) \quad (4)$$

where $v_f$ is the volume in which any central ion can move and

$$\Lambda = \frac{h}{(2\pi mkT)^{1/2}} \quad (5)$$

where $h$ is Planck's constant, $m$ is the mass of a particular ion, $k$ is Boltzmann's constant, and $T$ is the absolute temperature. The exponential term is still the energy of the system when all the ions are situated at lattice sites. The $N_+!$ and $N_-!$ are the entropy factors. Note that this partition function is formally similar to that of an Einstein crystal, except for the factorials. We need only define $v_f$ to specify completely our partition function. $v_f$ is defined as

$$v_f = \int_{\text{cell}} \exp\{-(\varphi(\mathbf{r}) - \varphi(\mathbf{0}))/kT\}\, d\mathbf{r} \quad (6)$$

or for a spherically symmetric potential

$$v_f = 4\pi \int_{\text{cell}} e^{-(\varphi(r) - \varphi(0))/kT} r^2 dr \quad (7)$$

In Fig. 1 the central ion is at P, a distance $r$ from the center of the shell formed by its j-th neighbors. The area of the ring shown on the surface of the sphere is $2\pi a_j^2 \sin\theta d\theta$. The number of neighbors in this area is

$$C_j \frac{2\pi a_j^2 \sin\theta d\theta}{4\pi a_j^2} = \frac{C_j}{2}\sin\theta d\theta \quad (8)$$

and the potential energy of interaction between the ion at P and the j-th neighbors in the ring is $u(R_j)\cdot C_j \sin\theta d\theta/2$ where $R_j^2 = r^2 + a_j^2 - 2a_jr\cos\theta$. The total interaction energy between the ion at P and all of its $c_j$ j-th neighbors in the shell is

$$\varphi_j(r) = \frac{c_j}{2}\int_0^\pi u(R_j)\sin\theta d\theta \quad (9)$$

The total interaction energy between the ion at P and all of its shells is

(9) T. L. Hill, "Statistical Thermodynamics," Addison-Wesley Publishing Co., Inc., Reading, Mass., 1960.

(10) R. H. Wentorf, R. J. Buehler, J. O. Hirschfelder, and C. F. Curtiss, *J. Chem. Phys.*, **18**, 1484 (1950).

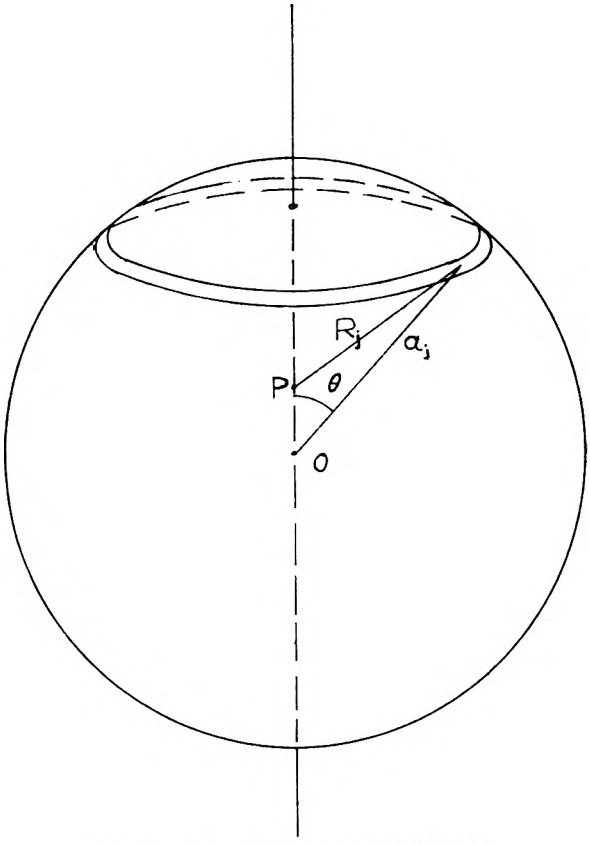


Fig. 1.—A central ion and its j-th shell.

$$\varphi(r) = \sum_{j=1}^{\infty} \varphi_j(r) \qquad (10)$$

We must now assume a form for $u(R_j)$. We first assume that it consists of two parts, a short-range potential and a long-range potential. As indicated above we assume that the long-range contribution is coulombic and can be written as

$$u(R_j) = (-1)^j \frac{z^2\epsilon^2}{R_j} \qquad (11)$$

where $z$ is the valence of the ion, $\epsilon$ is the charge on the electron. The short-range contribution should introduce a strong repulsive force at small values of $r$, indicating the improbability of the ions to inter-penetrate. It would perhaps be most suitable to assume a Lennard-Jones type of potential, but for convenience we shall ignore any short-range attractive part and use a hard sphere potential for the repulsive part. $u(R_j)$ is then

$$\begin{aligned} u(R_j) &= (-1)^j z^2\epsilon^2/R_j \qquad r < a - \sigma \\ &= +\infty \qquad r > a - \sigma \end{aligned} \qquad (12)$$

where sigma is the sum of the radii of the positive and negative ions.

Let us assume that the crystalline form of the crystal state of the liquid is simple cubic. Most alkali halide salts have this form. $\varphi(r)$ then becomes

$$\begin{aligned} \varphi(r) &= \frac{\epsilon^2}{2} \sum_{j=1}^{\infty} (-1)^j c_j \int_0^{\pi} \frac{\sin\theta d\theta}{(r^2 + a_j^2 - 2ra_j\cos\vartheta)^{1/2}} \\ &= -\frac{\epsilon^2}{2a}\left\{\frac{6}{\sqrt{1}} - \frac{12}{\sqrt{2}} + \cdots\right\} = -\frac{\epsilon^2\alpha}{a} \\ & \qquad\qquad r < a - \sigma \\ &= +\infty \qquad\qquad r > a - \sigma \end{aligned} \qquad (13)$$

where $\alpha$ is the Madelung constant of the particular lattice, in the present case, simple cubic. This, of course, is the potential inside a uniformly charged sphere and could have been written down immediately. It is this natural occurrence of the Madelung constant which eliminates any problem due to the coulombic potential. This simple result indicates that the Coulomb potential, aside from scaling thermodynamic quantities, does not directly influence the motion of an ion in its cell. Therefore, a molten salt may be approximated by a hard sphere fluid in certain cases. This has, in fact, been done with some success in the past, and the fact that the potential inside a uniformly charged sphere is constant furnishes an explanation for its success. The applicability of this fact is made clear by the present treatment.

$v_f$ now becomes

$$v_f = 4\pi \int_0^{a-\sigma} r^2 dr = \frac{4\pi v}{3}\left[1 - \left(\frac{v^*}{v}\right)^{1/3}\right]^3 \qquad (14)$$

where $v^* = \sigma^3$. This form for $v_f$ occurs in an approximation of the Lennard-Jones–Devonshire theory due to Prigogine and Mathot.[11] The occurrence of this form in the present development is not due to an approximation, but occurs because the electrostatic potential inside a uniformly charged sphere is a constant. The partition function for the model is

$$Q(N_+, N_-, T) = \frac{2}{N_+!N_-!}\left[\frac{v_f}{\Lambda_+^3}\right]^{N_+}\left[\frac{v_f}{\Lambda_-^3}\right]^{N_-} e^{\alpha\epsilon^2 N/2akT} \qquad (15)$$

From this we can derive all the thermodynamic properties of the model. Some will be derived in the next section.

## III

We shall derive the equation of state for this model. It is well known from statistical mechanics that[9]

$$p = kT\left(\frac{\partial \ln Q}{\partial v}\right)_{N,T} \qquad (16)$$

This immediately yields

$$pv = RT\left[1 - \left(\frac{v^*}{v}\right)^{1/3}\right]^{-1} - \frac{\epsilon^2\alpha N^{4/3}}{6v^{1/3}} \qquad (17)$$

This equation of state consists of two parts, a hard sphere part and one due to the energy of the system when all the ions are situated on lattice sites. It

(11) I. Prigogine and V. Mathot, *J. Chem. Phys.*, **20**, 49 (1952).

has been pointed out by Bockris and Richards[12] that fused salts obey an equation of state of hard spheres fairly well. This is an example of the successful approximation of a fused salt as a hard sphere fluid. This provides some evidence that our simple model may be satisfactory for fused salts. Equation 17 may be rearranged to illustrate the law of corresponding states for fused salts as stated by Reiss, Mayer, and Katz.[13] They have shown that the reduced variables for fuses salts are $z^2\epsilon^2/\sigma kT$ and $v^*/v$. The equation of state in these reduced variables is

$$\frac{pv^*}{kT} = \frac{(v^*/v)}{[1 - (v^*/v)^{1/3}]} - \frac{\alpha}{6}\left(\frac{\epsilon^2}{\sigma kT}\right)\left(\frac{v^*}{v}\right)^{4/3} \quad (18)$$

In Fig. 2 we have plotted this reduced equation of state. In it we have plotted $pv^*/kT$ *vs.* $v/v^*$ for fixed $z^2\epsilon^2/\sigma kT$. From this we were able to determine the critical constants for fused salts. The critical constants are

$$\frac{\epsilon^2}{\sigma kT_c} = 13.1; \quad \frac{p_c v^*}{kT_c} = 9.0 \times 10^{-3}; \quad \frac{v_c}{v^*} = 15 \quad (19)$$

which give for computation

$$T_c = \frac{12.76}{\sigma} \times 10^3; \quad v_c = 15\sigma^3; \quad p_c = \frac{149.5}{\sigma^4} \times 10^2 \quad (20)$$

If $\sigma$ has units of Angstroms, $T_c$ is in °K., $V_c$ in cm.$^3$, and $P_c$ in atmospheres. The values of the critical constants calculated from these equations are listed in Table I. Carlson, Eyring, and Ree[5] also have calculated critical constants and their results are compared with those of the present paper in Table II. They report values for only four salts. The values of Carlson, Eyring, and Ree corresponding to eq. 19 are 16.7, 10.2 × $10^{-3}$, and 13.4, respectively. These are average values for the four salts. Unfortunately these data are not known experimentally. The agreement between our results and theirs seems to indicate that both calculated sets have some reliability. An advantage to the present approach is that there are no empirical parameters to fit to data. These are the only estimates of critical constants of fused salts of which the author is aware.

TABLE I

CALCULATED CRITICAL CONSTANTS

| Salt | $a$ (Å.) | $T_c$ (°K.) | $V_c$ (cm.$^3$) | $p_c$ (atm.) |
|---|---|---|---|---|
| LiF | 2.01 | 6350 | 122 | 910 |
| LiCl | 2.57 | 4960 | 254 | 343 |
| LiBr | 2.75 | 4640 | 312 | 261 |
| LiI | 3.02 | 4220 | 413 | 180 |
| NaF | 2.31 | 5530 | 185 | 525 |
| NaCl | 2.81 | 4540 | 333 | 240 |
| NaBr | 2.98 | 4280 | 398 | 190 |
| NaI | 3.23 | 3950 | 505 | 137 |
| KF | 2.67 | 4780 | 285 | 294 |
| KCl | 3.14 | 4060 | 464 | 154 |
| KBr | 3.29 | 3880 | 534 | 128 |
| KI | 3.53 | 3610 | 660 | 96 |
| RbF | 2.82 | 4520 | 336 | 236 |
| RbCl | 3.29 | 3880 | 534 | 128 |
| RbBr | 3.43 | 3720 | 608 | 108 |
| RbI | 3.66 | 3490 | 735 | 83 |

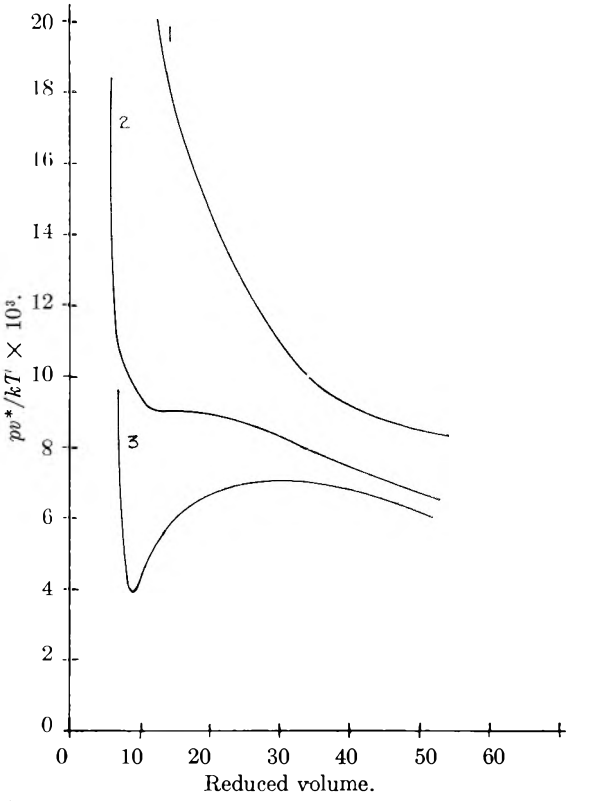


Fig. 2.—$pv^*/kT$ *vs.* $v/v^*$: curve 1, $\epsilon^2/\sigma kT$ = 12.0; curve 2, $\epsilon^2/\sigma kT$ = 13.1; curve 3, $\epsilon^2/\sigma kT$ = 13.5.

TABLE II

COMPARISON OF CRITICAL CONSTANTS WITH CARLSON, EYRING, AND REE'S RESULTS

| | $T_c$ (°K.) | $p_c$ (atm.) | $V_c$ (cm.$^3$) |
|---|---|---|---|
| NaCl | | | |
| This paper | 4540 | 240 | 333 |
| C., E., and R. | 3600 | 235.5 | 293 |
| KCl | | | |
| This paper | 4060 | 154 | 464 |
| C., E., and R. | 3092 | 135.5 | 431 |
| NaBr | | | |
| This paper | 4280 | 190 | 398 |
| C., E., and R. | 3364 | 186.1 | 342 |
| KBr | | | |
| This paper | 3880 | 128 | 534 |
| C., E., and R. | 3060 | 118.3 | 482 |

Now we shall derive the equation for the vapor pressure of a fused salt. We shall do this by equating the chemical potential of the liquid to that of the vapor in equilibrium with it. It is known experimentally that alkali halides exist in the gas phase as diatomic molecules, so the vapor phase will be considered to be an ideal diatomic gas.

(12) J. O'M. Bockris and N. E. Richards, *Proc. Roy. Soc.* (London), **A241**, 44 (1957)

(13) H. Reiss, S. W. Mayer, and J. L. Katz, *J. Chem. Phys.*, **35**, 820 (1961).

Miller and Kusch[14] have found that alkali halide vapors are associated into clusters of diatomic molecules, but we shall ignore this added complication. The chemical potential of an ideal diatomic gas is

$$\mu(T,p) = \ln p - \ln\left[\frac{2\pi(m_1 + m_2)\,kT}{h^2}\right]^{3/2} kT - \ln\frac{8\pi^2 IkT}{h^2} + \ln(1 - e^{-h\nu/kT}) - \frac{D_0}{kT} \quad (21)$$

The chemical potential of the liquid phase is found from eq. 22

$$\mu = kT\left(\frac{\partial \ln Q}{\partial N}\right)_{V,T} \quad (22)[9]$$

Setting $\mu_{gas} = \mu_+ + \mu_-$ gives, after some algebra

$$\log P = \log\left\{\frac{(M/m_+m_-)^{3/2}(8\pi k)^{1/2}\,hI\,(7.6 \times 10^{-4})}{v_f^2\,\epsilon^2}\right\} + \frac{0.434\left(D_0 - \frac{\alpha\epsilon^2}{a}\right)}{kT} + 0.217 \log T \quad (23)$$

where $P$ has units of mm., $M$ is the mass of the diatomic molecule, $I$ is its moment of inertia, $\nu$ is its fundamental vibrational frequency, and $D_0$ is the energy necessary to separate the molecule into its constituent ions, not atoms, at 0°K. Note that this is not the usual definition of this quantity. Experimentally, vapor pressure curves for molten salts are of the form $\log P = A + B/T + C \log T$. This curve allows one to calculate several thermodynamic quantities from a knowledge of the molecular and crystal parameters.

Equation 23 can be compared to experimental vapor pressure curves, but the values of $v_f$ are not known with sufficient accuracy to be useful. Since the liquid does not possess the ordered structure of the solid, $\alpha$ can hardly be expected to have the same numerical value as the Madelung constant of the crystal. Because of this, $v_f$ and $\alpha$ have been treated as adjustable parameters and eq. 23 has been fitted to experimental curves. The data were taken from reference 15. For KCl, $v_f = 0.28 \times 10^{-25}$ cm.$^3$ and $\alpha = 1.1$, and for NaBr, $v_f = 0.78 \times 10^{-25}$ cm.$^3$ and $\alpha = 1.1$. Similar values would have been found for the other salts of this class. These values of $v_f$ differ from those found by Bockris and Richards[12] by a factor of approximately ten. Their experimental error was large however.

Instead of varying $\alpha$ and $v_f$, we may investigate $\alpha$ alone by considering the slope of $\log P$ *vs.* $1/T$. If the boiling points are known, values of $\Delta S_v$, the entropy of vaporization, may be calculated and compared to experiment. This is a well-tabulated thermodynamic quantity and provides an indirect discussion of eq. 23. The value of $\alpha$ has been set equal to the Madelung constant and the results are listed in Table III. As is to be expected, values of $\alpha$ somewhat less than this give reasonable agreement.

TABLE III

CALCULATED ENTROPIES OF VAPORIZATION

| Salt | $D_0$ (kcal./mole)[16] | $a$ (Å.)[17] | $T_b$ (°K.)[18] | $\Delta S_v$ (calcd.) (e.u.) | $\Delta S_v$ (obsd.)[18] (e.u.) | Obsd./calcd. |
|---|---|---|---|---|---|---|
| LiF | 180.5 | 2.01 | 1954 | 55.9 | 26.1 | 0.47 |
| LiCl | 150 | 2.57 | 1655 | 46.2 | 21.8 | .47 |
| LiBr | 144 | 2.75 | 1583 | 42.8 | 22.4 | .52 |
| LiI | 135 | 3.02 | 1444 | 40 0 | 28.2 | .70 |
| NaF | 151 | 2.31 | 1977 | 51.2 | 25 | .49 |
| NaCl | 130 | 2.81 | 1738 | 44.4 | 23.5 | .53 |
| NaBr | 124 | 2.98 | 1665 | 42.9 | 23.2 | .54 |
| NaI | 117.5 | 3.23 | 1577 | 39.9 | 24.2 | .61 |
| KF | 136 | 2.67 | 1775 | 46.3 | 23.3 | .50 |
| KCl | 115 | 3.14 | 1680 | 41.9 | 23.1 | .55 |
| KBr | 110 | 3.29 | 1656 | 39.5 | 22.4 | .56 |
| KI | 104 | 3.53 | 1597 | 38.2 | 21.7 | .57 |
| RbF | 131 | 2.82 | 1681 | 45.0 | 23.50 | .52 |
| RbCl | 110 | 3.29 | 1654 | 40.5 | 22.32 | .55 |
| RbBr | 105.5 | 3.43 | 1625 | 39.6 | 22.84 | .58 |
| RbI | 99.5 | 3.66 | 1577 | 37.8 | 22.80 | .60 |

The last thermodynamic quantity which will be calculated and compared to experiment is the entropy of fusion. We shall use the very simple Lennard-Jones theory of melting to do this. The chemical potential of the liquid phase is set equal to that of the solid phase. We need only assume a partition function for the solid in equilibrium with the liquid. Lennard-Jones assumed that the crystal could be approximated as an Einstein crystal. This gives

$$\Delta S_f = 3R \ln \frac{\nu^K}{\nu^L} + R \quad (24)$$

where $\nu^K$ is the Einstein frequency of the crystal and $\nu^L$ is given by eq. 25.

$$\nu^L = \left(\frac{2kT}{\pi m}\right)^{1/2} v_f^{-1/3} \quad (25)$$

where $m$ is the geometric mean of the positive and negative ion. Equation 25 is the expression obtained in the harmonic oscillator approximation to the Lennard-Jones–Devonshire theory and we shall simply use it formally. The Lennard-Jones theory of melting is discussed in reference 19. The only modification used in the present treatment is to consider a two-component system. Equation 24 has been used to calculate entropies of fusion of several alkali halides. The results are listed in Table IV. This table is incomplete compared to Table III since the Einstein temperatures or Debye temperatures are not known for all the alkali halide salts. Several points of explanation must be

(14) R. C. Miller and P. Kusch, *J. Chem. Phys.*, **25**, 860 (1956).

(15) J. O'M. Bockris, ed., "Modern Aspects of Electrochemistry," Vol. 2, Academic Press, Inc., New York, N. Y., 1959.

(16) L. Brewer and E. Brackett, *Chem. Rev.*, **61**, 425 (1961).

(17) L. Pauling, "The Nature of the Chemical Bond," 3rd Ed., Cornell University Press, Ithaca, New York, 1960.

(18) "American Institute of Physics Handbook," McGraw-Hill Book Co., Inc., New York, N. Y., 1957.

(19) R. H. Fowler and E. A. Guggenheim, "Statistical Thermodynamics," Cambridge, London, 1939.

mentioned with this table. For the latter three salts we have used values of $\theta_D$ equal to 180, 130, and 115 in that order. There was no particular reason for choosing these values. The values of $v_f$ taken from Bockris and Richards were not accurate enough to use more than one or two figures and most of the values are close to $8 \times 10^{-25}$. The Einstein temperature was taken to be $^3/_4\,\theta_D$.[5] Two sets of experimental values are included because of the rather large discrepancy in the reported results.

TABLE IV

CALCULATED ENTROPIES OF FUSION

| Salt | $\theta_D$[18] | $\Delta S_f$ (obsd.), e.u.[18] | $\Delta S_f$ (obsd.), e.u.[20] | $\Delta S_f$ (calcd.), e.u. | Calcd./ obsd.[18] | Calcd./ obsd.[20] |
|---|---|---|---|---|---|---|
| NaCl | 281 | 6.3 | 6.23 | 5.7 | 0.90 | 0.91 |
| KCl | 227 | 5.8 | 6.01 | 4.8 | .83 | .80 |
| KBr | 177 | 7 | 6.06 | 5.2 | .74 | .86 |
| KI | 115–200 | .. | 6.02 | 4.2 | .. | .70 |
| RbBr | 120–135 | 3.9 | 5.77 | 4.6 | 1.18 | .80 |
| RbI | 110–118 | 3.27 | 5.73 | 4.7 | 1.44 | .82 |

## IV

Probably the most important result of this treatment is that it shows that the Coulomb potential, aside from setting the scale on which thermodynamic properties are measured, does not directly influence the motion of an ion, indicating that a molten salt can be approximated by a hard sphere fluid in certain cases. This is a result of the fact that the potential inside a uniformly charged sphere is a constant.

Critical constants of fused salts have not yet been measured, and this treatment provides a straightforward method for estimating these quantities.

This theory imposes an artificial order upon the liquid state and this has appeared in the calculation of the entropies of vaporization. With less order, $\alpha$ could decrease and this would improve the results. Also, a consideration of the association of the molecules in the vapor phase might lead to better agreement with experiment. It was the purpose of this paper to present a simple non-empirical theory, however, and so this was not done.

The most obvious modification of this treatment is to consider the presence of holes in a molten salt. Salts expand about 20% upon melting and yet the distance between neighboring ions increases by only 1 or 2%.[15] The Lennard-Jones–Devonshire theory has been modified to include holes in the system and this modification begins with eq. 1 by allowing for the case where $N_+ + N_-$ is less than the number of lattice sites. This then becomes a lattice statistics problem and this has been treated by means of various approximations.[21]

**Acknowledgment.**—The author is indebted to Prof. T. L. Hill for helpful discussions.

(20) A. S. Dvorkin and M. A. Bredig, *J. Phys. Chem.*, **64**, 269 (1960).

(21) H. M. Peek and T. L. Hill, *J. Chem. Phys.*, **18**, 1252 (1950); G. E. Blomgren, *ibid.*, **34**, 1307 (1961).

# THE THERMODYNAMICS OF THE THERMAL DECOMPOSITION OF ACETIC ACID IN THE LIQUID PHASE[1]

BY JAMES A. KNOPP, WILLIAM S. LINNELL, AND WILLIAM C. CHILD, JR.

*Department of Chemistry, Carleton College, Northfield, Minnesota*

*Received March 23, 1962*

Equilibrium constants for the thermal decomposition of liquid acetic acid into acetic anhydride and water were determined over the temperature range 169–248°. From the temperature dependence of the equilibrium constant, $\Delta H^0$ for the decomposition of two moles of acetic acid was found to be 15.22 ± 0.28 kcal., which is in good agreement with the calorimetric value, when the latter is corrected for heats of mixing. $\Delta F^0$ for the reaction was combined with free energies of formation from the literature to give −117.3 kcal./mole as the standard free energy of formation of liquid acetic anhydride at 25°.

The discovery[2] that liquid propionic acid is thermodynamically unstable at temperatures as low as the normal boiling point led us to suspect that acetic acid also is unstable at corresponding temperatures, even though previous measurements of critical constants,[3] liquid density,[3] and vapor pressure[3–5] at high temperature failed to reveal any decomposition. The products of the thermal decomposition of propionic acid in the liquid phase are propionic anhydride and water.[2] By analogy, acetic acid would decompose according to the reaction

$$2CH_3COOH = (CH_3CO)_2O + H_2O \quad (1)$$

By measuring the equilibrium constant for this reaction at several temperatures, one can calculate $\Delta F^0$ and $\Delta H^0$ for the reaction and eventually the free energy of formation of acetic anhydride, for which there is no value presently available.[6]

## Experimental

**Purification of Acetic Acid.**—Analytical Reagent grade acetic acid was purified by refluxing for about one day with an amount of acetic anhydride calculated to react with the water present. The acid then was subjected to fractional distillation at atmospheric pressure, and the middle fraction was used in the thermal decomposition experiments. It was found that if even a slight excess of anhydride was used, the acetic acid after fractional distillation contained a low concentration of anhydride. The amount of anhydride added therefore was adjusted to give a final batch of acid

(1) Taken in part from the senior honors thesis of J. A. Knopp.

(2) W. C. Child, Jr., Ph.D. Thesis, University of Wisconsin, 1955, and later unpublished work.

(3) S. Young, *Sci. Proc. Roy. Dublin Soc.*, **12**, 374 (1910).

(4) D. R. Stull, *Ind. Eng. Chem.*, **39**, 517 (1947).

(5) A. E. Potter, Jr., and H. L. Ritter, *J. Phys. Chem.*, **58**, 1040 (1954).

(6) J. H. S. Green, *Quart. Rev.* (London), **15**, 125 (1961).

which contained either water and anhydride at mole fractions of about $1 \times 10^{-4}$ and $3 \times 10^{-4}$, respectively, or water at mole fractions ranging up to $2 \times 10^{-3}$ (anhydride concentration negligible). Determination of these values is described in the section on analyses. It was necessary to have low initial concentrations of water and anhydride to avoid repression of the decomposition reaction.

**Thermal Decomposition.**—Although several methods were employed for equilibrating samples of acetic acid at high temperature and then quenching the samples, only the final method, used for the quantitative data reported here, is described. Acetic acid (3–4 ml.) was distilled on a vacuum line into a Pyrex sample tube, which was 16 mm. in diameter and 9 cm. in length and had a small thermocouple well along the axis of the tube. At one end of this tube there was a 5-cm. length of capillary tubing leading to a break seal, which could be fractured with the aid of a glass enclosed iron rod and a magnet. After filling, the tube was sealed off from the vacuum line and placed inside an electrically heated, crucible-type furnace with the break seal at the top. This seal was connected to another section of the vacuum line, which contained a U-trap partially filled with glass beads. After an appropriate equilibration time at high temperature (see Table I), the break seal was fractured, and the sample quickly distilled into the U-trap, which was maintained at −196°. It is estimated that the time required to freeze the entire sample was 10 to 15 sec. Finally, the sample was warmed and distilled into another tube, which was sealed from the line. The sample was held at −80° until the time of the analysis.

TABLE I

RESULTS OF EQUILIBRIUM STUDIES

| Temp., °C. | Equilibration time, hr. | $X_{an} \times 10^3$ | $X_w \times 10^3$ | $K \times 10^6$ | log $K_{obsd.}$ − log $K_{calcd.}$ |
|---|---|---|---|---|---|
| 168.9 | 5 | 0.94 | 0.77 | 0.73 | 0.000 |
| 169.1 | 3 | .95 | .80 | 0.76 | .019 |
| 169.6 | 2 | .94 | .81 | 0.76 | .009 |
| 196.8 | 2 | .82 | 2.35 | 1.94 | − .017 |
| 197.1 | 2 | .75 | 2.64 | 1.99 | − .012 |
| 197.9 | 3 | .855 | 2.40 | 2.07 | − .007 |
| 215.7 | 1.5 | 1.94 | 1.88 | 3.67 | − .017 |
| 218.9 | 2 | 2.08 | 2.02 | 4.24 | .001 |
| 222.7 | 1.5 | 1.69 | 2.53 | 4.32 | − .039 |
| 224.8 | 2 | 1.61 | 3.21 | 5.24 | .015 |
| 226.0 | 3 | 1.77 | 3.09 | 5.51 | .022 |
| 244.8 | 1 | 3.03 | 2.87 | 8.80 | − .021 |
| 245.1 | 1 | 3.03 | 2.97 | 9.10 | − .009 |
| 246.5 | 1 | 2.76 | 3.59 | 10.05 | .021 |
| 247.5 | 1 | 2.82 | 3.59 | 10.26 | .016 |
| 247.7 | 0.6 | 3.17 | 3.08 | 9.88 | − .003 |
| 247.8 | 1.7 | 2.82 | 3.64 | 10.40 | .019 |

Temperatures were measured with an iron–constantan thermocouple calibrated at the melting points of benzoic acid, tin, and cadmium. Thermocouple e.m.f.'s were measured with a Leeds and Northrup No. 7552 potentiometer. To prevent a temperature drop off at the top of the sample tube, heater windings were more closely spaced at the top than at the bottom of the furnace. The temperature of the upper sample tube, which contained a relatively small quantity of vapor, was held no more than 5° above the temperature of the liquid. The latter temperature was maintained constant to ±0.2° with the help of a proportional controller. The uncertainty in the reported temperatures is estimated at ±0.4°.

**Analyses for Acetic Anhydride and Water.**—The ultraviolet spectrum of a previously heated sample of acetic acid exhibited a strong absorbance relative to pure acetic acid in the region, 250–280 mμ. The shape of the spectrum was identical to that of acetic anhydride in acetic acid. After a small amount of anhydrous sulfuric acid in acetic acid was added to the sample, the absorbance dropped to zero. These observations were taken to support the hypothesis that the products of the thermal decomposition are acetic anhydride and water.

The mole fraction of anhydride was determined by measuring the absorbance of the sample at one or more of the following wave lengths: 256, 260, and 265 mμ. The absorbance values were converted to mole fractions by use of Beer's law plots. The standard solutions used for the Beer's law data were made by adding from a microburet known volumes of acetic anhydride to a weighed quantity of acid in a glass-stoppered, 1-cm. spectrophotometer cell. The anhydride contained 1.7% water (as determined by the method of Bruckenstein[7]), which was taken into account in the calculations. A Beckman DU spectrophotometer was employed for all absorbance measurements. The uncertainty in the values for the mole fraction of anhydride is estimated as ±2%.

To determine the mole fraction of water, it was necessary only to find the amount of water remaining in a sample after the addition of a small amount of anhydrous sulfuric or perchloric acid in acetic acid, which causes rapid reaction of anhydride with water at room temperature. The mole fraction of the excess water then was added to the mole fraction of anhydride, determined previously, to give the mole fraction of the total water present. The excess water was measured by a spectrophotometric titration with acetic anhydride in the presence of the acid catalyst.[7] This operation was carried out in a drybox during humid weather. In those cases in which the original acetic acid contained a slight excess of acetic anhydride, the result of the titration was a negative quantity of water, which was treated in the calculations exactly as in the other cases. The maximum uncertainty in the mole fraction of total water varies from ±3 to ±5%, because the excess water is a varying fraction of the total, and because the drybox operation was not always successful in preventing absorption of atmospheric moisture.

## Results and Discussion

The results of seventeen experiments in the temperature range 169–248° are given in Table I. Equilibrium constants for the decomposition of acetic acid were calculated according to the equation

$$K = \frac{X_{an} X_w}{(X_{ac})^2} \qquad (2)$$

where $X_{an}$, $X_w$, and $X_{ac}$ represent the mole fractions of acetic anhydride, water, and acetic acid, respectively. Although the ratio of water to anhydride varied considerably from experiment to experiment, the measured equilibrium constant was independent of this ratio. The results of a set of four experiments at ~174°, conducted during the humid summer months, were discarded in favor of the three listed experiments at 169°, which were performed during the dry winter period. These measurements at the lowest temperatures, where the extent of decomposition is relatively slight, are the most susceptible to errors from the absorption of moisture from the air during the water titration. The equilibrium constants calculated from the first experiments were about 20% larger than those predicted from the final plot of log $K$ *vs.* $1/T$, and the discrepancy is attributed to this cause. In addition, the results of an experiment at 197° and one at 248° were omitted, because the calculated equilibrium constants differed from those read from the log $K$ plot by 12 and 23%, respectively, considerably more than the estimated maximum random error.

Since there is a vapor phase in the sample tube, it is possible that the experimentally determined equilibrium constant might differ significantly from

(7) S. Bruckenstein, *Anal. Chem.*, **31**, 1757 (1959).

the true constant for the liquid phase. To investigate this possibility, the Henry's law constants for water in acetic acid and acetic anhydride in acetic acid were calculated, by the method described below, for a temperature of 245°, at which the fraction of the sample in the vapor phase is greatest. Using these values, the known vapor pressure of acetic acid at 245°, and the volumes of liquid and vapor phases in a typical experiment at 245°, the difference between equilibrium constants determined with and without a vapor phase was calculated and found to be negligible. To confirm this conclusion, the amount of sample used in the experiment at 245.1° (see Table I) was adjusted so that the ratio of vapor volume to liquid volume was approximately one-fifth that of the other experiments near this temperature. The resulting equilibrium constant was not out of line with the others.

It is believed that the equilibrium constants obtained are thermodynamic constants. That is, the mole fractions are equal to activities, provided that the proper choice of standard states is made. The equilibrium system at all temperatures consists of a very dilute solution of water and acetic anhydride in acetic acid. One therefore reasonably can expect water and acetic anhydride to obey Henry's law and acetic acid to obey Raoult's law. This fact suggests that the standard states for water and acetic anhydride be chosen as the hypothetical states in which the fugacities of the two components are equal to their Henry's law constants. The standard state for acetic acid is logically the pure liquid. With this choice, the activities of the three components approach the respective mole fractions in the very dilute solutions.

A straight line was fitted to the values of log $K$ and $1/T$ by the method of least squares. The result is

$$\log K = -3326.5/T + 1.385 \qquad (3)$$

The deviations between calculated and observed values of log $K$ are included in Table I. The average deviation is ±0.014 log unit, which corresponds to a deviation in $K$ of ± 3.2%, well within the estimated error. Extrapolation of eq. 3 to the normal boiling point of acetic acid, 118.1°, yields a value of $K$ of $7.6 \times 10^{-8}$. Absolutely pure acetic acid therefore should decompose to the extent of 0.028% at the boiling point, if held at this temperature for a sufficiently long time. Recently Bruckenstein[8] has noticed that after the careful purification of acetic acid, the last step of which involves fractional distillation, very small and approximately equimolar amounts of anhydride and water are present.

From eq. 3 one obtains the thermodynamic quantities, $\Delta H^0 = 15.22 \pm 0.28$ kcal., and $\Delta S^0 = 6.3 \pm 0.6$ e.u. for the decomposition of two moles of acetic acid. The uncertainties were obtained from the 90% confidence level in the least squares treatment. From calorimetric measurements, Kistiakowsky and co-workers[9] found that $\Delta H$ for the reaction

$$2CH_3COOH(l) = (CH_3CO)_2O(l) + H_2O(l) \qquad (4)$$

is 13.96 kcal. at 30°. In order to make a comparison between the two values of $\Delta H$, one must take into account not only the different temperatures but also the different standard states used. Kistiakowsky, *et al.*, employed the pure liquids as the standard states. Our standard states for enthalpy are, for water and acetic anhydride, the infinitely dilute solution in acetic acid, and for acetic acid, the pure liquid. Thus the two $\Delta H$'s should differ by the sum of the heats of mixing of water and acetic acid, and acetic anhydride and acetic acid, to form the infinitely dilute solutions in acetic acid. Either of these heats of mixing is related to partial molar enthalpies by the equation

$$\Delta H_{mix} = \bar{H}_2^* - \bar{H}_2^{\Delta} \qquad (5)$$

in which $\Delta H_{mix}$ is the heat of mixing per mole of solute (water or anhydride), $\bar{H}_2^*$ is the partial molar enthalpy of the solute at infinite dilution, and $\bar{H}_2^{\Delta}$ is the molar enthalpy of the pure solute.

To obtain the heat of mixing of water in infinitely dilute acetic acid, several methods of calculation and sources of data have been used. The first calculation is based on data of Keily and Hume,[10] who measured the decrease in temperature on adding small quantities of water to a fixed amount of acetic acid. From Fig. 3 of their paper, $(\partial T/\partial V_w)_\infty$ was evaluated for use in the equation[10]

$$\bar{H}_w^* - \bar{H}_w^{\Delta} = -\left(\frac{\partial T}{\partial V_w}\right)_\infty \frac{M_w C_p}{d_w} \qquad (6)$$

to yield the desired heat of mixing. Here $(\partial T/\partial V_w)_\infty$ is the rate of change of temperature with volume of water added to a fixed quantity of acetic acid, evaluated at infinite dilution, $M_w$ and $d_w$ are the molar weight and density of water, and $C_p$ is the sum of the heat capacities of the solution and the calorimeter. The calculated heat of mixing is 1030 cal. per mole of water.

A second value for this heat of mixing was obtained from the activity coefficients for the system water–acetic acid at two temperatures, by use of the equation

$$\left(\frac{\partial \ln \gamma_w^*}{\partial T}\right)_p = \frac{\bar{H}_w^{\Delta} - \bar{H}_w^*}{RT^2} \qquad (7)$$

where $\gamma_w^*$ is the activity coefficient, based on Raoult's law, for water in an infinitely dilute solution of water in acetic acid. The two values of $\gamma_w^*$ employed are 2.71 at 25.0°[11] and 1.91 at 99.0°.[12] On the assumption that the heat of mixing is independent of temperature, the resulting value is 1040 cal./mole.

An attempt was made to obtain a third value from the heats of dilution for this system measured by Payn and Perman[13] over the temperature range 20–70°. However, it was found that the scatter in the data precluded accurate extrapolations to infinite dilution. An approximate value of 700 cal./

(8) S. Bruckenstein, private communication.

(9) J. B. Conn, G. B. Kistiakowsky, R. M. Roberts, and E. A. Smith, *J. Am. Chem. Soc.*, **64**, 1747 (1942).

(10) H. J. Keily and D. N. Hume, *Anal. Chem.*, **28**, 1294 (1956).

(11) R. S. Hansen, F. A. Miller, and S. D. Christian, *J. Phys. Chem.*, **59**, 391 (1955).

(12) J. Marek, *Coll. Czech. Chem. Commun.*, **21**, 269 (1956).

(13) R. C. Payn and E. P. Perman, *Trans. Faraday Soc.*, **25**, 599 (1929).

mole at 25° was obtained. It was noted that the heats of mixing increase with temperature, contrary to the general rule that solutions approach ideal behavior more closely as the temperature increases. The first two results therefore are regarded as the most reliable, and the final value selected for this heat of mixing is 1030 cal. per mole of water.

The corresponding heat of mixing for acetic anhydride in acetic acid was estimated from the temperature decreases observed by Greathouse and co-workers[14] on mixing the anhydride with the acid. The method of calculation was identical to that employed in first calculation of the heat of mixing of water and acetic acid, and the resulting value is 430 cal. per mole of acetic anhydride. The error in this value may be as large as 20%, because the temperature changes were small and the heat capacity of the calorimeter was not given.

Addition of the two heats of mixing to the $\Delta H$ determined by Kistiakowsky, *et al.*,[9] gives 15.4 kcal. as the value of $\Delta H^0$ at 30° for the decomposition reaction, based on the standard states employed in this research. The correction to Kistiakowsky's value is particularly large because both solutes in this system exhibit significant positive deviations from Raoult's law. It is not possible to convert accurately the above value of $\Delta H^0$ to 210°, the average temperature of the thermal decomposition experiments, because only $\Delta C_p$ for reaction 4 at 30° can be obtained from literature values. Using 40.2,[15] 29.5,[16] and 18.0[16] cal./deg. mole for the heat capacities at 30° of acetic anhydride, acetic acid, and water, respectively, $\Delta C_p$ is found to be −0.8 cal./deg. $\Delta H^0$ at 210° would therefore be smaller than $\Delta H^0$ at 30° by about 0.1 kcal. The heats of mixing also would if anything be smaller at the higher temperature. It would seem that in any case the variation of $\Delta H^0$ with temperature is slight. This conclusion is further supported by the fact that log $K$ for the thermal decomposition is a linear function of $1/T$, within experimental error. Therefore, the agreement between the $\Delta H^0$ obtained from this research, 15.2 kcal., and the calorimetric value seems satisfactory.

On the assumption that $\Delta H^0$ and $\Delta S^0$ for the decomposition reaction do not vary with temperature, one can readily calculate $\Delta F^0$ for the reaction at 25° and from this the standard free energy of formation of acetic anhydride at 25°, since the free energies of formation of acetic acid and water are known. The calculated $\Delta F^0$ at 25° is 13.3 kcal. Since this value refers to the standard states employed in this research, it must be corrected to the usual standard states, the pure liquids. This again involves a correction for water and one for acetic anhydride and requires a knowledge of $k_2/p_2^{\Delta}$, the ratio of the Henry's law constant for the solute in acetic acid to the vapor pressure of the pure solute. Since this ratio is equal to $\gamma_2^*$, the activity coefficient already discussed, it can be found readily.

$\gamma_w^*$ is 2.71 at 25°, as discussed earlier. This value leads directly to $\Delta F$ for the process,

$$H_2O(l, \text{v.p.} = k_w, 25°) \longrightarrow H_2O\ (l, \text{v.p.} = p_w^{\Delta}, 25°) \quad (8)$$

which is the desired result. The left side of this equation refers to water in a hypothetical state in which it exerts a vapor pressure equal to the Henry's law constant, while the right side refers to pure water exerting its real vapor pressure. The calculated $\Delta F$ for the process is −590 cal.

$\gamma_{an}^*$ at 25° must be calculated from the value at 99.0°, which is 2.21.[12] The calculation is made by use of eq. 7 applied to acetic anhydride; $\bar{H}_{an}^{\Delta} - \bar{H}_{an}^*$ for this calculation already has been obtained. The result is $\gamma_{an}^* = 2.55$ at 25°, and the correction to the free energy change accompanying the decomposition reaction is −560 cal.

Addition of these two corrections to the experimentally determined $\Delta F°$ gives 12.2 kcal. as the standard free energy change for the reaction at 25° when the standard states for reactant and products are the pure liquids. This value now can be combined with the standard free energies of formation of water and acetic acid, −56.7[15] and −93.1[6] kcal./mole, respectively, to give −117.3 kcal./mole as the standard free energy of formation of liquid acetic anhydride at 25°.

By use of the above corrected $\Delta F^0$ for the reaction at 25° and the known[9] $\Delta H^0$, $\Delta S^0$ is found to be 5.9 e.u., based on the conventional standard states. This value in turn is combined with the standard entropies of water and acetic acid, 16.7[16] and 38.2[6] e.u./mole, respectively, to give 65.6 e.u./mole for the standard entropy of acetic anhydride at 25°.

A comparison of the magnitudes of the $\Delta H^0$ and $T\Delta S^0$ terms for the decomposition shows that $\Delta H^0$ is by far the more important. This means that the slight instability of acetic acid can be related primarily to bond energies. The $T\Delta S^0$ contribution, although small, decreases the stability. Kistiakowsky and co-workers,[9] in their study of the heats of hydrolysis of acetic and methyl-substituted acetic anhydrides, found no correlation between $\Delta H$ and increasing methyl substitution (*i.e.*, increasing positive inductive effect of the substituent). An investigation of the thermal decomposition of several substituted acetic acids is planned to determine whether a trend becomes apparent when the $T\Delta S^0$ contribution is included.

**Acknowledgment.**—Financial support from the Research Corporation, the Petroleum Research Fund of the American Chemical Society, and the National Science Foundation is gratefully acknowledged. We are indebted to Dr. Robert Kolenkow and Mr. Arthur Hay for the design and construction of the proportional temperature controller used in this research.

(14) L. H. Greathouse, H. J. Janssen, and C. H. Haydel, *Anal. Chem.*, **28**, 357 (1956).

(15) N. M. Philip, *Proc. Indian Acad. Sci.*, **9A**, 109 (1939).

(16) F. D. Rossini, *et al.*, "Selected Values of Chemical Thermodynamic Properties," Circular 500, National Bureau of Standards, Washington, D. C., 1952.

# CHANGES IN LENGTH AND INFRARED TRANSMITTANCE DURING THERMAL DEHYDRATION OF POROUS GLASS AT TEMPERATURES UP TO 1200°

BY THOMAS H. ELMER, IAN D. CHAPMAN, AND MARTIN E. NORDBERG

*Research & Development Division, Corning Glass Works, Corning, New York*

*Received March 24, 1962*

Infrared spectra and length changes were measured as a plate of porous glass was heated *in vacuo* from room temperature to 1200°. Shrinkage is shown to be due to rearrangement of the silica network brought about by reaction between silanol groups on the surface to form strong Si–O–Si bridges and water. The elimination of water on heating is shown by infrared measurements to occur at temperatures up to that corresponding to complete consolidation. Changes in intensity and assignment of the infrared bands observed during degassing and rewetting of the porous glass are discussed.

## Introduction

The numerous publications dealing with the surface chemistry of silica gel and porous glass show that there exists considerable interest in these materials. Investigations have shown that these materials contain appreciable amounts of silanol (hydroxyl) groups on the surfaces. In recent studies porous glass has been used successfully as adsorbent for studying changes in infrared spectra of physically adsorbed molecules. Folman and Yates[1] also included water in their adsorption studies. The thermal dehydration of porous glass up to 400° has been investigated by Kiselev and Lygin.[2] Little and Mathieu[3] also studied the thermal dehydration of porous glass. It was felt valuable to use infrared spectroscopy to provide information during the course of dehydration, together with length change measurements up to consolidation of the porous glass to see if correlation exists between length change and loss of water from the porous glass.

## Experimental

**Samples.**—The porous glass used in this study was in the form of thin plates, 3.5 cm. × 1.5 cm. × 0.25 mm. Porous glass is an intermediate glass obtained by heat treating and leaching a special soft alkali borosilicate glass.[4] One phase, which is rich in boric oxide and alkali, is leached out to leave a porous high-silica structure. The composition of porous glass on the basis of ignited weight is 96% $SiO_2$, 3% $B_2O_3$, 0.5% $R_2O_3$ + $RO_2$ (chiefly $Al_2O_3$ and $ZrO_2$), and traces of $Na_2O$ and $As_2O_3$.

**Infrared Measurements.**—The porous glass plate was inserted in a cell containing a fused quartz window. The cell was connected to a mechanical pump which could evacuate the system to a pressure of 0.2 mm. The cell was placed inside a Vycor Brand Code 7913 glass tube which protruded from an electric furnace capable of attaining 1200°. Temperatures were measured with a Chromel–Alumel thermocouple. All infrared spectra were recorded at room temperature with a Perkin-Elmer Model 21 infrared spectrophotometer with sodium chloride optics.

**Length Measurements.**—The length changes observed during heating were obtained by measuring with a travelling microscope the distance between two index marks, 3 cm. apart, on the surface of the plate in the cell under vacuum. All measurements were made after the porous glass had cooled to room temperature. The length measurement for the wet sample involved placing the plate in a Petri dish partially filled with distilled water to obtain a "wet" reading.

**Procedure.**—The cell containing the porous glass plate was placed in the furnace at the predetermined temperature and was pumped for 1 hr. (longer in some cases). The cell then was sealed by means of a glass stopcock, removed from the furnace and vacuum attachment, and allowed to cool to room temperature. After making both infrared and length change measurements the cell again was placed in the furnace and pumped at the next higher temperature. The procedure was repeated until the porous glass was completely consolidated.

## Results and Discussion

**Length Change Measurements.**—The distance between two points on the plate was measured after it first had been immersed in water, after both air drying and pumping at room temperature, and after pumping while being heated at 100° intervals from 100 to 1200°. The results are shown graphically in Fig. 1. The 0.4% decrease in length between AB is a phenomenon commonly observed during drying of porous materials, particularly in the ceramic field. It has been studied recently by Amberg and McIntosh[5] and Folman and Yates.[1] The former two investigators[5] point out that contraction occurs on desorbing water from a porous glass rod initially in an 87% relative humidity atmosphere due first to a deepening of the menisci formed in the pores and the decreasing spreading force of the adsorbed film in filled pores, the increasing value of the negative pressure as reversible desorption takes place, and finally the increase in surface free energy as desorption takes place from the walls of the pores. The destruction of concave menisci results in a loss of capillary forces and causes a slight expansion which is observed by an increase in length of the porous glass rod, but the net process is a contraction which Amberg and McIntosh report to be about 0.2%. It is not clearly known whether all the physically adsorbed water is removed even at 200° (see Infrared Measurements) and it may well be that the small contractions observed up to 200° are due to the final stages of the above process as the last traces of physically adsorbed water are removed.

Above 200° other factors must cause the small but steady contraction that occurs up to about 900°. Young[6] has found that above *ca.* 180° silanol groups on a silica gel start to condense to form silica–oxygen bonds and water. Wolf and Beyer[7] point out that DeBoer and co-workers,[8,9]

(1) M. Folman and D. J. C. Yates, *Trans. Faraday Soc.*, **54**, Part II, 1684 (1958).

(2) A. V. Kiselev and V. I. Lygin, *Proc. Second Intern. Congr. Surface Activity*, **2**, 204 (1957).

(3) L. H. Little and M. V. Mathieu, *Actes Congr. Intern. Catalyse, 2e, Paris*, **1**, 771 (1960).

(4) M. E. Nordberg, *J. Am. Ceram. Soc.*, **27**, 299 (1944).

(5) C. H. Amberg and R. McIntosh, *Can. J. Chem.*, **30**, 1012 (1952).

(6) G. J. Young, *J. Colloid Sci.*, **13**, 67 (1958).

(7) F. Wolf and H. Beyer, *Z. anorg. allgem. Chem.*, **300**, 33 (1959).

(8) J. H. DeBoer, *Angew. Chem.*, **70**, 389 (1958).

(9) J. H. DeBoer, M. E. H. Hermans, and J. M. Vleeskens, *Proc. Koninkl. Ned. Akad. Wetenschap.*, **B60**, 45, 54 (1957).

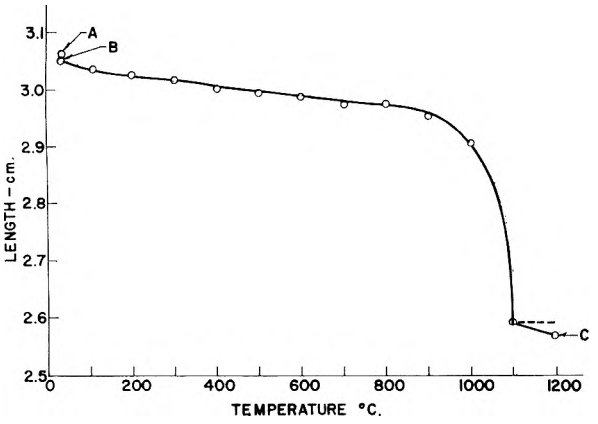


Fig. 1.—Length of porous glass at room temperature as a function of successive heating *in vacuo* at temperatures from 25 to 1200°. Warpage of the sample above 1100° caused point C to be low in value. It normally would be expected to fall on the dotted line.

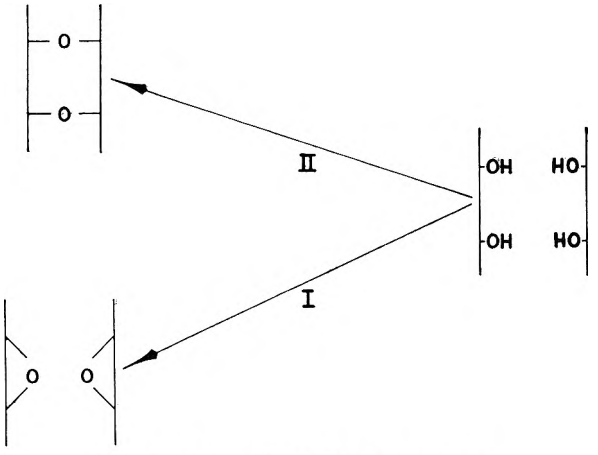


Fig. 2.—Thermal dehydration reactions.

whose work with silica gel agrees with that of Kohlschütter and Kämpf,[10] showed that the thermal dehydration of silanol surfaces can be represented by two different reactions as illustrated schematically in Fig. 2. According to reaction I two surface Si–OH groups on a particle can react with each other to form an Si–O–Si bridge and water. In this reaction both the pore volume and internal surface area remain constant, but the surface has changed chemically, becoming more hydrophobic. Reaction II (Fig. 2) involves the dehydration between two Si–OH groups on surfaces belonging to different particles. It results in a decrease in internal surface area (sintering). De Boer and co-workers showed that the siloxane groups formed during dehydration reaction I can be hydrated with water to silanol groups, but those produced by reaction II cannot be broken.

Above 900° the shrinkage process is greatly accelerated. At these high temperatures the silanol concentration in the porous plate also decreases markedly as will be shown later, and this confirms that shrinkage can be accounted for by rearrangement of the silica structure due to condensation reactions between silanol groups on the surface of the porous glass. Wolf and Beyer[7] point out that at very high temperatures the loss in water from silica gel is not large enough to explain the rapid decrease in internal surface area and pore volume and suggest the following reaction scheme to explain this.

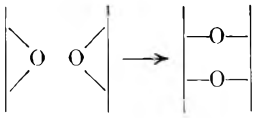


III

The fact that we have observed little change in the water absorption bands in relatively thick porous glass measured both after 900° heating and after plunging into a furnace above 1100° to rapidly consolidate the glass leads one to conclude that the sintering reaction under these conditions probably is due chiefly to joining of the silica surfaces as indicated by reaction III, described by Wolf and Beyer.

**Infrared Measurements.**—Infrared spectra were measured between 1.2 and 5.0 $\mu$. The sharp absorption band observed at around 2.7 $\mu$ is due to stretching vibrations of relatively unassociated OH groups. Overtones of the fundamental O–H vibration band also were observed in the region of 1.4 and 2.2 $\mu$. Absorption bands at 3.64 and 3.95 $\mu$ are due to boric oxide in the structure of the glass. The main band of interest is the band between 2.7 and 3.0 $\mu$. The broadness of this band is a common phenomenon in OH systems that are strongly associated by hydrogen bonding. The asymmetric decrease in the width of the band as consolidation proceeds is one of the significant observations in this work. This phenomenon generally is thought to be due to condensation reactions between silanol groups or removal of physically adsorbed water.

Young[6] points out that all of the truly physical adsorbed water is removed from the silica surface by evacuation at room temperature. Benesi and Jones,[11] who worked with silica gel, agree with Young and state that adsorbed water is completely removed by evacuation at room temperature within the limits of their means of detection. Benesi and Jones base their conclusion upon the appearance and disappearance of a strong absorption band at about 6.1 $\mu$ due to a $\nu_2$ fundamental for water when an evacuated film of grade 950 silica gel was exposed to water vapor and then vacuum pumped. It was not possible with our cell and with the thickness of the plate used to follow the infrared transmittance curve beyond 4.8 $\mu$ and hence this observation could not be confirmed for porous glass in this work. However, Little and Mathieu,[3] who used a thinner sample and $CaF_2$ optics, note the presence of a band at 6.1 $\mu$ which decreases sharply in intensity up to 200°. Furthermore, from studies in this and other laboratories, activation temperatures of about 180° are needed to obtain maximum water vapor adsorption on porous glass at low relative pressures. It is difficult to see why this should be so if all the physically adsorbed water has been driven off at room temperature and no condensation reaction is postulated below 180°. Also, the

(10) H. W. Kohlschütter and G. Kämpf, *Z. anorg. allgem. Chem.*, **292**, 298 (1957).

(11) H. A. Benesi and A. C. Jones, *J. Phys. Chem.*, **63**, 179 (1959).

bands in the region around 2.8 $\mu$ are decreasing in width below 200° and above room temperature, indicating a loss of water from one source or another from within the porous glass. Therefore, one can conclude that physically adsorbed water is present in porous glass at temperatures up to 200°. Due to scattering, which seemed to be unavoidable in the case of the silica gel used by Benesi and Jones, satisfactory observations in the region of 6.1 $\mu$ were not possible, and as Miller[12] points out, due to the great difference in absorbancy index for the stretching and bending vibration in water molecules, amounts of water too small to show a noticeable band at about 6.1 $\mu$ will cause an appreciable absorption at 2.8–2.9 $\mu$.

The condensation reaction between adjacent silanol groups on the surface will occur first between closest neighbors which hence are also the most hydrogen-bonded species. Hence, as the temperature is raised, the band decreases asymmetrically in width as association decreases. This is clearly shown in the spectra taken following heat treatments up to 400° (Fig. 3A). Above this temperature both the peak height and the width of the band decrease, the latter in a fashion not explained on the basis of the decrease in peak height. The peak also is displaced from 2.7 to 2.64 $\mu$ as the plate is heated from 500 to 1000° (Fig. 3B). The band disappears completely at above 1000° leaving only the background caused by the fused silica cell. In the case of additional plates which were heated rapidly to consolidation temperatures without thorough degassing the residual peaks observed after consolidation were all at 2.73 $\mu$. The displacement of the peak to higher wave lengths observed in the final consolidated glass probably is due to modification of the stretching vibrations of OH groups by the closer packing of oxygens in the glass structure. It would, of course, have been predicted from the study by Rundle and Parasol[13] of O–H stretching vibrations and bond distances. The 2.73 $\mu$ band also is present in fused quartz[14] and fused silica.[15]

The effect of heating at 800° followed by the admitting of water vapor at $p$ = 4.6 mm. at room temperature is shown in Fig. 4. The peak at 2.67 $\mu$ moves to a higher wave length and eventually becomes lost as water is physically absorbed and complex hydrogen bonding occurs. The diminution in the intensity of the so-called $OH_{free}$ band on adsorption of water reported by Sidorov[16] for porous glass heated at 300, 540, and 650° and reacted with water vapor at $p$ = 16 mm. at room temperature was not observed. Instead it was found that the intensity of the OH peak increased as the sample was exposed to water, as shown in Fig. 4. This increase can be explained by the breaking of oxygen bonds to form silanol groups as per reaction I in Fig. 2.

The effect of prolonged heating of another plate of porous glass, also 0.25 mm. thick, indicated

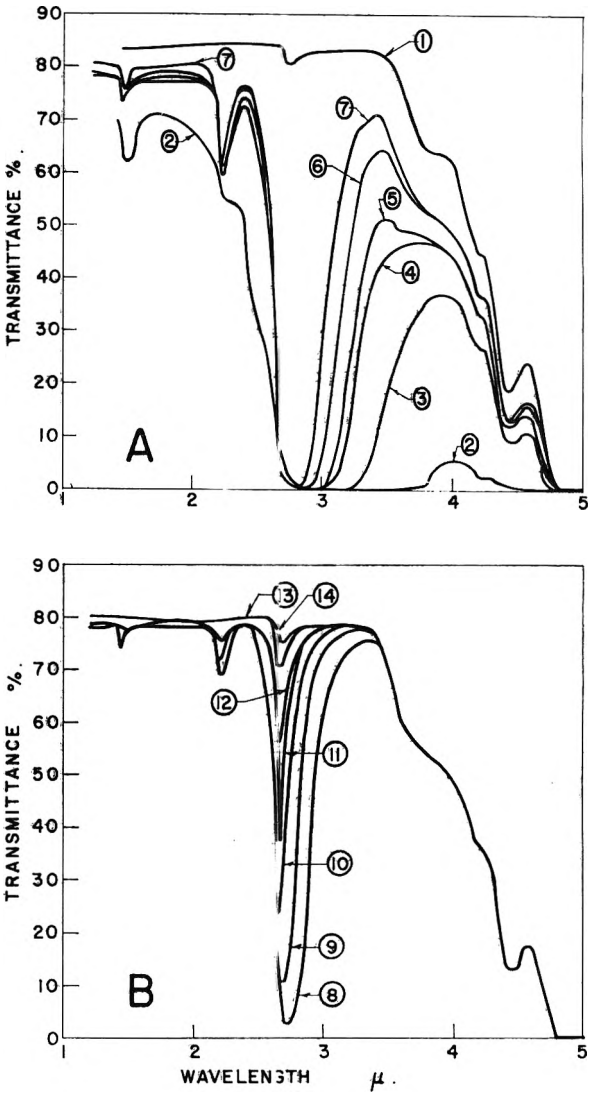


Fig. 3.—Infrared spectra at room temperature of porous glass after successive heating *in vacuo* at temperatures from 25 to 1200°: 1, empty cell; 2, water saturated; 3, 25°; 4, 100°; 5, 200°; 6, 300°; 7, 400°; 8, 500°; 9, 600°; 10, 700°; 11, 800°; 12, 900°; 13, 1000°; 14, 1100 and 1200°.

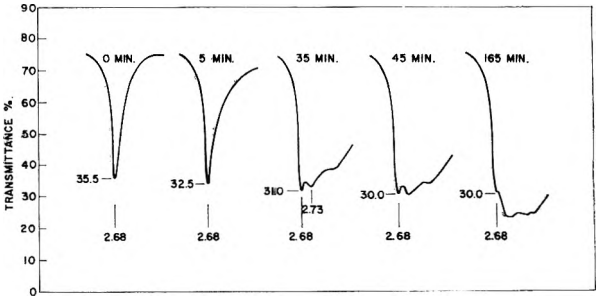


Fig. 4.—Infrared spectra at room temperature between 2.5 and 3 $\mu$ of porous glass heated to 800° and exposed to water vapor at pressure 4.6 mm. for the times indicated.

that there is not a great deal of difference between a 1-, 8-, and 24-hr. bake in the amount of water driven off. This indicates that there is a finite amount of water which can be removed at a given temperature and that a steady state is achieved in less than 1 hr.

(12) J. G. Miller, *J. Phys. Chem.*, **65**, 800 (1961).
(13) R. E. Rundle and M. Parasol, *J. Chem. Phys.*, **20**, 1487 (1952).
(14) R. V. Adams and R. W. Douglas, *J. Soc. Glass Tech.*, **43**, 147 T (1959).
(15) C. J. Parker, Corning Glass Works, private communication.
(16) A. N. Sidorov, *Opt. Spectr.*, **VIII** [6], 424 (1960).

# HIGH-FIELD CONDUCTANCE OF POLYVALENT ELECTROLYTES. I. APPARATUS AND EXPERIMENTAL TECHNIQUES: THE WIEN EFFECT IN SOME 2–2 AND 3–3 ELECTROLYTES

BY GORDON ATKINSON[1] AND MASATOKI YOKOI

*Department of Chemistry, The University of Michigan, Ann Arbor, Michigan*

*Received April 9, 1962*

An apparatus for the measurement of high-field (Wien effect) conductance in electrolyte solutions has been constructed. The apparatus possesses certain advantages of simplicity of construction and operation over ones previously described. To show the utility of the measurement the Wien effects for $CuSO_4$, Cu *m*-benzenedisulfonate, (CuBDS), La $Co(CN)_6$, and La naphthalenetrisulfonate (LaNTS) have been measured in water at 25°. By combining the Onsager first and second Wien effect theories, it is possible to obtain an association constant for these four salts from the Wien effect measurement. These constants are compared with those derived for the same salt from low-field conductance measurement and a tentative explanation of the differences is offered.

Since Wien's early measurements[2] on the effect of high-field gradients on electrolyte conductance, this technique has promised much information to investigators. Interest was intensified by the theoretical contributions of Falkenhagen[3] and Onsager[4] on the strong electrolyte effect (first Wien effect) and of Onsager[5] on the dissociation field effect (second Wien effect). The effect of the increasing field gradient on the total destruction of the time of relaxation drag and partial destruction of the electrophoretic drag seemed to promise increased understanding of these effects in low-field conductance. The dissociation field effect seemed certain to lead to a much better understanding of weak electrolyte behavior.

Unfortunately, the field gradients necessary to produce measureable conductance changes, particularly in strong electrolytes, were so high as to make the measurements incredibly difficult in the 1930's. One can only admire the perseverence of the earlier investigators in the face of such great experimental problems. The few results of this early work are ably summarized by Eckstrom and Schmeltzer.[6]

The great advances in electronic techniques encouraged by World War II revolutionized the approaches to this problem. In particular, the great improvement in pulse generation and measurement techniques engendered by radar research promised to alleviate two of the greatest experimental difficulties: the heating effect of long excitation and the detection of resistance change with short time excitation.

Patterson realized the potentialities of the new techniques and in a fine series of papers[7] beginning in 1952, reopened the field of Wien effect measurements as a worthy tool for solution chemists. At the risk of doing his work an injustice, Patterson's main contributions can be classified as developing a usable precision apparatus[8a] and recognizing that the Onsager theories of the first and second Wien effects could be combined to give a much better explanation of salts like $CuSO_4$.[8b]

Much of Patterson's work on symmetrical electrolytes is summarized in one paper.[9] Recently he has been concerned with more complicated chemical problems such as the $NH_3$–$H_2O$ and $CO_2$–$H_2O$ equilibria and has applied high-field techniques to the investigation of these important problems.[10,11]

Although Patterson investigated the conductance of some associated 2–2 and 3–3 electrolytes using a combined Onsager theory for the first and second Wien effects, the results had some discouraging aspects. For example, the high-field method gave an association constant ($K_A$) of 2850 for $LaFe(CN)_6$ in water[12] as compared to James' value of 5500.[13] Even with $CuSO_4$ the discrepancy between $K_A$'s determined by high-field and low-field techniques was noticeable.[14]

It was difficult at the time to do much more with the data because of the uncertainty in the application of the Debye–Hückel–Onsager solution theories to such high-charge salts. Recently, however, it has been demonstrated that there exist 2–2 salts far less associated than any others previously investigated.[15] In fact, even 3–3 salts much less associated in water than the ferricyanides and cobalticyanides seem possible. The properties of these substances—transition metal salts of *m*-benzenedisulfonic acid, 4,4′-biphenyldisulfonic acid, and 1,3,6-naphthalenetrisulfonic acid—have been investigated in water and, in some cases, mixed solvent systems by low-field conduct-

(1) Department of Chemistry, University of Maryland, College Park, Maryland.

(2) M. Wien, *Ann. Phys.*, **83**, 327 (1927).

(3) H. Falkenhagen, *Physik Z.*, **32**, 353 (1931).

(4) H. S. Harned and B. B. Owen, "The Physical Chemistry of Electrolytic Solutions," 2nd Ed., Reinhold Publ. Corp., New York, N. Y., 1950, p. 95.

(5) L. Onsager, *J. Chem. Phys.*, **2**, 599 (1934).

(6) H. C. Eckstrom and C. Schmeltzer, *Chem. Revs.*, **24**, 367 (1939).

(7) J. A. Gledhill and A. Patterson, Jr., *J. Phys. Chem.*, **56**, 999 (1952).

(8) (a) J. A. Gledhill and A. Patterson, Jr., *Rev. Sci. Instr.*, **20**, 960 (1919); (b) F. E. Bailey, Jr., and A. Patterson, Jr., *J. Am. Chem. Soc.*, **74**, 4428 (1952).

(9) A. Patterson, Jr., *Proc. Natl. Acad. Sci.*, **39**, 146 (1953).

(10) D. Berg and A. Patterson, Jr., *J. Am. Chem. Soc.*, **75**, 5731 (1953).

(11) K. Wissbrun, D. M. French, and A. Patterson, Jr., *J. Phys. Chem.*, **58**, 693 (1954).

(12) D. Berg and A. Patterson, Jr., *J. Am. Chem. Soc.*, **75**, 1484 (1953).

(13) C. W. Davies and J. C. James, *Proc. Roy. Soc.* (London), **A195**, 116 (1948).

(14) D. Berg and A. Patterson, Jr., *J. Am. Chem. Soc.*, **74**, 4704 (1952).

(15) G. Atkinson, M. Yokoi, and C. J. Hallada, *ibid.*, **83**, 1570 (1961).

ance.[15-18] The data were analyzed by means of the new Fuoss–Onsager theory and reasonable values of $\Lambda^0$, $a^0$ were obtained. At the same time some older data on 2–2 and 3–3 salts were reanalyzed using the extended theory and better values of $K_A$ found.

It seemed important then to investigate the high-field conductance of these salts with the following questions in mind.

1. How well does the Onsager high-field theory apply to an essentially unassociated 2–2 salt such as Cu *m*-benzenedisulfonate?

2. For associated 2–2 salts and 3–3 salts, how close together are the association constants from high-field measurements and low-field measurements?

This paper describes the tentative answers to these questions from the examination of two pairs of salts: $CuSO_4$ and CuBDS; $LaCo(CN)_6$ and LaNTS.

## Experimental

**Equipment.**—On examining the apparatus used by Patterson, it seemed possible to make some simplifications. For his high-field pulse generator, Patterson used an MIT Model 9 Radar pulse modulator and power supply weighing almost 2000 pounds. The bulk of this weight is necessary because of the high repetition rate needed in radar operation (in this case up to 2000 p.p.s.) However, high-field conductance normally is carried out as a "single-shot" measurement so that heating effects can be allowed to dissipate between measurement pulses. Therefore a much smaller and simpler high-field pulse generator and power supply were designed using common "soft tube" pulser circuitry.[19] The schematic is given in Fig. 1. The pulser generates 2.5-μsec. pulses from 0.1 to 20 kv. in amplitude. For the measurement bridge, the "relative bridge" of Patterson was adapted as is shown in Fig. 2. Where Patterson used hand-made differential pulse transformers (DPT) for his detecting system, we decided to confine ourselves to commercially available components and have used both the resistive pickoff (A detector) and various types of DPT pick-offs (B detector). Both varieties have their advantages but we have found that the resistive pick-off functions best in the lower voltage range and the DPT best in the higher range. For best results from DPT it is necessary to damp carefully the primaries and secondary windings of all commercial transformers used to date. Otherwise the ringing caused by the shock excitation of the primaries by the HV pulse and saturation of the transformer core makes accurate measurements very tedious. With the "A" detector the differential amplifier of the Model 502 scope functioned very well and no phasing problems were noted. For maximum sensitivity, careful calibration and balancing of the amplifier was necessary. It was found that the pulse transformers used were phased very adequately for DPT operation. Since the 502 is a dual beam scope, one beam normally was used for the bridge detector and the second for applied pulse measurement. Using a type P7 medium-persistence phosphor, balance was easily made by watching successive single shot pulses. When balance was reached, the oscilloscope Land camera was used to record the balance point and HV pulse simultaneously. The applied voltage is measured using a Tektronix Model P6014 HV probe.

**Auxiliary Equipment.**—The conductance cells were flask type cells with very heavy electrode construction. The electrodes were made and assembled as described by Patterson[7] and then sealed into the cell. The electrodes were 2 cm. in diameter and the spacing was maintained at 1.000 ± 0.001 mm. by a surface-ground iron spacer until the cells were made and annealed. The spacers and clamps were

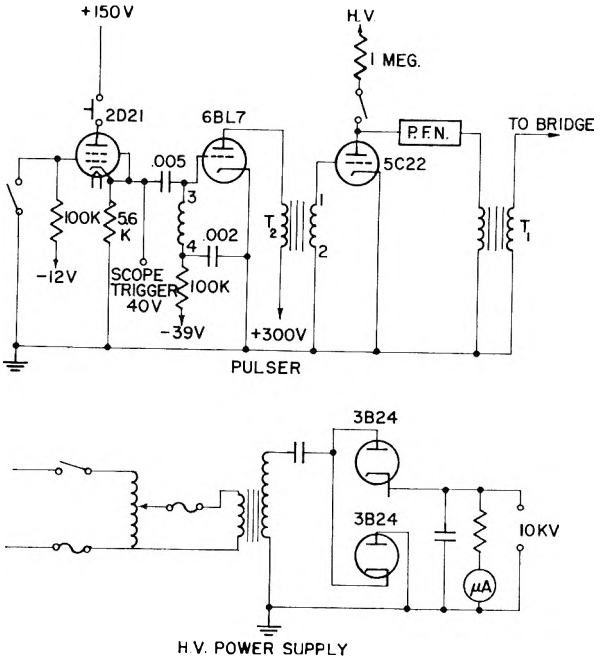


Fig. 1.—Pulse generator circuits. $T_1$, pulse transformer WE D-164661; $T_2$, blocking oscillator transformer Rad Lab 176 Aw 2F; PFN, pulse forming network, Sprague 10E4-2.2-375-20P.

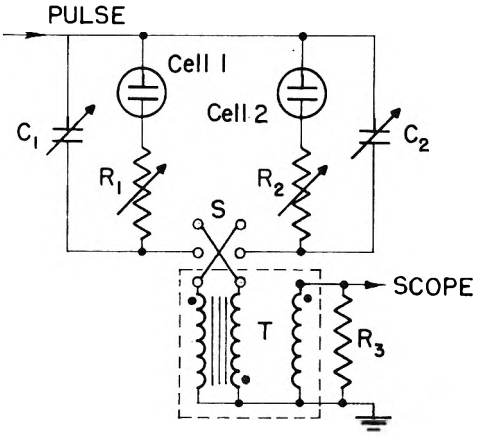


Fig. 2.—"Relative" Wien effect bridge. $C_1$, $C_2$, Jennings Model ATC vacuum variable capacitors (15–74 mmf., 30 kv.); $R_1$, $R_2$, General Radio Model 670F resistance boxes (0–111 Ω in 0.1 Ω steps); S, Leeds and Northrup DPDT knife switch; T, Raytheon UX-7307 pulse transformer. When resistive pick-off used, matched GR Model 500 resistors were placed in series with $R_1$ and $R_2$ and a signal taken from each to opposing sides of the scope differential amplifier. $R_3$, variable damping resistor for transformer secondary; Scope, Tektronix Model 502 dual-beam, high-sensitivity oscilloscope with Mod 104 and P7 phosphor.

then dissolved with $HNO_3$ and the cells exhaustively steam cleaned. Even with the utmost precautions in manufacture, the final pairs of cells do not have exactly the same cell constant but will differ by as much as 3%. Each cell constant therefore is evaluated independently using both a Jones Bridge and the low-field pulse generator bridge. It also was found that there is an apparent small but reproducible change of cell constant with applied pulse voltage. This may be calibrated using the Onsager first Wien effect theory for KCl solutions.

The constant temperature bath is a 50-gallon fish tank containing 45 gallons of Wemco C transformer oil kept dry with silica gel. The temperature is maintained at 25 ± ± 0.01° with a very conventional mercury thermoregulator–electronic relay arrangement. The bath fluid is circulated at a high rate of speed by an external centrifugal pump

(16) C. J. Hallada and G. Atkinson, *J. Am Chem., Soc.*, **83**, 3759 (1961).

(17) M. Yokoi and G. Atkinson, *ibid.*, **83**, 4367 (1961).

(18) G. Atkinson and C. J. Hallada, *ibid.*, **84**, 721 (1962).

(19) G. N. Glasoe and J. V. Lebacqz, "Pulse Generators," McGraw-Hill Book Co., New York, N. Y., 1948.

(Gorman-Rupp Model 2812). The cells are clamped into bakelite clamps and fit into a bakelite platform holding two magnetic stirrers driven by a single motor through a gear drive. Stirring the solutions at a high rate of speed made no measureable difference in the resistance but greatly decreased the temperature effect of the HV pulsing. At the very highest applied voltage (20 kv.) 30 sec., at most, was required for the resistance of the solution to return to its prepulse value. The resistance of the individual cells can be varied between 500 and 2500 ohms without adversely affecting the pulse shape. However, the lowest resistance that the maximum output voltage can be applied to is approximately 1000 ohms.

As is shown in the Appendix, the use of a standard solution in one arm of the bridge and the unknown in the other does not give a real "relative" measurement. This procedure, however, does decrease spurious readings due to polarization and heating effects. Morever, it makes it possible to use HV capacitors of reasonable size (and cost) in the bridge.

**Measurement Procedures.**—The cells are thoroughly cleaned, dried, and weighed. Solvent water is then run into them from a double column of mixed bed ion-exchange resin[20a] through a Millipore filter.[20b] The operation is carried out under nitrogen. The water used has a specific conductance $\leq 0.2 \times 10^{-6}$ ohm$^{-1}$. The cells are capped and placed in the constant temperature bath until temperature equilibrium is reached. Then the solvent resistance is measured for each cell, substituting a calibrated decade box for the other cell in the bridge circuit, and putting 30,000 ohms in parallel with the cell being measured. A concentrated stock solution of KCl then is added dropwise to the "standard" cell until the cell resistance desired is reached, as measured against the substituted decade. This then is repeated with the "unknown" cell using the stock unknown solution until the resistance of this cell approximately equals that of the unknown. These additions are made by weight and the molalities of the measured solutions converted to molarities using pycnometrically measured densities.

The high-field pulser then is turned on and pulses are applied to the bridge. At a given pulse voltage the bridge is balanced by the addition of $R$ to the "standard" side and simultaneous balancing of capacitance change. It is easy to distinguish $R$ imbalance from $C$ imbalance. Both types of detectors function in the way described by Patterson[7] in this respect. Two readings of $\Delta R$ are made at each voltage using the reversing switch. This serves to average out the small difference between the pick-off resistors or primary transformer windings. When the balance is reached a photograph is taken. It usually is possible to divide the smallest unit on the decade box (0.1 ohm) further by taking photographs on either side of the balance point and interpolating. By suitable manipulation of the sensitivity control of the oscilloscope and careful calibration of the scope amplifier and HV probe, it is possible to measure the pulse amplitude to 0.5% or better. The final data then are a set of [$\Delta R$ (av.), $X$(appl.)].

At the end of each set of measurements (after the maximum voltage has been reached) the low-field resistance of each solution is remeasured. If it has changed more than 0.1% from its initial low-field value, the run is repeated with more frequent rechecking of the low-field resistance. At least two different concentrations of each salt were measured and at least two runs were made at each concentration of each salt.

The preparation and analysis of CuBDS and LaNTS were described previously, together with their low-field conductance.[15] The preparation, purification, and analysis of $CuSO_4$ and $LaCo(CN)_6$ have been described, as have their conductances.[21,22]

**Calculation of Results.**—The ($\Delta R$, $X$) data obtained in a measurement are converted to ($\Delta\Lambda/\Lambda(0)$, $X$) data in the manner described in the appendix. In this case we mean $\Delta\Lambda/\Lambda(0)$ to mean the "absolute" change of equivalent conductance.

$$\frac{\Delta\Lambda}{\Lambda(0)} = \frac{\Lambda(X) - \Lambda(0)}{\Lambda(0)}$$

where

$\Lambda(X)$ = equivalent conductance of "unknown" solution at field $X$

$\Lambda(0)$ = equivalent conductance of "unknown" solution at zero field (*i.e.*, low field).

The data for the four salts measured for two concentrations of each salt are given in Table I.

It is now of interest to compare these values with those predicted by the Onsager theories. One difficulty that troubles us in this comparison is the inconsistency between the high-field and low-field theories. That is, in its most recent form, the low-field theory for an unassociated electrolyte can be written[23]

$$\Lambda = \Lambda^0 - SC^{1/2} + EC \log C + JC \quad (2)$$

where

$\Lambda$ = low-field equivalent conductance at molar concn. $C$

$\Lambda^0$ = equivalent conductance at infinite dilution

$S$ = limiting low slope = $\alpha^*\Lambda^0 + \beta^*$

$E$ = $E_1\Lambda^0 - E_2$

$J$ = $\sigma_1\Lambda^0 + \sigma_2$ = function of $a_J$, the mean distance of closest approach

It has been conclusively demonstrated[15] that the extended terms ($EC$ log $C$ and $JC$) are absolutely necessary for a rational explanation of the behavior of 2–2 and 3–3 electrolyte. Unfortunately, the latest form of the Onsager high-field theory for unassociated symmetrical electrolytes[24] is in the form

$$\Lambda(X) = \Lambda^0 - S_X C^{1/2} \quad (3)$$

$\Lambda(X)$ = equivalent conductance at field $X$ and molar concn. $C$

$$S_X = \frac{\alpha^* 3g(x)}{2 - \sqrt{2}}\Lambda^0 + \frac{\beta^*}{\sqrt{2}}f(x)$$

where $f(x)$ and $g(x)$ are tabulated in ref. 4, p. 153. That is, only the $C^{1/2}$ term has been corrected for the effect of field and the corrections to the $E$ and $J$ terms are unknown.

A second plaguing problem concerns the need for activity coefficients when the effect of the high field on association is considered. We can assume the Debye–Hückel theory to hold at zero field but at high-field gradients with their distortion of the ion atmosphere, what can be assumed? One can say, first of all, that the very term activity coefficient is non-applicable to this non-equilibrium thermodynamic problem and should be discarded. "Screening coefficient" has been suggested as a useful replacement.[25] In the second place, we probably can believe that as the field, $X$, increases, the ion-atmosphere effect should be gradually destroyed and at very high fields the screening coefficients will approach one. This tells us that if we must make calculations using a concentration equilibrium constant, let us do it at the highest field obtainable.

With these reservations carefully in mind, let us examine the actual techniques used for the theoretical calculations.

**Case I. Unassociated Electrolytes.**—The simplest calculation would be

(20) (a) Barnstead Bantam Model 0808, Barnstead Still and Sterilizer Co., Boston 31, Mass.

(20) (b) Millipore Filter HAWPO 470C, Millipore Filter Corp., Bedford, Mass.

(21) B. B. Owen and R. W. Gurry, *J. Am. Chem. Soc.*, **60**, 3074 (1938).

(22) G. Atkinson, *ibid.*, **82**, 818 (1960).

(23) *E.g.*, R. M. Fuoss and F. Accascina, "Electrolytic Conductance," Academic Press, New York, N. Y., 1960, to which the reader is referred for a further explanation of the symbols.

(24) L. Onsager and S. K. Kim, *J. Phys. Chem.*, **61**, 198 (1956).

(25) Andrew Patterson, Jr., private communication.

TABLE I

EXPERIMENTAL DATA

PART A, 2–2 SALTS

CuBDS

$C = 1.6505 \times 10^{-4}$, $R(0) = 1654.7$ ohms; $C = 1.3691 \times 10^{-4}$, $R(0) = 1169.4$ ohms

| kv./cm. | $\%\left(\frac{\Delta\Lambda}{\Lambda(0)}\right)_{exp}$ | $\%\left(\frac{\Delta\Lambda}{\Lambda(0)}\right)_{calcd}$ $K_A = 62$ | kv./cm. | $\%\left(\frac{\Delta\Lambda}{\Lambda(0)}\right)_{exp}$ | $\%\left(\frac{\Delta\Lambda}{\Lambda(0)}\right)_{calcd}$ $K_A = 57$ |
|---|---|---|---|---|---|
| 13.0 | 0.385 | ... | 10.5 | 0.268 | ... |
| 29.0 | 1.147 | ... | 24.0 | 0.973 | ... |
| 44.0 | 1.693 | 1.755 | 37.0 | 1.555 | 1.600 |
| 60.0 | 2.099 | 2.144 | 47.0 | 2.002 | 1.994 |
| 76.0 | 2.347 | 2.426 | 59.0 | 2.316 | 2.352 |
| 90.0 | 2.596 | 2.616 | 72.0 | 2.623 | 2.657 |
| 102.0 | 2.777 | 2.749 | 84.0 | 2.877 | 2.888 |
| 116.0 | 2.885 | 2.879 | 93.0 | 3.060 | 3.038 |
| 128.0 | 2.995 | 2.973 | 104.0 | 3.188 | 3.194 |
| 141.0 | 3.074 | 3.064 | 116.0 | 3.389 | 3.341 |
| | $\bar{\delta} = 0.034$ | | | $\bar{\delta} = 0.026$ | |

$CuSO_4$

$C = 1.3525 \times 10^{-4}$, $R_0 = 1743.9$ ohms; $C = 1.9230 \times 10^{-4}$, $R_0 = 1251.7$ ohms

| kv./cm. | $\%\left(\frac{\Delta\Lambda}{\Lambda(0)}\right)_{exp}$ | $\%\left(\frac{\Delta\Lambda}{\Lambda(0)}\right)_{calcd}$ $K_A = 210$ | kv./cm. | $\%\left(\frac{\Delta\Lambda}{\Lambda(0)}\right)_{exp}$ | $\%\left(\frac{\Delta\Lambda}{\Lambda(0)}\right)_{calcd}$ $K_A = 210$ |
|---|---|---|---|---|---|
| 14 | 0.461 | ... | 10.5 | 0.330 | ... |
| 30 | 1.313 | 1.377 | 24 | 1.140 | ... |
| 46 | 1.948 | 2.032 | 37 | 1.852 | 1.815 |
| 61 | 2.450 | 2.485 | 50 | 2.449 | 2.436 |
| 79 | 2.792 | 2.882 | 65 | 2.898 | 2.983 |
| 91.5 | 3.086 | 3.108 | 78.5 | 3.309 | 3.380 |
| 105 | 3.290 | 3.312 | 88.5 | 3.584 | 3.625 |
| 118 | 3.463 | 3.484 | 99 | 3.817 | 3.859 |
| 130 | 3.662 | 3.617 | 109 | 4.069 | 4.057 |
| 142 | 3.792 | 3.730 | 120 | 4.288 | 4.246 |
| | $\bar{\delta} = 0.049$ | | | $\bar{\delta} = 0.044$ | |

PART B, 3–3 SALTS

$LaCo(CN)_6$

$C = 0.8180 \times 10^{-4}$, $R_0 = 1863.6$ ohms; $C = 1.1914 \times 10^{-4}$, $R_0 = 1345.0$ ohms

| kv./cm. | $\%\left(\frac{\Delta\Lambda}{\Lambda(0)}\right)_{exp}$ | $\%\left(\frac{\Delta\Lambda}{\Lambda(0)}\right)_{calcd}$ $K_A = 4500$ | kv./cm. | $\%\left(\frac{\Delta\Lambda}{\Lambda(0)}\right)_{exp}$ | $\%\left(\frac{\Delta\Lambda}{\Lambda(0)}\right)_{calcd}$ $K_A = 4800$ |
|---|---|---|---|---|---|
| 14.5 | 4.85 | ... | 11.0 | 1.35 | ... |
| 30.0 | 9.70 | 9.56 | 24.0 | 8.35 | ... |
| 43.0 | 13.61 | 13.72 | 36.0 | 12.44 | 12.29 |
| 60.0 | 17.14 | 17.57 | 47.0 | 16.39 | 16.35 |
| 74.0 | 19.30 | 19.74 | 60.0 | 19.56 | 19.92 |
| 89.0 | 21.05 | 21.47 | 70.0 | 22.01 | 22.08 |
| 100.5 | 22.27 | 22.45 | 81.0 | 23.73 | 23.99 |
| 110.0 | 23.26 | 23.11 | 90.0 | 25.09 | 25.26 |
| 122.0 | 24.07 | 23.79 | 99.0 | 26.29 | 26.31 |
| 138.0 | 24.72 | 24.47 | 111.0 | 27.59 | 27.47 |
| | $\bar{\delta} = 0.27$ | | | $\bar{\delta} = 0.15$ | |

LaNTS

$C = 1.0211 \times 10^{-4}$, $R_0 = 1759.5$ ohms; $C = 1.668 \times 10^{-4}$, $R_0 = 1170.4$ ohms

| kv./cm. | $\%\left(\frac{\Delta\Lambda}{\Lambda(0)}\right)_{exp}$ | $\%\left(\frac{\Delta\Lambda}{\Lambda(0)}\right)_{calcd}$ $K_A = 2850$ | kv./cm. | $\%\left(\frac{\Delta\Lambda}{\Lambda(0)}\right)_{exp}$ | $\%\left(\frac{\Delta\Lambda}{\Lambda(0)}\right)_{calcd}$ $K_A = 2450$ |
|---|---|---|---|---|---|
| 14.0 | 3.11 | ... | 11.0 | 2.11 | ... |
| 28.0 | 7.86 | ... | 22.0 | 6.02 | ... |
| 44.0 | 11.78 | 11.68 | 33.5 | 10.16 | 9.09 |
| 58.5 | 14.33 | 14.44 | 45.0 | 13.44 | 12.89 |
| 72.0 | 15.88 | 16.28 | 55.0 | 15.73 | 15.49 |
| 84.0 | 17.40 | 17.50 | 67.0 | 18.03 | 17.90 |
| 96.0 | 18.29 | 18.40 | 77.0 | 19.46 | 19.53 |
| 109.0 | 19.20 | 19.15 | 83.0 | 20.39 | 20.32 |
| 117.0 | 19.71 | 19.54 | 94.0 | 21.50 | 21.56 |
| 129.0 | 20.17 | 20.02 | 104.0 | 22.49 | 22.49 |
| | $\bar{\delta} = 0.14$ | | | $\bar{\delta} = 0.27$ | |

$$1.\quad \left[\frac{\Delta\Lambda}{\Lambda(0)}\right]_1 = \frac{[\Lambda^0 - S_x C^{1/2}] - [\Lambda^0 - (\alpha^*\Lambda^0 + \beta^*)C^{1/2}]}{\Lambda^0 - [\alpha^*\Lambda^0 + \beta^*]C^{1/2}} \qquad (4)$$

If we use $\Lambda(0)$ (measured) for the right hand numerator term and the denominator we are, in effect, using

$$2.\quad \left[\frac{\Delta\Lambda}{\Lambda(0)}\right]_2 = \frac{[\Lambda^0 - S_{(x)}C^{1/2}] - [\Lambda^0 - SC^{1/2} + EC\log C + JC]}{\Lambda^0 - SC^{1/2} + EC\log C + JC} \qquad (5)$$

At the "crossover point" (see ref. 15) where

$$EC\log C + JC = 0$$

then

$$\left[\frac{\Delta\Lambda}{\Lambda(0)}\right]_1 = \left[\frac{\Delta\Lambda}{\Lambda(0)}\right]_2 \qquad (6)$$

Further discussions of the unassociated case seems superfluous since none of the experimental results discussed here can be described well by this case.

**Case II. Associated Electrolytes.**—For the theoretical calculation of $\Delta\Lambda/\Lambda(0)$ for an associated electrolyte using an assumed $K_A(0)$ we must calculate $\Lambda(0)$ rather than use the measured value which is not, in general, compatible with the assumed $K_A(0)$. If we merely desire to calculate a theoretical curve using a $K_A(0)$ derived from low-field measurements, we can use $\Lambda(0)$ measured. However, the $K_A(0)$ must have been calculated by the extended theory for full thermodynamic significance. The mode of calculation becomes increasingly more important as we move away from 1–1 salts and the $C\log C$ and $C$ terms become important. We have adapted a form of calculation which is not completely consistent but which minimizes our lack of knowledge of the extended terms in the high-field equations. The calculation has been programmed for the IBM 704 computer and all calculations are done in this fashion.

Assuming a $K_A(0)$ and using $\Lambda^0$ and $a_J$ from the low-field data treatment, we calculate $\Lambda(0)$ in the following way.

$$\ln f_\pm(0) = \frac{-\kappa e^2}{2DkT(1 + \kappa a_J)} =$$

Debye activity coefficient (7)

$\gamma(0)$ = degree of dissociation

$$= \{-1.0 + [1.0 + 4.0\ K_A(0)\ Cf_\pm^2(0)]^{1/2}\}/[2.0K_A(0)\ Cf_\pm^2(0)] \quad (8)$$

$f_\pm$ and $\gamma(0)$ are calculated successively by the machine until they are consistent. Then

$$\Lambda(0) = [\Lambda^0 - SC_i^{1/2} + EC_i \log C_i + JC_i]/[1 + K_A(0)f_\pm^2 C_i] \quad (9)$$

This gives us the calculated conductance at zero field using the assumed $K_A(0)$. We then calculate

$$b = [9.6885Z^3 \times 10^3 \times X]/[DkT] \quad (10)$$

where $X$ is the field gradient in kv./cm., and $F(b)$ where

$$F(b) = 1.0 + \frac{b^2}{3} + \frac{b^3}{18} + \frac{b^4}{180} + \text{-------} \quad (11)$$

or

$$F(b) = \left(\frac{2}{\pi}\right)^{1/2} (8b)^{-3/4} \exp(8b)^{1/2} \left\{1 - \frac{3}{8(8b)^{1/2}} - \frac{15}{128(8b)} \text{---}\right\} \quad (12)$$

where (12) is used when $b > 0.32$. Now

$$K_A(X) = \frac{K_A(0)}{F(b)} \quad (13)$$

so that $\alpha(X)$ can be calculated from the calculated $K_A(X)$. Here we have generally assumed rather arbitrarily that $f_\pm = 1.0$ at $X > 20$ kv./cm. and have empirically calculated $f_\pm$ below this value.

Then

$$\kappa(X) = Z\left(\frac{4\pi e^2 Nz}{1000\ DkT}\right)^{1/2} (\gamma C)^{1/2} \quad (14)$$

$$f(x) = \text{from Wilson's table} \quad (15)$$

$$g(x) = \text{from Wilson's table} \quad (16)$$

Finally

$$\Lambda(X) = \left\{\Lambda^0 - \left[\left(\frac{3\alpha\Lambda^0 g(x)}{2 - \sqrt{2}}\right) + \frac{\beta}{2} f(x)\right] C_i^{1/2} + EC_i \log C_i + JC_i\right\} \Big/ [1 + K_A(x) f_\pm^2 C_i] \quad (17)$$

and our desired $\Delta\Lambda/\Lambda(0)$ can be calculated. As can be seen in eq. 17, we have arbitrarily added $EC_i \log C_i + JC_i$ term to the limiting high-field equation in the hope of partially correcting for these extended terms. It is obviously impossible to justify this on completely theoretical grounds. We can only claim a more realistic comparison and better data fitting.

## Discussion of Results

Table I gives data for two determinations on each of the four salts measured. The $\Delta\Lambda/\Lambda(0)$ values reported are "absolute" values calculated in the way described in the appendix. Figures 3 through 6 show the plots of $\Delta\Lambda/\Lambda(0)$ *vs.* field gradient from these data. At least three other runs were made on each salt at different concentrations. The results are so similar to these reported here that inclusion seemed unnecessary.

Theoretical curves calculated for two assumed $K_A$'s by the method discussed above as case II are given on each plot. To obtain a more accurate idea of $K_A$, eight or ten such calculations were made for each concentration and an interpolation was made for the "best" $K_A$ to fit the highest field gradient points.

Table II lists the $K_A$'s found in this fashion as well as the $\Lambda^0$ and $a_J$ used in the theoretical calculation. It also lists the $K_A$ from the low field conductance data for the same salt. All of the low-field data were recalculated using the Fuoss–Onsager extended conductance equation. For a more complete discussion of the low-field fitting, the previous papers should be consulted (ref. 15–18).

TABLE II

HIGH FIELD PARAMETERS

| Salt | Concn. (mole/l.) × 10⁴ | $\Lambda^0$ LF[d] | $a_J$(Å.) LF[d] | $K_A$ LF[d] | $K_A$ HF[d] |
|---|---|---|---|---|---|
| CuBDS[a] | 1.6505 | 114.47 | 4.95 | 0.0 | 62 |
| | 2.3691 | | | | 57 |
| $CuSO_4$[b] | 1.3525 | 133.95 | 5.37 | 191 | 210 |
| | 1.9230 | | | | 210 |
| LaNTS[a] | 1.0211 | 137.6 | 9.24 | 2765 | 2850 |
| | 1.6686 | | | | 2450 |
| $LaCo(CN)_6$[c] | 0.8180 | 163.6 | 11.70 | 4667 | 4500 |
| | 1.1914 | | | | 4800 |

[a] LF data recalculated from ref. 15. [b] LF data recalculated from ref. 21. [c] LF data recalculated from ref. 22. [d] LF = parameters derived from low-field conductance data by use of Fuoss–Onsager equation. HF = parameter derived from high-field conductance data.

The agreement between the low-field $K_A$ for the two 3–3 salts is very good. However, the $K_A$'s obtained for $CuSO_4$ are somewhat different. Finally, while the low-field work shows CuBDS to have essentially no association, the high-field work gives a sizeable $K_A$. This pattern has been repeated in further work to be published later. In general, the larger the $K_A$ the better the agreement between the two techniques. It does not seem possible to attribute this to a consistent experimental error since concentrations, method of detection, and even cells were changed. Furthermore, in the case where earlier data were available ($CuSO_4$) the two sets are in good agreement. An attempt to rationalize the problem by doubting the correctness of the Debye–Hückel activity coefficients used did not lead in the right direction. In addition, the variation of $K_A$ with concentration for a given salt was small enough as to seemingly absolve gross calculational blunders.

The most logical explanation seems to be more basic. Our feeling is that the dissociation field effect theory is a much better description for such high charge salts than is the first Wien effect theory. In a case where most of the conductance change is due to dissociation (*i.e.*, $K_A$ large), theory and experiment agree well. When $K_A$ becomes smaller and we become more dependent on the first Wien effect theory in its limiting law form, agreement is much worse. It seems reasonable that since the extended terms are absolutely necessary for an

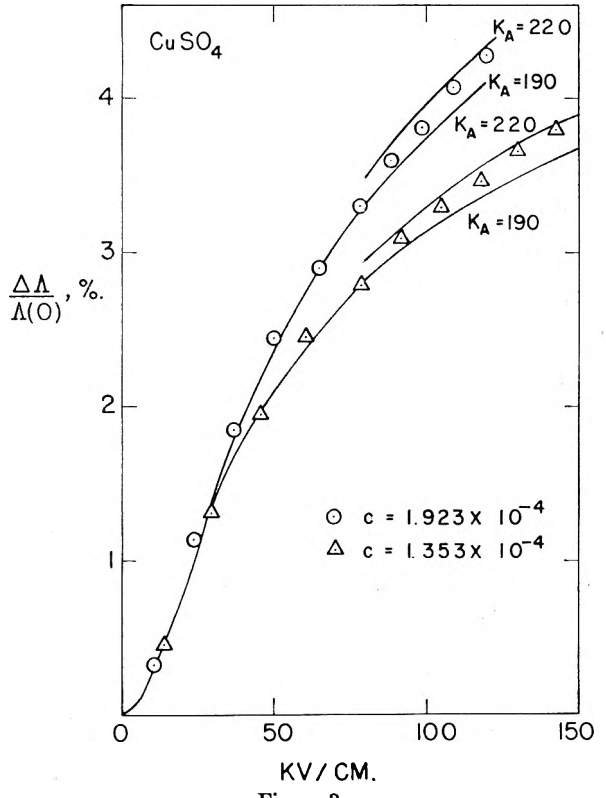

Figure 3

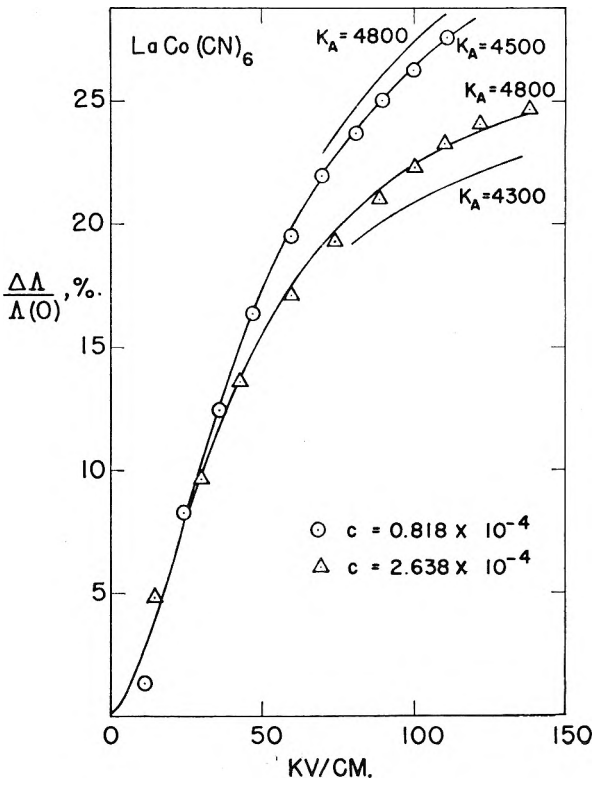

Figure 5

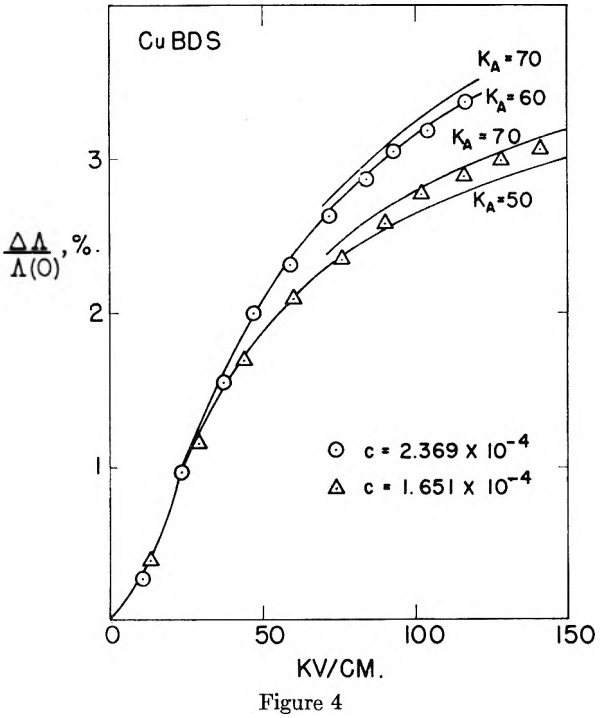

Figure 4

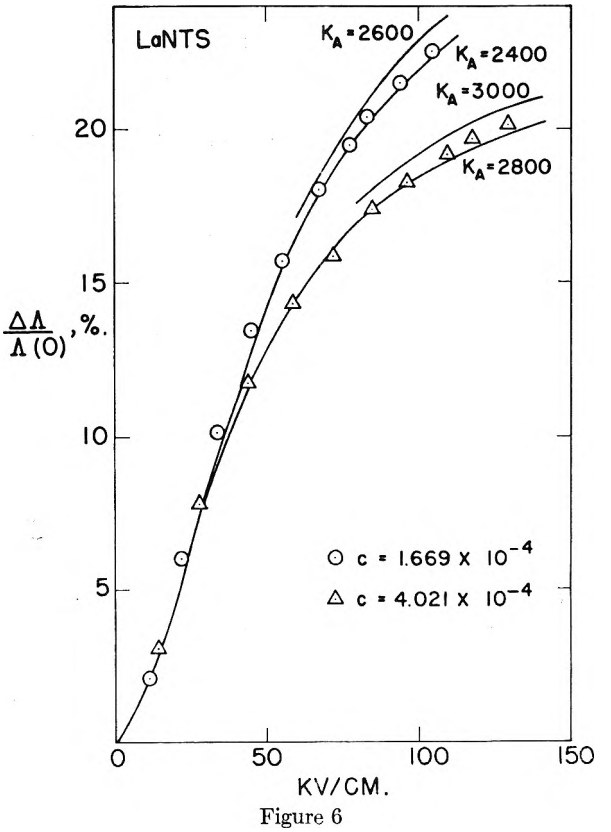

Figure 6

understanding of the low-field conductance of 2–2 and 3–3 salts, they are also necessary in the high-field case. This is a very simple critique and ignores the important problem of the screening coefficient. And, unfortunately, it is an explanation that is uncheckable at present since an extended first Wien effect theory is unavailable.

In conclusion, then, we have established the utility of high-field conductance in the measurement of large $K_A$'s. Its utility with respect to small $K_A$'s is, at present, dubious. We have extended the work to some high-charge salts in mixed solvents and have partially verified these prejudices. Preliminary results on some 1–1 salts in low di-

electric constant solvent mixtures indicate that the screening coefficient problem can become acute.

**Acknowledgment.**—The authors would like to acknowledge the support of the National Science Foundation (G 9974) and the Rackham School of Graduate Studies in this research. They express their appreciation of the aid given them by Ronald Keyes in the computer work and C. J. Hallada in the experimental work.

## Appendix

### "Relative" High-Field Conductance

Define the "relative" high-field conductance change by

$$\left(\frac{\Delta\Lambda}{\Lambda(0)}\right)_{\text{unkown}} - \left(\frac{\Delta\Lambda}{\Lambda(0)}\right)_{\text{ref}} = \left[\frac{\Delta\Lambda}{\Lambda(0)}\right]_{\text{rel}}$$

and denote the reference by primed quantities.

$$\left[\frac{\Delta\Lambda}{\Lambda(0)}\right]_{\text{rel}} = \left[\frac{L^*(X) - L^*(0)}{L^*(0)}\right] - \left[\frac{L'^*(X) - L'^*(0)}{L'^*(0)}\right]$$

where $L^* = L$ measured $- L$ solvent

$$= \frac{L^*(X)}{L^*(0)} - \frac{L'^*(X)}{L'^*(0)}$$

$$= \left[\frac{L(X) - L_s(X)}{L(0) - L_s(0)}\right] - \left[\frac{L'(X) - L_s(X)}{L'(0) - L_s(0)}\right]$$

assuming the solvent to be the same in both cells. Then

$$\left[\frac{\Delta\Lambda}{\Lambda(0)}\right]_{\text{rel}} = \left[\frac{L(X)}{L(0) - L_s(0)} - \frac{L'(X)}{L'(0) - L_s(0)}\right] - \left[\frac{L_s(X)}{L(0) - L_s(0)} - \frac{L_s(X)}{L'(0) - L_s(0)}\right]$$

and if $L'(0) \approx L(0)$ the second term cancels. If we also assume that

$$L_s(0) \ll L(0) \approx L'(0)$$

then

$$\left[\frac{\Delta\Lambda}{\Lambda(0)}\right]_{\text{rel}} = \frac{L(X)}{L(0)} - \frac{L'(X)}{L'(0)} = \frac{R(0)}{R(X)} - \frac{R'(0)}{R'(X)} = \left(\frac{R(0) - R(X)}{R(X)}\right) - \left(\frac{R'(0) - R'(X)}{R'(X)}\right)$$

This first term looks the same as the one used in ref. 7–9. It is not, since we do not know $R(X)$. All we know is $R(X) - R'(X)$. Only if we assume $R'(X) = R'(0)$ do we obtain the simpler formula previously used.

Now let $\Delta R = R'(X) - R(X)$ where $\Delta R$ is simply the resistance that must be added in series with the unknown cell to obtain balance at a given field, $X$. This is our experimental information. In practice we know $R(0)$ and $R'(0)$, and measure $\Delta R$. We also know $L$ solvent and the cell constants. By using the Onsager theory for the Wien effect in KCl, we can then calculate $\Delta\Lambda/\Lambda(0)$ for the unknown by a tedious but straight forward procedure. This was programmed for the IBM 704 computer.

---

# THE $\gamma$-RAY RADIOLYSIS OF METHYL SUBSTITUTED BORAZOLES[1]

BY CLARENCE J. WOLF AND RICHARD H. TOENISKOETTER

*Parma Research Laboratory, Union Carbide Corporation, Parma 30, Ohio*

*Received April 11, 1962*

The 100 e.v. yields of hydrogen, methane, and ethane from the cobalt-60 $\gamma$-ray radiolysis of N-trimethyl-, B-trimethyl-, and hexamethylborazole are independent of dose and dose rate. At 30°, the hydrogen, methane, and ethane yields are, respectively, 3.53, 0.015, and <0.01 for N-trimethylborazole; 1.65, 1.38, and 0.08 for B-trimethylborazole; and 0.45, 0.83, and 0.28 for hexamethylborazole. Hydrogen is the predominant product at −196 and −78°. Between −6 and 100° the methane yields from irradiated hexamethyl- and B-trimethylborazole change more with temperature than the corresponding hydrogen and ethane yields. Above 100°, however, the methane yields vary only slightly with temperature. The methane yield from N-trimethylborazole is low regardless of irradiation temperature.

Methyl-substituted borazoles provide a suitable system of compounds in which the relative effects of radiation on the B–C, N–C, C–H, B–H, and N–H bonds may be studied. The present paper describes the effects of dose, dose rate, and temperature on the gas yields from the cobalt-60 $\gamma$-ray irradiations of N-trimethyl-, B-trimethyl-, and hexamethylborazole.

(1) Presented in part before the Division of Physical Chemistry at the 139th National Meeting of the American Chemical Society, March, 1961, St. Louis, Missouri.

## Experimental

The borazoles were obtained by reduction or methylation of the corresponding trichloro derivatives. B-Trichloroborazole was obtained from the U.S. Borax Research Corporation. B-Trichloro-N-trimethylborazole was prepared by passing boron trichloride into a mixture of methylamine hydrochloride and boiling chlorobenzene.[2]

Treatment of B-trichloro-N-trimethylborazole with methylmagnesium bromide in diethyl ether[3] yielded hexa-

(2) C. A. Brown and A. W. Laubengayer, *J. Am. Chem. Soc.*, **77**, 3699 (1955).

methylborazole. This material was purified by repeated vacuum sublimation; m.p. 98–99°. B-Trimethylborazole was obtained in a similar manner from methylmagnesium bromide and B-trichloroborazole.[4] Its melting point after fractional distillation was 31–32°. Reduction of B-trichloro-N-trimethylborazole with lithium aluminum hydride in tetraethylene glycol dimethyl ether gave N-trimethylborazole in yield of 95%. The product was recovered from the reaction mixture by vacuum fractional distillation, b.p. 39–42° at 18 mm. It was redistilled at 745 mm. and the fraction boiling in the range 129–131° was collected. This compound melted between −2 and −1°.[5] B-Trimethyl- and N-trimethylborazole were further purified by trap-to-trap distillation in the vacuum line prior to use. Vapor pressure measurements indicated high states of purity for these compounds. The constancy of gas yields with varying dose and the reproducibility of results using different dose rates also gave assurance of minimal impurity levels in the samples.

Samples for irradiation were prepared in lots of eight. Pyrex sample tubes, 10 × 100 mm., were outgassed under high vacuum (usually overnight at pressures less than $10^{-5}$ mm.), cooled to −196°, and samples were introduced by sublimation or distillation. The tubes were sealed off at pressures less than $10^{-4}$ mm.

The samples, weighing between 0.5 and 1.2 g., were irradiated at the desired temperature in a 3200 curie cobalt-60 γ-ray source. The dose rate in the center of the source was $1.2 \times 10^{20}$ e.v./g.-hr. measured by means of a ferrous sulfate dosimeter assuming a ferric yield of 15.6.[6] All doses were corrected for the decay of the cobalt-60 source and for the difference between the electron density of the sample compared with that of the dosimeter.

The temperatures of samples irradiated above 30° (ambient source temperature) were controlled to about ±2°. The temperatures at −196, −78, −6, 0, and +6° were controlled by liquid nitrogen, solid carbon dioxide, melting aniline, melting ice, and melting benzene, respectively.

The irradiated samples were warmed or cooled to room temperature, opened in the vacuum system and, with the aid of a Toepler pump, the product gases were passed through a Dry Ice trap into a calibrated gas buret. Hydrogen, methane, and ethane were determined in a Beckman gas chromatograph employing an argon sweep and a temperature programmed column packed with Linde 5A Molecular Sieve.

## Results

**N-Trimethylborazole.**—The yield of hydrogen from liquid N-trimethylborazole at 30° is a linear function of dose to $1 \times 10^{21}$ e.v./g. and is independent of dose rate between $5 \times 10^{18}$ and $1 \times 10^{20}$ e.v./g.-hr. $G(H_2)$ was 3.53 molecules per 100 e.v., with a maximum deviation near 2%. At a dose of $3 \times 10^{21}$ e.v./g., the yield fell off to 3.4 molecules/100 e.v.

Within experimental error, the yields of methane and ethane are essentially independent of dose and dose rate: $G(CH_4) = 0.01$ and $G(C_2H_6) < 0.01$.

The temperature dependence of the hydrogen yield from irradiated N-trimethylborazole is shown in Fig. 1. All samples were irradiated to a total dose of $6 \times 10^{20}$ e.v./g. at a dose rate of $1.2 \times 10^{20}$ e.v./g.-hr. At −196°, $G(H_2) = 0.6$. Between −78 and 30°, $G(H_2)$ increases from 0.6 to 3.5 and appears to be practically independent of the irradiated phase (m.p. −1°). Above 30° the hydrogen yield increases more slowly to about 4.5 molecules per 100 e.v. at 200°. At temperatures above 150° the observed yields were corrected for thermal decomposition. Sealed tube pyrolysis of N-trimethylborazole produced hydrogen at a rate

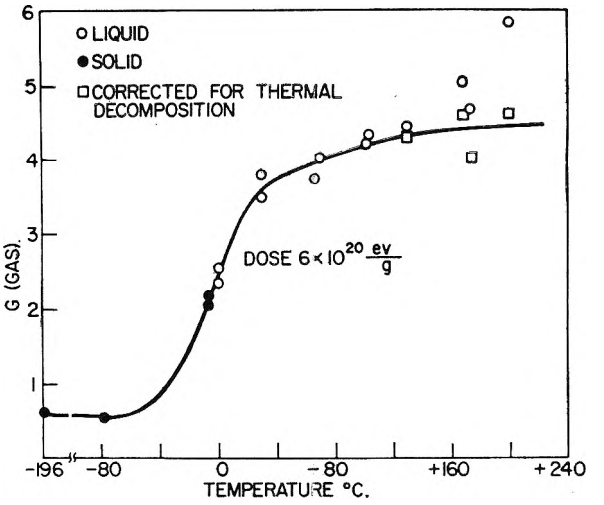


Fig. 1.—Effect of temperature on the hydrogen yield of irradiated N-trimethylborazole.

of 0.6 and 0.9 micromole per g. of sample per hr. at temperatures of 175 and 200°, respectively.

The methane and ethane yields from irradiated N-trimethylborazole are low at all temperatures; at 200° $G(CH_4) = 0.11$ and $G(C_2H_6) = 0.05$ molecule per 100 e.v.

**B-Trimethylborazole.**—At 30°, yields of hydrogen, methane, and ethane were essentially independent of dose rate between $5 \times 10^{18}$ and $1 \times 10^{21}$ e.v./g.-hr. For doses to $1.3 \times 10^{21}$ e.v./g. the yields were linear with dose with $G(H_2) = 1.65$, $G(CH_4) = 1.38$, and $G(C_2H_6) = 0.08$ molecules/100 e.v. Maximum deviations for these results were of the order of 2%. At a dose of $3 \times 10^{21}$ e.v./g., the hydrogen and methane yields dropped slightly to $G(H_2) = 1.6$ and $G(CH_4) = 1.3$. The yields as a function of irradiation temperature are shown in Fig. 2. The methane and ethane yields are quite small from irradiations at −196 and −78°. At approximately −6° the methane yield increases rapidly and appears to pass through a discontinuity at the melting point (32°). The ethane yield, however, is essentially independent of irradiation phase. $G(H_2)$ increases from 0.52 to 2.11 molecules per 100 e.v. in the temperature interval −196 to +80°.

The 200° irradiations gave significantly higher yields for all three gases than the corresponding 160° irradiations. Pyrolysis of B-trimethylborazole at 200° in a sealed tube for 8 hr. produced 1.8 micromoles of hydrogen per g. of sample and negligible amounts of methane and ethane. This accounts for only 2% of the hydrogen produced during irradiation at 200°. Thus, the sharp increase in yields is not due to the thermal decomposition of the borazole itself, although it could arise from thermal decomposition of some radiogenic product.

**Hexamethylborazole.**—The gas yields were linear functions of dose to $2 \times 10^{21}$ e.v./g. and were independent of dose rate between $5 \times 10^{18}$ and $1 \times 10^{20}$ e.v./g.-hr. $G(H_2)$, $G(CH_4)$, and $G(C_2H_6)$ are 0.45, 0.83, and 0.28 molecule per 100 e.v., respectively, at 30° It is interesting to note that the methane yield exceeds the hydrogen yield by a fac-

(3) G. E. Ryschkewitsch, J. J. Harris, and H. H. Sisler, *J. Am. Chem. Soc.*, **80**, 4514 (1958).

(4) D. T. Haworth and L. F. Hohnstedt, *ibid.*, **82**, 3860 (1960).

(5) T. C. Bissot and R. W. Parry, *ibid.*, **77**, 3481 (1955).

(6) C. J. Hochanadel and J. A. Ghormley, *J. Chem. Phys.*, **21**, 880 (1953).

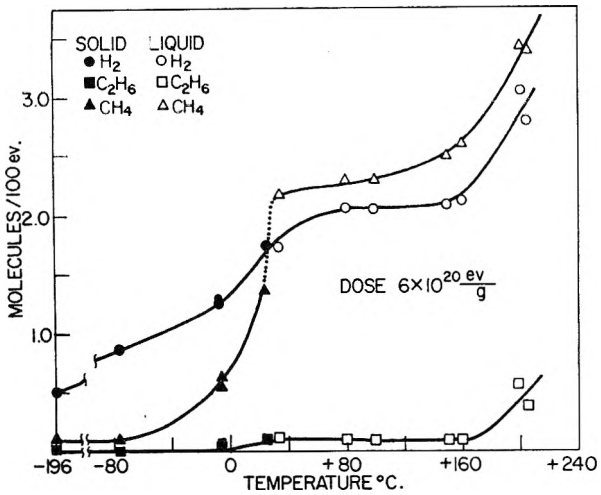


Fig. 2.—Effect of temperature on the gas yields of irradiated B-trimethylborazole.

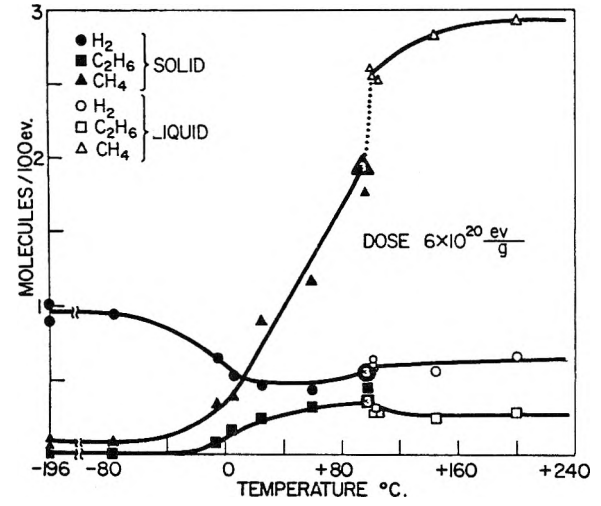


Fig. 3.—Effect of temperature on the gas yields from irradiated hexamethylborazole.

tor of almost two and that the ethane yield is appreciably higher than found from radiolysis of the other two borazoles.

The temperature dependences of the hydrogen, methane, and ethane yields are shown in Fig. 3. At low temperatures (−78 and −196°) hydrogen is the dominant product. Between −78 and 0° the hydrogen yield decreases somewhat and the methane and ethane yields begin to increase. The methane yield increases rapidly above 0° and appears to pass through a discontinuity at the melting point (99°) with $G(CH_4)$ increasing from 1.94 at 97° to 2.51 at 102°. Above the melting point methane is the principal product. The hydrogen and ethane yields do not change much between 30 and 200°. However, the data may suggest small abrupt shifts in the hydrogen and ethane yields at the melting point.

## Discussion

It generally is considered that primary processes in radiation chemistry, such as molecular detachment and formation of radicals, "hot" atoms, or ions, are independent of temperature. The relative importance of such processes cannot be evaluated from the present data. However, it may be assumed that the gas yields at low temperature (−196°) represent the maximum contributions of "molecular detachment" and "hot" atom reactions. The increase of most of the gas yields with increasing temperature then suggests the onset of secondary processes which are temperature dependent. Radical abstraction reactions satisfy this condition.

In the radiolysis of N-trimethyl- and B-trimethylborazole, therefore, the increase in hydrogen yields in the temperature range −78 to 30° may reasonably be attributed to an abstraction reaction, $H + RH \rightarrow H_2 + R$. Activation energies of about 10 kcal./mole[7] usually are found for gas phase reactions of this type. It should be noted also that the ratios of the hydrogen yields at 30° to those at −196° indicate that at the lower temperature most of the hydrogen atoms recombine with their partners.

Contrary to this behavior, the hydrogen yield from hexamethylborazole decreased with increasing temperature in the range −80 to 25°. This phenomenon could result from scavenging of hydrogen atoms by impurities or by some radiolytic product. If, at low temperatures, hydrogen molecules were produced by a process with inverse temperature characteristics, the hydrogen yield might be expected to decrease with increasing temperature. An ionic process characteristic of the hexamethylborazole medium might fulfill this requirement. However, at higher temperatures competition by the abstraction reaction $H + RH \rightarrow H_2 + R$ would be reflected by an increase in the hydrogen yield curve. Similar arguments could be applied to the possibility of methyl radical scavenging of hydrogen atoms. Although further speculation on the reactions producing hydrogen is unwarranted, the phenomenon does suggest competitive processes, the relative rates of which change with temperature. Similar effects were noted by Taylor, Mori, and Burton[8] in the radiolysis of neopentane.

The low yields at −196° of methane from B-trimethyl- and hexamethylborazole may be attributed to radical combination, $H + CH_3 \rightarrow CH_4$. The increase of these yields between about −80° and the melting points indicates the inception of an abstraction reaction, $CH_3 + RH \rightarrow CH_4 + R$, a process requiring some activation energy and, hence, becoming more favorable at higher temperatures. The abrupt increase in methane yields in the temperature regions near the melting points suggests that, in the solid state, many of the methyl radicals are trapped and eventually recombine with their partners. In the liquid state, however, the probability of methyl radicals escaping the cages in which they are formed, and producing methane *via* the abstraction reaction, is enhanced.

A probable source of ethane in irradiated B-trimethyl- and hexamethylborazole is *via* radical combination, $CH_3 + CH_3 \rightarrow C_2H_6$, in the spurs. However, the pronounced temperature dependence

(7) E. W. R. Steacie, "Atomic and Free Radical Reactions," 2nd Ed., Reinhold Publ. Corp., New York, N. Y., 1954, p. 496.

(8) W. H. Taylor, S. Mori, and M. Burton, *J. Am. Chem. Soc.*, **82**, 5217 (1960).

of the ethane yield from hexamethylborazole between −20 and 100° may be indicative of other reactions which produce ethane. In this regard, it should be noted that abstraction reactions of the type $CH_3 + RCH_3 \rightarrow C_2H_6 + R$ were shown by Rice and Teller[9] to be improbable on theoretical grounds. Significant low temperature yields could be expected if ethane were produced by a molecular process, but this was not observed.

The very low yields of methane and ethane from irradiated N-trimethylborazole indicate that among the competitive processes which determine the formation of free radicals, the probability of the $N-CH_3$ bond breaking is low. Whether the $N-CH_3$ bond in irradiated hexamethylborazole is similarly resistant to cleavage cannot be ascertained from the present data.

**Acknowledgment.**—The authors gratefully acknowledge the suggestions and comments given them during the course of this work by Dr. J. A. Ghormley of this Laboratory.

(9) F. O. Rice and E. Teller, *J. Chem. Phys.*, **6**, 489 (1938).

# COMBUSTION CALORIMETRY OF ORGANIC FLUORINE COMPOUNDS. THE HEATS OF COMBUSTION AND FORMATION OF THE DIFLUOROBENZENES, 4-FLUOROTOLUENE AND *m*-TRIFLUOROTOLUIC ACID[1]

BY W. D. GOOD, J. L. LACINA, D. W. SCOTT, AND J. P. MCCULLOUGH

*Contribution No. 115 from the Thermodynamics Laboratory of the Bartlesville Petroleum Research Center, Bureau of Mines, U. S. Department of the Interior, Bartlesville, Oklahoma*

*Received April 12, 1962*

The heats of combustion of five aromatic fluorine compounds were determined by a rotating-bomb method of combustion calorimetry. The suitability of *m*-trifluorotoluic acid ($\alpha, \alpha, \alpha$-trifluoro-*m*-toluic acid) as a reference substance for the combustion calorimetry of organic fluorine compounds was investigated. The following values, in kcal. mole$^{-1}$, are reported for the standard heats of formation, $\Delta Hf°_{298.15}$, from graphite and gaseous hydrogen, oxygen, and fluorine: 4-fluorotoluene(g), −34.01; 1,2-difluorobenzene(g), −67.65; 1,3-difluorobenzene(g), −71.35, 1,4-difluorobenzene(g), −70.69, and *m*-trifluorotoluic acid(c), −251.78.

Systematic investigations of the thermodynamic properties of organic fluorine compounds have been in progress in this Laboratory.[2,3] This paper reports measurements of the heats of combustion of five aromatic fluorine compounds: 4-fluorotoluene, the three isomeric difluorobenzenes, and *m*-trifluorotoluic acid ($\alpha,\alpha,\alpha$-trifluoro-*m*-toluic acid). The study of *m*-trifluorotoluic acid was undertaken because this compound was suggested as a reference substance for the combustion calorimetry of organic fluorine compounds by the Standing Commission on Thermochemistry of the International Union of Chemistry.[4]

## Experimental

**Apparatus and Procedures.**—The rotating-bomb calorimeter, BMR-2, and platinium-lined bombs have been described.[2,3] Bomb Pt-5, internal volume 0.352 l., was used for the experiments with 4-fluorotoluene. Modification of bomb Pt-5, before the experiments with the difluorobenzenes, increased the internal volume to 0.355 l. Bomb Pt-3b, internal volume 0.350 l., was used for the experiments with *m*-trifluorotoluic acid.

The basic procedures used in this investigation for the combustion calorimetry of organic fluorine compounds have been described.[2,3] The earlier experimental method developed for fluorine compounds of relatively low fluorine content[2] was used for 4-fluorotoluene. Sample containers were ampoules of fused quartz, and a small but significant thermochemical correction was applied for the reaction of fused quartz with the hydrofluoric acid produced by the combustion reaction. A later method which utilized sealed sample containers of polyester film[3] was used for the difluorobenzenes. The volatility of *m*-trifluorotoluic acid is low enough to make sample confinement unnecessary.

In all experiments with the organic fluorine compounds, the bomb initially contained 10 ml. of water. For the comparison experiments,[2] the bomb initially contained a solution of HF (or, for 4-fluorotoluene, HF and $H_2SiF_6$) which, upon dilution with water produced by the combustion of the sample, gave a solution of nearly the same amount and concentration as that obtained from combustion of the fluorine compound.

**Units of Measurement and Auxiliary Quantities.**—All data reported are based on the 1951 International Atomic Weights[5a] and fundamental constants[5b] and the definitions: 0°C. = 273.15°K.; 1 cal. = 4.184 j. (exactly). The laboratory standard weights had been calibrated at the National Bureau of Standards.

For reducing weights in air to weights *in vacuo*, correcting the energy of the actual bomb process to the isothermal bomb process, and correcting to standard states, the values summarized below, all for 25°, were used for density, $\rho$, specific heat, $c_p$, and $(\partial E/\partial P)_T$ of the various substances.

| | $\rho$, g. ml.$^{-1}$ | $c_p$, cal. deg.$^{-1}$ g.$^{-1}$ | $(\partial E/\partial P)_T$, cal. atm.$^{-1}$ g.$^{-1}$ |
|---|---|---|---|
| 4-Fluorotoluene | 0.990 | 0.374 | −0.0079 |
| 1,2-Difluorobenzene | 1.150 | .334 | − .0080 |
| 1,3-Difluorobenzene | 1.147 | .33 | − .0060 |
| 1,4-Difluorobenzene | 1.163 | .33 | − .0040 |
| *m*-Trifluorotoluic acid | 1.371 | .3 | − .0028 |

Materials.—The benzoic acid used was National Bureau

(1) This research was supported by the United States Air Force through the Air Force Office of Scientific Research of the Air Research and Development Command under Contract No. CSO-680-57-4. Reproduction in whole or in part is permitted for any purpose of the United States Government.

(2) W. D. Good, D. W. Scott, and Guy Waddington, *J. Phys. Chem.*, **60**, 1080 (1956).

(3) W. D. Good, D. R. Douslin, D. W. Scott, Ann George, J. L. Lacina, J. P. Dawson, and Guy Waddington, *ibid.*, **63**, 1133 (1959).

(4) Revue Analytique et Critique de Thermochimie Organique. Appendices au Premier Rapport de la Commission Permanente de Thermochimie, Paris, 1936.

(5) (a) E. Wichers, *J. Am. Chem. Soc.*, **74**, 2447 (1952). (b) F. D. Rossini, F. T. Gucker, Jr., H. L. Johnston, L. Pauling, and G. W. Vinal, *ibid.*, **74**, 2699 (1952).

of Standards Sample 39g, with a certified heat of combustion of 26.4338 ± 0.0026 abs. kj. $g.^{-1}$ (6317.83 ± 0.62 cal. $g.^{-1}$) under certificate conditions. Conversion from certificate conditions to standard conditions[6] gives −6312.97 ± 0.62 cal. $g.^{-1}$ for $\Delta Ec^\circ/M$, the energy of the idealized combustion reaction. The samples of succinic acid, auxiliary oil, polyester film, cotton thread, and filter paper fuse material have been described.[2,3] The value of $\Delta Ec^\circ/M$ for succinic acid is −3019.8 ± 0.4 cal. $g.^{-1}$.[3] Values of $\Delta Ec^\circ/M$ for the auxiliary oil obtained from two series of experiments chronologically close to those with 4-fluorotoluene and the difluorobenzenes were −10,984.8 ± 0.5 and −10.984.2 ± 0.5 cal. $g.^{-1}$, respectively. Attention is called to an obvious, but previously undetected, error in reference 3. The equation relating $\Delta Ec^\circ/M$ of the polyester film to relative humidity should be

$$\Delta Ec^\circ/M = -5476.1 + 0.2524 \text{ (relative humidity expressed in \%) cal. } g.^{-1}$$

Samples of 1,2-difluorobenzene, 1,3-difluorobenzene, 1,4-difluorobenzene, and 4-fluorotoluene were supplied by the Illinois State Geological Survey Division, through the courtesy of Dr. G. C. Finger. These materials were distilled in an efficient fractionating column by C. J. Thompson and H. J. Coleman of the Bartlesville Research Center. The purities of the samples of 1,2-difluorobenzene and 1,3-difluorobenzene were 99.998 ± 0.002 and 99.999 ± 0.001 mole %, respectively, and that of 4-fluorotoluene was 99.92 ± 0.04 mole %, as determined by calorimetric studies of melting point as a function of the fraction melted. Studies of the time–temperature freezing behavior[7] of 1,4-difluorobenzene did not give quantitative values of purity, but did give qualitative evidence of high purity. Recovery of the stoichiometrically expected quantities of hydrofluoric acid (100.0 ± 0.1%) in the combustion products of these materials is good evidence of the absence of non-isomeric impurity.

The sample of *m*-trifluorotoluic acid was prepared at the University of Colorado under the direction of Drs. J. D. Park and J. R. Lacher. Elemental analysis of the material as prepared was

| | Found | Calcd. for $C_8H_5F_3O_2$ |
|---|---|---|
| % C | 50.54 | 50.52 |
| % H | 2.96 | 2.65 |
| % F | 29.75 | 29.98 |

This material was purified by zone refining.[2] Passage of the molten zone down the column 30 times removed 0.01% of an indicator dye from approximately one fourth of the material. This portion of the material was used for the calorimetric measurements. The neutralization equivalent of the original material was 99.7% of the theoretical value, and that of the purified material was 100.0% of the theoretical value. Recovery of hydrofluoric acid from the combustion products was 100.0 ± 0.1% of the quantity expected from the stoichiometry of the combustion reaction.

## Results

**Calorimetric Results.**—Detailed results of calorimetric experiments selected as typical of each compound are given in Table I. The results of all experiments are summarized in Table II. The symbols in these tables are the same as those of reference 6. The values of $\Delta Ec^\circ/M$ for the compounds in Table I and II refer to the equations

4-Fluorotoluene

$$C_7H_7F(\text{liq.}) + 17/2\ O_2(g) + 67H_2O(\text{liq.}) = 7CO_2(g) + HF\cdot 70H_2O(\text{liq.}) \quad (1)$$

Difluorobenzenes

$$C_6H_4F_2(\text{liq.}) + 13/2\ O_2(g) + 59H_2O(\text{liq.}) = 6CO_2(g) + 2HF\cdot 30H_2O(\text{liq.}) \quad (2)$$

*m*-Trifluorotoluic acid

$$C_8H_5O_2F_3(c) + 15/2\ O_2(g) + 59H_2O(\text{liq.}) = 8CO_2(g) + 3HF\cdot 20H_2O(\text{liq.}) \quad (3)$$

**Derived Results.**—The molal values of $\Delta Ec^\circ$, the standard change in internal energy, and $\Delta Hc^\circ$, the standard heat of combustion (eq. 1, 2, and 3), are presented in Table III. The uncertainties indicated in Table III are the "uncertainty intervals," equal to twice the final over-all standard deviation of the mean. To calculate the values of the standard heat of formation, $\Delta Hf^\circ$, also given in Table III, values of heat of formation for carbon dioxide, water, and aqueous hydrofluoric acid were taken from N.B.S. Circular 500.[8] The values of standard heat of vaporization used to calculate heats of formation in the gaseous state were calculated from unpublished results of this Laboratory.

## Discussion

**Comparison with Previous Work.**—The only comparison of values possible is with those given in the early work of Swarts,[9] who reported the "heat of combustion at constant volume" for three of the compounds studied in this research. A comparison of results follows

| | $-\Delta Ec^\circ/M$, cal. $g.^{-1}$ This investigation | "Heat of combustion at constant volume," cal. $g.^{-1}$ Swarts | Difference, cal. $g.^{-1}$ |
|---|---|---|---|
| 4-Fluorotoluene | 8124.0 | 8196.5 | 72.5 |
| 1,4-Difluorobenzene | 6173.9 | 6188.5 | 14.6 |
| *m*-Trifluorotoluic acid | 4187.6 | 4248.8 | 61.2 |

It has been pointed out in reference 1 that the results of the present investigations on organic fluorine compounds are not strictly comparable with the results obtained by Swarts.

***m*-Trifluoric Acid as a Reference Substance.**—In 1936, the Standing Commission on Thermochemistry of the International Union of Chemistry suggested the investigation of *m*-trifluorotoluic acid as a reference substance for the combustion calorimetry of fluorine compounds. The purpose of reference substances, or "secondary standards," is to permit intercomparison of the results of different investigators for a particular class of compounds. When such substances have been tested adequately, results of calorimetry with them can serve as a criterion for judging the correctness of procedures followed and the accuracy of data obtained in the investigations.

As discussed by Beckers,[10] a reference substance must satisfy certain minimum requirements: (1)

(6) W. N. Hubbard, D. W. Scott, and G. Waddington, "Experimental Thermochemistry," F. D. Rossini, Editor, Interscience Publishers, Inc., New York, N. Y., 1956, Chapter 5, pp. 75–128.

(7) A. R. Glasgow, A. J. Streiff, and F. D. Rossini, *J. Res. Natl. Bur. Stds.*, **35**, 355 (1945).

(8) F. D. Rossini, D. D. Wagman, W. H. Evans, S. Levine, and I. Jaffe, "Selected Values of Chemical Thermodynamic Properties," N. B. S. Circular 500, 1952.

(9) G. Swarts, *J. chim. phys.*, **17**, 3 (1919).

(10) M. Beckers, *Bull. soc. chim. Belges*, **40**, 518 (1931).

TABLE I

SUMMARY OF TYPICAL COMBUSTION EXPERIMENTS[a]

| | 4-Fluoro-toluene | 1,2-Difluoro-benzene | 1,3-Difluoro-benzene | 1,4-Difluoro-benzene | *m*-Trifluoro-toluic acid |
|---|---|---|---|---|---|
| | Comparison experiments | | | | |
| $m'$ (benzoic acid), g. | 0.58248 | | 1.01363[b] | | 0.71270 |
| $m''$ (oil), g. | 0.38591 | | 0.15274 | | |
| $m'''$ (succinic acid), g. | | | | | 1.19179 |
| $m''''$ (fuse), g. | 0.00300[c] | | 0.00101[d] | | 0.00107[d] |
| $n^i$ ($H_2O$), moles | 0.5408 | | 0.5298 | | 0.5146 |
| $n^i$ (HF), moles | 0.007152 | | 0.021340 | | 0.030470 |
| $n^i$ ($H_2SiF_6$), moles | 0.000148 | | | | |
| $\Delta t_c$, deg. | 1.97599 | | 2.01368 | | 2.02141 |
| $m'\ \Delta Ec°/M$ (benzoic acid), cal. | −3677.1 | | −6399.0 | | −4499.3 |
| $m''\ \Delta Ec°/M$ (oil), cal. | −4239.1 | | −1677.7 | | |
| $m'''\ \Delta Ec°/M$ (succinic acid), cal. | | | | | −3599.0 |
| $m''''\ \Delta Ec°/M$ (fuse), cal. | −11.8 | | −4.1 | | −4.3 |
| $-\Delta E^f_{dec.}$ ($HNO_3$), cal. | −0.5 | | −0.6 | | −0.3 |
| $-\Delta E$, corr. to st. states, cal. | −8.3 | | −10.2 | | −13.7 |
| $-\Delta E_{ign.}$, cal. | −1.4 | | −0.4 | | −0.6 |
| $\varepsilon$ (cont.)($\Delta t_c$), cal. | 27.1 | | 28.1 | | 27.2 |
| $\varepsilon_{app.}$ (calor.)($-\Delta t$), cal. | −7911.1 | | −8063.9 | | −8090.0 |
| $\varepsilon_{app.}$ (calor.), cal. deg.$^{-1}$ | 4003.6 | | 4004.6 | | 4002.2 |
| | Combustion experiments | | | | |
| $m'$ (compound), g. | 0.88682 | 1.21293 | 1.21579 | 1.21840 | 1.93140 |
| $m''$ (oil), g. | 0.06444 | | | | |
| $m'''$ (polyester), g. (at % rel. hum.) | | 0.09701(24) | 0.09216(46) | 0.09254(46) | |
| $m''''$ (fuse), g. | 0.00286[c] | 0.00105[d] | 0.00091[d] | 0.00093[d] | 0.00115[d] |
| $n^i$ ($H_2O$), moles | 0.5523 | 0.5523 | 0.5523 | 0.5523 | 0.5523 |
| $\Delta t_c$, deg. | 1.97632 | 2.00732 | 1.99590 | 2.00134 | 2.01830 |
| $\varepsilon_{app.}$ (calor.)($-\Delta t_c$), cal. | −7912.4 | −8038.5 | −7992.8 | −8014.6 | −8077.6 |
| $\varepsilon$ (cont.)($-\Delta t_c$), cal. | −27.5 | −28.1 | −27.9 | −27.9 | −28.2 |
| $\Delta E_{ign.}$, cal. | 1.4 | 0.6 | 0.6 | 0.6 | 0.3 |
| $\Delta E$, corr. to st. states, cal. | 8.4 | 10.5 | 10.5 | 10.6 | 14.1 |
| $\Delta E^f_{hydr.}$ ($H_2SiF_6$), cal. | 5.4 | | | | |
| $\Delta E^f_{dec.}$ ($HNO_3$), cal. | 0.6 | 0.6 | 0.6 | 0.5 | 0.4 |
| $-m''\ \Delta Ec°/M$ (oil), cal. | 707.8 | | | | |
| $-m'''\ \Delta Ec°/M$ (polyester), cal. | | 530.6 | 503.6 | 505.7 | |
| $-m''''\ \Delta Ec°/M$ (fuse), cal. | 11.2 | 4.3 | 3.7 | 3.8 | 4.7 |
| $m'\ \Delta Ec°/M$ (compound), cal. | −7205.1 | −7520.0 | −7501.7 | −7521.3 | −8086.3 |
| $\Delta Ec°/M$ (compound), cal. g.$^{-1}$ | −8124.6 | −6199.9 | −6170.2 | −6173.1 | −4186.8 |

[a] The symbols used in this table are those of ref. 2. [b] For the experiments with the difluorobenzenes, one comparison experiment was matched with a combustion experiment for each of the three isomers. [c] Filter paper fuse. [d] Cotton thread fuse.

TABLE II

SUMMARY OF COMBUSTION EXPERIMENTS

| Compound | 4-Fluoro-toluene | 1,2-Difluoro-benzene | 1,3-Difluoro-benzene | 1,4-Difluoro-benzene | *m*-Trifluoro-toluic acid |
|---|---|---|---|---|---|
| | −8127.3 | −6199.9 | −6171.1 | −6174.8 | −4188.7 |
| | −8123.6 | −6200.6 | −6172.4 | −6173.5 | −4188.2 |
| | −8124.6 | −6199.9 | −6171.1 | −6174.5 | −4187.5 |
| $\Delta Ec°/M$ (compd.), cal. g.$^{-1}$ | −8123.0 | −6199.8 | −6167.6 | −6174.2 | −4187.7 |
| | −8122.2 | −6199.3 | −6170.7 | −6173.1 | −4186.5 |
| | −8123.4 | −6198.4 | −6170.2 | −6173.1 | −4186.8 |
| | | | −6169.3 | | |
| Mean value | −8124.0 | −6199.6 | −6170.3 | −6173.9 | −4187.6 |
| Std. dev. of the mean | ±0.7 | ±0.3 | ±0.6 | ±0.3 | ±0.3 |

it should be obtainable in a pure state; (2) it should be stable; (3) it should not be hygroscopic; (4) it should not be too volatile; (5) it should be easily compressed into pellets; and (6) it should ignite readily and react completely in the bomb. Both *m*-trifluorotoluic acid and *p*-fluorobenzoic acid, suggested in an earlier publication of this Laboratory,[2] satisfy these requirements. Both compounds are commercially available. *p*-Fluorobenzoic acid is purified readily by zone refining, but the crystal habit of *m*-trifluorotoluic acid makes purification by zone refining more difficult. The

TABLE III

DERIVED RESULTS AT 298.15°K., KCAL. MOLE$^{-1}$

| Compound | Condensed state | Values for condensed state: $\Delta Ec°$ | $\Delta Hc°$ | $\Delta Hf°$ | $\Delta Hv°$ | $\Delta Hf°$ (gas) |
|---|---|---|---|---|---|---|
| 4-Fluorotoluene | Liquid | −894.67 ± 0.17 | −895.56 ± 0.17 | − 43.43 | 9.42 ± 0.02 | −34.01 |
| 1,2-Difluorobenzene | Liquid | −707.33 ± .13 | −707.62 ± .13 | − 76.30 | 8.65 ± .02 | −67.65 |
| 1,3-Difluorobenzene | Liquid | −703.99 ± .17 | −704.28 ± .17 | − 79.64 | 8.29 ± .05 | −71.35 |
| 1,4-Difluorobenzene | Liquid | −704.39 ± .13 | −704.68 ± .13 | − 79.24 | 8.51 ± .05 | −70.69 |
| *m*-Trifluorotoluic acid | Solid | −796.14 ± .14 | −795.85 ± .14 | −251.78 | | |

apparent difficulty in preparing pure samples of *m*-trifluorotoluic acid is an undesirable characteristic for a proposed reference substance. Nevertheless, *m*-trifluorotoluic acid is satisfactory in other important respects, and the purity problem could be solved if an appropriate organization prepared a suitable large sample for distribution to qualified investigators.

# THERMODYNAMICS OF THE GOLD–NICKEL SYSTEM

BY GENE F. DAY[1a] AND RALPH HULTGREN[1b]

*Department of Mineral Technology, University of California, Berkeley, California*

*Received April 14, 1962*

The heats of formation of five gold–nickel alloys have been measured at 1150°K. by liquid tin solution calorimetry. The results have been correlated with other thermodynamic data and the equilibrium diagram for the gold–nickel system. Free energy, heat, and entropy values have been tabulated for the solid alloys. For a 10 atom % nickel alloy, the enthalpy relative to room temperature has been measured to 1250°K. for comparison with $\Delta C_p$ values in the literature. Lattice parameter and density measurements indicate that the vacancy concentration in the quenched alloys is not great, in contradiction to previously reported results.

## Introduction

The gold–nickel system has recently been investigated a number of times with the objective of elucidating crystal chemical principles. The system was chosen as an example of an endothermic alloy system, possessing a miscibility gap which closes above 1084°K. and a minimum in the liquidus and solidus curves[2] (Fig. 1). Results have been somewhat less than satisfying.

Flinn, Averbach, and Cohen[3] examined alloys for atomic arrangement by Fourier analysis of X-ray diffraction patterns. They found, to their surprise, evidence of short-range order rather than the expected tendency toward clustering (atoms surrounded preferentially by like atoms). They concluded that the quasichemical theory was not adequate and attributed the tendency to order to atomic size differences. However, a few years later Münster and Sagel[4] repeated the study and found clustering in the alloys.

Ellwood and Bagley[5] measured lattice parameters and densities of the alloys. At two compositions (20 and 90 atom % Ni) they concluded that about 3% of the lattice positions were vacant, while at other compositions X-ray densities agreed more nearly with measured densities. As has already been mentioned in a technical note,[6] this fact was not confirmed in this work.

Seigle, Cohen, and Averbach[7] report e.m.f. measurements of solid alloys. Free energies calculated from these data agree reasonably well with the miscibility gap boundaries except for $x_{Ni} < 0.3$. However, entropies and heats of formation derived from their temperature coefficients seem improbably high[8] as do $\Delta C_p$ values derived from the change of these quantities with temperature.[9]

Oriani and Murphy,[10] studying gold-rich and nickel-rich compositions (2–22 and 95–98 atom % Ni), found heats of formation of solid alloys much smaller than those indicated by Seigle, Cohen, and Averbach. In another investigation,[11] by direct reaction of the elements, they found heats of formation of liquid alloys much less endothermic than those of the solid state.

DeSorbo[12] and Oriani[13] measured heat capacities and heat contents of a single alloy (48.3 atom % Ni). DeSorbo found that between 13 and 298.15°K. a positive derivation from the Kopp–Neumann rule ($\Delta C_p > 0$) accounted for about 0.51 cal./g.-atom deg. of excess entropy for the alloy.

(1) (a) Graduate Research Engineer, Department of Mineral Technology, University of California. Berkeley. (b) Professor of Metallurgy, Department of Mineral Technology, University of California, Berkeley.

(2) M. Hansen, "Constitution of Binary Alloys," McGraw-Hill Book Co., New York, N. Y., 1958.

(3) P. A. Flinn, B. L. Averbach, and M. Cohen, *Acta Met.*, **1**, 664 (1953).

(4) A. Münster and K. Sagel, Paper 2D, Proceedings, Symposium No. 9, National Physical Laboratory. The Physical Chemistry of Metallic Solutions and Intermetallic Compounds, H. M. S. O., London, 1959.

(5) E. C. Ellwood and K. Q. Bagley, *J. Inst. Metals*, **80**, 617 (1952).

(6) G. F. Day, *ibid.*, **89**, 296 (1960–61).

(7) L. L. Seigle, M. Cohen, and B. L. Averbach, *J. Metals*, **4**, 1320 (1952).

(8) O. Kubaschewski and J. A. Catterall, "Thermochemical Data of Alloys," Pergamon Press, New York, N. Y., 1956.

(9) Selected Values for the Thermodynamic Properties of Metals and Alloys, 1955–1961, University of California, Minerals Research Laboratory.

(10) R. A. Oriani and W. K. Murphy, *Acta Met.*, **8**, 23 (1960).

(11) R. A. Oriani and W. K. Murphy, *J. Phys. Chem.*, **62**, 199 (1958).

(12) W. DeSorbo, *Acta Met.*, **3**, 227 (1955).

(13) R. A. Oriani, *ibid.*, **3**, 232 (1955).

Oriani measured heat contents above 273.15°K. by means of an ice calorimeter. Measurements could not be made between 373 and 1075°K. because of phase separation. Specimens dropped into the calorimeter from above 1075°K. were examined metallographically and found to be single phase. Above 1075°K. Oriani found $\Delta C_p > 0$, increasing to $\Delta C_p = 1.75$ at 1190°K.; he attributed the positive deviation to the imminence of the melting point.

In the work described here, the heats of formation of single phase Au–Ni alloys were determined by liquid tin solution calorimetry. The reliability of this type of measurement is usually greater than is obtainable from temperature coefficients of e.m.f. measurements. In addition, heat contents above room temperature were determined for an alloy composition ($x_{Ni} = 0.1$) where the miscibility gap caused no trouble.

With the aid of these and earlier cited data, a set of thermodynamic functions has been calculated for the solid phase which is consistent with the miscibility gap and which agrees well with the free energies determined by Seigle, *et al.*, for $x_{Ni} > 0.3$.

## Experimental

Gold and nickel of 99.95% purity were used. Weighed amounts of each were sealed in evacuated capsules of fused quartz, then heated to temperatures 50–150° above the liquidus for each composition. After several minutes of severe agitation at temperature, the capsules were plunged into cold water so that the ingots, which weighed from 5 to 10 g., would freeze with a minimum of macrosegregation. In every case the loss in weight amounted to less than 0.01%, so that the final composition was taken to be the same as that initially weighed out.

After cold working, the ingots were sealed in evacuated fused quartz tubes and homogenized for more than a week at temperatures about 50° below the solidus and were rapidly quenched. Filings were then taken from both ends of each ingot, annealed for 1 hr. in the single phase region, and quenched rapidly in cold water.

Back-reflection X-ray lines proved to be sharp, assuring homogeneity of the ingots. Precision lattice constants were determined from these lines. Values obtained were found to agree fairly well with those of Ellwood and Bagley, but follow a smoother curve with composition.[6]

Densities were determined by measuring the buoyancy of the ingots in distilled water.[6] These results indicated very few vacancies, in contradiction to the work of Ellwood and Bagley.

The liquid tin solution calorimeter has been described elsewhere,[14] so the procedure will be described only briefly.

Small chips of the alloys were encapsulated in gold foil to make samples about 5 mm. in diameter and weighing approximately 0.5 g. Specimens were introduced into the dispenser and held there at about 1150°K. for about 15 min. before being dropped into the calorimeter bath which was contained in the same evacuated space. Previous tests had shown that prolonged heating of the samples at 1150°K. produced negligible reaction between the alloy and gold foil. The tin bath was maintained at approximately 910°K.; at lower temperatures the pure nickel samples did not dissolve rapidly enough for accurate measurement of the heat evolved.

Heats of solution were determined in the usual manner. After correcting for the heat effect of the gold foil, heats of solution of alloys minus heats of solution of their components yielded heats of formation of the alloys at the initial temperature, about 1150°K. Concentrations of impurities in the tin bath were held below a total of 0.9 atom %. Within these limits their effect on the heat of solution of pure gold was found to be negligible; the heat of solution of nickel in tin was found to depend on the nickel concentration in the bath, however. A small correction was made for this dependence. The experimental results are shown in Tables I and II.

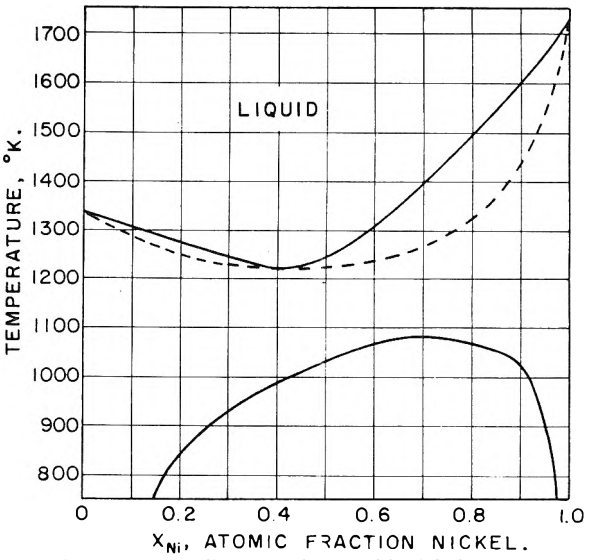


Fig. 1.—Phase diagram of the gold-nickel system.

TABLE I

HEATS OF SOLUTION AT 910°K. IN LIQUID TIN

| Sample | $T_i$, °K. | $T_f$, °K. | $x_{Ni}$ (in bath) | $\Delta H$, soln. cal./g.-atom |
|---|---|---|---|---|
| Au | 1143.2 | 909.8 | 0.000 | −4520 |
| | 1145.6 | 909.4 | .000 | −4534 |
| | 1144.8 | 912.4 | .000 | −4594 |
| | 369.3 | 908.7 | .0155 | −4575 |
| | 369.2 | 908.7 | .0155 | −4573 |
| Ni | 1147.1 | 910.6 | .0010 | −9866 |
| | 1147.1 | 916.0 | .0044 | −9866 |
| | 376.0 | 911.0 | .0062 | −9766 |
| | 369.1 | 910.2 | .0167 | −9558 |

TABLE II

HEATS OF FORMATION OF ALLOYS AT 1150°K.

| $x_{Ni}$ | $T_i$, °K. | $T_f$, °K. | $x_{Ni}$ (in bath) | Heats of soln.,[a] cal./g.-atom | $\Delta H$, form., cal./g.-atom |
|---|---|---|---|---|---|
| 0.1 | 1141.0 | 912.2 | 0.0001 | − 7293 | 601 |
| | 1146.6 | 911.4 | .0048 | − 7097 | 370 |
| 0.3 | 1137.5 | 912.6 | .0004 | − 9059 | 1288 |
| | 1140.5 | 913.5 | .0018 | − 9101 | 1323 |
| | 1146.3 | 911.6 | .0046 | − 9262 | 1445 |
| | 1155.3 | 914.8 | .0058 | − 9265 | 1412 |
| | 1149.4 | 914.8 | .0086 | − 9148 | 1355 |
| 0.5 | 1143.0 | 913.1 | .0012 | −10592 | 1683 |
| | 1140.9 | 914.2 | .0023 | −10882 | 2007 |
| | 1148.6 | 912.4 | .0039 | −10728 | 1800 |
| | 1155.8 | 916.5 | .0065 | −10967 | 2041 |
| | 1156.4 | 912.4 | .0069 | −10526 | 1571 |
| 0.7 | 1142.0 | 913.1 | .0024 | −11750 | 1758 |
| | 1147.7 | 912.6 | .0027 | −11577 | 1544 |
| | 1144.5 | 915.9 | .0077 | −11772 | 1860 |
| 0.9 | 1150.1 | 913.0 | .0010 | −11773 | 593 |
| | 1146.0 | 910.3 | .0036 | −11686 | 565 |
| | 1142.6 | 912.6 | .0038 | −11741 | 669 |

[a] For reaction $\text{Alloy}_{T_i} \rightarrow \text{Solution}_{T_f}$.

(14) R. L. Orr, A. Goldberg, and R. Hultgren, *Rev. Sci. Instr.*, **28**, 767 (1957).

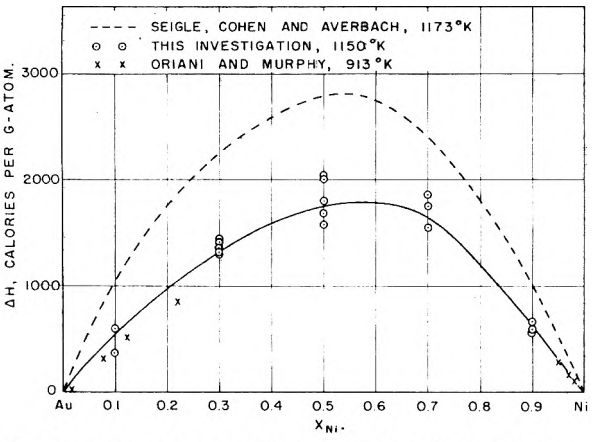


Fig. 2.—Integral heats of formation of solid Au–Ni alloys.

At 910°K. the heat of solution of gold in pure tin has been found to be −4560 cal./g.-atom, which is consistent with values measured at lower temperatures. At the same temperature, the heat of solution of nickel in tin may be represented by

$$\Delta\bar{H}_{Ni} = -9920 + 20500x_{Ni} \text{ cal./g.-atom}$$

Oriani and Murphy,[10] however, report that at 913°K.

$$\Delta\bar{H}_{Ni} = -9464 + 23770x_{Ni} \text{ cal./g.-atom}$$

Leach and Bever[15] have measured the heat of solution of nickel in tin as −7470 cal./g.-atom at 623°K., a value which seems unreasonably small despite the temperature difference. It should be noted that the heat of solution of nickel is less certain than that of gold due to the slow rate of solution of nickel in the tin bath.

Heats of formation of the alloys are plotted in Fig. 2 and are compared with heats of formation at other temperatures by Seigle, Cohen, and Averbach[7] and by Oriani and Murphy.[10]

Heat contents of the 10 atom % nickel alloy were measured using a diphenyl ether drop calorimeter described elsewhere.[16] This composition was chosen since the alloy should remain single phase during the measurements. Microscopic examination revealed no second phase present after dropping the alloy from a high temperature. Results are shown in Tables III and IV. The positive deviations from the Kopp–Neumann rule which were found are similar to those found by Oriani[13] at high temperatures for another composition. They indicate that heats of formation become increasingly endothermic at higher temperature. This accounts for the small difference between our measurements and those of Oriani and Murphy as shown in Fig. 2. Heat capacities of pure gold and pure nickel have been taken from tabulated values.[9]

## Selection of Thermodynamic Functions

In order to provide a consistent thermodynamic picture of the Au–Ni system, the free energies measured by Seigle, Cohen, and Averbach have been modified in the region $x_{Ni} < 0.3$ so as to bring them into agreement with the miscibility gap conditions. The new values of $\Delta\bar{F}_{Ni}$ are more negative and result in the integral free energy being 150 cal./g.-atom more negative at $x_{Ni} = 0.4$ than was originally reported.[7] Table V gives the thermodynamic functions resulting from these data and the measured heats of formation.

(15) J. S. L. Leach and M. B. Bever, *Trans. Met. Soc. AIME*, **215**, 728 (1959).

(16) R. Hultgren, P. Newcomb, R. L. Orr, and L. Warner, Paper 1H, Proceedings, Symposium No. 9, National Physical Laboratory, The Physical Chemistry of Metallic Solutions and Intermetallic Compounds, H. M. S. O., London, 1959.

TABLE III

MEASURED HEAT CONTENTS OF THE ALLOY $Au_{0.9}Ni_{0.1}$

| $T$, °K. | $H_T - H_{298}$ | $Y = \frac{H_T - H_{298}}{T - 298}$ |
|---|---|---|
| 757.6 | 2954 | 6.429 |
| 797.3 | 3224 | 6.459 |
| 887.1 | 3851 | 6.539 |
| 893.9 | 3905 | 6.555 |
| 1012.5 | 4728 | 6.619 |
| 1052.7 | 5040 | 6.680 |
| 1079.6 | 5260 | 6.731 |
| 1202.0 | 6202 | 6.862 |
| 1244.5 | 6532 | 6.902 |

TABLE IV

SMOOTHED VALUES OF THE ENTHALPY, HEAT CAPACITY AND $\Delta C_p$ FOR THE ALLOY $Au_{0.9}Ni_{0.1}$

| $T$, °K. | $H_T - H_{298}$ | $C_p$ alloy | 0.9 $C_{pAu}$ + 0.1 $C_{pNi}$ | $\Delta C_p$ |
|---|---|---|---|---|
| 800 | 3245 | 6.838 | 6.729 | 0.109 |
| 900 | 3940 | 7.055 | 6.857 | .198 |
| 1000 | 4655 | 7.280 | 6.987 | .293 |
| 1100 | 5395 | 7.609 | 7.115 | .494 |
| 1150 | 5780 | 7.793 | 7.178 | .615 |
| 1200 | 6180 | 8.040 | 7.241 | .799 |
| 1250 | 6590 | 8.387 | 7.312 | 1.075 |

TABLE V

SELECTED THERMODYNAMIC PROPERTIES OF SOLID Au–Ni ALLOYS AT 1150°K.

| $x_{Ni}$ | $\Delta F$ | $\Delta H$ | $\Delta S$ | $a_{Au}$ | $a_{Ni}$ |
|---|---|---|---|---|---|
| 0.00 | 0 | 0 | 0.00 | 1.000 | 0.000 |
| .10 | −450 | 550 | 0.87 | 0.916 | .310 |
| .20 | −620 | 970 | 1.38 | .839 | .519 |
| .30 | −685 | 1325 | 1.75 | .767 | .684 |
| .40 | −685 | 1590 | 1.98 | .711 | .788 |
| .50 | −640 | 1745 | 2.07 | .666 | .856 |
| | (±100) | (±100) | (±.15) | (±.025) | (±.025) |
| .60 | −570 | 1780 | 2.04 | 0.627 | 0.900 |
| .70 | −480 | 1645 | 1.85 | .594 | .926 |
| .80 | −370 | 1215 | 1.38 | .572 | .938 |
| .90 | −250 | 635 | 0.77 | .535 | .948 |
| 1.00 | 0 | 0 | 0.00 | .000 | 1.000 |

**Acknowledgments.**—Support by the Army Research Office, Durham, has made this project possible. The authors wish to thank Mr. R. L. Orr and Mr. P. D. Anderson for many helpful discussions and Mr. Stanley Ross for his valuable assistance.

# NOTES

## METHYLENE AND DIPHENYLMETHYLENE

By F. O. Rice[1] and John D. Michaelsen

*Chemistry Department, Catholic University, Washington 17, D. C.*

*Received November 2, 1961*

In this note we shall report some attempts to freeze out methylene and diphenylmethylene using the technique described by Rice and Freamo.[2] We are basing our conclusions on the possible occurrence of an irreversible low temperature phenomenon. This might be a color change or exothermicity of the deposit when allowed to warm to room temperature, after its original condensation on a liquid nitrogen-cooled finger.

Under the conditions of our experiments[2] we have not found any evidence of a frozen out methylene radical. We have performed a large number of experiments, using pure diazomethane in various carrier gases, but in no case did we notice phenomena that would indicate any sort of sharp transition when the deposit was allowed to warm to room temperature. In each case the pressure of the system increased slowly and smoothly and ethylene constituted more than 75% of the product.

With nitrogen as carrier gas and the furnace temperature at 650°, a mass spectrometric analysis of the gases showed

| Product | Mole % of total |
|---|---|
| Ethylene | 83 |
| Ethane | 8 |
| Acetylene | 4 |
| Propane | 3 |
| Propylene | 1 |
| $C_4$ and higher hydrocarbons | 1 |

Methylene can, of course, be frozen out[3] in a rigid medium but the amount is too small to be detected by our methods.

We next investigated diphenyldiazomethane in the hope that the diphenylmethylene radical could be stabilized at liquid nitrogen temperatures. The parent substance was prepared according to the method given in *Org. Syn.*, **24**, p. 53; following these directions (without change) we obtain approximately a 70% yield of the burgundy-red diazomethane; this was stored at −78°.

### Experimental

In the first series of experiments, diphenyldiazomethane which had been deposited on a cold finger filled with liquid nitrogen was illuminated by a high pressure mercury arc lamp. A high-melting (150–156°) yellow solid was obtained, which seems to be benzophenone azine (m.p. 164°). Presumably this is formed by the reactions[4]

$$(C_6H_5)_2C{=}N{\equiv}N \xrightarrow{h\nu} (C_6H_5)_2C + N_2$$

$$(C_6H_5)_2C + (C_6H_5)_2C{=}N{\equiv}N \longrightarrow (C_6H_5)_2C{=}N{-}N{=}C(C_6H_5)_2$$

In a second series of experiments diphenyldiazomethane was introduced at room temperature and vaporized by passing through a furnace at 460°. The effluent gases condensed on a liquid nitrogen cooled finger as a yellow solid. After crystallizing, this substance had a melting point of 113° and proved to be fluorene[5] (which is isomeric with diphenylmethylene) since admixture of synthetic fluorene did not change the melting point. Based on the amount of diphenyldiazomethane decomposed, the yield of fluorene was greater than 60%; it is independent of the furnace temperature.

Since we could detect absolutely no effect on warming the condensate we are postulating that the diphenyl methylene isomerizes either while still in the gas phase or immediately on condensing, according to the equation

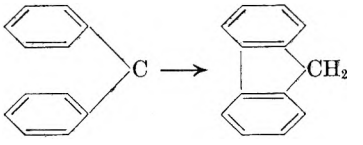


In an attempt to demonstrate exothermicity, blue $N_2O_3$ was deposited on the yellow solid on the liquid nitrogen cooled finger and the mixture warmed; the resulting pressure–temperature curve was the same as that obtained in pure $N_2O_3$, whereas if the warming of the yellow condensate was exothermic, the heating of the combined condensate would have resulted in the sudden volatilization of $N_2O_3$.

(1) Chemistry Department, Georgetown University, Washington 7, D. C.

(2) F. O. Rice and M. J. Freamo, *J. Am. Chem. Soc.*, **73**, 5529 (1951).

(3) (a) T. D. Goldfarb and G. C. Pimentl, *ibid.*, **82**, 1865 (1960); (b) G. W. Robinson and M. McCarty, Jr., *ibid.*, **82**, 1859 (1960).

(4) (a) W. B. De More, H. O. Pritchard, and N. Davidson, *ibid.*, **81**, 5874 (1959); (b) W. Fielding and H. O. Pritchard, *J. Phys. Chem.*, **64**, 278 (1960).

(5) Compare with ref. 3b; apparently when the pyrolysis is carried out at a much lower temperature than in our experiments the azine is formed.

## HYDROGEN EXCHANGE IN BENZYL MERCAPTAN STUDIED BY NUCLEAR MAGNETIC RESONANCE

By M. Sheinblatt and Z. Luz

*Weizmann Institute of Science, Rehovoth, Israel*

*Received November 20, 1961*

Relatively few works were published on the exchange reactions of sulfur-bonded hydrogen. Hobden, *et al.*,[1] measured the distribution coefficient of hydrogen between ethyl mercaptan and water, but the kinetics and mechanisms of the exchange were not studied. Geib[2] showed that the rate of exchange of deuterium between $H_2S$ and methanol is measurable only below −80°. In the present note a study on the hydrogen exchange in benzyl

(1) F. W. Hobden, E. F. Johnston, L. H. P. Weldon, and C. L. Wilson, *J. Chem. Soc.*, 61 (1939).

(2) K. H. Geib, *Z. Elektrochem.*, **45**, 648 (1939).

mercaptan (B.M.) by the n.m.r. technique[3] is described.

The n.m.r. spectrum of neutral B.M. consists of a doublet due to the methylene group, a triplet due to the thiol group, and a single line due to the aromatic protons. The spectra of the methylene and thiolic group show a second-order splitting, since the spin–spin interaction is not negligible in comparison to the chemical shifts of the two groups. The addition of both acid and base to neutral B.M. causes the resonance lines of the methylene and the thiol to broaden. These changes in the line shape can be interpreted in terms of the average lifetime, $\tau$, of the thiolic hydrogen between successive exchanges. In practice only the methylene doublet was used.[4]

Pure B.M. was purchased from Fluka A. G. and was distilled in vacuum under nitrogen. No degassing of the samples was carried out before use. Acidic solutions of B.M. were prepared by dissolving anhydrous silver perchlorate in neutral B.M. The resulting precipitate of silver salt was removed by several centrifugations and the titers of the supernatants were determined by titration against an aqueous-ethanol solution of NaOH using thymol blue as indicator. Basic solutions of B.M. were prepared by the addition of known quantities of Triton B (benzyltrimethylammonium hydroxide) solution in methanol to neutral B.M. These solutions contained, therefore, certain amounts of $CH_3OH$, about 0.5% by volume for the most basic solution studied.

N.m.r. spectra of these solutions were recorded and the line shape interpreted to give values for the specific rate of exchange of the thiolic hydrogen, $1/\tau$. (For definition of specific rate see ref. 5).

The experimental results show that $1/\tau$ increases linearly with the acid concentration, being practically zero for neutral B.M. This behavior can be explained in terms of the reaction

$$C_6H_5CH_2SH_2^+ + C_6H_5CH_2SH \xrightarrow{k_I} C_6H_5CH_2SH + C_6H_5CH_2SH_2^+ \quad (1)$$

The slope of the line describing the dependence of $1/\tau$ upon the acid concentration gives $k_I$. It was found that

$$k_I = 1.35 \times 10^2 (M^{-1}\ \text{sec.}^{-1})$$

The results for the basic range show that the addition of base, up to $1.2 \times 10^{-3}$ $M$, does not affect the spectra of B.M. Further addition of base results in the broadening of the lines of the spectra. $1/\tau$ calculated from the line shape is linearly dependent on the base concentration in excess of $1.2 \times 10^{-3}$ $M$. The exchange reaction in basic solution is

$$C_6H_5CH_2S^- + C_6H_5CH_2SH \xrightarrow{k_2} C_6H_5CH_2SH + C_6H_5CH_2S^- \quad (2)$$

There are however two experimental difficulties in obtaining the rate constant of this reaction. (a) Basic solutions of B.M. are unstable. This is manifested by changes with time of the line shape of the resonances of both the thiol and methylene groups in basic solutions of B.M. Triton B solutions were found to be more stable than other bases tried ($CH_3ONa$ and $C_6H_5CH_2SK$). (b) The fact that the addition of less than $10^{-3}$ $M$ of base does not affect the rate of exchange can be attributed to the presence of a small amount of acidic impurities ($\approx 10^{-3}$ $M$) in the original B.M. This assumption is supported by experiments with B.M. that was first kept for several hours over anhydrous $K_2CO_3$. In this case the intercept was much closer to zero but on the other hand these solutions were more unstable and therefore could not be studied quantitatively. The slope of $1/\tau$ as a function of base concentration above $10^{-3}M$ of base is used as an approximate measure of the rate constant of reaction 2, giving $k_2 \sim 6 \times 10^5$ $M^{-1}$sec.$^{-1}$.

The above interpretation of the experimental results could in principle be checked by conductance measurements in B.M. solutions; however, such measurements were not carried out.

(3) J. A. Pople, W. G. Schneider, and H. J. Bernstein, "High-resolution Nuclear Magnetic Resonance," McGraw-Hill Book Co., Inc., New York, N. Y., 1959, p. 454.

(4) A. Loewenstein and S. Meiboom, *J. Chem. Phys.*, **27**, 1067 (1957).

(5) Z. Luz, D. Gill, and S. Meiboom, *ibid.*, **30**, 1540 (1959).

## PHOTO-INDUCED BINDING OF FLUORESCEIN DYES TO ZINC OXIDE[1]

By Gerald Oster and Mark Wasserman[2]

*Department of Chemistry, Polytechnic Institute of Brooklyn, Brooklyn, N. Y.*

*Received January 5, 1962*

During the course of studies in the binding of dyes to solid substrates we noticed that for fluorescein and its halogenated derivatives the rate of binding is considerably increased if the dye is illuminated by visible light. The effect is particularly noticeable with zinc oxide powder as the substrate although, as will be demonstrated, the effect does not arise from the photochemical properties of the substrate itself.

It is the purpose of the present paper to describe some of the kinetic aspects of this unusual reaction. In particular, we are concerned with which excited state of the dye is involved in the reaction. The kinetics of photoreduction of fluorescein and its halogenated derivatives[3,4] have established that the long-lived (probably triplet) state of the excited dye is responsible for the electron abstraction from the mild reducing agent present during the photoreduction. As will be seen, the same excited state is involved in photobinding to solid surfaces. Those substances which retard photoreduction also retard photobinding and in the same quantitative manner.

### Experimental

Materials.—Fluorescein and its halogenated derivatives were sodium salts obtained from Fisher Scientific (National Aniline, histological grade). Most of the quantitative studies were carried out with rose bengal (2′,4′,5′,7′-tetraiodo-3,4,5,6-tetrachlorofluorescein).

(1) Presented at the New York–New Jersey Regional Meeting of the American Chemical Society, January 22, 1962. Supported in part by the United States Air Force through the Air Force Cambridge Contract No. 19(604)-3065.

(2) On the National Science Foundation Summer Chemistry Program of the Polytechnic Institute of Brooklyn while a senior at the Brooklyn Technical High School.

(3) G. Oster and A. H. Adelman, *J. Am. Chem. Soc.*, **78**, 913 (1956).

(4) A. H. Adelman and G. Oster, *ibid.*, **78**, 3977 (1956).

The zinc oxides employed were of two types; one is Analytical Reagent from Mallinckrodt Chemical Company and the other is Florence Green Seal 8 obtained from the New Jersey Zinc Company. This latter material is made by heating zinc oxide in the presence of zinc vapor. With the use of wire meshes only particules between mesh sizes No. 100 to No. 200 where chosen (approximate mean diameter of zinc oxide particles 110 $\mu$). Aluminum oxide ("activated alumina") was obtained from Alcoa. All other chemicals were Eastman C.P. grade.

The nitrogen employed is prepurified Airco and further purified to remove any traces of oxygen by passing through a chromous chloride solution.

**Procedure.**—All dye solutions were made up in 0.1 *M* phosphate buffer at pH 7.0. The solid substrate powder was introduced into the cylindrical reaction cell (10 cm. high and 5 cm. diameter) fitted with a polyethylene cap to allow nitrogen to be bubbled through the suspension. The bubbling was carried out 15 min. prior to and during the irradiation so as to agitate the suspension as well as to flush the system free of oxygen.

The cell was illuminated with a 500-watt tungsten lamp slide projector provided with the appropriate filters. Using a green interference filter (Baird Associates) which is 80% transmitting at its peak (539 m$\mu$) it was found with a calibrated thermopile (Eppley Laboratories) that the intensity of light falling on the cell is $9.2 \times 10^{-9}$ einsteins/cm.$^2$/sec.

After illumination of the system for a particular period, the samples were centrifuged at 3000 r.p.m. for 30 min. so as to obtain a clear, non-turbid supernatant above the colored ZnO sediment. The optical density of the carefully removed supernatant was determined in a Carey Model 14 spectrophotometer.

In one experiment the system was illuminated with a medium pressure mercury lamp (General Electric AH4) fitted with a Wood's glass filter to isolate the 365 m$\mu$ line.

All the above solutions were in 0.1 *M* phosphate buffer at pH 7.0.

## Results

In the concentrations employed (below $10^{-4}$ *M*) all the dyes obey Beer's law. In the absence of light, rose bengal and the other fluorescein dyes do not adsorb to zinc oxide over the time periods (up to 4 hr.) involved in the present work. With orange light (obtained with a Corning No. 3486 filter which cuts off light below 520 m$\mu$) there is a considerable photobinding effect as manifested by a decrease in optical density of the supernatant of the centrifuged sample. Resuspending the dyed solid particles and heating the system at 100° for 1 hr. gave practically 100% recovery of the adsorbed dye, the dye being unchanged in spectrum.

Under green monochromatic light at 539 m$\mu$ (the dye absorbs maximally at 548 m$\mu$ with a molar extinction coefficient of $8.5 \times 10^4$) it was established that the quantum yield for disappearance of the dye, averaged over 1 hr. of illumination, is $1.2 \times 10^{-4}$. This value is only approximate since the powder (Analytical Reagent grade ZnO, 1.5 mg./ml.) scatters light and considerably complicates the photometry of the system.

The rate of photobinding is proportional to the zinc oxide content up to about 1.5 mg./ml., after which it appears to be insensitive to the concentration of powder present.

Trace amounts (of the order of $10^{-5}$ *M*) of potassium iodide and *p*-phenylenediamine retard the reaction. The rate is reduced to one-half its normal value in the presence of $1.0 \times 10^{-4}$ *M* KI. Less than one-hundredth this concentration of *p*-phenylenediamine was equally effective.

Qualitatively similar results to those described above were obtained for other members of the fluorescein family (using the appropriate transmitting filters) including erythrosin B, phloxine B, eosin Y, and fluorescein along with its dihalogenated derivatives. On the other hand, no member of the thiazine, acridine, or azo families of dyes of the many examined were found to give the photobinding effect.

Bubbling a 50–50 mixture of oxygen and nitrogen through the illuminated solution resulted in a decreased optical density, but this is due entirely to irreversible photooxidation of the dye since the result was independent of the presence of zinc oxide.

Ultraviolet irradiation with 365 m$\mu$ where the dye does not absorb appreciably gave no reaction. This was the case for both types of zinc oxide. When an aqueous suspension of zinc oxide in water is illuminated with ultraviolet radiation in the presence of oxygen, hydrogen peroxide is produced.[5] However, in our case, the absence of oxygen, due to the constant flushing with nitrogen, prevents this reaction from occurring.

The zinc oxide powders were subjected to high vacuum with heating to remove gases and then used for the dye studies. It was found that the rate of binding was unaffected by such treatment.

Aluminum oxide served equally well as zinc oxide for the photobinding studies.

Illumination with orange light of rose bengal and of zinc oxide under nitrogen prior to their mixture, produced no effect unless the mixture was further illuminated.

## Discussion

The photobinding effect does not involve the photoexcitation of the solid substrate. Although certain zinc oxides are photoconductors, their spectral sensitivity[6,7] generally lies at shorter wave lengths than the light employed to excite rose bengal. Although the zinc oxide with excess zinc could be sensitive to blue light, the pure zinc oxide would be sensitive only to ultraviolet light. Furthermore it is unlikely that alumina would be sensitive to visible light, yet it was also a suitable substrate. Illumination with ultraviolet light undoubtedly excites both types of zinc oxide, but does not produce photobinding.

The photoconduction of zinc oxides can be sensitized by dyes.[8,9] Photobinding is apparently unrelated to this phenomenon in that in our case the dye is not initially adsorbed to the solid. Furthermore, dye-sensitized photoconductivity can be carried out with dyes such as methylene blue and acriflavine which we found exhibit no photobinding.

The retardation of photobinding with small concentrations of potassium iodide and especially of *p*-phenylenediamine clearly indicates that the long-lived excited species of the dye is involved in the reaction.[3,4] The Stern–Volmer quenching con-

(5) M. C. Markham and K. J. Laidler, *J. Phys. Chem.*, **57**, 363 (1953).

(6) P. Miller in "Semiconducting Materials," Butterworths, London, 1951.

(7) R. Arneth quoted by G. Heiland, E. Mollwo, and F. Stöckman in Vol. 8 of "Solid State Physics" F. Seitz and D. Turnbull, Ed., Academic Press, New York, N. Y., 1959.

(8) E. K. Putseiko and A. N. Terenin, *Dokl. Akad. Nauk SSSR*, **90**, 1005 (1953).

(9) C. J. Young and H. G. Greig *R.C.A. Rev.*, **15**, 469 (1954).

stant for the long-lived excited state was found to be $1.0 \times 10^7$ l./mole. The lifetime is computed to be $1.5 \times 10^{-3}$ sec. assuming that every diffusional encounter ($6.6 \times 10^9$/sec./l. for a 1 *M* solution) between quencher and excited molecule is effective. It is significant that the concentrations of retarders for this reaction are close to those for the retardation of the photoreduction of the fluorescein-type dyes. It appears that the triplet species of these dyes have a strong affinity for the solid substrates. Thionine dyes in the long-lived state undergo certain photochemical reactions when bound to specific high polymers.[10] In the present case, however, the long-lived species wanders through the solution until it encounters a solid particle; failing such an encounter during 1 msec. it drops to the ground state. This may account for the low quantum yield of photobinding for rose bengal. This is approximately $^1/_{300}$ that of the maximum (extrapolated to infinite reducing agent concentration) for photoreduction.

Increasing the amount of zinc oxide should increase the chance of such an encounter and hence, increase the rate of the reaction. However, the system is unaffected by concentrations of the powder beyond 1.5 mg. per ml. due to the light scattering by the suspended substrate which decreases the amount of light allowed into the solution.

For zinc oxide powder of this mesh size, the surface area is estimated from extrapolation of published data on zinc oxide powder[11] to be about 100 cm.$^2$/g. For a 10-ml. solution of rose bengal at $10^{-5}$ *M* in the presence of 15 mg. of zinc oxide, complete binding takes place with prolonged illumination. That is, $4 \times 10^{16}$ molecules are bound per cm.$^2$ of surface. Since the dye molecules occupy an area of the order of 100 Å.$^2$, it is obvious that multilayer adsorption occurs. Apparently the light-excited dye has an affinity for solids coated with adsorbed dye as well as for the original solid substrates.

(10) N. Wotherspoon and G. Oster, *J. Am. Chem. Soc.*, **79**, 3992 (1957).

(11) C. W. Siller, *ibid.*, **65**, 431 (1943).

## RADIOLYSIS OF TOLUENE: MECHANISM OF FORMATION OF BENZYL RADICALS

BY L. H. GALE, B. E. GORDON, G. STEINBERG, AND C. D. WAGNER

*Shell Oil Company, Martinez, California, and Shell Development Company, Emeryville, California*

*Received January 11, 1962*

Toluene in the liquid phase reacts under ionizing radiation to give hydrogen and polymeric products. The dimeric materials have been shown by Hoigné and Gäumann[1] to consist of bibenzyl, the benzyltoluenes, and the six bitolyls. Bridge[2] and Chilton and Porter[3] have shown that ionizing radiation acting on toluene in a solid matrix at low temperature generates benzyl radicals, and the bibenzyl appears to be formed by combination of the benzyl radicals.[1] When isolated molecules of toluene in the gas phase are ionized by energetic electrons in a mass spectrometer, the principal fragment ion is the cyclic tropylium ion, $C_7H_7^+$, as shown by Meyerson and Rylander.[4] (They found by isotopic means that the probability of loss of the single hydrogen to form the ion is the same for all types of hydrogen on toluene, and that all carbon atoms in the $C_7H_7^+$ ion are equivalent.)

Although at 25° some of the benzyl radicals are undoubtedly formed by hydrogen abstraction by tolyl radicals,[1] they also must be formed by a direct process. They may be formed directly by detachment of an alpha hydrogen from an excited toluene molecule, as in (a), or by rearrangement of the tropylium ion on neutralization by an electron, as

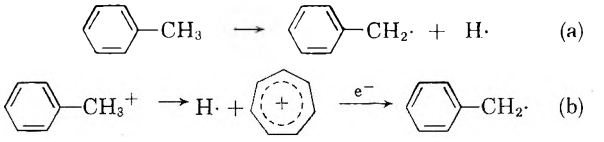


in (b). In the present study, toluene-$\alpha$-$C^{14}$ was irradiated with 3 Mev. electrons in order to differentiate between these paths of reaction.

### Experimental

A sample of two microcuries of toluene-$\alpha$-$C^{14}$ (Research Specialties Co., Richmond, California) was diluted with 71 g. of research grade toluene, and placed in a circulation system containing an irradiation cell.[5] The cell was cooled to −30° and degassed by successive addition and removal of dry, oxygen-free nitrogen while the liquid was circulated through the cell.

The irradiation was conducted with a 45-$\mu$amp. 3-Mev. electron beam, collimated by a 1/2 in. o.d. pipe before striking the thin window of the cell. An irradiation time of 4800 sec. gave an estimated dose of $8 \times 10^8$ rad.

Toluene was separated from the heavier material by distillation, and the dimer fraction was recovered from the residue by several gas chromatographic separations on a 6-mm. diameter × 1.5 m. silicone column at 170°.

The recovered fraction (151 mg.) was diluted with 299 mg. of bibenzyl (Eastman Kodak White Label) and oxidized by chromic acid. The resulting benzoic acid was purified by sublimation, yielding 307 mg. of material (51%). Most of this (274 mg.) was degraded by the Schmidt reaction to aniline (86%) and carbon dioxide (82%), which in turn were converted to acetanilide and barium carbonate.

TABLE I

SPECIFIC ACTIVITIES OF SCHMIDT DEGRADATION PRODUCTS

| Starting material | Products | μc./mole |
|---|---|---|
| Bibenzyl–benzyl-toluene-bitolyl | Benzoic acid | 0.42 ± 0.03 |
| | Acetanilide | 0.000 ± 0.0015 |
| | Barium carbonate | 0.37 ± 0.01 |
| Toluene | Benzoic acid | 2.47 |
| | Acetanilide | 0.000 ± 0.0051 |
| | Barium carbonate | 2.21 |

### Results and Discussion

The benzoic acid was derived solely from the bibenzyl, since the dimeric acids from the other dimers were discarded. All of the activity was found in the carboxyl carbon. The reduced specific activity in the carbon dioxide may be due to dilution of the sample by atmospheric carbon dioxide

(1) J. Hoigné and T. Gäumann, *Helv. Chim. Acta.*, **44**, 2141 (1961).

(2) N. K. Bridge, *Nature*, **185**, 30 (1960).

(3) H. T. Chilton and G. Porter, *J. Phys. Chem.*, **63**, 904 (1959).

(4) S. Meyerson and P. N. Rylander, *J. Am. Chem. Soc.*, **79**, 842 (1957); *J. Chem. Phys.*, **27**, 901 (1957).

(5) The apparatus was described previously: C. D. Wagner, *J. Phys. Chem.*, **64**, 231 (1960).

or self-absorption in the barium carbonate suspension counting technique.

The absence of activity in the ring excludes a symmetrical intermediate such as the tropylium ion in the formation of benzyl radicals in the liquid phase. Therefore, it is concluded that the direct mechanism for formation of benzyl radicals is by direct C–H scission and does not involve tropylium ion.

A check was made on the possibility that rearranged toluene could be found in the radiolysis. Oxidation of a sample of the toluene following radiolysis, and measurement of the activity in the ring and carboxyl by the same method, gave an upper limit of $G = 0.025$ for such a rearrangement reaction.

## FREE ENERGY OF FORMATION OF MOLYBDENUM OXIDE AND CARBIDE

By Molly Gleiser and John Chipman

*Department of Metallurgy, Massachusetts Institute of Technology, Cambridge, Mass.*

*Received January 18, 1962*

Despite their growing importance as useful materials, little has been learned concerning the thermodynamic properties of the metallic carbides. A knowledge of their free energies at elevated temperature need not await the results of calorimetric investigations since in many cases it is possible to obtain dependable values through simple equilibrium measurements. This paper presents the results of such a study.

When a metal and two other solid phases comprising its oxide and carbide are brought into equilibrium with a gas phase, the free energies of formation of both the oxide and the carbide are determined by the partial pressures of CO and $CO_2$ and their known thermodynamic properties. If the free energy of formation of the oxide is known, a simple measurement of the total pressure fixes that of the carbide. The oxide and carbide must be in general the most metal-rich stable compositions of the system and the solubility of each in the metal must be small. In the case of molybdenum, this last requirement is filled.[1] The oxide phase is $MoO_2$, while the carbide is the metal-rich extreme of the solid solution the composition of which varies from $Mo_{2.21}C$ to $Mo_{1.98}C$. This nonstoichiometric composition[2-4] will be designated "$Mo_2C$" for present purposes, and its molar thermodynamic properties will be taken as those associated with 1 g.-atom of C.

**Method.**—The apparatus consisted of a gas-tight porcelain tube, closed at one end, and resting inside a platinum-wound furnace. The rest of the apparatus was made entirely of Pyrex glass, fused to the porcelain tube. It comprised a mercury manometer, a vacuum tap, and a ground-glass stopper *via* which specimens would be inserted. It was found that with the system evacuated no change in pressure could be detected by the mercury manometer over a 24-hr. period. One day was roughly the time taken for an experiment. The temperature was measured and controlled with a platinum–rhodium thermocouple placed outside the reaction chamber, which had been shown to agree with another couple inside the chamber. Both couples were accurate within 2° at the melting point of Au.

The sample consisted of Mo, $MoO_2$, and "$Mo_2C$," whose X-ray diffraction patterns gave no indication of any impurities. Complete dissolution of "$Mo_2C$" in nitric acid indicated the absence of carbon. These were intimately mixed together, pressed into a pellet, and put on a piece of molybdenum foil in an alumina boat. This was placed in the reaction chamber, which was evacuated and closed. The sample was heated to about 850°. The gas evolved was pumped off and the sample left at this temperature for 2 days. A further small amount of gas was evolved and this also was pumped off. This procedure removed water vapor and other extraneous gases from the system.

The sample was heated to a fixed temperature and readings of the mercury manometer were taken until a constant pressure was reached. The temperature was raised slightly in order to increase the gas pressure, dropped back to its original value, and a new constant pressure obtained. The equilibrium lies between these two pressures. The system then was completely evacuated and the process repeated, the second equilibrium being always in excellent agreement with the first. This procedure removed any further gaseous impurities and indicated the independence of the equilibrium pressure upon composition of the sample.

An X-ray diffraction pattern of the quenched sample at the end of the experiment showed only Mo, $MoO_2$, and "$Mo_2C$" present. Complete solution of the sample in nitric acid without residue indicated the absence of carbon.

A series of equilibrium pressures was obtained in this fashion at different temperatures from 926 to 1068°. During the first experiments an alumina rod was placed inside and along the porcelain reaction chamber. This was removed at the end of the experiment and examined visually for traces of carbon which could have formed by disproportionation of carbon monoxide, resulting in an alteration of the equilibrium pressure. Only the most minute traces of carbon were ever formed.

To obtain gas samples for analysis, the ground-glass stopper was replaced by a rubber stopper through which passed a thin silica sampling tube, one end of which was centered over the sample, the other end being connected to a sampling bulb. When the total pressure in the furnace became equal to the equilibrium pressure measured previously, a small gas sample was quickly withdrawn through the silica tube so that the equilibrium was not disturbed perceptibly. The sample was collected over a mercury reservoir and analyzed in an Orsat apparatus, using a standard procedure[5] in which the $CO_2$ was absorbed in a potassium hydroxide solution and the CO in an acid cuprous chloride solution. The samples were found to consist of CO and $CO_2$ and a small unanalyzed residue comprising always between 2 and 3% of the sample. The recorded partial pressures in Table I have been corrected accordingly, and the ratios $p_{CO_2}/p_{CO}$ have been used to obtain values of the free energy[6] shown in Fig. 1.

### Discussion

Complete thermodynamic data on $MoO_2$ were summarized in the recent work of King, Weller, and Christensen,[7] who based their free energy values entirely on calorimetric data. Earlier equilibrium studies of the reaction

$$MoO_2 + 2H_2 = Mo + 2H_2O$$

were reviewed by Gokcen[8] along with his own data on this equilibrium. Of the four sets of data con-

(1) M. Hansen, "Constitution of Binary Alloys," McGraw-Hill Book Co., New York, N. Y., 1958, p. 371.

(2) T. Takei, *Sci. Repts. Tohoku Imp. Univ.*, **17**, 939 (1928).

(3) A. Westgren and G. Phragmén, *Z. anorg. allgem. Chem.*, **156**, 27 (1926).

(4) W. P. Sykes, K. R. Van Horn, and C. M. Tucker, *Trans. Am. Inst. Min. Met. Engrs.*, **117**, 173 (1935).

(5) Burrell, "Manual for Gas Analysts," Catalogue No. 80, Burrell Technical Supply Co., Pittsburgh, Penna.

(6) "Selected Values of Chemical Thermodynamic Properties," Series III, Natl. Bur. of Standards, 1949.

(7) E. G. King, W. W. Weller, and A. U. Christensen, Bureau Mines Rept. Investigations 5664, 1960.

(8) N. A. Gokcen, *Trans. Am. Inst. Min. Met. Engrs.*, **197**, 1019 (1953).

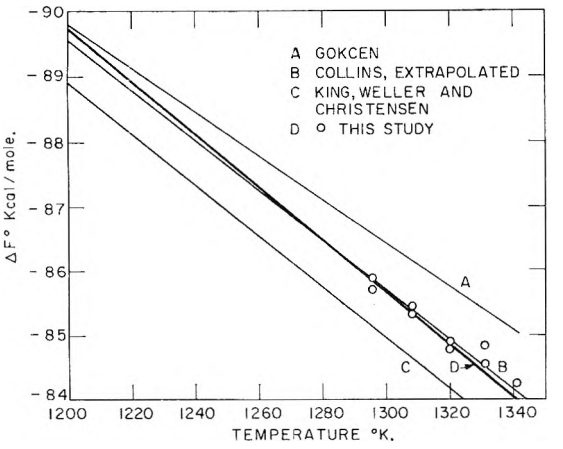


Fig. 1.—Free energy of formation of $MoO_2$.

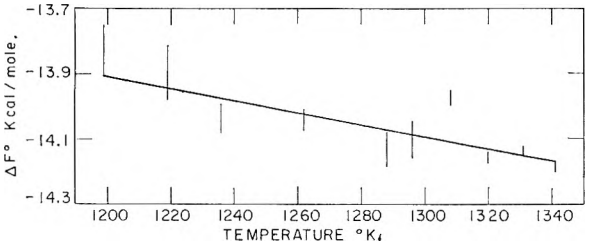


Fig. 2.—Free energy of formation of $Mo_2C$.

sidered, only that of Collins[9] has a slope nearly compatible with the calorimetric value for the entropy.

TABLE I

GASEOUS EQUILIBRIA WITH $MoO_2$–Mo–"$Mo_2C$"

| Temp., °K. | Corrected pressures, mm. $p_{CO} + p_{CO_2}$ | $p_{CO_2}/p_{CO}$ |
|---|---|---|
| 1199 | 64.0–68.4 | ... |
| 1219 | 91.9–97.6 | ... |
| 1236 | 121.8–126.3 | ... |
| 1262 | 195.7–200.1 | ... |
| 1288 | 296.8–308.5 | ... |
| 1296 | 342.1–356.8 | 0.393–0.405 |
| 1308 | 444.6–452.8 | .389–.399 |
| 1320 | 507.0–513.5 | .399–.406 |
| 1331 | 610.1–617.1 | .372–.391 |
| 1341 | 703.7–708.6 | .387 |

The agreement among the several sets of data shown in Fig. 1 is fairly good, especially at the lower temperatures. Our data are represented best by line D, whose slope is based on the calorimetric entropies. Its equation for the range 1200–1350°K. is

$$MoO_2;\ \Delta F_f^0 = -137{,}890 + 40.18T \text{ cal./mole}$$

On the same basis its heat of formation at 298.15°K. is −141.5 kcal./mole. The corresponding calorimetric value[6] is −140.8 kcal./mole.

The free energy of formation of "$Mo_2C$" has been determined by Schenck, Kurzen, and Wesselcock[10] and by Browning and Emmett.[11] The method of Schenck, *et al.*, consisted in determining the equilibrium of the system, Mo–$CH_4$–$H_2$–"$Mo_2C$." Unfortunately they used a static system in which considerable thermal segregation of the gases must have occurred. This was evidenced by the fact that their measurements of the C–$H_2$–$CH_4$ equilibrium by the same method are not in agreement with the presently accepted data for this system. Browning and Emmett[11] studied the same equilibrium using a dynamic method. Their results lead to an impossibly large entropy change of about 26 e.u. for the reaction 2Mo(s) + C(s) = $Mo_2C$(s).

The observed total pressures of Table I and values of $p_{CO_2}/p_{CO}$ read from the experimental data represented by line D of Fig. 1 yield values for the free energy of formation of "$Mo_2C$" shown in Fig. 2. Here, as before, "$Mo_2C$" signifies the Mo-rich extremity of the solid solution field including that composition. The results in the range 1200–1340°K. are given by

$$\text{"}Mo_2C\text{"};\ \Delta F_f^0 = -11{,}710 - 1.83T \text{ cal.}$$

In the absence of other data on this compound, these figures may be used as roughly valid at lower temperatures and the heat of formation as approximately −11.7 kcal.

**Acknowledgments.**—The authors wish to thank the National Science Foundation for sponsoring this project, John C. d'Entremont for assistance in constructing and controlling a furnace, and Frank Haynes, without whose sarcasm and wit this work would not have been carried out.

(9) B. T. Collins, Sc.D. Thesis, Massachusetts Institute of Technology, Cambridge, Mass., June, 1949.

(10) R. Schenck, F. Kurzen, and H. Wesselcock, *Z. anorg. allgem. Chem.*, **203**, 159 (1932).

(11) L. C. Browning and P. H. Emmett, *J. Am. Chem. Soc.*, **74**, 4773 (1952).

## THE DIFFUSION OF THIOUREA IN WATER AT 25°

BY DAVID B. LUDLUM, ROBERT C. WARNER, AND HOMER W. SMITH[1]

*Department of Physiology and Biophysics and Department of Biochemistry, New York University School of Medicine, New York, N. Y.*

*Received January 19, 1962*

Interest in the penetration of biological membranes by urea and thiourea has led us to search the literature for values of the diffusion coefficients of these compounds. Although excellent data are available for urea,[2,3] no comparable information appears to have been published for thiourea. Therefore, the diffusion coefficient of this compound has been obtained as a function of concentration and a comparison has been made with similar data for urea. This comparison is related to differences in other properties of these compounds known to affect diffusion and permeation.

### Experimental

**Diffusion Measurements.**—All measurements were made on a parallel beam Gouy diffusion apparatus described in a preceding publication.[4] Design and operation of such

(1) This investigation was supported in part by the New York Heart Association, the National Science Foundation, and PHS Research Grant RG-6967.

(2) L. J. Gosting and D. F. Akeley, *J. Am. Chem. Soc.*, **74**, 2058 (1952).

(3) D. F. Akeley and L. J. Gosting, *ibid.*, **75**, 5685 (1953).

(4) R. C. Warner, *J. Biol. Chem.*, **229**, 711 (1957).

equipment has been reviewed recently by Gosting,[5] and standard technique was used throughout.

Green light from an AH-4 mercury lamp was isolated with a Wratten 77-A filter. The optical distance, $b$, was determined for this wave length by measuring the deviation of the slit image resulting from the introduction of a small glass prism at the angle of maximum deviation in the position of the diffusion cell. The optical properties of the prism itself were determined independently on two separate occasions by its manufacturer, the Perkin-Elmer Corporation, on their Guild-Watts spectrometer. The cell thickness, $a$, was determined by direct measurement with a traveling microscope.

Experiments were performed at 25.00° in a thermostat controlled to within ±0.002°. Temperature was determined on a thermometer calibrated against a National Bureau of Standards resistance thermometer.

Diffusion was carried out in a Tiselius cell with reference windows for Rayleigh optics. After an hour had been allowed for thermal equilibration, a boundary was formed between the more concentrated solution on the bottom and the less concentrated solution on the top. Then the boundary was sharpened through a fine glass capillary siphon for 30 to 60 min. under observation through the Rayleigh system.

Time was recorded from the moment when siphoning was discontinued and the capillary withdrawn. From 10 to 15 Gouy photographs were obtained over a period of about 4 hr. in each experiment. Rayleigh photographs were taken during or shortly after completion of boundary sharpening for determination of the total fringe number, $J$, which was about 150 for the thiourea experiments.

The apparent diffusion coefficient, $D'$, was calculated from fringes 0 to 50 for each Gouy photograph, averaged, and plotted against the reciprocal of the elapsed time. Extrapolation to the $y$-axis then yielded a corrected value of the diffusion coefficient. The corresponding starting time correction was of the order of 20 sec.

Solutions.—Highest purity thiourea from Eastman was recrystallized from reagent grade methyl alcohol and dried to constant weight at 60° *in vacuo*. Its melting point was 178–179° with some slight decomposition. Reagent grade urea, similarly recrystallized (melting point 132.5–132.9°) and reagent grade sucrose were used for standard diffusion experiments. All solutions were made up to volume in calibrated glassware with air-saturated distilled water.

## Results

Optical constants and results from standard diffusion experiments are given in Table I below. Experiments with thiourea are summarized in Table II. In these tables, $C_1$ and $C_2$ are the concentrations of the more dilute and more concentrated solutions, respectively, in moles per liter; $\Delta n/\Delta C$ is the refractive index increment for $\lambda$ = 5461 Å.; and $D$ is the diffusion coefficient corrected by extrapolation to $1/t = 0$.

TABLE I

CALIBRATION OF DIFFUSION EQUIPMENT

Optical constants: $a$ = 2.5065 ± 0.0005 cm.; $b$ = 148.01 ± 0.08 cm. Standard diffusion experiments at 25.00°

| | Sucrose | Urea |
|---|---|---|
| $C_1$, moles/l. | 0 | 0 |
| $C_2$, moles/l. | 0.043784 | 0.25018 |
| $\Delta n/\Delta C$, l./mole | $4.895 \times 10^{-2}$ | $8.594 \times 10^{-3}$ |
| $\Delta n/\Delta C$, lit. value | $4.895 \times 10^{-2}$[6] | $8.602 \times 10^{-3}$[2] |
| $D$, cm.²/sec. | $5.140 \times 10^{-6}$ | $1.365 \times 10^{-5}$ |
| $D$, lit. value | $5.170 \times 10^{-6}$[3] | $1.371 \times 10^{-5}$[2] |

Data from Table II are plotted in Fig. 1, together with corresponding data for urea from reference 2. Also plotted in the same figure are points calculated from the theoretical equation $D = D_0 (1 + C\,\partial \ln y/\partial C)$, where $D_0$ is the diffusion coefficient at infinite dilution and $y$ is the activity coefficient on the $C$ scale referred to infinite dilution. These points are taken from Gosting and Akeley's paper on urea and calculated from the thermodynamic data of Redlich, *et al.*, for thiourea.[2,7]

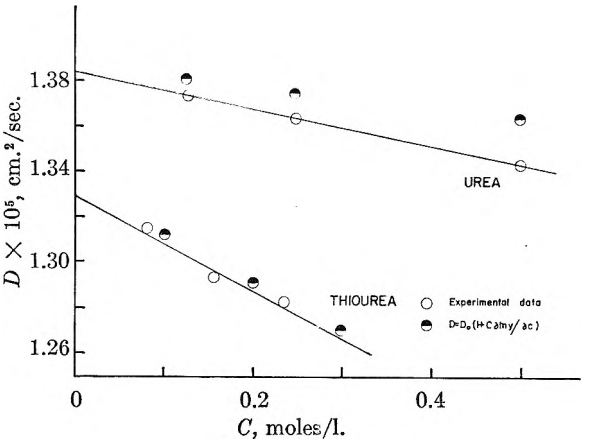


Fig. 1.—Dependence of diffusion coefficient on concentration at 25°; data for urea taken from work of Gosting and Akeley.[2]

TABLE II

DIFFUSION OF THIOUREA IN WATER AT 25.00°

| $C_1$, moles/l. | $C_2$, moles/l. | $\overline{C}$, moles/l. | $\Delta n/\Delta C$, l./mole | $D$, cm.²/sec. |
|---|---|---|---|---|
| 0 | 0.15775 | 0.07887 | $2.038 \times 10^{-2}$ | $1.314 \times 10^{-5}$ |
| .07887 | .23662 | .15775 | $2.035 \times 10^{-2}$ | $1.294 \times 10^{-5}$ |
| .15775 | .31549 | .23662 | $2.035 \times 10^{-2}$ | $1.283 \times 10^{-5}$ |

## Discussion

The first point to be considered is the calibration of the apparatus. As indicated in Table I, diffusion coefficients have averaged 0.6% lower than values reported in the literature for convergent beam equipment. The optical distance, $b$, which enters as a squared term in the calculation of the diffusion coefficient, is the factor most likely to be involved in such a difference. Accordingly, the constants of the glass prism used to calibrate the equipment were redetermined. Substitution of the confidence limits on these values leads to an estimate of $b$ good to within 0.05%. It seems unlikely, therefore, that this difference has resulted from an incorrect determination of the properties of the prism, but no other explanation has been forthcoming.

Physical constants for urea and thiourea are compared below in Table III.

Longsworth[10] recently has discussed the molecular parameters affecting the extrapolated diffusion coefficient, $D_0$. To the extent that small molecules follow the Stokes–Einstein relationship, the product, $D_0 \bar{V}_2^{1/3}$, is a constant independent of the nature of the solute. In practice, as Longsworth has shown, values of $D_0 \bar{V}_2^{1/3}$ increase linearly with $D_0$ for a variety of simple sugars, amino acids, and other compounds.

Among similar substances, an increase in hydration accompanying an increase in polarity or an in-

(5) L. J. Gosting in M. L. Anson, K. Bailey, and J. T. Edsall, ed., "Advances in Protein Chemistry," Vol. XI, Academic Press, Inc., New York, N. Y., 1956, p. 429.

(6) J. M. Creeth, *J. Phys. Chem.*, **62**, 66 (1958).

(7) O. Redlich, C. M. Gable, L. T. Beason, and R. W. Millar, *J. Am. Chem. Soc.*, **72**, 4161 (1950).

(8) "International Critical Tables," Vol. III, McGraw-Hill Book Co., Inc., New York, N. Y., 1928, p. 111.

TABLE III

| | Urea | Thiourea |
|---|---|---|
| Molecular weight | 60.05 | 76.12 |
| $\bar{V}_2$, cc./mole | 44.2[2] | 53.6[8] (at 15°) |
| Dipole moment in dioxane, Debye units[9] | 4.56 | 4.89 |
| $D_0$, cm.²/sec. | $1.382 \times 10^{-5}$ | $1.329 \times 10^{-5}$ |
| $D_0\bar{V}_2^{1/3}$ | 48.9 | 50.3 |

crease in asymmetry lowers the $D_0\bar{V}_2^{1/3}$ product. When urea and thiourea are compared on this basis, the increase in partial molar volume of thiourea over urea is paralleled by a decrease in the diffusion coefficient. However, the $D_0\bar{V}_2^{1/3}$ product is larger for thiourea in spite of its lower diffusion coefficient. This difference probably is not significant in terms of differences in hydration or symmetry.

The dependence of diffusion coefficient on concentration has been related to the dependence of activity coefficient and viscosity on concentration.[11,12] As shown in Fig. 1, good agreement is obtained with experimental data for thiourea with the equation: $D = D_0(1 + C\,\partial \ln y/\partial C)$, which would attribute the entire variation in diffusion coefficient to the thermodynamic term, $C\,\partial \ln y/\partial C$. Actually, this agreement probably is partly fortuitous in that changes in viscosity of the solution have been neglected in the equation.

(9) W. D. Kumler and G. M. Fohlen, *J. Am. Chem. Soc.*, **64**, 1944 (1942).

(10) L. G. Longsworth in T. Shedlovsky, "Electrochemistry in Biology and Medicine," John Wiley and Sons, Inc., New York, N. Y., 1955, p. 225.

(11) L. Onsager and R. M. Fuoss, *J. Phys. Chem.*, **36**, 2689 (1932).

(12) A. R. Gordon, *J. Chem. Phys.*, **5**, 522 (1937).

## BINDING ENERGIES OF THE GASEOUS ALKALINE EARTH HALIDES[1]

BY THOMAS E. BRACKETT AND ELIZABETH B. BRACKETT

*Department of Chemistry, William Marsh Rice University, Houston, Texas*

*Received January 19, 1962*

Cubicciotti[2] has calculated the binding energies of the gaseous alkaline earth halides, using Rittner's[3] method. This calculation, which is based on an ionic model, generally includes a term of the form $Ae^{-r/\rho}$ for the repulsion energy. The agreement of these calculations with experimental values was not satisfactory. However, Cubicciotti showed that the substitution of an $Ar^{-n}$ term for the repulsion energy gave very good agreement. It seemed worthwhile to investigate the matter further, as the $Ae^{-r/\rho}$ form is generally found satisfactory for expressing repulsion energies.

The binding energy for an alkaline earth halide molecule, at 0°K., assuming a linear, ionic model, may be written as

$$W = -\frac{7}{2}\frac{e^2}{r} + 2\mu\left[-\frac{7}{4}\frac{e}{r^2} + \frac{\mu}{8r^3} + \frac{\mu}{2\alpha}\right] + Ae^{-r/\rho}$$

where $\alpha$ is the polarizability of the halide ion, $r$ is the internuclear distance, and $\mu$ the induced dipole moment at each halide ion. All terms higher than dipole terms have been neglected. The induced dipole moment is written

$$\mu = \alpha\left[\frac{7}{4}\frac{e}{r^2} - \frac{2\mu}{8r^3}\right]$$

The second term accounts for the effect of the induced dipole of one halide ion upon the electric field at the other halide ion.

The requirement $(dW/dr)_{r=r_0} = 0$ allows one to evaluate the term for the repulsion energy.

$$Ae^{-r/\rho} = \rho\left[\frac{7}{2}\frac{e^2}{r_0^2}\left(1 + \frac{7}{2}\alpha\frac{(16r_0^3 + \alpha)}{(4r_0^3 + \alpha)}\right)\right]$$

The additional requirement $d^2W/dr^2 = k$, where $k$ is the vibrational force constant for the stretching frequency, allows one to evaluate $\rho$ directly. However, for the four salts for which $k$ is known,[4,5] the $\rho$-values range from 0.34 to 0.52. It was decided to evaluate $\rho$ empirically using a single value, $\rho = 0.27$ Å., for all of the alkaline earth halides. Certainly a better agreement could be obtained if a slightly different value of $\rho$ was assigned for each halide ion, but other uncertainties in our calculation would make such a treatment unwarranted at this time.

The polarizabilities used are those calculated by Pauling[6] and the internuclear distances have been measured by Akishin and Spiridonov[7] by the electron diffraction method. Their estimated uncertainty in $r$ is 0.02 to 0.03 Å.

The calculated values for $W$, the binding energy, are shown in Table I, along with the recently revised experimental values.[8] The agreement is satisfactory, except for the beryllium halides. In this case one might expect a strictly ionic model to be inadequate. The results of both of Cubicciotti's calculations are included for comparison.

The major differences between our calculation and the calculation which Cubicciotti found to be unsatisfactory lie in (a) the inclusion of the dipole–dipole term in the energy, (b) different values for the polarizabilities, (c) different values for the parameter $\rho$, and (d) the inclusion of the term $\mu\alpha/4r^3$ in the calculation of the induced dipole moment. The effect of the dipole terms, (a) and (d), is not insignificant, amounting to 60 kcal. in some cases, down to 1 or 2 kcal. for others.

The choice of polarizabilities deserves some comment because the values used by Cubicciotti, calculated from the indices of refraction of alkali halide crystals,[9] are some 10 to 40% smaller than those calculated for the free ions by Pauling from the theory of the quadratic Stark effect. We have calculated the energy of the alkaline earth halides using the Tessman, Kahn, and Shockley values for the polarizabilities. The polarization terms in the energy are found to be lower, and the parameter $\rho$ must decrease accordingly. Thus the agreement with experimental values is about the same, as

(1) This research was supported by the National Aeronautics and Space Administration.

(2) D. Cubicciotti, *J. Phys. Chem.*, **65**, 1058 (1961).

(3) E. S. Rittner, *J. Chem. Phys.*, **19**, 1030 (1951).

(4) A. Buchler and W. Klemperer, *J. Chem. Phys.*, **29**, 121 (1958).

(5) S. P. Randall, F. T. Greene, and J. L. Margrave, *J. Phys. Chem.*, **63**, 758 (1959).

(6) L. Pauling, *Proc. Roy. Soc.* (London), **A114**, 191 (1927).

(7) P. A. Akishin and V. P. Spiridonov, *Kristallografiya*, **2**, 475 (1958).

(8) L. Brewer, G. R. Somayajulu, and E. Brackett, *Chem. Rev.*, in press.

(9) J. R. Tessman, A. H. Kahn, and W. Shockley, *Phys. Rev.*, **92**, 890 (1953).

TABLE I

ENERGIES (KCAL./MOLE) OF THE REACTION $MX_2(g) = M^{++}(g) + 2X^-(g)$ FOR THE ALKALINE EARTH HALIDES

| | Calcd.[a] | Exptl.[b] | Calcd.[c] | Calcd.[d] |
|---|---|---|---|---|
| $BeF_2$ | 741 | 773 | 662 | 748 |
| $BeCl_2$ | 715 | 683 | 623 | 707 |
| $BeBr_2$ | 678 | 660 | 606 | 675 |
| $BeI_2$ | 654 | 635 | 565 | 624 |
| $MgF_2$ | 599 | 615 | 560 | 591 |
| $MgCl_2$ | 549 | 543 | 511 | 533 |
| $MgBr_2$ | 524 | (522) | 490 | 513 |
| $MgI_2$ | 510 | 500 | 473 | 500 |
| $CaF_2$ | 509 | 522 | 484 | 502 |
| $CaCl_2$ | 465 | 460 | 442 | 455 |
| $CaBr_2$ | 447 | 443 | 426 | 438 |
| $CaI_2$ | 429 | (422) | 409 | 425 |
| $SrF_2$ | 487 | 490 | 465 | 482 |
| $SrCl_2$ | 434 | (437) | 416 | 427 |
| $SrBr_2$ | 419 | 417 | 402 | 413 |
| $SrI_2$ | 403 | (398) | 386 | 400 |
| $BaF_2$ | 462 | 469 | 445 | 463 |
| $BaCl_2$ | 409 | 414 | 393 | 404 |
| $BaBr_2$ | 392 | 394 | 377 | 389 |
| $BaI_2$ | 377 | (374) | 363 | 377 |

[a] This work. [b] These experimental values have been revised recently[8] and thus are different from those given by Cubicciotti. [c] Values calculated by Cubicciotti using an $Ae^{-r/\rho}$ repulsion term. [d] Values calculated by Cubicciotti using an $Ar^{-n}$ repulsion term.

long as $\rho$ assumes a value of 0.24 Å., instead of 0.27 Å. Cubicciotti used the values for $\rho$ determined[10] for the alkali halide crystals; 0.313 Å. for the fluorides, 0.318 Å. for chlorides, 0.325 Å. for bromides, and 0.332 Å. for iodides.

Apparently the binding energy for the gaseous alkaline earth halides can be successfully calculated on the basis of an ionic model, with the possible exception of the beryllium salts.

(10) D. Cubicciotti, *J. Chem. Phys.*, **31**, 1646 (1959); **33**, 1579 (1960).

## THE KINETICS OF THE DECARBOXYLATION OF OXANILIC ACID IN ETHERS AND IN THE MOLTEN STATE

BY LOUIS WATTS CLARK

*Department of Chemistry, Western Carolina College, Cullowhee, N. C.*

*Received January 20, 1962*

Kinetic studies have been reported previously on the decarboxylation of oxanilic acid in aniline,[1] *o*-toludine,[1] *o*-ethylaniline,[1] quinoline,[2] 8-methylquinoline,[2] anisole,[3] phenetole,[3] $\beta$-chlorophenetole,[3] and N,N-dimethylaniline.[3] In the aryl-alkyl ethers,[3] the reaction appeared to proceed by an activated-complex mechanism analogous to that which had been proposed previously for malonic acid.[4] The data for the reaction in aromatic amines, however, could not be reconciled with such a mechanism.[3]

In an effort to gain more insight into the unsolved problems connected with this reaction additional studies have been carried out in this Laboratory on the decarboxylation of oxanilic acid in the molten state, as well as in five additional solvents, *n*-butyl ether, *n*-amyl ether, *n*-hexyl ether, *bis*-(2-chloroethyl) ether, and dibenzyl ether. The results of this investigation are reported herein.

(1) L. W. Clark, *J. Phys. Chem.*, **65**, 572 (1961).
(2) L. W. Clark, *ibid.*, **65**, 1460 (1961).
(3) L. W. Clark, *ibid.*, **65**, 2271 (1961).
(4) G. Fraenkel, R. L. Belford, and P. E. Yankwich, *J. Am. Chem. Soc.*, **76**, 15 (1954).

### Experimental

**Reagents.**—Reagent grade oxanilic acid, 100.0% assay, was used in this research. The solvents were either reagent grade or highest purity chemicals. Immediately before the beginning of each experiment each solvent was distilled at atmospheric pressure, approximately 60 ml. of constant-boiling liquid being collected in the dried reaction flask.

**Apparatus and Technique.**—The apparatus and technique used in studying the decarboxylation of oxanilic acid in solution (involving measuring the volume in ml. of $CO_2$ evolved at different time intervals) has been described previously.[5] The temperature of the thermostat (controlled to within $\pm 0.05°$) was determined by means of a thermometer calibrated by the U. S. Bureau of Standards. The buret used to collect the evolved $CO_2$ likewise was calibrated by the Bureau of Standards. In each experiment a 0.2948-g. sample of oxanilic acid (the amount required to yield 40.0 ml. of $CO_2$ at STP on complete reaction) was introduced in the usual manner into the reaction flask containing about 60 ml. of solvent saturated with dry $CO_2$ gas.

The study of the decarboxylation of molten oxanilic acid was carried out in the same manner as was that of molten picolinic acid.[6]

### Results

The decarboxylation of oxanilic acid in the molten state as well as in the five ethers mentioned was studied at three different temperatures over approximately a 20° temperature interval. Duplicate experiments were performed at each temperature. The log $(V_\infty - V_t)$ *vs.* $t$ was linear over practically the entire course of the reaction. The average rate constants, calculated in the usual manner from the slopes of the experimental logarithmic plots, are brought together in Table I. The parameters of the Eyring equation, based upon the

TABLE I

APPARENT FIRST-ORDER RATE CONSTANTS FOR THE DECARBOXYLATION OF OXANILIC ACID IN THE MOLTEN STATE AND IN SEVERAL ETHERS

| System | Temp., °C. | $k \times 10^4$, sec.$^{-1}$ | Av. deviation |
|---|---|---|---|
| Molten oxanilic acid | 152.38 | 10.87 | 0.05 |
| | 161.12 | 28.7 | .1 |
| | 166.96 | 54.0 | .1 |
| Bis-(2-chloroethyl) ether + oxanilic acid | 138.0 | 4.82 | .03 |
| | 147.8 | 9.10 | .04 |
| | 159.9 | 19.2 | .1 |
| *n*-Butyl ether + oxanilic acid | 120.37 | 0.88 | .01 |
| | 127.60 | 1.60 | .02 |
| | 138.02 | 3.64 | .03 |
| *n*-Amyl ether + oxanilic acid | 138.04 | 3.92 | .03 |
| | 147.95 | 9.84 | .05 |
| | 156.2 | 19.3 | .1 |
| *n*-Hexyl ether + oxanilic acid | 139.32 | 3.34 | .02 |
| | 149.73 | 11.6 | .1 |
| | 158.63 | 31.5 | .1 |
| Dibenzyl ether + oxanilic acid | 131.44 | 1.46 | .02 |
| | 140.22 | 3.94 | .03 |
| | 150.12 | 11.5 | .1 |

(5) L. W. Clark, *J. Phys. Chem.*, **60**, 1150 (1956).
(6) L. W. Clark, *ibid.*, **66**, 125 (1962).

data in Table I, are shown in Table II, along with corresponding data obtained previously for the reaction in several other solvents.

TABLE II

KINETIC DATA FOR THE DECARBOXYLATION OF OXANILIC ACID IN THE MOLTEN STATE AND IN SEVERAL POLAR LIQUIDS

| Solvent | $\Delta H^*$, kcal./mole | $\Delta S^*$, e.u./mole | $\Delta F^*_{150°}$, kcal./mole |
|---|---|---|---|
| Bis-(2-chloroethyl) ether | 21.4 | −22.4 | 30.9 |
| *n*-Butyl ether | 25.1 | −13.9 | 31.0 |
| *n*-Amyl ether | 28.3 | − 6.6 | 31.1 |
| β-Chlorophenetole[3] | 31.3 | + 0.7 | 31.0 |
| Phenetole[3] | 32.6 | + 4.0 | 30.9 |
| Anisole[3] | 35.6 | +11.1 | 31.0 |
| Dibenzyl ether | 36.8 | +14.2 | 30.8 |
| N,N-Dimethylaniline[3] | 37.6 | +15.3 | 31.1 |
| Melt | 40.1 | +21.4 | 31.0 |
| *n*-Hexyl ether | 40.1 | +22.1 | 30.8 |
| *o*-Ethylaniline[1] | 45.5 | +34.3 | 31.0 |
| *o*-Toluidine[1] | 47.8 | +39.9 | 30.9 |
| Aniline[1] | 49.8 | +46.3 | 30.2 |

## Discussion of Results

The parameters of the Eyring equation for the decarboxylation of oxanilic acid in the molten state as well as in twelve organic solvents are listed in Table II. The solvents are arranged in the order of increasing enthalpy of activation, which is likewise that of increasing entropy of activation. An enthalpy–entropy plot of the data given in Table II yields a straight line, indicating that the reaction takes place in each case by the same mechanism.[7] This mechanism is very likely similar to that of the malonic acid decomposition, an activated complex being formed *via* the electrophilic polarized carbonyl carbon atom of the acid and an unshared pair of electrons on a nucleophilic atom of solvent.[4] If this is the case, it would be expected that the $\Delta H^*$ of the reaction would decrease as the nucleophilicity of the solvent increases.[8] It has been noted previously[3] that the $\Delta H^*$ of the oxanilic acid reaction in aromatic amines is higher than would be expected on the basis of the proposed mechanism (see Table II). Very possibly, in the reaction in ethers, unionized oxanilic acid takes part in the rate-determining step, whereas, in more strongly basic solvents, ionization of the oxanilic acid takes place and the anion is the entity involved in the reaction.

The value of $\Delta S^*$ is a measure of the relative complexity of the activated complex.[9] In general, an increase in size or steric hindrance of either solute or solvent will bring about a decrease in $\Delta S^*$, and *vice versa*. It will be seen from the data in Table II that the reaction in the smallest ether is accompanied by the lowest value of $\Delta H^*$, and also the largest negative value of $\Delta S^*$. As the size of the solvent molecule increases it appears that the size of the complex decreases. Two factors may contribute to increase the size of the activated complex—polymerization of the solvent and polymerization of the solute. Monobasic acids exist largely as dimers. Ethers associate to a certain extent through dipole–dipole interaction. The extent of association would tend to decrease as the number of carbon atoms increases. These two sets of conditions would help to account satisfactorily for the data involving the ethers shown in Table II. In the case of the amines we find a large $\Delta H^*$ accompanied by a large positive value of $\Delta S^*$ (see Table II). The aromatic amines have fewer carbon atoms than the ethers and show little association. Furthermore, if the anion of oxanilic acid is the entity reacting it would not dimerize. These two factors would contribute to decrease the size of the activated complex, giving rise to a large positive value of $\Delta S^*$.

The slope of the enthalpy–entropy plot of the data in Table II turns out to be 423. This corresponds to the isokinetic temperature, that is, the temperature at which the rate of reaction is the same in all solvents.[7] This is also the temperature at which $\Delta F^* = \Delta H_0^*$, where $\Delta H_0^*$ is the enthalpy change corresponding to zero change of entropy. The experimental enthalpy change corresponding to $\Delta S^* = 0$ is 31.0 kcal./mole. The isokinetic temperature, 423°K., is 150°, which is very nearly the melting point of oxanilic acid. It will be seen in Table II that the $\Delta F_{150°}^*$ for the decarboxylation of molten oxanilic acid, as well as for the reaction in all the solvents listed (aniline excepted), turns out to be 31.0 kcal./mole within plus or minus one or two tenths. The discrepancy in the case of aniline is probably due to some error in the data.

**Acknowledgment.**—The support of this research by the National Science Foundation, Washington, D. C., is gratefully acknowledged.

(7) J. E. Leffler, *J. Org. Chem.*, **20**, 1202 (1955).

(8) K. J. Laidler, "Chemical Kinetics," McGraw-Hill Book Co., Inc., New York, N. Y., 1950, p. 138.

(9) S. Glasstone, J. K. Laidler, and H. Eyring, "The Theory of Rate Processes," McGraw-Hill Book Co., Inc., New York, N. Y., 1941, p. 22.

## THE EFFECT OF ELECTROLYTES ON THE SOLUTION CHROMOTROPISM OF BIS-(*meso*-2,3-DIAMINOBUTANE)-NICKEL (II) IONS

BY D. L. LEUSSING, J. HARRIS,[1] AND P. WOOD

*National Bureau of Standards, Washington, D. C.*

*Received January 26, 1962*

The bis-C-methylethylenediamine complexes of nickel(II) have been found to exhibit a yellow diamagnetic form in solution in addition to the normal blue paramagnetic form.[2] Increasing substitution favors diamagnetism so that the C,C′-TetraMeen[3] complex is present completely in the diamagnetic form but with *meso*- and *racemic*-bn both forms are present in appreciable amounts at room temperature. Ahmed and Wilkins[4] report that the addition of sodium perchlorate to nitrate solutions of $Ni(rac\text{-bn})_2^{++}$ causes the proportion of the yellow form to increase. Similar behavior has been reported by Jorgensen[5] with nickel(II) and trien

(1) NBS Summer Student, 1961.

(2) F. Basolo, Y. T. Chen, and R. K. Murmann, *J. Am. Chem. Soc.*, **76**, 956 (1954).

(3) en = ethylenediamine, bn = *m*-2,3-diaminobutane, pn = propylenediamine, C,C′-TetraMeen = C,C′-tetramethylethylenediamine, trien = triethylenetetramine.

(4) A. K. Shamsuddin Ahmed and R. G. Wilkins, *J. Chem. Soc.*, 2901 (1960).

(5) C. Klixbull Jorgensen, *Acta Chem. Scand.*, **11**, 399 (1957).

and by Sone and Kato[6] for hot solutions of $Nien_2^{++}$ and $Nipn_2^{++}$.

In order to learn more about this interesting property we have examined the spectra and determined the formation constants of the nickel(II) complexes with *meso*-bn at 25° in various salt solutions.

### Experimental

*meso*-2,3-Diaminobutane dihydrochloride was prepared according to the method of Dickey, Fickett, and Lucas.[7] Analysis by potentiometric titration with standard silver nitrate solution indicated a purity of 99.2%.

The formation constants were calculated from the results of the usual pH-titration experiments which yielded $\bar{n}$ values and the corresponding free ligand concentrations at 25.0°. The primary medium in all experiments was a solution 0.080 *M* in bn·2HCl and 0.013 *M* in $NiCl_2$, which also contained added electrolyte. A standardized 1.00 *M* solution of sodium hydroxide was the titrant. In those experiments where the concentration of added electrolyte was 1.00 *M* or greater the titrant also was made up to contain the same concentration of electrolyte as the test solution. Equilibrium was attained within the time of mixing. With the perchlorate solutions, a saturated sodium chloride salt bridge was used to connect the solution being titrated with an external saturated calomel electrode. In the perchlorate medium it was found impossible to obtain useful results regarding the stability of the tris complex, since the perchlorate of this ion is only slightly soluble.

Spectrophotometric measurements were made, using a Cary Model 14 spectrophotometer with a cell compartment thermostated at 25.0°. In the solutions where the added electrolyte was 0.10 *M* sodium nitrate the spectra of $Nibn^{++}$, $Nibn_2^{++}$, and $Nibn_3^{++}$ were obtained on solutions in which $\bar{n}$, the average number of bn molecules bound per nickel(II) ion, was 0.35, 2.04, and 3.05. For the first case a solution containing 0.10 *M* potassium nitrate and a concentration of nickel chloride equal to that of the uncomplexed nickel(II) in the sample solution was used as the reference solution to subtract out the contribution of the free nickel ions. Similar measurements were made using en to obtain the spectra of the complexes with this latter ligand. The extinction coefficients calculated for the maxima corresponding to those of the paramagnetic species are given in Table I.

TABLE I

THE POSITIONS AND EXTINCTION COEFFICIENTS CORRESPONDING TO THE ABSORPTION MAXIMA OF THE PARAMAGNETIC NICKEL(II) COMPLEXES 0.10 *M* $KNO_3$, 25°

| | λ, mμ | ε | λ, mμ | ε | λ, mμ | ε |
|---|---|---|---|---|---|---|
| $Nien^{++}$ | 970 | 5.6 | 616 | 4.3 | 370 | 7.6 |
| $Nibn^{++}$ | 965 | 5.7 | 623 | 4.2 | 372 | 7.3 |
| $Nien_2^{++}$ | 927 | 6.5 | 568 | 5.4 | 354 | 11.4 |
| $Nibn_2^{++}$ | 935 | 5.1 | 570 | 4.5 | 360 | 12.4 |
| $Nien_3^{++}$ | 884 | 7.1 | 543 | 6.8 | 345 | 12.0 |
| $Nibn_3^{++}$ | 915 | 8.3 | 557 | 7.9 | 353 | 14.0 |

For the other salt solutions only the absorbance of the bis species at 442 mμ was obtained. This wave length corresponds to the ligand-field maximum of the diamagnetic species. In those experiments where potentiometric data were obtained (see Table III) the absorbance was determined when $\bar{n}$ was within 1–2% of 2.00.[8] For the remaining solutions a spectrophotometric titration was conducted. An aliquot of a solution containing known amounts of nickel chloride and bn·2HCl was placed in a cylindrical optical cell, which in turn was placed in the sample compartment of the spectrophotometer. The aliquot was of such a volume that the cell was not completely filled, leaving room for additional liquid. The openings in the sample cell holder through which the light beam passes were masked so that the light beam did not strike the meniscus of the solution. The solution then was titrated with base dispensed with a microburet. The spectrum in the region of 442 mμ was scanned for each increment of base. The extinction coefficients at 442 mμ are given in Table II. Because finite increments of base were added, the possibility exists that measurements were made either slightly before or slightly after the point corresponding exactly to the formation of $Nibn_2^{++}$. For this reason the extinction coefficients for these experiments tend to be low but because the titration points were sufficiently close the maximum relative error in the extinction coefficients is 10 to 15%. This error is acceptable for the present comparison purposes and is indicated in Table II for the experiments so affected.

### Results and Discussion

In Table I the low extinction coefficients of $Nibn_2^{++}$ at its two long wave length maxima are apparent. The low results are due to the presence of an appreciable proportion of the diamagnetic isomer which does not absorb in this region. The extinction coefficients of only the spin-free isomer, $\epsilon_{sf}$, were estimated by assuming that $\epsilon_{sf935}$ is equal to the average of $\epsilon_{965}$ and $\epsilon_{915}$ for the mono and tris bn complexes and, similarly, $\epsilon_{570}$ for the bis is equal to the average of the extinction coefficients for the second peaks of the lower and higher complexes. Applying this procedure to the en system gives a calculated value of 6.4 for $\epsilon_{927}$ of $Nien_2^{++}$ compared to 6.5 observed and a calculated value of 5.5 for $\epsilon_{568}$ compared to 5.4 observed, so this method appears to give reasonably good values.

The ratio $\epsilon_{sf965obs}/\epsilon_{sf965calc}$ for $Nibn_2^{++}$ is 0.73 and the ratio $\epsilon_{sf570obs}/\epsilon_{sf570calc}$ is 0.75. Thus, the results at both wave lengths are in good agreement and indicate about 74% of the bis complex to be spin-free. Using this fraction the extinction coefficient of the spin-paired form of $Nibn_2^{++}$ at 442 mμ, $\epsilon_{sp442}$, was calculated from the result given in Table II for 0.10 *M* $NaNO_3$. In this calculation the value of $\epsilon_{442sf}$ was assumed to be 1.4, which is the value for $Nien_2^{++}$ at this wave length. This choice is justified because of the close similarity of the spectra of the en and bn nickel(II) complexes (with the exception of the 442 mμ peak) and, owing to its low value, the results are not sensitive to relatively large variations in the assumed value of $\epsilon_{sf442}$. The calculated value of $\epsilon_{sp442}$ is 88. This value is somewhat higher than the value 66 for $Ni(C,C'\text{-TetraMeen})_2^{++}$ at its 434 mμ maximum. Both of these values lie well within the range reported by Holm[9] for various diamagnetic nickel(II) salicylaldimine complexes.

Finally, the relative proportions of the spin-paired and spin-free forms of $Nibn_2^{++}$ in the various media were calculated using the observed extinction coefficients of 442 mμ and the values assigned above to the isomers.[10] These results also are given in Table II.

These results show that not only do perchlorate ions affect the equilibrium between the two forms but other salts do as well. Even chloride ions in high concentration bring about an appreciable increase in the fraction of the diamagnetic species.

(6) K. Sone and M. Kato, *Z. anorg. allgem. Chem.*, **301**, 277 (1959).

(7) F. H. Dickey, W. Fickett, and H. J. Lucas, *J. Am. Chem. Soc.*, **74**, 944 (1952).

(8) An exception was made with perchlorate because of precipitation in this region of $\bar{n}$. Spectra were obtained on solutions in which $\bar{n}$ was 1.53 and the absorbance of $Nien^{++}$ was taken into account in the calculations.

(9) R. H. Holm, *J. Am. Chem. Soc.*, **83**, 4683 (1961).

(10) The intrinsic values of $\epsilon_{sf}$ and $\epsilon_{sp}$ are most likely insensitive to the medium changes judging from the behavior of the en and Tetra-Meen complexes. In 3.0 *M* NaCl, $\epsilon_{884}$ and $\epsilon_{543}$ for $Nien_3^{++}$ were found to be 7.2 and 6.7, respectively, and in 1.9 *M* $NaNO_3$, $\epsilon_{432}$ for $Ni(Tetra\text{-}Meen)_2^{++}$ was found to be 70.

TABLE II

ESTIMATION OF RELATIVE PROPORTIONS OF THE SPIN-FREE AND SPIN-PAIRED FORMS OF $Nibn_2^{++}$

$T = 25°$

| Added electrolyte | Obsd. extinction coefficient of $Nibn_2^{++}$ at 442 mμ | Fraction spin-free | Fraction spin-paired |
|---|---|---|---|
| 0.10 *M* NaCl | 24 | 0.74 | 0.26 |
| 1.0 *M* NaCl | 21–24 | .77–0.74 | .23–0.26 |
| 3.0 *M* NaCl | 33 | .64 | .36 |
| Nearly satd. NaCl | 43–49 | .52– .45 | .48– .55 |
| 0.10 *M* $NaNO_3$ | 24 | (.74) | (.26) |
| 1.25 *M* $NaNO_3$ | 30 | .67 | .33 |
| 0.10 *M* $NaClO_4$ | 22–25 | .76– .73 | .24– .27 |
| 1.0 *M* $NaClO_4$ | 30 | .67 | .33 |
| 1.0 *M* KI | 35–40 | .61– .55 | .39– .45 |
| 1.0 *M* $Na_2SO_4$ | 22–25 | .76– .73 | .24– .27 |

However, the fact that an increase in the chloride in concentration from 0.3 to 3.0 *M* produces a relative increase of only 50% in the fraction of the spin-paired form shows that the interaction is weak. The large monovalent anions have a greater effect while the divalent sulfate ions have a negligible effect, at least up to 1.0 *M* concentrations. We attribute this behavior either to actual or to incipient ion-pair formation.

In the classical cases of ion-pair formation between oppositely charged multivalent ions the electrostatic forces are strong enough to overcome the individual ionic hydration energies. On the other hand, the solvation energy is low along the axis perpendicular to the coördination plane of the diamagnetic nickel(II) complex[11] and it is reasonable to expect that in this case weak association also can occur with oppositely charged ions provided their solvation energies are small enough so that the sum of the ionic hydration energies (which promotes dissociation) is less than the electrostatic attractive force. Thus, weakly solvated cations would interact more strongly with the large anions than with the small anions which have higher hydration energies. This argument is similar to that discussed regarding the solubilities of salts[12] and, indeed, those salts having the greatest effect, $ClO_4^-$ and $I^-$, also have the greatest tendency to form precipitates with the nickel(II)–bn complexes. In connection with the trien system, Jorgensen[5] also has invoked ion-pair formation.

The formation constants obtained for various media are given in Table III. It is seen that all the *Q*-values increase appreciably as the salt concentration increases. The changes can be accounted for to a large extent by considering changes only in the activity of the free ligand. The ratio of the constants for the formation of a given complex, $MA_n^{++}$, in two different media is given by

$$R_n = (Q_n)_1/(Q_n)_2 = \left(\frac{\gamma MA_n}{\gamma M \gamma n_A}\right)_2 \left(\frac{\gamma M \cdot \gamma n_A}{\gamma MA_n}\right)_1$$

(11) D. Dyrssen and M. Hennicks, *Acta Chem. Scand.*, **15**, 47 (1961).

(12) D. L. Leussing, "Treatise on Analytical Chemistry," I. M. Kolthoff and P. J. Elving, Ed., Vol. I, Part I, Interscience, Publishers, Inc. New York, N. Y., 1959.

TABLE III

THE FORMATION CONSTANTS OF THE Ni(II)-*meso*-2,3-DIAMINOBUTANE COMPLEXES

$T = 25°$; initially: 0.08 *M* bn·2HCl, 0.13 *M* $NiCl_2$

| Added electrolyte | $pK_{1a}$ | $pK_{2a}$ | Log $Q_1$ | Log $Q_2$ | Log $Q_3$ |
|---|---|---|---|---|---|
| 0.10 *M* $NaNO_3$ | 6.92 | 9.99 | 6.97 | 12.72 | 15.52 |
| 1.25 *M* $NaNO_3$ | 7.03 | 9.96 | 7.23 | 13.20 | 16.36 |
| 0.10 *M* NaCl | 6.92 | 9.97 | 6.99 | 12.83 | 15.66 |
| 3.0 *M* NaCl | 7.09 | 10.13 | 7.57 | 14.08 | 17.90 |
| 1.0 *M* $NaClO_4$ | 6.91 | 9.87 | 6.97 | 13.66 | ... |

where the $\gamma$ represent the activity coefficients of the various species. If to a first approximation the quotient $(\gamma MA_n)_2(\gamma M)_1/(\gamma MA_n)_1(\gamma M)_2$ is equal to unity, then $R_n$ is equal to $(\gamma^n A)_1/(\gamma^n A)_2$. From this it results that $R_1 = R_2^{1/2} = R_3^{1/3}$. Comparing 0.10 and 1.25 *M* nitrate media the observed values are 0.56, 0.33, and 0.14 for $R_1$, $R_2$, and $R_3$, respectively. The square and cube roots of the last two quantities, 0.57 and 0.52, are in satisfactory agreement with the observed value of $R_1$. For 0.10 and 3.0 *M* chloride, the observed ratios, $R_1$, $R_2$, and $R_3$, are 0.26, 0.057, and 0.006, while $R_2^{1/2}$ and $R_3^{1/3}$ are 0.24 and 0.18. In these figures no exceptional increase in the value of $Q_2$ with increasing salt concentration is manifested as would be the case if strong ion-pair formation occurred. Thus, as was concluded from the spectral results, only weak ion-pairs are formed.

Conductivity measurements on $Nien_2^{++}$ and $Ni(C,C'\text{-TetraMeen})_2^{++}$ solutions also indicate that association of anions with the latter diamagnetic species possibly occurs. In 0.10 *M* solutions at 22° the molar conductivities of the chlorides were found to be 223 for $Nien_2^{++}$ and 139.5 for $Ni(C,C'\text{-TetraMeen})_2^{++}$. The former value is typical of those for di–univalent salts while the latter is closer to those for uni–univalent salts.

## THE HEAT CAPACITY OF THE SILVER CHALCOGENIDES, $Ag_{1.99}S$, $Ag_{1.99}Se$, AND $Ag_{1.88}Te$ FROM 16 TO 300°K.[1]

BY PATRICK N. WALSH, EDWARD W. ART, AND DAVID WHITE

*Cryogenic Laboratory, Department of Chemistry, The Ohio State University, Columbus, Ohio*

*Received January 30, 1962*

The heat capacities of the sulfide, selenide, and telluride of silver have been measured from the liquid hydrogen region to room temperature to determine whether any macroscopic reordering processes which would affect the electrical properties of these semiconductors occur in this temperature range. The magnitudes of the heat capacities of these compounds at low temperatures are also of considerable interest because of their possible significance in thermoelectric cooling.

Prior to this work, the only investigation of the heat capacities of the silver chalcogenides at low temperatures was that of Gul'tyaev and Petrov.[2] They measured the heat capacities of $Ag_2S$ and

(1) This work was supported by the Wright Air Development Division, Air Research and Development Command, United States Air Force.

(2) P. V. Gul'tyaev and A. V. Petrov, *Soviet Phys. Solid State* (Fiz. Tverd. Tela), **1**, 330 (1959).

$Ag_2Te$ from 80 to 300°K. Unfortunately their measurements have uncertaintities of 3–7%, and the stoichiometry of the compounds is not given. Earlier investigations consist primarily of heat capacity measurements above 273°K. for what were assumed to be the three stoichiometric compounds, $Ag_2S$[3–5], $Ag_2Se$[4], and $Ag_2Te$[5,6].

**Apparatus and Procedure.**—The heat capacity measurements on all three compounds were carried out in "Solid Calorimeter No. 3" using the apparatus and procedure previously described by Johnston and Kerr.[7] The temperatures reported are based on the thermodynamic temperature scale established by Rubin, Johnston, and Altman.[8] Although the calorimeter had previously been calibrated,[9] the calibration was rechecked before and after use over the entire temperature range.

The samples, originally in the form of small ingots, were crushed in an atmosphere of argon to a particle size of approximately $^1/_{16}$ in. before loading in the calorimeter. In order to ensure good thermal contact between the sample and the resistance thermometer (wound outside the calorimeter), the calorimeter was filled with helium to a pressure of one atmosphere before sealing.

**Materials.**—The silver chalcogenides used in this investigation were specially prepared from materials with an initial purity of 99.99 mole % or better, by the Ohio Semiconducting Company. Spectral analysis of these compounds indicated that the impurities introduced in preparation were negligible. The compounds, however, were non-stoichiometric; the compositions as established by chemical analysis[10] were $Ag_{1.99}S$, $Ag_{1.99}Se$, and $Ag_{1.88}Te$. The uncertainty of the analyses was ±0.01 mole of silver per mole of sulfur, selenium, or tellurium.

The silver sulfide and selenide were n-type semiconductors,[11] and presumably single phase systems. The silver telluride was a p-type semiconductor with a room temperature crystal structure corresponding to that of hessite.[10] Although the phase diagram for the Ag–Te system is quite uncertain,[11] it is likely that our sample of silver selenide was a single phase solid solution. The stoichiometry of the telluride was also confirmed by phase equilibria studies[10] using a silver–telluride e.m.f. cell of the type previously used by Kiukkola and Wagner.[12]

**Experimental Results and Calculations.**—The heat capacity measurements were made using as samples 232.045 g. (0.94041 mole) of silver sulfide, 226.659 g. (0.77189 mole) of silver selenide, and 227.651 g. (0.68942 mole) of silver telluride. The molecular weights were taken as 246.75 for $Ag_{1.99}S$, 293.64 for $Ag_{1.99}Se$, and 330.21 for $Ag_{1.88}Te$. The experimental heat capacities expressed in defined thermochemical calories (1 cal. = 4.1840 absolute joules) are given in Table I.

No anomalies were observed in any of the three compounds in the temperature range 16 to 300°K. Any defects in the lattice apparently remain frozen in and there are no first-order transitions characteristic of changes in crystal structures. In the

TABLE I

HEAT CAPACITY OF $Ag_{1.99}S$, $Ag_{1.99}Se$, AND $Ag_{1.88}Te$

| $T$ av., °K. | $C_p$, cal. mole$^{-1}$ deg.$^{-1}$ | $T$ av., °K. | $C_p$, cal. mole$^{-1}$ deg.$^{-1}$ |
|---|---|---|---|
| $Ag_{1.99}S$ | | $Ag_{1.99}Se$ | |
| 13.23 | 2.04 | 41.33 | 8.62 |
| 14.14 | 2.43 | 45.93 | 9.65 |
| 15.56 | 3.17 | 50.73 | 10.49 |
| 16.95 | 3.40 | 56.03 | 11.37 |
| 19.60 | 4.46 | 60.06 | 11.84 |
| 21.58 | 4.87 | 64.82 | 12.55 |
| 23.17 | 5.23 | 71.24 | 13.20 |
| 23.91 | 5.49 | 77.13 | 13.72 |
| 25.14 | 5.70 | 82.85 | 14.18 |
| 27.26 | 6.14 | 88.23 | 14.73 |
| 28.22 | 6.39 | 91.96 | 14.80 |
| 29.67 | 6.57 | 101.25 | 15.37 |
| 32.87 | 7.18 | 109.88 | 15.77 |
| 36.62 | 7.88 | 120.90 | 16.25 |
| 40.85 | 8.53 | 129.13 | 16.53 |
| 45.56 | 9.05 | 137.34 | 16.76 |
| 55.91 | 10.21 | 145.99 | 17.00 |
| 61.58 | 10.88 | 155.32 | 17.29 |
| 69.85 | 11.69 | 159.87 | 17.40 |
| 72.16 | 11.89 | 170.60 | 17.58 |
| 76.86 | 12.22 | 178.89 | 17.80 |
| 80.78 | 12.44 | 187.75 | 17.99 |
| 84.38 | 12.70 | 197.36 | 18.13 |
| 86.74 | 12.92 | 207.49 | 18.31 |
| 91.04 | 13.34 | 207.83 | 18.28 |
| 97.29 | 13.46 | 216.34 | 18.41 |
| 97.41 | 13.74 | 217.27 | 18.45 |
| 112.46 | 14.19 | 235.28 | 18.59 |
| 123.49 | 14.77 | 240.89 | 18.69 |
| 128.81 | 14.99 | 246.28 | 18.78 |
| 135.47 | 15.13 | 258.04 | 18.97 |
| 141.10 | 15.31 | 264.47 | 19.12 |
| 148.96 | 15.57 | 271.07 | 19.22 |
| 149.41 | 15.64 | 277.34 | 19.24 |
| 155.47 | 15.76 | 283.48 | 19.33 |
| 161.71 | 15.95 | | |
| 167.65 | 16.08 | $Ag_{1.88}Te$ | |
| 177.17 | 16.20 | 16.16 | 1.78 |
| 184.62 | 16.41 | 17.91 | 2.40 |
| 192.46 | 16.62 | 19.90 | 3.15 |
| 200.15 | 16.70 | 22.10 | 3.86 |
| 210.18 | 16.99 | 24.65 | 4.70 |
| 217.08 | 17.14 | 27.37 | 5.39 |
| 224.87 | 17.28 | 30.25 | 6.13 |
| 241.00 | 17.49 | 33.50 | 7.05 |
| 245.33 | 17.53 | 36.82 | 7.95 |
| 254.37 | 17.66 | 40.44 | 8.76 |
| 260.17 | 17.72 | 45.36 | 9.74 |
| 268.66 | 17.85 | 50.09 | 10.54 |
| 282.40 | 18.01 | 55.49 | 11.45 |
| 296.15 | 18.19 | 60.59 | 12.16 |
| | | 65.52 | 12.69 |
| $Ag_{1.99}Se$ | | 71.65 | 13.34 |
| 16.66 | 2.26 | 84.83 | 14.42 |
| 18.53 | 3.05 | 97.60 | 15.16 |
| 20.57 | 3.75 | 109.38 | 15.63 |
| 22.63 | 4.38 | 126.51 | 16.33 |
| 24.74 | 4.95 | 145.70 | 16.82 |
| 27.00 | 5.54 | 154.12 | 17.06 |
| 29.87 | 6.20 | 161.87 | 17.16 |
| 33.20 | 7.00 | 170.15 | 17.40 |
| 37.00 | 8.19 | 185.28 | 17.66 |

(3) M. Bellati and S. Lussana, *Atti ist. Veneto, ser. 6*, **7**, 1051 (1888–1889).

(4) A. F. Kapustinsky and B. K. Veselovshi, *J. Phys. Chem. U.S.S.R.*, **11**, 68 (1938).

(5) W. A. Tilden, *Phil. Trans. Roy. Soc.* (London), **201A**, 37 (1903); **203A**, 139 (1904).

(6) L. Rola, *Nuovo Cimento*, [6] **9**, 197 (1915).

(7) H. L. Johnston and E. C. Kerr, *J. Am. Chem. Soc.*, **72**, 4988 (1950).

(8) T. Rubin, H. L. Johnston, and H. Altman, *ibid.*, **72**, 3401 (1951).

(9) H. W. Goldstein, E. F. Neilson, P. N. Walsh, and D. White, *J. Phys. Chem.*, **63**, 1445 (1959).

(10) Unpublished results of P. M. Harris and G. E. MacWood, Dept. of Chemistry, The Ohio State University.

(11) F. C. Kracek and C. J. Ksanda, *Trans. Am. Geophys. Union*, **21**, 363 (1940).

(12) K. Kiukkola and C. Wagner, *J. Electrochem. Soc.*, **104**, 379 (1957).

TABLE I (*Continued*)

| $T$ av., °K. | $C_p$, cal. mole$^{-1}$ deg.$^{-1}$ | $T$ av., °K. | $C_p$, cal. mole$^{-1}$ deg.$^{-1}$ |
|---|---|---|---|
| $Ag_{1.88}Te$ | | $Ag_{1.86}Te$ | |
| 192.59 | 17.73 | 245.72 | 18.51 |
| 200.58 | 17.89 | 251.79 | 18.64 |
| 207.64 | 17.99 | 257.70 | 18.79 |
| 214.12 | 18.13 | 269.38 | 19.16 |
| 220.67 | 18.22 | 277.27 | 19.28 |
| 226.05 | 18.30 | 283.34 | 19.51 |
| 233.15 | 18.39 | 289.54 | 19.70 |
| 244.47 | 18.57 | 296.16 | 19.92 |

case of the telluride there is an unusual increase in the heat capacity in the vicinity of 265°K. This rise is reminiscent of a premelting phenomenon and may be associated with the high temperature transition which occurs at approximately 410°K. A similar effect has been observed by Boettcher.[13]

TABLE II

THERMAL FUNCTIONS FOR $Ag_{1.99}S$, $Ag_{1.99}Se$, AND $Ag_{1.88}Te$

| $T$, °K. | $C_p$ cal. deg.$^{-1}$ mole$^{-1}$ | $S_T^0$ cal. deg.$^{-1}$ mole$^{-1}$ | $H_T - H_0^0$, cal. mole$^{-1}$ | $-(F_T - H_0^0)/T$ cal. deg.$^{-1}$ mole$^{-1}$ |
|---|---|---|---|---|
| | | $Ag_{1.99}S$ | | |
| 15 | 2.77 | 1.144 | 12.33 | 0.328 |
| 20 | 4.35 | 2.166 | 30.19 | 0.985 |
| 30 | 6.73 | 4.411 | 86.33 | 1.534 |
| 40 | 8.38 | 6.585 | 162.3 | 2.528 |
| 50 | 9.68 | 8.600 | 252.8 | 3.544 |
| 60 | 10.76 | 10.462 | 355.1 | 4.543 |
| 70 | 11.66 | 12.190 | 467.3 | 5.515 |
| 80 | 12.40 | 13.797 | 587.7 | 6.451 |
| 90 | 13.06 | 15.297 | 715.2 | 7.351 |
| 100 | 13.60 | 16.702 | 848.4 | 8.217 |
| 120 | 14.52 | 19.265 | 1130.0 | 9.848 |
| 140 | 15.29 | 21.562 | 1428.3 | 11.361 |
| 160 | 15.91 | 23.645 | 1740.5 | 12.768 |
| 180 | 16.37 | 25.546 | 2063.5 | 14.082 |
| 200 | 16.78 | 27.293 | 2395.6 | 15.318 |
| 220 | 17.15 | 28.911 | 2734.5 | 16.482 |
| 240 | 17.45 | 30.416 | 3080.8 | 17.580 |
| 260 | 17.72 | 31.822 | 3432.5 | 18.621 |
| 280 | 17.98 | 33.145 | 3789.4 | 19.611 |
| 298.16 | 18.20 | 34.278 | 4118.0 | 20.467 |
| 300 | 18.21 | 34.392 | 4151.3 | 20.555 |
| | | $Ag_{1.99}Se$ | | |
| 17 | 2.37 | 0.979 | 11.92 | 0.275 |
| 20 | 3.51 | 1.457 | 20.77 | 0.415 |
| 30 | 6.27 | 3.438 | 70.59 | 1.085 |
| 40 | 8.50 | 5.555 | 144.7 | 1.937 |
| 50 | 10.37 | 7.660 | 239.4 | 2.872 |
| 60 | 11.85 | 9.680 | 350.8 | 3.842 |
| 70 | 13.05 | 11.609 | 475.6 | 4.816 |
| 80 | 13.98 | 13.413 | 610.9 | 5.778 |
| 90 | 14.71 | 15.104 | 754.5 | 6.721 |
| 100 | 15.32 | 16.687 | 904.6 | 7.640 |
| 120 | 16.21 | 19.563 | 1220.4 | 9.393 |
| 140 | 16.87 | 22.114 | 1551.5 | 11.032 |
| 160 | 17.39 | 24.402 | 1894.3 | 12.562 |
| 180 | 17.83 | 26.476 | 2246.7 | 13.994 |
| 200 | 18.18 | 28.372 | 2606.8 | 15.338 |
| 222 | 18.49 | 30.119 | 2973.6 | 16.603 |
| 240 | 18.77 | 31.740 | 3346.1 | 17.798 |
| 260 | 19.03 | 33.253 | 3729.2 | 18.910 |
| 280 | 19.27 | 34.672 | 4107.1 | 20.004 |
| 298.16 | 19.47 | 35.890 | 4458.8 | 20.935 |
| 300 | 19.49 | 36.009 | 4494.8 | 21.027 |
| | | $Ag_{1.88}Te$ | | |
| 16 | 1.70 | 0.631 | 7.39 | 0.169 |
| 20 | 3.16 | 1.169 | 17.13 | .312 |
| 30 | 6.26 | 3.064 | 64.90 | .901 |
| 40 | 8.69 | 5.211 | 140.1 | 1.708 |
| 50 | 10.61 | 7.364 | 237.0 | 2.624 |
| 60 | 12.07 | 9.434 | 350.8 | 3.587 |
| 70 | 13.17 | 11.380 | 477.2 | 4.563 |
| 80 | 14.03 | 13.196 | 613.5 | 5.529 |
| 90 | 14.71 | 14.889 | 757.2 | 6.475 |
| 100 | 15.26 | 16.468 | 907.2 | 7.396 |
| 120 | 16.09 | 19.328 | 1221.3 | 9.151 |
| 140 | 16.68 | 21.859 | 1549.3 | 10.792 |
| 160 | 17.12 | 24.119 | 1887.5 | 12.322 |
| 180 | 17.52 | 26.159 | 2233.9 | 13.748 |
| 200 | 17.88 | 28.054 | 2587.9 | 15.114 |
| 220 | 18.20 | 29.773 | 2948.7 | 16.379 |
| 240 | 18.50 | 31.369 | 3315.7 | 17.554 |
| 260 | 18.85 | 32.862 | 3689.0 | 18.673 |
| 280 | 19.38 | 34.277 | 4071.0 | 19.738 |
| 298.16 | 19.98 | 35.512 | 4428.3 | 20.660 |
| 300 | 20.05 | 35.635 | 4465.1 | 20.751 |

The heat capacities of the silver sulfide and telluride reported here differ by as much as a few per cent from those previously reported by Gul'tyaev and Petrov.[2] We have not presented a detailed comparison with this earlier work because of the large uncertainties, previously mentioned, contained therein. It is of interest to note the unusually large values of the heat capacities of the three compounds at low temperatures. At 20°K. they are 4.35, 3.51, and 3.16 cal. deg.$^{-1}$ for the sulfide, selenide, and telluride, respectively.

The thermal functions for the chalcogenides were calculated from the smoothed heat capacity data extrapolated to 0°K. using a Debye function. These heat capacities together with the derived thermodynamic data are given in Table II at various integral values of the temperature. The entropies of the silver sulfide, selenide, and telluride at 298.16°K., assuming no zero point entropies, are 34.278, 35.890, and 35.512 ± 0.08 cal. deg.$^{-1}$ mole$^{-1}$, respectively. The Debye $\theta$'s used in the calculations were 70, 85, and 96° for the sulfide, selenide, and telluride, respectively, and were obtained from the heat capacities at the lowest temperatures. Between 0 and 15° these Debye functions contribute 1.139, 0.975, and 0.631 cal. deg.$^{-1}$ mole$^{-1}$, respectively, to the entropies of these compounds.

## Discussion

The standard entropies of the three silver chalcogenides at 298°K. can be compared with values derived from electrochemical measurements. Such a comparison is shown in Table III. Kimura[14] and Goates, *et al.*,[15] measured the temperature variation of the e.m.f. of the reaction

$$2Ag(c) + H_2S(g) \longrightarrow H_2(g) + Ag_2S(c) \qquad (1)$$

(13) A. Boettcher, *Z. angew. Phys.*, **7**, 478 (1955).

(14) G. Kimura, *Bull. Inst. Phys. Chem. Res. Tokyo*, **13**, 464 (1934).

(15) J. R. Goates, A. G. Cole, E. L. Gray, and N. D. Faux, *J. Am. Chem. Soc.*, **73**, 707 (1951).

in the vicinity of 298°K. Kiukkola and Wagner[12] measured the e.m.f. of the cell reactions

$$2Ag(c) + S(l) \longrightarrow Ag_2S(c) \qquad (2)$$

and

$$2Ag(c) + Se(l) \longrightarrow Ag_2Se(c) \qquad (3)$$

at temperatures above the melting points of sulfur and selenium. They derived the 298°K. entropy of $Ag_2Se(c)$ listed in Table III. The entropy change for reaction 2 at the temperature of their measurements was derived from the slope of a plot of $\Delta F$ *vs.* $T$ (data from Table III, ref. 13) and corrected to 298°K. using the entropy increment tables of Kelley.[16] Combining $\Delta S_{298}^0$ so derived with the standard entropies of the elements[17] yields the value listed in Table VII. The data on the silver–tellurium system[12] are insufficient to allow a comparison.

TABLE III

COMPARISON OF EXPERIMENTAL VALUES OF $S_{298.16}^0$ FOR THE SILVER CHALCOGENIDES

| | $S_{298}^0$, cal. deg.$^{-1}$ mole$^{-1}$ | | |
|---|---|---|---|
| | $Ag_2S$ | $Ag_2Se$ | $Ag_{1.88}Te$ |
| Kimura[14] | 34.5 | .. | .. |
| Goates, *et al.*[15] | 33.6 | .. | .. |
| Kiukkola and Wagner[12] | 33.9 | 35.8 | .. |
| This investigation | 34.3 | 35.9 | 35.5 |

The agreement among the various investigations cited in Table VII is within the uncertainty of the measurements and supports the assumption of no zero point entropy used in our calculation of thermodynamic properties.

(16) K. K. Kelley, U.S. Bur. Mines Bull., 584, 1960.

(17) D. R. Stull and G. C. Sinke, "Thermodynamic Properties of the Elements," American Chemical Society, Washington, D. C., 1956.

## ION-EXCHANGE MEMBRANES. IV.[1] UNIVALENT CATION TRANSFER RATES

BY J. CIRIC AND W. F. GRAYDON

*Department of Chemical Engineering, University of Toronto, Toronto, Canada*

*Received February 1, 1962*

Previous reports[2] in this series have discussed the measurement of sodium–hydrogen cation-exchange rates across membranes of the homogeneous polystyrenesulfonic acid type. This report is concerned with cation transfer rates and electrical resistances for a number of univalent cations: hydrogen, lithium, potassium, sodium, and ammonium.

### Experimental

**Membranes.**—The membranes used in this work were prepared following the procedures previously described.[3-5] The methods used for the determination of moisture content and exchange capacity also have been given.

**Diffusion Measurements.**—A two-compartment lucite cell, previously described,[2] was used to measure the rates of diffusion. Each compartment, separated from the other one by the ion-exchange membrane, contained at zero time 10 ml. of 0.1 *M* solution of hydrochloric acid or alkali chloride. Thus two ionic species were allowed to counterdiffuse across the membrane for several 5-min. periods, until a constant flux was obtained. The counter-diffusion then was allowed to proceed for various time intervals. At the end of each interval the contents of the compartments were analyzed by titration, in the case of hydrogen ion, or by flame photometry, in the case of alkali ions.

**Resistance Measurements.**—The membrane resistance was measured using an a.c. bridge with Wagner earth and capacitance balance. A Hewlett-Packard oscillator with a frequency range of 6–600,000 c.p.s. was used as the signal source. Null points were determined using a type 304H Du Mont oscilloscope. Membrane strips between electrode clamps were used for the resistance determination. Each measurement was done on a leached sample supported in the vapor phase above pure water at 25°. The membrane showed negligible variation in resistance measured, when the frequency was varied from 500–5000 c.p.s. Variations in the membrane strip length between clamps caused no change in resistance per centimeter, indicating a negligible contact resistance. For example, an 8.0-cm. distance between clamps showed a resistance of 7720 ohms or 965 ohms/cm. and a 4.4-cm. length showed a resistance of 4320 ohms or 980 ohms/cm. The major source of error in the calculation of specific resistances is the uncertainty in the strip dimensions, particularly in the length between electrode clamps. The error in dimension measurements is estimated at ±1%.

### Results and Discussion

The characteristics of the membranes used in this work are given in Table I.

TABLE I

MEMBRANE CHARACTERISTICS

| Membrane no. | Nominal cross-linking, mole % DVB | Capacity, meq./g. | Moisture content g. $H_2O$/g. membrane substance[a] | Thickness, cm. |
|---|---|---|---|---|
| 1 | 6 | 2.80 | 0.927 | 0.0131 |
| 2 | 6 | 1.76 | .483 | .0078 |
| 3 | 4 | 1.57 | .398 | .0069 |
| 4 | 4 | 1.30 | .322 | .0080 |

± 0.0002

[a] Moisture content is based on the weight of membrane substance dried at 110° to constant weight.

The diffusion coefficients, given in Table II, have been obtained using the equation

$$D = \frac{VL}{2A} \frac{\Delta \ln \frac{\Delta c_0}{\Delta c_f}}{\Delta t} \qquad (1)$$

where

$L$ = membrane thickness, cm.
$A$ = membrane area = $\pi$ cm.$^2$
$V$ = volume of the half-cell = 10 cm.$^3$
$\Delta c_0$ = difference in concn. of the diffusing species between half cells at zero time = 0.1
$\Delta c_f$ = difference in concn. of the diffusing species between half cells at time $t$
$t$ = time in minutes

The plots of log $(\Delta c_0/\Delta c_f)$ *vs.* time, calculated from the analytical results, are shown in Fig. 1. The values of $D$ are obtained from the slopes of the linear plots and are subject to no assumptions as to the diffusion process or the concentration gradient in the membrane.[2]

(1) This report is abstracted from the thesis of J. Ciric submitted for the degree of Doctor of Philosophy, University of Toronto, October, 1956.

(2) R. J. Stewart and W. F. Graydon, *J. Phys. Chem.*, **60**, 750 (1956).

(3) I. H. Spinner, J. Ciric, and W. F. Graydon, *Can. J. Chem.*, **32**, 143 (1954).

(4) W. F. Graydon and R. J. Stewart, *J. Phys. Chem.*, **59**, 86 (1955).

(5) W. F. Graydon, U.S. Pat. No. 2,877,191, March 10, 1959.

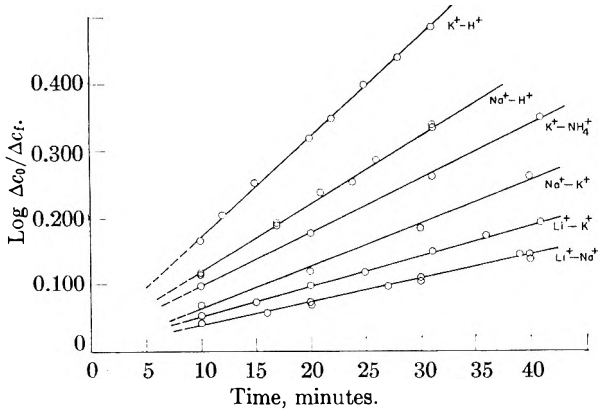


Fig. 1.—Ion transport rates, membrane 2: $\Delta c_0$ is the original ion concentration difference across the membrane (0.100 $N$); $\Delta c_f$ is the final concentration difference; temperature 25°.

TABLE II

DIFFUSION COEFFICIENTS

| Ion pair | $D \times 10^5$ for membrane no. 1 | 2 | 3 | 4 |
|---|---|---|---|---|
| $K^+$–$N^+$ | 9.17 | 3.91 | 2.59 | 1.29 |
| $NH_4^+$–$H^+$ | | 3.81 | | |
| $Na^+$–$H^+$ | 6.86 | 2.63 | 1.74 | 0.884 |
| $Li^+$–$H^+$ | 4.27 | 1.52 | 1.06 | 0.518 |
| $Na^+$–$K^+$ | | 1.62 | | |
| $Na^+$–$NH_4^+$ | 4.53 | 1.62 | 1.12 | 0.601 |
| $Li^+$–$K^+$ | | 1.21 | | |
| $Li^+$–$NH_4^+$ | 3.22 | 1.25 | 0.80 | 0.428 |
| $Na^+$–$Li^+$ | 2.46 | 0.89 | 0.568 | 0.295 |
| $NH_4^+$–$K^+$ | 5.30 | 2.17 | 1.34 | 0.770 |

From the data of Table II, diffusion coefficients for single ions can be calculated using the relationship[6]

$$D = \frac{2D_{i_1} D_{i_2}}{D_{i_1} + D_{i_2}} \qquad (2)$$

The values of diffusion coefficients, calculated in such a manner, are listed in Table III.

TABLE III

SINGLE ION DIFFUSION COEFFICIENTS

| Ion | $D \times 10^5$ for membrane no. 1 | 2 | 3 | 4 |
|---|---|---|---|---|
| $H^+$ | 28.0 | 11.0 | 7.00 | 3.70 |
| $K^+$, $NH_4^+$ | 5.50 | 2.20 | 1.40 | 0.77 |
| $Na^+$ | 3.90 | 1.50 | 0.96 | 0.50 |
| $Li^+$ | 2.32 | 0.86 | 0.57 | 0.29 |

It may be seen from Table III that the ratios of the single ion diffusion coefficient values are quite independent of membrane cross-linking and capacity. For the four membranes, these ratios may be calculated: $D_{H^+}/D_{K^+} = 5.0 \pm 0.2$, $D_{H^+}/D_{Na^+} = 7.3 \pm 0.1$, $D_{H^+}/D_{Li^+} = 12.5 \pm 0.3$. These ratios are quite similar to the ratios of ionic equivalent conductances in concentrated salt solutions. It has been shown previously[2] that the apparent diffusion coefficients ($Na^+$–$H^+$) for any membrane of this type may be estimated from the capacity and moisture content of the membrane in hydrogen form. From the relation[2] further estimates can be made for the cation transfer rates of other ions.

(6) K. S. Spiegler and C. D. Coryell, *J. Phys. Chem.*, **57**, 687 (1953).

Examples of the results obtained from the resistance measurements are given in Table IV.

TABLE IV

RESISTANCE OF MEMBRANES[a]

| Membrane no. | Ionic form | Measured specific resistance, ohm cm. | Calcd. $\frac{2.66}{D_i}$, ohm cm. |
|---|---|---|---|
| 1 | $H^+$ | 7.4 | 9.5 |
| | $K^+$ | 31.0 | 48.4 |
| | $NH_4^+$ | 27.7 | ... |
| | $Na^+$ | 48.8 | 68.2 |
| | $Li^+$ | 69.7 | 114.8 |
| 3 | $H^+$ | 25.9 | 38.0 |
| | $K^+$ | 98.4 | 190.0 |
| | $NH_4^+$ | 92.7 | ... |
| | $Na^+$ | 167 | 277.0 |
| | $Li^+$ | 266 | 466.0 |

[a] Strip dimensions for resistance measurements were about 0.06 × 0.6 × 7 cm.

The above values indicate the variation in membrane resistance with capacity and cross-linking. They may be compared, for example, with data for a phenolic membrane which showed intermediate values.[7]

It is of interest to compare the results of the measurements of diffusion and electrical resistance. Use is made of the Nernst–Einstein equation[7]

$$D_m = 2.66 \times 10^{-4} \frac{\kappa}{c_i} \qquad (3)$$

where

$\kappa$ = specific conductance = reciprocal of the specific resistance

$D_m$ = true diffusion coefficient of a cation in the membrane interior, related to the diffusion coefficient of eq. 1 and 2, by the relation

$$D_i = D_m \frac{c_i}{c_e} \qquad (4)$$

$c_i$ = concn. of the diffusing cation in the membrane interior

$c_e$ = exterior concn. = 0.1 mole/l.

By substituting (4) in (3), the specific resistance can be calculated from the apparent diffusivities of single ions. The appropriate quantities appear in the third column of Table III. Because of the simplicity of the treatment and in particular the neglect of variations in membrane composition and water transport, it is not surprising that there are considerable differences between the values in column 3 and those in column 4.

It is to be expected that the electrical resistance values calculated from diffusion should be higher than those measured directly as a result of water transport. Values for the water transport under conditions comparable to those of the electrical resistance measurements are known for sodium resin.[8] The water velocity was found to be approximately $^1/_2$ of the ion velocity for all membranes. Similar results have been obtained for the potassium form of these membranes.

(7) W. T. Grubb, *ibid.*, **63**, 55 (1959).

(8) R. J. Stewart and W. F. Graydon, *ibid.*, **61**, 164 (1957).

Although the water transports are not known precisely under the conditions of the diffusion and the electrical resistance measurements, a calculation can be made for the potassium ammonium cross diffusions. If it be assumed that the water transport for this cross diffusion is zero, then the rate of potassium–ammonium interchange may be calculated assuming a conductance relative to water of one-half that measured relative to the membrane. For membrane 1 the calculated apparent diffusion coefficient for potassium–ammonium exchange is $4.54 \times 10^{-5}$ cm.$^2$/sec. That found was $5.30 \times 10^{-5}$ cm.$^2$/sec. For membrane 3: calculated 1.40; found 1.34. The difference in water transport seems to be the major effect in the differences between diffusion and electrical resistance measurements.

**Acknowledgment.**—The authors are indebted to the Ontario Research Foundation, the National Research Council, Ottawa, and the President's Advisory Committee on Scientific Research, University of Toronto, for financial support.

## ELECTRON IMPACT SPECTROSCOPY OF PROPYLENE SULFIDE[1]

By Brice G. Hobrock and Robert W. Kiser

*Department of Chemistry, Kansas State University, Manhattan, Kansas*

*Received February 9, 1962*

We currently are investigating a number of organic sulfides. Gallegos and Kiser[2,3] recently have reported mass spectrometric data for ethylene sulfide and other saturated heterocyclic sulfur compounds. These authors also have reported this type of information for propylene oxide[4] and recently we have studied some of the straight-chain sulfides and disulfides.[5] Electron impact data for a missing member of this important series of sulfides, propylene sulfide, is herein reported.

Mass spectra and appearance potentials were determined using a time-of-flight mass spectrometer. The instrumentation has been described previously.[4] The sample of propylene sulfide, obtained from Aldrich Chemical Co., was found to be quite pure by gas–liquid partition chromatographic analysis, and therefore was used as received.

Mass spectra were obtained at 70 e.v. Appearance potentials were determined using the extrapolated voltage difference method,[6] the technique of Lossing, Tickner, and Bryce,[7] and the energy compensation method.[8] The voltage scale was calibrated by mixing xenon with the sample of propylene sulfide.

A partial mass spectrum for propylene sulfide is given in column 2 of Table I. To our knowledge, the mass spectral cracking pattern for this compound has not been reported previously. The measured appearance potentials are given in column 3 and the proposed processes in column 4. The heats of formation for the various ions consistent with the proposed processes are given in the last column. The heats of formation were calculated using a value of 19.7 kcal./mole for propylene sulfide. This value was estimated using Franklin's method.[9] The value of 8.6 e.v. reported for the ionization potential of propylene sulfide is new and compares favorably with the values reported for ethylene sulfide and trimethylene sulfide and with the estimated values given in Table II. The results shown in Table II were calculated in the same manner as those for ethylene oxide and propylene oxide.[4]

$m/e$ = **15.**—This ion is $CH_3^+$. The appearance potential is reported, but a process for the formation of $CH_3^+$ was not assigned, since the energetics do not distinguish between several possibilities.

$m/e$ = **26.**—The only ion of $m/e$ = 26 that can be formed from propylene sulfide is $C_2H_2^+$. If one considers $CH_3S$ + H as neutral products, $\Delta H_f^+$ ($C_2H_2$) = 337 kcal./mole; this is somewhat high in comparison to the value of 317 kcal./mole reported by Field and Franklin.[10]

TABLE I

MASS SPECTRUM AND APPEARANCE POTENTIALS OF THE PRINCIPAL IONS OF PROPYLENE SULFIDE

| $m/e$ | Relative abundance | Appearance potential (e.v.) | Process | $\Delta H_f^+$ (kcal./mole) |
|---|---|---|---|---|
| 15 | 5.9 | 18.1 ± 0.4 | $C_3H_6S \rightarrow CH_3^+ + ?$ | |
| 26 | 9.8 | 17.7 ± .4 | $\rightarrow C_2H_2^+ + CH_3S + H$ | 337 |
| 27 | 19.3 | 17.2 ± .3 | $\rightarrow C_2H_3^+ + CH_2S + H$ | 288 |
| 29 | 5.0 | | | |
| 30 | 3.2 | | | |
| 37 | 5.2 | 22.2 ± .5 | $\rightarrow C_3H^+ + S + H_2 + 3H$ | 322 |
| 38 | 8.7 | 19.2 ± .4 | $\rightarrow C_3H_2^+ + SH + H + H_2$ | 379 |
| | | | $\rightarrow C_3H_2^+ + H_2S + 2H$ | 363 |
| 39 | 50.0 | 15.9 ± .2 | $\rightarrow C_3H_3^+ + H_2 + H + S$ | 281 |
| 40 | 9.2 | 14.4 ± .3 | $\rightarrow C_3H_4^+ + S + H_2$ | 298 |
| 41 | 100.0 | 11.5 ± .2 | $\rightarrow C_3H_5^+ + SH$ | 253 |
| 42 | 7.7 | | | |
| 44 | 3.0 | | | |
| 45 | 53.6 | 14.1 ± .2 | $\rightarrow CHS^+ + C_2H_4 + H$ | 279 |
| | | | $\rightarrow CHS^+ + C_2H_3 + H_2$ | 280 |
| 46 | 45.8 | 12.4 ± .3 | $\rightarrow CH_2S^+ + C_2H_2 + H_2$ | 251 |
| 47 | 14.3 | 13.5 ± .2 | $\rightarrow CH_3S^+ + C_2H_2 + H$ | 224 |
| 48 | 3.6 | | | |
| 57 | 3.8 | | | |
| 58 | 8.9 | 15.6 ± .4 | $\rightarrow C_2H_2S^+ + CH_3 + H$ | 295 |
| 59 | 27.2 | 12.3 ± .3 | $\rightarrow C_2H_3S^+ + CH_3$ | 271 |
| 60 | 2.6 | | | |
| 69 | 2.5 | | | |
| 71 | 2.9 | | | |
| 73 | 10.3 | 11.2 ± .3 | $\rightarrow C_3H_5S^+ + H$ | 226 |
| 74 | 95.9 | 8.6 ± .2 | $\rightarrow C_3H_6S^+$ | 217 |
| 75 | 6.6 | | | |
| 76 | 5.2 | | | |

$m/e$ = **27.**—A value of 288 kcal./mole is calculated for $\Delta H_f^+$($C_2H_3$) assuming that the formation of

(1) This work was supported by the U. S. Atomic Energy Commission under Contract No. AT(11-1)-751 with Kansas State University. It comprises a portion of a dissertation to be presented by B. G. Hobrock to the Graduate School of Kansas State University in partial fulfillment of requirements for the degree of Doctor of Philosophy.

(2) E. J. Gallegos and R. W. Kiser, *J. Phys. Chem.*, **65**, 1177 (1961).

(3) E. J. Gallegos and R. W. Kiser, *ibid.*, **66**, 136 (1962).

(4) E. J. Gallegos and R. W. Kiser, *J. Am. Chem. Soc.*, **83**, 773 (1961).

(5) B. G. Hobrock and R. W. Kiser, *J. Phys. Chem.*, in press (1962).

(6) J. W. Warren, *Nature*, **165**, 811 (1950).

(7) F. P. Lossing, A. W. Tickner, and W. A. Bryce, *J. Chem. Phys.*, **19**, 1254 (1951).

(8) R. W. Kiser and E. J. Gallegos, *J. Phys. Chem*, **66**, 947 (1962).

(9) J. L. Franklin, *Ind. Eng. Chem.*, **41**, 1070 (1949).

(10) F. H. Field and J. L. Franklin, "Electron Impact Phenomena and the Properties of Gaseous Ions," Academic Press, Inc., New York, N. Y., 1957.

TABLE II

MOLECULAR IONIZATION POTENTIALS OF SOME THIACYCLOALKANES (IN E.V.)

| Molecule | | Calculated[a] | | Measured |
|---|---|---|---|---|
| *b* | 1.55 | 1.55 | 1.28 | |
| *c* | 1.99 | .. | .. | |
| *e* | 13.31 | 13.31 | 13.04 | |
| *f* | 10.46 | 8.87 | 8.87 | |
| $CH_2—CH_2S$ | 9.08[b] | (8.87) | (8.87) | 8.87[b] |
| $CH_3CHCH_2S$ | 9.02 | 8.38 | 8.51 | 8.6[c] |
| $CH_2CH_2CH_2S$ | 8.43[b] | .. | .. | 8.64[d] |

[a] The first column gives the parameters due to Franklin (see ref. 11); the second and third columns assume that the $-CHCH_2S$ unit may be treated as a group and the other parameters are those given by Franklin. [b] See ref. 2. [c] This work. [d] L.D. Isaacs, W. C. Price, and R. G. Ridley, "Vacuum Ultraviolet Spectra and Molecular Ionization Potentials," in "The Threshold of Space," Edited by M. Zelikoff, Pergamon Press, Ltd., London, 1957, pp. 143–151.

$C_2H_3^+$ from propylene sulfide is accompanied by the neutral fragments $CH_2S$ + H. This value is in good agreement with that of 280 kcal./mole reported by Field and Franklin.[10]

*m/e* = **37.**—The formation of $C_3H^+$ from propylene sulfide appears to occur by the process in Table I. The abundance of this ion was quite small and therefore the appearance potential was rather difficult to measure; however, fair agreement is obtained assuming that the neutral fragments S + $H_2$ + 3H are formed. We calculate $\Delta H_f^+(C_3H)$ = 322 kcal./mole; 309 kcal./mole is reported by Field and Franklin.[10]

*m/e* = **38.**—$C_3H_2^+$ is believed to be formed by a process which includes the neutral fragments $H_2S$ + 2H. The heat of formation for $C_3H^+$ calculated from the energetics for this process is 363 kcal./mole, in good agreement with the literature value of 360 kcal./mole.[10] Another process which cannot be entirely ruled out, as indicated by the energetics, is $C_3H_6S \rightarrow C_3H_2^+ + SH + H + H_2$; this leads to $\Delta H_f^+(C_3H_2)$ = 379 kcal./mole.

*m/e* = **39.**—The energetics indicate that $C_3H_3^+$ is formed by a process which includes the neutral fragments $H_2$ + H + S. The heat of formation calculated for $C_3H_3^+$ is 281 kcal./mole, in agreement with the literature.[10]

*m/e* = **40.**—The ion at *m/e* 40 is $C_3H_4^+$ and the thermochemical calculations result in $\Delta H_f^+(C_3H_4)$ = 298 kcal./mole, assuming the neutral fragments to be S + $H_2$.

*m/e* = **41.**—This ion is the dominant specie in the propylene sulfide mass spectrum and can only be $C_3H_5^+$. Only fair agreement between $\Delta H_f^+(C_3H_5)$ = 253 kcal./mole and various literature values[10] is noted for the process $C_3H_6S \rightarrow C_3H_6^+ +$ SH, but the energetics rule out any other process.

*m/e* = **45.**—If the formation of $CHS^+$ from propylene sulfide is accompanied by the neutral fragments $C_2H_4$ + H, $\Delta H_f^+(CHS)$ = 279 kcal./mole, which is in good agreement with the heats of formation for this ion obtained by Gallegos and Kiser[2,3] for other sulfur-containing heterocyclics and values obtained by us for straight-chain sulfides.[5] Also possible, however, is a process in which the neutral fragments $C_2H_3$ + $H_2$ are formed. From the energetics for this process, $\Delta H_f^+(CHS)$ = 280 kcal./mole.

*m/e* = **46.**—This ion is quite abundant in the mass spectrum of propylene sulfide and can only be $CH_2S^+$. From the measured appearance potential $\Delta H_f^+(CH_2S)$ = 251 kcal./mole if the accompanying neutral fragments are $C_2H_2$ + $H_2$. This is somewhat high in comparison to values given by Gallegos and Kiser[2,3] but other processes are eliminated by the energetics.

*m/e* = **47.**—A heat of formation of 224 kcal./mole is calculated for $CH_3S^+$ if the neutral fragments are $C_2H_2$ + H. This result is in good agreement with the literature value of 222 kcal./mole.[10]

*m/e* = **58.**—The ion of *m/e* = 58 is $C_2H_2S^+$ and is thought to be formed by the process shown in Table I. The heat of formation of $C_2H_2S^+$ = 295 kcal./mole is somewhat higher than those reported by Gallegos and Kiser[2,3] but other processes are indicated by energetic considerations to be less probable.

*m/e* = **59.**—This ion is thought to be formed by the removal of a $CH_3$ group from the parent molecule. $\Delta H_f^+(C_2H_3S)$ = 271 kcal./mole agrees rather poorly with literature values,[4] but any other process is less probable, as indicated by the thermochemical calculations.

*m/e* = **73.**—Abstraction of a hydrogen atom from $C_3H_6S^+$ results in the ion *m/e* = 73. We calculate $\Delta H_f^+(C_3H_5S)$ = 226 kcal./mole. The heat of formation of this ion has not been determined previously.

*m/e* = **74.**—This is the parent molecule-ion from propylene sulfide. Using the experimentally determined ionization potential, $\Delta H_f^+(C_3H_6S)$ = 217 kcal./mole. This is in good agreement with the value of 220 kcal./mole calculated from the trimethylene sulfide study.[3] This also indicates that our estimation of the heat of formation of propylene sulfide gave a reasonable value.

(11) J. L. Franklin, *J. Chem. Phys.*, **22**, 1304 (1954).

## THE AFFINITY OF HYDROHALIC ACIDS FOR TRI-*n*-OCTYLAMINE

BY ARCHIE S. WILSON AND NED A. WOGMAN

*Hanford Laboratories Operation, General Electric Company, Richland, Washington*

*Received February 13, 1962*

The salts of high molecular weight tertiary amines are soluble in a variety of organic solvents which are immiscible with water. This property of the amines has made possible the extraction of metallic complex ions and other anions from acidic aqueous solutions.[1-3]

We have been interested in understanding the factors which are important in these extractions. In the course of our study, we have measured the affinity of the hydrohalic acids for tri-*n*-octylamine (TOA) dissolved in a variety of solvents and at different concentrations. In addition to the affinity measurements, the extraction of the

(1) E. L. Smith and J. E. Page, *J. Soc. Chem. Ind.*, **67**, 48 (1948).

(2) W. E. Keder, J. C. Sheppard, and A. S. Wilson, *J. Inorg. Nucl. Chem.*, **12**, 327 (1960).

(3) F. L. Moore, "Liquid Extraction with High-Molecular-Weight Amines," NAS-NS-3101 (1960).

hydrohalic acids into aromatic solvent solutions of TOA also has been measured as a function of aqueous acid concentrations.

### Experimental

**A. Chemicals.**—TOA, obtained from the Chemical Procurement Co., contained a colored impurity which was removed by crystallizing the amine hydrochloride etherate four times from ether at −30°. The amine was obtained by neutralization of this salt and had an equivalent weight of 339.7 ± 0.8 g. as determined by the method of C. D. Wagner, *et al.*[4]

No secondary or primary amine was detected in the TOA, which analyzed: C, 81.72; H, 14.58; and N, 4.02. The index of refraction was $1.447^{25}_{D}$ as compared to the literature[5] value, $1.450^{19.5}_{D}$.

Hydrofluoric and hydrochloric acids were Baker and Adamson's C.P. grade and were used as received. Hydrobromic acid, Baker and Adamson's reagent grade, was purified by aerating with $H_2S$, distilling, and collecting the fraction boiling at 126 ± 1°. Hydriodic acid solutions were prepared from diluted Merck's reagent grade acid by $H_2S$ aeration and boiling to coagulate the sulfur and to remove $H_2S$. The solutions, free of $S^{-2}$ and $SO_4^{-2}$ were filtered and used the same day.

Toluene and xylene, Baker and Adamson's purified grade, cyclohexane, Eastman's spectro grade, and nitrobenzene, Eastman's White Label grade, were used as received. Commercial Solvents' manufacturing grade 2-nitropropane was distilled and the fraction boiling at 119.3–119.5° was used. Water was triply distilled.

**B. Procedure.**—The TOA solutions were prepared volumetrically from weighed amounts of the amine. Measured volumes of a TOA solution and water were equilibrated with enough acid to convert half of the amine to its salt and the pH of the resulting aqueous phase was determined with a Beckman Zeromatic meter using a saturated calomel electrode and a glass electrode. Titrations of the pure solvents showed that almost no acid was extracted. In the acid extraction experiments, the acid concentration in each phase was determined by standard acidimetry. All experiments were conducted at 25.0°.

### Results and Discussion

**Affinity Constants.**—The reactions of aqueous solutions of HCl, HBr, and HI with the amine, A, can be considered to form the amine salt, AHX, according to this equation: $\underline{A} + H^+ + X^- = \underline{AHX}$ where the underlined terms indicate the organic phase. The affinity constant, $K$, in terms of activities, $a$, molarities, $c$, and molar activity coefficients, $y$, can be written as: $K = (c_{\underline{AHX}}/c_{\underline{A}}a_{H^+}a_{X^-})(y_{\underline{AHX}}/y_{\underline{A}})$. When $c_{\underline{AHX}} = c_{\underline{A}}$, the half titration point, the apparent affinity constant, $K' = y_{\underline{A}}K/y_{\underline{AHX}}$, equals $1/a_{H^+}a_{X^-}$. Under these conditions $\log K' = -2$ pH since $a_{H^+} = a_{X^-}$.

For hydrofluoric acid, $\log K'$ was calculated by equating activities to concentrations and assuming that the amine salt was $AH(HF_2)$. This assumption was justified by the shape of the HF curve in Fig. 1. In this calculation a value of the aqueous HF concentration of 0.166 $M$ from Fig. 1 corresponds to the half titration point. The values of $a_{H^+}$ and $a_{HF_2^-}$ were calculated by the simultaneous solution of the equations involving the ionization constants of HF and $H_2F_2$[6] and the stoichiometric and charge balance relationships. The calculations yielded $a_{H^+} = 0.0125$, $a_{HF_2^-} = 0.00450$, and $\log K'_{H_2F_2} = 4.25$.

(4) C. D. Wagner, R. H. Brown, and E. D. Peters, *J. Am. Chem. Soc.*, **69**, 2609 (1947).

(5) O. Westphal and D. Jerchel, *Ber.*, **73B**, 1002 (1940).

(6) W. M. Latimer, "Oxidation Potentials," Prentice Hall, Inc., Englewood Cliffs, N. J., 1952, p. 52.

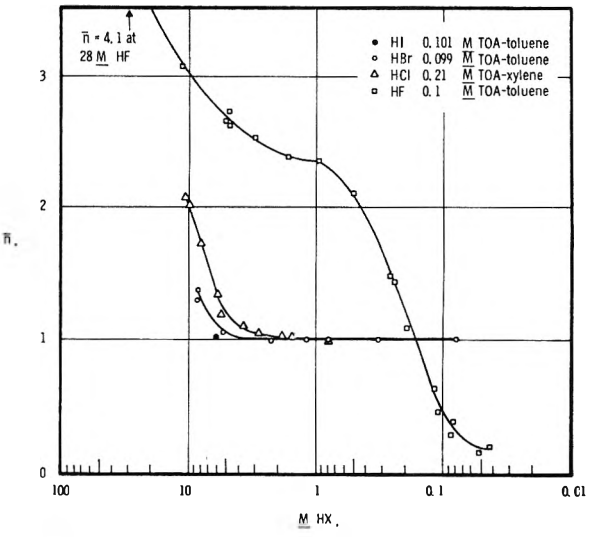


Fig. 1.—The extraction of the hydrohalic acids by TOA with $\bar{n}$, moles of acid to moles of amine, plotted *vs.* aqueous acid concentration.

In Table I are listed the apparent affinity constants at three different TOA concentrations in four different solvents for the hydrohalic acids. The $K'$ values for the two lower TOA concentrations increase in each solvent in the order HCl, HBr, HI. This observation, that the largest ion has the greatest tendency to extract from the aqueous phase into the organic phase, is that expected as recently discussed by Diamond and Tuck.[7] Moreover, a linear relationship exists between $\log K'$ and the crystal ionic radius of the halide ion for a given solvent and TOA concentration. A comparison of the difference between $\log K'$ values for two different solvents at a given TOA concentration shows that the difference does not vary greatly with hydrohalic acid.

The observation that the apparent affinity constants increase with an increase in the concentration of TOA can be rationalized on the basis that multiple ion clusters are present at these TOA concentrations.[8]

The results in Table I show that $K'$ increases as the dielectric constant of the solvent increases. Moreover, if $\log K'$ for hydrochloric acid is plotted *vs.* the dielectric constant of the solvent for 0.1 $M$ TOA in cyclohexane and toluene, 0.08 $M$ TOA in carbon tetrachloride,[9] and 0.02 $M$ TOA in benzene,[10] the data fit a straight line.

**Acid Extraction.**—The extraction behavior of the hydrohalic acids, except hydrofluoric acid, shown in Fig. 1, indicates that at aqueous concentrations below 2 $M$ the ratio of moles of acid to moles of amine in the organic phase ($\bar{n}$) does not exceed unity. There is no excess acid extracted until higher aqueous acid concentrations are reached. Thus, at an aqueous concentration of hydrochloric acid of 10 $M$, $\bar{n}$ is two. In the case of nitric acid extraction of TOA, it was concluded

(7) R. M. Diamond and D. G. Tuck, "Progress in Inorganic Chemistry," Interscience Publishers, New York, N. Y., 1960, p. 122.

(8) R. M. Fuoss and F. Accascina, "Electrolytic Conductance," Interscience Publishers, Inc., New York, N. Y., 1959.

(9) J. Bizot and B. Tremillon, *Bull. soc. chim. France*, 122 (1959).

(10) L. Newman and P. Klotz, *J. Phys. Chem.*, **65**, 795 (1961).

TABLE I
LOG $K'$

| Acid | TOA, $M$ | Solvent: Cyclohexane | Toluene | 2-Nitropropane | Nitrobenzene |
|---|---|---|---|---|---|
| $H_2F_2$ | 0.1 | ... | 4.25 | ... | ... |
| HCl | 0.1 | 3.03 | 4.87 | 8.44 | 8.60 |
| | 0.2 | 3.35[a] | 5.25 | 8.81 | 9.22 |
| | 1.0 | 5.14[b] | 5.94 | 9.24[c] | 9.10[c] |
| HBr | 0.1 | 4.11 | 6.08 | 8.91 | 9.68 |
| | 0.2 | 4.55[a] | 6.68 | 9.89 | 10.19 |
| | 1.0 | 6.87[a] | 7.69 | 11.00[c] | 10.84[c] |
| HI | 0.1 | 5.95 | 7.98 | 10.78 | 11.34 |
| | 0.2 | 6.84[a] | 8.80 | 11.59 | 12.27 |
| | 1.0 | 9.40[a] | 10.23 | 10.87[a] | 12.90[c] |
| Dielectric constant | | 2.02 at 20° | 2.38 at 25° | 25.52 at 20° | 34.82 at 25° |

[a] Two organic phases formed during titration. [b] Three organic phases formed during titration. [c] The concentration of amine was 0.6 $M$ rather than 1.0 $M$.

by Shevchenko, *et al.*,[11] that the species $(AHHO_3)$-$HNO_3$ was important. Similar species for the hydrohalic acids also may be considered.

It appears from Fig. 1 that the stronger the acid, the less likelihood there is of excess acid extraction. Hydrofluoric acid presents a unique case because apparently the extracted species, even in low aqueous acid concentration, does not predominate as AHF, but most likely it is $AH(HF_2)$. The value of $\bar{n}$ rises as high as four when the amine solution is equilibrated with 28 $M$ hydrofluoric acid.

**Acknowledgments.**—We wish to express our thanks to Mrs. W. G. Artman, who assisted in the laboratory. This work was performed under Contract No. AT(45-1)-1350 for the U. S. Atomic Energy Commission.

(11) V. P. Shevchenko, V. S. Shmidt, E. A. Nenarokomov, and K. A. Petrovd, *Zh. Neorgan. Khim.*, **5**, 1852 (1960).

## PROTON CHEMICAL SHIFTS IN PI COMPLEXES

BY J. C. SCHUG AND R. J. MARTIN

*Gulf Research & Development Company, Pittsburgh, Pennsylvania*

*Received February 15, 1962*

The fact that certain species form pi complexes[1] with aromatics and olefinic hydrocarbons is well established. However, only few of the known complexes have been studied in any detail. The dependence on electronic environment of the chemical shifts obtained from high-resolution nuclear magnetic resonance experiments[2] makes that technique an attractive one for such studies. In this note, we present a brief study of the proton chemical shifts in aqueous silver ion complexes of cyclohexene, *cis*-2-butene, benzene, and toluene.

### Experimental

All experiments were performed in an air-conditioned room, whose temperature was regulated to within ±2°F. Aqueous ($D_2O$) silver nitrate solutions of known concentration (0.6 to 6.0 moles/l.) were saturated with the desired hydrocarbon. The proton magnetic resonance spectra of the aqueous solutions were observed at a frequency of 40 Mc.p.s. with a Varian Model V 4300 spectrometer. All chemical shifts were measured relative to the impurity $H_2O$ signal by the sideband technique, using an electronic counter to measure the modulation frequency. From the ionic diamagnetic susceptibilities given by Selwood[3] and the $H_2O$ susceptibility given by Pople, *et al.*,[2] it was established that the chemical shifts between the $H_2O$ signals of the ionic solutions and that of pure water were satisfactorily accounted for by bulk susceptibility corrections[2] alone.

For the studies on the aromatics, we also measured the total amount of hydrocarbon taken up by each solution. This was done by extracting the hydrocarbon from the aqueous solution with isooctane[4] and determining the amount of extracted hydrocarbon from the intensity of an infrared absorption band (14.85 $\mu$ for benzene and 13.75 $\mu$ for toluene) and a previously prepared calibration curve.

### Results

The n.m.r. spectra of the olefin-containing aqueous solutions were independent of the $AgNO_3$ concentration, indicating the presence of a single species, presumably the 1:1 complex. The pertinent chemical shift data for the olefinic hydrocarbons are given in Table I. The data in column three of this table are in fair agreement with the findings of Powell and Sheppard.[5] The values of $\delta$ in the final column are the changes in chemical shift due to complex formation. This symbol will be used for the same purpose throughout the remainder of the note. For the two olefins, the $\delta$-values of corresponding protons (relative to the double bond) are very similar; it is inferred that this will be true of other olefins as well.

The n.m.r. spectra of the aromatic-containing aqueous solutions varied with the $AgNO_3$ concentration, but every spectrum contained only a single absorption due to aromatic protons. These features can be understood in terms of rapid exchange between several different species in equilibrium with one another.[6] Andrews and Keefer have studied[4] the equilibria in these systems and found evidence for the existence of free aromatic, 1:1 complex, and 1:2 complex, *i.e.*, Ar, $Ar{\cdot}Ag^+$, and $Ar{\cdot}Ag_2^{++}$. Furthermore, they were able to evaluate the two appropriate equilibrium constants for both benzene and toluene.

In such equilibrium systems, the observed chemical shift of a particular proton type can be written as an average of those in the various species[6]; *i.e.*

$$\langle\delta\rangle = \chi_0\delta_0 + \chi_1\delta_1 + \chi_2\delta_2 \qquad (1)$$

In this expression, the brackets signify the observed shifts; $\chi_0$ and $\delta_0$ represent, respectively, the fraction of hydrocarbon which is uncomplexed and the chemical shift of that form; $\chi_1$, $\delta_1$, $\chi_2$, and $\delta_2$ have similar meanings for the 1:1 and 1:2 complexes, respectively. In the following discussion, all shifts are referred to the uncomplexed molecules, whose shifts from the reference $H_2O$ signal

(1) R. S. Mulliken, *J. Am. Chem. Soc.*, **72**, 600 (1950); **74**, 811 (1952); *J. Phys. Chem.*, **56**, 801 (1952).

(2) J. A. Pople, W. G. Schneider, and H. J. Bernstein, "High-Resolution Nuclear Magnetic Resonance," McGraw-Hill Book Co., Inc., New York, N. Y., 1959.

(3) P. W. Selwood, "Magnetochemistry," 2nd Ed., Interscience Publishers, New York, N. Y., 1956, p. 78.

(4) L. J. Andrews and R. M. Keefer, *J. Am. Chem. Soc.*, **71**, 3644 (1949); **72**, 3113 (1950).

(5) D. B. Powell and N. Sheppard, *J. Chem. Soc.*, 2519 (1960).

(6) Reference 2, Chapter 10.

were taken from the tabulation by Pople, *et al.*[7] Thus, $\delta_0 = 0$ by definition.

In order to calculate the fractions $\chi_1$ and $\chi_2$ for a particular solution, the equilibrium constants must be known. The only values available, those of Andrews and Keefer,[4] proved to be inapplicable in our more concentrated solutions: the total hydrocarbon concentrations calculated from their constants were larger by factors of two to three than those determined in the present experiments. Since the evaluation of equilibrium constants was not our prime concern, we chose to analyze the data in a simpler manner.

Using parentheses to denote concentrations and defining total aromatic concentration by

$$(\mathrm{Ar})_T = (\mathrm{Ar}) + (\mathrm{Ar}\cdot\mathrm{Ag}^+) + (\mathrm{Ar}\cdot\mathrm{Ag}_2^{++}) \quad (2)$$

we can write eq. 1 in the form

$$(\mathrm{Ar})_T \langle\delta\rangle = \delta_1(\mathrm{Ar})_T - \delta_1(\mathrm{Ar}) + (\mathrm{Ar}\cdot\mathrm{Ag}_2^{++})[\delta_2 - \delta_1] \quad (3)$$

Plots of the product $[(\mathrm{Ar})_T \langle\delta\rangle]$ *vs.* $(\mathrm{Ar})_T$ for the aromatic protons of benzene and toluene are shown in Fig. 1. The units used are moles/l. for concentrations and cycles/sec. for chemical shifts. All toluene data have been scaled up by a factor of two in both directions to permit the plotting of both cases on the same scale. The observed shifts for the toluene $CH_3$ protons were all $\lesssim 1$ c.p.s.; since these are of the same order as the expected error, no conclusions could be drawn from them.

In view of eq. 3, the near linearity of the plots indicates that the concentration of 1:2 complex is never very large in either case. Then, the slopes of the straight lines give $\delta_1$, the chemical shifts of the 1:1 complexes relative to the uncomplexed molecules. These are −15.6 c.p.s. (−0.39 p.p.m.) for benzene and −17.1 c.p.s. (−0.43 p.p.m.) for toluene. These conclusions were strengthened by some parallel experiments on the solubility of benzene in aqueous $NaNO_3$ solutions. It was found that maximum benzene solubility occurs in pure water, and the solubility decreases at higher $NaNO_3$ concentrations. If the same trend occurs for the concentration of free aromatic, (Ar), in the $AgNO_3$ solutions, then the straight lines obtained cannot be due to approximate cancellation of the last two terms in eq. 3.

## Discussion

Two factors that could contribute appreciably to the chemical shifts found here are transfer of electrons from the hydrocarbon to the silver ion, and polarization effects. As to the first of these, if in each 1:1 complex, 0.1 to 0.2 electron were transferred to the silver ions, the entire chemical shifts could be explained.[8,9] However, this would not substantially affect the polarization effects, which we believe to be most important.

To estimate the polarization effects, the structure of the aqueous benzene·$Ag^+$ complex was assumed to be the same as that found[10] for crystalline

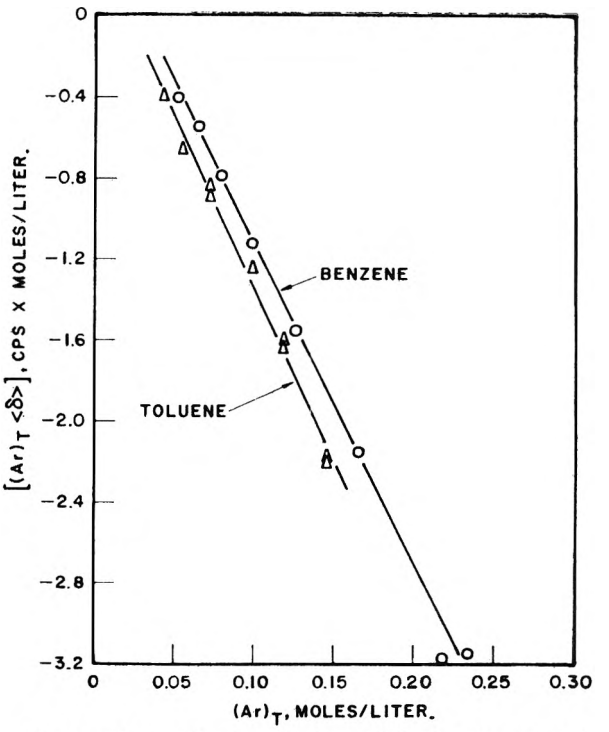


Fig. 1.—Plots of $[(\mathrm{Ar})_T \langle\delta\rangle]$ *vs.* $(\mathrm{Ar})_T$ for the aromatic protons of benzene and toluene. All toluene data have been scaled up by a factor of two on both axes. Observed chemical shifts, $\langle\delta\rangle$, are in cycles per second from the uncomplexed species, measured at 40 Mc.p.s. Total aromatic concentrations, $(\mathrm{Ar})_T$, are in moles per liter.

benzene·$Ag^+ClO_4^-$. Small changes in this structure will not affect our results. The electric fields at the protons of the aqueous benzene complex were estimated as arising from a charge distribution consisting of a point-positive charge at the position of the $Ag^+$ ion and two concentric hemispheric shells containing a uniform negative charge density and a uniform density of oriented point dipoles. The concentric shells were attempts to include the average effects of other ions and of nearby solvent molecules. The effects of the electric fields on the proton chemical shifts were estimated from the relation derived by Buckingham.[11] Some calculated results are given in Table II, where $N_A$ represents the total number of negative ions on the ionic hemisphere and $N_\mu$, the total number of water molecule dipoles on the hydration hemisphere. The protons are labeled so that proton 1 is closest to the bond occupied by the $Ag^+$ ion,[10] proton 2 is on the next carbon atom away, and proton 3 is farthest from the $Ag^+$ ion. The calculated shifts are appreciable and can easily explain the observed ones, which are about −0.40 p.p.m.

Polarization of the pi-electrons also could result in further contributions, due to changes in the ring current effect. However, using a dipole approximation of this effect,[12] we estimated that, although this may cause sizable chemical shifts in the individual protons, the effect on the average would be quite small.

(7) Reference 2, p. 263. These data were checked in this Laboratory.

(8) G. Fraenkel, R. E. Carter, A. McLachlan, and J. H. Richards, *J. Am. Chem. Soc.*, **82**, 5846 (1960).

(9) C. MacLean and E. L. Mackor, *Mol. Phys.*, **4**, 241 (1961).

(10) H. G. Smith and R. E. Rundle, *J. Am. Chem. Soc.*, **80**, 5075 (1958).

(11) A. D. Buckingham, *Can. J. Chem.*, **39**, 1158 (1960).

(12) H. M. McConnell, *J. Chem. Phys.*, **27**, 226 (1957).

The situation for toluene is quite comparable to that for benzene and needs no further discussion here.

TABLE I

PROTON CHEMICAL SHIFTS IN OLEFIN·$Ag^+$ COMPLEXES

| Complex | Proton | Chemical shifts in p.p.m., from internal $H_2O$: Aqueous complex | Free hydrocarbon[a] | δ, p.p.m. |
|---|---|---|---|---|
| $Ag^+$·*cis*-2-butene | CH | −1.37 | −0.72 | −0.65 |
| | $CH_3$ | +2.93 | +3.08 | −0.15 |
| $Ag^+$·cyclohexene | CH | −1.60 | −0.91 | −0.69 |
| | α-$CH_2$ | −2.60 | +2.74 | −0.14 |
| | β-$CH_2$ | +3.00 | +3.00 | 0.00 |

[a] Measured in dilute $CCl_4$ solution, corrected for bulk susceptibility.

TABLE II

CALCULATED CHEMICAL SHIFTS (IN P.P.M.) FOR BENZENE·$Ag^+$ COMPLEX, RELATIVE TO FREE BENZENE

| Proton[a] | $N_A = 0$ $N_\mu = 0$ | 0.2 1.0 | 0.2 3.0 | 0.5 1.0 | 0.5 3.0 | Experimental[b] |
|---|---|---|---|---|---|---|
| 1 | −0.87 | −0.63 | −0.39 | −0.50 | −0.27 | −0.65 |
| 2 | − .52 | − .42 | − .33 | − .36 | − .27 | − .15 |
| 3 | − .42 | − .32 | − .27 | − .26 | − .21 | − .00 |
| Av. | −0.60 | −0.46 | −0.33 | −0.37 | −0.25 | −0.39 |

[a] Proton 1 is closest to the $Ag^+$ ion; and proton 3, farthest from it. [b] The individual values are the shifts observed for the olefins (*cf.* Table I); and the average, that for benzene.

For the olefin complexes, no structures are known, but it is reasonable to suppose that the silver ion is located relative to the double bond in much the same manner as in benzene.[10] If this is true, then the calculated shifts for protons 1, 2, and 3 of Table II should roughly apply to the olefinic, alpha, and beta protons, respectively, of the olefins. On comparing Tables I and II, it is seen that order of magnitude agreement obtains, but that the calculated effects do not fall off sufficiently rapidly with distance from the $Ag^+$ ion. Approximate corrections for changes in the neighbor-anisotropy shielding[12] do not substantially improve the agreement.

In all cases, polarization effects also could be felt *via* changes in the hybridization of the carbon atomic orbitals, but we are presently unable to estimate this effect.

Because the polarization effects cannot be more accurately calculated, it is clear that no reliable estimates can be made for the amount of charge-transfer in the ground states of these complexes.

**Acknowledgments.**—The authors are gratetul to Dr. N. D. Coggeshall for his continuous encouragement, to Mr. L. R. Cousins for the infrared data, and to a referee for several helpful comments.

## SUBLIMATION AND DECOMPOSITION STUDIES ON BORON NITRIDE AND ALUMINUM NITRIDE[1]

BY LLOYD H. DREGER, V. V. DADAPE, AND JOHN L. MARGRAVE

*Department of Chemistry, University of Wisconsin, Madison, Wisconsin*

*Received February 27, 1962*

Langmuir free-evaporation rates for solid BN and AlN were measured with a microbalance built inside a vacuum system. This system has been used previously for several Knudsen effusion and Langmuir studies at high and low temperatures.[2]

### Experimental Techniques and Materials

The experimental technique was similar to that reported by Dreger and Margrave[2] where a sample of known surface area was suspended from the balance into an inductively heated carbon susceptor furnace by a tungsten wire hook in the case of the BN and a tungsten wire basket for the AlN. No reactions of the nitrides with tungsten were observed.

Temperatures were measured with a Leeds and Northrup optical pyrometer and the usual corrections for windows and mirror absorptions were made. The furnace tube acted essentially as a black body radiation source and was regarded as such.

The BN samples were 99.0+% pure, with oxide as a likely contaminant, and consisted of thin plates sawed from a compressed BN block.

The AlN sample was 99.0+% pure compressed powder, with Al being the most likely contaminant.

In the Langmuir free-evaporation technique,[3] the rate of weight loss, $m$, in g./cm.$^2$-sec., is related to the equilibrium vapor pressure by the equation

$$P_{\text{exptl.}} = \alpha_s P_{\text{eq}} = m\sqrt{\frac{2\pi RT}{M}}$$

where $\alpha_s$ is the sublimation coefficient and $M$ is the weighted average molecular weight of the subliming species. For simple substances, $\alpha$ is sometimes equal to unity and the experimental pressure is then equal to the equilibrium pressure. However, this is not the case for BN and AlN.

**Sublimation and Decomposition of Boron Nitride.**—The behavior of BN at high temperatures has been previously studied by Lorenz and Woolcock[4] who measured directly the pressure of $N_2$ at equilibrium over BN from 1968 to 2318°K. From their data, Kelley[5] deduced a heat of formation of BN of −32 kcal./mole on the basis of the slope of a log $K$ *vs.* $1/T$ plot. A more modern treatment of these data may be made utilizing free energy functions.

With the experimental $N_2$ pressures of Lorenz and Woolcock[4] and an estimated change of free energy function of −42.3 cal. deg.$^{-1}$ mole$^{-1}$ for the decomposition reaction, one calculates $\Delta H_f^\circ{}_{298} = -50 \pm 5$ for BN(s) as shown in Table I. More negative heats may be obtained by revising the high temperature thermal data for B(s) and BN(s) which are only measured up to 1600°K.

Dworkin, Sasmor, and Van Artsdalen[6] measured the heat of formation of BN by oxygen bomb calorimetry and found $\Delta H_f^\circ{}_{298}$ to be −60.3 kcal./mole with possible errors due to incomplete burning. This value, −60 ± 1 kcal./mole, has recently been confirmed by measuring the heat of the direct nitridation of boron,[7] by another study in which

(1) Abstracted in part from the thesis presented by Lloyd H. Dreger in partial fulfillment of the requirements for the Doctor of Philosophy degree at the University of Wisconsin, 1961.

(2) L. Dreger and J. Margrave, *J. Phys. Chem.*, **64**, 1323 (1960), and earlier papers.

(3) J. L. Margrave, in "Physico-Chemical Measurements at High-Temperatures," edited by Bockris, White, and Mackenzie, Butterworths, 1959, Chapter 10.

(4) R. Lorenz and J. Woolcock, *Z. anorg. allgem. Chem.*, **176**, 289 (1928).

(5) K. K. Kelley, U.S. Bureau of Mines Bull. 407 (1937), as cited in NBS Circular 500.

(6) A. S. Dworkin, D. J. Sasmor, and E. R. Van Artsdalen, *J. Chem. Phys.*, **22**, 837 (1954).

(7) G. L. Gal'chenko, A. N. Kornilov, B. I. Timofeev, and S. M. Skuratov, *Proc. Acad. Sci. USSR, Chem. Sect.*, **106**, 1016 (1959); p. 635 in English transl.

BN was oxidized in $O_2$[8] and by a calorimetric study of the reaction $2BN + 3F_2 \rightarrow 2BF_3 + N_2$.[9] Thus, one must regard the Lorenz and Woolcock data as incorrect unless major changes in the high temperature thermal functions are postulated.

TABLE I

HEAT OF FORMATION OF BN(s) FROM EQUILIBRIUM MEASUREMENTS OF LORENZ AND WOOLCOCK

$2BN(s) \rightarrow 2B(amorp) + N_2(g)$

| $T$, °K. | $P_{N_2}$, mm. | $\Delta H^0_{298}$, kcal./mole $N_2$ |
|---|---|---|
| 1968 | 23 | 96.9 |
| 2018 | 26 | 98.9 |
| 2013 | 27 | 98.5 |
| 2073 | 31 | 100.9 |
| 2093 | 43 | 100.6 |
| 2163 | 67 | 102.0 |
| 2158 | 70 | 102.0 |
| 2203 | 79 | 103.1 |
| 2243 | 97 | 104.0 |
| 2318 | 158 | 105.3 |

Av. $\Delta H^0_{298}$ = 101.2 kcal./mole $N_2$ (or 50.6 kcal./mole BN)

Hoch and White[10] have studied the decomposition of BN in carbon Knudsen cells and support a value of $\Delta H_f^0{}_{298} = -60$ kcal./mole for BN from the slope of a log $P$ *vs.* $1/T$ plot for the reaction

$$BN(s) \longrightarrow B(s) + 1/2\ N_2(g)$$

although their absolute pressures are too low by a factor of 3 to 10,000 times depending upon the hole size.

Schissel and Williams[11] in a mass spectrometric study of the thermal decomposition of BN report no evidence for complex molecular species and support a heat of formation of about −60 kcal./mole. A low $\alpha$ was not considered.

In this work BN was studied over the temperature range 1421–2031°K. Considerable scattering was observed during the first experiments until a preliminary treatment for removal of $B_2O_3$ impurity in the sample was adopted. The results are summarized in Table II assuming the reaction to be

$$2BN(s) \rightleftarrows 2B(amorp.) + N_2(g)$$

$N_2(g)$ was assumed to be the only significant volatile species since the study of Schissel showed no appreciable BN(g) at these temperatures. The data of Hoch and White[10] were corrected for the hole to surface area ratio for better comparison with the Langmuir data presented here. With the heat of formation at 298°K. as −60.3 kcal./mole for BN,[6-9] and free energy functions from Stull and Sinke,[12] Evans, Wagman, and Prosen,[13] and Wise, Altman, and Margrave,[14] one may compute the equilibrium decomposition pressures. The experimental $N_2$ pressures are lower than those calculated for equilibrium and indicate an apparent heat of decomposition at 298°K., assuming $\alpha_s = 1$ in the range 135–150 kcal./mole $N_2$. From typical data of Hoch and White,[10] one calculates $\Delta H_{298}{}^{app}$ with $\alpha_s = 1$, as 145.

TABLE II

EXPERIMENTAL DECOMPOSITION PRESSURES OF $N_2$ OVER BN

$2\ BN(s) \rightarrow 2B(amorp.) + N_2(g)$

| Temp., °K. | Measured $P_{N_2}$, mm. | $\Delta H_{298}{}^{app}$; ($\alpha_s = 1$) kcal./mole $N_2$ |
|---|---|---|
| 1421 | $1.42 \times 10^{-6}$ | 130.3[a] |
| 1465 | $8.86 \times 10^{-7}$ | 122.3[a] |
| 1567 | $1.64 \times 10^{-6}$ | 128.7[a] |
| 1598 | $3.01 \times 10^{-7}$ | 136.6 |
| 1628 | $1.05 \times 10^{-6}$ | 135.1 |
| 1671 | $4.52 \times 10^{-6}$ | 133.8[a] |
| 1677 | $1.49 \times 10^{-6}$ | 137.9 |
| 1685 | $1.22 \times 10^{-6}$ | 139.3 |
| 1725 | $2.51 \times 10^{-6}$ | 140.0 |
| 1758 | $3.69 \times 10^{-6}$ | 141.4 |
| 1777 | $1.51 \times 10^{-5}$ | 137.9 |
| 1779 | $1.17 \times 10^{-5}$ | 139.0 |
| 1868 | $4.13 \times 10^{-5}$ | 141.2 |
| 1868 | $2.87 \times 10^{-5}$ | 142.5 |
| 1871 | $7.23 \times 10^{-6}$ | 147.9 |
| 1913 | $5.88 \times 10^{-5}$ | 143.2 |
| 1914 | $2.54 \times 10^{-5}$ | 146.5 |
| 1914 | $4.12 \times 10^{-5}$ | 144.6 |
| 1982 | $3.60 \times 10^{-5}$ | 150.3 |
| 1987 | $5.91 \times 10^{-5}$ | 148.7 |
| 2003 | $7.91 \times 10^{-5}$ | 148.7 |
| 2003 | $1.07 \times 10^{-4}$ | 147.6 |
| 2003 | $7.71 \times 10^{-5}$ | 149.0 |
| 2018 | $6.70 \times 10^{-5}$ | 150.5 |
| 2031 | $1.82 \times 10^{-4}$ | 147.5 |
| 2031 | $1.09 \times 10^{-4}$ | 149.5 |

[a] Given 0 weight in calculations.

In an extended decomposition run at 2000°K. on a BN sample where about 25% of the sample was decomposed, the sample was found to be heavily coated with boron. It also was observed that, when BN was heated rapidly to temperatures over 2500°K. *in vacuo* in a solar mirror, only $N_2$ was evolved and no appreciable solid deposit was detected on a Pyrex balloon. These experiments would tend to confirm the absence of BN(g) in the vapor phase.

During the extended heating, the rate of weight loss decreased as a function of time until it approached a constant rate determined by the vapor pressure of boron as given by Stull and Sinke.[12] This would indicate that the $N_2$ molecule is hindered in escaping from the BN surface by the coating of the sample with a layer of boron. For this reason, new BN samples were used for each of several runs in an attempt to eliminate this problem. It was necessary to degas each sample at 1800°K. for about an hour before starting a run in order to remove any $B_2O_3$ impurity but the amount of boron coating the sample at the end of

(8) Private communication, American Cyanamid Company, Stamford, Connecticut.

(9) S. S. Wise, W. N. Hubbard, H. Feder, and J. L. Margrave, Argonne National Laboratory, Report 6472, January, 1962.

(10) M. Hoch and D. White, "The Vaporization of Boron Nitride and Aluminum Nitride," ASTIA Unclassified Report 142616, October 29, 1956; Technical Research Report MCC-1023-TR-216, Ohio State University, Research Foundation, October 29, 1956.

(11) P. Schissel and W. Williams, *Bull. Am. Phys. Soc.*, **4**, 139 (1959).

(12) D. R. Stull and G. Sinke, "Thermodynamic Properties of the Elements," Advances in Chemistry Series, No. 18, A. C. S. (1956).

(13) W. H. Evans, D. D. Wagman, and E. J. Prosen, National Bureau of Standards Report No. 6252, December 15, 1958.

(14) S. S. Wise, R. Altman, and J. L. Margrave, *J. Phys. Chem.*, **64**, 915 (1960).

this time was small. The correction for the effect of the boron layer formed was about a factor of 2 in the highest temperature runs. From the corrected data one concludes that $\Delta H_f^0{}_{298}$ of BN $\leq -60 \pm 2$ kcal./mole.

Holden, Speiser, and Johnston[15a] and Johnston and Marshall[15b] have suggested a relationship between $\Delta H_{app}$, $\Delta H_{eq}$, and $\alpha_s$, a mean sublimation coefficient. One may extend this idea and define

$$\Delta H_{298}{}^{apparent} - \Delta H_{298}{}^{eq} = -RT \ln \alpha_s{}^n = \Delta F^{activation}$$

where $n$ is the number of moles of subliming species. $\Delta H_{298}{}^{apparent}$ is the apparent heat of reaction as derived from free energy functions and the experimental vapor pressures, and $\Delta H_{298}{}^{eq}$ is the equilibrium heat of reaction.

Assuming $\alpha$ to have the form

$$\alpha_s = e^{-\Delta H^{act}/RT}\, e^{\Delta S^{act}/R}$$

one expects a plot of ln $\alpha$ *vs.* $1/T$ to have a slope equal to $-\Delta H^{act}/R$ and an intercept of $\Delta S^{act}/R$.

Log $\alpha$ was found to vary from $-2.01$ at 2000°K. to $-2.18$ at 1400°K., which yields $\Delta H^{act} = 3.9 \pm 2$ kcal./mole and $\Delta S^{act} = -7.3 \pm 1$ e.u.

**Sublimation and Decomposition of Aluminum Nitride.**—Hoch and White[10] also have studied AlN using carbon Knudsen cells. They suggest the reaction

$$2AlN(s) \rightleftarrows 2Al(g) + N_2(g)$$

The existence of gaseous AlN molecules has not been clearly established and one may safely assume that AlN(g) is negligible as a vapor species.[11]

The standard heat of formation of solid AlN has been determined by Neugebauer and Margrave[16] by direct nitridation of aluminum in a bomb calorimeter as $-76.5$ kcal./mole and this value recently has been confirmed.[17] Other determinations by Neumann, Kroger, and Haebler[18] ($-57.4$ kcal./mole); by Fichter and Jenney[19] ($-71.5$ kcal./mole); and by Schissel and Williams[11] ($-63$ kcal./mole) are apparently in error. With $-76.5$ kcal./mole as the heat of formation, together with data on Al and $N_2$ from Stull and Sinke,[12] one computes the heat of the decomposition reaction, $\Delta H^0{}_{298}$, as 308 kcal./mole $N_2$.

AlN was studied over the temperature range 1450 to 1870°K. and the decomposition pressures are summarized in Table III. The data of Hoch and White were again corrected for the hole to surface area ratio for better comparison with the Langmuir data. From the available free energy functions[17,20] and the known heat of formation, one may calculate the equilibrium Al and $N_2$ pressures. The experimentally observed pressures are lower and indicate an apparent $\Delta H_{298}$ in the range 365–387 kcal./mole $N_2$ if $\alpha_s = 1$. If AlN vaporizes stoichiometrically, one may show that

(15) (a) R. B. Holden, R. Speiser, and H. L. Johnston, *J. Am. Chem. Soc.*, **70**, 3897 (1948); (b) H. L. Johnston and A. L. Marshall, *ibid.*, **62**, 1382 (1940).

(16) C. A. Neugebauer and J. L. Margrave, *Z. anorg. allgem. Chem.*, **290**, 82 (1957).

(17) A. D. Mah, E. G. King, W. W. Weller, and A. U. Christensen, U. S. Bureau of Mines Rept. Invest. 5716 (1961).

(18) B. Neumann, C. Kroger, and H. Haebler, *Z. anorg. allgem. Chem.*, **204**, 81 (1932).

(19) F. Fichter and E. Jenney, *Helv. Chim. Acta*, **5**, 448 (1922).

(20) R. Mezaki and J. L. Margrave, unpublished work, University of Wisconsin, 1961.

TABLE III

EXPERIMENTAL DECOMPOSITION PRESSURE DATA FOR AlN

$$2AlN(s) \rightarrow 2Al(g) + N_2(g)$$

| $T$, °K. | Measured $P_{mm}{}^{total}$ | $\Delta H_{298}{}^{app}$; ($\alpha_s = 1$), kcal./mole $N_2$ |
|---|---|---|
| 1450 | $6.07 \times 10^{-9}$ | 387.4[a] |
| 1590 | $1.32 \times 10^{-6}$ | 373.6 |
| 1590 | $1.04 \times 10^{-6}$ | 375.9 |
| 1635 | $6.89 \times 10^{-6}$ | 367.9 |
| 1635 | $9.16 \times 10^{-6}$ | 365.1 |
| 1647 | $6.61 \times 10^{-6}$ | 370.9 |
| 1762 | $1.03 \times 10^{-4}$ | 367.6 |
| 1762 | $1.05 \times 10^{-4}$ | 367.6 |
| 1762 | $1.23 \times 10^{-4}$ | 365.7 |
| 1869 | $6.63 \times 10^{-4}$ | 368.1 |
| 1870 | $6.00 \times 10^{-4}$ | 371.7 |

[a] Given 0 weight in calculations.

$$\alpha_s{}^3 K_{eq} = 0.148\, P^3{}_{total}$$

For the same relationship discussed previously

$$\Delta H_{298}{}^{apparent} - \Delta H_{298}{}^{eq} = -RT \ln \alpha_s{}^n$$

where $n = 3$ and $\alpha_s$, is a mean sublimation coefficient, one calculates log $\alpha_s = -3.13$ at 1590°K. and $-2.46$ at 1869°K., leading to $\Delta H^{act} = 33 \pm 6$ kcal./vaporizing molecule and $\Delta S^{act} = 6 \pm 4$ e.u./vaporizing molecule. The data of Hoch and White,[10] when treated in a similar manner, give $\alpha$-values that are in agreement with this work. Hildenbrand[21] has found $\alpha \approx 2.2 \times 10^{-3}$ for AlN decomposition from torque Knudsen measurements.

In the case of AlN, the problem of a non-volatile metal layer does not exist. X-Ray studies indicated that the lattice constant of AlN did not change detectably during evaporation and so it may be assumed that Al and $N_2$ are evolved in a stoichiometric ratio. However, one might expect different values for the sublimation coefficients of Al(g) and $N_2$(g) on an AlN surface. No effort has been made to distinguish the two sublimation coefficients but a large difference seems unlikely because of the essentially congruent vaporization observed.

## Conclusions

Both BN and AlN appear to undergo decomposition at higher temperatures to the elements, but at rates which are only about $10^{-2}$–$10^{-3}$ of the thermodynamically expected rates. There is no evidence for appreciable BN(g) or AlN(g) at temperatures up to 2000°K.

A similarly low sublimation coefficient for $Mg_3N_2$ has been reported by Soulen, Sthapitanonda, and Margrave.[22] These reports are to be contrasted with Knudsen studies of TiN and ZrN made by Hoch, Dingledy, and Johnston,[23] where the sublimation coefficient is reported as unity. Actually, the range of hole sizes used merely proves $\alpha_s \geq 10^{-3}$ and recent Langmuir studies on TiN[24] indicate $\alpha_s \approx 10^{-1}$. Both TiN and ZrN form defect lattices

(21) D. Hildenbrand, Aeronutronic Technical Report No. U-1497, December 15, 1961.

(22) J. R. Soulen, P. Sthapitanonda, and J. L. Margrave, *J. Phys. Chem.*, **59**, 132 (1955).

(23) M. Hoch, D. Dingledy, and H. Johnston, *J. Am. Chem. Soc.*, **77**, 304 (1955).

(24) L. Dreger and J. Margrave, unpublished work, 1960.

from which nitrogen probably is freer to escape than from the more strictly stoichiometric crystal lattices of BN, AlN, and $Mg_3N_2$.

A possible mechanism by which metal nitrides could undergo decomposition to the elements with escape of nitrogen molecules and sometimes metal atoms to the gas phase might involve these steps: (1) escape of metal and nitrogen atoms from crystal ledges or imperfections to adsorbed positions on the surface; (2) equilibration of atoms in the adsorbed layer to yield $N_2$ molecules adsorbed and metal crystal nuclei if the metal is sufficiently non-volatile (like boron); (3) escape of adsorbed $N_2$ and adsorbed metal atoms to the gas phase.

**Acknowledgments.**—The authors wish to acknowledge the financial support of this research by the Wisconsin Alumni Research Foundation, the National Aeronautics and Space Administration and its sub-contractor, the Callery Chemical Company, and the Atomic Energy Commission.

## CRACKING OF HYDROCARBONS OVER A PROMOTED ALUMINA CATALYST

BY J. H. SINFELT AND J. C. ROHRER

*Esso Research and Engineering Co., Linden, N. J.*

*Received March 1, 1962*

Alumina possesses some catalytic activity for cracking reactions of saturated hydrocarbons.[1-3] The presence of halogens (Cl or F) has been shown to promote the cracking activity of alumina,[1,2] presumably because of an increase in the number or strength of acid sites on the surface. To obtain further information regarding the nature of cracking reactions over halogen-promoted alumina, data have been obtained on the kinetics of cracking of *n*-heptane and methylcyclopentane over an alumina catalyst containing 1.2 wt. % chlorine. For the most part, the reactions were carried out in the presence of hydrogen, with one of the objectives of the study being the determination of the effects of hydrogen pressure on reaction rates and product distribution.

### Experimental

**Procedure.**—The *n*-heptane and methylcyclopentane were contacted with the catalyst in the presence of hydrogen, using a flow reactor technique described elsewhere.[4,5] The reaction products were analyzed by a procedure, also described elsewhere,[5] consisting of a combination of chromatographic columns coupled directly to the reactor outlet.

**Materials.**—Phillips pure grade *n*-heptane and methylcyclopentane (> 99 mole % pure) were used throughout. Both these hydrocarbons and the hydrogen were dried to less than 5 p.p.m. water using procedures described previously.[4,5] The alumina catalyst used in this study contained 1.2 wt. % chlorine. The catalyst was calcined in air for 4 hr. at 593°, and had a surface area of 210 $m.^2/g$. Prior to calcination, X-ray diffraction data obtained in this Laboratory showed the alumina to be β-alumina trihydrate, a form of alumina which has been described elsewhere.[6]

### Results

When *n*-heptane or methylcyclopentane is passed over the catalyst used in this work, the observed reactions are essentially limited to cracking. The reaction products are mixtures of paraffins and olefins, the former resulting in large part from hydrogenation of the latter when the reactions are carried out in the presence of hydrogen. In the case of *n*-heptane, cracking refers to the production of olefins and paraffins of lower carbon number than the reactant. In the case of methylcyclopentane, cracking refers to the production of hexenes and hexanes as well as lower carbon number paraffins and olefins. At the low conversion levels (1 to 12%) studied in the present work, the average distribution of the products by carbon number is shown below

| | *n*-Heptane | Methylcyclopentane |
|---|---|---|
| $C_1$ | 17 | 12 |
| $C_2$ | 23 | 17 |
| $C_3$ | 27 | 10 |
| $C_4$ | 23 | 22 |
| $C_5$ | 10 | 2 |
| $C_6$ | | 37 |

With respect to other reaction products, trace amounts of isoheptanes, toluene, methylcyclohexane, and dimethylcyclopentanes were observed in the products from *n*-heptane. Trace quantities of cyclohexane and benzene were observed in the products from methylcyclopentane.

A complete resolution of the paraffins and olefins was not obtained by the analytical procedure used in this work. However, in the case of *n*-heptane some data were obtained at 527° on the relative amounts of propane and propylene in the reaction products. Of particular interest is the effect of hydrogen pressure on the ratio of propane to propylene, as shown below

| $p_H$, atm. | Propane/propylene |
|---|---|
| 2 | 0.5 |
| 20 | 5.0 |

Increasing the hydrogen pressure tenfold thus increases the ratio of propane/propylene tenfold. However, the ratios are about 70-fold lower than the equilibrium ratios[7] at these conditions. Similar results have been observed previously when cracking methylcyclopentane over a pure alumina.[3]

Rates of cracking of *n*-heptane and methylcyclopentane are shown in Table I as a function of temperature and hydrogen partial pressure. The reaction rates were measured at low conversion levels (1 to 12%) and were evaluated using the relation

$$r = \frac{F}{W}\Delta x \qquad (1)$$

where $F$ represents the feed rate of the hydrocarbon reactant in g. moles per hour, $W$ is the weight of catalyst in grams, and $\Delta x$ is the fraction of the hy-

(1) C. G. Myers and G. W. Munns, Jr., *Ind. Eng. Chem.*, **50**, 1727 (1958).

(2) K. W. McHenry, R. J. Bertolacini, H. M. Brennan, J. L. Wilson, and H. S. Seelig, Paper No. 117, Section II, "Proceedings of the Second International Congress on Catalysis," Paris, France, 1960.

(3) J. H. Sinfelt and J. C. Rohrer, *J. Phys. Chem.*, **65**, 2272 (1961).

(4) J. H. Sinfelt, H. Hurwitz, and J. C. Rohrer, *ibid.*, **64**, 892 (1960).

(5) J. H. Sinfelt and J. C. Rohrer, *ibid.*, **65**, 978 (1961).

(6) H. C. Stumpf, A. S. Russell, J. W. Newsome, and C. M. Tucker, *Ind. Eng. Chem.*, **42**, 1398 (1950).

(7) "Selected Values of Physical and Thermodynamic Properties of Hydrocarbons and Related Compounds," API Research Project 44, Carnegie Press, Inc., New York, N. Y., 1953.

drocarbon reactant which is converted to products of the cracking reaction.

The rates of cracking are higher in the presence of hydrogen and increase with increasing hydrogen pressure. The data suggest that the effect of the partial pressure of the hydrocarbon reactant is small. Throughout the range of conditions studied, the rate of cracking of *n*-heptane is lower than that of methylcyclopentane. Furthermore, the data on the effect of temperature on the reaction rates indicate an apparent activation energy of 43 kcal./mole for *n*-heptane as compared to 30 kcal./mole for methylcyclopentane.

## Discussion

Cracking reactions of hydrocarbons over acidic catalysts are generally interpreted in terms of carbonium ion mechanisms.[8] According to carbonium ion theory, the rate of cracking is related to the ease of formation of carbonium ions. Hydrocarbons containing a tertiary hydrogen atom form ions more readily than those containing only primary and secondary hydrogen atoms. This offers an explanation for the higher rate and the lower apparent activation energy of cracking of methylcyclopentane as compared to *n*-heptane, since the former contains a tertiary hydrogen atom.

TABLE I

SUMMARY OF CRACKING RATES OF *n*-HEPTANE ($n$-$C_7$) AND METHYLCYCLOPENTANE (MCP)

| | Temp., °C. | | | | | | |
|---|---|---|---|---|---|---|---|
| | 471 | 471 | 471 | 471 | 471 | 499 | 527 |
| Cracking of $n$-$C_7$ | | | | | | | |
| $H_2$ pressure, atm. | 0[b] | 2.0 | 6.0 | 20.0 | 17.0 | 17.0 | 17.0 |
| $n$-$C_7$ pressure, atm. | 1.0 | 1.0 | 1.0 | 1.0 | 3.7 | 3.7 | 3.7 |
| Rate, $r$, $\times 10^3$ [a] | 2.5 | 4.2 | 7.5 | 9.9 | 10 | 28 | 74 |
| Cracking of MCP | | | | | | | |
| $H_2$ pressure, atm. | 0[b] | 2.0 | 6.0 | 20.0 | 17.0 | 17.0 | 17.0 |
| MCP pressure, atm. | 1.0 | 1.0 | 1.0 | 1.0 | 3.5 | 3.5 | 3.5 |
| Rate, $r$, $\times 10^3$ [a] | 12 | 19 | 26 | 26 | 28 | 64 | 118 |

[a] Gram moles converted per hr. per g. of catalyst. [b] $N_2$ at 2.0 atm. substituted for $H_2$.

In comparing the rates and activation energies for the cracking of *n*-heptane and methylcyclopentane, it appears that a compensation effect exists. Thus, in the Arrhenius relation, $k = k_0 \exp(-E/RT)$, the preëxponential factor $k_0$ for methylcyclopentane would appear to be about 2000 times lower than for *n*-heptane. This conclusion is derived from the data on the temperature dependence of the rate of cracking at 17 atm. hydrogen pressure. Here the rates of cracking have been treated like rate constants, since the rates appear to be nearly zero order with respect to both hydrogen and hydrocarbon pressures at this level of hydrogen pressure. Thus, while the activation energy for cracking of methylcyclopentane is 13 kcal./mole lower than for cracking of *n*-heptane, the lower preëxponential factor for the former largely compensates for this, so that the differences in rates are not many-fold. A compensation effect also has been noted by Franklin and Nicholson[9] for the cracking of hydrocarbons over silica–alumina.

The effect of hydrogen pressure on the paraffin-to-olefin ratio in the reaction products is further evidence for the hydrogenation activity of alumina catalysts, which has been noted before.[10,11] The promotional effect of hydrogen pressure on the rate of cracking at the lower hydrogen pressures conceivably could be explained in several ways[3]: Increasing hydrogen pressure might serve to increase surface acidity (concentration of protons), to increase the rate of desorption of products *via* hydrogenation, or possibly to free the surface of carbonaceous residues which lower catalyst activity.

(8) H. H. Voge, "Catalysis," Vol. 6, Reinhold Publ. Corp., New York, N. Y., 1958, p. 445.

(9) J. L. Franklin and D. E. Nicholson, *J. Phys. Chem.*, **61**, 814 (1957).

(10) V. C. F. Holm and R. W. Blue, *Ind. Eng. Chem.*, **43**, 501 (1951).

(11) S. W. Weller and S. G. Hindin, *J. Phys. Chem.*, **60**, 1501 (1956).

# OXIDATION–REDUCTION ANALYSIS OF CRYOGENICALLY STABLE PRODUCTS OF DISSOCIATED WATER VAPOR

BY HENRY M. GLADNEY AND DAVID GARVIN[1]

*Frick Chemical Laboratory, Princeton University, Princeton, New Jersey*

*Received March 1, 1962*

Deposits having similar characteristics may be obtained by trapping at 77°K. the products from discharged water vapor[2-4] or hydrogen peroxide[5] and from the reactions of hydrogen atoms with either oxygen[3,6,7] or ozone.[6,8,9] The deposits, in part crystalline and in part glassy, recrystallize with evolution of oxygen upon warming,[1-3,6] and, when melted, form concentrated solutions of hydrogen peroxide. The deposit from discharged water vapor is weakly paramagnetic.[10,11] Similar oxygen evolution and recrystallization was observed when mixtures of hydrogen peroxide vapor and oxygen were frozen at 4°K.[12] This method, however, failed to produce gas-evolving solids at 77°K.

In view of these results, we have undertaken chemical analyses of the frozen deposits to determine whether or not there is present a species stable only at low temperature and what relation it has to the oxygen evolution.

## Experimental

Degassed water was vaporized, metered through a capillary (0.31 g./hr.) into a low pressure (0.1 to 0.4 mm.) flow

(1) National Bureau of Standards, Washington 25, D. C.

(2) (a) W. H. Rodebush, C. W. J. Wende, and R. W. Campbell, *J. Am. Chem. Soc.*, **59**, 1924 (1937); (b) R. A. Jones and C. A. Winkler, *Can. J. Chem.*, **29**, 1010 (1951).

(3) M. A. Hogg and J. E. Spice, *J. Chem. Soc.*, 3971, (1957).

(4) P. Giguere, *Discussions Faraday Soc.*, **14**, 104 (1953).

(5) J. S. Batzold, C. Luner, and C. A. Winkler, *Can. J. Chem.*, **31**, 262 (1953).

(6) J. D. McKinley, Jr., and D. Garvin, *J. Am. Chem. Soc.*, **77**, 5802 (1955).

(7) K. H. Geib and P. Harteck, *Ber.*, **65**, 1551 (1932).

(8) N. I. Kobosev, I. T. Skorokodov, L. I. Nekrasov, and E. I. Makarova, *Zh. Fiz. Khim.*, **31**, 1843 (1957).

(9) P. Giguere and D. Chin, *J. Chem. Phys.*, **31**, 1685 (1959).

(10) R. Livingston, J. Ghormley, and H. Zeldes, *ibid.*, **24**, 483 (1956).

(11) A. I. Gorbanev, S. D. Kaitzmazov, A. M. Prokhodov, and A. B. Tsentsiper, *Zh. Fiz. Khim.*, **31**, 515 (1957).

(12) J. W. Edwards, Chapter 8 in "Formation and Trapping of Free Radicals," A. M. Bass and H. P. Broida, Editors, Academic Press, New York, N. Y., 1960, pp. 288–292; J. W. Edwards and J. S. Hashman, Am. Chem. Soc. Abstracts of 132d Natl. Meeting, Sept., 1957, p. 42-S.

TABLE I

OXIDATION AND REDUCTION TITERS (as $H_2O_2$) AND OXYGEN EVOLVED FROM THE PRODUCTS OF WATER VAPOR DISRUPTED BY AN ELECTRODELESS DISCHARGE[a]

| Run | Trap size and method | Melted sample: Total liquid products g./hr. | Melted sample: Oxygen evolved mmoles/hr. | Melted sample: $H_2O_2$, mmoles/hr. | Frozen sample: Oxygen evolved mmoles/hr. | Frozen sample: $H_2O_2$ mmoles/hr. | $\Delta H_2O_2/O_2$ equiv./mole |
|---|---|---|---|---|---|---|---|
| | | | Reduction | | | | |
| 1 | S $I^-$ | 0.274 | 0.610 | 4.46 | | 4.78 | 1.05 |
| 1′ | S $I^-$ | .278 | .630 | 4.44 | | 4.76 | 1.02 |
| 2 | S As | .289 | .625 | 4.28 | | 4.52 | 0.77 |
| 3 | S $I^-$ | .289 | .617 | 4.47 | | 4.63 | .52 |
| 3′ | S As | .278 | .608 | 4.49 | | 4.73 | .79 |
| 6 | L $I^-$ | .291 | .680 | 4.42 | | 4.81 | 1.15 |
| 6′ | L $I^-$ | .292 | .685 | 4.56 | | 4.83 | 0.79 |
| 9 | L As[b] | | .625 | 4.21 | 0.6 | 4.16 | − .16 |
| 9′ | L As[b] | | .617 | 4.38 | 0.6 | 4.41 | .10 |
| | | | Oxidation | | | | |
| 4 | S | 0.295 | 0.601 | 4.40 | | 4.51 | 0.37 |
| 4′ | S | .276 | .596 | 4.12 | | 4.41 | .97 |
| 5 | L | .290 | .646 | 4.37 | | 4.48 | .34 |
| 5′ | L | .291 | .668 | 4.44 | | 4.58 | .42 |
| 7 | L | .274 | .611 | 4.22 | | 4.25 | .10 |
| 7′ | L | | .625 | 4.25 | | 4.29 | .13 |
| 8 | L[b] | | .621 | 4.32 | 4.3 | 4.36 | .12 |
| 8′ | L[b] | | .625 | 4.56 | 4.4 | 4.59 | .10 |
| 10 | L[b] | | .626 | 4.76 | 4.8 | 5.02 | .83 |
| I | L[b,c] | | .054 | 0.726 | | 0.770 | 1.72 |
| II | L[b,c,d] | | .042 | 0.745 | | 0.733 | −0.57 |

[a] The numbering of the runs indicates the sequence of experiments. Runs with the same arabic numeral were performed on the same day. In column 2 "S" means a 45-cc. trap, "L" a trap of 149 or 161 cc. capacity. [b] Reagent added dropwise to frozen material. [c] Recalculation of results in Table II, ref. 6, for oxidation experiments on the H + $O_2$ reaction. Numbers are all per mole of $O_2$ used in the reaction. [d] Procedure used in analysis of frozen sample considered questionable.

system, disrupted by a 2.45 kMc. electrodeless discharge and then trapped in a detachable U-shaped trap immersed in liquid nitrogen. Non-condensable products were pumped away during deposition. The solids were either colorless or had a slight yellowish tinge.

Analyses consisted of either an oxidation or a reduction assay and a measurement of the evolved oxygen. All the chemical analyses were excess reagent–back-titration procedures. Some samples were analyzed after they had evolved gas and melted. For others an excess of the reagent was added to the frozen sample while the trap was kept at liquid nitrogen temperature. Two procedures were used for adding reagents to the frozen samples. The solution either was poured in quickly, or it was added dropwise from a weight buret to the cooled trap while the latter was connected to the gas measuring system. This second method allowed a measurement of the total gas evolved during sample decomposition and analytical reaction. Sample handling procedures were modeled on those reported earlier.[6]

The oxidation analyses were made with 0.4 *N* ceric sulfate in 3 *N* sulfuric acid, back-titrated with 0.2 *N* sodium arsenite. Two types of reduction analyses were used. In the first, acidified 1 *N* potassium iodide was added, the liberated iodine being measured with 0.3 *N* sodium thiosulfate. In the second, an excess of basic 2 *N* sodium arsenite was used, the back-titration being made with 0.4 *N* ceric sulfate.

## Results and Discussion

The results are collected in Table I. Each line presents the analyses of two samples, one treated with reagent after melting the sample, the other treated while frozen. Titers were calculated as moles of peroxide, *i.e.*, two electron changes for both oxidation and reduction. In addition, there are included in the table results of oxidation studies on the H + $O_2$ reaction, which were incorrectly reported earlier.[6]

The main limitation on the accuracy of these measurements is the reproducibility of the samples. This may be estimated from pairs of values for the same type of analysis in experiments made on the same day, *e.g.*, columns 3, 4, 5, and 7 for pair 1, 1′. These pairs show an average deviation of ±12 parts per thousand. The reproducibility from day to day is poorer than this and probably is strongly affected by variations in flow rates, power supplied to the discharge, and trapping efficiency. A reproducibility of 12 parts per thousand in peroxide content means that a difference in titers of the frozen and warmed samples of 0.1 mmole/hr. is significant.

The experiments show the presence of a species stable only at low temperature that undergoes typical chemical reactions. The differences in peroxide titer for frozen and melted samples were 3 to 8% of the residual peroxide in the reduction studies and 1 to 7% in the oxidations. The mole fractions of this species in the total deposit (considering the oxygen as a separate component) ranged up to 0.03, an order of magnitude greater than that indicated by paramagnetic resonance studies.

The relative oxidation and reduction equivalents of the cryogenic material cannot be determined precisely because of the great variability of the results. This variability may be due to erratic formation or preservation in the solid (by isolation) or, it may be due to an effective competition between the thermal decomposition of the species and its reaction with the oxidation–reduction reagent

during the warmup period. The argument of competition suggests that the upper limit of the titers be used. This yields a reduction/oxidation ratio of 5/4 (or roughly 1/1), while average values (for the runs in which the reagent was added in bulk and which meet the significance level cited above) lead to a 2/1 ratio. These results seem to rule out a chain reaction decomposition of hydrogen peroxide, and, coupled with the high mole fractions, a direct correlation with the species causing paramagnetism. On this basis we are led to suggest that the species is molecular. The isomeric peroxide postulated by Geib and Harteck[7] fits the 1/1 ratio, and the quasimolecular $H_2O_3$ is consistent with 2/1.

No direct relation between oxygen evolution and the difference in titers was found. However, the few cases in which oxygen evolution was measured concurrently with the oxidation of the frozen samples show a curious effect. The total oxygen values may be attributed to the oxidation reaction. Were the evolved oxygen independent of the cryogenic species an additional 0.6 mmole would be expected. The cause of this deficit during *oxidation* is not clear, further studies being indicated.

**Acknowledgment.**—We are indebted to Professor Clark M. Bricker and Dr. John D. McKinley, Jr., for many helpful suggestions. H. M. G. thanks the National Woodrow Wilson Fellowship Foundation for its support during the period of this work. The support of the U.S. Air Force Office of Scientific Research under Contract AF 18 (603)-134 with Princeton University is gratefully acknowledged.

## HEAT OF REACTION OF FLUORINE WITH GRAPHITE[1]

BY RICHARD F. PORTER[2] AND DAVID H. SMITH

*Department of Chemistry, Cornell University, Ithaca, N. Y.*

*Received March 10, 1962*

Fluorine is known to react with graphite to form condensed compounds.[3] Thermochemical data for the reactions are not generally available. At temperatures between 500 and 1000°K., $CF_3$–$CCl_3$(g) reacts with graphite with the elimination of one F atom and one Cl atom to form $CF_2$=$CCl_2$(g).[4] Since this reaction appeared to provide a suitable means for determining the heat of reaction of $F_2$(g) with graphite, a further quantitative examination of the reaction was undertaken.

### Experimental

The experimental procedure has been described.[4] Reactant $CF_3$–$CCl_3$(g) was passed into a graphite effusion cell packed with small chips of graphite. Reactant and product gases leaving the cell were then analyzed mass spectrometrically. The leak rate was regulated to provide a pressure of $CF_3$–$CCl_3$ between about $10^{-8}$ and $10^{-5}$ atm. within the cell. At these pressures the gas is assumed to obey Knudsen flow conditions. A small impurity of $CF_2Cl$–$CFCl_2$ was present in the reaction gas and it was therefore necessary to observe a fragment ion, $CCl_3^+$, as a measure of the $CF_3$–$CCl_3$(g) rather than the $C_2F_3Cl_2^+$ ion which is common to both isomers. For $CF_2$=$CCl_2$, the $C_2F_2Cl_2^+$ ion was observed.

### Results and Discussion

Pressure dependence data are shown in Fig. 1. The curve shows a simple first-order pressure dependence at low pressures, but tends toward a lower order at high pressures. The stoichiometry of the reaction is best described by the equation

$$CF_3\text{–}CCl_3(g) + \text{graphite} \longrightarrow CF_2{=}CCl_2(g) + (F + Cl)\text{graphite} \quad (1)$$

where the last term in the equation represents F and Cl atoms chemically bound to graphite. Second law heats for reaction 1 were obtained for a series of flow rates. The quantity $\log I_{C_2F_2Cl_2^+}/I_{CCl_3^+}$, which is proportional to $\log K_{eq}$ is plotted *vs.* $1/T$ in Fig. 2. Reliable values of $\Delta H_1^0$ could only be obtained when the operating pressure of $CF_3$–$CCl_3$ was in the range corresponding to the first-order region (see Fig. 1). During these experiments, an increase in $C_2F_2Cl_2^+$ intensity with increase in cell temperature was followed by a decrease in $CCl_3^+$ intensity, indicating that the total pressure was remaining nearly constant. From these determinations, we obtain $\Delta H_1^0 = 18.7 \pm 2.0$ kcal./mole reactant in the temperature range 840–1140°K. A trend toward higher values (20–28 kcal.) was observed for higher flow rates of $CF_3$–$CCl_3$. These data were not considered significant since the reaction apparently is not at equilibrium under these conditions. This presumably is the reason for the high value (29 kcal.) originally reported.[4]

The reaction of the isomer $CFCl_2$–$CF_2Cl$ with graphite was also investigated. In this case the reaction at low pressure of $CF_2Cl$–$CFCl_2$ is represented by the equation

$$CF_2Cl\text{–}CFCl_2(g) + \text{graphite} \longrightarrow CF_2{=}CFCl(g) + 2Cl(\text{graphite}) \quad (2)$$

For temperature dependence measurements, intensities of $C_2F_3Cl^+$ and $CFCl_2^+$ were observed for product and reactant, respectively. Second law data for this reaction also are illustrated in Fig. 2.

To obtain the heat of reaction of fluorine with graphite, we consider reactions 1 and 2 and the subsequent thermochemical data

Reaction 1: $\Delta H_1^0 = 18.7 \pm 2.0$ kcal./mole (this work)

Reaction 2: $\Delta H_2^0 = 10.5 \pm 1.5$ kcal./mole (this work)

$$Cl_2(g) + CF_2{=}CFCl(g) \longrightarrow CF_2Cl\text{–}CFCl_2(g) \quad \Delta H_3^0 = -48.8 \text{ kcal./mole}^5 \quad (3)$$

$$Cl_2(g) + CF_2{=}CCl_2(g) \longrightarrow CF_2Cl\text{–}CCl_3(g) \quad (4)$$
$$\Delta H_4^0 = -41.1 \text{ kcal./mole}^5$$

Combination of $\Delta H_2^0$ and $\Delta H_3^0$ gives for the reaction

(1) Supported by the Advanced Research Projects Agency.

(2) Alfred P. Sloan Fellow.

(3) W. Rüdorff and G. Rüdorff, *Chem. Ber.*, **80**, 417 (1947).

(4) D. R. Bidinosti and R. F. Porter, *J. Am. Chem. Soc.*, **83**, 3737 (1961).

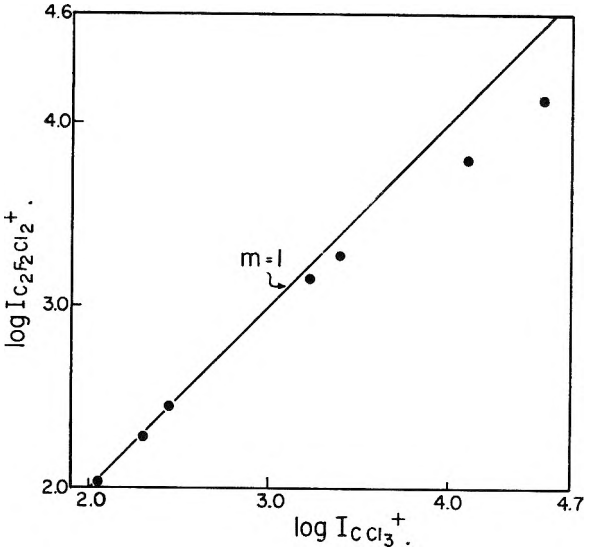


Fig. 1.—Pressure dependence data for the reaction of $CF_3$–$CCl_3$(g) with graphite. Electron energy = 50 v., reaction temperature 915°K.

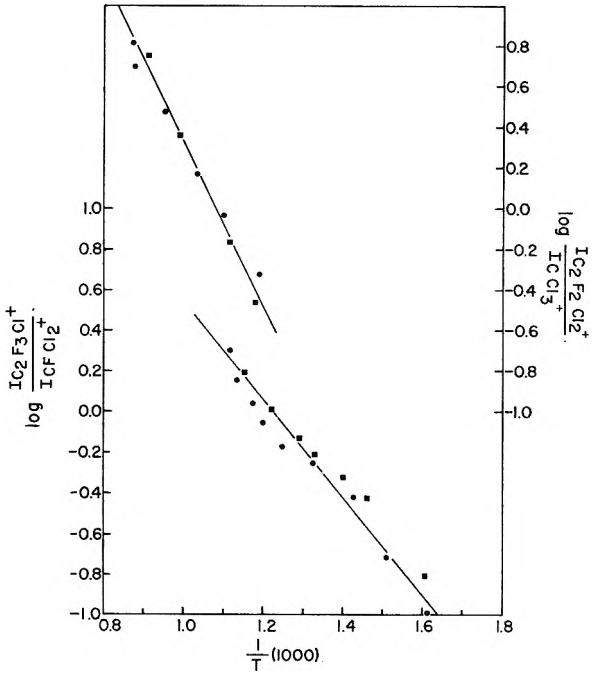


Fig. 2.—Temperature dependence data for the reactions of $CF_3$–$CCl_3$(g) and $CF_2Cl$–$CFCl_2$(g) on graphite. Ionizing electron energies were 50 and 75 v., respectively. A small correction has been applied to the intensities of $C_2F_2Cl_2^+$ and $C_2F_3Cl^+$ due to ion fragmentation of reactant gases. Squares and circles represent independent sets of data.

$$2Cl(\text{graphite}) \longrightarrow Cl_2(g) + \text{graphite} \quad (5)$$
$$\Delta H_5^0 = +38.3 \text{ kcal./mole}$$

Combination of data for reactions 1 and 4 gives for the reaction

$$CF_3\text{–}CCl_3(g) + \text{graphite} + Cl_2(g) \longrightarrow CF_2Cl\text{–}CCl_3 + (F + Cl)\text{graphite} \quad (6)$$
$$\Delta H_6^0 = -22.4 \text{ kcal./mole}$$

Heats of formation computed from bond additivity considerations[6] give $\Delta H_f^0$ ($CF_2$–$ClCCl_3$) = $\Delta H_f^0$ ($CF_3$–$CCl_3$) = 46.8 kcal. Combining this latter quantity with values of $\Delta H_5^0$ and $\Delta H_6^0$, we obtain for the reaction

$$F_2(g) + \text{graphite} \longrightarrow 2F(\text{graphite}) \quad (7)$$
$$\Delta H_7^0 = -100.2 \text{ kcal./mole } F_2$$

The uncertainty in $\Delta H_7^0$ is estimated to be about ±6 kcal., and results largely from the use of empirical bond energies in the computation. In view of this, heat capacity corrections to $\Delta H_1^0$ and $\Delta H_2^0$ were considered insignificant. The availability of experimental heats of formation of $CF_3$–$CCl_3$ and $CF_2$=$CCl_2$ should diminish the uncertainty.

In the reaction of $CF_2Cl$–$CFCl_2$ with graphite, the only observable product in addition to $CF_2$=CFCl was HCl(g). This is attributed to a reaction with hydrogen in graphite, which can diffuse into the reaction zone. The pressure of HF(g) in the reaction of $CF_3$–$CCl_3$ with graphite, however, was small compared to that of HCl(g) (as noted by the $HF^+/HCl^+$ ratio). Thus it appears that most of the reacted fluorine remains in the graphite. It should be noted that the total amount of $CF_3$–$CCl_3$(g) that has reacted during the course of the experiment was less than $10^{-3}$ mole, although at least a mole of solid carbon was available for reaction. Since so little fluorine is finally present in the graphite, we cannot demonstrate whether a new phase such as $C_4F$ has been formed. For our purposes, it is perhaps only meaningful to consider that the reaction involves the bonding of fluorine atoms to active sites in the graphite, or to active surface sites. Comparison of these data with calorimetric heats may provide information that will allow us to distinguish between a surface reaction and one involving internal sites.

It should be noted that reaction 1 must have a positive entropy change of the order of 20–25 e.u. at 1000°K. This probably is due in part to break-up of the graphite structure on the bonding of fluorine and chlorine atoms. The ease of removal of an F atom in reaction 1 must reflect the ease of removal of chlorine on the adjacent carbon atom. If we assume that the rate determining step is the transfer of a chlorine atom to graphite, an upper limit of 30 kcal. for the activation energy is obtained by combining $\Delta H_5^0$ with a dissociation energy of $Cl_2$ of 58 kcal. and a bond strength of 78 kcal. in chloroethanes.[6]

**Acknowledgment.**—We wish to thank Professor W. T. Miller for samples of $CF_3$–$CCl_3$ and $CF_2Cl$–$CFCl_2$ used in this work.

(5) J. R. Lacher, J. J. McKinley, C. Walden, K. Lea, and J. D. Park, *J. Am. Chem. Soc.*, **71**, 1337 (1949).

(6) C. R. Patrick, "Advances in Fluorine Chemistry," Vol. 2, Butterworths, 1961.

## THE VAPOR PRESSURE OF GERMANIUM TELLURIDE[1]

BY CHIKARA HIRAYAMA

*Westinghouse Research Laboratories, Pittsburgh 35, Pennsylvania*

*Received March 28, 1962*

The germanium–tellurium system and the thermoelectric properties of germanium telluride have

been reviewed recently by Miller.[2] Only a single compound, GeTe, with a melting point of 725°, has been known to be present in this system.[3] However, a recent detailed study[4] of this system has shown the compound to be congruent melting and of composition $GeTe_{1.025}$. Germanium telluride undergoes a phase transformation[5] at about 440° from the low-temperature rhombohedral form to the cubic.

The thermodynamic properties of GeTe(g) have been computed by Kelley,[6] based on the spectroscopic data[7] for this compound. The thermodynamic properties of GeTe(s) are still lacking.

In view of the interesting thermoelectric properties of the "pure" and bismuth-doped GeTe[2] at temperatures above 400°, we have undertaken to measure the vapor pressure of germanium telluride. The heat of sublimation thus enables one to calculate the thermodynamic properties of GeTe(s). This information adds further to the high temperature thermodynamic properties and volatility characteristics of intermetallic compounds of tellurium.

## Experimental

The apparatus consisted of a 30-in. long vertical tube. This tube consisted of a 22 in. long, flanged Pyrex brand pipe of 1.5 in. i.d. (Corning Glass Works), to which was sealed a flat-bottomed 8 in. long mullite tube of 1-1/8 in. i.d. A stainless steel flange, through which passed the iron–constantan thermocouple and a hook for suspending the sample, was sealed to the flanged top of the Pyrex tube. A gasket of Viton-A (E. I. duPont) was used to facilitate a vacuum seal. The tube was connected to a vacuum system just below the flanged top. Allowance was made also for introduction of argon to the system to break the vacuum.

The mullite section was heated by raising a tube furnace over it. The temperature of the furnace was controlled to ±2°, or better, and the bottom 4-in. section of the tube was at the same temperature.

The Knudsen effusion cells were machined from graphite rods supplied by the National Carbon Company. The dimensions were 1-1/8 in. high, 3/4 in. diameter with wall thickness of approximately 3/16 in. The cap, on which was drilled the orifice, was approximately 1/4 in. thick. Three different orifice diameters were used, namely, 0.250, 0.125, and 0.0625 in. The Clausing correction[8] was used to calculate the effective orifice area. The cells were heated above 800° *in vacuo* of approximately $1 \times 10^{-6}$ mm. for several hours until constant weight was obtained.

To obtain the effusion rate, the Knudsen cell was contained in a silica cup which was placed on a platinum pan. The pan then was lowered into the mullite tube. The thermocouple was placed adjacent to the cell. The system was flushed several times with oxygen-free argon, and finally filled with the latter. The sample then was heated by raising the furnace over the tube and allowed to come to constant temperature. The time required was 20 to 30 min. The system subsequently was evacuated to about $3 \times 10^{-5}$ mm. in about 3 min. The pressure during any run was maintained between $5 \times 10^{-6}$ and $3 \times 10^{-5}$ mm. Check runs indicated no detectable loss of material during the heat-up time in the argon atmosphere. Each run was terminated by breaking the vacuum with argon, and lowering the furnace to cool the tube with a forced draft. The effusion rate was determined from the weight loss over the heating period under vacuum.

The germanium telluride was prepared[9] similarly to that described by Johnston and Sestrich[10] from stoichiometric amounts of germanium and tellurium, and the material was crushed and ground to a powder. A wet analysis indicated 36.2% Ge and 63.75% Te (theoretical: Ge = 36.21%, Te = 63.79%). An X-ray powder diffraction pattern indicated no unreacted metals present, and the lattice parameter agreed with that reported[10]; *i.e.*, $\bar{a} = 5.98$ Å.

Separate samples of germanium telluride were volatilized at 525 to 650°. The X-ray diffraction patterns of the condensate indicated the presence of GeTe only. Because we do not have mass spectroscopic data, the volatile species is assumed to be the monomer GeTe.

## Results

The results of the determinations are summarized in Table I, with the data recorded in the order of runs. The vapor pressure was calculated with the aid of the equation

$$p = 0.02255(m/At)(T/M)^{1/2} \qquad (1)$$

where $p$ is in atmospheres, $m$ the weight loss in grams, $t$ the effusion time in seconds, $A$ the effective orifice area, $T$ the absolute temperature, and $M$ the molecular weight of GeTe. The pressure in mm. also is recorded.

A least squares treatment of the data in Table I gave the equation

$$\log p_{atm.} = -(10{,}255 \pm 451)1/T + 8.255 \pm 0.598 \qquad (2)$$

with a linear regression coefficient of 0.992. The good linear relationship of the data obtained with cells of three different effective orifice areas shows that the accommodation coefficient is very close to unity. In view of the small ratio of orifice area to surface area of the vaporizing solid, it can be concluded that the equilibrium vapor pressure of germanium telluride is identical to the measured dynamic pressure, $p$.

TABLE I
VAPOR PRESSURE OF GeTe

| $T$, °K. | Time, sec. | Wt. loss, mg. | Eff. orifice area, cm.² × $10^2$ | $p$, mm. | $p$, atm. |
|---|---|---|---|---|---|
| 725 | 10300 | 10.2 | 2.784 | $1.16 \times 10^{-3}$ | $1.52 \times 10^{-6}$ |
| 702 | 13520 | 5.4 | 2.784 | $4.60 \times 10^{-4}$ | $6.05 \times 10^{-7}$ |
| 751 | 8360 | 22.2 | 2.784 | $3.17 \times 10^{-3}$ | $4.17 \times 10^{-6}$ |
| 767 | 5150 | 18.2 | 2.784 | $4.26 \times 10^{-3}$ | $5.61 \times 10^{-6}$ |
| 787 | 3480 | 23.8 | 2.784 | $8.34 \times 10^{-3}$ | $1.10 \times 10^{-5}$ |
| 680 | 18900 | 2.0 | 2.784 | $1.19 \times 10^{-4}$ | $1.57 \times 10^{-7}$ |
| 816 | 2100 | 38.4 | 2.784 | $2.27 \times 10^{-2}$ | $2.99 \times 10^{-5}$ |
| 796 | 6060 | 16.4 | 0.444 | $2.08 \times 10^{-2}$ | $2.74 \times 10^{-5}$ |
| 837 | 3310 | 44.6 | 0.444 | $1.06 \times 10^{-1}$ | $1.39 \times 10^{-4}$ |
| 823 | 3340 | 28.5 | 0.444 | $6.69 \times 10^{-2}$ | $8.80 \times 10^{-5}$ |
| 683 | 10620 | 4.7 | 14.11 | $9.94 \times 10^{-5}$ | $1.31 \times 10^{-7}$ |

The heat of sublimation over the temperature range studied has a constant value, $\Delta H_{sub.} = 46.86$

(1) This work was supported in part under a contract with the Bureau of Ships.

(2) R. C. Miller, in "Thermoelectricity: Science and Engineering," Ed. R. R. Heikes and R. W. Ure, Jr., Interscience Publishers, New York, N. Y., 1961, pp. 434–439.

(3) M. Hansen and K. Anderko, "Constitution of Binary Alloys," 2nd Ed., McGraw-Hill Book Co., New York, N. Y., 1958.

(4) J. P. McHugh and W. A. Tiller, *Trans. Met. Soc. A.I.M.E.*, **218**, 187 (1960).

(5) K. Schubert and H. Fricke, *Z. Metal.*, **44**, 459 (1953).

(6) K. K. Kelley, "Contributions to the data on theoretical metallurgy," U.S. Bur. Mines, Bull. No. 584, 1960.

(7) G. Herzberg, "Molecular Spectra and Molecular Structure. I. Spectra of Diatomic Molecules," 2nd Ed., D. Van Nostrand Co., New York, N. Y., 1950.

(8) S. Dushman, "Scientific Foundations of Vacuum Technique," John Wiley and Sons, Inc., New York, N. Y., 1949, p. 99.

(9) The GeTe was kindly supplied by Mr. Y. Ichikawa, Westinghouse Electric Corporation, Youngwood, Pennsylvania.

(10) W. D. Johnston and D. E. Sestrich, *J. Inorg. Nucl. Chem.*, **15**, 229 (1961).

± 2.06 kcal./mole. From the heat capacity of GeTe(g) given by Kelley,[6] and a reasonable estimate of 13.5 cal./deg. mole for the average heat capacity of GeTe(s) between 298.16° and the median experimental temperature of 758°K., the standard heat of sublimation is 49.0 ± 2 kcal./mole.

From the heats of dissociation[11] for GeTe(g) and $Te_2$(g), their spectroscopic data,[7] and the heats of sublimation for germanium[12] and tellurium,[13] the standard heat of formation for GeTe(s) is calculated as

$$Ge(g) \longrightarrow GeTe(s)$$
$$\Delta H = -49.0 \pm 2 \text{ kcal./mole} \quad (1)$$

$$Ge(g) + Te(g) \longrightarrow GeTe(g)$$
$$\Delta H = -94.6 \pm 9 \text{ kcal./mole} \quad (2)$$

$$1/2\ Te_2(g) \longrightarrow Te(g)$$
$$\Delta H = 26.2 \pm 2 \text{ kcal./mole} \quad (3)$$

$$Ge(s) \longrightarrow Ge(g)$$
$$\Delta H = 91.5 \pm 3 \text{ kcal./mole} \quad (4)$$

$$Te(s) \longrightarrow 1/2\ Te_2(g)$$
$$\Delta H = 34.8 \text{ kcal./mole} \quad (5)$$

$$Ge(s) + Te(s) \rightarrow GeTe(s)$$
$$\Delta H^0 = 8.9 \pm 9 \text{ kcal./mole}$$

The entropy of sublimation of GeTe is 42.1 e.u., and using the data of Stull and Sinke[14] the entropy change for reactions 4 and 5 are 32.7 and 20.2 e.u., respectively. The standard entropy of formation is therefore $\Delta S^0 = 0.6$ e.u. The standard free energy of formation is $\Delta F^0 = 8.7 \pm 9$ kcal./mole. There is a large uncertainty in $\Delta F^0$ due to uncertainties in the dissociation energies, which probably results in the positive free energy.

(11) A. G. Gaydon, "Dissociation Energies and Spectra of Diatomic Molecules," Chapman and Hall, Ltd., London, 1953.

(12) A. W. Searcy and R. D. Freeman, *J. Chem. Phys.*, **23**, 88 (1955).

(13) I. V. Korneeva, A. S. Pashinkin, A. V. Novoselova, and Yu. A. Priselkov, *Zh. Neorg. Khim.*, **2**, 1720 (1957).

(14) D. R. Stull and G. C. Sinke, "Thermodynamic Properties of the Elements," Advances in Chemistry Series, 1959.

## A SPECTROPHOTOMETRIC METHOD FOR DETERMINATION OF FORMATION CONSTANTS OF LEAD HALIDE COMPLEXES IN FUSED SODIUM NITRATE-POTASSIUM NITRATE

BY J. D. VAN NORMAN[1] AND R. A. OSTERYOUNG

*Department of Chemistry, Rensselaer Polytechnic Institute, Troy, New York*

*Received March 10, 1962*

### Theoretical

Duke and Iverson[2] have shown that the successive formation constants for chloro and bromo complexes of lead and cadmium in molten nitrate media may be evaluated by measuring the increase in solubility of the metal chromate as a function of added halide. Duke determined the solubility of the metal chromate by sampling and subsequent analysis. The development of a high temperature spectrophotometric technique suggested that an *in situ* analysis could be performed using the absorption peak of the chromate ion in the fused $NaNO_3$-$KNO_3$ mixture. Investigation showed that chromate ion could be accurately determined spectrophotometrically in the presence and absence of halide ion and in the presence of excess lead nitrate.

In the presence of excess lead ion the chromate ion concentration will be defined by the solubility product

$$K_{sp} = [Pb^{+2}][CrO_4^{-2}] \quad (1)$$

If now halide ion is added, some of the lead chromate solid will dissolve due to formation of $PbX_n^{2-n}$ species. The following expression holds if only species of the form $PbX_n^{2-n}$ exist

$$[Pb]_{total} = [Pb^{+2}] + [PbX^+] + [PbX_2] + \ldots [PbX_n^{2-n}] \quad (2)$$

The successive formation constants for lead halide complexes, $K_1$, $K_2$, $K_3$,. . .,$K_n$ are expressed as

$$K_1 = \frac{[PbX^+]}{[Pb^{+2}][X^-]} \quad (3)$$

$$K_2 = \frac{[PbX_2]}{[PbX^+][X^-]} \quad (4)$$

$$K_3 = \frac{[PbX_3^-]}{[PbX_2][X^-]} \quad (5)$$

Substitution of eq. 3–5 into eq. 2 results in the equation

$$\frac{[Pb]_{total}}{[Pb^{+2}]} = 1 + K_1[X^-] + K_1K_2[X^-]^2 + K_1K_2K_3[X^-]^3 \ldots \quad (6)$$

A function $K_{sp}'$ now is defined as

$$K_{sp}' = [Pb]_{total}\,[CrO_4^{-2}] \quad (7)$$

By multiplying the numerator and denominator of equation 6 by $[CrO_4^{-2}]$ and introducing a function $F_0$ the following can be written.

$$F_0 = K_{sp}'/K_{sp} = 1 + K_1[X^-] + K_1K_2[X^-]^2 + K_1K_2K_3[X^-]^3 \ldots \quad (8)$$

If a function $F_1$ is defined by

$$F_1 = \frac{F_0 - 1}{[X^-]} \quad (9)$$

and $F_1$ is plotted *vs.* $[X^-]$ the intercept of the plot as $[X^-]$ goes to zero will be $K_1$. If $F_2$ is now defined as

$$F_2 = \frac{F_1 - K_1}{[X^-]} \quad (10)$$

(1) Brookhaven National Laboratory, Upton, New York.

(2) F. R. Duke and M. L. Iverson, *J. Phys. Chem.*, **62**, 417 (1958).

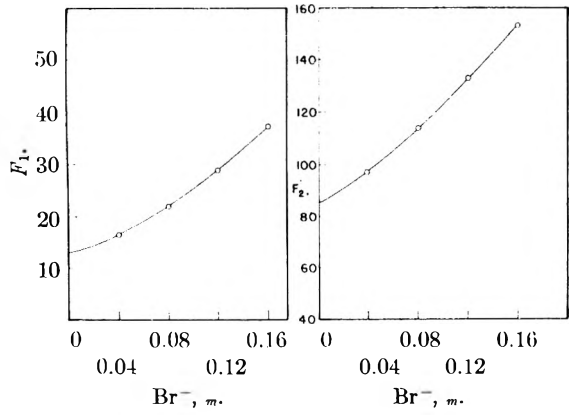


Fig. 1.—Typical plots of $F_1$ and $F_2$.

a plot of $F_2$ *vs.* $[X^-]$ will have an intercept of $K_1K_2$. A similar function $F_3$ will yield $K_1K_2K_3$. This method is similar to that used by DeFord and Hume.[3]

Since $[Pb]_{total}$ is the lead present initially plus what lead dissolved as a result of adding halide ion

$$[Pb]_{total} = [Pb^{+2}]_o + [CrO_4^{-2}]_f - [CrO_4^{-2}]_o \quad (11)$$

where the subscript o denotes the original concentrations before halide addition and the subscript f denotes the final concentrations. The halide ion concentration $[X^-]$ is taken as the total halide added since it is always in greater than 40-fold excess, generally more than 100-fold excess.

### Experimental

Lead chromate and lead nitrate were equilibrated with the equimolar mixture of $NaNO_3$ and $KNO_3$ at 300° to form a master solution. A series of solutions of known halide ion concentration was prepared by direct addition of the potassium halide. These solutions were equilibrated at 285° for 4 hr. and a portion then was transferred to preheated 2-mm. quartz optical cells which were placed in a high temperature spectrophotometer furnace and the solutions equilibrated at 275° for 2 more hr. The spectrophotometer was a modified Beckman DU similar to those described by Sundheim and Greenberg[4] and Gruen.[5] Experimental details are given by Osteryoung, Van Norman, and Christie.[6] A slight precipitate of lead chromate generally formed which did not completely settle out during the time of equilibration. The absorbance readings were corrected for absorption by the solid by subtracting the absorbance of the solution at 550 mμ, where chromate ion does not absorb. Corrections were of the order of 3 to 5%. Absorbances were always taken *vs.* a cell containing the pure equimolar mixture of the nitrates.

### Results

The chromate ion concentrations were calculated from absorbance readings using a molal extinction coefficient of 6600 at 370 mμ at 275°. Beer's law plots at 360, 370, and 380 mμ were linear. The $[Pb^{+2}]_o$ was calculated from the original chromate ion concentration (in the absence of halide ion) using a $K_{sp}$ of $1.62 \pm 0.02 \times 10^{-7}$ on the molal scale at 275°. Since excess lead ion generally was added to lower the absorbance due to chromate ion to a determinable level, this $K_{sp}$ was checked over a range of $Pb^{+2}$ concentrations of $4.03 \times 10^{-4}$ to $1.3\ 10^{-3}$ *m*. Figure 1 shows typical plots for the $F_1$ and $F_2$ functions obtained. The formation constants for the lead-chloro complexes calculated from an average of three separate experiments are $K_1 = 11$, $K_2 = 4$, and $K_3 = 5$. The comparable values for the lead-bromo complexes are 13, 6, and 4, again an average of three separate experiments. As this method involves the method of successive intercepts any error in the first formation constant will manifest itself in the second formation constant. The errors thus are multiplied. Therefore, the limits of error placed on the formation constants are $K_1$, ±20%, $K_2$, ±50%, and $K_3$, ±100%.

These results compare quite favorably with the values found by Duke[2] for the lead-chloro complex at the same temperature of 8, 3, and 1; and 13, 2, and 1 for the lead-bromo complexes. Duke and Garfinkel[7] have evaluated the first two formation constants for the lead-bromo complexes using an e.m.f. technique and have found $K_1 = 14.2$ and $K_2 = 6.2$ at 306°. Christie and Osteryoung[8] obtained formation constants for the lead-chloro complexes in fused $LiNO_3$–$KNO_3$ eutectic at 180° using a polarographic technique. They found $K_1 = 42$ and $K_2 = 3$. Braunstein, *et al.*,[9] have pointed out that the formation constants calculated by Duke and co-workers and Christie and Osteryoung are in error due to incorrect analysis of the data. They also state that the errors in the first formation constants of the lead halide complex determined by Duke[2] due to the analysis of the data are much less than the experimental errors because of the low solubility of lead chromate. Calculations show that the errors in the first formation constants of the lead halide complexes in the present work arising from using the simplified analysis of the data previously described in this paper rather than the method recommended by Braunstein are much less than the experimental errors, again due to the low solubility of lead chromate. Braunstein also recommended that the slope of the plot of log $F_0$ *vs.* $[X^-]$ be used to calculate $K_1$. This procedure was tried and made no difference in the values of $K_1$ obtained.

The method described in this paper is useful for studying complex ion formation of metal ions which form slightly soluble salts with colored anions such as chromate, permanganate, and dichromate ions.

**Acknowledgment.**—This work was supported in part by the U. S. Atomic Energy Commission, Contract AT(30-3)-241, Troy, New York.

(3) D. D. DeFord and D. N. Hume, *J. Am. Chem. Soc.*, **73**, 5321 (1951).

(4) B. R. Sundheim and J. Greenberg, *Rev. Sci. Instr.*, **27**, 703 (1956).

(5) D. M. Gruen, *Nature*, **178**, 1181 (1956).

(6) R. A. Osteryoung, J. D. Van Norman, and J. H. Christie, Final Report, Contract No. AT(30-3)-241, September, 1959; see also J. D. Van Norman, Ph.D. Thesis, Rensselaer Polytechnic Institute, 1959.

(7) F. R. Duke and H. M. Garfinkel, *J. Phys. Chem.*, **65**, 1627 (1961).

(8) J. H. Christie and R. A. Osteryoung, *J. Am. Chem. Soc.*, **82**, 1841 (1960).

(9) J. Braunstein, M. Blander, and R. M. Lindgren, *ibid.*, **84**, 1529 (1962).

# CALCULATIONS OF ENTANGLEMENT COUPLING SPACINGS IN LINEAR POLYMERS

BY HERSHEL MARKOVITZ,[1] THOMAS G FOX,[1] AND JOHN D. FERRY

*Mellon Institute, Pittsburgh, Pennsylvania and Department of Chemistry, University of Wisconsin, Madison, Wisconsin*

*Received March 24, 1962*

Several different quantities and symbols have been introduced in the literature to characterize the density of points of entanglement (or coupling) in a linear amorphous polymer of sufficiently high molecular weight. Their definitions have been based on different viewpoints which are in some respects inconsistent. With the hope of reducing the attendant confusion, we summarize here the various practices which have arisen and propose a uniform usage.

In all cases, the calculation of the threshold for an entanglement network has been based on the theory of gelation due to a cross-linking process,[2] as though the coupling loci were equivalent to cross-links. Gelation theory shows that an infinite network will be formed from a monodisperse system if one *cross-linkage* is introduced on the average for two primary molecules; equivalently stated, since there is one *cross-linked unit* on each of the joined molecules in the cross-linkage, there is an average of one cross-linked unit on each primary molecule. In a polydisperse system, the criterion is one cross-linked unit per primary molecule *on a weight-average basis*. The cross-linking is, of course, assumed to be random.

**Methods for Characterizing Entanglement Spacing. A. From Viscosity–Molecular Weight Data.**—The viscosity for a homogeneous series of flexible chain molecules in bulk or at a fixed diluent concentration is observed to increase with the 3.4 power of the molecular weight $M$ providing $M \geq M_c$. Abruptly for $M \leq M_c$, a less severe dependence of the viscosity on the chain length is found. The observed critical molecular weight, designated as $M_c$, is a characteristic of the polymer's chemical structure. The corresponding chain length at its "break point," designated as $Z_c$, is equal to $n_a M_c/M_0$, where $M_0$ is the molecular weight of the monomer unit and $n_a$ is the number of chain atoms per unit.

The entanglement spacing has been variously computed from $M_c$ as follows:

1. The molecular weight at the break point ($M_c$) was identified *directly* with the average molecular weight between entanglements. The symbol $K$ was used for its reciprocal.[3] Accordingly, the observed $Z_c$ at the break point was identified with the average number of chain atoms between entanglements.[4]

2. On the basis of the hypothesis that there exist both retarding and accelerating elements,[5] the observed value of $M_c$ at the break point was identified as $2M_e$, where $M_e$ denotes[6] the average molecular weight between entanglements. Such a factor of 2 has alternatively been introduced on the hypothesis that the entanglements which change the character of the viscosity–molecular weight relationship at $M_c$ must be located near the middle of the chain.[7] In this assignment, the average degree of polymerization between entanglement points, denoted[6] as $Z_e$, is $M_e/M_0$. Thus, for polymers with two chain atoms per monomer unit $Z_c$ in (A1) is four times $Z_e$ defined here.

**B. From the Pseudo-equilibrium Modulus or Compliance.**—Another method for estimating the entanglement spacing involves the value of the storage modulus $G'(\omega)$, the relaxation modulus $G(t)$, the storage compliance $J'(\omega)$, or the creep compliance $J(t)$ in the region of the time or frequency scale where the slope is very small and undergoes an inflection. Taking this value as a pseudo-equilibrium modulus, $G_e$, or compliance, $J_e$, one can calculate an average molecular weight, $M_e'$, or degree of polymerization, $Z_e'$, between coupled units from rubber elasticity theory: $M_e' = Z_e' M_0 = \rho RTJ_e = \rho RT/G_e$, where $\rho$ is the density, $R$ is the gas constant, and $T$ is the absolute temperature.[8,9] There is no uncertainty involving a factor of 2 in these calculations. However, there is usually considerable doubt in selecting a suitable magnitude of $G_e$ or $J_e$.

**C. From the Loss Compliance.**—The position and value of the maximum of the loss compliance, $J''(\omega)$, also have been employed[6,7] to estimate the entanglement spacing. The values obtained here involve assumptions similar to those used in treating the dependence of viscosity on molecular weight.

**Comments and Recommendations.**—There are two important inconsistencies in the references cited. One is arbitrary: the use of the symbol $Z$ to denote number of chain atoms[4] and alternatively degree of polymerization.[6] There is a difference of a factor of 2 in vinyl polymers, 3 in polyethylene oxide, 4 in Hevea rubber, and larger factors in polyesters. Since the number of chain atoms is the more useful basis of comparison among different polymers, *we propose to express spacings on this basis in the future, but adopt a new symbol* $\Lambda$ *for the average number of chain bonds between coupling entanglements.*

The second inconsistency, a more basic discrepancy, involves the question of whether the break point in the dependence of viscosity on molecular weight should be identified with $\Lambda$ or $2\Lambda$. From the analogy with gelation theory, the reasons previously given for including a factor of 2 do not appear to be valid. Accordingly, pending the development of rigorous theories and/or a comprehensive body of experimental data relating $\Lambda$ to the observed $M_c$ in the viscosity–molecular weight relation, to the aforementioned inflection point in

(1) The support of the Office of Naval Research is acknowledged.

(2) P. J. Flory, "Principles of Polymer Chemistry," Cornell University Press, Ithaca, N. Y., 1953, p. 357 ff.

(3) F. Bueche, *J. Chem. Phys.*, **20**, 1959 (1952).

(4) T. G Fox and S. Loshack, *J. Appl. Phys.*, **26**, 1080 (1955).

(5) F. Bueche, *ibid.*, **26**, 738 (1955).

(6) J. D. Ferry, "Viscoelastic Properties of Polymers," John Wiley and Sons, New York, N. Y., 1961, p. 287.

(7) R. S. Marvin in J. T. Bergen, ed., "Viscoelasticity: Phenomenological Aspects," Academic Press, New York, N. Y., 1950, p. 48.

(8) H. Mark and A. V. Tobolsky, "Physical Chemistry of High Polymer Systems," Interscience Publishers, New York, N. Y., 1950, p. 344.

(9) J. D. Ferry, R. F. Landel, and M. L. Williams, *J. Appl. Phys.*, **26**, 359 (1955).

TABLE I

REVISED VALUES OF Λ, THE AVERAGE ENTANGLEMENT SPACING, IN CHAIN ATOMS

| | Dependence of $\eta$ on $M$[v] | Inflection of viscoelastic properties[w] | Max. in $J^x$ $J''_m$ | $\omega_m$ | |
|---|---|---|---|---|---|
| Polystyrene | 730(f, 217°)[a] | 610($E$, w, 100°, $3.5 \times 10^3$)[b] | | | |
| | | 320($E$, f, 110°, $3.5 \times 10^3$)[c] | | | |
| Polyvinyl acetate | 680(f, 160°)[d] | 338($E$, f, 50°, $1.8 \times 10^4$)[e] | 480 | 1040 | (90°)[f] |
| Polyisobutylene | 608(f, 217°)[a] | 240($E$, w, −30°, $2.4 \times 10^5$)[g] | | | |
| | | 320($E$, w, −30°, $5.6 \times 10^4$)[h] | | | |
| | | 320($J'$, w, 90°, $5.6 \times 10^4$)[i] | 500 | 820 | (50°)[i] |
| Hevea | | 296($G'$, r, −30°, $6 \times 10^4$)[j] | 272 | 400 | (−50°)[k] |
| | | 120; 400($G'$, w, −30° −)[k] | | | |
| | | 480($D$, w, −, −)[l] | | | |
| Polyethylene oxide | | 200($J'$, w, 70°, $7.8 \times 10^4$)[m] | | | |
| Polydimethyl siloxane | 950(f, 25°)[a] | 320($J'$, w, 25°, $1.3 \times 10^5$)[n] | | | |
| Polymethyl methacrylate | | 88($D$, f, 140°, $8.2 \times 10^4$)[o] | | | |
| | | 74($E$, −, 135°, −)[p] | | | |
| Polymethyl acrylate | | | 400 | 760 | (f, 80°, $5.3 \times 10^4$)[q] |
| Poly-*n*-butyl methacrylate | | | 368 | 640 | (f, 125°, $4.3 \times 10^4$)[r] |
| Poly-*n*-hexyl methacrylate | | | 720 | 1080 | (f, 105°, $4.7 \times 10^4$)[s] |
| Poly-*n*-octyl methacrylate | | | 1320 | 2320 | (f, 90°, $3.8 \times 10^4$)[t] |
| Poly-*n*-docosyl methacrylate | | | 5000 | 19200 | (w, 60°, −)[u] |

[a] T. G Fox and S. Loshaek, *J. Appl. Phys.*, **26**, 1080 (1955). [b] H. Fujita and K. Ninomiya, *J. Polymer Sci.*, **24**, 433 (1957). [c] A. V. Tobolsky and K. Murakami, *ibid.*, **40**, 443 (1959). [d] T. G Fox and H. Nakayasu, unpublished. [e] K. Ninomiya, *J. Colloid Sci.*, **14**, 49 (1959). [f] M. L. Williams and J. D. Ferry, *ibid.*, **9**, 474 (1954). [g] R. D. Andrews and A. V. Tobolsky, *J. Polymer Sci.*, **7**, 221 (1951). [h] E. Catsiff and A. V. Tobolsky, *J. Colloid Sci.*, **10**, 375 (1955). [i] E. R. Fitzgerald, L. D. Grandine, Jr., and J. D. Ferry, *J. Appl. Phys.*, **24**, 650 (1953). [j] L. J. Zapas, S. L. Shufler, and T. W. DeWitt, *J. Polymer Sci.*, **18**, 250 (1955). [k] A. R. Payne, in "Rheology of Elastomers," ed. by P. Mason and N. Wookey, Pergamon Press, London, 1958, p. 86. There appear to be two distinct pseudo-equilibrium moduli in the data. [l] F. Bueche, *J. Polymer Sci.*, **25**, 305 (1957). [m] T. P. Yin, S. E. Lovell, and J. D. Ferry, *J. Phys. Chem.*, **65**, 534 (1961). [n] D. J. Plazek, W. Dannhauser, and J. D. Ferry, *J. Colloid Sci.*, **16**, 101 (1961). [o] F. Bueche, *J. Appl. Phys.*, **26**, 738 (1955). [p] J. R. McLoughlin and A. V. Tobolsky, *J. Colloid Sci.*, **7**, 555 (1952). [q] M. L. Williams and J. D. Ferry, *ibid.*, **10**, 474 (1955). [r] W. C. Child, Jr., and J. D. Ferry, *ibid.*, **12**, 327 (1957). [s] W. C. Child, Jr., and J. D. Ferry, *ibid.*, **12**, 389 (1957). [t] W. Dannhauser, W. C. Child, Jr., and J. D. Ferry, *ibid.*, **13**, 103 (1958). [u] P. R. Saunders and J. D. Ferry, *ibid.*, **14**, 239 (1959). [v] In parentheses we have indicated type of sample and temperature of measurement. [w] In parentheses we have indicated which property, type of polymer, approximate temperature where inflection was measured, and weight- or viscosity-average number of chain atoms in polymer sample used. [x] Where no entry appears in another column, we indicate type of polymer sample, temperature, and average chain length. Type of polymer: w, whole; r, rough fraction; f, fraction. Viscoelastic property measurement: $E$, longitudinal relaxation modulus; $J'$, storage shear compliance; $G'$, storage shear modulus; $D$, longitudinal creep compliance.

the modulus or compliance, and to the maximum in the loss compliance, we suggest that all lengths calculated by (A2) and (C) above should be multiplied by 2; it follows that no correction of this sort is required in the length computed by (A1) and (B).

In accord with these considerations, we identify Λ with $Z_e$ in (A1), with $2n_aZ_e$ in (A2), with $n_aZ_e' = n_a\rho RT/M_0G_e$ in (B), and with $2n_aZ_e$ in (C). We further recommend that *the method of computation of* Λ *be given explicitly in all cases, together with other pertinent details such as the temperature of measurement and information characterizing the molecular weight, molecular weight distribution, degree of branching, and stereochemical structure of the polymer samples on which the data were obtained.*

Some values recalculated on this basis from a recent compilation,[10] together with other recent literature values, are given in Table I. The data on the dependence of the zero-shear viscosity on molecular weights all were obtained on fractions at the temperatures indicated. The viscoelastic function whose inflection point was observed is indicated in the next column. Here most of the data were obtained on unfractionated polymers, and for each the viscosity- or weight-average number of chain atoms is indicated if known. Although the point of inflection frequently is determined from a reduced plot, we have indicated here a temperature in whose neighborhood the actual data were obtained. In most cases the curves do not have a point of zero slope so that the choice of a value of $J_e$ is at best subject to considerable uncertainty and sometimes may be unjustified. The method employing the maximum in $J''(\omega)$ involves the same data as used in the inflection point method at a somewhat different temperature where both kinds of information are available; otherwise more detailed information is indicated.

The values of Λ in Table I are generally of the order of $10^2$ to $10^3$. Values obtained by different methods on the same type of polymer generally differ by no more than a factor of three; in some cases the agreement is much better. It is clear that a better theoretical basis for these methods as well as accurate evaluations of Λ at the same temperature by all three methods on the same series of polymers covering a range of $M$ and/or of molecular weight distribution are required before final conclusions can be drawn concerning their interrelationships.

(10) J. D. Ferry, ref. 6, p. 289.

# 1961 DIRECTORY OF GRADUATE RESEARCH

The newest edition of this unique directory is the fifth to be prepared by the ACS Committee on Professional Training. It covers the 1959–60 and 1960–61 academic years and provides a useful reference to:

**—degrees available**
**—fields of interest and publications of 3702 faculty members**

in 273 departments or divisions of chemistry, biochemistry, and chemical engineering in United States universities offering the Ph.D. degree.

**Under each department heading, degrees offered and fields of specialization appear first. Then faculty members are listed alphabetically with an up-to-date record on their education...general fields of major research interest...subjects of current research...publications during the past two years. You can clearly determine where your own field of interest is most actively represented.**

The table of contents lists universities under the three main groups. There is another index by faculty names. A summary table also shows for each graduate department of chemistry the number on the faculty, number of Ph.D.'s in each department, graduate enrollment, and Ph.D. degrees granted in 1959–60 and 1960–61. It offers as a starting point a quick comparison by size.

If you counsel students or seek an advanced degree yourself, or if you are interested in knowing the kind of research done in certain academic centers, for whatever purpose, then this book will answer your questions and save you time.

**529 pages.** **Paper bound.** **Price: $4.00**

*Order from:*

**Special Issues Sales, American Chemical Society**
**1155 16th Street, N. W., Washington 6, D. C.**